



UNIVERSITY OF
LIVERPOOL

Characterising Load-Induced Changes in 3D
Cultured Mesenchymal Stem Cells Through
Collagen Isoform Composition and
Arrangement

Thesis submitted in accordance with the requirements of the
University of Liverpool for the degree of Doctor in Philosophy

By

Adam Jacques Janvier

September 2021

Abstract

Tissue engineering has been highlighted as a potential regenerative medicine therapy for the regeneration of musculoskeletal tissues, many of which have poor healing capacity. Currently there is no 'gold standard' approach to tissue engineering with many researchers investigating the effects of different stimuli on different cells in different culture environments. One of these stimuli is mechanical stimulation, a variety of which naturally occur in the body. Mechanical stimulation is often used in tissue engineering to recapitulate the structure, extracellular matrix composition (ECM) and biomechanics of tissues such as tendon, bone and cartilage. The extracellular matrix of these tissues is primarily composed of one fibril forming collagen, for tendon and bone this is collagen type I whilst for cartilage it is collagen II. However an array of additional collagen isoforms play important roles in ECM architecture and maturation.

The aim of this thesis was to investigate if collagen synthesis can be used to assess human mesenchymal stem cells (hMSCs) differentiation in response to different mechanical stimulation. Typically tissue engineering studies use the most populous ECM components to highlight the success of the engineered tissues, whilst this makes sense it neglects the minor ECM components. For musculoskeletal tissues fibril forming collagens are routinely the dominant component of the ECM, however without the minor collagens these structure would not function appropriately. The composition of collagens varies across all musculoskeletal tissues, therefore by investigating the complete collagen composition the differentiation of the cells can be identified and the quality of the tissue being engineered can be established. Tensile stimulation, hydrostatic pressure and microgravity were applied to hMSCs seeded within fibrin hydrogels, chosen as it acts as a blank slate material for collagen investigation. These mechanical stimuli were selected as they have all routinely been used to show enhanced or inhibited MSC differentiation, offering a well-established set of mechanical stimulations to investigate their role in the differentiation of hMSCs and how the subsequent collagen production can be used to identify it. Molecular (qPCR and western blot), imaging (histology, TEM and fluorescence) and structural (mechanical testing and μ CT) analytical techniques have been used to assess what collagens have been produced and how this relates to the structural development of the engineered tissue.

The cell embedded hydrogels had varying responses to the different percentages of cyclic tensile stimulation (0%, 3%, 5% and 10%). These specific strains were selected to assess how

Abstract

hMSCs would respond to the static culture (0%), low physiological dynamic strain (1-4%), high physiological dynamic strain (5-6%) and degenerative dynamic strain (>6%). The 0% and 10% strain groups indicated some osteogenic differentiation through Alizarin red staining and ALP analysis from the culture media. Suggesting that physiologically relevant dynamic strain inhibited osteogenic differentiation. 3% cyclic strain saw a two-fold increase in maximum stress and a slight decrease in fibril diameter compared to the control. The 5% strain group saw increases in tendon collagens COL3A1 and COL11A1 as well as tenogenic markers SCXA and TNMD though expression of the negative tendon marker COL2A1 was also increased. At the protein level collagen II was downregulated whilst collagen III was upregulated compared to the control. The fibril diameter and fibre alignment was found to be highest in the 10% strain group, typically a marker of increased mechanical properties, however with 10% strain only the rate of stress relaxation was increased compared to other groups with a decrease in maximum stress compared to the 3% strain group.

The microtissues used for hydrostatic pressure were cultured in one of three culture medias, basic, chondrogenic or osteogenic and with one of four hydrostatic pressure condition, control, 100 kPa, 200 kPa or 300 kPa. The effects of hydrostatic pressure was largely overridden by the differentiation media supplements with the basic media group showing the biggest changes in response to different levels of hydrostatic pressure. The chondrogenic media group displayed the highest level of COL1A1, COL2A1 and COL10A1 suggesting that the hMSCs within this media group were undergoing hypertrophy. At the protein level no microtissues saw significance within a media group suggesting that hydrostatic pressure was not influencing the collagen synthesis of the hMSCs as much as the media types. The μ CT analysis showed within the media groups the density of the mineralised particles was largely unchanged for the basic media, chondrogenic media and control and 100 kPa osteogenic media samples with the osteogenic 200 and 300 kPa being near two fold greater than all other conditions, suggesting that with appropriate media the higher loading regimens generated a more developed mineralised structure than the lower hydrostatic pressure.

It appeared that the microgravity microtissues were all pre-disposed to spontaneously differentiate towards the osteogenic lineage as seen through the collagen gene expression. Further ALP concentration in the media increased in all culture condition across the three week culture period. PCA analysis showed evidence that the static culture was acting separately from the dynamic and microgravity culture suggesting that the increased nutrient diffusion within the RCCS 4H bioreactor was having a significant effect on the culture.

Abstract

Analysis of the ratio of COL14A1 to COL12A1 was used to demonstrate which culture was the most mature, COL14A1 indicating immaturity and COL12A1 maturity. The microgravity group had the least developed ECM due to the highest ratio, whilst the static group had the most developed ECM due to the lowest ratio. This was further supported through the PCA analysis highlighting COL12A1 as one of the largest contributing variables to the statics groups separation from the other two. This indicated that increased nutrient diffusion was inhibiting the maturation of the MSCs compared to static culture and microgravity was amplifying this effect.

Contents

Abstract	i
Contents	i
Index of Figures	vii
Index of Tables	x
Index of Equations.....	xi
List of Abbreviations.....	xii
List of Poster Presentations.....	xvi
List of Oral Presentations	xvi
List of Travel Awards	xvi
List of Publications	xvi
Acknowledgements.....	xvii
1. Chapter 1	1
1.1. Introduction.....	2
1.2. Tissue Engineering.....	3
1.2.1. Overview	3
1.2.2. Scaffolds	5
1.2.2.1. Hydrogels.....	5
1.2.2.1.1. Natural hydrogels.....	6
1.2.2.1.2. Synthetic hydrogels	8
1.2.2.1.3. Decellularised tissue.....	9
1.2.2.2. Bio-Printing.....	9
1.2.3. Bioreactors	13
1.2.3.1. Mechanical stimulation bioreactors.....	13
1.3. Mesenchymal Stem Cells.....	16
1.3.1. Mechanical Regulation of Mesenchymal Stem Cell Differentiation.....	19
1.4. Tendon	23
1.4.1. Function.....	23
1.4.2. Structure.....	23
1.4.2.1. ECM of Tendon.....	24
1.4.2.1.1. Collagens of Tendon	25
1.4.3. Mechanical Properties.....	26
1.4.4. Tendon Tissue Engineering.....	29
1.5. Bone	33

Contents

1.5.1.	Function.....	33
1.5.2.	Structure.....	33
1.5.2.1.	ECM of Bone	35
1.5.2.1.1.	Collagens of Bone	37
1.5.3.	Cells of the Bone.....	39
1.5.4.	Bone Tissue Engineering.....	42
1.6.	Cartilage	46
1.6.1.	Function.....	46
1.6.2.	Structure.....	46
1.6.2.1.	ECM of Cartilage	47
1.6.2.1.1.	Collagens of Cartilage	49
1.6.3.	Cartilage Tissue Engineering.....	52
1.7.	Collagen	56
1.7.1.	Collagen Types – Structure and Function	61
1.7.1.1.	Fibril Forming Collagens	64
1.7.1.2.	FACIT Collagens	66
1.7.1.3.	Basement Membrane Collagen	67
1.7.1.4.	Hexagonal Networking Forming Collagen	68
1.7.1.5.	Microfibrillar Collagens	68
1.7.1.6.	Anchoring Collagen.....	70
1.7.1.7.	MACIT Collagens.....	71
1.7.1.8.	Multiplexin Collagens	71
1.7.2.	Collagen Synthesis.....	73
1.8.	Summary	76
1.9.	Hypothesis.....	76
1.10.	Aims.....	76
2.	Chapter 2	77
2.1.	Materials	78
2.2.	Methods and Optimisation	81
2.2.1.	Cell Culture	81
2.2.2.	hMSC Validation	82
2.2.2.1.	hMSC FACS Verification	82
2.2.2.2.	Tri-Linage Differentiation Assay	83
2.2.2.3.	Conclusion	86

Contents

2.2.3.	Fibrin Hydrogel Formation Optimisation.....	87
2.2.3.1.	Tensile Fibrin Hydrogel Generation.....	88
2.2.3.2.	Hydrostatic Pressure and Microgravity Fibrin Hydrogel Generation.....	91
2.2.4.	Histology.....	93
2.2.4.1.	Calcium Quantification with Alizarin Red	96
2.2.4.2.	Alkaline Phosphatase Assay.....	96
2.2.5.	Protein Extraction and Western Blotting	97
2.2.6.	RNA Extraction and qPCR	102
2.2.7.	Transmission Electron Microscopy.....	105
2.2.8.	CNA35 Collagen-Probe	108
2.2.9.	Mineralised Hydrogel Imaging by Micro-Computed Tomography	117
2.2.10.	Tensile Mechanical Testing	119
2.3.	Statistical Analysis	121
3.	Chapter 3.....	123
3.1.	Introduction.....	124
3.1.1.	Bioreactors for Tendon Tissue Engineering.....	124
3.2.	Hypothesis.....	125
3.3.	Aims.....	125
3.4.	Bioreactor Chamber Fabrication	126
3.4.1.	3D Printing.....	126
3.4.2.	3D Printed Culture Chamber Validation	129
3.4.2.1.	6-Way Tensile Arm Displacement	129
3.4.2.2.	Chamber Cytotoxicity	129
3.5.	Results	131
3.5.1.	Development of Bioreactor Chamber	131
3.5.1.1.	Anchor Post Design.....	131
3.5.1.2.	Initial Concept Designs for 3D Printed Posts and Loading Supports	132
3.5.1.3.	Bioreactor Chamber Design mark 1.....	135
3.5.1.4.	Bioreactor Chamber Design mark 2.....	137
3.5.1.4.1.	Updated Anchor Posts.....	139
3.5.1.5.	Bioreactor Chamber Design Mark 2.1	140
3.5.1.6.	Final Anchor Frame Design.....	145
3.5.1.7.	3D Printed Culture Chamber Validation	147
3.5.1.7.1.	Well Displacement.....	147

Contents

3.5.1.7.2. Lactate Dehydrogenase Assay	148
3.6. Discussion	149
3.6.1. Conclusion	150
4. Chapter 4	151
4.1. Introduction.....	152
4.2. Hypothesis	158
4.3. Aims.....	158
4.4. Experimental Setup	158
4.4.1. Chamber Run design	158
4.4.2. Tensile Stimulation	159
1.1.1. Histology.....	161
1.1.2. Alkaline Phosphatase Assay	163
1.1.3. Tendon Gene Expression	164
1.1.4. Complete Tendon Collagen Composition Expression	166
1.1.5. Transmission Electron Microscopy Analysis	168
1.1.6. CNA35 Collagen-Probe Analysis	170
1.1.7. Tensile Mechanical Testing	173
1.2. Discussion.....	176
1.2.1. Conclusion	180
5. Chapter 5	181
5.1. Introduction.....	182
5.2. Hypothesis.....	184
5.3. Aims.....	184
5.4. Experimental setup	185
5.4.1. Hydrostatic Pressure	185
5.4.2. Hydrostatic Pressure Loading Regime	186
5.5. Results	188
5.5.1. Hydrogel weight and Appearance	188
5.5.2. Histology.....	190
5.5.2.1. H&E.....	190
5.5.2.2. Alcian Blue	191
5.5.2.3. Alizarin Red.....	192
5.5.2.4. Picrosirius Red	194
5.5.3. Alkaline Phosphatase Assay	195

Contents

5.5.4.	Hydrostatic Pressure Collagen Gene Response	196
5.5.5.	Collagen Composition in Response to Hydrostatic Pressure	198
5.5.6.	Micro-Computed Tomography	200
5.6.	Discussion	204
5.6.1.	Conclusion	208
6.	Chapter 6	209
6.1.	Introduction	210
6.2.	Hypothesis	214
6.3.	Aims	214
6.4.	Experimental Design	215
6.4.1.	Microgravity Culture	215
6.5.	Results	216
6.5.1.	Hydrogel Weight and Appearance	216
6.5.2.	Histology	217
6.5.3.	Alkaline Phosphatase Assay	218
6.5.4.	Microgravity Collagen Gene Response	219
6.5.5.	Collagen Composition in Response to Microgravity	222
6.5.6.	Micro-Computed Tomography	224
6.6.	Discussion	226
6.6.1.	Microgravity Culture Differentiation	227
6.6.2.	Static Culture Differentiation	228
6.6.3.	Dynamic Culture Differentiation	229
6.6.4.	Conclusion	230
7.	Chapter 7	231
7.1.	Conclusion and Future Work	235
8.	Chapter 8	236
8.1.	Appendix A – Histology reagent recipes	237
8.2.	Appendix B – Designed Primer Parameters	239
8.3.	Appendix C – Analysis of Primer Efficiencies and Melt Peaks	240
8.4.	Appendix D – Determination of House Keeper Genes	242
8.5.	Appendix E – CNA35 reagent recipes	243
8.6.	Appendix F – CNA35 image acquisition	244
8.7.	Appendix G – μ CT Analysis Macro for Hydrogel Mineralisation	245
8.8.	Appendix H – μ CT Analysis Macro for Hydrogel Density	249

Contents

8.9.	Appendix I – Original Picrosirius red images for hydrostatic pressure study	252
9.	References.....	253

Index of Figures

Figure 1.1. Example of a 3D bio printer	10
Figure 1.2. The differentiation potential of MSCs.....	17
Figure 1.3. Schematic of the hierarchical structure of collagen in tendon	24
Figure 1.4. Schematic stress-strain curve for tendon	27
Figure 1.5. Schematic of viscoelastic loading regimen.....	28
Figure 1.6. Suture repair of torn patellar tendon	29
Figure 1.7. Image of tissue engineered tendon in stretch bioreactor.....	31
Figure 1.8. Schematic of the interior of cortical and trabecular bone	34
Figure 1.9. Schematic of collagen I fibril with hydroxyapatite crystals	36
Figure 1.10. Schematic of osteoblast to osteocyte cycle	40
Figure 1.11. Schematic of osteoclast activation.....	41
Figure 1.12. Schematic of osteoclast adhered to the surface of bone.....	42
Figure 1.13. Damaged cartilage repair techniques	53
Figure 1.14. Schematic of the collagen triple helix	61
Figure 1.15. Schematic of collagen α -chain primary structures and functional domains	63
Figure 1.16. Schematic of fibrillar forming collagen	65
Figure 1.17. Schematic of FACIT collagens.....	66
Figure 1.18. Schematic of the collagen basement membrane subcategory.....	67
Figure 1.19. Schematic of collagen type VIII and X hexagonal lattices	68
Figure 1.20. Schematic of microfibril collagen	69
Figure 1.21. Schematic of collagen type VII	70
Figure 1.22. Schematic of MACIT collagens	71
Figure 2.1. Human mesenchymal stem cells.....	81
Figure 2.2. Flow cytometric analysis of minimal stem cell markers.....	83
Figure 2.3. Histological analysis of trilineage differentiation.....	86
Figure 2.4. Effects of thrombin concentration of fibrin formation	87
Figure 2.5. Protein concentration from fibrin hydrogels	97
Figure 2.6. Collagen extraction flow diagram.	98
Figure 2.7. Gel and membrane setup for electrophoretic transfer.....	100
Figure 2.8. Example of western blot	101
Figure 2.9. Thermal profile for qPCR.....	103
Figure 2.10. Axis the fibrin hydrogels were cut along for TEM	105
Figure 2.11. TEM image processing	107
Figure 2.12. 1% agarose gel electrophoresis of DNA	109
Figure 2.13. SDS-PAGE gel of extracted protein from CNA35 culture.....	111
Figure 2.14. Nanodrop results to investigate the success of the DyLight 488 binding	112
Figure 2.15. Schematic of the sample preparation process for vibrotome sectioning	114
Figure 2.16. Anchor point region and Mid region highlight on fibrin hydrogel	115
Figure 2.17. CNA35 mage opened in Image J.....	115
Figure 2.18. Colour key for OrientationJ.....	116
Figure 2.19. Example arrangement of samples in imaging tube for μ CT.	117
Figure 2.20. Schematic of fibrin hydrogel within paper frame.	119
Figure 2.21. Tensile Mechanical testing.....	119

Index of Figures

Figure 3.1. Bioreactor chamber CAD during design process in Creo Parametric.	126
Figure 3.2. CAD on CURA software	127
Figure 3.3. Schematic of displacement measurements for chamber validation.....	129
Figure 3.4. Schematic of the anchor posts from culture plate to bioreactor.....	133
Figure 3.5. Anchor post in EBERS TC3 chamber	134
Figure 3.6. Initial design of 3D printed bioreactor chamber	136
Figure 3.7. Bioreactor chamber mark 2	138
Figure 3.8. Render of updated anchor posts.....	139
Figure 3.9. Render of updated bioreactor chamber and anchor posts.....	140
Figure 3.10. Dimensions of bioreactor chamber body mark 2.1.....	141
Figure 3.11. Final design of 3D printed culture chamber.....	143
Figure 3.12. Anchor frame	145
Figure 3.13. Dimensions of anchor frame.....	145
Figure 3.14. Flow of anchor frames from contraction to loading	146
Figure 3.15. Linear displacement of the 6-way tensile arm	147
Figure 3.16. LDH assay for bioreactor chamber.....	148
Figure 4.1. Tensile stimulation experimental run	159
Figure 4.2. Bioreactor chambers and EBERS TC-3 in non-humidified incubator.....	160
Figure 4.3. Histological analysis of tissue engineered tendons.....	162
Figure 4.4. Alkaline phosphatase expression of tissue engineered tendons	163
Figure 4.5. Gene expression analysis of tendon differentiation genes.....	164
Figure 4.6. Gene expression analysis of collagen isoform composition.....	165
Figure 4.7. Western blot analysis of tendon collagen isoforms	167
Figure 4.8. TEM analysis of tissue engineered tendons	169
Figure 4.9. Tissue engineered tendons stained with CNA35 collagen-probe	171
Figure 4.10. CNA35 collagen fibre analysis	172
Figure 4.11. Stress vs strain profiles for all tissue engineered tendon	174
Figure 4.12. Viscoelastic profiles of tissue engineered tendons	175
Figure 4.13. The stress relaxation profiles	175
Figure 5.1. Hydrostatic pressure bioreactor setup.	185
Figure 5.2. Representative images of microtissues.....	188
Figure 5.3. Weight of microtissues.....	189
Figure 5.4. H&E staining of microtissues.....	190
Figure 5.5. Alcian blue staining of microtissues	191
Figure 5.6. Alizarin red staining of microtissues	192
Figure 5.7. Alizarin red assay for osteogenic microtissues.....	193
Figure 5.8. Picosirius red staining of microtissues.....	194
Figure 5.9. Graphs of alkaline phosphatase media content.....	195
Figure 5.10. Collagen gene expression for hydrostatic pressure regimen	197
Figure 5.11. Densitometry of collagen types for hydrostatic pressure regimen.....	199
Figure 5.12. Representative μ CT images of microtissues	202
Figure 5.13. μ CT analysis of hydrostatic pressure microtissues.....	203
Figure 6.1. Free fall microgravity bioreactor setup.....	213
Figure 6.2. Size and weight of microgravity microtissues	216
Figure 6.3. Histological sections of microtissues.....	217

Index of Figures

Figure 6.4. ALP activity in the media of static, dynamic and microgravity.....	218
Figure 6.5. Collagen gene expression for microgravity microtissues	220
Figure 6.6. Ratio of COL14A1 to COL12A1	221
Figure 6.7. PCA of microgravity collagen gene expression	221
Figure 6.8. Densitometry of collagen extracted from microgravity microtissues.....	223
Figure 6.9. μ CT analysis of microgravity microtissues	225
Figure 8.1. Example of primer efficiency calculation	241
Figure 8.2. Graphical representation of GeNorm calculation	242
Figure 8.3. Acquisition information for CNA35 collagen probe staining.....	244
Figure 8.4. Original Picosirius red images of microtissues.....	252

Index of Tables

Table 1.1. Table of collagen types and the associated category	57
Table 2.1. Tissue processing protocol for fibrin hydrogels	94
Table 2.2. Antibodies	101
Table 2.3. Primer sequences for investigated genes.	104
Table 3.1. Design iterations of the 3D printed posts	132
Table 3.2. Full components list for the bioreactor chamber.....	144
Table 4.1. Published work on cyclic tensile stimulation for tendon tissue engineering	154
Table 8.1. Table of primers used and their parameters.....	239
Table 8.2. Table of macro used to determine hydrogel mineralisation.....	245
Table 8.3. Table of macro used to determine hydrogel density.	249

Index of Equations

Equation 1. Total protein in volume.....	116
Equation 2. Amount of DyLight 488.....	116
Equation 3. Volume of dye to add.....	116
Equation 4. Molar protein concentration.....	117
Equation 5. Molecules of dye per mole protein.....	118
Equation 6. Stress.....	124
Equation 7. Strain.....	124
Equation 8. Hysteresis.....	124
Equation 9. Percentage energy loss.....	124
Equation 10. Rate of change of stress.....	124
Equation 11. Young's modulus.....	124
Equation 12. Porosity.....	144

List of Abbreviations

ACI	Autologous chondrocyte implantation
ALP	Alkaline phosphatase
ANK	Ankylosis
ANOVA	Analysis of variance
ATP	Adenosine triphosphate
BBPER	BugBuster protein extraction reagent
BCA	Bicinchoninic acid
BMP1	Bone morphogenetic protein 1
BSA	Bovine serum albumin
BSP	Bone sialoprotein
c-fms	Colony stimulating factor 1 receptor
CAD	Computer aided design
CAII	Carbonic anhydrase II
Clp	Chloroproline
DHh	Desert Hedgehog
DLP	Digital light process
DMEM	Dulbecco's modified Eagle's Medium
DMF	Dimethylformamide
DMLS	Polyjet, direct metal laser sintering
DMP1	Dentin matrix protein-1
DMSO	Dimethyl Sulfoxide
DNA	Deoxyribonucleic acid
EBM	Electron beam melting
ECM	Extracellular matrix
EDTA	Ethylenediaminetetraacetic acid
ENPP1	Ectonucleotide pyrophosphatase/phosphodiesterase 1
ER	Endoplasmic reticulum
F-actin	Filamentous actin

List of Abbreviations

FACIT	Fibril associated collagen with interrupted triple helix
FACS	Fluorescence-activated cell sorting
FBS	Foetal calf serum
FFF	Fused filament fabrication
FGF	Fibroblast growth factors
FKBP	FK506 binding proteins
Flp	Fluoroproline
flp	Fluoroproline
FSC	Forward light scatter
FZ	Frizzled
GAG	Glycosaminoglycan
Gly	Glycine
H&E	Haematoxylin and eosin
H ⁺ -ATPase	H ⁺ -adenosine triphosphate
Hh	Hedgehog
hMSC	Human mesenchymal stem cell
HPC	Hydrostatic pressure chamber
HSP47	Heat shock protein 47
Hyp	Hydroxyproline
IBMX	3-Isobutyl-1-methylxanthine
IFM	Interfascicular matrix
IGF-1	insulin-like growth factor
IHh	Indian Hedgehog
ISS	International Space Station
ITS	Insulin-Transferred-Sodium
LDH	Lactate dehydrogenase
Lgr	Leucine-rich repeat-containing G-protein-coupled receptors
LOX	Lysyl oxidase
M-CSF	Macrophage-colony stimulating factor
MACIT	Membrane associated collagen with interrupted trip helix

List of Abbreviations

MAPK	Mitogen activated protein kinase
MCTS	Multicellular tumour spheroids
MEMS	Micro-electromechanical system
MEPE	Matrix extracellular phosphoglycoprotein
MGP	Matrix Gla protein
MJF	Multi jet fusion
MMP	Matrix metalloproteinase
MSC	Mesenchymal stem cell
MSCRAMM	Microbial surface component recognising adhesive matrix molecule
mTLD	Mammalian tolloid
NBF	Neutral buffer formalin solution
OPG	Osteoprotegerin
OPN	Osteopontin
PA	Polyacrylamide
PBS	Phosphate-buffered saline
PC	Phenol chloroform
PCA	Principle component analysis
PCL	Polycaprolactone
PCM	Pericellular matrix
PDGF	Platelet-derived growth factor
PDMS	Polydimethylsiloxane
PEEK	Polyether ether ketone
PEG	Polyethylene glycol
PGA	Polyglycolide
PLA	Polylactic acid
PPIase	Peptidyl prolyl cis-trans isomerases
Pro	Proline
Pt	Porosity
Ptc	Patched
qPCR	quantitative polymerase chain reaction

List of Abbreviations

RANKL	Receptor activator of nuclear factor- κ B ligand
RCCS	Rotating cell culture system
RNA	Ribonucleic acid
Rspo	R-spondins
SDFT	Superficial digital flexor tendon
SHh	Sonic Hedgehog
SIBLINGs	Small integrin-binding ligands N-linked glycoproteins
SLA	Stereolithography
SLRP	Small leucine-rich proteoglycans
SLS	Selective laser sintering
Smo	Smoothened
Sox9	SRY-Box Transcription Factor 9
SSC	Side light scatter
STL	StereoLithography
STLV	Slow-turning lateral vessel
STZ	Superficial zone
TANGO1	Transport and Golgi organisational protein 1
TBS	Tris-buffered saline
TEM	Transmission electron microscopy
TGF- β	Transforming growth factor-beta
TLL-1	Tolloid like 1
TNAP	Tissue-nonspecific alkaline phosphatase
TNG	Trans-Golgi network
TSP	Thrombospondin
Vp	Pore volume
Vt	total volume
VTCs	Vesicular tubular cluster
vWF-A	Type A domains of von Willebrand factor
Wnt	Wingless-type MMTV integration site
μ CT	Micro-computed tomography

List of Poster Presentations

Mercia stem cell conference 2016, Manchester, UK – Bioreactors for engineering 3D musculoskeletal tissues: how does mechanical stimulation affect collagen isoform expression?

UKSB 2017, Loughborough, UK – How does mechanical loading of 3D biomimetic scaffolds effect collagen production?

TCES 2017, Manchester, UK – Bioreactors for engineering 3D musculoskeletal tissues: how does mechanical stimulation affect collagen isoform expression?

FIRM 2017, Girona, Spain – How does mechanical loading of 3D biomimetic scaffolds effect collagen production?

TERMIS world congress 2018, Kyoto, Japan – 3D printed bioreactors for tendon tissue engineering: characterising load-induced changes by the ‘collagen barcode’

BSMB 2019, Liverpool, UK – Mechanical stimulation for tissue engineering: characterising load-induced changes by the ‘collagen barcode’.

List of Oral Presentations

FIRM 2017, Girona, Spain – How does mechanical loading of 3D biomimetic scaffolds effect collagen production?

Tendon UK 2018, Oxford, UK – 3D printed bioreactors for tendon engineering: characterising load induced changes by the ‘collagen barcode’

List of Travel Awards

TCES travel bursary 2018 – Attendance to Tendon UK 2018

List of Publications

Janvier AJ, Canty-Laird E, Henstock JR. (2020) A universal multi-platform 3D printed bioreactor chamber for tendon tissue engineering. *Journal of Tissue Engineering*. 2020 10.1177/2041731420942462

Janvier AJ, Pendleton EG, Mortensen LJ, Green DC, Henstock JR, Canty-Laird E. (2021) 3% cyclic strain improves tensile strength, whilst 10% strain increases collagen fibril diameter and fibre alignment in de-novo cell-engineered tendons. *International Journal of Molecular Sciences*. *Submission pending*.

Acknowledgements

This PhD would not have been possible without the generous funding from the University of Liverpool. I would also like to acknowledge the Royal Societies support funding for the EBERS TC3 Bioreactor.

Before I started my PhD I had never held a pipette let alone culture cells. I would therefore like to first thank my supervisors Dr James Henstock and Dr Elizabeth Canty-Laird for the initial faith they showed in me and the continued support, guidance and patience throughout. Without them there would be no PhD, I am forever grateful.

I would like to thank the technical staff at the William Henry Duncan Building for their training and maintenance of all the systems I used throughout my work. Miss Marion Pope for her expertise's in TEM and the Leahurst Campus for the use of their facilities. The team at the Cell Sorting and Isolation Facility for their help with flow cytometry and Professor Rob Van 'T Hof's group for their expertise on μ CT.

I would like to thank my colleagues who I have met during my time at the William Henry Duncan Building, ensuring we laughed as much as we stressed. In particular I would like to thank Shahjahan Shigdar, Lorenzo Ramos, Lina Abdul-Kadir, Conor Sugden, Danielle O'Loughlin, and Daniel Green. My former flat mates Euan Owen and Francesca Manuela Johnson de Sousa Brito deserve a special mention, you both supported me through the hardest periods of my PhD, the time I spent living with you both was some of the most enjoyable of my life and a period I will always look back on fondly.

Finally I would like to thank my friends and family. The Gittings family have allowed me to write my thesis at their home during the COVID-19 pandemic and have made me feel so welcome and comfortable, truly thank you. My parents, Tina and Richard and siblings, Myles and Jessica, have only ever shown encouragement and support even when I doubted myself, I wouldn't have been able to complete this without you guys. I would like to especially thank my girlfriend Harriet, you have an ability to calm me like no one else and make me laugh without trying, thank you.

Chapter 1

General Introduction

1.1. Introduction

In response to changes during development, ageing and illness the cells of a tissue will react by changing the extra cellular matrix (ECM), this may have a positive impact such as increased hydroxyapatite during bone development (Long, 2011) or a negative impact such as increased collagen I in osteoarthritic cartilage (Lahm et al., 2010). One of the key components of the ECM of musculoskeletal tissues is collagen, of which there is at least 28 different types with each type performing a different specific function within the ECM (Ricard-Blum, 2011). The presence and proportion of the different collagen types varies between tissues, for example in tendon types I, II, III, V, XI, XII and XIV are present with type I accounting for >90% of the collagen whilst in cartilage types I, II, VI, IX, X, XI, XII, XIV are present with type II accounting for >90% of the collagens (Thorpe et al., 2013, Sophia Fox et al., 2009). The specific collagen composition has the potential to be used to identify the tissue. One of the key regulators of collagen is the mechanical forces applied to the tissue, which has been shown to regulate cell differentiation and subsequent protein synthesis (Sarasa-Renedo and Chiquet, 2005). For example higher tensile strain rates applied to tendon will result in an increase in collagen I, this will result in an increase in stiffness of the tissue therefore enabling the tissue to better cope with the force, this is seen during exercise (Carroll et al., 2017). However excessive force leads to cell death and eventual tissue rupture (Wang, 2006), appropriate mechanical stimulation is required to grow healthy tissue.

Tissue engineering is the *in vitro* development of native tissues. This can be achieved in multiple ways, one such approach is the use of a 3D biomimetic scaffold seeded with cells and exposed to chemical and/or mechanical stimulation in order to develop the targeted tissue. Mesenchymal stem cells (MSCs) are one of the most frequently used cell types for musculoskeletal tissue engineering as they possess the potential to differentiate down a large number of cell lineages including tenogenic, osteogenic, chondrogenic, adipogenic and myogenic (Dominici et al., 2006). The differentiation of MSCs is well characterised through the use of media supplements and the application of mechanical stimulation, with different stimuli better suited for different tissues, for example compression stimulation has been found to induce osteogenic differentiation whilst inhibiting adipogenic differentiation (Rath et al., 2008, Li et al., 2013) Mechanical stimulation is typically applied through the use of a bioreactor, these are specialised devices that are designed to apply a specific function to biological systems such as tensile strain, hydrostatic pressure or microgravity. The mechanical stimulation is received by the cell through mechanotransduction, this may be

through cell membrane deformation, cytoskeleton deformation or protein unfolding amongst others and results in the activation of signalling pathways such as the p38 MAPK pathway (Deng et al., 2008).

There are many material options for the 3D culture of cells both naturally derived and synthetic, one of the most widely used is fibrin . Fibrin is formed at wound sites and is generated through the selective cleavage of the glycoprotein fibrinogen by the protease thrombin (Brown and Barker, 2014). The key advantages of fibrin include the well-established approach in the field, pre-existing use as a natural scaffold in the body, cell adhesion and that it can be considered a blank slate material enabling investigation of an ECM solely produced by the cells (Paxton et al., 2012).

The assessment of successful tissue engineering is typically done by investigating the production of ECM products that are widely found in a tissue, this approach excludes a number of important and less populous ECM components such as the minor collagen types. In tendon tissue engineering for example collagen I and III (the most abundant) are typically assessed for success excluding types II, V, XI, XII and XIV, however without the other types the type I and III fibrils would not form correctly resulting in a non-functional tissue. It is therefore necessary to assess all collagen types within the tissue engineered structure to assess the success. The specific collagen types and their proportion detected can then be used to define the cell differentiation and the tissue generated.

1.2. Tissue Engineering

1.2.1. Overview

Tissue engineer is a branch of regenerative medicine that first emerged as a potential solution to aid in the repair and restoration of damage tissue and organs which, still to this day, is widely provided by donations (Lanza et al., 2020). The shortage of donors coupled with the increasing number of people of the donor waiting list and the ever-increasing aging population acts as a major limiting factor to the effectiveness of tissue and organ donations. In the USA there are over 113,000 people on the transplant waiting list with around 17,000 people waiting for over five years (OPTN, 2020). The effectiveness of tissue engineering as a replacement for organ and tissue donations has been limited, though there has been a few clinical successes such as INTEGRA, used for skin repair, and Osteopore, applied during craniofacial bone surgery. Whilst the regenerative medicine applications are continued to be

tackled newer approaches which utilise tissue engineering are beginning to be used such as the emerging culture meat field (Ben-Arye and Levenberg, 2019).

Tissue engineering was first proposed in the 1970/80s where initial studies focused on seeding cells onto existing biological scaffolds to generate new functioning tissue. One example by Green (1977) saw chondrocytes seeded onto decalcified bone to repair cartilage defects. Whilst these results were not satisfactory the principles helped to develop the basis for tissue engineering. The field then moved towards using biocompatible scaffolds to grow cells and develop the ECM. Early work looked to use natural scaffolds, such as collagen and fibrin, on which cells were seeded with the potential to act as replacements for tissue such as skin. The study by Vacanti (1988) was the next key work in the emerging field, here the author moved away from using natural scaffolds to seed the cells onto specifically designed scaffold that had appropriate chemical and physical properties for the tissue of interest. In 1981 the first engineered tissue transplantation, artificial skin for burn injuries, was developed by Burke et al. (1981), here the dermal and epidermal layers were separated to two scaffolds, the dermal was made up of bovine collagen and chondroitin 6-sulfate from shark cartilage whilst the epidermal was made of medical grade Silastic. As the field progressed so did the engineered tissue. In 1999 the first laboratory grown organ, an artificial bladder, was implanted into patients (Atala et al., 2006). The artificial bladders were generated from a collagen and polyglycolic acid scaffold and seeded with urothelial and muscle cells, however there have been numerous obstacles that have since been identified and slowly overcome (Adamowicz et al., 2017). Whilst the use of tissue engineering has not progressed as rapidly in medicine as initially expected it is currently used for cartilage, bone, skin, bladder, vascular graft and cardiac tissues in modern medicine (Colombo et al., 2017, Lanza et al., 2020).

As the tissue engineering field developed so did the applications, one of the key techniques to emerge was organoids for enhanced *in vitro* studies. Organoids are miniature tissue engineered versions of organs that are generated by cells by mimicking organogenesis with uses including drug screening and development (Sasai et al., 2012). This enables a study to more closely resemble the *in vivo* environment than the traditional 2D culture. These tissue engineered approaches allow for a more rapid understanding of diseases such as cancer and dementia, whilst also reducing the need for animal testing. With continued development, patient specific research may become a reality, featuring patients derived cells with organ-on-a-chip or 3D tissue engineered models to identify genetic triggers for specific diseases helping to speed up and specify diagnosis.

Whilst the applications for tissue engineering vary the basis in which the structures are generated are relatively consistent. The tissue engineered structure is typically formed from a population of cells within a 3D environment. The 3D structure is then cultured under controlled conditions designed to optimise desirable outcomes such as cell differentiation, protein synthesis and structural development. To achieve a robust product initial experimental criteria need to be defined including 3D scaffold, cell type, and culture environment.

1.2.2. Scaffolds

Cells within an *in vivo* environment operate in a highly developed 3D structure that has evolved to deliver a specific function, it is therefore impossible to re-create this same environment in 2D cell culture. Tissue engineering better replicates the *in vivo* environment by culturing the cells within a 3D structure, of which there is a wide variety that have been utilised to develop the lab based engineered tissues. The cell-cell and cell-ECM interaction is driven by the 3D structure in which the cell reside, with increased development of the 3D structure material leading to a promotion in proliferation, migration and matrix production. There is therefore a wide range of 3D cell culture techniques including decellularised ECM and natural/synthetic hydrogels. The natural hydrogel fibrin has been used throughout the present study due to the well-established application for a range of different tissues types (Osathanon et al., 2008, Heher et al., 2015, Almeida et al., 2016, Gonzalez de Torre et al., 2016, Carroll et al., 2017), natural biocompatibility and cell adhesion properties (Almelkar et al., 2014) and, most importantly, offering a blank slate for collagen synthesis and detection (Paxton et al., 2012). This section introduces a number of different biomaterials available for 3D cell culture including fibrin.

1.2.2.1. Hydrogels

Hydrogels are 3D polymeric structures that are primarily made up of water and can incorporate and facilitate cells and proteins. Hydrogels can be broken down into two categories, synthetic (e.g. polyacrylamide and polyethylene glycol) and natural polymers (e.g. collagen, fibrin, alginate and hyaluronic acid) (Lee and Kim, 2018). The choice of hydrogel depends on the users preference towards 2D and 3D culture, the tissue aiming to be engineered with different materials enabling cells to adhere in a variety of ways, different levels of stability in culture and the structural properties of the material. Fabrication of the hydrogels is enabled by chemical or physical cross-link methods (Khunmanee et al., 2017).

1.2.2.1.1. Natural hydrogels

Fibrin is formed naturally at wound sites (Weisel and Litvinov, 2013) where the serine protease thrombin selectively cleaves two small amino acid sequence in the amino-termini of the A α and B β chain of the dimeric glycoprotein fibrinogen. Successful cleavage exposes polymerisation sites, resulting in the formation of fibrin molecules that interact through disulfide bonds (Brown and Barker, 2014). Factor XIIIa is activated by thrombin and increases the fibrin stability by introducing ϵ -N-(γ -glutamyl)-lysyl crosslinks between residues in the γ - and α -chains of fibrin monomers (Byrnes et al., 2015). The ratio of thrombin to fibrinogen dictates the fibril size and pore sizes (Lawrie et al., 1998). The pore size is important for sufficient nutrient uptake and cell transport. Larger pores allow for increased cell growth rates however this must be achieved without compromising the structural integrity (Chiu et al., 2012). Once formed fibrin will naturally contract, closing the wound site in an *in vivo* environment. The contraction is utilised during tissue engineering by casting the fibrin between two posts which causes the material to generate a rod like structure similar to that of tendon, bone or muscle. Cells can be either mixed with the raw components of the fibrin hydrogel prior to gelation and therefore cast within as the gel polymerises or seeded on top of the formed fibrin where the cells will then migrate through the structure.

Fibrin's role within the body as a natural scaffold makes it appealing as a hydrogel due to its cell adhesion properties resulting in the material being widely used in studies investigating cell-mediated collagenous tissue assembly (Bian et al., 2012, Paxton et al., 2012). Fibrin hydrogels exhibit viscoelastic properties with low stiffness, therefore limiting its effectiveness as a replacement material for damaged tissue. The long term culture of fibrin is restricted by the material's high susceptibility to protease mediated degradation however additives to the culture media such as 6-amino-n-caproic acid inhibits the fibrin degradation (Kupcsik et al., 2009).

Collagen is one of the most abundantly utilised hydrogels for tissue engineering musculoskeletal tissue such as bone, tendon and ligament (Antoine et al., 2014). Collagen type I is widely used due to the relative ease of extraction with the most common source being rat-tail tendons, typically collagen type I is extracted using a solution of acetic acid and pepsin and stored in a low pH solution at a low temperature to prevent spontaneous fibril formation (Walters and Stegemann, 2014). By raising the temperature and pH the collagen will undergo gelation and form a 3D structure, cells can either be pre-mixed with the liquid collagen or seeded on top of the gelled collagen. Similarly to fibrin, collagen will form a rod

like structure if generated about two fixed posts. Through temperature controlled gelation the collagen I fibrils thickness can be altered, changes in fibril thickness can help control structural properties, cellular migration and morphology (Doyle et al., 2015).

Collagen II has been utilised at a lower extent for hydrogel formation, primarily in cartilage tissue engineering. Collagen type II has been extracted from chicken sternum to generate hydrogels (Vidal Bde and Mello, 2016). Comparison between the collagen I and II hydrogels showed that the structure of collagen type II more appropriately mimicked the ECM of cartilage and promoted cartilage gene expression highlighting the importance of hydrogel material choice (Vidal Bde and Mello, 2016, Lazarini et al., 2017). The key advantages of using collagen based hydrogels is the cytocompatibility, cell adhesion and viscoelastic structural properties. The collagen based hydrogels do feature some disadvantages including low stiffness, batch to batch variation and limited long term stability. Some of these disadvantages can be alleviated with chemical cross-linking however this can drastically change the degradability of the structure whilst only slightly improving the structural stiffness (Bian et al., 2009).

Other ECM derived hydrogels feature collagen types within the solution, this includes the commercially available Matrigel which is extracted from Engelbreth-Holm-swarm mouse sarcoma tumours and includes collagen type IV along with other basement membrane components. Matrigel again has low structural mechanical properties and high batch to batch variation. This coupled with the tumorigenic origin has resulted in high levels of uncertainty in tissue engineering studies and the requirement of more tuneable hydrogels. One of the main targets of tissue engineering is to regenerate the native ECM found in healthy tissue. ECM derived hydrogels present the initial culture with these components from the initial hydrogel formation by generating the hydrogel from solubilised and polymerised native ECM. This results in a hydrogel that retain the full biochemical complexity of the native tissue without the tumorigenic origin of Matrigel (Saldin et al., 2017). Many tissues have been solubilised for ECM hydrogels such as the esophagus (Keane et al., 2015), heart (Seif-Naraghi et al., 2013) and tendon (Farnebo et al., 2014) typically using a pepsin based approach, however each tissue requires different digestion times, concentrations, pH among other process parameters.

Whilst collagen and fibrin feature similar structural and cell adhesion characteristics, other natural polymers do not and require modifications to enable their use as a hydrogels, this includes alginate and hyaluronic acid. Hyaluronic acid, a nonsulfated glycosaminoglycan

composed of a repeating disaccharide unit of glucuronate and N-acetylglucosamine (Meyer, 1958), is found in a wide range of tissues including cartilage, skin and the brain and has been shown to play roles in development and healing (Fraser et al., 1997). The biggest advantage to using hyaluronic acid hydrogels is the tunability of the structure, these modifications include enabling cell adhesion, release of growth factors and other proteins and manipulation of the mechanical properties of the structure (Burdick and Prestwich, 2011). CD44 expression has been found to induce cell adhesion to hyaluronic acid hydrogels through reduced material stiffness enabling integrin based adhesion, suppression of CD44 was found to impair cell adhesion (Kim and Kumar, 2014).

Alginate is a polysaccharide derived from brown algae that consists of β -D-mannuronic acid M units and α -L-guluronic acid G units which assembles as block copolymers (Martinsen et al., 1989, Augst et al., 2006). Alginate forms a hydrogel through ionic crosslinks between the G units generated using divalent cations (e.g. calcium, magnesium and barium) (Augst et al., 2006). By rapidly forming the cross linked structure cells can be encapsulated for 3D culture, alginate then offers the ability to easily dissolve allowing for cell recovery, though as the cells cannot degrade the hydrogel they remain relatively rounded meaning this structure is most suited to chondrogenic 3D culture but has limited application for other cell types.

1.2.2.1.2. Synthetic hydrogels

Synthetic polymers offer highly tuneable structures; materials include polyacrylamide (PA) and polyethylene glycol (PEG). PA hydrogels are generated by reacting acrylamide monomer and bisacrylamide crosslinker in the presence of ammonium persulfate and tetramethyl ethylene-diamine (Caliari and Burdick, 2016). PEG forms a hydrogel when combined with a crosslinking substrate such as (meth)acrylates, alternatively when combined with diacrylate the mixture forms a gel when exposed to UV light (Caliari and Burdick, 2016). The advantages of PA derive from the well-established fabrication protocols which allows to dictate the mechanical properties of the structure and the ease of protein coupling (Pelham and Wang, 1997, Tse and Engler, 2010). The structure of the PA hydrogel is highly directable and the cell adhesion is pre-determined this enables a more complete understanding of the cellular response when compared to a natural polymer derived hydrogel. However PA hydrogels cannot be used for 3D encapsulation of cells due to the toxicity of the hydrogel precursors, therefore this synthetic polymer is used with 2D culture where the adhesion layer is finely tuneable (Caliari and Burdick, 2016). PEG is considered a blank slate material which again allows for high modification to the structural and biological properties. As a basic material

PEG does not offer many advantageous properties but with the addition of modification materials the structure becomes highly adaptable and useful for a wide range of applications (Kong et al., 2017).

1.2.2.1.3. Decellularised tissue

Decellularised tissue is a highly attractive form of 3D cell culture as it offers the most close-to-nature mechanical and biological properties of all 3D structures (Chan and Leong, 2008). Decellularised tissues have been used to tissue engineer heart valves (Knight et al., 2008), vessels (Borschel et al., 2005), nerves (Hall, 1997) and tendons (Ingram et al., 2007). Decellularisation of tissue is achieved through a multi-step process that involves lysing cell membranes through freeze thaw cycles or ionic/non-ionic solution before separating the cellular components from the tissue by enzymatic method such as trypsin/EDTA treatment. The cytoplasmic and nuclear cellular components are then solubilised and removed using specific detergents (Chan and Leong, 2008). Ionic detergents, such as SDS, are the most robust at removing cells however these ionic solutions also remove GAGs and growth factors from the ECM, should these components be required a non-ionic solution, such as Triton X-100, can be used in place, though these do not decellularise the tissue as effectively (Reing et al., 2010, White et al., 2017). By removing the cellular components from the tissue the process also removes the allogenic or xenogeneic cellular antigens that may otherwise result in immune rejection upon implantation. The decellularised tissue can then be repopulated with the patient's cells generating a structure that closely replicates the originally damaged tissues structure, however this technique requires surgery to acquire the scaffold. The decellularised tissue may not be entirely decellularised which may result in immune rejection and the seeded cells may not be evenly distributed across the structure leading to an inhomogeneous distribution and therefore incomplete tissue (Zheng et al., 2005). One of the main draw backs from tissue decellularization is the protocol variation between different tissue types, therefore requiring empirical experimentation and optimisation before the tissue can be used (Heath, 2019). A set of minimum criteria have been established to standardise the decellularization of tissues; 1) less than 50 ng double stranded DNA/mg dry ECM, 2) <200 base pair DNA fragment length and 3) lack of visible nuclear material when stained with DAPI or H&E (Crapo et al., 2011).

1.2.2.2. Bio-Printing

One of the major issues with scaffolds used in tissue engineering is the variation seen during the fabrication of the 3D structure. This can be due to batch to batch variation when using

naturally derived materials or due to the operator, who when dispensing and incubating the components will inevitably incur variation from scaffold to scaffold. A potential solution to the human lead variation is automation, with bioprinting offering an automated scaffold manufacturing process.

Bioprinting is a relatively new form of 3D printing (Fig.1.1), this form of additive manufacturing works in a very similar way to standard 3D printing in that the component to be manufactured is generated on a computer system and then printed using the selected material in a layer by layer deposition process. The material is then crosslinked using chemical, UV or heat approaches to solidify the structure ready for use (Ozbolat et al., 2016). Where bio-printing differs from standard 3D printing is that the components being printed are designed for tissue engineering, typically as scaffolds for cells to grow on or in. If the material used for printing contains live cells it is referred to as bioinks (Hospodiuk et al., 2017), bioinks may also contain growth factors and ECM components (Ozbolat et al., 2016). A wide range of materials are available for bio printing and are similar to those already used as hydrogels for tissue engineering, including natural polymers such as agarose, alginate, chitosan, collagen, Matrigel, fibrin, gelatin and hydroxyapatite and synthetic polymers such as graphene, PLA and Pluronic F127 (Aldrich, 2020), with each material better suited to different forms of bio printing and for different types of targeted tissues.



Figure 1.1. Example of a 3D bio printer, the Cellink Box X (left) and a bioprinted hydrogel (right) (Cellink, 2021).

The types of bio printing can be split into two broad groups, the nozzle based and the light based, with nozzle based including inkjet and extrusion and light base including laser assisted, digital light processing (DLP) and volumetric. The original bio-printing technique was the inkjet method developed by Thomas Boland in the early 2000s (Mironov et al., 2003).

Cells were encapsulated within a hydrogel solution and were stored within a sterile cartridge, the cartridge was connected to the printer which secreted the bioink as droplets of a controlled size. The droplets were dispensed in a predetermined pattern to produce the computer generated design and the bioink was crosslinked as required. This method prints designs quickly, is relatively low cost due to the simple design and retains a high cell viability (80-90%) (Mandrycky et al., 2016). However due to the technique used to control the droplet size and shape, micro-electromechanical system (MEMS), high viscosity materials cannot be used with this technique, the viscosity of the material is not only affected by the materials properties but also the cell density, a higher number of cells increases the viscosity therefore the cell density is limited by the technique to approximately 1×10^6 cells/ml (Pepper et al., 2012). The method has also been shown to induce the settling effect; initially the cells are well mixed within the cartridge, however as the printing progresses the cells begin to settle within the cartridge, leading to uneven cell distribution and eventual clogging of the system as the cell density increases at the nozzle (Pepper et al., 2012).

Extrusion printing was developed in order to print the more viscous materials. Either an air-force pump or screw plunger is used to continuously force the material through the nozzle, this results in a continuous cylindrical line of bioink being dispensed onto the build plate, the bioink is then crosslinked as required to form the structure intended. This method allows for a much wider range of bioinks to be used and at a higher cell density than the inkjet method. This method is limited by the resolution of the printer and the geometry it is able to achieve. To improve the complexity of geometries extrusion printers typically come with multiple nozzles to allow for the printing of multiple materials in parallel, this allows for a support structure to be generated around the scaffold, once printing is complete the support structure can be dissolved away leaving the desired scaffold. High levels of shear force are seen as the material is extruded through the nozzle, this leads to relatively high cell death during the fabrication.

Laser assisted printing originated from laser direct write (Bohandy et al., 1986) and laser induced transfer technologies (Duocastella et al., 2007, Kattamis et al., 2007). The laser is fired at an energy absorbing layer, such as gold or titanium, known as the donor layer. The laser is fired at the desired location on the donor layer causing the portion of the donor layer to vaporise and generate a high pressure bubble at the interface with the scaffold material. The material falls as a droplet onto the build plate and is crosslinked to form the desired structure. As no nozzle is involved much higher viscosity material can be used and no mechanical stress is seen between the nozzle and cells therefore there is a higher cell viability

(95%). However the effects of the laser on the cells is still not fully understood and is more expensive due to the more complex system (Mandrycky et al., 2016).

DLP bioprinting works in a similar way to laser assisted printing in that a photocurable resin is cured by a light source to a defined shape. However where as laser assisted focuses on a specific position to cure before moving onto the next position, DLP cures the entire layer immediately therefore printing at a much faster rate than laser assisted and subjecting the cells within the bioink to shorter periods of intense light (Ngo et al., 2018, Lu et al., 2006). DLP bioprinting generates the structure through the use of a digital micro mirror device (DMD) which consists of a group of micro sized, controllable mirrors. The mirrors rotate to control the path of the light onto the photocurable resin, the light is then directed as defined by a computer software to generate a specific structure. The resolution of the system is defined by the DMD and is typically on the micron scale (Ngo et al., 2018). DLP does not use a nozzle and therefore sees higher cell viability (85-95%) than nozzle based bioprinters (Zhang et al., 2020).

Volumetric bioprinting looks to move away from the layer by layer approach of other printing types and instead generate the entire structure at once. It is argued that this approach will reduce the stress imposed on the cells during the relatively slow fabrication of the structure. The instant fabrication means more complex hollow structures with overhangs can be manufactured without out the need for a support structure (Kelly et al., 2019). Volumetric bioprinting works by the controlled projection of a series of 2D patterned optical light fields within a volume of a photopolymer. The 2D light patterned acts cumulatively to produce an optical 3D dose distribution that triggers the polymerisation of the irradiated material into the desired shape (Bernal et al., 2019, Loterie et al., 2018).

The generation of 3D scaffolds by the researcher inevitably leads to variation between samples, by utilising bio printers the variability between samples and studies will dramatically reduce allowing for more comparable and trustworthy results. The ever developing bioprinting technology is making more complex and higher quality building a reality, and with the ability to share designs and ideas between labs, comparable approaches can be more widely used across research. Tissue engineering is only around 40 years old, and with the continued emergence of newer technologies the automation and reproducibility of lab grown tissues will continue to grow, potentially helping to generate an environment closer to that of the target tissue.

1.2.3. Bioreactors

Bioreactors have been developed to enable high expansion of adherent cultured cells that is otherwise a limitation with 2D approaches. This is achieved by the tight control and monitoring of the environmental conditions (e.g. pH, temperature, mechanical stimuli, nutrient supply and waste removal) and can be applied using a stir tank bioreactor in which adherent cells are cultured on a microcarrier system in suspension culture, drastically reducing the number of tissue culture plastic vessels required. Through the high level of control and experimental automation the reproducibility is dramatically increased, this has led to the industrial utilisation of large-scale bioreactors for fermentation processing, water treatment, food processing and the production of pharmaceuticals and recombinant proteins (Martin et al., 2004). At the research level smaller bioreactors are utilised to apply *in vivo* conditions to cell cultures, driving the cells to proliferate, differentiate and produce targeted ECM to generate the engineered tissue (Liu et al., 2010b). Mechanical stimulation bioreactors fall into the category of research bioreactors, and are used to replicate the mechanical forces experienced by the targeted tissue *in vivo* such as tensile stimulation by tendons and hydrostatic pressure by cartilage.

1.2.3.1. Mechanical stimulation bioreactors

A wide range of commercial and custom designed bioreactors are available for mechanical stimulation. These bioreactors are designed to replicate the *in vivo* mechanical loads applied to cells including tensile stimulation, shear force and hydrostatic pressure as well as environmental forces such as microgravity. The application of mechanical stimulation and the subsequent biochemical response is known as mechanotransduction, whilst the exact process is not fully understood, studies have shown that integrins, cadherins, ion channels, focal adhesion and growth factors/receptors play a role in the process (Sarasa-Renedo and Chiquet, 2005). The activation of these mechanotransduction receptors activates cell signalling cascades which may involve nuclear factor kappa B, MAPK, protein kinase C pathway, Rho-dependent kinase (Sarasa-Renedo and Chiquet, 2005).

For tensile stimulation a range of commercial bioreactors are available, these include the EBERS TC3, CellScale MCT6, BioDynamic 5200 and the Flex Cell Tissue train. A wide range of custom built bioreactors have been utilised for studies as shown by Juncosa-Melvin et al. (2006), Morita et al. (2013), Youngstrom et al. (2016) and Brandt et al. (2018). All tensile stimulation bioreactor share similar design characteristics: a culture chamber enabling tensile stimuli to be applied to the cells in a sterile environment, with the force applied by a

linear actuator controlled by displacement software. Tensile stimulation is usually applied by stretching the sample by a fixed amount, the sample may be cells within a 3D structure (Youngstrom et al., 2015, Janvier et al., 2020) or cells adhered to a flexible membrane as a monolayer (Juncosa-Melvin et al., 2006). In the case of the 3D cell culture, the samples are attached to the bioreactor at the structures two extremes, this may be by a grip or a post system. For both 2D and 3D tensile stimulation one end is typically fixed and the opposite end is attached to a linear actuator (though both ends can be attached to two linear actuators), the linear actuator is then electronically driven to stretch the sample by a fixed amount. The amount of tensile stimulation applied is usually calculated as the strain placed on the sample, this strain is the percentage change from the original length of the sample, more advanced systems may have a load cell built in to record the amount of force being applied. The tensile stimulation can be applied as a constant force where the only variable is the amount of strain or as a dynamic force where as well as strain the frequency and duration of the cyclic loading is also a variable.

Compressive forces are detected by cells throughout the body particularly by chondrocytes (Responte et al., 2012). There are two main options to replicate compressive forces *in vitro*, direct compression and hydrostatic pressure. Direct compression involves physically pressing the cell culture structure with a solid object whilst hydrostatic pressure involves increasing the volumetric pressure the sample is cultured in. Both commercial and custom direct compression and hydrostatic pressure bioreactors are available. Examples for commercially available direct compression bioreactors include the CellScale MCTX and EBERS TC3 with compression grips and examples of custom are presented in studies by Cochis et al. (2017), Meinert et al. (2017). Examples of commercially available hydrostatic pressure bioreactors include the TGT Cartigen, CellScale MCTR, EBERS TC3 with hydrostatic pressure chamber and Flexcell's FX-5000C and custom are presented in studies by Reinwald et al. (2015), Correia et al. (2012)).

Direct compression bioreactors typically work via a piston system. Here a sterile end is driven down onto the test sample in a uniaxial direction, this requires the sample to all be uniform in size and shape with a flat surface at the top and bottom of the structure ensuring the load is evenly applied and the sample does not move. Hydrostatic pressure bioreactors typically work by applying compressed air into the system to increase the atmospheric pressure around the sample. As the entire atmospheric pressure within the culture environment is increased the load is applied uniformly across the sample (Reinwald et al., 2015). Hydrostatic

pressure has also been shown to enhance the transfer of small molecules such as O₂ and CO₂ (Portner et al., 2005). The hydrostatic pressure systems require a large compressed air tank as well as a culture chamber that is able to withstand the high pressures applied. Other hydrostatic pressure systems, such as the EBERS TC3 hydrostatic pressure chamber, utilise a piston which presses against a flexible membrane wall of the culture chamber, by reducing the volume of the culture chamber the hydrostatic pressure increases, this type of system is limited by the amount of pressure able to be applied as high pressure levels see the liquid environment leak out. Both the piston based and compressed air systems are operated electronically allowing the applied load to be easily controlled. For piston based systems the load is measured as piston displacement, through a mounted pressure gauge the change in pressure can be monitored. Many systems have been designed to use existing well plates or petri dishes, therefore the transfer of samples from non-stimulated culture to pressurised culture is relatively straightforward. The pressure can be applied as a constant (Tworkoski et al., 2018) or as a cyclic profile (Henstock et al., 2013) where along with the pressure the frequency and duration are also variables.

Some custom built compression bioreactor have been designed to allow for shear forces to be applied in tandem with the compressive forces (Meinert et al., 2017, Cochis et al., 2017), this helps to mimic mechanical environment such as the knee where compressive loads are applied to the cartilage whilst the synovium also applies shear force to the tissue (Escamilla, 2001). Shear force is also seen in other tissues such as blood vessels (Lu and Kassab, 2011). Shear based bioreactors have been developed commercially, for example the CellScale Vitroflow, and work in a similar way to a rocker plate. Other systems apply shear force by rotating samples within a drum, this includes the Synthecon RCC 3D cell culture system. As well as the ability to apply shear force the Synthecon RCC 3D can also place samples within microgravity, this is achieved by manipulating the rotational speed so that samples placed within the rotation drum are in constant free fall therefore dramatically reducing the gravitational force applied to the samples. The rotation is electronically controlled, to generate the microgravity environment, the rotational drum should be entirely filled with cell culture medium and all air bubbles removed from the system, which then attaches to the rig and can begin rotation. The Synthecon RCC does not control temperature, humidity, O₂ or CO₂ conditions and therefore must be placed within an incubator during use to achieve the required conditions. These type of bioreactors allow researchers to investigate how environment factors, such as microgravity, affect the proliferation, differentiation and ECM production of the cells encapsulated within the system. The Synthecon RCC is the most

commonly used system to apply microgravity to 3D cell cultures, as shown from the authors literature review being used in approximately 70% of all studies investigating the effects of microgravity on 3D cell culture between January 2015 and August 2020. The second most frequently used is the custom designed random position machine (RPM) which has been used in 29% of studies, here the whole system is constantly reorientating with respect to earths gravitation field, resulting in the average gravitational force acting on the samples to be less the 1 g (Benavides Damm et al., 2014).

The use of bioreactors allows specific stimuli that occur within the native environment to be replicated in a controlled *in vitro* environment. This may result in an over simplified culture as within a biological system these stimuli will not occur in isolation, however this does allow the researcher to better understand the role these stimuli play. The choice of cell type is equally as important as the stimuli being applied and the scaffold being used as different cells will have different responses to specific loading. MSCs act as an ideal starting cell for load based experimentation due to the MSCs multipotent characteristics enabling the cells to respond to the varying stimuli by differentiating down different lineages.

1.3. Mesenchymal Stem Cells

MSCs are a multipotent cell that have the potential to differentiate down a variety lineages to form skeletal cell types, the lineages including osteogenic, chondrogenic, adipogenic and tenogenic (Fig.1.2) (Dominici et al., 2006, Archer and Ralphs, 2010). Tendon, bone and cartilage have been investigated throughout the experimental sections of this thesis and so have been specifically discussed in sections 1.4, 1.5 and 1.6. MSCs have been isolated *in vitro* from a number of sources including the umbilical cord, placenta, fat and skin however the most studied source is the bone marrow derived MSC (Zuk et al., 2002, da Silva Meirelles et al., 2006). Within the bone marrow, MSCs account for 0.001-0.01% of the nucleated cell population (Pittenger et al., 1999, Jiang et al., 2002) and therefore require a multistep process to extract the cell from the bone marrow source. Initially the bone marrow is flushed and dispensed over tissue culture plastic where, after a set period of time, the adherent cells are retained and the non-adherent cells, such as red blood cells, are discarded. The population of adherent cells can then be verified as MSCs through a variety of methods however the most common is the tri-lineage assay. Here the cells must be able to differentiate down all three of the adipogenic, chondrogenic and osteogenic lineage (Pittenger et al., 1999, Jiang et al., 2002). Characterisation kits are another option for MSC verification with the minimum criteria being defined by Dominici et al. (2006). 95% of the

cell population must express CD73, CD90 and CD105 whilst less than 2% of the cell population should express CD11b, CD34, CD45, CD79A and HLA-DR. The criteria defined in the verification kit has been disputed as a range of cells may express the markers, for example CD90 is expressed by fibroblasts in culture (Saada et al., 2006, Powell et al., 2011).

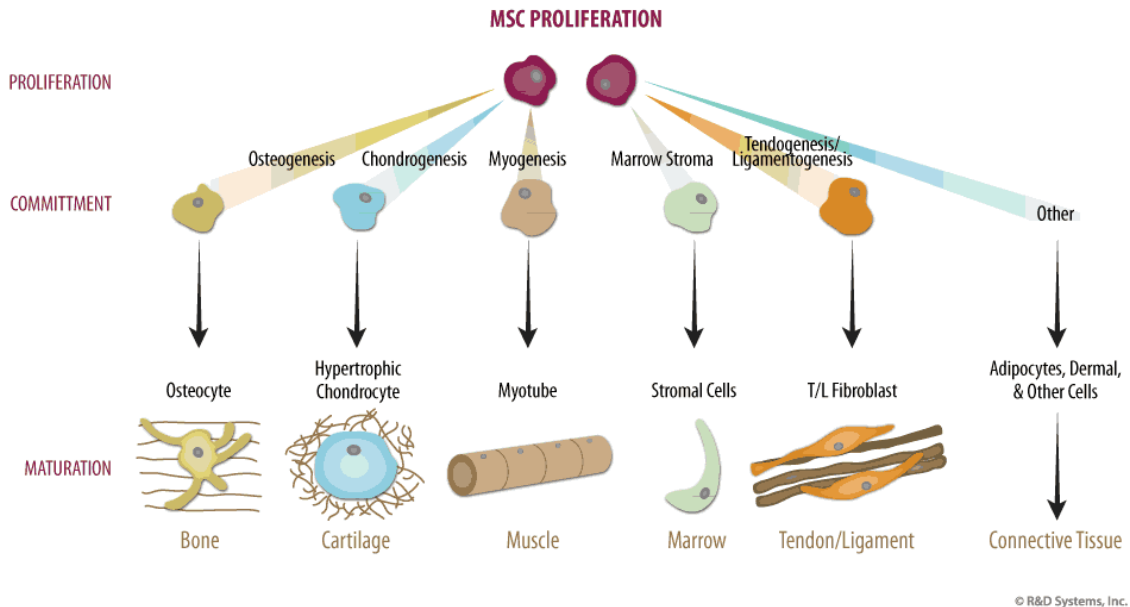


Figure 1.2. The differentiation potential of MSCs, captured from Chan et al. (2007).

The differentiation fate of the MSC is determined by a number of factors including chemical and physical stimuli and involves a two-step process; lineage commitment and maturation. A number of signalling pathways have been shown to be involved in osteogenic, chondrogenic and tenogenic differentiation including transforming growth factor-beta (TGF- β)/BMP signalling, Wnt signalling, Hh signalling, Notch, Hippo and FGF (Chen et al., 2016). The TGF- β superfamily consists of three subtypes: TGF- β 1, TGF- β 2 and TGF- β 3 (Chen et al., 2012, Lorthongpanich et al., 2019). This group of growth factors is widely involved in cell proliferation and cell differentiation, however the effect may be dose dependent, for example low doses of BMP2, along with rosiglitazone (an antidiabetic drug), have been shown to induce adipogenic differentiation whilst high doses of BMP2 accelerate chondrogenic and osteogenic differentiation (zur Nieden et al., 2005). TGF- β s bind to the appropriate serine-threonine kinase receptor and activate canonical Smad-dependent pathways (including TGF- β /BMP ligands, receptors and Smads) and non-canonical Smad-independent signalling pathways, such as p38 mitogen activated protein kinase (MAPK) pathway (Deng et al., 2008), resulting in the regulation of osteogenic genes (e.g. Runx2), chondrogenic genes (e.g. Sox9) and tenogenic genes (e.g. SCX).

The Wnt proteins bind to Frizzled (FZ) 7-transmembrane spanning receptors and activate the canonical Wnt/ β -catenin pathway and the Wnt/ β -calcium pathway (Kohn and Moon, 2005, Cadigan and Peifer, 2009). The Wnt proteins that belong to the canonical group are: Wnt1, Wnt2, Wnt2b/13, Wnt3, Wnt3a, Wnt8a/d, Wnt8b, Wnta10a, Wnta10b, Wnt9a.14, Wnt9b/15 and Wnt16 and the noncanonical group: Wnt4, Wnt5a, Wnt5b, Wnt6, Wnt7a, Wnt11 and Wnt16 (Ackers and Malgor, 2018). The Wnt signalling pathway has been previously shown to facilitate osteogenic and chondrogenic differentiation (Kirton et al., 2007, Park et al., 2015) and inhibit tenogenic differentiation (Kishimoto et al., 2017).

The Hedgehog family of secreted proteins consist of three orthologues: Sonic Hedgehog (SHh), Indian Hedgehog (Ihh) and Desert Hedgehog (Dhh) (Chen et al., 2016). Through binding of Hedgehog precursor to membrane proteins, Patched (Ptc) and Smoothed (Smo), the transcription factors Gli1, Gli2 and Gli3 are activated and regulate the expression of Hedgehog targeted genes (Deng et al., 2008). Hedgehog and BMP signals have been shown to cross-talk resulting in Smad modulation which in turn results in the promotion of osteogenic differentiation (Spinella-Jaegle et al., 2001). Hedgehog signalling is an important regulator of chondrogenesis with Ihh highly expressed by prehypertrophic chondrocytes and osteoblasts at puberty (Kindblom et al., 2002) though the regulation of the cell types is not identical. Osteoblast differentiation is controlled by Runx2 expression (Yuan et al., 2016) whilst prehypertrophic chondrocyte differentiation is regulated by PTHrP (Williams et al., 2018). Ihh signalling is mediated by Wnt/ β -calcium signalling during osteoblast differentiation (Hill et al., 2006) whilst Wnt/ β -calcium acts upstream and in parallel to Ihh in chondrocyte survival and hypertrophy, respectively (Mak et al., 2006). Hedgehog signalling has been shown to be present at the insertion site of tendon-bone during cell differentiation (Liu et al., 2013) and found via the primary cilia, to be a mechanosensitive pathway during tendon-bone healing (Carbone et al., 2016), suggesting it plays an important role during tendon development particularly at the bone attachment site.

Activation of the Hippo pathway negatively regulates the expression of the yes associated protein (YAP), a key transcriptional co-factor that has been shown to be involved in stem cell fate (Zhao et al., 2011a). YAP and its paralogue transcriptional co-activator with PDZ-binding motif (TAZ) are thought to shuttle between the cytoplasm and the nucleus and interact with transcription factors, regulating their activity and therefore cell differentiation (Karystinou et al., 2015). Low expression of YAP and TAZ has been shown to promote adipogenesis and chondrogenesis in MSCs whilst high expression drives MSCs towards osteogenesis (Hong et al., 2005, Zhong et al., 2013, Karystinou et al., 2015).

The notch signalling pathway involves the single transmembrane proteins Notch and Notch ligand (Delta/Serrate/LAG-2, DSAL protein) (Lin and Hankenson, 2011). These proteins regulate cell differentiation through cell-cell communication and have been shown to both suppress and induce osteogenic differentiation by inhibiting Wnt/ β -catenin signalling (Deng et al., 2008) whilst promoting BMP2 signalling (Shimizu et al., 2011). Similarly during chondrogenesis Notch signalling is necessary to initiate differentiation but must be switched off to allow chondrogenesis to proceed (Oldershaw and Hardingham, 2010).

1.3.1. Mechanical Regulation of Mesenchymal Stem Cell Differentiation

Each signalling pathway does not function in isolation but works with other pathways to drive the differentiation of MSCs, the activation of the pathways is driven by stimuli found in the tissue microenvironment. Stimuli can comprise biological factors such as ageing and chemical cues including the addition of TGF- β *in vitro* which initiates and maintains chondrogenic differentiation of MSCs through the stimulatory activities on MAPK and modulation of Wnt signalling (Tuli et al., 2003). Mechanical factors also act to drive MSC differentiation and include a range of stimuli including cell morphology, mechanical forces, ECM components and geometric structures. The process through which mechanical factors influence cell changes via intercellular biochemistry and gene expression is known as mechanotransduction (Wang et al., 2009). These mechanical factors arise from the MSCs not acting in isolation but physically interacting with components of their microenvironment, with changes to the microenvironment directing the MSC fate. This has been demonstrated by Engler et al. (2006), here the matrices the MSCs adhered to varied in stiffness, the cells then differentiated into either neuron cells when on the elastic matrix (0.1-1 kPa), myocytes when on the stiffer matrix (8-17 kPa) or osteoblasts on the stiffest matrix (25-40 kPa). The main cellular components that mediate mechanical forces from the ECM are integrin and cadherin receptors which facilitate cell adhesion to the ECM by binding to proteins and are able to transmit forces by physical interaction with the actin cytoskeleton (Alenghat and Ingber, 2002, Schwartz, 2010, Schwartz and DeSimone, 2008). Mechanical stimulus results in the activation of mechanosensitive ion channels, heterotrimeric G proteins, protein kinases and other membrane-associated single transducer molecules. This sees the downstream activation of signalling cascades which results in mechanical stimulation dependant cellular changes (Chien, 2007). The interaction with the structural cytoskeleton can dictate the cell shape which can then lead to the differentiation of the MSC; if the MSC

is to differentiate down the chondrogenic lineage it becomes round (Johnstone et al., 1998, Erickson et al., 2002) whereas if the MSC spreads out it may develop into an osteoblast (McBeath et al., 2004). The cytoskeleton can generate a response to mechanical forces, as the load will deform the structure. Through this deformation, proteins associated with the cytoskeleton will also deform which, under the right conditions, may cause the protein to unfold and present a new binding site, this then may lead to the activation of signalling pathways through the phosphorylation of proteins (Vogel and Sheetz, 2009).

External mechanical forces act on musculoskeletal tissues through development and maturation. Various forces are experienced by the different tissues dependant on the role the tissue plays to maintain homeostasis, this includes tensile loading on tendons and muscle (Magid and Law, 1985, Wang, 2006) and hydrostatic pressure on bone and cartilage (Gurkan and Akkus, 2008, Montagne et al., 2017). The application of constant tensile stimulation to MSCs has been shown to promote endogenous BMP-2 expression, osteogenic gene expression and calcium deposition (Sumanasinghe et al., 2006, Byrne et al., 2008, Qi et al., 2008, Hanson et al., 2009, Rui et al., 2011). The upregulations of the MAPK pathway has been seen with cyclic tensile strain (Ward et al., 2007) suggesting its importance as a key mechanotransductive pathway in tensile stimulation. The magnitude of the tensile strain has been found to regulate the MSC differential fate with high tensile strain resulting in myogenesis and low tensile strain osteogenesis (Jang et al., 2011). Tensile stimulation deforms the tissue and therefore the cells bound to the actin cytoskeleton, therefore resulting in a cell response, hydrostatic pressure is a non-deforming mechanical stimulus and therefore regulates cell fate in a different way. In chondrocytes static hydrostatic pressure inhibits the Na/K and Na/K/2Cl pump whilst enhancing the Na/H exchange (Browning et al., 1999, Hall, 1999). There is evidence to suggest that hydrostatic pressure regulates hypertrophy with the application of cyclic hydrostatic pressure resulting in a decrease in hypertrophic markers collagen X and IHH in MSC pellet culture (Vinardell et al., 2012).

MSCs detect and respond to external mechanical signals in a number of ways through mechanotransduction, these include cell membrane components and intracellular components. The regulation of many ions across the cell membrane is highly controlled through ion channels. Some of these ion channels have been found to activate or deactivate when the cell is exposed to mechanical stretch (Campbell et al., 2008). The importance of these ion channels has been shown with cyclic tensile loading of MSCs, by blocking the ion channels through the stretch-activated ion channel inhibitor gadolinium chloride, it was found that proteoglycan production was significantly decreased (McMahon et al., 2008).

Integrins detect the deformation to the ECM through binding sites with multiple or single ECM components. The response of the integrin to the mechanical stimuli has little direct control over the cell behaviour, instead the mechanical signals transmitted to the integrin from the ECM results in the formation of protein complexes that in turn trigger signalling cascades within the cell (Giancotti and Ruoslahti, 1999). Integrins help to regulate cell-ECM interaction, cadherins help to regulate cell-cell interactions. The cadherins bind to other cadherins on other cells in a homophilic manner extracellularly, whilst also binding to the actin cytoskeleton intracellularly, this allows the cells to interact with other cells in response to mechanical stimulation, therefore directing the cell populations differentiation (Steward and Kelly, 2015).

The cell membrane mechanoreceptors transmit the mechanical stimuli to intracellular sensors. One of the key responders is the actin-rich stress fibres which bind to the transmembrane integrins at prominent membrane-substratum adhesion sites known as focal adhesions (BurrIDGE et al., 1988). The stress fibres are myosin associated, contractile bundles of filamentous actin that assemble in stress sensing cells (Wong et al., 1983). The application of mechanical stresses results in the remodelling of the actin skeleton and thus the focal adhesion sites. The intracellular response leads to a number of signal transduction pathways including kinase activation (Akt, MAPK and FAK) and β -Catenin. MAPKs are serine/threonine protein kinases which are essential to mechanosensing, for example ERK1/2 is necessary for strain response by osteoblasts (Rubin et al., 2002), and without, osteogenic differentiation of MSCs through TGF- β is not possible (Arita et al., 2011). The interaction of different intracellular responses results in different cell fate, for example mechanical activation of Akt (a serine/threonine kinase) increases β -Catenin activation which results in inhibited adipogenic differentiation of MSCs (Sen et al., 2008). Further focal adhesion kinases are concentrated near focal adhesions and are associated with a number of signalling proteins including phosphatidylinositol 3-kinases (PI3K), and paxillin (Cukierman et al., 2001, HehlGans et al., 2007). Through interactions with these signalling proteins, the focal adhesion kinases form a functional network of integrin stimulated signalling pathways that result in downstream activation of the MAPK pathways (Chatzizacharias et al., 2008). Extra and Intracellular mechanotransduction is a complex process that involves a number of cell membrane mechanoreceptors and the activation of multiple signalling pathways. Through the appropriate activation the MSC begins to differentiate down a specific lineage and, under the right conditions, results in the further activation of signalling pathways and maturation of the cell within the lineage.

The 3D culture of MSCs has been routinely used to investigate the role of mechanical stimulation in a controlled research environment. Different types of mechanical stimulation has been applied to 3D MSCs culture generating different differential responses from the cells. Tensile stimulation has been shown to upregulate osteogenesis and tenogenesis whilst inhibiting adipogenesis (Simmons et al., 2003, Sen et al., 2008). Studies have shown that the amount of tensile strain applied can drive the type of differentiation seen, with 3% being shown to favour osteogenic differentiation and 10% tenogenic differentiation both seeing increases in COL1A1 and osteogenic or tenogenic markers (Altman et al., 2002, Chen et al., 2008, Zhang et al., 2008, Jagodzinski et al., 2004). The profile in which the tensile stimulation is applied has been shown to be critical in the long term differentiation of the cells with constant force of 6.7 N leading to a reduced production of collagen after 21 days compared to the unloaded scaffold, suggesting cyclic loading is essential to targeted differentiation.

Hydrostatic pressure has been used to drive the chondrogenic and osteogenic differentiation of MSCs, again it has been shown that the rate and level at which the force is applied results in varying effects of the MSCs. Chondrocytes are typically exposed to high magnitudes of hydrostatic pressure (>1 MPa) (Zhang et al., 1998), loads lower than what is seen in chondrogenesis have been shown to upregulate osteogenic markers ALP and RUNX2, suggesting the MSCs are differentiating down the osteogenic lineage (Liu et al., 2009a). Increasing the level of hydrostatic pressure has been found to induce chondrogenic differentiation, Saha et al. (2017) found that 1 MPa saw upregulation of SOX9, and the downregulation of COL10A1, indicating that not only was hydrostatic pressure driving the chondrogenic differentiation but also inhibiting hypertrophy. Higher levels of hydrostatic pressure, 10 MPa, has again been shown to drive chondrogenic differentiation with increases in GAG production and collagen II synthesis (Steward et al., 2014). It appears that lower levels of either tensile loading or hydrostatic pressure favour osteogenic differentiation, whilst higher results in different forms of differentiation, demonstrating the variable role mechanical stimulation can play in the differentiation of MSCs in 3D culture.

The multiple lineage potential coupled with the well-established response to mechanical stimulation of MSCs has made the cell an ideal candidate when investigating tissue engineering of different musculoskeletal tissues. Within this study the generation of tissue engineered bone, tendon and cartilage has been investigated through the application of tensile stimulation (tendon) and hydrostatic pressure (bone and cartilage). An review of the native tissue and tissue engineered approaches is established in the subsequent sections.

1.4. Tendon

1.4.1. Function

Tendons are dense, organised, fibrous soft tissues that connect muscle to bone. The primary function of tendon is transmitting force produced by muscle to bone enabling joint motion (Robert et al., 1974). Whilst tendon encompasses a wide range of tissues found throughout the body each specific tendon has differences (e.g. composition and shape) that help it to adapt to the environment it is located in (Sharma and Maffulli, 2006, Thorpe et al., 2010, Thorpe et al., 2014). For example the human Achilles tendon and the equine superficial digital flexor tendon (SDFT) require energy storage properties. Therefore whilst the primary function of tendon is force transmission, the conflicting functions, including tensile resistance and energy storage, requires a specialised structure. Tendon is mainly composed of water, which accounts for 55-70% of the wet weight (Gomes et al., 2015). The major ECM component is collagen, accounting for 60-85% of the dry weight which enables the tendon to withstand high strain rates and prevents the loss of contractile energy during movement (Kjaer, 2004). The presence of a viscous matrix enables the collagen fibres to slide and provides the tendon with an increased range of movement and viscoelastic properties (Shepherd and Screen, 2013).

1.4.2. Structure

Tendons are composed of a complex hierarchical structure (Fig.1.3), surrounding the tendon is the paratenon and epitenon whilst the endotenon resides within, these are the main blood vessel and nerve containing regions. The paratenon is the outer most structure and is composed of loose connective tissue. It is found away from joints and facilitates movement in the subcutaneous position. The epitenon surrounds the collagen fascicles and is a layer of connective tissue that is continuous with the endotenon, also known as the interfascicular matrix (IFM) (Thorpe et al., 2015). Whilst the paratenon and epitenon contain the majority of the blood vessels and nerves a percentage does reside within the fascicles, this number varies between tendon types, for examples the human Achilles tendon has regions of high vascularisation (insertion and origin points) with avascular regions (the mid region) (Theobald et al., 2005). The primary cell found in tendon is the tenocyte (a tendon specific fibroblast) and is thought to account for approximately 95% of the cells with endothelial cells, progenitor cells and chondrocytes making up the other 5% (Franchi et al., 2007). Tenocytes are thought to derive from a mesenchymal origin with the progenitor cell differentiation regulated by a number of transcription factors including Six1, Six2, EphA4, Eya2, follistatin,

tenascin, mohawk and scleraxis (Aslan et al., 2008, Jelinsky et al., 2010). The tenocytes are either located as groups in the IFM between the collagenous fascicles or within the collagenous fascicles. The tenocytes found in the IFM (termed interfascicular tenocytes) are relatively plump and round whilst those within the fascicles (termed intarfascicular tenocytes) are elongated with an extended nuclei and a complex network of cytoplasmic processes extending through the ECM to other tenocytes via gap junctions (McNeilly et al., 1996). The tenocyte's role is to produce the relevant ECM as well as repair and maintain the tendon tissue (Franchi et al., 2007, Kannus, 2000).

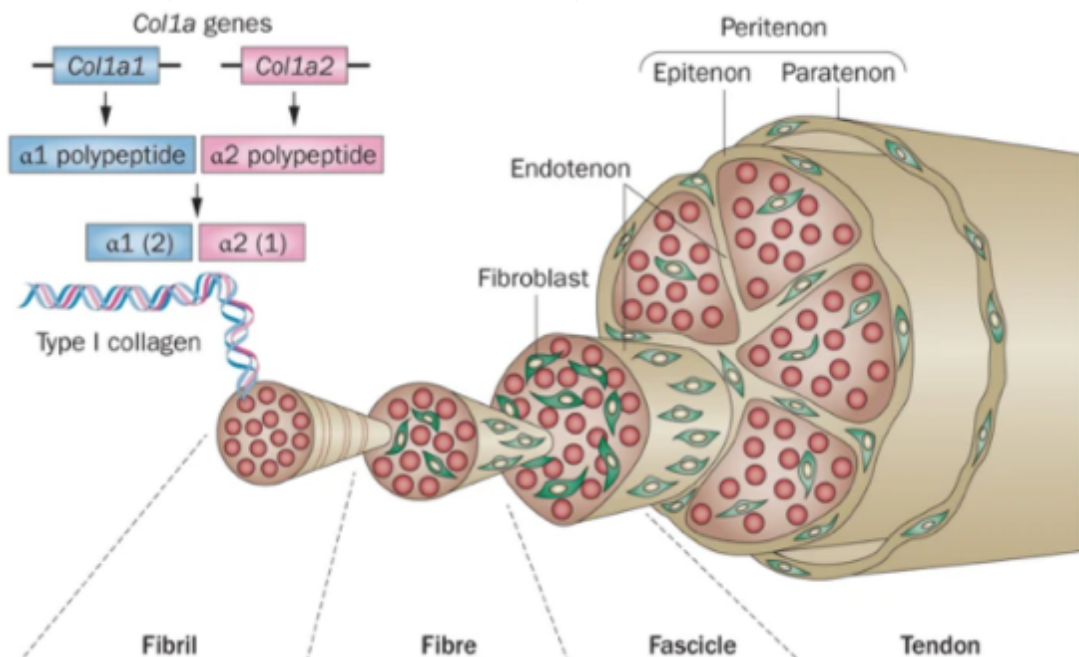


Figure 1.3. Schematic of the hierarchical structure of collagen in tendon. Captured from Nourissat et al. (2015).

1.4.2.1. ECM of Tendon

Whilst the ECM of tendon is composed mostly of collagen other molecules also reside within this space. Proteoglycans are the predominant class of glycoproteins and are classified into two groups, the small leucine-rich proteoglycans (SLRPs) and the large aggregating proteoglycans (Parkinson et al., 2011). Of the proteoglycans, the SLRP decorin is the most common accounting for 80% of the proteoglycan content in tendon (Samiric et al., 2004a, Thorpe et al., 2013), other SLRP include biglycan, fibromodulin, lumican and keratocan (Rees et al., 2009). These proteoglycans are prevalent in collagen-rich tissues, with a horseshoe shaped protein core featuring a leucine-rich repeat which is involved in binding to collagen (Henry et al., 2001, Vogel et al., 1984, Hedbom and Heinegard, 1989, Rada et al., 1993). The SLRPs have been shown to help regulate collagen organisation (Danielson et al., 1997). Aggrecan and versican are the large aggregating proteoglycans found in the tendon (Vogel

et al., 1994, Campbell et al., 1996, Rees et al., 2000, Samiric et al., 2004b). Due to the negatively charged glycosaminoglycan (GAG) chains attached to the core proteins of the large aggregating proteoglycans, they have the ability to attract and bind water within the ECM of tendon aiding the biomechanical properties, particularly the compressive properties (Rees et al., 2002, Marcelino et al., 1999, Rhee et al., 2005). Other non-collagenous proteins include elastin, link protein, cartilage oligomeric matrix-protein, tenascin-C fibronectin, tenomodulin, COMP, lubricin, undulin and thrombospondin-1 (Thorpe et al., 2013, Kannus, 2000, Parkinson et al., 2011). These proteins are involved in matrix-matrix, cell-matrix organisation or cell-matrix signalling (Parkinson et al., 2011).

1.4.2.1.1. Collagens of Tendon

The most prevalent component of the tendon ECM is collagen and as with every tissue the composition of collagen types found in tendon is specific to tendon. Collagen types I, III, V, XI, XII and XIV make up the tendon collagen composition (Riley et al., 1994, Thorpe et al., 2013) with type I accounting for 95% of the collagen in tendon (Screen et al., 2015). Within tendon there are two collagen subcategories, fibril forming (I, II, III, V, XI) and FACIT (XII and XIV). The fibril forming collagens are secreted into the ECM by the tenocytes and spontaneously assemble into parallel fibrils stabilised by intra and intermolecular covalent crosslinking (Anttinen et al., 1977, Canty and Kadler, 2005). These fibrils bunch together forming the fibres which form the fascicles and finally the tendon (Fig.1.11). Collagen type I fibrils are the main contributor to the tendons mechanical properties providing the tendon with tensile strength. The other collagens within the ECM all play an important, and often overlooked, role to maintain tendon homeostasis. Collagen type III is the second most abundant collagen in the tendon ECM, accounting for up to 10% of the total collagen content (Kadler et al., 1990). Type III is always associated with type I collagen and forms smaller diameter fibrils than type I (Rees et al., 2002). Type III is found in high concentrations at wound sites (Voleti et al., 2012) and in the vascular wall (Buckley et al., 2013). Elaborating from the prevalence of type III suggests that type III fibrils have greater flexibility than the type I fibrils, therefore increasing the tendon's flexibility (Parkin et al., 2017). However an increased ratio of type III to type I in the tendon is seen with ageing and increased pathology (Smith et al., 1999, Goncalves-Neto et al., 2002).

Type V and XI act as regulatory collagens within the structure. Collagen type V is mostly located in the core of collagen I fibres and plays a critical role during the early process of fibril nucleation, type I fibre diameter regulation and organisation (Connizzo et al., 2015). The

collagen V fibrils incorporate into the collagen I fibres, with the triple helix present in the core of the fibre and the N-terminal propeptides (containing a thrombospondin or von Willebrand factor C domain) extending outward to the gap zone of the collagen I structure. Through interactions with the exposed N-terminal the collagen V fibrils help to regulate the collagen I fibre development (Birk, 2001). A reduction in collagen V fibrils sees a reduction in overall fibres and an increased fibre diameter, resulting in a major change to the mechanical properties of tendon (Segev et al., 2006, Wenstrup et al., 2011, Sun et al., 2015). Collagen type XI is expressed in developing tendons and plays a similar role to collagen type V (Wenstrup et al., 2011). Similarly to collagen type V, type XI's triple helix is located in the core of the collagen I fibre and the N propeptides extends outward to the gap, the N propeptides contains a thrombospondin like domain and is thought to inhibit lateral growth as well as regulate fibril assembly (Seet et al., 2017). Type V and XI are structurally and functionally homologous and are now considered a single collagen type with multiple tissue-specific isoforms (Hoffman et al., 2010).

The two FACIT collagens (XII and XIV) share a similar role within the tendon though feature different expression patterns during tendon development (Zhang et al., 2005). Both FACIT collagens bind to the surface of the collagen fibrils and due to the large globular N-terminal domains interact with other components of the tendons ECM. Type XII has been shown to be expressed throughout tendon development and into adulthood though the expression is significantly decreased in adulthood (Zhang et al., 2003, Walchli et al., 1994, Gordon et al., 1996). Type XIV is involved in linear fibril growth (Zhang et al., 2005) by limiting the fibril diameter through the prevention of lateral fusion of adjacent fibrils through interaction between one of the non-collagenous terminals and collagen I fibrils, and has been shown to be highly expressed during embryogenesis before a sharp decrease in expression (Young et al., 2000, Young et al., 2002). Type XIV interacts with other ECM components such as collagen IV, heparin and decorin (Brown et al., 1993) and various mesenchymal and epithelial cells (Ehnis et al., 1996).

1.4.3. Mechanical Properties

Tendons are predominantly loaded along the long axis in tension, however some tendons have the additional role of energy storage to aid in locomotion (Biewener, 1998). Uniaxial tensile testing gives an insight into the tendon's mechanical properties. Fig.1.4 shows a typical stress-strain curve for tendon, depicting the typical non-linear response as four distinct regions. The initial region is known as the toe region. As the tendons structure is

primarily made of collagen type I the elasticity of the structure is relatively low (though higher for energy storing tendons). To overcome this limitation the collagen fibrils arrange into a crimp structure, as loading is applied the crimp straightens out and there is some reordering of the collagen fibres until it is aligned in the direction of loading, resulting in a period of relatively high elongation for low stress (Screen et al., 2004). Following the toe region is the heel region. Here the stiffness begins to rise due to further reordering of the collagen fibrils and straightening of kinks in the gaps of the D period (Misof et al., 1997). Once the collagen fibres are appropriately arranged the response enters the linear region. Here due to the composite structure of tendon (collagen and proteoglycans) the matrix undergoes a combination of extension and sliding of the collagen fibres (Screen, 2009). Eventually the load becomes great enough that the tendon begins to fail, usually seen as a pulling apart of collagen fibres, resulting in a gradual decrease in the recorded force rather than a sudden breakage (Screen et al., 2004).

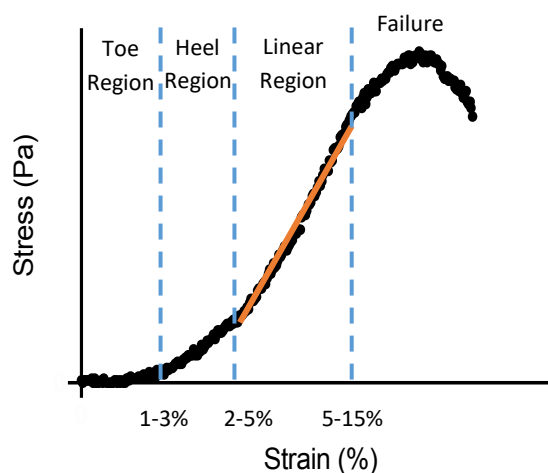


Figure 1.4. Schematic stress-strain curve for tendon. The toe region, heel region, linear region and point of failure have been highlighted and typical strains at each region shown.

Due to its structure and composition tendon is a viscoelastic material, therefore a tendon exhibits both viscous and elastic mechanical behaviour. This results in the mechanical properties of the tendon being rate of force dependant. Viscoelastic properties can be observed through hysteresis, creep and stress relaxation, all three properties apply some form of load to the sample for a set period of time and demonstrate how the materials response changes with time.

Hysteresis is shown by applying a load to a sample over a period of time and then unloading the sample for the same period of time (Fig.1.5.Ai). A perfectly elastic material will have an

identical loading and unloading curve, whereas a viscoelastic materials unloading curve will not follow the loading curve (Fig.1.5.Aii), the area between the loading and unloading curve is the energy lost during the loading cycle. In tendon, hysteresis is thought to occur due to the movement of water through the tissue and the reordering of the fibre structure (Thorpe et al., 2013).

Creep is tested for by applying a constant load to the sample and the extension is monitored over a set period of time (Fig.1.5.Bi). If the sample is viscoelastic the material will continue to elongate until it fails despite no increase in load or the recorded extension stabilises (Fig.1.5.Bii).

Stress relaxation is shown by displacing the sample by a fixed amount over a set period of time (Fig.1.5.Ci), and measuring the change in force. A typical viscoelastic response will see the stress decrease until it levels off and reaches equilibrium (Fig.1.5.Cii).

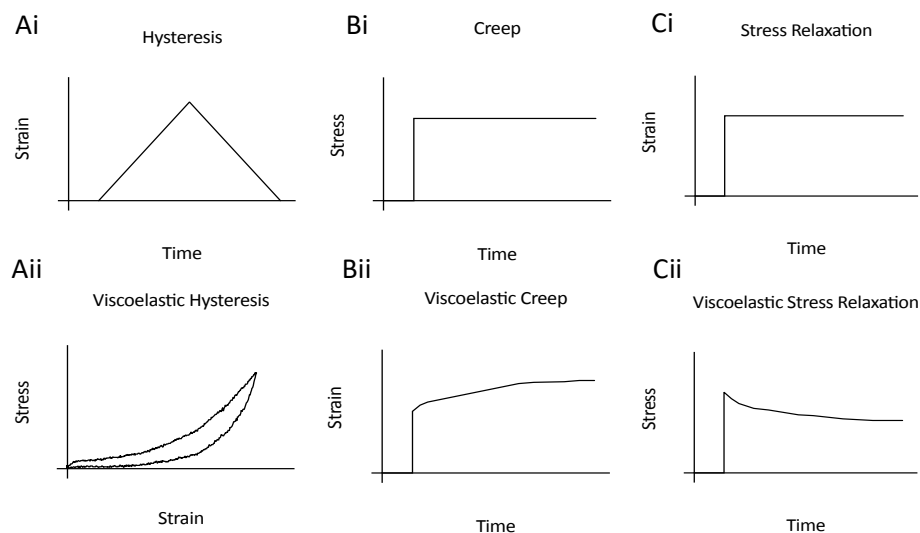


Figure 1.5. Schematic of viscoelastic loading regimen graphs (Ai, Bi and Ci) and viscoelastic material response graphs (Aii, Bii and Cii). Viscoelastic hysteresis data points taken from section 4.4.9.

1.4.4. Tendon Tissue Engineering

Tendons are susceptible to injury during overuse and overloading particularly in athletes, this can lead to pathological changes within the tendons structure that results in tendinopathy (Kaux et al., 2011). Due to the poor vascular supply in tendons repair following rupture is slow and leaves an impaired structure. The most common technique used to repair ruptured tendons is primary suture (Fig.1.6) or autologous transfer, however these techniques result in reduced mechanical strength of the tissues due to scar formation, infection, donor site morbidity and limited availability of autografts (Glass et al., 2014). Tissue engineered tendon therefore offer a potential alternative for the current gold standard. Alternatively improved tissue engineered tendon (closer to native tissue) gives researchers an *in vitro* model that can be used to investigate drug approaches, rehabilitation or cell therapies.

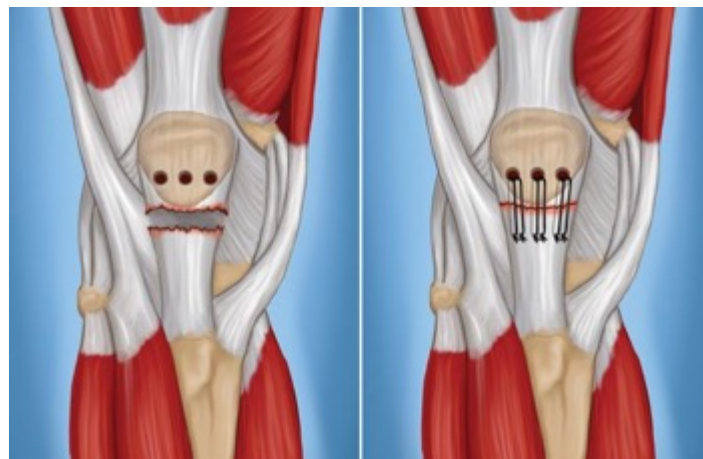


Figure 1.6. Suture repair of torn patellar tendon. Holes are drilled into the kneecap and sutures are threaded through the tendon and into the holes to pull the tendon back into position. Adapted from (Wilkerson, 2016).

The natural polymer is fibrin is one of the most widely used biomaterials for tendon tissue engineering, Breidenbach et al. (2015) showed that after 2-3 weeks the cells degrade the fibrin scaffold and replace it with collagen fibrils, this also shows an improved mechanical strength compared to collagen scaffolds. Yeung et al. (2015) showed that the collagen fibrils generated during collagen gelation are random in size and orientation whilst the collagen fibrils generated by cells in both fibrin and collagen hydrogels are narrow and aligned to the long axis of the structure. The cells in the collagen hydrogel appear stellate in shape with numerous projections similar to a 2D culture, whilst the cells in fibrin hydrogels appeared

more similar to *in vivo*, with cylindrical shape aligned to the loading axis. Therefore fibrin is a better model for tendon development.

An alternative natural polymer is collagen type I which is frequently used as it is the primary biological component of the tendon's ECM (Young et al., 1998, Awad et al., 1999, Bagnaninchi et al., 2007), and has shown to increase healing and function in damaged rabbit Achilles when seeded with MSCs (Young et al., 1998). However the initially formed structure is not aligned and instead made up of randomly orientated fibrils with impaired mechanical strength compared to native tendon (Bagnaninchi et al., 2007). Hybrid structures have been utilised to overcome some of these issues using other natural and synthetic polymers, this includes a collagen-silk (Chen et al., 2010), collagen-GAG (Caliari et al., 2011) and collagen-poly(l-lactide-co- ϵ -caprolactone) (Xu et al., 2013), all having seen increased mechanical strength and alignment compared to solely collagen structures.

In tissue engineering, tenocytes, fibroblast and MSCs have been the most widely used cell type (Engebretson et al., 2015). MSCs have been shown to be the better option as, whilst tenocytes do produce the correct ECM they proliferate at a much slower rate than MSCs. Tenocyte seeded Polyglycolide (PGA) fibres have been shown to generate high amounts of ECM after 10 weeks but do not have a high mechanical strength (Cao et al., 2004). When the tenocyte seeded PGA scaffold where implanted into rabbits the structure began to resemble that of native tendon however the PGA generated an immune response (Cao et al., 2002). Alternatively MSC seeded collagen scaffolds have shown a positive increase in mechanical strength but do not show improved cell morphology or alignment suggesting limited tenogenic differentiation (Awad et al., 1999). To further drive the differentiation and ECM production chemical and mechanical stimuli have been applied to the tissue engineered tendons.

Whilst most tissues receive a range of mechanical forces tendons mostly undergo stretch and relaxation as they transfer loads from the muscle to the bone (Kannus, 2000). The most common *in vitro* force applied to tissue engineered tendon is tensile stimulation which is normally applied in the longitudinal direction (Calve et al., 2004). Mechanical stimulation is applied using bioreactors, this can be either to 2D monolayers or 3D cell cultures (Fig.1.7). Appropriate mechanical stimulation for human tendons has been proposed to be up to 6% strain, above this strain rate the tendon ECM begins to degenerate (Wang, 2006). This has been supported with *in vitro* studies showing improved cell morphology with 5% strain at 1Hz (Sensini et al., 2019) and increased expression of tendon specific markers; scleraxis,

tenascin C, collagen I, collagen III, tenomodulin and VEGFA with 4% strain at 0.5Hz (Wu et al., 2017). However degenerative strain rates (>6%) have shown to increase the production of tendon degenerative markers, the study by Wang et al. (2003a) saw an increase in cyclooxygenase 1 and 2, prostaglandin E2 which are related to tendon inflammation when the tendons were strained at 12%. Further 9% strain has been shown to significantly increase the c-Jun N-terminal kinase pathway activation, which can lead to apoptosis (Arnoczky et al., 2002), separately Kearney et al. (2008) showed that 7.5% strain resulted in increased rates of apoptosis.

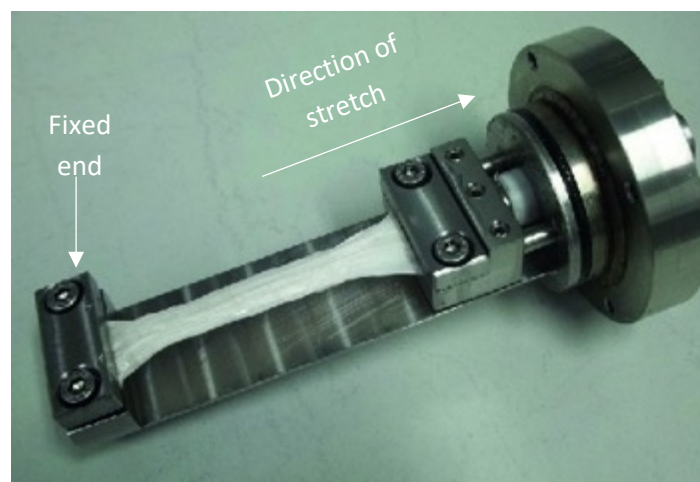


Figure 1.7. Image of tissue engineered tendon in stretch bioreactor. MSCs seeded onto a decellularised tendon and subjected to 24hrs of uniaxial stretch. Adapted from (Burk et al., 2016).

Currently no study has produced a tissue engineered tendon that has been adopted widely for tendon repair surgery, however progress has been made through the investigation of different cell sources, a variety of scaffolds and the stimuli used during cell culture giving a more complete understanding of how these cells proliferate, differentiate and produce ECM for tendon regeneration, though more still needs to be done. Whilst the tissue engineered tendon is becoming a more usable tool, further studies are required to confirm the long-term usage and biosafety of the structure before it can be considered for tendon repair. The application of mechanical stimulation for tendon tissue engineering is proving to be essential. With induced differentiation of cells towards tenocytes, improved mechanical properties and upregulation of tendon specific markers, the use of tensile stimulation has been shown on multiple occasions to promote the regeneration of the tendon ECM (Carroll et al., 2017, Wu et al., 2017, Sensini et al., 2019). Whilst progress is being made important markers within the ECM are not being investigated, these include the complete collagen composition found within healthy tissue. By focusing on the major components of the ECM

a skewed view of what is being generated is being established, for example only investigating the collagen I concentration is not effective if none of the regulatory collagens (V, XI, XII, or XIV) are investigated as the collagen I may be forming in-correctly, rendering the tissue useless. The field of tendon tissue engineering is promising, though no one protocol has proven to be optimal for the tissue generation, continued development of the biomaterial selection, media formulation and culture dynamics are required to create a truly effective engineered tendon.

1.5. Bone

1.5.1. Function

The adult bone can be split into two main types, the cortical bone and trabecular bone (Mizokami et al., 2017) with the structure containing three main compartments, the extracellular organic matrix, bone cells and extracellular minerals (An and Martin, 2003). The conventional function of bone is to act as a static support structure for organs that govern the body's movement (An and Martin, 2003). Cortical bone forms at sites of high load and is therefore very dense, it provides support for locomotion and other motor functions. Conversely trabecular bone is far less dense, forming the inner core of long bones and cranial plates and being in closer contact with vascular spaces (Li et al., 2017a).

Whilst the conventional functions have long been known more recent studies have eluded to a wider-ranging role for bone to help maintain the body's homeostasis, these roles (termed extraskeletal functions) include haematopoiesis, immune activity, energy metabolism and brain function (Asada et al., 2015, Han et al., 2018). The extraskeletal functions are mediated by bone-derived factors.

1.5.2. Structure

Bones are formed by the process of either endochondral or intermembranous ossification. Flat bones (calvariae of the skull, mandible or maxilla) form by intramembranous ossification, where MSCs differentiate directly into bone cells generating the bone ECM immediately (Ralston, 2017). Alternatively other bone forms by endochondral ossification, here an initial cartilage template forms before vascular tissue develops containing osteoprogenitor cells, the cartilage is then replaced by mineralised tissue at the middle and ends of developing bones. The growth plate (or epiphyseal plate), a thin layer of cartilage, is present throughout childhood and regulates the growth of the bone, here chondrocytes divide in the proliferation zone and migrate towards the centre of the bone where they enlarge and form hypertrophic chondrocytes in the hypertrophic zone. The hypertrophic chondrocytes subsequently die and the surrounding matrix calcifies before being removed by osteoclasts and are replaced with mature bone, this process stops during puberty as hormones prevent the chondrocyte cell division from occurring (Ralston, 2017).

From the developing bone two main structural types form, the trabecular and cortical bone. Woven bone is a third less common type which forms during development and at wound sites but does not require a preliminary cartilage template and therefore forms quickly, however this results in a weak structure that is replaced by cortical or trabecular bone (Sommerfeldt and Rubin, 2001). Trabecular bone is made up of plates and rods which generate a honeycomb structure (Fig.1.8) providing adequate structural support (Khurana, 2009).

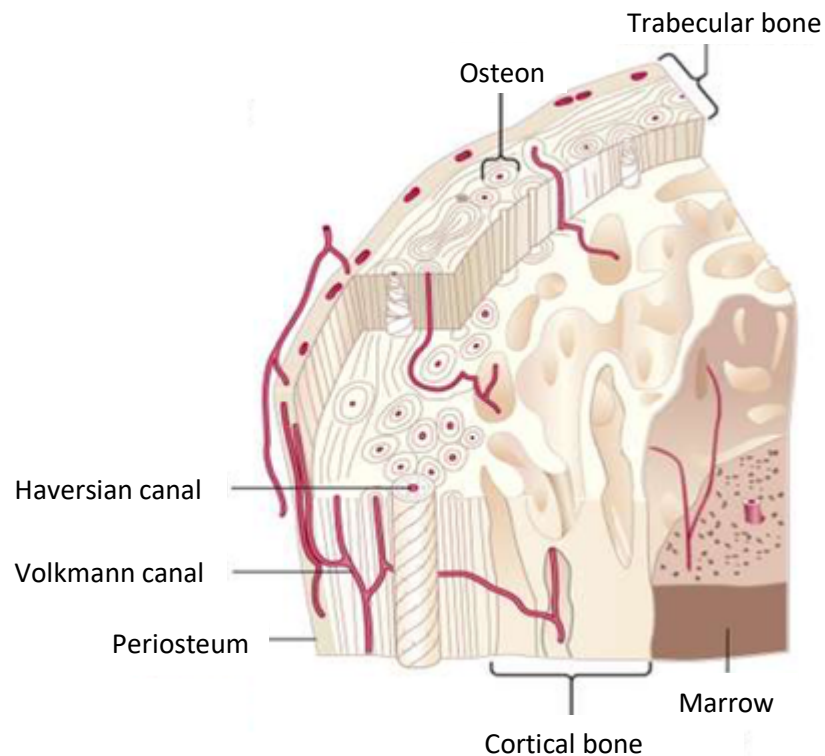


Figure 1.8. Schematic of the interior of cortical and trabecular bone (Adapted from Whedon and Heaney (2019)).

Bone marrow and blood vessels reside within the trabecular bone which has a lower calcium content and greater water content than cortical bone, allowing trabecular bone to act as a shock absorber that transfers the mechanical loads from the articular surface to the cortical bone (Ott, 2018). Trabecular bone does not possess the same strength as cortical bone as it is not as compact and dense. This more porous structure gives trabecular bone a much greater surface area resulting in a higher turnover compared to cortical bone (Parfitt, 2002). Cortical bone is composed of densely packed fibrils which form concentric lamellae that in turn form cortical osteons. Between the lamellae reside the lacunae, here osteoblasts become trapped within their secreted mineralised tissue and differentiate into less active osteocytes (Sommerfeldt and Rubin, 2001, Clarke, 2008, Bilezikian et al., 2008, Bonewald and Johnson, 2008). The cortical osteons make up the Haversian system which surrounds the

Haversian canal. Blood vessels and nerves feature within the Haversian canal and through connections form the Volkmann's canals (Fig.1.8). It is via these connections that the osteocytes communicate within the bone, utilising the canaliculi. Through these connections the osteocytes act as mechanosensors and help regulate the remodelling of the bone (Florencio-Silva et al., 2015). The high density of cortical bone imbues it with high mechanical strength and generates the protective functions of the tissue (Bilezikian et al., 2008).

1.5.2.1. ECM of Bone

The ECM of bone is, as with all tissue, a collection of components that each provide the tissue with specific functions. Within bone the ECM provides mechanical stability, cell-cell communication (Fan et al., 2014), acts as a repository for growth factors (ten Dijke and Arthur, 2007, Zhu and Clark, 2014, Wang et al., 2008) and offers the driving force for organogenesis (Sakai et al., 2003). Three main cell types reside within bone, the osteoblasts, osteoclasts and osteocytes. The ECM of bone therefore needs to provide the appropriate environment for these cell types to function efficiently. Bone is formed through the deposition of calcium phosphate onto a collagenous matrix by the osteoblasts. The calcium phosphate deposition is regulated through the crosslinking of the collagen fibres which is provided by lysyl oxidase (LOX) (Wassen et al., 2000, Bailey et al., 1993). The density of the bone is therefore regulated by the LOX-mediated intra/intermolecular covalent crosslinking of collagen and elastin (Knott and Bailey, 1998). Transversely the density of bone can be reduced via the activity of the osteoclasts. Here hydrogen ions and cathepsins/matrix metalloproteinases (MMPs) are secreted into the ECM and result in bone reabsorption (Blair et al., 1989, Vaananen et al., 2000, Oxlund et al., 1995). Bone homeostasis is therefore achieved through appropriate osteoblast and osteoclast activity.

The ECM of bone is made up of organic (40%) and inorganic compounds (60%) (Lin et al., 2020). The main inorganic compound is hydroxyapatite ($\text{Ca}_5(\text{PO}_4)_3\text{OH}$) (Ramesh et al., 2018), whilst the organic compounds are mainly collagen (90%) with small amounts of non-collagenous proteins (10%). Hydroxyapatite is deposited during biomineralisation, this process is controlled by interactions between matrix and minerals such as amino acids present in non-collagenous proteins and sees hydroxyapatite deposited onto a collagenous matrix (Fig.1.9) (Lin et al., 2020).

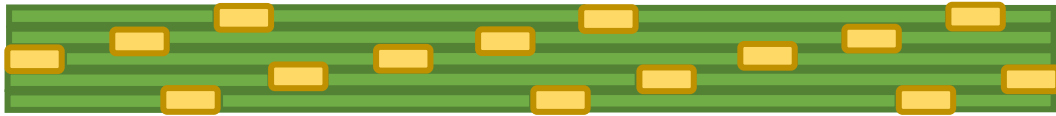


Figure 1.9. Schematic of collagen I fibril with hydroxyapatite crystals occupying the gaps generated by the staggered arrangement of the collagen triple helices (collagen green, hydroxyapatite crystals yellow).

The non-collagenous proteins can be classified into four groups: γ -carboxyglutamate-containing proteins, proteoglycans, glycoproteins and small integrin-binding ligands N-linked glycoproteins (SIBLINGs) (Paiva and Granjeiro, 2017). The γ -carboxyglutamate-containing proteins include osteocalcin which is specifically expressed by osteoblasts and contains three Gla residues enabling osteocalcin to bind to calcium and regulate calcium metabolism by mediating its association with hydroxyapatite (Mizokami et al., 2017). Periostin is mainly secreted by osteoblasts in long bones (Wen et al., 2018) and is an adhesion molecule required for collagen fibrillogenesis and to maintain bone strength (Wen 2018). Matrix Gla protein (MGP) is synthesised by osteoblast, osteoclasts and chondrocytes and is involved in inhibiting bone formation and mineralisation (Kaipatur et al., 2008).

SLPRs play a major role in the bone ECM by interacting with cell surface receptors and cytokines to regulate normal and pathological cellular behaviour (Lin et al., 2020). Biglycan and decorin are class I SLPRs and are both required for collagen fibrillogenesis and bone formation (Moorehead et al., 2019, Coulson-Thomas et al., 2015). Biglycan is expressed during cell proliferation and mineralisation whilst decorin is continuously expressed from the initial bone matrix deposition (Lin et al., 2020). Keratocan, mainly expressed by osteoblasts, promotes the mineral deposition rate and helps to regulate bone formation (Coulson-Thomas et al., 2015). Asporin binds to collagen type I fibrils and promotes collagen mineralisation (Kalamajski et al., 2009).

The glycoproteins include osteonectin, thrombospondin and r-spondins. Osteonectin is highly expressed by osteoblasts and through binding to collagen and hydroxyapatite crystals helps to regulate the release of calcium, therefore influencing the mineralisation of collagen (Rosset and Bradshaw, 2016). The thrombospondin family comprises of TSP1 to TSP5, is expressed by osteoblasts during bone development and has been shown to have an involvement in cell differentiation and the maintenance of bone mass (Delany and Hankenson, 2009, Hankenson et al., 2000). R-spondins are widely expressed throughout bone formation and maintenance and can be split into four groups (Rspo1-4) (Lin et al., 2020). R-spondins reinforces the wntless-type MMTV integration site (Wnt)/ β -catenin

signalling pathway through leucine-rich repeat-containing G-protein-coupled receptors 4, 5, and 6 (Lgr4/5/6) and therefore act as regulators for bone development and remodelling (Shi et al., 2017).

Finally the SIBLINGs are found predominantly in mature bone and include bone sialoprotein (BSP), osteopontin (OPN), dentin matrix protein-1 (DMP1) and matrix extracellular phosphoglycoprotein (MEPE). BSP is required for osteoblast differentiation and initiation of matrix mineralisation (Marinovich et al., 2016). Similarly OPN help to promote bone formation, mineralisation and remodelling, during which OPN regulates osteoclastogenic and osteoclast activity which contributes to bone formation and resorption (Singh et al., 2018). DMP1 and MEPE are mainly expressed by fully differentiated osteoblasts and have been show to regulate phosphate metabolism and matrix mineralisation (Zelenchuk et al., 2015).

1.5.2.1.1. Collagens of Bone

The main organic component of bone is collagen, specifically collagen type I (accounting for 90% of the collagens). As with other tissue multiple types of collagen occur within the bones ECM and all offer an important role to maintain the bones homeostasis throughout its life cycle. The collagen matrix in bone is very dense, aiding the bones mechanical and structural properties (Tzaphlidou, 2008). The other fibrillar collagens along with type I that occur in bone are type II, III, V, XI and XIV, the FACIT collagens are type IX, XII and XIV whilst type VI occurs as the microfibrillar collagen and type X as the Hexagonal network-forming collagen (Tzaphlidou, 2005). The collagen type I arrangement in bone is not as uniformly distributed as in tendon, though it does maintain a regular parallel pattern (Tzaphlidou, 2008). The collagen type I fibrils form the classical banding pattern where gaps form due to the staggered arrangement. In bone the collagen fibrils mineralise due to the formation of hydroxyapatite crystals in the gap regions (Fig.1.9). These hydroxyapatite crystals grow and interlink generating a interpenetrating organic-inorganic nanocomposite (Hansma et al., 2006). Collagen type I does not itself induce the hydroxyapatite nucleation (Glimcher, 1989), here other components of the ECM, such as osteonectin (Clarke, 2008), drive the process of fibril mineralisation whilst the collagen I fibrils act as templates (Tomoaia and Pasca, 2015).

Collagen type III occurs in small concentration in bone and similarly with tendon, is associated with collagen type I fibrils. In bone collagen type III has been shown to play a key role in skeletal development especially in the growth acceleration of osteoblasts (Maehata et al., 2007) and the preservation of osteogenic differentiated mesenchymal stem cells (Chen

et al., 2007). Collagen type V appears to play a regulatory role for the collagen fibres forming in the centre of the collagen I fibril bundles and working to organise the orientation and diameter. This is achieved via the collagen V fibril extending to the surface of the collagen I fibre, limiting the growth of the fibrils (Mak et al., 2016). A hybrid of collagen type V and XI has been shown in the bone ECM with the triple helix structure of $[\alpha 1(XI)_2]\alpha 2(V)$ (Niyibizi and Eyre, 1994), demonstrating the shared regulatory role of collagen V and XI in the bone ECM. The fibril forming collagen, type XXIV appears in the developing bone's ECM and has been shown to represent a marker for osteoblast differentiation and bone formation (Wada et al., 2006, Matsuo et al., 2008). Type XXIV is predominantly expressed in tissues containing type I and V, though its biological role has not yet been elucidated (Karsdal, 2019, Misawa et al., 2014).

Collagen type VI is a microfibril collagen and is located in the pericellular matrix (PCM). It is particularly present in the PCM of chondrocytes and therefore is thought to aid in the endochondral ossification of the growth plate (Alexopoulos et al., 2009). It has also been shown to feature in the PCM of pre-osteoblasts migrating to bone-forming sites (Izu et al., 2016). Due to the globular domain collagen VI interacts with multiple components of the ECM (Chen et al., 2015, Doane et al., 1998, Howell and Doane, 1998) enabling cell-matrix interactions and has been shown to interact with collagen XII during the formation of bone (Izu et al., 2016).

The FACIT collagens type XII and XIV operate in bone in a similar way as in tendon. In dense connective tissue both type XII and XIV bind to collagen I fibrils via the collagenous domain and helps to regulate the organisation of the fibril bundles through the large non-collagenous arm and its interactions with other ECM components (Chiquet et al., 2014). The two collagens have been shown to have temporal expression, with type XIV being expressed in a few specific areas during embryonic development whilst type XII is more widely expressed and continues to be so throughout bone development (Walchli et al., 1994). Collagen XII has been previously shown to localise at bone-forming sites with collagen XII deficient mice showing impaired osteoblast arrangement and therefore reduced bone mass and strength (Izu et al., 2012).

Collagen type II, IX, X and XI are the characteristic collagens of cartilage and are covered in more detail in section 1.6.2.1.1 of this chapter. Type X is produced by hypertrophic-preossifying cartilage, therefore this collagen is highly expressed before endochondral ossification. Collagen IX binds to surface of collagen II fibrils, the major collagen fibrils found

in cartilage. The collagen II fibrils generate an appropriate environment for the chondrocytes to operate and the growth plate to develop. Collagen IX offers an attachment site for other components of the ECM (Pihlajamaa et al., 2004, Tillgren et al., 2009, Parsons et al., 2011). Type XI, like type V, forms fibrils in the core of the collagen II fibres which extend to the surface, the extension features a thrombospondin-like domain which works to maintain the space and diameter of the collagen II fibrils (Kadler et al., 2008). Collagen type X is secreted into the ECM by hypertrophic chondrocytes, and in healthy tissue is localised to the calcifying zone of the growth plate. The collagen X multimer assembles into a hexagonal lattice which is thought to play a role in endochondral ossification by facilitating the process of calcification and the normal distribution of matrix vesicles and proteoglycans (Kwan et al., 1991, Chan et al., 1995, Kwan et al., 1997). Type X deficiency results in abnormal trabecular bone production in mice (Kwan et al., 1997) and therefore appears to play a major role in the transition between cartilage to bone, though its exact role is still yet to be determined (Shen, 2005).

1.5.3. Cells of the Bone

Osteoclasts, osteoblasts and osteocytes are the main cells types found in bone and other mineralised tissue. To achieve homeostasis all the cells types must work optimally, balancing the deposition and reabsorption of the mineralised tissue.

Osteoblasts are the bone forming cells, are mononucleated and derived from mesenchymal stem cells (MSCs) (Komori, 2006, Chen et al., 2016, Modder and Khosla, 2008, Liu et al., 2009c). Osteoblasts generate bone through the synthesis and secretion of bone ECM proteins which in turn enable the mineralisation of the ECM (Huang et al., 2007). The pre-osteoblasts bind through integrins to vitronectin generating a monolayer linked by cadherins (Schneider et al., 2001, Ferrari et al., 2000), the osteoblasts, once activated, then secrete bone ECM proteins in order to generate bone (Fig.1.10). The osteoblasts secrete ectoproteins including, tissue-nonspecific alkaline phosphatase (TNAP) which hydrolyses inorganic pyrophosphate (PP_i an inhibitor of hydroxyapatite formation) resulting in the production of phosphate for the formation of hydroxyapatite, therefore playing a crucial role in the mineralisation of the ECM (Moss et al., 1967, Majeska and Wuthier, 1975, Johnson et al., 2000, Hessle et al., 2002, Murshed et al., 2005). Progressive ankylosis gene (ANK) exports pyrophosphate generated intracellularly to the ECM and is primarily localised to the plasma membrane (Hakim et al., 1984, Kanaujiya et al., 2018). A number of signalling pathways, including TGF- β , BMP signalling, hedgehog (Hh), Wnt signalling, Notch and fibroblast growth

factors (FGFs) are involved in the differentiation and function of pre-osteoblasts to mature osteoblasts (Chen et al., 2016). Whilst the primary function of osteoblasts is the generation and remodelling of bone, they also act as regulators of bone reabsorption through regulation of osteoclast development. This is achieved through the secretion of macrophage-colony stimulating factor (M-CSF) and receptor activator of nuclear factor- κ B ligand (RANKL), both essential in osteoclastogenesis (Suda et al., 1999) and the secretion of osteoprotegerin (OPG), a decoy receptor for RANKL (Lacey et al., 1998). Once osteoblasts have completed their main function they either undergo programmed cell death (apoptosis) (Jilka et al., 1998), become bone lining cells (Manolagas, 2000) or are entrapped within the mineralised matrix and become osteocytes (Rodan and Martin, 1981) (Fig.1.10).

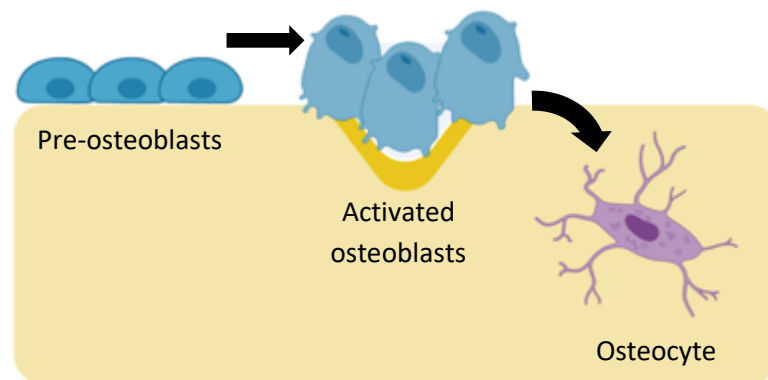


Figure 1.10. Schematic of osteoblast to osteocyte cycle. Pre-osteoblasts form monolayer on surface of bone, activated osteoblasts remodel bone and osteocyte become "trapped" within self-generated mineralised tissue. Created with BioRender.com. Osteocytes are small dendritic-like cells and are the most abundant cells in bone, accounting for 95% of cells in an adult skeleton (Franz-Odenaal et al., 2006). Through long thin processes which run through canals called canaliculi, osteocytes connect with other osteocytes and other cells on the surface of the bone. The system of connecting processes is known as the lacuna canalicular system and acts as a metabolic exchange which allows the osteocytes to sense and respond to stimuli by regulating osteoblasts and osteoclasts via the release of soluble mediators (Baud, 1968, Goldring, 2015). Osteocytes have been shown to respond to mechanical stimulation through the production of RANKL and therefore to regulate osteoclast differentiation in response to mechanical stimulus (Xiong et al., 2011).

Osteoclasts are a large multinucleated cell derived from haematopoietic stem cells that reabsorb bone and occur as a much lower percentage of bone cells than osteoblasts and osteocytes (Bilezikian et al., 2008). Osteoclast differentiation is dependent on two essential cytokines, M-CSF and RANKL, both secreted by osteoblasts and osteocytes (Han et al., 2018).

Osteoclast precursor cells interact with bone marrow stem cells via the RANKL and RANK receptor whilst M-CSF interacts with colony stimulating factor 1 receptor (c-fms) stimulating the proliferation and survival of the osteoclast precursor, motility and cytoplasmic spreading of mature osteoclasts and induces expression of receptor activator of RANK (Insogna et al., 1997, Arai et al., 1999, Teitelbaum and Ross, 2003). This results in the fusion of osteoclast precursor cells into mature osteoclasts (Fig.1.11). The stimulation of the RANK pathway by RANKL is negatively regulated by a decoy receptor, OPG which is expressed by osteoblasts

(Boyce and Xing, 2008).

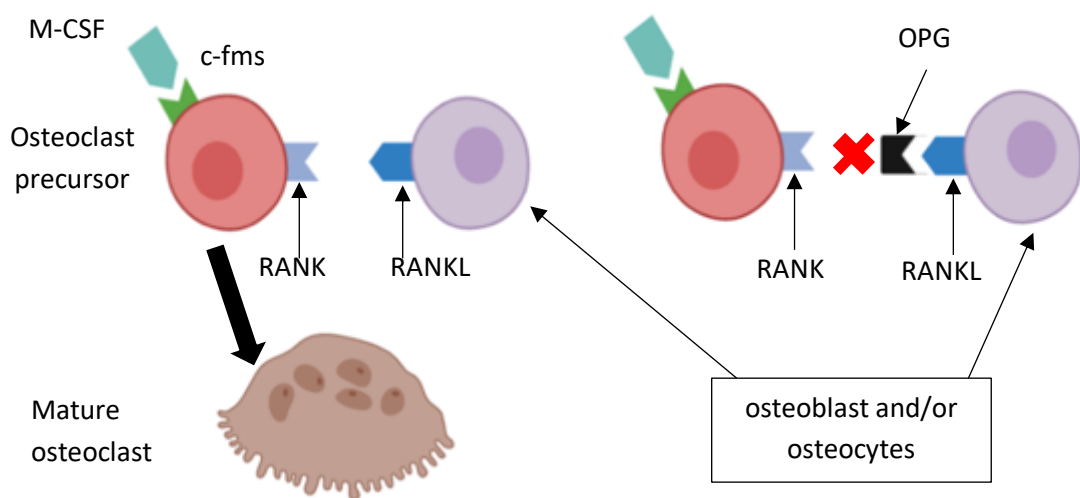


Figure 1.11. Schematic of osteoclast activation via RANK and c-fms receptors. Osteoblasts and osteocytes regulate the maturation of osteoclasts through the expression of c-fms, RANKL and OPG. Created with Biorender.

Osteoclasts work to reabsorb bone through degradation of the organic and inorganic phases (Teitelbaum, 2000). This is only achieved when the osteoclasts have adhered to the surface of the bone. Once adhered the osteoclasts begin the resorption process by first polarising. This is achieved through the clustering of the integrin $\alpha\beta3$ at adhesive sites called podosomes (Teitelbaum, 2000) (Fig.1.12). The podosomes enable osteoclast polarisation and allows the cell to adhere and spread out on the mineralised surface, sealing the osteoclast onto the bone. Bone reabsorption is achieved by the secretion of proteases (mainly cathepsin K) which dissolve the underlying bone, releasing the minerals into the extracellular space located in the sealed area under the osteoclasts ruffled plasmalemma (ruffled boarder), and resulting in the osteoclasts sitting in cavities known as the Howship's lacuna (Holtrop and King, 1977, Chambers, 2000). The seal formed between the osteoclast and the bone is made up of podosomes rich in filamentous actin (f-actin) which forms a ring

adjacent to the ruffled border (Vaananen and Horton, 1995, Chellaiah et al., 2000). The low pH in the Howship's lacuna is generated by the active secretion of protons driven by the activity of carbonic anhydrase II (CAII) and the vacuolar H⁺-adenosine triphosphate (H⁺-ATPase) pump, both located in intracellular vacuoles (Fig.1.12) (Baron et al., 1985, Blair et al., 1989, Schlesinger et al., 1997, Vaananen et al., 2000). The pH within the osteoclast is maintained by an energy dependent chloride/bicarbonate (Cl⁻/HCO₃⁻) exchange (Teti et al., 1989). The osteoclasts release hydrogen ions into the cavity resulting in a low pH which leads to the acidification and solubilisation of the mineral phase of bone into Ca²⁺, H₃PO₄, H₂CO₃ and H₂O (Chatterjee et al., 1992), exposing the organic phase. The degraded mineral is endocytosed by the osteoclasts and released into the ECM at the osteoclasts antiresorptive surface (Salo et al., 1997, Stenbeck and Horton, 2004). The released product is again degraded in secondary lysosomes, transcytosed and secreted via the secretory domain of into the osteocyte microenvironment (Soysa and Alles, 2016).

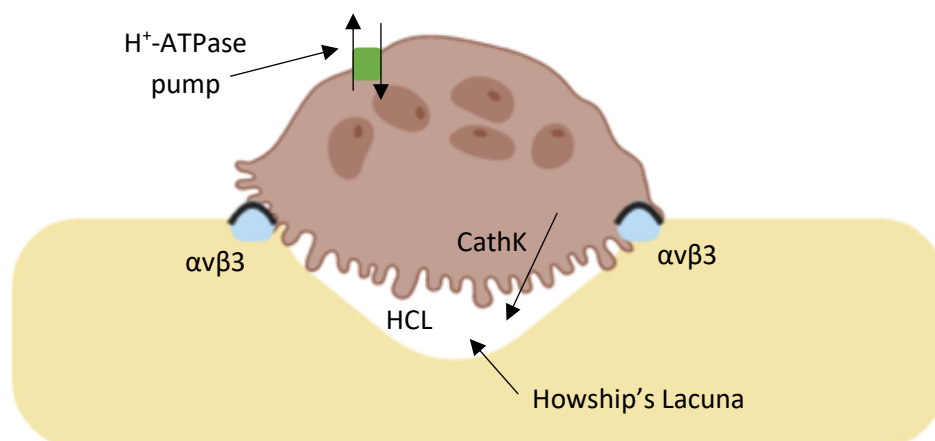


Figure 1.12. Schematic of osteoclast adhered to the surface of bone via integrin $\alpha v \beta 3$. Bone reabsorption is achieved through the secretion of hydrochloric acid and cathepsin K, producing an acidic environment within the Howship's Lacuna. Created with BioRender.com.

1.5.4. Bone Tissue Engineering

Following fracture, bone usually takes between six and eight weeks to heal, this may be delayed by the thickness of the cortical bone or unfavourable biological (e.g. osteoporosis) and mechanical (e.g. excessive fracture movement) environments, additionally other influences could result in delayed repair including age, alcohol, tobacco, steroid abuse, infection, type I diabetes and nutrient deficiency (Kostenuik and Mirza, 2017). These unfavourable factors may result in impaired fracture healing leading to delayed union or in some cases non-union of the damaged bone. Poor healing of the bone presents the surgeon

with challenges during operation due to the difficulty in re-routing and generating appropriate healing of the structure. Bone grafts have been developed to improve the treatment of impaired fracture repair with techniques including allografts and autografts. Allografts, the implantation of a grafts source from a non-identical donor, have the advantages of no morbidity of the donor site and unlimited use of the material, however this method has a number of drawbacks including graft rejection, disease transmission and potential loss of mechanical and cellular properties due to the sterilisation and storage process (Sohn and Oh, 2019). The current gold standard is autografts, the transplantation of tissue from one region of the body to another. This method is considered the gold standard due to their established osteoinductive and osteoconductive properties whilst eliminating any immune rejection (Perez et al., 2018). Whilst autografts appear as an ideal solution there are some drawbacks: donor site morbidity, donor site muscle weakness and potential surgical complications (though these are present for allografts also). Coupled with the initial drawbacks, after 10 years of implantation up to 60% of both graft types have been shown to fail to integrate resulting in non-union and late graft fracture (Soucacos et al., 2006). Tissue engineering is emerging as an alternative methods to those currently being used to treat damaged bones as well enabling *in vitro* research into diseases and drug responses.

There have been a number of cell types used for bone tissue engineering including osteoblasts, however due to the difficulty of harvesting and expanding, studies have focused more on osteo progenitor cells (Perez et al., 2018). MSCs have been the most widely used cell type for bone tissue engineering, with different sources having varying potential as a therapeutic option. Bone marrow derived MSCs have been shown to be more efficient at differentiating into osteoblasts than adipose derived (Han et al., 2014). Adipose derived MSCs do not demonstrating much success when directly grafted onto critical sized bone defects (Peterson et al., 2005), however they have shown some promise as a potential option. Cui et al. (2007) showed repair to a cranial bone defect in a canine model using osteogenically differentiated adipose derived MSCs grafted onto a coral biomaterial whilst *in vivo* studies have shown bone regeneration with adipose derived MSCs combined with specialised biomaterials (Lendeckel et al., 2004, Mesimaki et al., 2009). In comparison bone marrow derived MSCs have been shown to be successful when treated onto large bone defects with complete fusion five to seven months post treatment and good integration with no further fractures six to seven years after treatment (Marcacci et al., 2007). Similarly Kim et al. (2009) showed accelerated fracture repair two months after treatment with osteogenic differentiated bone marrow derived MSCs encased in fibrin. Whilst bone marrow derived

MSCs show a lot of promise the main limitations arise from the cell harvesting from older patients (Mareschi et al., 2006), donor site morbidity and reduced regenerative ability with extended expansions (Both et al., 2011). Other MSC sources include dental pulp (Lindroos et al., 2008, Kanafi et al., 2014), synovial membrane derived (De Bari et al., 2001, Sakaguchi et al., 2005) and umbilical cord derived (Chen et al., 2013, Dilogo et al., 2017).

Both synthetic (Polycaprolactone (PCL)) and natural (fibrin, collagen) polymers have been used for bone tissue engineering. PCL is the most heavily researched synthetic polymer for bone tissue engineered due to its high permeability, thermal stability and aliphatic semi-crystalline structure (Woodruff and Hutmacher, 2010). Calvert et al. (2000) showed that PCL maintained its mechanical properties for up to 6 months before degrading over a 2 year period. Natural polymers such as collagen and fibrin have been widely studied, but due to the low mechanical strength of the structure they are not suitable as load bearing replacement but more readily used as 'glues'. Oh et al. (2014) found that fibrin is the superior material for *in vitro* bone regeneration due to greater absorption of fibronectin, more proliferation of large MC3T3-E1 pre-osteoblasts and increased osteoblast differentiation shown by higher expression of Runx2, more alkaline phosphatase (ALP) production and greater calcium deposition. Composite materials can be made by combining ceramics and polymers, enabling control over degradation, improving mechanical strength and biocompatibility.

During culture of the tissue engineered bone, growth factors, that are stored within the bone *in vivo*, are added as supplements to the cell culture media, these include BMPs, FGF, Platelet-derived growth factor (PDGF), TGF- β and insulin-like growth factor (IGF-1). Only two growth factors are currently FDA approved, BMP-2 and BMP-7 (Cahill et al., 2015), though a range have been shown to play an important role in osteogenesis, BMP-2, 4, 5, 6 and 7. A randomised study in which 120 patients were treated with BMP-7/collagen constructs saw a significant increase in bone union (86.7%) compared to the alternative therapy (68.3%) (Calori et al., 2008). BMP-2 has been shown to not be essential during prenatal limb formation but essential during postnatal fracture healing (Wang et al., 2011). BMP-2 has been shown to increase the expression of collagen I and ALP when used to stimulate MC3T3 cells (Nohe et al., 2002). Further FGF-2 and IGF-1 have both been shown to increase the expression of osteogenic differentiation genes Runx2 and CDH11, whilst BMP-2 and FGF-2 both increase the expression of WNT5A and LEF1 both of which are developmental genes that regulate cell fate and patterning during embryogenesis (Robubi et al., 2014). TGF- β 1 has been shown to play an important role in the migration of MSCs to the site of the defect

whilst IGF-1 has been shown to be highly responsible for creating the osteogenic environment in which the MSCs differentiate down the osteogenic lineage (Perez et al., 2018).

Mechanical stimulation bioreactors have been used to further mimic the microenvironment of bone for tissue engineering. Stretch based bioreactors effect the proliferation and ECM production of osteoblasts, with low strain magnitudes (0.8%) having higher ALP production and higher strain rates (3.2%) showing the highest production of collagen I, osteocalcin and Runx2 (Zhu et al., 2008). Perfusion bioreactors have been utilised for bone tissue engineering due to the size of the structure, static cultures have been found to be limited in size due to the nutrient diffusion for the highly metabolic requirements of the bone cells (Grayson et al., 2011). On top of the increased perfusion, this type of bioreactor system induces fluid shear stress on the cells, therefore mechanically stimulating the cells in culture. The perfusion bioreactors utilise a pump, a culture media revisor, a tubing circuit and cartridges, chamber or columns that hold scaffolds (Martin et al., 2004, Chen and Hu, 2006, Yeatts and Fisher, 2011). When used to culture tissue, engineered bone studies have shown that ALP production is increased compared to static culture (Goldstein et al., 2001, Gomes et al., 2003, Wang et al., 2003b), further osteopontin has been shown to increase with flow perfusion (Holtorf et al., 2005a, Holtorf et al., 2005b). Using perfusion systems has also shown the production of a more uniform ECM compared to a static culture (Holtorf et al., 2005b, Sikavitsas et al., 2005, Porter et al., 2007). Hydrostatic pressure bioreactors have been shown to have varying effects on osteogenic development dependant on the frequency and the amount of pressure applied to the cell culture. Stavenschi et al. (2018) found that the most robust pro-osteogenic response was found with 300 kPa applied at 2 Hz , the highest pressure applied at the highest frequency in this study, however low pressures (10 kPa) still drove osteogenic lineage commitment.

Due to the diversity of potential solutions a greater understanding for bone tissue engineering is required. This is currently being achieved through the trial and application of different cells types including osteoblasts, bone marrow derived MSCs and adipose derived MSCs. Additionally the culture of these cells is continuously being improved through the addition of growth factors and mechanical stimulation environments used to mimic the healthy bone environment. Through a combination of materials, cell types and culture conditions, tissue engineered bone, in many different forms, will become a viable alternative for bone regeneration.

1.6. Cartilage

1.6.1. Function

There are three types of cartilage found in the human body, elastic, hyaline and fibrous each exhibiting different functions as a result of the differing ECM which is optimal to the location it is found in. Elastic cartilage is yellow in appearance, located in the outer ear and predominantly feature elastin in the ECM making it the most pliable of the cartilage types (Watkins, 2009). Fibrocartilage is located at tendon and ligament bone attachment sites and features the highest amount of collagen type I in healthy cartilage, making it very tough and strong (Benjamin and Ralphs, 2004). Hyaline cartilage is the most prevalent type of cartilage in the body, the embryonic skeleton is composed of hyaline cartilage that undergoes calcification to form bone. Hyaline cartilage is present in human adults at the end of ribs, in the nose and at the end of long bones as articular cartilage, (Pollard et al., 2017). The primary function of articular cartilage is the dissipation of mechanical loads (compressive (Eisenberg and Grodzinsky, 1985), shear (Parsons and Black, 1979) and tensile loads (Korhonen and Jurvelin, 2010)) from the bone by acting as a shock absorber and the facilitation of synovial joints to articulate by providing a site of low friction (Hardingham, 2010). In the adult human body articular cartilage can be expected to experience loads of 3.5 times the person's bodyweight at the knee, 3.3 times the bodyweight at the hip and 2.5 times at the ankle (Mow et al., 1984). Due to the high loads that are applied to the articular cartilage, it is essential that the biochemical and mechanical characteristics are maintained to allow for proper function. Cartilage observes viscoelastic behaviour during loading that allows the force to be appropriately absorbed. The structure of articular cartilage is vital for this (Boettcher et al., 2016).

1.6.2. Structure

Cartilaginous tissue features a specialised ECM generated by chondrocytes, the sole terminally differentiated cell within the structure. The precursor cell to the chondrocyte is the chondroblast, which themselves are derived from mesenchymal cells. As the chondroblasts generate the ECM they become separated from each other and become embedded within cavities within the matrix known as lacunae. The chondroblasts then terminally differentiate into chondrocytes. SRY-Box Transcription Factor 9 (Sox9) is essential to MSC differentiation down the chondrogenic lineage. No other transcription factor has been shown to effect chondrogenic cell fate as much as Sox9 (Lefebvre and Smits, 2005), however other transcription factors from the Pax, Hox, forkhead-helix and homeodomain

families have been shown to effect cell migration, proliferation, survival and condensation (Mundlos and Olsen, 1997). Following Sox9 driven differentiation of MSCs into chondroblasts, the cartilage ECM begins to develop. As this progresses the chondroblasts differentiate into chondrocytes. Here the cells continue to express Sox9 along with L-Sox5 and Sox6. The chondrocytes feature large endoplasmic reticulum and a highly developed Golgi apparatus required for extensive protein synthesis. The chondrocytes found within the lacunae organise themselves into distinct populations derived from the same original chondroblast referred to as isogenous groups (Armiento et al., 2019).

The structure of the different types of cartilage is different, though the composition is similarly made up of ground substances (polysaccharides), fibrous proteins and interstitial fluid (Armiento et al., 2019). Cartilage becomes avascular during maturation therefore requires nutrition diffusion from surrounding tissue, such as the synovial fluid at the knee joint. Elastic cartilage features a structure mainly composed of collagen type II and elastin fibres which form a dense structure orientated in multiple directions. There are a low number of isogenous groups which feature large chondrocytes in between the fibres (Nielsen and Bytzer, 1979). Fibrocartilage is located at the attachment site of dense connective tissue such as tendon where it enables the tissue to resist compression thanks to the large number of proteoglycans (Benjamin and Ralphs, 1998, Benjamin and Ralphs, 2004). The structure resembles that of connective tissues, with thick densely-packed fibres and featuring the highest concentration of collagen type I in cartilage with a low concentration of ground substances (Armiento et al., 2019). The number of chondrocytes in fibrocartilage is lower than in other cartilage types with the chondrocytes aligning with the thick collagen fibres (Benjamin and Ralphs, 2004). Hyaline cartilage is the most common type of cartilage, receives high loads throughout its life cycle and acts as the precursor to bone formation during endochondral ossification.

1.6.2.1. ECM of Cartilage

Collagen type II and aggrecan are the most abundant proteins in the ECM of hyaline cartilage. The structure is highly regulated offering specific functional properties to the tissue. Water is the primary component of hyaline cartilage, accounting for 70-80% of the wet weight. The dry weight is mainly composed of collagen (50-75%) and proteoglycans (15-30%) (Darling and Athanasiou, 2003). It is the combination of collagen and proteoglycans within the hyaline cartilage structure that imbues it with the appropriate mechanical properties. SLRP are the only type of proteoglycans present in hyaline cartilage, and are large macromolecules made

up of a protein core with one or more polysaccharide chains (glycosaminoglycans (GAGs)) covalently attached. The chains can be made up of more than 100 monosaccharides and extend out from the protein core and remain separated by charge repulsion (Sophia Fox et al., 2009). The ECM of articular cartilage contains multiple proteoglycans including aggrecan, decorin, biglycan and fibromodulin with aggrecan representing the most abundant and largest structure. Aggrecan features more than 100 chondroitin sulfate and keratan sulfate chains and interacts with hyaluronan via the N-terminal G1 domain whilst the C-terminal G3 domain binds to ECM molecules such as tenascins and fibulins to form large proteoglycan aggregates which are stabilised by cartilage link proteins (Hardingham, 1979, Casscells, 1990). Through the development of these proteoglycan aggregates within the intrafibrillar space, aggrecan generates a negative charge providing cartilage with osmotic properties that draws water into the tissue which is crucial to the structures ability to withstand compressive forces (Sophia Fox et al., 2009). SLRP class I-IV have been detected within the ECM of cartilage (Aspberg, 2016). These include decorin and biglycan from class I. Both SLRP feature chondroitin sulfate chains at the N-terminal (one chain in decorin, two chains in biglycan). Decorin binds to collagen fibrils at the D period via its core protein and through its N-terminal GAG (e.g. dermatan sulfate), decorin plays a role in fibril assembly *in vitro*, resulting in slower fibrillar assembly (Yamaguchi et al., 1990, Ruhland et al., 2007). Similarly to decorin, biglycan binds to collagen fibrils and is highly expressed in the pericellular matrix where it interacts with collagen type VI, linking it with collagen type II (Wiberg et al., 2001, Wiberg et al., 2002, Wiberg et al., 2003). Biglycan has been shown to regulate innate immunity through activation of TLR2 and TLR4 signalling, which may be involved in the inflammation of the joint (Schaefer et al., 2005). The class II proteoglycans include fibromodulin which features tyrosine residues at the N-terminal. Fibromodulin binds to the gap region of fibril forming collagens where it inhibits and therefore regulates the formation of fibrils (Hedbom and Heinegard, 1989). Epiphykan is a class III proteoglycan that fluctuates in expression throughout the cartilage lifecycle. It is highly expressed in the growth plate and in developing bones but expression in articular cartilage reduces with maturation (Onnerfjord et al., 2012). The class IV SLRP chondroadherin has been shown to be involved in cell adhesion through $\alpha 2\beta 1$ integrins (Haglund et al., 2013). Though proteoglycans are not the main component of the cartilage ECM they provide vital functions as structural components, regulators of other ECM proteins, regulators of growth factors and regulation of innate immunity ensuring the tissue operates optimally.

1.6.2.1.1. Collagens of Cartilage

The main component of mature hyaline cartilage ECM is collagen, specifically collagen type II accounting for more than 90% of the collagen content (Eyre, 2002). Other minor collagens are required to ensure cartilage functions correctly, these minor collagens include type I, V, VI, IX, X, XI and XII (Luo et al., 2017). Whilst collagen type XII is expressed across a wide range of tissue, especially those containing collagen type I, collagens II, VI, IX, X and XI are predominantly localised to cartilage. The role of collagen type II in cartilage is similar to that of collagen type I in tendon as it is the primary fibre-forming collagen in healthy cartilage. Collagen type II therefore is the main structural component supplying tensile strength to the ECM as well as a binding structure for other ECM proteins. The collagen type II fibrils are thinner than collagen type I fibrils. A reduction of collagen type II in the ECM of hyaline cartilage results in excessive production of collagen I and III, this can lead to diseases such as osteoarthritis (Mundlos et al., 1996, Lorenz et al., 2014). Collagen type II forms as a homotrimer of three $\alpha 1(\text{II})$ chains encoded by the COL2A1 gene in humans.

Collagen VI is the sole member of the microfibrillar group and is formed through the combination of six different alpha chains ($\alpha 1-6(\text{VI})$) (Fitzgerald et al., 2008), which go through a complex multistep process of intracellular assembly before secretion into the ECM (Knupp et al., 2006). In cartilage collagen VI is primarily expressed in the chondrocyte pericellular matrix (Keene et al., 1988). Whilst the functional role of the pericellular matrix is still not fully known (Grassel and Aszódi, 2016) it is hypothesised that due to it completely surrounding chondrocytes within healthy cartilage it helps to regulate the biochemical, biophysical and biomechanical signals that the cells receives (Guilak et al., 2006). The collagen VI fibrils interact with hyaluronan (Kielty et al., 1992), decorin (Bidanset et al., 1992) and fibronectin (Chang et al., 1997) to anchor the chondrocytes to the ECM (Sherwin et al., 1999). A study by Wiberg et al. (2003) found that collagen VI binds to collagen II fibres through biglycan whilst other proteoglycans bind to the collagen VI scaffold. These proteoglycans help to organise the collagen II fibres which generates a healthy ECM, therefore the author hypothesise that collagen VI acts as a scaffold to bring the regulatory proteoglycans into close proximity with the collagen II fibres. A deficiency in collagen VI has been shown to delay cell differentiation and proliferation which subsequently leads to delayed and decreased cartilage development, and spontaneous development of osteoarthritis (Alexopoulos et al., 2009).

Collagen XI is distributed across multiple tissues however the triple helical composition is specific to cartilage. In developing cartilage it is made up of $\alpha 1(XI)$ and $\alpha 2(XI)$ and a third chain, $\alpha 1(II)$. In mature cartilage collagen XI forms in two distinct heterotrimeric molecules, $\alpha 1(XI)\alpha 2(XI)\alpha 3(XI)$ or the hybrid molecule $\alpha 1(XI)\alpha 3(XI)\alpha 1(V)$. The function of this hybrid is currently unknown. As the cartilage continues to mature the amount of $\alpha 2(XI)$ in the collagen XI fibrils decreases whilst $\alpha 1(V)$ increases (Wu et al., 2009). Type XI forms uniformly thin fibrils which act as the basic structure for type II fibrils in developing cartilage (Kadler et al., 2008, Fernandes et al., 2007, Vaughan-Thomas et al., 2001) and resides in the core of collagen II fibres. Collagen XI features a thrombospondin-like domain which extends from the core of the collagen II fibres. It is thought that through the extension of this domain, collagen XI helps to regulate the spacing and diameter of the collagen II fibrils as well as inhibit lateral growth (Seet et al., 2017). In a study by Li et al. (2018) collagen XI has been shown to have strong chondrogenic effects through the promotion of cell proliferation and ECM production, specifically synthesis of collagen II, SOX9 and aggrecan.

The FACIT collagens found within cartilage are type IX and XII, with collagen IX being the primary FACIT collagen found in hyaline cartilage accounting for 1% of the collagen content (Martel-Pelletier et al., 2008). Whilst type XII was initially thought to be absent in cartilage it has been shown to occur in small quantities (Watt et al., 1992). Collagen IX assembles from three alpha chains $\alpha 1(XI)$, $\alpha 2(XI)$ and $\alpha 3(XI)$ and features a hinge-like globular non-collagenous region at the N-terminal of the $\alpha 1$ chain (Shaw and Olsen, 1991). During embryonic development collagen IX is widely distributed and binds to the collagen II fibrils, through interactions with other ECM components via the hinged N-terminal and alongside the collagen XI fibrils, collagen IX regulates the fibril orientation generating the appropriate heterofibril network (Eyre et al., 2002). One of the key interactions collagen IX makes is with cartilage oligomeric protein which influences the diameter of the type II fibrils (Blumbach et al., 2009). In mature hyaline cartilage collagen IX is present in specific regions of the tissue rather than widely occurring (Hagg et al., 1998b). Collagen XI alpha chains consist of three triple helix domains (COL1, COL2 and COL3) which are separated and flanked by non-collagenous domains (NC-1, NC-2, NC-3 and NC-4), with the NC-4 domain only present on the $\alpha 1$ chain and allowing for interactions with the ECM. The COL2 domain of the $\alpha 3(XI)$ chain covalently bonds to the N-telopeptide of the $\alpha 1(II)$ chain and the COL2 (IX) domain of the $\alpha 2(XI)$ chain forms an intra-molecular covalent bond to the C-telopeptide of the $\alpha 1(II)$ chain (Diab et al., 1996). The NC-4 projection into the ECM is achieved via a kink between the COL2 and COL3 domains. Collagen XII is highly distributed in the superficial zone of developing

cartilage especially in areas of highly organised fibrils, suggesting that collagen XII plays a role in the development, alignment and stabilisation of the superficial zone of hyaline cartilage (Gregory et al., 2001). Similarly to collagen XI, collagen XII binds to the surface of collagen II fibrils and via a hinge in the structure the N-terminal domain extends into the ECM. Through the extension collagen XII has been shown to bind to decorin, fibromodulin (Font et al., 1996) and COMP (Agarwal et al., 2012).

Collagen X is a member of the hexagonal network forming collagens and is primarily found in the calcified zones of cartilage, this may be during endochondral ossification or in calcifying regions of mature cartilage where it is seen as a marker for cartilage degeneration (Boos et al., 1997). In healthy mature cartilage, collagen X should only account for around 1% of the total collagen content (Eyre, 2002). Collagen X is predominantly expressed in the hypertrophic zone of cartilage. Here chondrocytes undergo hypertrophy and differentiate into hypertrophic chondrocytes. During hypertrophic differentiation chondrocytes enlarge by up to 20 fold, which also sees the development of a granular cell surface and protrusion of numerous microvilli which release matrix vesicles required for matrix mineralisation (Wuthier, 1988, Mackie et al., 2008). Sox9 continues to drive chondrocyte differentiation and is expressed by early hypertrophic chondrocytes but expression ceases in late hypertrophic chondrocytes (Zhao et al., 1997, Hattori et al., 2010). The reduction in the expression of Sox9 is mediated by the increased expression of osteogenic genes including Runx2, osterix, osteopontin and bone sialoprotein (Komori, 2010). Runx2 promotes the expression of collagen X and the maturation of hypertrophic chondrocytes (Wang et al., 2004, Stricker et al., 2002). Furthermore, Runx2 induces the expression of VEGFA and MMP13. VEGFA is required for the invasion of capillaries into the hypertrophic cartilage (Gerber et al., 1999, Carlevaro et al., 2000, Zelzer et al., 2001), Mmp13 loosens the matrix of the hypertrophic cartilage to allow the invasion of bone marrow sprouts (Inada et al., 2004). The hypertrophic chondrocytes develop the required ECM for mineralisation and undergo apoptosis, laying a cartilage template for bone formation (Shapiro et al., 2005). Whilst the role of collagen X is still unknown (Shen, 2005) it is thought to play a major role in endochondral ossification through the facilitation of calcification and the normal distribution of matrix vesicles and proteoglycans at the growth plate, with deficiencies in collagen X, resulting in abnormal bone development (Kwan et al., 1997).

1.6.3. Cartilage Tissue Engineering

Defects to articular cartilage may result in significant pain and reduction in function of the joint with long lasting treatment not currently available. This is a particular problem for younger patients who may require repeat treatment to alleviate the symptoms, and the inevitable development of osteoarthritis (Robertsson et al., 2007, Julin et al., 2010). There are several surgical options for such defects; bone marrow stimulation treatment, direct chondral replacement and cell-culture treatment (Fig.1.13). The most commonly used technique is microfracture, a form of bone marrow stimulation, here micro pores are drilled into the subchondral bone to allow blood and bone marrow to infiltrate, clot and stimulate cartilage repair (Steadman et al., 1999). A less widely used technique, autologous chondrocyte implantation (a cell-culture treatment), harvests cartilage from non/low weight bearing regions, isolates and expands the chondrocytes, before re-implantation into the defect (Brittberg et al., 1994). Mosaicplasty, a direct chondral replacement treatment (not recommended for use on cartilage showing signs of osteoarthritis, rheumatoid arthritis, infection or tumour growth), involves the extraction of cartilage plugs from non/low weight bearing regions and implantation into the lesions (Hangody et al., 2004). The production of fibrocartilage during repair and treatment is a major barrier in long term viability (Redman et al., 2005) therefore new treatments are being pursued with 3D tissue engineering a potential option (Francis et al., 2018). Similarly with bone and tendon tissue engineering, MSCs have emerged as the most frequently used cell type for cartilage, partially due to the range of sources and ease of culture in addition to the well-established ability for chondrogenic differentiation (Rada et al., 2009, Ronziere et al., 2010). The most frequently utilised MSC sources are bone marrow and adipose with adipose derived MSCs showing more superior chondrogenic differentiation compared to bone marrow derived (Strioga et al., 2012, Jang et al., 2015). Chondrocytes have also been utilised for cartilage tissue engineering, though isolation from articulating surfaces is difficult therefore other regions have been used including cartilage from the nose and ear as the chondrocytes from these regions are easier to harvest and proliferate at a greater rate, it is unclear whether these cells would produce the appropriate cartilage (Van Osch et al., 2004, El Sayed et al., 2010, El Sayed et al., 2013, Lohan et al., 2014).

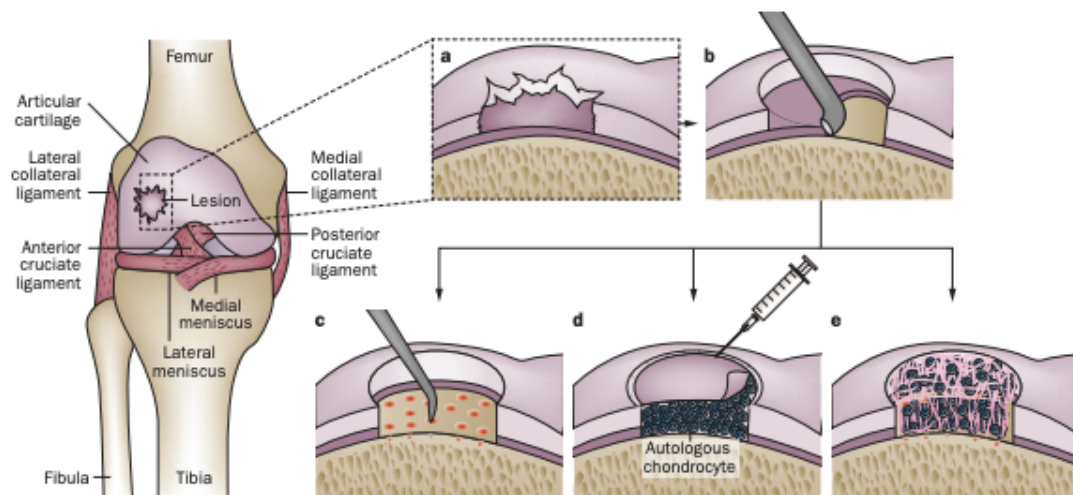


Figure 1.13. Damaged cartilage repair techniques. (a) full thickness focal chondral lesion. (b) debrided lesion. (c) The microfracture techniques for MSC repair from bone marrow. (d) Autologous chondrocyte implant sealed with collagen glue. (e) Tissue engineered cartilage plug generated from *in vitro* culture of chondrocytes in hydrogel and secured in place with fibrin glue. Adapted from (Makris et al., 2015).

For chondrogenic culture, specific growth factors are added to the culture medium in place of foetal calf serum as the composition and concentration of the serum varies from batch to batch, instead TGF- β and IGF are regularly added to the media to induce differentiation. TGF- β is necessary for chondrogenic differentiation of MSCs and has been shown to inhibit chondrogenic hypertrophy for at least seven weeks, though not entirely as the MSCs still express hypertrophy-related genes including collagen type X, ALP, MMP13, VEGF, PTHR1 and Runx2 (Mueller and Tuan, 2008, McCarthy et al., 2012, Giuliani et al., 2013). Other growth factors have been shown to have differing effects on the differentiation and subsequent ECM production of MSCs down the chondrogenic lineage, FGF-2 has been shown to prime MSCs for chondrogenic differentiation through the increased expression of Sox9 and formation of chondrogenic specific ECM (Solchaga et al., 2005, Solchaga et al., 2010, Hagmann et al., 2013, Somoza et al., 2014). BMPs have been shown to play a major role in endochondral bone formation driving cells along the osteochondral pathway (O'Connor et al., 2000). BMP-1 and 2 have been found to upregulate proteoglycan and collagen expression from chondrocytes (O'Connor et al., 2000, Pecina et al., 2002, Gooch et al., 2002, Valcourt et al., 2002), BMP-7 inhibited collagen I formation and fibroblast infiltration *in vivo* (Kaps et al., 2002) and treatment with BMP-12 and 13 has shown increased production of GAGs, though this was less so than BMP-12 (Gooch et al., 2002). However BMP-4 has shown an increase in bone formation, suggesting that the type of BMP is important to maintain the desired lineage (Pecina et al., 2002, Luyten et al., 1992), a study by Kuroda et al. (2006) showed that BMP-4

enhanced chondrogenesis and significantly improved articular cartilage repair in rats, suggesting that further work is required to fully evaluate the role BMPs can play in the controlled differentiation of MSCs to chondrocytes.

A number of different types of bioreactors have been used to mimic the cartilage *in vivo* environment for *in vitro* experiments, this includes hydrostatic pressure, compression and shear bioreactors. Compression bioreactors are regularly used for tissue engineering cartilage to replicate the compressive forces applied to the articular cartilage of the knee joint, these loads are typically in the range of 0.5-7.7 MPa (Afoke et al., 1987, Mow and Wang, 1999, von Eisenhart et al., 1999), with the average deformation of the articular cartilage being 13% of its initial thickness (Chung and Burdick, 2008). Cyclic compression has been shown to increase the Young's modulus of the constructs whilst also increasing the production of cartilage oligomeric matrix protein and collagen type II and IX (Ng et al., 2009). The frequency at which the compression is applied at can help drive the differentiation, with low frequency (1 Hz) causing MSCs to differentiate down the chondrogenic lineage and high frequencies (100 Hz) resulting in osteogenic differentiation (Cashion et al., 2014). Many groups have seen increases in cartilage specific matrix components such as collagen II, GAGs and aggrecan (Nebelung et al., 2011, Correia et al., 2016, Gharravi et al., 2012, Gharravi et al., 2016), however direct compression does have disadvantages; the applied pressure is not uniform with the highest pressure being seen at the centre of the sample, the transfer of nutrients and waste across the sample is limited with the centre receiving very little and storing a high amount of waste production (Li et al., 2017b).

Hydrostatic pressure bioreactors look to mimic the hydrostatic forces sensed by the cartilage *in vivo*, here under the applied force the fluid flows out of the cartilage and into the joint space, however this is controlled by the small effective pore size of the cartilage preventing rapid fluid flow. This results in the pressure increasing with each cycle of pressure applied and is thought to be applied at 7-10 MPa (Stockwell, 1971, Hall et al., 1996). The application of the hydrostatic pressure can have varying effects on the cellular response, Smith et al. (1996) found that a monolayer of articular chondrocytes exposed to cyclic 10 MPa hydrostatic pressure at 1 Hz for four hours increased the expression of collagen II and aggrecan whilst the static loaded group saw a decrease in collagen II expression. The positive effects of hydrostatic pressure are also seen in 3D culture, Kawanishi et al. (2007) showed that chondrocytes cultured in pellet culture and loaded with 5 MPa at 0.5 Hz see a 4 fold increase in collagen II and a 5 fold increase in aggrecan gene expression compared to the non-loaded controls. Further, differentiation genes have shown significant increases within

cyclic hydrostatic pressure environments,. Sakao et al. (2008) saw significant increase in the expression of Sox9 and collagen II by synovium derived MSCs cultured in hydrostatic pressure.

Shear stress is seen in cartilage during the loading and unloading phase (Wang and Peng, 2015), and has been shown to affect chondrocytes through changes in membrane potential, solute transport or cellular deformation (Sharifi and Gharravi, 2019). A number of studies have shown positive changes in the chondrogenic gene production and ECM development with shear bioreactors (Waldman et al., 2003, Frank et al., 2000, Jin et al., 2003, Jin et al., 2001), while Cochis et al. (2017) used a shear-compression bioreactor that enabled the two stimuli to act simultaneously, here they saw significant chondrogenesis in the stimulated group compared to the non-stimulated group. Certain types of fluid shear bioreactors and microgravity bioreactors work in a similar way, the constructs are cultured within a vessel and shear is applied through either the rotation of the vessel itself or the rotation of a mixer.

Due to the long lasting impairment seen at damaged cartilage, the use of grafts from healthy locations on the patient's body is not an ideal solution as the graft site will likely remain impaired for the remainder of their life. Tissue engineering offers the option to source pre-chondrogenic cells from a self-replenishing site, such as adipogenic tissue, and culture the graft artificially. Similarly to bone, different damage types seen on cartilage require different procedures to repair. A range of materials with different properties (mechanical and chemical) are therefore required to successfully restore the cartilage, however one of the current issues with cartilage tissue engineering is the progression of the chondrocytes towards hypertrophy. Recent studies have suggested that different growth factors and chemical supplements may be able to dictate the cellular fate, whilst others point towards a combined mechanical stimulation approach. It is clear that only by better re-creating the healthy native chondrogenic environment, both chemically and mechanically, will more successful tissue engineering cartilage be generated, this will most likely require a combination of the chemical supplements and the mechanical environments supplied by bioreactors.

1.7. Collagen

To date there are known to be at least 28 different types of collagen and as outlined in section 1.4, 1.5 and 1.6 the different types of collagen feature in varying proportions in different tissue types. Each collagen type exhibits a specific characteristic that enables the tissue it features in to perform appropriately (Kadler et al., 2007, Gordon and Hahn, 2010, Ricard-Blum, 2011, Johnstone, 2000). There is potential to use the collagens found in specific musculoskeletal tissues as a marker for the quality of tissue engineered tissue, this is currently not being fully utilised as most studies focus on the major collagen type of the tissue or a type specific to the study. By investigating the complete collagen composition the researcher can establish the developmental stage of the tissue, infer the phenotype of the cells and determine what tissue has been generated within the study.

Collagen is the most abundant structural protein found in vertebrates (Landis and Jacquet, 2013). In humans, collagen is known to comprise of one-third of the total protein and is the most prevalent component of the extracellular matrix (ECM) (Shoulders and Raines, 2009). In some tissues, such as tendon and the organic components of bone, collagen potentially accounts for more than 90% of the structure (Friess, 1998). Whilst being present across a wide variety of tissues, collagen has not been detected in a small number, these include the nail plate and hair shaft (Lee et al., 2006, Rice, 2011). Each collagen type exists within a subcategory of fibrillar or non-fibrillar collagen, with the non-fibrillar having further subcategories: fibril associated collagen with interrupted triple helix (FACIT), hexagonal network-forming, basement membrane, microfibrillar, anchoring fibrils, membrane associated collagen with interrupted triple helix (MACIT) and multiplexins (van Huizen et al., 2019). Table 1.1 lists the different collagen types and the subcategory they fall into.

Changes in collagen composition within a particular tissue can be a result of development, degradation and regeneration. The cells found within the tissue will naturally turn over the proteins within the ECM to ensure the tissue health and homeostasis, and an imbalance to this protein turnover may result in an impaired function of the tissue (Karsdal et al., 2017).

Table 1.1. Table of collagen types and the associated category, adapted from Canty and Kadler (2005) and van Huizen et al. (2019).

Type	Human Genes	Category	Triple helix composition	Tissue distribution	References
I	COL1A1, COL1A2	Fibril-forming	$[\alpha 1(I)]_2, \alpha 2(I)$	Fibrils in tendon, ligament, bone, skin, cornea and blood vessel walls	(Myers et al., 1981, Chu et al., 1982)
II	COL2A1	Fibril-forming	$[\alpha 1(II)]_3$	Fibrils in Cartilage	(Miller and Matukas, 1969)
III	COL3A1	Fibril-forming	$[\alpha 1(III)]_3$	Forms heterotypic fibrils with type I	(Cameron et al., 2002)
IV	COL4A1, COL4A2, COL4A3, COL4A4, COL4A5, COL4A6	Basement membrane	$[\alpha 1(IV)]_2, \alpha 2(IV)$ $\alpha 3(IV), \alpha 4(IV), \alpha 5(IV)$ $[\alpha 5(IV)]_2, \alpha 6(IV)$	Basement membranes	(Timpl et al., 1981, Timpl and Brown, 1996)
V	COL5A1, COL5A2, COL5A3	Fibril-forming	$[\alpha 1(V)]_3$ $\alpha 1(V)]_2, \alpha 2(V)$ $\alpha 1(V), \alpha 2(V), \alpha 3(V)$	Forms heterotypic fibrils with type I	(Birk, 2001)
VI	COL6A1, COL6A2, COL6A3, COL6A4	Microfibrillar	$\alpha 1(VI), \alpha 2(VI), \alpha 3(VI)$ $\alpha 1(VI), \alpha 2(VI), \alpha 4(VI)$	Fine microfibrils with ubiquitous distribution	(Kielty et al., 1992)

Chapter 1

VII	COL7A1, COL7A2	Anchoring fibrils	$[\alpha 1(\text{VII})]_3$ $[\alpha 1(\text{VII})]_2, \alpha 2(\text{VII})$	Forms anchoring fibrils in skin at the dermal/epidermal junction	(Keene et al., 1987)
VIII	COL8A1, COL8A2	Hexagonal network-forming	$[\alpha 1(\text{VIII})]_3$ $[\alpha 1(\text{VIII})]_2, \alpha 2(\text{VIII})$	3D hexagonal lattice is Descemet's membrane in the eye	(Kapoor et al., 1986, Kapoor et al., 1988, Stephan et al., 2004)
IX	COL9A1, COL9A2	FACIT	$\alpha 1(\text{IX}), \alpha 2(\text{IX}), \alpha 3(\text{IX})$	Associated with type II	(Olsen, 1997, Shimokomaki et al., 1990)
X	COL10A1	Hexagonal network-forming	$[\alpha 1(\text{X})]_3$	Hexagonal lattice in the hypertrophic cone of the growth plate	(Kwan et al., 1991)
XI	COL11A1, COL11A2, COL11A3	Fibril-forming	$\alpha 1(\text{XI}), \alpha 2(\text{XI}), \alpha 3(\text{XI})$	Forms heterotypic fibrils with type II	(Mendler et al., 1989)
XII	COL12A1	FACIT	$[\alpha 1(\text{XII})]_3$	Associated with type I	(Keene et al., 1991, Nishiyama et al., 1994)
XIII	COL13A1	MACIT	$[\alpha 1(\text{XIII})]_3$	Transmembrane and possibly involved with cell adhesion	(Latvanlehto et al., 2003)

Chapter 1

XIV	COL14A1	FACIT	$[\alpha 1(XIV)]_3$	Associated with type I	(Young et al., 2000, Young et al., 2002)
XV	COL15A1	Multiplexins	$[\alpha 1(XV)]_3$	Specialised basement membrane, cleaved to produce antiangiogenic fragments (restin)	(Myers et al., 1996, Ramchandran et al., 1999)
XVI	COL16A1	FACIT	$[\alpha 1(XVI)]_3$	Components of specialised fibrillin-rich microfibrils in skin and type II collagen fibrils in cartilage	(Kassner et al., 2003)
XVII	COL17A1	MACIT	$[\alpha 1(XVII)]_3$	Transmembrane component of hemidesmosomes (cell-cell junction), which attach epidermis to basement membrane in skin	(Hopkinson et al., 1998)
XVIII	COL18A1	Multiplexins	$[\alpha 1(XVIII)]_3$	Cleaved to produce antiangiogenic fragment (endostatin)	(Sasaki et al., 1998)
XIX	COL19A1	FACIT	$[\alpha 1(XIX)]_3$	Radially distributed aggregates formed by association at one end <i>in vitro</i>	(Myers et al., 2003)
XX	COL20A1	FACIT	$[\alpha 1(XX)]_3$	Associated with type I	(Koch et al., 2001)
XXI	COL21A1	FACIT	$[\alpha 1(XXI)]_3$	Fibril associated, widespread expression pattern	(Fitzgerald and Bateman, 2001)
XXII	COL22A1	FACIT	$[\alpha 1(XXII)]_3$	Located in specific tissue junctions and may be associated with microfibrils	(Koch et al., 2004)

Chapter 1

XXIII	COL23A1	MACIT	$[\alpha 1(\text{XXIII})]_3$	Transmembrane collagen identified in cell culture	(Banyard et al., 2003)
XXIV	COL24A1	Fibril-forming	$[\alpha 1(\text{XXIV})]_3$	Associated with type I	(Koch et al., 2003)
XXV	COL25A1	MACIT	$[\alpha 1(\text{XXV})]_3$	Transmembrane collagen, cleaved from present in Alzheimer's amyloid plaques in neurons	(Hashimoto et al., 2002)
XXVI	COL26A1	FACIT	$[\alpha 1(\text{XXVI})]_3$	Expressed in testis and ovary of adult tissue	(Sato et al., 2002)
XXVII	COL27A1	Fibril-forming	$[\alpha 1(\text{XXVII})]_3$	Widespread expression in cartilage	(Boot-Handford et al., 2003, Pace et al., 2003)
XXVIII	COL28A1	Multiplexins	$[\alpha 1(\text{XXVIII})]_3$	Beaded filament forming	(Veit et al., 2006)

1.7.1. Collagen Types – Structure and Function

All collagen types share a structural motif that has become the hallmark of the protein: the collagen triple helix (Fig.1.14). The triple helix structure is composed of three parallel polypeptide strands in a left-handed helical conformation coil with a one-residue stagger to form a right-handed triple helix (Shoulders and Raines, 2009). Each left handed helix is one of three procollagen alpha chains that compose the triple helix.

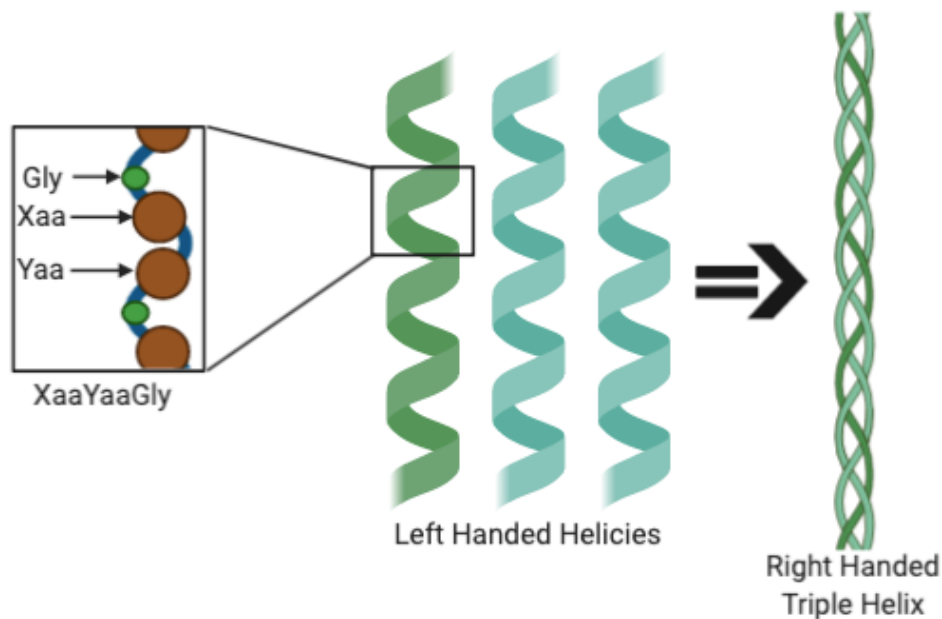


Figure 1.14. Schematic of the collagen triple helix showing the Gly-X-Y sequence within the left handed triple helices. The three left-handed triple helices (either three different alpha chains, two different alpha chains or one alpha chain) wind together and pack tightly at the Gly residues generating the right handed triple helix. Adapted from Fidler et al. (2018). Created with BioRender.com.

Every third residue within the triple helix is Glycine (Gly) due to the tight packing of the helices. This results in a repeating Gly-X-Y sequence, where X and Y can be any amino acid but are most often proline (Pro) and hydroxyproline (Hyp) respectively. Therefore the most common sequence is ProHypGly accounting for 10.5% of all triples (Ramshaw et al., 1998). The number of triple helices found in each collagen varies from type to type; in some less common types of collagen the triple helical domain accounts for less than 10% of the amino acids in the mature protein whilst the mature forms of fibrillar collagens are formed of essentially a long triple helix made up of over 1000 amino acids (Ricard-Blum, 2011). The primary structure of the collagen type varies across all alpha chains. The triple helix structure features across the collagen superfamily with every member containing at least one triple-

helical domain. The collagens also contain nontriple-helical domains which act as building blocks with the other ECM protein. The structure of the collagen alpha chains is depicted in Fig.1.15.

In the triple-helical domains the three alpha chains supercoil around each other to form the right handed triple helix with the adjacent alpha chains linked together by an intermolecular backbone of N-H...O=C hydrogen bonds. To form the triple helix two structural events must occur: the three chain must form in a staggered arrangement with one residue rising in the direction of the helical axis approximately 0.29 nm in relation to the next residue, and every third residue in the strand must be placed near the common helical axis due to the close packing of the three chains. This packing is achieved by the repetitive Gly-X-Y sequence where the smallest amino acid (Gly) occurs in this position (Bella, 2016), and correct alignment during in-cell synthesis of the collagen structures.

The amino acids located in the X and Y positions of the alpha chain sequence are most commonly Pro or Hyp (Ramshaw et al., 1998). This leads to a reduction in the entropic cost for collagen folding as the abundance of the Pro and Hyp residues pre-organises the helical conformation in the unfolded state and primes it for the folded state (Cram, 1988). However, the presence of Pro results in some detrimental effects to the triple helix folding and stability. All peptide bonds in collagen are trans, however Pro has a secondary amino group which forms tertiary amides within a protein resulting in a population of both trans and cis isomers. Before a sequence featuring Pro can form into a triple helix all cis peptide bonds must isomerize to trans peptide bonds (Kersteen and Raines, 2001). Isomerisation of cis to trans bonds in the unfolded alpha-chains acts as a rate-limiting step for triple helix formation (Bachinger et al., 1978, Bachinger et al., 1980, Bruckner and Eikenberry, 1984, Bachinger, 1987). The isomerisation is catalysed by the peptidyl prolyl cis-trans isomerases (PPIase) of which three PPIase families exist in the cell: cyclophilins, FK506 binding proteins (FKBP) and parvulins (Ishikawa and Bachinger, 2013).

The presence of hydroxylated proline in the Y position dramatically increases the thermal stability of the triple helix; for example a (ProProGly)₁₀ sequence has a melt temperature of 31-41°C whilst a (ProHypGly)₁₀ sequence has a melt temperature of 61-69°C (Holmgren et al., 1999). If the Hyp features in the X position ((HypProGly)₁₀) no helix will form (Inouye et al., 1976). These results led to the hypothesis that the 4R configuration of a prolyl hydroxyl group is the sole contributor to water mediated hydrogen bonds that ensure the stable folding of the triple helix.

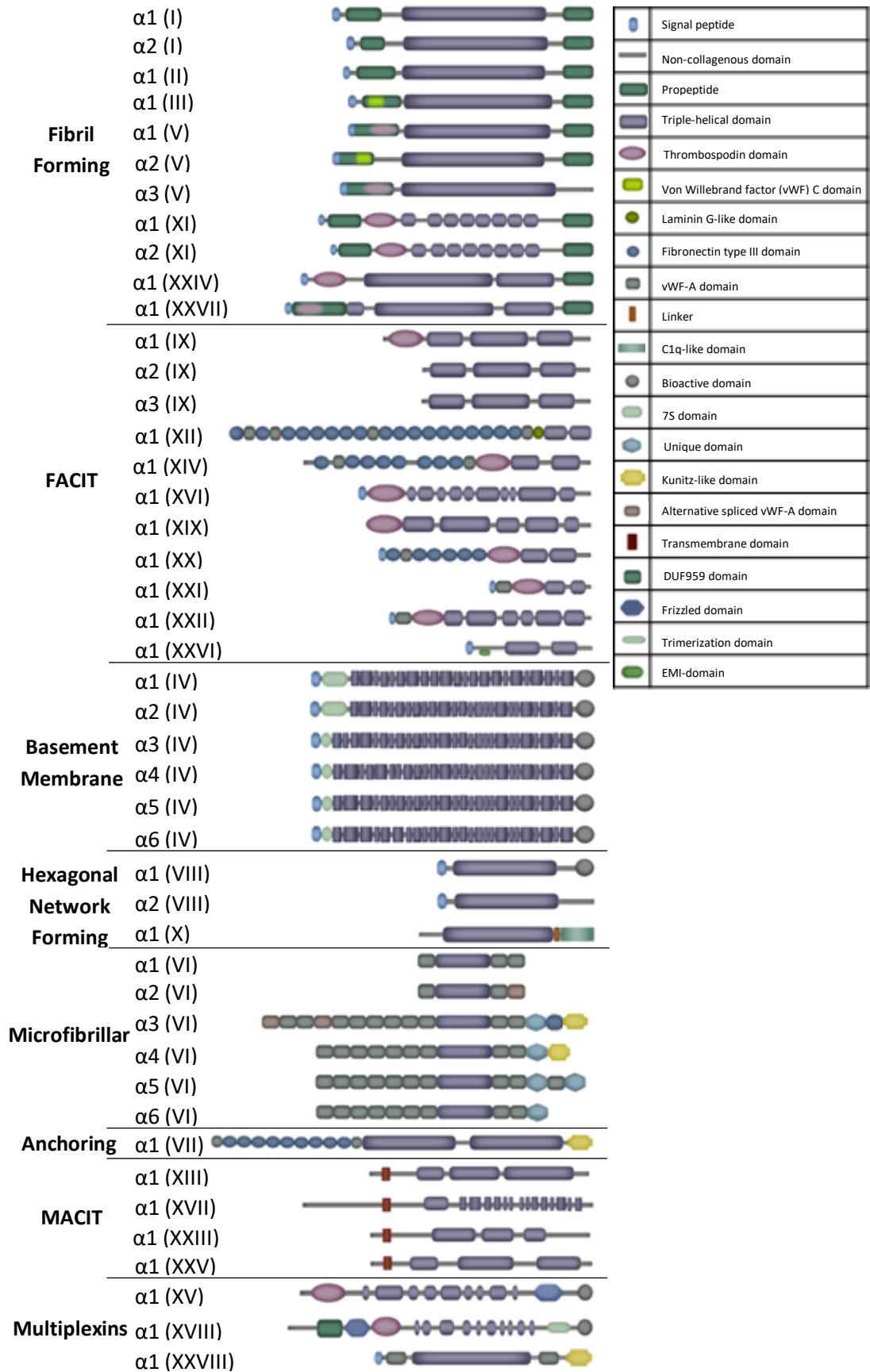


Figure 1.15. Schematic of collagen α -chain primary structures and functional domains.

Adapted from Karsdal (2019)

The frequency of Hyp in most natural collagen is too low to support the extensive network of water bridges (Shoulders and Raines, 2009). This hypothesis was further tested by replacing the Hyp residue with (2S,4R)-4-fluoroproline (Flp) generating a sequence of (ProFlpGly)₁₀. Fluoro groups do not form strong hydrogen bonds, however the (ProFlpGly)₁₀ sequence generated a hyperstable triple helix (melt temperature of 91°C) therefore water bridges cannot be fundamental to the stability of the triple helix (Holmgren et al., 1999). Further work by Bretscher et al. (2001) replaced the Hyp with (2S,4S)-4-fluoroproline (flp) a diastereomer of Flp, which resulted in the triple helix not forming. This highlighted that the stereochemistry of electronegative substituents at the 4-position of the Pro ring are important in the stability of the triple helix and therefore the residue in the Y position stabilises the triple helix via a stereo-electronic effect. The stereo-electronic effect is due to the preference of the residue to one of two major pyrrolidine ring puckers (C^γ-exo and C^γ-endo). Hyp and Flp cause an imposition of a C^γ-exo pucker on the pyrrolidine ring via the gauche effect resulting in the pre-organisation of the main chain angle to the residue in the Y position of the triple helix, therefore stabilising the triple helix (DeRider et al., 2002). This has been further supported by insertion of (2S,4R)-4-chloroproline (Clp) in the Y position which resulted in a stable triple helix (melt temperature of 52°C (Shoulders et al., 2008)), Clp like Flp and Hyp has a strong preference for the C^γ-exo ring pucker supporting the hypothesis that the triple helix is stabilised by a stereo-electronic effect.

1.7.1.1. Fibril Forming Collagens

Whilst the hallmark of the collagen structure is the triple helix motif, the overall structure of the different collagen types changes dramatically between each subcategory (Fig.1.15). Due to the abundance of collagen type I, fibril forming collagens occur the most frequently across vertebrates. The fibril forming collagens are rod-like with a large triple helical domain made of approximately 1000 amino acids per polypeptide chains. The non-collagenous domains are composed of a specific C-terminal and a variant dependant N-terminal which is either completely or partially removed during collagen processing (Bella and Hulmes, 2017). To form fibrils, these collagen triple helices arrange into longitudinally staggered arrays of molecules which generate the distinct banding pattern known as the D-period (Fig.1.16) (Birk and Bruckner, 2005), these staggered molecules are held together and stabilised by covalent intramolecular cross-links (Barnard et al., 1987, Bailey, 2001, Magnusson et al., 2003). The collagen molecules are themselves approximately 300 nm long with a width of 1.5 nm, these molecules are then staggered with respect to the neighbouring collagen molecule at a fixed

length equal to multiple of the size of the D-period (Hodge and Schmitt, 1960, Kadler et al., 1996, Christiansen et al., 2000, Zhao et al., 2011b).

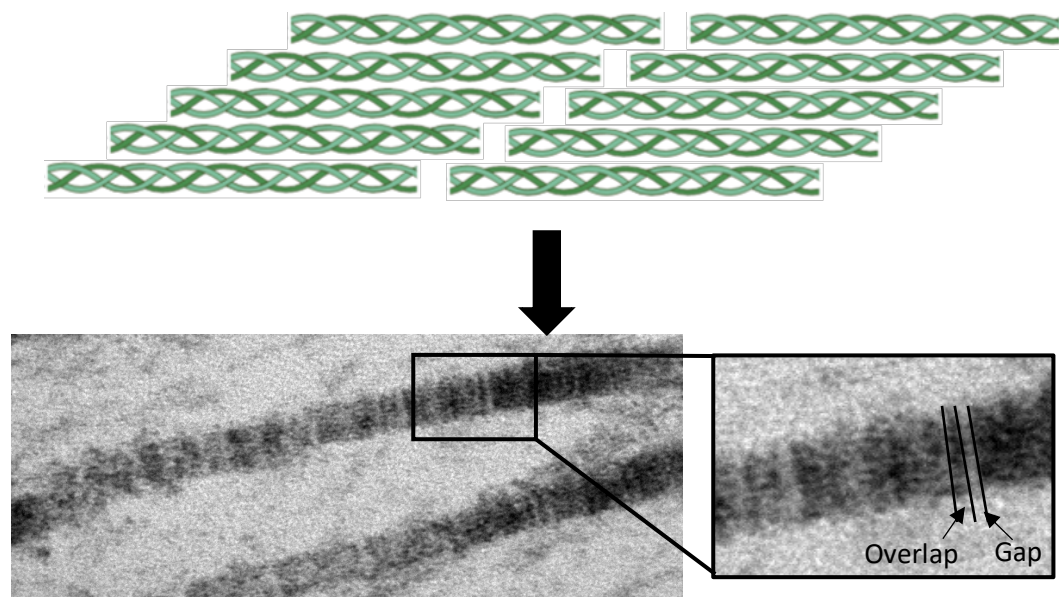


Figure 1.16. Schematic of fibrillar forming collagen triple helices arranged in staggered pattern. The staggered pattern generates the D-period banding pattern seen on collagen fibrils due to the presence of gaps and overlaps in the network. TEM images taken from section 4.4.7. Collagen drawings created with BioRender.com.

Collagen types I, II, III, V, XI, XXIV and XXVII make up the fibril forming collagen subgroup where types I, II and III are the major fibril forming collagens, type V and XI the minor fibril forming collagens and types XXIV and XXVII functions are still being investigated (Bella and Hulmes, 2017). The different types of fibril forming collagens are located across connective tissues with type I appearing in tendon, bone and skin, type II predominantly in cartilage, and type III (along with type I) forming the main structural component in the blood vessel. The main fibril forming collagens imbue the tissue with the required mechanical properties to ensure the appropriate function, whilst the minor fibril forming collagens act as regulatory proteins for the major fibril forming collagens helping to maintain the fibril diameter and orientation. It is therefore incorrect to consider a collagen fibre to be composed of one collagen type, as whilst the fibre may predominantly feature one fibril forming collagen, other fibril forming collagens are required to ensure the tissue functions correctly (Bella and Hulmes, 2017). The percentage of the different fibril forming collagens found in specific tissues varies between tissue function, development, ageing, disease and regeneration (Ricard-Blum, 2011, Mienaltowski and Birk, 2014).

1.7.1.2. FACIT Collagens

Whilst the fibril forming collagens possess a long triple helix domain, the FACIT collagens contain short triple helical domains (200 amino acids in collagen IX (Von der Mark, 2006)) interspersed with non-helical domains (the interrupted helix). These interruptions give the collagen specific properties required in the tissue it resides in, which may result in intramolecular flexibility or specific proteolytic cleavage (Gelse et al., 2003). The FACIT collagens do not form fibrils as the fibril forming collagens do, but instead, bind to specific regions on the fibril forming collagens (Fig.1.17) which leads to altered surface properties and assembly of the fibrils (Birk and Brückner, 2011). FACIT collagens form covalent lysine-derived crosslinks to the N-telopeptide of the fibril forming collagen. The NC3 domain features a hinge which allows a large N-terminal domain to 'reach out' from the fibril where it interacts with other matrix components (Vaughan et al., 1988).

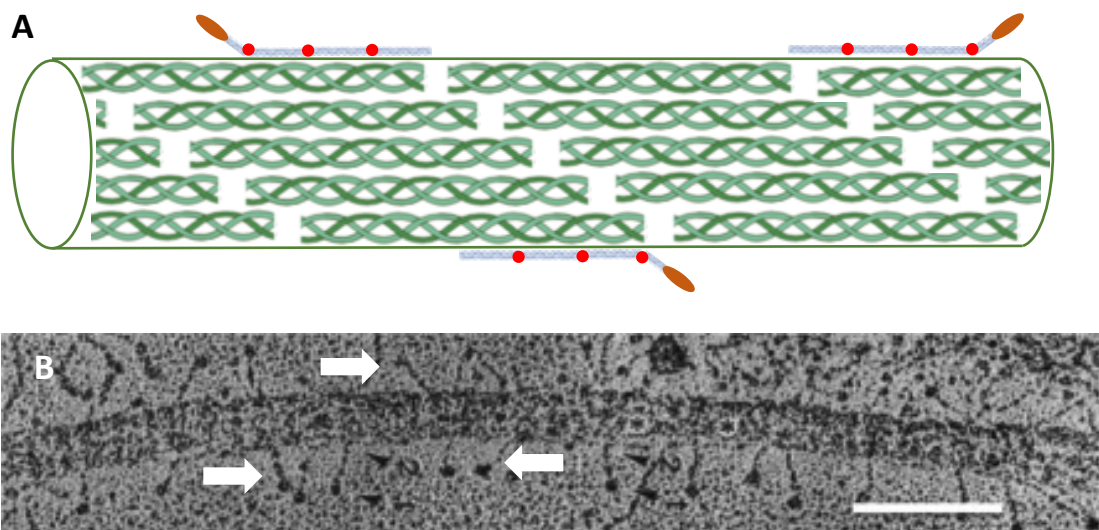


Figure 1.17. Schematic of FACIT collagens attached to surface of a collagen fibril, triple helix interruptions are displayed as red circles whilst the globular N-terminal domain is shown as an orange oval (A). Rotary-shadowed images of type II collagen fibril with type IX (FACIT) collagen molecules attached to the surface. White arrows indicate type IX. Scale bar=100nm (B), adapted from Vaughan et al. (1988). Created with BioRender.com.

1.7.1.3. Basement Membrane Collagen

Collagen type IV is the only collagen to make up the basement membrane sub category. There are six alpha chains that combine to generate the collagen IV triple helix. The combination of the six different alpha chains depends on the tissue the collagen is located in, for example $\alpha 1(\text{IV}) [\alpha 2(\text{IV})]_2$ is found in the liver, whilst $\alpha 3(\text{IV}) \alpha 4(\text{IV}) \alpha 5(\text{IV})$ is found in the kidney, lung and neuromuscular junction (Miner, 2011). As with all collagen types the structure is composed of a triple helix with non-collagenous domains at either end of the helix. The triple helix is a long chain (approximately 1400 amino acids) with 21-26 short non-collagenous interruption giving the structure flexibility (Khoshnoodi et al., 2008). The ends of the triple helix are composed of a short N-terminal non-collagenous 7S domain and a C-terminal globular non-collagenous domain, both of which are required for collagen IV network formation (LeBleu et al., 2007). Once the triple helix is formed, two collagen IV monomers associate via the C-terminal trimers forming a dimer. Four protomers then form cross links at the N-terminal 7S region forming the collagen IV tetramer. As more and more protomers bind a polygonal lattice forms generating the basement membrane network to which other basement membrane molecules such as Laminins bind (Fig.1.18) (Mak and Mei, 2017).

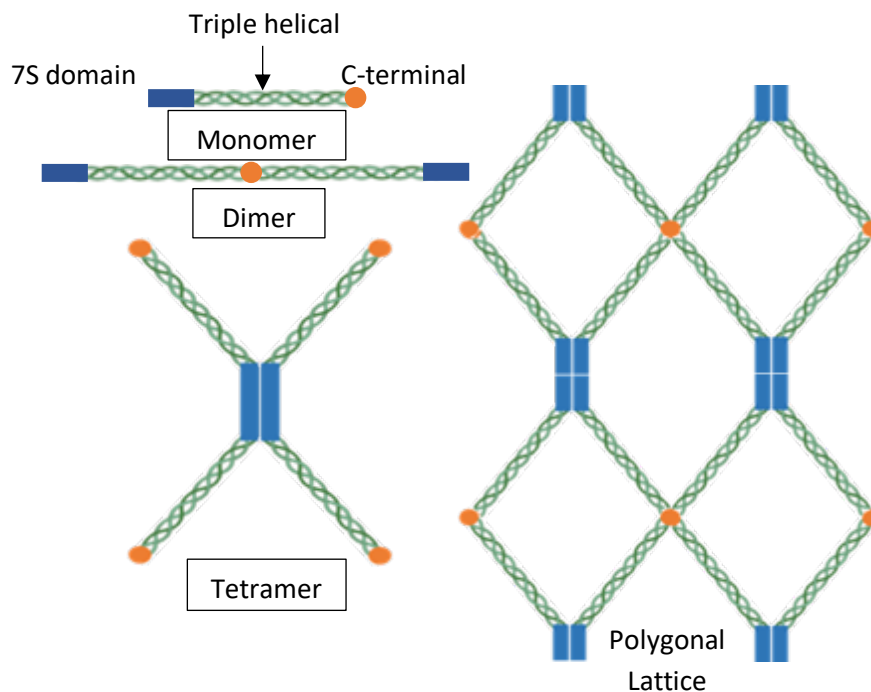


Figure 1.18. Schematic of the collagen basement membrane subcategory. The collagen forms as the protomer before associating with a second collagen IV protomer at the C-terminal (the dimer). The dimers then associate with other dimers via the 7S domain forming a tetramer which then proceed to form the polygonal lattice. Created with BioRender.com.

1.7.1.4. Hexagonal Networking Forming Collagen

There are two hexagonal network forming collagens; type VIII and type X, and this subcategory is sometimes combined with collagen type IV as the network forming collagens. Both are short chain collagens which form hexagonal lattices within the tissue (Fig.1.19). Type VIII collagen is found predominantly in the Descemet's membrane, the basement membrane that separates the corneal endothelial cells from the stroma. Type X is secreted by hypertrophic chondrocytes during endochondral bone formation (Sutmuller et al., 1997). The triple helical domain of both type VIII and X collagens features eight imperfections in the Gly-X-Y repeat (Knupp and Squire, 2003). Type VIII molecules bind to form four molecule tetrahedrons which subsequently bind laterally with multiple tetrahedrons to generate the hexagonal lattice (Hansen et al., 2019). Collagen type X generates a hexagonal lattice structure by forming multiple hexagonal multimers through the non-collagenous globular NC1 domain, which then associate by interaction between juxtaposed triple helix domains (Chan et al., 1995).

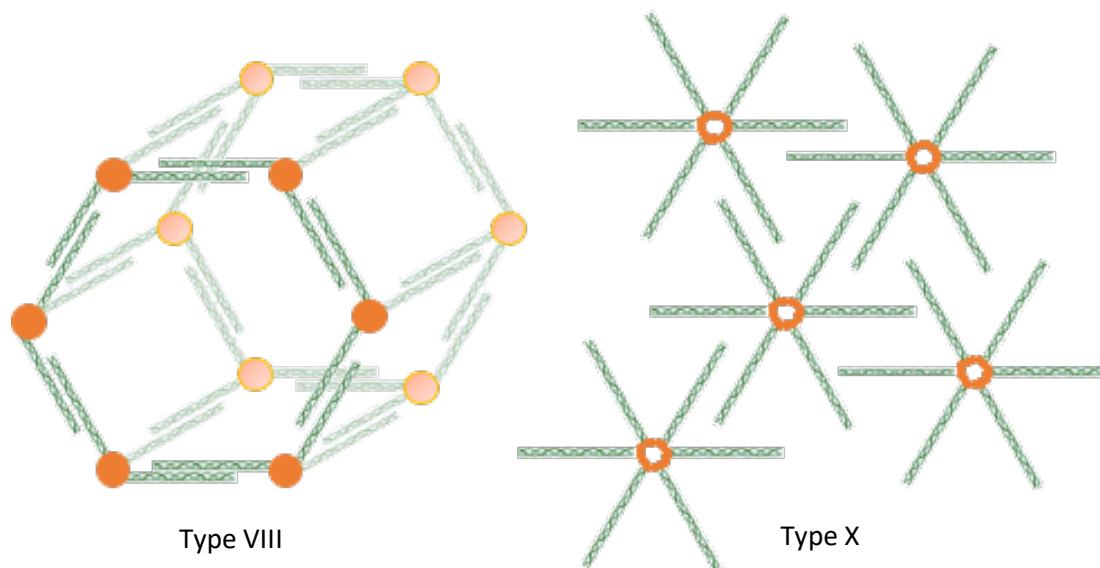


Figure 1.19. Schematic of collagen type VIII and X hexagonal lattices. Created with BioRender.com.

1.7.1.5. Microfibrillar Collagens

Similarly with the basement membrane collagen, the microfibrillar collagen is made up of one collagen type (VI) which has six different alpha chains. Initially the α_1 , α_2 and α_3 were thought to be the only chains, subsequently the α_4 , α_5 and α_6 chains were discovered in 2008, these chains are homologous to α_3 (Fitzgerald et al., 2008, Gara et al., 2008, Fitzgerald et al., 2013). The α_4 chain is not present in humans due to a chromosome inversion rendering the COL6A4 gene non-functional (Gara et al., 2008). Similarly to type IV, the alpha chains

form the triple helix in different combinations in different tissues (Sabatelli et al., 2011). The microfibrillar collagen is found across a variety of tissues including the lung, blood vessels and cartilage (Kuo et al., 1997) and is located near the basement membrane. The microfibrillar structure contains many binding sites for basement membrane proteins such as collagen type IV, decorin, fibronectin and integrin (Kuo et al., 1997, Bidanset et al., 1992, Carter, 1982, Fitzgerald et al., 2008). Each alpha chain contains a short collagenous region with globular regions at both the N- and C-termini (Baldock et al., 2003). The $\alpha 1$ and $\alpha 2$ chains contain one N-terminal subdomain and two C-terminal subdomain which are homologous to type A domains of von Willebrand factor (vWF-A). The $\alpha 3$ chain, and therefore the $\alpha 4$, $\alpha 5$ and $\alpha 6$ chains, are much longer than the $\alpha 1$ and $\alpha 2$ chains, containing 10 N-terminal subdomains and five C-terminal subdomains including two vWF-A like domains (Lamande et al., 2006). The structure forms intracellularly by two monomers associating in an antiparallel fashion to generate a dimer. Tetramers then form by two dimers arranging in a side-by-side alignment. The tetramers are then secreted into the ECM and form a microfibril via end-to-end association through non-covalent bonds with other tetramers (Fig.1.20) (Sun et al., 2019).

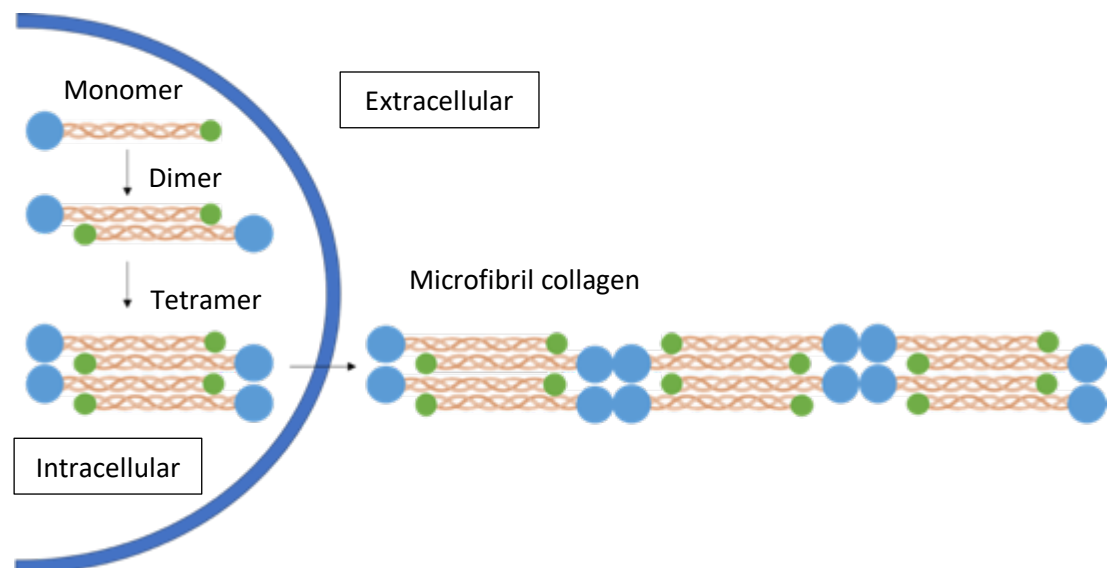


Figure 1.20. Schematic of microfibril collagen production. Within the cell monomers are generated, two monomers then bind to form a dimer. The dimer then undergoes further translation and two bind to form a tetramer. The tetramer is secreted from the cell and binds to other tetramers via non-covalent bonds to form the microfibril. Created with BioRender.com.

1.7.1.6. Anchoring Collagen

Collagen type VII is the only collagen found in the anchoring collagens subcategory. The triple helix is a homotrimer composed of three $\alpha 1$ chains. The anchoring collagen consists of a central collagenous domain flanked by the non-collagenous N- and C-terminal. The collagenous domain is made up of a long triple helix (1530 amino acids) with 19 imperfections offering the collagen structure flexibility (Christiano et al., 1994b). The most notable feature of the anchoring collagen is the non-collagenous 'hinge' region, located in the middle of the triple helix, which is made up of 39-amino acids. The N-terminal is relatively large (145 kDa) and made up of sub-molecules with homology to known adhesive proteins including cartilage matrix protein, nine fibronectin type III-like domains and a short cysteine and proline rich region (Christiano et al., 1992). The C-terminal is conversely small (30 kDa) with a sub-molecule homologous to the Kunitz protease inhibitor molecule (Christiano et al., 1994a). The anchoring collagen forms in the ECM where initially two collagen VII molecules form an anti-parallel dimer with the N-terminal exposed at both ends (Sakai et al., 1986). A portion of the C-terminal is then proteolytically removed and the structure stabilised by inter-molecular disulphide bonds (Colombo et al., 2003). Multiple dimers then align laterally to form the anchoring fibril (Fig.1.21) (Chung and Uitto, 2010). The anchoring collagen appears predominantly in the skin, anchoring the lower portion of the dermal-epidermal basement membrane to the underlying papillary dermis (Chung and Uitto, 2010).

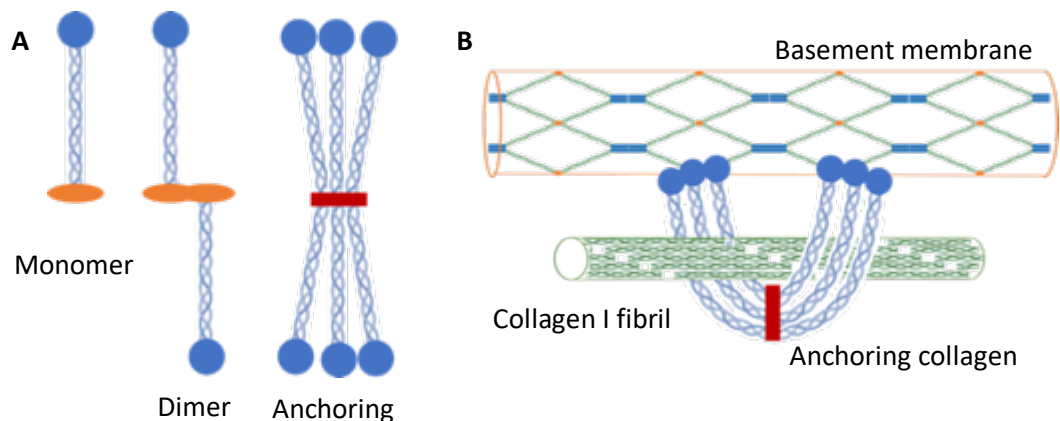


Figure 1.21. Schematic of collagen type VII. (A) The monomer forms a antiparallel dimer with a second monomer at the C-terminal (orange oval is NC2 domain). The C-terminal is partially proteolytically removed and multiple dimers bond to form the anchoring fibril (red band is post cleaved NC2 domain). (B) The anchoring fibril then anchors ECM proteins to the basement membrane. Created with BioRender.com.

1.7.1.7. MACIT Collagens

The MACIT collagens are type II transmembrane proteins (N-terminal is located intracellularly, C-terminal is located in the ECM) composed of a short N-terminal, a hydrophobic single-span transmembrane domain and the triple helical domain with three non-collagenous interruptions allowing the structure to bend (Fig.1.22) (Hagg et al., 1998a, Hashimoto et al., 2002, Banyard et al., 2003). Despite sharing a closely homologous structure, the collagens that make up the MACIT subgroup feature across different tissues. The most widespread MACIT is type XIII, which is expressed by cells of mesenchymal and epithelial origin and accumulates in low amounts (Peltonen et al., 1999, Sund et al., 2001, Ylonen et al., 2005, Latvanlehto et al., 2010). Type XXIII is primarily expressed by fibroblasts (Koch et al., 2006) whilst the types of cells that express type XXV change with ageing. During development the protein is expressed by the peripheral nervous system and the neuromuscular junction, then in adulthood it is exclusively produced by central neurons (Hashimoto et al., 2002, Goncalves et al., 2019, Tanaka et al., 2014). Type XVII is involved in the linkage between the ECM and intracellular regions of the epidermal (Diaz et al., 1990).

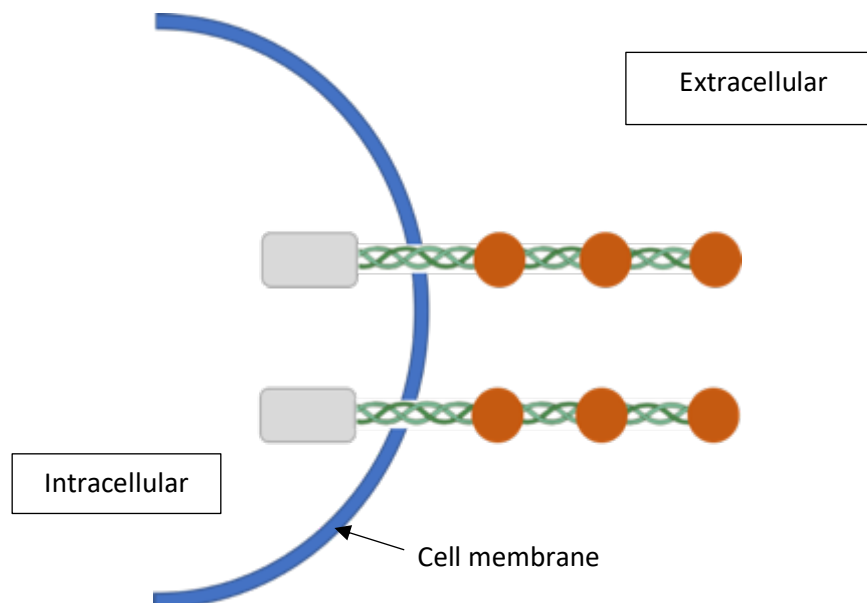


Figure 1.22. Schematic of MACIT collagens spanning the intra and extracellular matrix through the cell membrane. Created with BioRender.com.

1.7.1.8. Multiplexin Collagens

The multiplexin collagens share a multidomain structure with an interrupted triple helix resulting in flexibility (Myers et al., 1992, Rehn et al., 1994, Rehn and Pihlajaniemi, 1994). The N- and C-terminals are similar across the collagens with the N-terminal domain

composed of a laminin-G-like thrombospondin-1 homologous domain and the C-terminal domain featuring a endostatin or restin motif (Rehn and Pihlajaniemi, 1994). The multiplexins are the only collagens that feature a proteoglycan domain, which occurs as different forms of glycosaminoglycans (either heparan sulphate or chondroitin sulphate) (Iozzo and Schaefer, 2015). The multiplexin collagens are widely distributed in normal tissues where they associate with endothelial, epithelial, nerve, muscle and fat cells (Saarela et al., 1998, Hagg et al., 1997). Type XV is located at the interface between the basement membrane and fibrillar collagen network, linking the fibrillar collagens to the basement membrane. It is not considered an integral component of the basement membrane (Amenta et al., 2005, Rasi et al., 2010, Lisignoli et al., 2009). Type XVIII is an integral part of the basement membrane binding different basement membrane components together (Sasaki et al., 1999, Sasaki et al., 2000).

1.7.2. Collagen Synthesis

The biosynthesis of collagen is well characterised for the fibril forming collagens, however it is less well known for the non-fibril forming types. This section will discuss in detail the process for the synthesis of the fibril forming collagens, and where available the synthesis of the other collagen types. As previously stated the mature collagen structure varies across all collagen types with the collagen triple helix acting as the consistent motif present. This triple helix is formed of three alpha chains unique to the specific collagen and can form as a homotrimer or heterotrimer. The alpha chains form as procollagen which is cotranslationally translocated into the lumen of the endoplasmic reticulum (ER) where it folds and undergoes post translational modification due to the presence of a variety of enzymes including prolyl 4-hydroxylases, prolyl 3-hydroxylases and lysyl hydroxylases for hydroxylases of the Y position proline (Heard et al., 2016), GLT25D1 and GLT25D2 for glycosylation (Schegg et al., 2009) and peptidyl proline *cis-trans* isomerase (Ishikawa and Bachinger, 2013). Heat shock protein 47 (HSP47), a molecular chaperone, is also required during the synthesis of collagen, ensuring correct folding of the procollagen. HSP47 binds to the surface of the collagen stabilising the triple helix and preventing lateral aggregation within the ER that is otherwise induced due to the hydrophobic nature of collagen (Ito and Nagata, 2017).

Once translation in the ER is complete the three alpha chains assemble at the C-propeptides region forming inter-chain disulphide bonds (Bourhis et al., 2012). The triple helix then forms in a zipper-like manner from the C-terminal to the N-terminal forming the procollagen trimer (Engel and Prockop, 1991). Once the stable procollagen trimer is formed it is transported from the ER to the cis-Golgi. HSP47 travels with procollagens from the ER to the cis-Golgi at which point it dissociates and is recycled (Satoh et al., 1996). The length of the procollagen trimer is approximately 300 nm which is too large for the on average 60-80 nm diameter COPI and COPII coated vesicles (Bonfanti et al., 1998, Miller and Schekman, 2013), suggesting that the procollagen is transported via a specialised system. Transport and Golgi organisational protein 1 (TANGO1), an ER-exit site protein, has been identified as a key factor in the trafficking of procollagen (Bard et al., 2006, Saito et al., 2009). TANGO1 features an SH3-like domain which has been shown to bind to procollagen VII in the lumen, whilst the second coiled coil domain of TANGO1 binds to the protein cTAGE5 in the cytoplasm (Santos et al., 2015). The C-terminal proline rich domains of both TANGO1 and cTAGE5 then interact with the COPII coated proteins Sec23A and Sec24C (Saito et al., 2009, Saito et al., 2011), which leads to the nucleation of the proteins generating the complex that drives procollagen VII export from the ER (Malhotra et al., 2015, Miller and Schekman, 2013). TANGO1 knockout

in mice has shown defective sorting and exporting of many collagen types (Wilson et al., 2011) further supporting the role of TANGO1 in the connection of procollagen between the ER and cytoplasmic components. However *in vitro* studies have shown that TANGO1 knockdown does not affect procollagen export from the ER (Saito et al., 2009, Nogueira et al., 2014).

Procollagen has been suggested to be transported from the ER to the Golgi via cytoplasmic vesicular tubular cluster (VTCs) which are surrounded by small vesicles (Bonfanti et al., 1998) and requires both COPI (mediates the retrograde transport of ER resident proteins (Murshid and Presley, 2004)) and COPII (involved in the export of proteins from the ER). This hypothesis of large vesicles used to transport procollagen between the ER and Golgi has been disputed by a number of studies. McCaughey et al. (2019) proposes that the procollagen is trafficked via a 'short-loop' pathway between the ER and Golgi, whilst Santos et al. (2015) suggests that the procollagen is trafficked via ER-Golgi intermediate compartment-membrane derived megacarriers; however the process is still not completely understood and may be a combination of the hypotheses (Omari et al., 2020).

The transport of collagen (and other proteins) through the Golgi stacks in mammalian cells is still not fully understood (Malhotra and Erlmann, 2015), although a study by Bonfanti et al. (1998) showed that the procollagen I trimer remains in a Golgi cisterna lumen rather than in transport vesicles at the perimeter of the cisterna. They go further to suggest that progression is due to the cisternal maturation model, here the cargo remains in the lumen whilst the cisternae themselves progress through the stack (cis-to-trans direction) and 'mature' through recycling of their resident enzymes (Beznoussenko et al., 2014). The maturation model has continued to be challenged with reports of megacarriers, tubules, rim progression and direct/transient connections between cisternae (Glick and Nakano, 2009, Lavieu et al., 2013, Beznoussenko et al., 2014) suggesting that the maturation model is not solely correct. Whilst the exact process of transportation through the Golgi is still unknown it appears that it is not a singular process but a range of different processes may all be required for the efficient processing of specific proteins of different sizes and complexity.

Fibrillar procollagen processing involves the removal of the globular N- and C- propeptides by the enzymes N- and C- proteinases respectively (Leung 1979). The activity of the enzymes is provided by different molecules; C-proteinases activity is provided by members of the metalloproteinase family, bone morphogenetic protein 1 (BMP1), mammalian tolloid (mTLD) and tolloid like 1 (TLL-1) (Li et al., 1996, Kessler et al., 1996, Scott et al., 1999, Hartigan et al.,

2003) whilst N-proteinase activity is provided by members of the ADAMTS family; ADAMTS-2, ADAMTS-3 and ADAMTS-14 (Colige et al., 1997, Fernandes et al., 2001, Colige et al., 2002). The removal of the C-propeptides triggers the self-assembly of the collagen into fibrils due to the large reduction in critical concentration required for fibril assembly (Kadler et al., 1987, Hulmes et al., 1989). Assembly of fibrils begins within the plasma membrane and continues as the collagen is secreted into the ECM (Canty et al., 2004). The major fibril forming collagens (I, II, and III) undergo the stated processing whilst the minor fibril forming collagens (V and XI) undergo a more complex process. Here furin-like cleavage plays a major role in the pro α 1(V), pro α 1(XI) and pro α 2(XI) chains and BMP1/mTLD cleave the pro α 2(V) chain as well as within the large N-terminal regions of the pro α 1(V), pro α 1(XI) and pro α 2(XI) chains (Hulmes, 2008), with both enzymes cleaving at the C-propeptide (Unsold et al., 2002). Furthermore BMP1/mTLD cleave procollagen VII, showing that this process is not exclusive to fibril forming collagen (Hopkins et al., 2007).

Secretion from the cell into the extracellular matrix requires transport of the protein from the Golgi to the plasma membrane. There are numerous exits routes, however the most well understood is the clathrin-coated, vesicle mediated transport of cargo from the trans-Golgi network (TGN) to the endosomes, lysosomes and plasma membrane (Bard and Malhotra, 2006, De Matteis and Luini, 2008, Guo et al., 2014, Kienzle and von Blume, 2014). The sorting and transportation of proteins to the relevant position of the cell is a complex process, for example mature epithelial cells and neurons have functional and morphological polarization and therefore require the protein to be secreted at a specific region of the cell (Pakdel and von Blume, 2018). The mechanism of how collagen is sorted at the TGN remains unknown (Pakdel and von Blume, 2018). Transport of procollagen from the TNG to the plasma membrane before secretion into the ECM has been suggested to be via carriers that are generally tubular-saccular but are heterogeneous in shape. These clathrin-coated carriers are 300-1700 nm in length and form via the detachment of larger regions of the TGN (Polishchuk et al., 2003).

Before the mature collagen fibrils are generated, a precursor suprastructure is first assembled called the protofibrils (Birk and Trelstad, 1986, Birk et al., 1989). These fibrils are immature, short and feature small uniform diameters (diameter: \sim 20 nm, length: 4-12 μ m length (Birk and Brückner, 2011)). The protofibrils are secreted into the developing ECM where they are stabilised through interactions with other ECM components including FACIT collagens and small leucine-rich proteoglycans (SLRP). The mature fibril is assembled by end-to-end, lateral association of the protofibrils (Birk and Brückner, 2011).

1.8. Summary

Collagen is one of the major structural proteins found in the body and is known to occur as at least 28 different isoforms. The concentration of different types of collagen found in tissues varies, with the major fibril forming collagens typically accounting >90% of the dry protein weight of musculoskeletal tissues. This has led to many researchers considering the synthesis of these collagens as a key marker for successful tissue engineering, however the role of the minor collagens is key to achieve tissue homeostasis.

From early embryogenesis to maturation musculoskeletal tissue undergo a variety of mechanical forces that help to direct the differentiation of the cell found within the tissues. These mechanical stimuli also drive the production of collagens, acting as a key regulator for the appropriate development of the structures. The use of such mechanical stimulations in tissue engineering is key to achieve an appropriate engineered tissue. A number of bioreactors are now commercially available and regularly custom built to provide specific mechanical stimuli to tissue cultures, which has resulted in more organised ECMs, increases in differential markers and inhibitory effects on others. The magnitude, frequency and duration of a specific mechanical force has been found to have differing effects on the cells fate. This thesis will focus on how changes to these mechanical forces results in changes to the collagen synthesis and arrangement within tissue engineered structures.

1.9. Hypothesis

Mesenchymal stem cells will generate varying concentrations of the major and minor types of collagen in response to different mechanical stimuli. This composition can be used to identify the differentiation of the cells and the quality of the tissue engineered structure generated.

1.10. Aims

- To investigate the potential of 3D printing as a manufacturing technique for novel approaches to tissue engineering.
- Investigate the role of a variety of mechanical stimulations on MSC differentiation and collagen synthesis.

Chapter 2

Materials, Methods and Optimisation

2.1. Materials

Materials are listed below and grouped by supplier:

Abcam – Anti-collagen α 1(I) antibody (ab138492), Anti-collagen α 1(III) antibody (ab7778), Anti-collagen α 1(V) antibody (ab112551), Anti-collagen α 1(X) antibody (ab182563), Anti-collagen α 1(XI) antibody (ab64883), Anti-collagen α 1(XII) antibody (ab121304), Anti-collagen α 1(XIV) antibody (ab101464), Biebrich scarlet (ab146312).

Accu.co.uk – Grub screw (SSU-M5-30-A2), M3 thread insert (HSTI-M3-A2), M5 thread insert (HSTI-M5-A2), Thumb screw (SKT-M3-10-A1).

Agar scientific – ‘Diatome’ ultra-diamond knife (AGG3397), 200 mesh copper grid (AGG2700C).

BD Bioscience – BD™ CompBeads (552843).

Benam – XTC-3D oxirane resin (XTC-3D)

Bio-Rad – Criterion Blotter (1704071), Criterion Vertical Electrophoresis system (1656001), iScript (1708891).

Cambridge bioscience – Zymo Direct-zol DNA/RNA Miniprep (R2080).

Cole Palmer – Luer Lock adapter (OU-30800-00), 0.2-um syringe filter (16534-----K).

Don Whitley Scientific – Bellow (SP-90.007.06).

Farnell – Sylgard 184 (I0I697).

Fisher Sci – Nuclease free water (11538646).

Gibco – DMEM (11880028), FCS (A3160802, Lot- 42F7584K).

Greiner – T-flasks (660175).

Li-cor – Chameleon 800 Pre-stained Protein Ladder (929-800000), IRDye® 800CW Donkey anti-Mouse IgG Secondary Antibody (926-32212), IRDye® 800CW Donkey anti-Rabbit IgG Secondary Antibody (926-32213), REVERT Total Protein Stain (926-11021), REVERT Wash Solution (926-11012).

Lonza – Bone marrow aspirate (Pt-2501).

Merck – Amicon Ultra-15 centrifuge filter unit (UFC901008).

Millipore – BugBuster Ni-NTA His-Band purification kit (70751), RIPA buffer (20-188).

New England BioLabs – BamHI-FI (R3136), PstI-HF (R3140), Cutsmart buffer (B72042).

Peprotech – TGF- β 3 (100-36E).

Promega – PureYield plasmid miniprep (A1223).

Qiagen – COL5A1 primer (NM_000093), COL6A1 primer (NM_001848), COL9A1 primer (NM_001851), COL14A1 primer (NM_021110), COL24A1 primer (NM_152890), DCN primer (NM_133503) RNeasy Mini kit (74104), SXCA primer (NM_001080514), TNMD primer (NM_022144), QIAGEN TissueRuptor II (9002757).

R&D Systems – MSC verification kit (FMC020).

RS Components – Loctite super glue (787-7406), M3 screw (280-981), M5 thumb nut (664-4886), Polycarbonate sheet (681-665).

Santa Cruz – Anti-collagen α 1(II) antibody (sc-52658), Anti-collagen α 1(VI) antibody (sc-377143), Anti-collagen α 1(IX) antibody (sc-376969).

Sigma Aldrich – Acid Fuchsin (F8129), Alcian blue 8GX (A5268), Alizarin red S (A5533), Aluminium ammonium sulphate (A2140), Aniline blue (415049), β -glycerophosphate (G9422), Bradford reagent (B6916), Bovine serum albumin (A2153), Chloroform, Dexamethasone (D4902), Direct red 80 (365548), Dimethyl sulfoxide (D2650), DPX mounting solution (06522), Eosin Y (E4009), Ethanol (459844), Ferric chloride (236489), Fibrinogen (341573), Fibronectin (F4759), Formaldehyde (F8775), Glacial acetic acid (10000631011), Glycerol (G9012), Haematoxylin (H3136), Hydrochloric acid (320331), Hydrogen peroxide (H1009), Indomethacin (17378), Insulin (I6634), Isopropyl B-d-1-thiogalactopyranoside (420322), Isopropanol (I9516), Insulin Transferred Sodium (I3146), L-ascorbic acid (A92902), LB Broth (L3522), L-Glutamine (G7513), Nitrocellulose membrane (WHA10401403), Paraffin wax (327204), Pellet pestles Z359971, Pepsin (P7012), Picric acid solution (P6744) Phosphomolybdic acid (221856), Phosphotungstic acid (P4006), Phloxine B (P4030), Sodium azide (S2002), Sodium chloride (S7653), Sodium iodate (S4007), SYBR Green JumpStart *Taq* ReadyMix (S4438), Tissue processing cassette (H0542), Trypsin (59427C), Thrombin (T4648), Tris HCL, Trisma-base (T1503), Tween 20 (P1379), Xylene (534056), 4X SDS sample buffer (70607-3), 6-aminocaproic acid (A2504), 3-Isobutyl-1-methylxanthine (I5879).

Simply Bearings – O-ring (3 mm diameter, 134 mm bore VITON)

SLS – Methanol (34860).

TAAB Laboratories Equipment Ltd – Acetone (A018), Borax (B021), Epoxy resin (T001, D025, M011, D032), Ethanol (E047), Glutaraldehyde (G002), Maleic acid (M003), Methanol, Osmium tetroxide buffer (O001), Reynolds lead citrate stain (L037), Sodium cacodylate (S011), Toluidine blue (SD211), Uranyl acetate (U007).

ThermoFisher – Antibiotic-Antimitotic (15240062), Anti-collagen α 1(XXIV) antibody (MA5-24533), DAPI (D1306), Designed primers, DNA gel loading dye (R0611), (6X) DyLight 488 NHS ester dye (46402), EDTA (15576028), Foetal calf serum (A3160802), GelCode Blue Stain Reagent (24590), Low melting point agarose (16520100), Mini Gel Tank (A25977), Non-essential amino acids (11140035), Novex Sharp Pre-stained Protein Standard (LC5800), Novex Tris-Glycine SDS running buffer (LC2675), Novex™ WedgeWell™ 4 to 12%, Tris-Glycine (XP04120BOX), Nuclease free water (11538646), NuPAGE LDS Sample Buffer (NP0007), NuPage Sample Reducing Agent (10X) (NP0004), NuPAGE Transfer Buffer (20X) (NP0006), NuPAGE Tris-Acetate SDS Running Buffer (10X) (LA0041), NuPAGE 3-8% Tris-Acetate midi protein gels (WG1603A), Phalloidin 647 (A22287), Pierce BCA assay kit (23227), Pierce Bovine Serum Albumin Standard Pre-Diluted Set (23208), Pierce Dimethylformamide (20673), Pierce LDH assay kit (88953), Superfrost Plus Adhesion Microscope Slides (J1800AMNT), TrackIt 1Kb Plus DNA ladder (10488085), TRizol (15596026), 4-12% tri-glycine WedgeWell gel (XP04122BOX).

VWR – PegGREEN (732-3196).

3DGBIRE – PLA filament, Nylon Filament.

2.2. Methods and Optimisation

2.2.1. Cell Culture

Human mesenchymal stem cells (hMSCs), from bone marrow, were used in all tissue engineering experiments. The hMSCs were purchased as four 10 ml aspirates from Lonza. All four aspirates were donated from a single normal (non-diabetic) adult. The human bone marrow was withdrawn from bilateral punctures of the posterior iliac crests from the donor in the US, before being shipped as aliquots to UK on dry ice.

The mononuclear count provided by the supplier was 2.6×10^7 cells/ml. Before plating the cells the required number of tissue culture vessels was determined from the mononuclear cell count as 1×10^5 mononuclear cells/cm². The final cell count was found to be 1.554×10^9 cells, therefore a surface area of 14,505 cm² or 90 T175 flasks was required.

The flasks were coated in 10 ml of sterile fibronectin to a final concentration of 10 ng/ml and left for one hour at room temperature. The fibronectin solution was removed and 15 ml of low glucose, phenol free Dulbecco's modified Eagle's Medium (DMEM) containing 10% foetal calf serum (FBS), 1% L-Glutamine, 2% Antibiotic-Antimitotic and 1% Non-essential Amino Acids was added to each flask, this media was designated basic media throughout the rest of the study. Approximately 600 μ l of the bone marrow aspirate was added to each flask. The flask was gently mixed and incubated at 37°C in a humidified environment (5% CO₂, 21% O₂) for seven days. During the initial culture, hMSCs adhered to the fibronectin coated tissue culture plastic while red blood cells floated in the basic media, which prevented visualisation of the hMSCs adhered to the flasks. After seven days, 50% of the basic media was replaced and the flasks were again incubated at 37°C in a humidified environment (5% CO₂, 21% O₂) for a further seven days. Finally 100% of the basic media was replaced and hMSCs could be visualised (Fig.2.1).

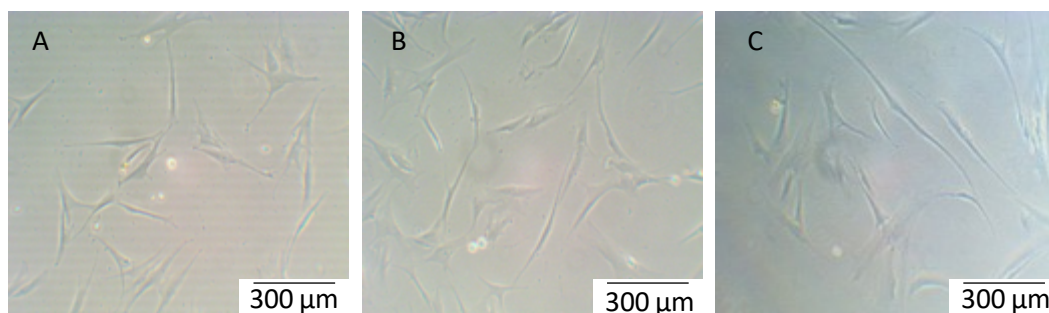


Figure 2.1. Human mesenchymal stem cells following isolation from bone marrow aspirate. A) 14 days post adherence, B) 16 day post adherence, C) 18 days post adherence. Scale bars represent 300 μ m.

Once the hMSCs had reached confluence they were passaged and stored in liquid nitrogen at P0. Confluence density was confirmed using a microscope with 10x objective. The basic media was removed and each flask washed in 10 ml of Phosphate buffered saline (PBS). Once washed the PBS was replaced with 7 ml PBS + 3 ml 10x Trypsin. The flasks were then incubated at 37°C in a humidified environment (5% CO₂, 21% O₂) for 5 minutes to dissociate the cells from the flask. The flasks were “tapped” to dissociate any cells still adhered to the flask before aspirating the cell solution into a 50 ml sterile centrifuge tube containing 5 ml basic media. The flask was washed with 10 ml basic media which was also added to the 50 ml sterile centrifuge tube. The cell solution was then spun down at 500 g for 5 minutes to pellet the cells. The supernatant was poured away and the cell pellet was re-suspended in 20 ml basic media. The cell number was determined using a haemocytometer on 10 µl samples. Cells were re-pelleted by centrifuging at 500 g for 5 minutes and re-suspended in 10% Dimethyl Sulfoxide (DMSO) + 90% FBS at 400,000 cells/ml and stored in liquid nitrogen until required.

2.2.2. hMSC Validation

Fluorescence-activated cell sorting (FACS) and the tri-lineage assay was used to characterise the cells extracted from the bone marrow aspirates as hMSCs.

2.2.2.1. hMSC FACS Verification

An MSC verification kit was used to define the cells grown from the bone marrow aspirate. The kit contains the MSC markers that have been defined by Dominici et al. (2006) as the minimum criteria to class the cells as MSCs. The markers include CD73, CD90, CD105 and a cocktail of negative markers: CD11b, CD34, CD45, CD79A and HLA-DR. All positive markers are required to be expressed by >95% of the population and the negative marker cocktail at <2% of the population to meet the criteria requirements.

The verification kit was run on the cells extracted from the bone marrow aspirate at passage 1 (P1). The cells not used for the verification kit were taken forward to be used in the tensile stimulation experiment. Antibody compensation was performed using BD™ CompBeads following the manufactures protocol: 100 µl of staining buffer was added to one flow cytometry tube per antibody. One drop (approximately 60 µl) of the BD™ CompBeads Negative Control and one drop of the BD CompBeads Anti-Mouse Ig was added to each tube and vortexed. 10 µl of each antibody supplied in the MSC verification kit was added to the appropriately labelled flow cytometry tube, including an unstained tube. The tubes were

incubated in the dark for 45 minutes at room temperature. After incubation 2 ml of staining buffer was added to each tube, the tubes were centrifuged at 200 g for 10 minutes. The supernatant was discarded and the bead pellet was re-suspended in 500 μ l of staining buffer. Each tube was run on the BD FACS Canto II flow cytometer and the singlet bead population was gated based on forward light scatter (FSC) and side light scatter (SSC) characteristics. Once compensation gates were acquired the process was applied to the cell population. The P1 cells were disassociated from tissue culture plastic via trypsin (as stated in section 2.2.1) and counted using a haemocytometer. 100,000 cells were transferred into a 1.5 ml centrifuge tube with 100 μ l of staining buffer and 10 μ l of each antibody. The tube was vortexed and incubated at room temperature in the dark for 45 minutes. The centrifuge tube was spun down at 200 g for 10 minutes and the supernatant was discarded. The cell pellet was re-suspended in 500 μ l of staining buffer and transferred to a flow cytometry tube. The marker expression was analysed by the BD FACS Canto II flow cytometer and measured against the compensation beads gating. Analysis was completed using FlowJo software. Fig.2.2 shows the expression for each marker from the verification kit. The positive markers were found to be present in >95% of the cell population (CD73 99.07%, CD90 99.55% and CD105 98.57%) meeting the criteria as defined by Dominici et al. (2006), however the negative marker cocktail was found to be 2.83%, which marginally exceeds the criteria.

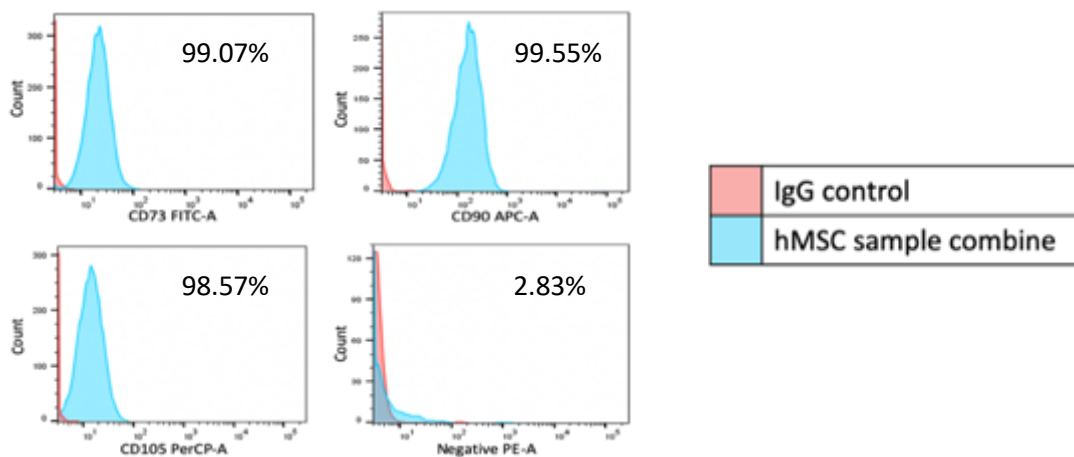


Figure 2.2. Flow cytometric analysis of minimal stem cell markers as defined by Dominici et al. (2006) expressed by P1 hMSCs. Red peaks represent IgG controls, blue peaks represents hMSCs.

2.2.2.2. Tri-Linage Differentiation Assay

The cells extracted from the bone marrow aspirate were grown to P2 before being disassociated from the tissue culture plastic by trypsin. Cells were re-plated in triplicate at seeding densities based on the required differentiation. For both osteogenic and adipogenic

differentiation the cells were seeded in monolayer in the wells of a 6-well plate. For osteogenic differentiation, cells were seeded at 3,000 cells/cm² and cultured in osteogenic media containing DMEM, 10% FBS, 1% L-Glutamine, 2% Antibiotic-Antimitotic, 1% Non-essential Amino Acids, 100 nM dexamethasone, 10 mM β -glycerophosphate and 50 μ M L-ascorbic acid (Jaiswal et al., 1997). For adipogenic differentiation the cells were seeded at 10,000 cells/cm² and cultured in adipogenic media containing DMEM, 10% FBS, 1% L-Glutamine, 2% Antibiotic-Antimitotic, 1% Non-essential Amino Acids, 1 μ M dexamethasone, 100 μ M indomethacin, 10 μ g/ml insulin and 500 μ M 3-Isobutyl-1-methylxanthine (IBMX) (Cheng et al., 2009). Chondrogenic differentiation required the cells to be present in a 3D arrangement, this was achieved by suspending 500,000 cells in 500 μ l of basic media in a 1.5 ml screw cap centrifuge tube. The sample was then centrifuged at 240 g generating a pellet of cells. The supernatant was removed and carefully replaced with chondrogenic media without disrupting the pellet. The chondrogenic media contained DMEM, 1% L-Glutamine, 2% Antibiotic-Antimitotic, 1% Non-essential Amino Acids, 100 nM dexamethasone, 10 ng/ml TGF- β 3, 1% Insulin-Transferred-Sodium (ITS), 25 μ g/ml L-ascorbic acid (Murdoch et al., 2007). Control groups were cultured identically to differentiated groups, but in basic media. Osteogenic and adipogenic media were changed twice a week for 21 days and chondrogenic media changed every other day for 21 days. To assess differentiation the groups were stained with Alizarin Red for osteogenic differentiation where calcium deposits stain red, Oil-Red-O for adipogenic differentiation where the lipid droplets stain red or Alcian blue for chondrogenic differentiation where the glycosaminoglycans are stained blue. For Alizarin Red the culture media was removed from the culture well and the cell monolayer was washed in three changes of PBS. The monolayer was fixed in 1% neutral buffer formalin solution (NBF) for 30 minutes. The monolayer was carefully washed with distilled water so as to not disrupt the cells (some disruption of the cells was observed) and stained with 2% Alizarin Red S solution (pH 4.1-4.3) (recipe in section 2.2.4) for 45 minutes in the dark at room temperature. The cells were washed a further three times with distilled water and imaged. For Oil-Red-O staining the monolayer was washed with three changes of PBS and fixed with 1% NBF for 30 minutes. Once fixed the cells were washed with distilled water, 60% isopropanol was then added to each well and the culture plate was incubated at room temperature for 5 minutes. The 60% isopropanol was removed and 0.18% Oil-Red-O solution (0.288 g Oil-red O mixed with 100 ml isopropanol to generate a stock solution). 30 ml of stock solution was mixed with 20 ml distilled water (generating 0.18% oil-red O solution) was the added to the culture plate, which was incubated at room temperature for 15 minutes. The

monolayers were washed with two changes of distilled water before the addition of haematoxylin for 1 minute. The cells were washed a further four times and then imaged. For Alcian blue staining the cell pellets were washed in three changes of PBS and fixed in 1% NBF for 60 minutes before paraffin embedding using the Leica ASP300 tissue processor (Leica Microsystems, UK) and Leica EG1150 tissue embedder (Leica Microsystems, UK) (explained in more detail in section 2.2.4). After the pellets were embedded, 6 μm sections were cut using the Leica RM2265 (Leica Microsystems, UK) and mounted on Superfrost Plus Adhesion Microscope Slides. Sections were deparaffinised in two changes of xylene (5 minutes each), rehydrated in 70%, 90% and 100% ethanol (5 minutes each) and washed in running tap water for 2 minutes. Sections were stained in 1% Alcian blue solution (recipe in appendix A) for 30 minutes and washed for a further 2 minutes in running tap water. Sections were dehydrated in 90% ethanol and two changes of 100% ethanol (30 seconds each) and cleared in two changes of xylene (1 minutes each). Sections were mounted with DPX mounting solution and imaged. Fig.2.3 shows representative images from each of the differentiation stains. Higher levels of staining were seen in each differentiation group. Low levels of calcium staining was detected in the control group with far higher seen in the osteogenic differentiated group. The chondrogenic differentiated pellet was more structurally stable with a complete Alcian blue staining whilst the control group generated a less complete pellet culture with fainter staining. There was no lipid droplet staining detected in the control group, whilst the adipogenic differentiated group had a high level of staining. This demonstrated that the cells had the potential to differentiate down the osteogenic, adipogenic and chondrogenic lineages.

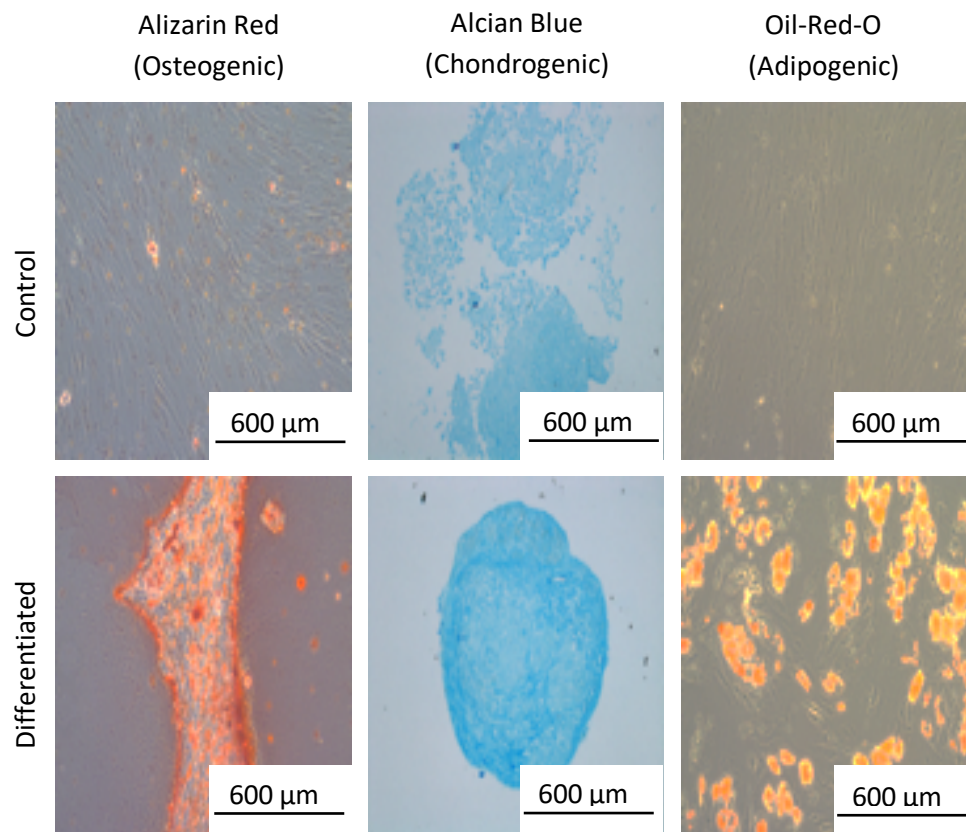


Figure 2.3. Histological analysis of trilineage differentiation potential of P1 hMSCs. Representative images are shown for cells after induced osteogenic, chondrogenic or adipogenic differentiation (Differentiated) and non-differentiated cells (Control) with appropriate staining. Cells differentiated down the osteogenic lineage were stained for calcium deposits using alizarin red. Cells differentiated down the chondrogenic lineage were stained for GAG formation using Alcian blue. Cells differentiated down the adipogenic lineage were stained for lipid droplets using oil-red-O staining. n=3 repeats from same donor, scale bars represent 600 μm .

2.2.2.3. Conclusion

From the flow cytometry analysis and the tri-lineage images it can be seen that the cells extracted from the bone marrow aspirate met the majority of the criteria needed to define the cells as MSCs. The only criteria not seen was the population of cells expressing the negative marker exceeding 2%, however this was exceeded by less than 1% (this may be contamination of other cell types). As all other criteria was met and the negative criteria was exceeded by less than 1% it was concluded that a mixed population of cells was present with the majority of the population being hMSCs.

2.2.3. Fibrin Hydrogel Formation Optimisation

Fibrin was chosen as the 3D biomimetic material used throughout the experimental runs for all mechanical stimuli as it has been previously used for tissue engineering of tendon, bone and cartilage (the musculoskeletal tissues investigated throughout this study) (Eyrich et al., 2007, Wang et al., 2010, Almeida et al., 2016) and that it acts as a blank slate for collagen synthesis, where the only detected collagen is that produced by the cells. The recipe used to generate the fibrin hydrogels was consistent across experiments, however the culture environment altered between the tensile stimulation (3D printed chamber), the hydrostatic pressure (24-well plates) and the microgravity groups (12-well plate and rotation drums). Tensile stimulation required rod like structures, similar to that of native tendon, whilst the hydrostatic pressure and microgravity required a free swelling samples, designated microtissues. Detailed methods for generation of the tensile stimulation fibrin hydrogels can be found in section 2.2.3.1 and for the hydrostatic pressure and microgravity samples can be found in section 2.2.3.2.

Fibrin is formed by the coagulation of the protein fibrinogen due to the enzyme thrombin. By mixing cells with the solution before it polymerises, a 3D network of suspended cells is formed that can be mechanically stimulated. The basis for the fibrin recipe was built on published work previously completed by members of our group (Kharaz et al., 2016), with a final protocol established following optimisation through a titration of thrombin with consistent fibrinogen and cell suspension of 1×10^6 cells/ml (10-80 μ l of 200 U/ml thrombin with 250 μ l of 20 mg/ml fibrinogen and 600 μ l cell suspension) a volume of 50 μ l was taken forward following optimisation (Fig.2.4).

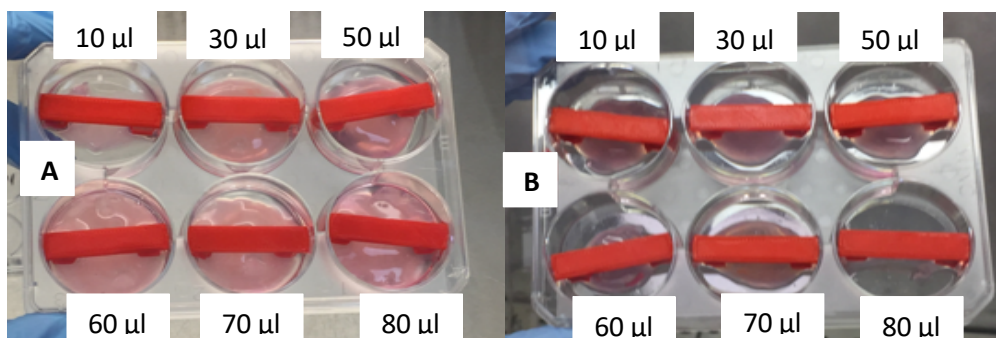


Figure 2.4. Effects of thrombin concentration of fibrin formation. Fibrin gels formed between early anchor post design, used for tensile stimulation optimisation. (A) End of week one, the 10 μ l group formed the smallest hydrogel and contracted the most. (B) End of week two, the 80 μ l group was almost completely degraded and 10 μ l group hadn't changed from week

one, the 50 μl and 60 μl produced the best hydrogels. 50 μl was taken forward due to slightly longer coagulation time.

For the final experiments with mechanical stimulation, the ratio of cell suspension, fibrinogen and thrombin was maintained at 12:3:1 using the same batches of fibrinogen, thrombin and MCS. All samples were generated with the same initial volume of fibrin though in different seeding environments which is explained in detail in the following sections. All fibrin protocols were based around the following protocol: in a well plate a layer of sterile 4% agarose was dispensed and set, this layer was then washed with sterile PBS. The hMSCs were disassociated from the tissue culture plastic *via* the trypsin method (see section 2.2.1) and counted using a haemocytometer. For the final hydrogels 1.25×10^6 cells/ml were used; this equated to 5×10^5 cell/hydrogel. Once the cells were counted and suspended in the correct volume of basic media, 75 μl (20 mg/ml) fibrinogen was added to each well. 300 μl of the cell suspension was added to the fibrinogen and mixed by pipetting up and down. 25 μl (200 U) of thrombin was then added to each well and mixed with a sterile 10 μl pipette tip. The plates were then placed into the incubator at 37°C, 5% CO₂ for one hour, or until polymerised. Once the fibrin had formed the edges were scored with a pipette tip to detach the fibrin from the edge of the well and encourage contraction. Each well was filled with basic culture media (volume depended on experimental group) containing fresh 800 μM L-ascorbic acid and 1 mg/ml 6-aminocaproic acid. Media was changed and the fibrin was scored with a pipette tip every other day during the contraction phase (contraction phase was one week for hydrostatic pressure and microgravity and two weeks for tensile stimulation). After the contraction phase the fibrin hydrogels were placed into the experimental environment as defined in the sections 2.2.3.1 and 2.2.3.2.

2.2.3.1. Tensile Fibrin Hydrogel Generation

Cells were grown as describe in section 2.2.1. Briefly hMSCs were thawed at passage 1 and grown in T175 flasks to passage 3. The cells were cultured in basic medium at 37°C in normoxia and 5% CO₂. Once the required cell number was achieved to enable formation of 30 fibrin hydrogels (>15,000,000 cells), the hMSCs were dissociated from the tissue culture plastic and counted. Cells were diluted to 1.25×10^6 cells/ml, which was the required concentration for the fibrin hydrogels. The ratio of components to generate the fibrin hydrogel was maintained from section 2.2.3: 75 μl (20 mg/ml) fibrinogen, 25 μl (200 U) Thrombin and 300 μl cells diluted in basic medium.

The anchor frames (describe in detail in section 3.5.1.6) were used to generate the tendon like structures that were subjected to tensile stimulation. Before use the anchor frames and spar covers were washed in PBS and then sterilised in 70% ethanol by submerging for 30 minutes within a BSC. After 30 minutes they were removed from the 70% ethanol with sterile forceps and placed on sterilised paper. The anchor frames and spar covers were then sprayed with 70% ethanol and left to dry for an hour. Whilst drying the six well plates were prepared. 1 ml of sterile 4% agarose was carefully dispensed into the base of each well of five 6-well plates (30 wells in total), ensuring the agarose set level across the base. Once dry, an anchor frame was moved into each well. The spar covers were then placed in position over the breakable spars and a further 2.5 ml of sterile 4% agarose dispensed around the anchor frame and spar cover ensuring no agarose moved into the centre of the anchor frame. The agarose was then left to set for 15 minutes. Once the 4% agarose was set, 300 μ l of sterile PBS was dispensed the middle of each anchor frame to confirm that the agarose had set without forming any escape routes that the fibrin may run down before polymerising. If any PBS did escape the well the escape route was filled in with more sterile 4% agarose and re-tested to ensure the well was watertight. The well was then washed in 3 changes of 3 ml sterile PBS and the plate left with the final change of sterile PBS until required.

To generate the fibrin hydrogels, first the sterile PBS was removed from all wells. Next 25 μ l (200 U) thrombin was dispensed into the centre of each anchor frame. 300 μ l of the suspended cells (1.25×10^6 cells/ml) was then added each anchor frame (5×10^5 cells/hydrogel). Finally 75 μ l (20 mg/ml) fibrinogen was dispensed into each anchor frame. The six well plates were then moved to an incubator operating at 37°C in normoxia and 5% CO₂. The samples were left for one hour to allow the fibrin to fully polymerise. Once polymerised, using a 10 μ l pipette tip, the edges of the fibrin were scored away from the anchor frame to encourage contraction and covered in 3 ml of basic medium. 1 mg/ml 6-aminocaproic acid was added to the culture medium to inhibit fibrin degradation during the contraction phase (first two weeks) (Kupcsik et al., 2009). The medium was changed and the fibrin hydrogels scored every 48 hours during the contraction phase. The fibrin hydrogels reached ideal contraction after two weeks and were ready to be moved into the 3D printed culture chamber.

Before the fibrin hydrogels could be moved into the bioreactor chamber it was sterilised with 70% ethanol; initially all components were disassembled and washed individually in 70% ethanol before drying within a sterile cell culture hood for one hour. Once dry the parts were assembled and washed a second time in 70% ethanol and left to dry in the sterile cell culture

hood for a further hour. Once dry the culture wells were washed 3 times with PBS and two 0.2 μm syringe filters attached to the lid for sterile air flow. Once washed the PBS was discarded and the bioreactor chamber was ready to use.

To transfer the fibrin hydrogels from the six well plate to the bioreactor chamber, the spars covers were first removed and the agarose seal was broken with sterile forceps. The anchor frame and fibrin hydrogel was then moved to a sterile petri dish again using the sterile forceps. The 90° attachment arms (which had been sterilised in the same method as the anchor frames) were installed onto the anchor frames and the system was picked up using sterile forceps and moved into the designated culture well.

To decide which fibrin hydrogel went into which well, each culture well was given a number (control chamber 1-6, tensile chamber one 7-12, tensile chamber two 13-18 and tensile chamber three 19-24) and each fibrin hydrogel given a number 1-30. The fibrin hydrogel numbers were then randomised using an online random number sequence generator (Random.org). The first number of the sequence was then assigned to well number one (i.e. control chamber well one).

Once in the bioreactor chamber the spars were broken using sterile scissors leaving the fibrin hydrogel to support itself between the anchor frame. The lid was fitted and secured using thumb screws, creating an airtight seal with the O-ring. The hydrogels were cultured in 3.5 ml of basic medium with 800 μM of L-ascorbic acid which was added fresh during every media change, there was no 6-aminocaproic acid in the culture media during the loading phase. Medium continued to be changed every 48 hours. The bioreactor chambers with fibrin hydrogels installed were incubated in non-humidified incubator at 37°C in 5% CO₂.

2.2.3.2. Hydrostatic Pressure and Microgravity Fibrin Hydrogel Generation

The method for generating the fibrin hydrogel was the same for both the hydrostatic pressure stimulation and the microgravity culture experiments. Cells were grown as described in section 2.2.1. Briefly hMSCs were thawed at passage 1 and grown in T175 flasks to passage 3. The cells were cultured in basic medium at 37°C in normoxia and 5% CO₂. Once the required cell number was achieved for the fibrin hydrogels, the hMSCs were dissociated from the tissue culture plastic and counted. Cells were diluted to 1.25x10⁶ cells/ml, this was the required concentration for the fibrin hydrogels. The ratio of components to generate the fibrin hydrogel was maintained from section 2.2.3, 75 µl (20 mg/ml) fibrinogen, 25 µl (200 U) thrombin and 300 µl cells diluted in basic medium.

Before the fibrin hydrogels were generated the well plates were prepared. Initial culture was done within 48 well plates as this was found to generate optimum hydrogel size. 100 µl of sterile 4% agarose was added to each well and left to set, forming a non-adherent base layer with a curved meniscus. Once set, 500 µl of sterile PBS was added to each well to wash away any unset agarose, the PBS was then removed. 25 µl (200 U) thrombin was then dispensed into each well, to this 300 µl (1.25x10⁶ cell/ml) of cells in basic medium (5x10⁵ cells/hydrogel) was added and mixed. Finally 75 µl (20 mg/ml) fibrinogen was added and mixed. The 48 well plate was then moved to an incubator operating at 37°C in normoxia and 5% CO₂. The samples were left for one hour to allow the fibrin to fully polymerise. Once polymerised, using a sterile 10 µl pipette tip, the edges of the fibrin were scored away from the well wall to encourage contraction and the samples then covered in 100 µl of basic medium. 1 mg/ml 6-aminocaproic acid was added to the culture medium to inhibit fibrin degradation during the contraction phase (first week) (Kupcsik et al., 2009). The medium was changed and the fibrin hydrogels scored every 48 hours during the contraction phase to prevent sticking and ensure consistent hydrogel morphology. The fibrin hydrogels reached optimum contraction after one week and were now designated microtissues. The microtissues were either moved into a 24 well plate for hydrostatic pressure conditions or into 12 well plates for static and dynamic microgravity condition. The hydrogels to be cultured under microgravity conditions were moved to the microgravity chamber.

Before the microtissues were moved into the 24 well plate 100 µl of sterile 4% agarose was dispensed into each well and left to set before washing with sterile PBS, the microtissues were then gently transferred into the 24 well plate using passive suction with a 5 ml pipette

tip. Similarly for the 12 well plates 200 μ l of sterile 4% agarose was dispensed into each well and washed with sterile PBS. The samples within the 24 well plates (hydrostatic pressure) were cultured with 500 μ l of appropriate media (chondrogenic, osteogenic or basic) with 800 μ M of L-ascorbic acid added fresh during each media change. In the microgravity group the samples were cultured in basic media with 800 μ M of L-ascorbic acid which was added fresh during each media change. 1 mg/ml 6-aminocaproic acid was not added after the initial one-week contraction period for either hydrostatic or microgravity microtissues.

To generate the equal ratio of media for the different microgravity microtissues (microgravity, dynamic and static), 27 microtissues were cultured in 54 ml media within the microgravity chamber, whilst 24 static and dynamic microtissues were cultured in 2 ml within 12 well plates (two 12 well plates per condition); a ratio of 2 ml of culture media per microtissue in all groups. Media continued to be changed every 48 hours for the hydrostatic pressure experiment and every third day for the microgravity groups. The well plates were cultured within an incubator operating at 37°C in normoxia and 5% CO₂, whilst the microgravity chamber was attached to the microgravity bioreactor and cultured in an incubator operating at 37°C in normoxia and 5% CO₂.

2.2.4. Histology

The same five histological stains (haematoxylin and eosin (H&E), Alcian blue, Alizarin Red and Picrosirius Red) were applied to all experimental groups. Microtissues in the hydrostatic groups were washed with three changes of PBS in the culture plates, fixed with 1% NBF for 30 minutes at room temperature, washed a further three times with PBS and stored in 0.01% sodium azide in PBS at 4°C until required. The microgravity microtissues were fixed and stored in the same way as the hydrostatic pressure microtissues, except the microtissues in the Synthecon microgravity bioreactor were first removed from the rotation drums and placed into a 24 well plate (one microtissue per well). The tensile stimulation samples were washed in three changes of PBS and fixed with 1% NBF for 30 minutes directly within the 3D printed bioreactor chamber whilst still attached to their anchor frames. Once fixed the samples were transferred to two 24 well plates (one sample per well), washed a further three times with PBS and stored in 0.01% sodium azide in PBS at 4°C. The fixed samples were washed with two changes of PBS before being placed into tissue processing cassettes (one cassette per experimental condition). The cassettes were placed into a beaker filled with 100 ml of 70% ethanol for short term storage (<2 hours). The cassettes were then placed into the Leica ASP300 tissue processor (Leica Microsystems, UK) and processed with the protocol shown in Table 2.1.

Table 2.1. Tissue processing protocol for fibrin hydrogels

Step	Chemical	Step duration
1	70% Ethanol	30 minutes
2	90% Ethanol	30 minutes
3	100% Ethanol	10 minutes
4	100% Ethanol	10 minutes
5	100% Ethanol	10 minutes
6	100% Ethanol	10 minutes
7	Xylene	30 minutes
8	Xylene	30 minutes
9	Paraffin wax	2 hours
10	Paraffin wax	2 hours
	Total time	6 hours and 40 minutes

After processing the samples were removed from the cassettes and embedded in paraffin wax using the Leica EG1150 tissue embedder (Leica Microsystems, UK). Embedded samples were sectioned using the Leica RM2265 microtome (Leica Microsystems, UK) generating 6 μm sections. Sections were mounted onto Superfrost Plus Adhesion Microscope Slides and dried at 37°C overnight. For all stains, sections were deparaffinised in two changes of xylene (5 minutes each), rehydrated in 70%, 90% and 100% ethanol (5 minutes each) and washed in running tap water for 2 minutes. The following protocols were then used for each stain:

Alcian Blue staining – Following deparaffinisation the slide was placed into Alcian blue solution for 30 minutes at room temperature. After the 30 minutes had elapsed the sample was placed under running tap water for two minutes to wash away excess and unbound dye. Finally the sample was rinsed in distilled water before being dehydrated and mounted as outlined below.

Alizarin Red staining – Following deparaffinisation the slide was placed into Alizarin red solution (pH 4.3-4.5) for two minutes before excess stain was shaken and the slide was blotted dry. The sample was then dehydrated and mounted as outlined below.

H&E staining – Following deparaffinisation the cell nucleus was stained by submerging the sample in Mayer's haematoxylin solution for five minutes. The sample was then washed in running tap water for one minute and then differentiated in 0.3% acid alcohol for 30 seconds. The sample was then washed again in running tap water for 5 minutes and counter stained in eosin for three minutes. The excess eosin was washed off by dipping the slide in distilled water before dehydrating and mounted as outlined below.

Picrosirius Red staining – Following deparaffinisation the cell nucleus was stained by submerging the slide in Weigert's haematoxylin for eight minutes. Once the eight minutes had passed the sample was washed in running tap water for 10 minutes before submerging in picrosirius red solution for one hour at room temperature. After one hour the sample was washed in two changes of acidified water before dehydration and mounting as outlined below.

Dehydration and mounting – Following staining all sections were dehydrated in 90% ethanol and two changes of 100% ethanol (30 seconds each) and cleared in two changes of xylene (1 minutes each). Sections were mounted with DPX mounting solution and imaged. H&E, Alcian blue and Alizarin red images were acquired using the Nikon Eclipse Ci, picrosirius red images were acquired using an Olympus BX60 in both brightfield and polarized light. All microscopy images were taken using either a x4 or x10 objective.

2.2.4.1. Calcium Quantification with Alizarin Red

After the hydrostatic pressure loading regime was completed, six samples from the osteogenic media group were randomly selected. The samples were submerged in 1ml of sterile PBS and washed in three changes three times. Once washed the samples were fixed in 1% NBF for 30 minutes at room temperature and washed again in three changes of sterile PBS. The samples were then stained with 1% Alizarin red solution (pH 4.1-4.3) for one hour at room temperature followed by washing in three changes of sterile PBS. The first two PBS washes were for one hour at room temperature, whilst the third wash was overnight at 4°C. The osteogenic samples were imaged using a dissection microscope fitted with an HD digital camera. Quantification of stained calcium in the osteogenic samples was achieved by de-staining the samples in 5% cetylpyridinium chloride solution for 24 hours at 4°C, yielding a purple solution containing the cetylpyridinium-Alizarin complex, which was quantified at 562 nm. Following the de-stain, some calcium deposits strongly associated with the matrix remained stained. Standard curve was generated using 1% Alizarin red serial diluted in 5% cetylpyridinium chloride (Henstock et al., 2014).

2.2.4.2. Alkaline Phosphatase Assay

Culture medium was collected at seven day time points throughout the experimental run for all loading conditions (tensile, hydrostatic pressure and microgravity) From the collected culture medium 50 µl was dispensed into a 96 well plate, along with 100 µl of p-nitrophenyl phosphate, a phosphatase substrate that turns yellow (λ_{max} = 405 nm) when dephosphorylated by alkaline phosphatase after 10 minutes of incubation at room temperature. Standard curves were generated with known concentration of bovine mucosa alkaline phosphatase enzyme.

2.2.5. Protein Extraction and Western Blotting

Complete extraction of collagen requires the addition of an enzyme as it is largely insoluble, therefore simple grinding and suspending in lysis buffer would not give an accurate representation of the collagen composition. Collagen solubilisation was done by digesting the sample with the enzyme pepsin. In weak acid pepsin cleaves the N- and the C-terminal telopeptides of the collagen molecule isolating the soluble triple helix from the insoluble telopeptides (Qian et al., 2017).

To optimise the pepsin digest a number of pepsin ($\geq 2,500$ U/mg) concentrations were trialled: 25, 50, 100 and 1000 $\mu\text{g}/\text{ml}$. The pepsin was suspended in a 0.5 M acetic acid with 25 mM Ethylenediaminetetraacetic acid (EDTA) solution, based on the solution used by ChandraRajan (1978). Optimisation samples were generated by culturing fibrin hydrogels (protocol as defined in section 2.2.3.1) between posts for two weeks in basic media with the addition of 800 μM L-ascorbic acid (refreshed every 48 hours). After pepsin digestion was complete the protein concentration was measured using the Bradford assay: the sample was diluted 1:10 in distilled water and dispensed in triplicate into a 96-well plate. 200 μl of Bradford reagent was then added to each well. Absorbance was measured at 470 nm using the SPECTROstar Nano microplate reader (BMG LABTECH), this measured the total protein found in the sample. The standard curve was generated with a serial dilution of bovine serum albumin (BSA) (0-1000 μg). As can be seen in Fig.2.5, as pepsin concentration decreased the extracted protein concentration increased. As 25 $\mu\text{g}/\text{ml}$ pepsin produced the highest protein concentration it was chosen as the concentration for experimental protein extraction. It should be noted that no concentration below 25 $\mu\text{g}/\text{ml}$ was tested and this may further increase the collagen yield from the digested tissue.

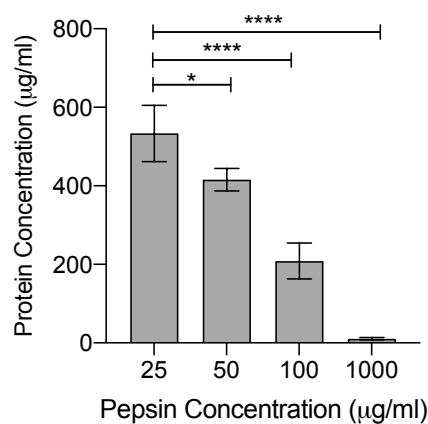


Figure 2.5. Protein concentration from fibrin hydrogels with varying pepsin concentration. Statistical significance measured using one way Anova with Tukey's multiple comparisons (**** $P < 0.001$, **** $P < 0.01$, * $P < 0.5$).

At the end of each experimental run, samples were removed from culture, weighed, snap frozen and stored at -80°C before digestion. Fig.2.6 outlines the 7 step process for digestion and protein extraction. For SDS page analysis, expression of collagen types was normalised to total protein, therefore soluble proteins were extracted (step 5a) before the samples were digested by pepsin, which degrades non-triple helical proteins. Soluble protein extraction was achieved by thawing the sample on ice and homogenising with a motorised pellet pestle. The homogenised sample was then suspended in $75\ \mu\text{l}$ of RIPA buffer and vortexed. The sample was centrifuged at $10,000\ \text{g}$ for 10 minutes at 4°C to separate the insoluble protein (pellet) from the soluble protein (supernatant); the soluble protein was removed and stored in a appropriately labelled tube at -20°C . The insoluble protein was suspended in the pepsin solution ($25\ \mu\text{g}/\text{ml}$ pepsin, $0.5\ \text{M}$ acetic acid and $20\ \text{mM}$ EDTA) and placed on a plate shaker overnight at 4°C . the digested sample then followed steps 5b and 6 with each NaCl molarity taking 12 hours to complete. The undigested sample was re-digested with fresh pepsin solution and again taken through steps 5b and 6. All extracted protein (both soluble and insoluble) were then combined at step 7.

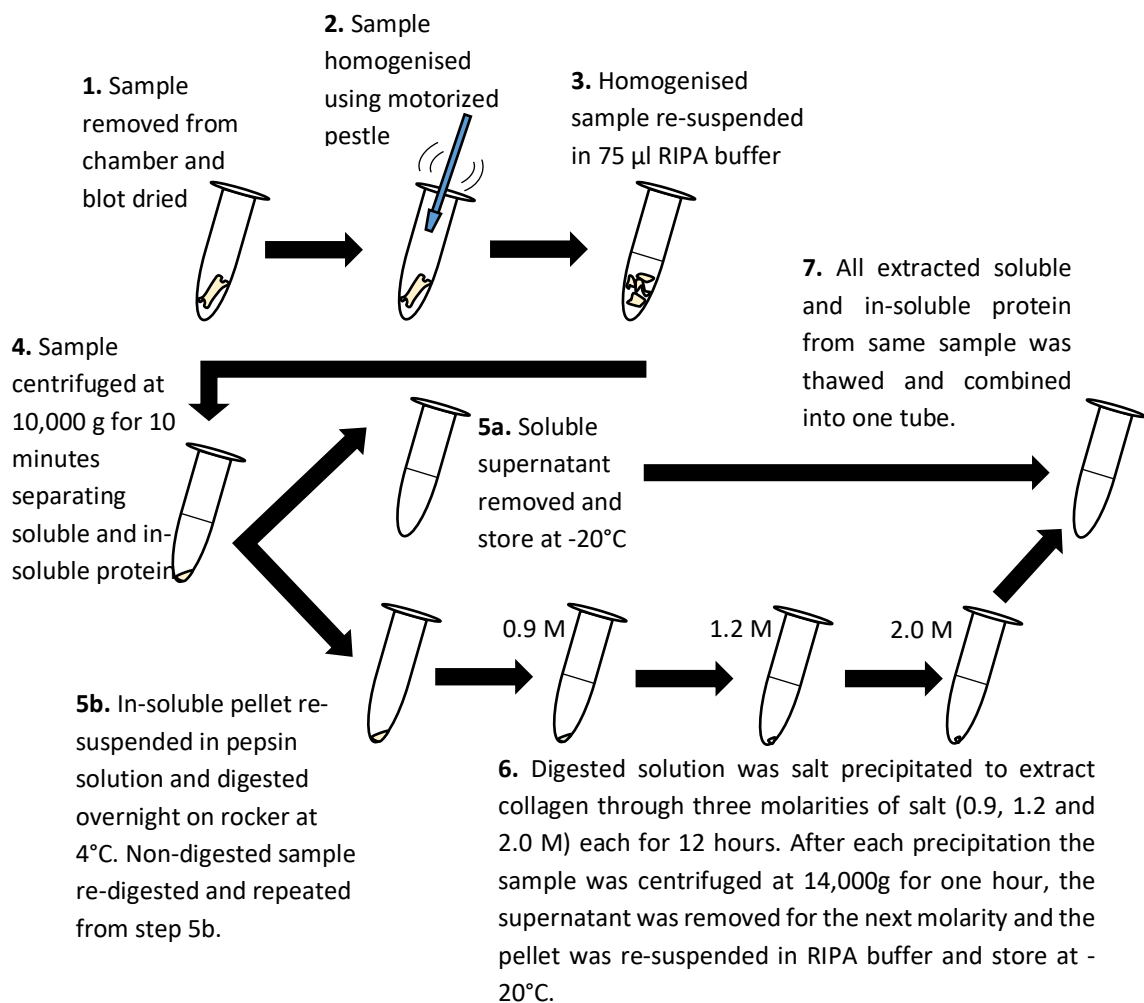


Figure 2.6. Collagen extraction flow diagram.

Protein content was measured using the Pierce BCA protein assay following the manufacturer's protocol. The BCA assay uses bicinchoninic acid (BCA) to detect the reduction of Cu^{2+} to Cu^{+} by protein in an alkaline medium. The assay works through two steps; the first step is the chelation of copper with protein in the alkaline environment, which results in a light blue complex and is known as the biuret reaction, where peptides containing three or more amino acid residues form a complex with cupric ions. The second step is used to enhance the detectability 100 times, compared to the first step alone. Here the colour of the complex is developed by reacting with BCA, generating an intense purple colour which forms due to the chelation of two BCA molecules with one cuprous ion. The BCA/copper complex exhibits strong linear absorbance at 562 nm with increasing protein concentration. The protein concentration was measured using the SPECTROstar Nano microplate reader (BMG LABTECH).

The protein concentration was used to determine the volume of the sample required for SDS page. For SDS page electrophoresis, 26 well, 1 mm, NuPAGE 3-8% Tris-Acetate midi protein gels were used with the Criterion Vertical Electrophoresis system. Tris-acetate gels were selected as they allow for the running of larger proteins with a range from 30-500 kDa. The proteins analysed throughout this study range from 35 to 333 kDa allowing for complete analysis with one gel type. Protein samples were thawed on ice, 15 μg of protein removed from stock and added to an appropriately labelled 1.5 ml centrifuge tube; stock sample was then returned to -20°C storage. 3.75 μl of NuPAGE LDS Sample Buffer and 1.5 μl of NuPAGE Sample Reducing Agent (10X) was added to the protein sample and the volume made up to 15 μl with distilled water. The samples were vortexed and heated to 70°C for 10 minutes to denature the protein. Once heated the samples were quickly centrifuged to collect any condensation generated during heating. The Tris-acetate gel was loaded into the Criterion system, as per the manufacturer's instructions and the tank filled with NuPAGE Tris-Acetate SDS Running Buffer (10X) diluted to 1x with distilled water. 5 μl of the Chameleon 800 Pre-stained Protein Ladder was added to the first well, then the reduced samples added to the remaining 25 wells in blocks of four or three depending on experiment, i.e. for the tensile stimulation experiment, wells were loaded as: protein ladder, Control A, 3% A, 5% A, 10% A, Control B, 3% B, 5% B, 10% B and so on. Electrophoresis was carried out at 150 V for one hour. During the run the Criterion Blotter was prepared for the protein transfer. The sponges and filter paper were submerged in NuPAGE Transfer Buffer (20X) diluted to 1X in 850 ml distilled water and 100 ml methanol. Once the run was complete the gels were removed from the chamber, broken out of the cassette and placed into the transfer system via the gel

and membrane setup as defined by Bio-Rad (Fig.2.7). Nitrocellulose membranes were used for transfers throughout this study.

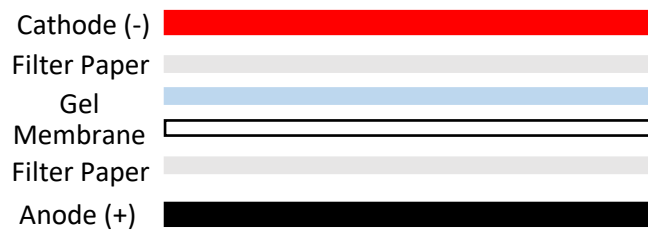


Figure 2.7. Gel and membrane setup for electrophoretic transfer.

Once the gel and transfer membranes were arranged correctly they were installed into the Criterion Blotter system and the tank was filled with 1x NuPAGE Transfer Buffer. Protein was transferred at 10 V for two hours, the gel was then discarded and the transfer membrane was washed in distilled water before being stained with REVERT Total Protein Stain. The membrane was incubated with the stain in the dark at room temperature for 5 minutes on a rocker plate. Once stained, the REVERT solution was thoroughly decanted and the membrane rinsed twice with REVERT Wash Solution. The membrane was imaged using the 700 nm channel on the Odyssey CLx imaging system (Li-cor, Nebraska, USA) generating a fluorescent image for the total protein on the membrane (example shown in Fig.2.8A). The membrane was briefly washed in distilled water before being blocked for one hour at room temperature with 5% reconstituted dehydrated milk in TBS-T.

The blocking buffer was removed and the membrane was incubated overnight at 4°C with the appropriate antibody diluted in 5% reconstituted dehydrated milk in TBS-T (antibody dilutions are shown in Table 2.2) The primary antibody was removed and the membrane washed three times with TBS-T before incubating at room temperature for one hour in the appropriate secondary antibody (Table 2.2) diluted in 5% reconstituted dehydrated milk in TBS-T at 1:10,000. The secondary antibody was removed and the membrane washed a further three times with TBS-T. The membrane was imaged using the Odyssey CLx imaging system at 800 nm (example shown in Fig.2.8B). Densitometry was performed on the acquired images using the Empiria software (Li-cor, Nebraska, USA) with the targeted protein expression normalised to the total protein expression.

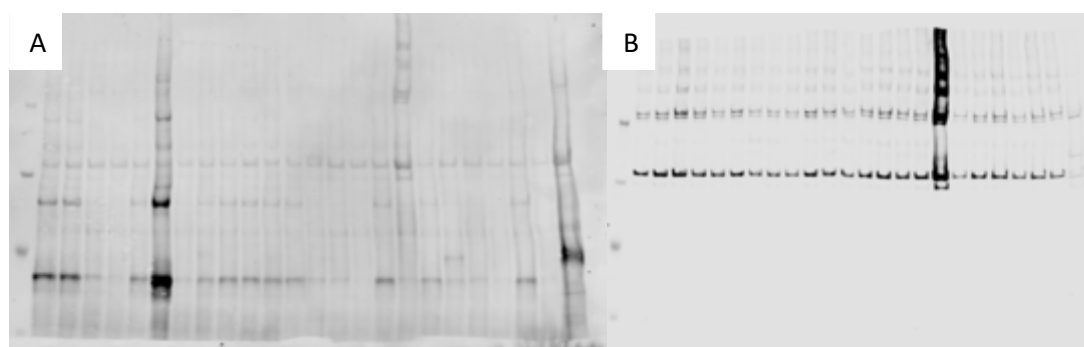


Figure 2.8. Example of western blot for chondrogenic media samples stimulated under hydrostatic pressure. (A) REVERT total protein stain of membrane, (B) Collagen I α 1 probe on membrane.

Table 2.2. Antibodies product number, supplier, dilutions and appropriate secondary antibody.

Protein	Product number/Supplier	Dilution	Secondary Antibody
Collagen α 1(I)	ab138492/Abcam	1:1000	926-32213/Li-cor
Collagen α 1(II)	sc-52658/Santa Cruz	1:500	926-32212/Li-cor
Collagen α 1(III)	ab7778/Abcam	1:1000	926-32213/Li-cor
Collagen α 1(V)	ab112551/Abcam	1:500	926-32212/Li-cor
Collagen α 1(VI)	sc-377143/Santa Cruz	1:500	926-32212/Li-cor
Collagen α 1(IX)	sc-376969/Santa Cruz	1:500	926-32212/Li-cor
Collagen α 1(X)	ab182563/Abcam	1:1000	926-32213/Li-cor
Collagen α 1(XI)	ab64883/Abcam	1:500	926-32212/Li-cor
Collagen α 1(XII)	ab121304/Abcam	1:500	926-32213/Li-cor
Collagen α 1(XIV)	ab101464/Abcam	1:500	926-32212/Li-cor
Collagen α 1(XXV)	MA5-24533/ThermoFisher	1:500	926-32212/Li-cor

2.2.6. RNA Extraction and qPCR

RNA was extracted from all sample by transferring fibrin hydrogels from culture to an RNase and DNase free 2 ml centrifuge tube. For the tensile stimulated samples, each strain rate was applied for a final two hours before transfer to the centrifuge tube, whilst hydrostatic microtissues underwent a final one hour stimulation. All control and microgravity microtissues were transferred directly to the centrifuge tubes. 300 μ l of TRIzol was added to each centrifuge tube and samples were frozen at -80°C . To extract RNA, samples were first thawed on ice, then homogenised using the QIAGEN TissueRuptor II before being drawn up into a 1 ml syringe and passed through a 23 gauge needle into a fresh 1.5 ml centrifuge tube. RNA was extracted using the phenol chloroform method: 60 μ l of chloroform was added to each homogenised sample in a 1.5 ml centrifuge tube. The samples were vortexed for 15 seconds before incubating at room temperature for 3 minutes. After incubation the samples were centrifuged at 12,000 g for 15 minutes at 4°C . The upper aqueous layer was transferred to a fresh RNase and DNase free 1.5 ml centrifuge tube, to which 150 μ l of 100% isopropanol was added. The samples were left for 15 minutes at room temperature to precipitate the RNA. Samples were then centrifuged at 12,000 g for 10 minutes at 4°C , the supernatant was removed and discarded. 300 μ l of 75% ethanol was added to each sample to wash the pellet. The samples were briefly vortexed and then spun down at 7,500 g for 10 minutes, the supernatant was removed and discarded and the wash step was repeated. Samples were left to air dry for 10 minutes in a fume hood before re-suspending RNA pellet in 11 μ l ultra-pure water. The quality and quantity of RNA was measured using the SPECTROstar Nano 2000 nanodrop (Thermo Scientific). 260/280 ratios between 1.6-2.1 were deemed acceptable. cDNA was synthesised using the Bio-rad iScript kit in a 20 μ l reaction with 0.2-1 μ g total RNA. The 20 μ l reaction comprised 0.1-11 μ l extracted RNA, 1 μ l iScript Reverse Transcriptase, 4 μ l 5x iScript Reaction Mix and was made up to 20 μ l with Nuclease free water. The reaction was ran using the Veriti™ 96-well Thermal Cycler (Applied Biosystems, ThermoFisher). Samples were initially primed at 25°C for 5 minutes, reverse transcription was applied at 46°C for 20 minutes before the reverse transcriptase was inactivated at 95°C for 1 minute. Samples were then stored at -20°C until required.

The qPCR reaction was ran using a Stratagene MX3005P instrument, where each sample is present within a well of a 96-well plate. Each well contained 10 ng (0.2-3 μ l) cDNA, 0-2.8 μ l (depending on sample volume) distilled water, 5 μ l SYBR Green JumpStart *Taq* ReadyMix, 1 μ l 10 μ M Forward Primer, 1 μ l 10 μ M Reverse Primer and 1x reference dye (ROX). Fig.2.9 shows the thermal profile for qPCR reactions. Initial denaturing occurs during segment 1

were samples are heated to 95°C for 5 minutes; following this 40 cycles were applied during segment 2 starting with denaturing at 95°C for 10 seconds, annealing at 55°C for 10 seconds and extension at 68°C for 30 seconds. The melt peaks were then generated during segment 3. qPCR data was analysed using the efficiency corrected Δ CT method (Pfaffl et al., 2004, Svec et al., 2015).

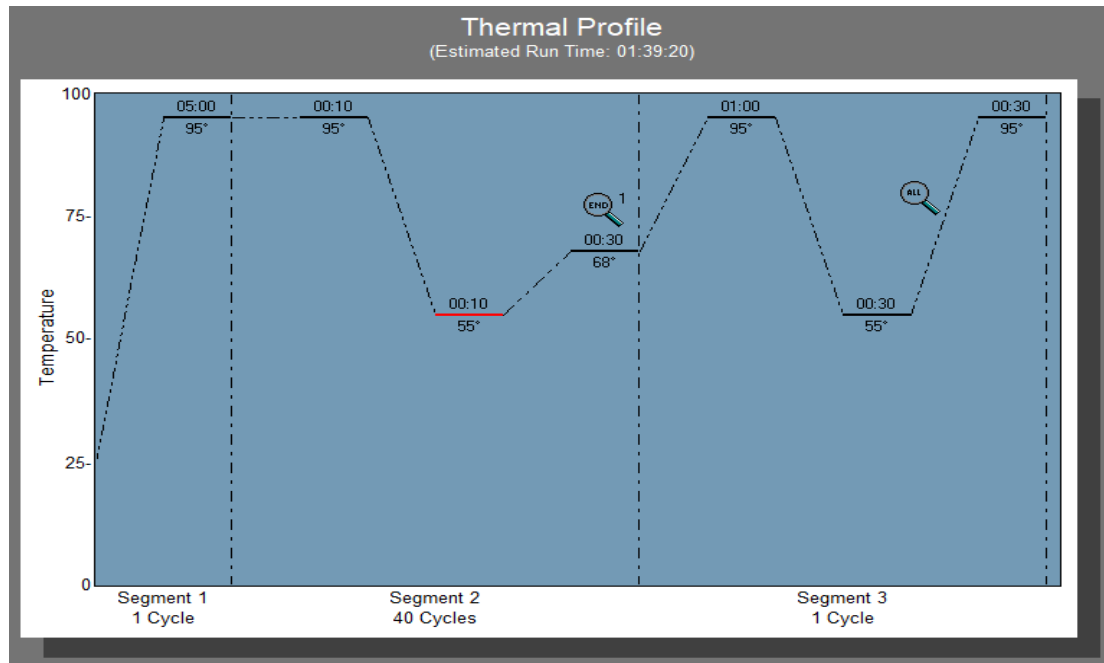


Figure 2.9. Thermal profile for qPCR.

Primers used were either designed in-house or purchased from QIAGEN (sequence not provided) as shown in Table 2.3. Primer sequences were designed using Primer-Blast (NCBI) or taken from published work. Sequence quality was confirmed using the IDT OligoAnalyzer tool and the ThermoFisher oligo design tool (primer parameters shown in Appendix B). Primers were tested for efficiency and melt peaks before use in experiments, Appendix C details efficiency and melt peak analysis. The most suitable housekeeper genes for each mechanical stimulation was confirmed using GeNorm (see Appendix D) and was found to be YWHAZ for tensile stimulation and GAPDH for hydrostatic pressure and microgravity.

Table 2.3. Primer sequences for investigated genes.

Gene	Forward	Reverse	Origin
COL1A1	CGGCTCCTGCTCCTCTTAG	CACACGTCTCGGTCATGGTA	(Naranda et al., 2016)
COL2A1	CCAGATTGAGAGCATCCGC	CCAGTAGTCTCCACTCTTCC AC	(Naranda et al., 2016)
COL3A1	GGGTGAGAAAGGTGAAGG AG	CATTACTACCAGGAGGACC AG	Designed
COL5A1		NM_000093, QIAGEN	QIAGEN
COL6A1		NM_001848, QIAGEN	QIAGEN
COL9A1		NM_001851, QIAGEN	QIAGEN
COL10A1	GCAACTAAGGGCCTCAATG G	CTCAGGCATGACTGCTTGA C	Designed
COL11A1	AATGGAGCTGATGGACCAC A	TCCTTTGGGACCGCCTAC	(Karaglani et al., 2015)
COL12A1	TTTAGTTAGCACAGCGGGC A	CGCTCGAAATACACAGCAG C	Designed
COL14A1		NM_021110, QIAGEN	QIAGEN
COL24A1		NM_152890, QIAGEN	QIAGEN
DCN		NM_133503, QIAGEN	QIAGEN
SCXA		NM_001080514, QIAGEN	QIAGEN
TNMD		NM_022144, QIAGEN	QIAGEN
GAPDH	ATGGGGAAGGTGAAGGTC G	TAAAAGCAGCCCTGGTGAC C	Designed
YWHAZ	CCGTTACTTGGCTGAGGTT G	TGCTTGTTGTGACTGATCGA C	(Lemma et al., 2016)

2.2.7. Transmission Electron Microscopy

Transmission electron microscopy (TEM) was performed externally at the department of Veterinary Pathology and Public Health, Leahurst Campus, University of Liverpool by Miss Marion Pope. Method for fixation, sectioning and imaging was provided by Miss Marion Pope. Samples were prepared in the Institute of Ageing and Chronic disease before being shipped to be imaged.

At the end of the three week loading phase during run 4, 5 and 6 one sample was randomly selected from each group, the media was removed and the sample was washed in three changes of sterile PBS within the bioreactor chamber. Once washed the samples were fixed in 2.5% glutaraldehyde in 0.1 M sodium cacodylate buffer (pH 7.4) for four hours. After four hours the tissue engineered tendon were removed from the anchor frame and placed into labelled 1.5 ml Eppendorf's with 1 ml of fresh glutaraldehyde buffer. The samples were then shipped for imaging.

Once at the Leahurst campus the samples were cut into five pieces all approximately 1.6 mm long (maximum embedding length 2 mm), along the transverse axis (Fig.2.10). The samples were washed in 0.1 M sodium cacodylate buffer for 30 minutes, and underwent a secondary fixation and contrast stain in 1% osmium tetroxide buffer for one hour. The samples were again washed in the 0.1 M sodium cacodylate buffer before 'en bloc' staining with 2% uranyl acetate in 0.69% maleic acid (pH 4.5).

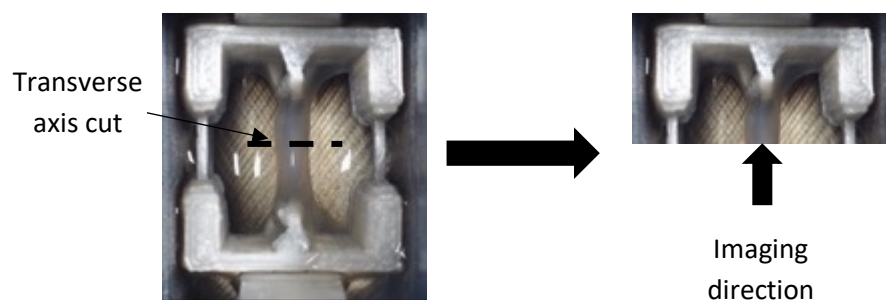


Figure 2.10. Axis the fibrin hydrogels were cut along for TEM analysis and direction fibrin hydrogel was imaged in.

Upon completion of the fixation process the samples were dehydrated through two changes of ascending ethanol concentration of 50%, 70% and 90% for five minutes each, three changes of 100% ethanol for ten minutes each and three changes of 100% acetone for five minutes each.

After the samples had been dehydrated, Taab epoxy resin was used to infiltrate the samples with ascending resin-acetone mixes with an initial ratio of 1:3 resin to acetone for one hour, then 2:2 resin to acetone for one hour, 3:1 resin to acetone for one hour and finally 100% resin for two hours.

Resin infiltrated samples were left to polymerise overnight at 60°C. Once polymerised the samples were sectioned. For Toluidine blue staining the samples were sectioned to semi-thin sections (0.5 μm) on a Reichert-Jung Ultracut ultramicrotome (Leica Microsystems) and stained with 1% Toluidine blue in 1% borax. Toluidine blue staining was used to highlight areas of collagen deposition to allow for more targeted TEM imaging.

For TEM the samples were cut to ultrathin sections (60-90 nm) with a 'Diatome' ultra-diamond knife on a Reichert-Jung Ultracut ultramicrotome and mounted on a 200 mesh copper grid. The sample was contrast stained with saturated soluble uranyl acetate in 50% methanol for 5 minutes, followed by Reynolds lead citrate stain for 5 minutes. All TEM images were taken using the Phillips EM208S transmission electron microscope at 80 kV (ThermoFisher, Massachusetts, USA). To correctly measure the samples the magnification was calibrated. For the x110,000 objective, 23 spheres with known diameter of 0.09 μm diameter were imaged using the EM208S transmission electron microscope. The calibration images were imported to Image J/Fiji (Schindelin et al., 2012) and the known diameter was used to correctly set the scale bar for subsequent image analysis.

All image analysis was completed using Image J/Fiji (Fig.2.11), first the images were imported to the programme and the 100 nm scale bar was correctly set to 113.84 nm. The extreme intensities in the image was next removed by despeckling followed by noise smoothing by applying a Gaussian's blur. The cleaner image then had the sigma value (radius) set to 1 and a threshold was taken to minimise fibril merging. The thresholded image was then made binary and using the ctrl + f shortcut the empty spaces in the fibrils were filled. Any fibrils that remained merged following the previous processing were separated by applying a watershed to the image. To measure the fibrils the measurements were set to "acquiring the area", "shape description", "perimeter" and "fit ellipse". Finally the fibrils were measured by selecting "show outlines", "display results" and "exclude on edges".

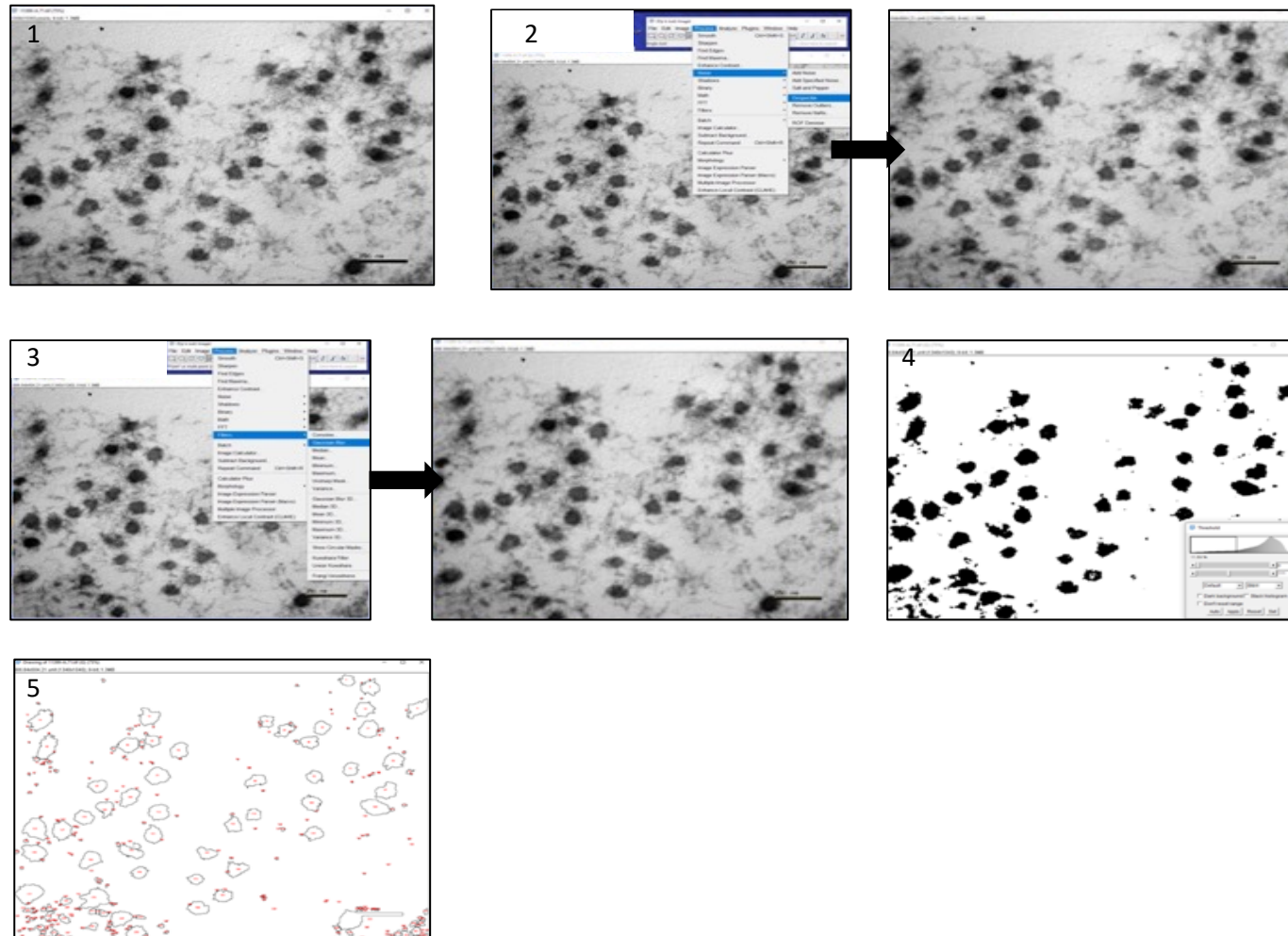


Figure 2.11. TEM image processing. 1) TEM images opened in ImageJ, 2) images despeckled, 3) Guassians blur applied to smooth noise, 4) threshold of images acquired, 5) TEM fibril analysis complete, all measurements taken and fibrils assigned numbers. Scale bars represent 100 nm.

2.2.8. CNA35 Collagen-Probe

The CNA35 collagen probe was used to image collagen generated by MSCs in response to tensile stimulations within fibrin hydrogels. The CNA35 collagen probe was used in place of traditional antibody staining as it is non-specific and so highlights all fibrillar collagen within the structure rather than the antibody specific isoform. The probe is approximately five times smaller than antibodies that bind to collagen therefore making staining of 3D structures more comprehensive as a greater proportion of collagen fibrils are exposed to the probe (Megens et al., 2007).

To generate the CNA35 collagen-probe, a plasmid vector, pQE-30, containing CNA35 (provided by the Mangus Höök group, Texas A&U University to Dr Elizabeth Laird (supervisor)) was added to *Escherichia coli* on ice, the mixture was heat shocked at 42°C for 30 seconds. Colonies were grown up on LB-ampicillin plates overnight. A single colony was selected and added to 25 ml of LB broth and incubated overnight at 37°C, 250 rpm. The following day the 25 ml culture was inoculated with 500 ml LB broth and grown further at 37°C, 250 rpm. The OD600 value was monitored until it reached 0.1. Once the OD600 value reached 0.1, 1 mM Isopropyl B-d-1-thiogalactopyranoside (IPTG) was added to the culture inducing protein expression (CNA35). The culture was grown for six hours at 37°C, 250 rpm.

To confirm the protein had been produced by the bacteria, a sample of the DNA was run on a 1% agarose gel. DNA was extracted using PureYield plasmid Minipreps following the manufacturer's protocol. 5 ml of 2x YT medium was inoculated with 50 ml of the bacterial culture overnight at 37°C. The following day 5 ml of the overnight culture was centrifuged at 8000 rpm for 3 minutes at room temperature. The pellet was then re-suspended in 250 µl buffer P1 and transferred to a 1.5 ml centrifuge tube. 250 µl of buffer P2 was added and mixed by inverting the tube until the solution turned blue. The sample was then incubated at room temperature for 5 minutes. 350 µl of buffer N3 was added and mixed by inverting tube until the solution turned colourless. The sample was then centrifuged at 8000 rpm for 10 minutes. The supernatant was added to a QIAprep spin column and centrifuged at 8000 rpm for 30-60 seconds before the flow through was discarded. The QIAprep spin column was washed with 500 µl buffer PE and re-centrifuged as before. The QIAprep spin column was moved to a collection tube and centrifuged at 8000 rpm for 1 minutes to remove residual wash buffer. The QIAprep spin column was placed into a clean 1.5 ml centrifuge tube and 60 µl buffer EB was added and incubated at room temperature for 1 minute before centrifuging for a further minute, the solution was taken forward for DNA analysis. DNA concentration

was found to be 57.9 ng/ μ l using the SPECTROstar Nano 2000 nanodrop (ThermoFisher, Massachusetts, USA).

The DNA was cut using two enzymes, BamHI-FI and PstI-HF, and ran on a 1% agarose gel. The gel was made by dissolving 1 g of agarose in 100 ml TAE buffer. Once dissolved the 1% agarose solution was poured into a gel mold and 5 μ l of PeqGREEN was added and mixed in, a comb was placed in position and the gel was left to set (approximately 30 minutes). 17.3 μ l (1 μ g DNA) of the sample was mixed with 5 μ l cutsmart buffer and 1 μ l of each enzyme, the sample was then diluted with 25.7 μ l of sterile distilled water to generate a 50 μ l sample. The solution was incubated at 37°C for 15 minutes. 10 μ l of DNA Gel Loading Dye (6x) was added to the sample. 10 μ l of TrackIt 1 Kb Plus DNA ladder was dispensed into the first well of the 1% agarose gel and 60 μ l of the sample into the second well. The gel was run at 90 V for 40 minutes and then imaged using the Chemicdoc Chemiluminescence imager (Bio-Rad) as shown in Fig.2.12. Two bands appear on the gel, one near 4000 bp and one near 900 bp. This agrees with what was expected to be seen; once cut by the BamHI-FI and PstI-HF enzymes the vector pQE-30 should appear at 3461 bp and the cut away CNA35 should appear at 948 bp, therefore the vector appeared to have been successfully taken up by the bacteria.

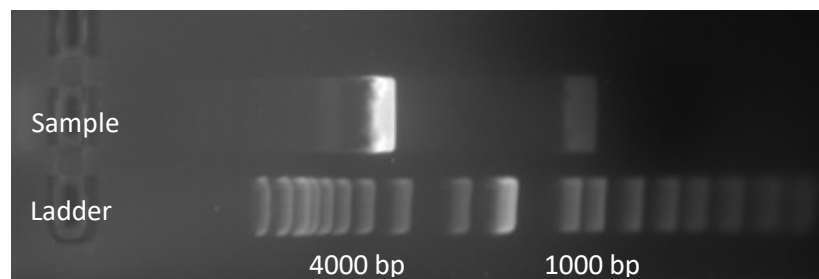


Figure 2.12. 1% agarose gel electrophoresis of DNA extracted from bacteria grown with CNA35 plasmid. Two products on gel at approximately 3500bp and 900bp, the two products are consistent with the pQE30 vector (3461 bp) and CNA35 (948 bp).

The protein was extracted and purified from the culture broth (475 ml remaining after DNA analysis) using the BugBuster Ni-NTA His-Bind purification kit. 40 ml aliquots were dispensed into 50 ml centrifuge tubes and centrifuged at 10,000 g for 10 minutes. The supernatant was removed and stored as lysate 1. The pellets were combined and resuspended with BugBuster protein extraction reagent (BBPER). 5ml of BBPER was added per 1 g of cell pellet. Benzonase nuclease was added to the suspended cells as 1 μ l per ml of BBPER. The cell suspension was incubated on a shaking platform on a low setting (approximately 25 rpm), at room temperature for 20 minutes (suspension should no longer be viscous due to the benzonase

nuclease). The suspension was transferred to a centrifuge tube and spun down at 16,000 g, 4°C for 30 minutes to remove insoluble cell debris. The soluble protein supernatants were pooled together in a fresh tube and the cell debris was re-suspended as lysate 2.

The supernatants were next passed through a chromatography column to filter the soluble protein (reagent listed in Appendix E). 1 ml of 50% Ni-NTA His bind slurry was added to 4 ml of the binding buffer and mixed gently. The resin was left to settle by gravity and then 4 ml of the supernatant was removed and added to a capped column. Imidazole was then added to the soluble protein solution to a final concentration of 10 mM. The solution was run through the chromatography column, followed by two washes with 8 ml of wash buffer (wash flow through kept as wash 1 and wash 2). Protein was then eluted through six runs of 1 ml elution buffer, each elution was stored separately as elution 1-6.

Protein content was investigated using SDS page (Fig.2.13). Samples (lysate 1, lysate 2, wash 1, wash 2, elution 1, elution 2, elution 3, elution 4, elution 5 and elution 6) were diluted with 4x SDS sample buffer and heated at 85°C for 3 minutes. Gel electrophoresis was performed using the Mini Gel Tank with 4-12% Tris-glycine WedgeWell gels, 10 µl of Novex Sharp Pre-stained Protein Standard was loaded in wells 1 and 6 and 40 µl of the samples loaded in wells 2-5 (lysate 1 and 2, wash 1 and 2) and 7-12 (elution 1-6). The Mini Gel Tank was filled with 1x Novex Tris-Glycine SDS running buffer and gels ran at 225 V for 40 minutes. Once ran the gel was removed from the Mini Gel Tank and washed three times (5 minutes per wash) in distilled water. The gel was then incubated on a rocking plate in GelCode Blue Stain Reagent for one hour at room temperature. Once stained the gel was imaged using the Chemidoc chemiluminescence imager (Bio-Rad, California, USA) (Fig.2.13). Based on the SDS page results, eluates 3 and 4 were pooled and taken forward to generate the collagen probe, other elutions were stored at -20°C.

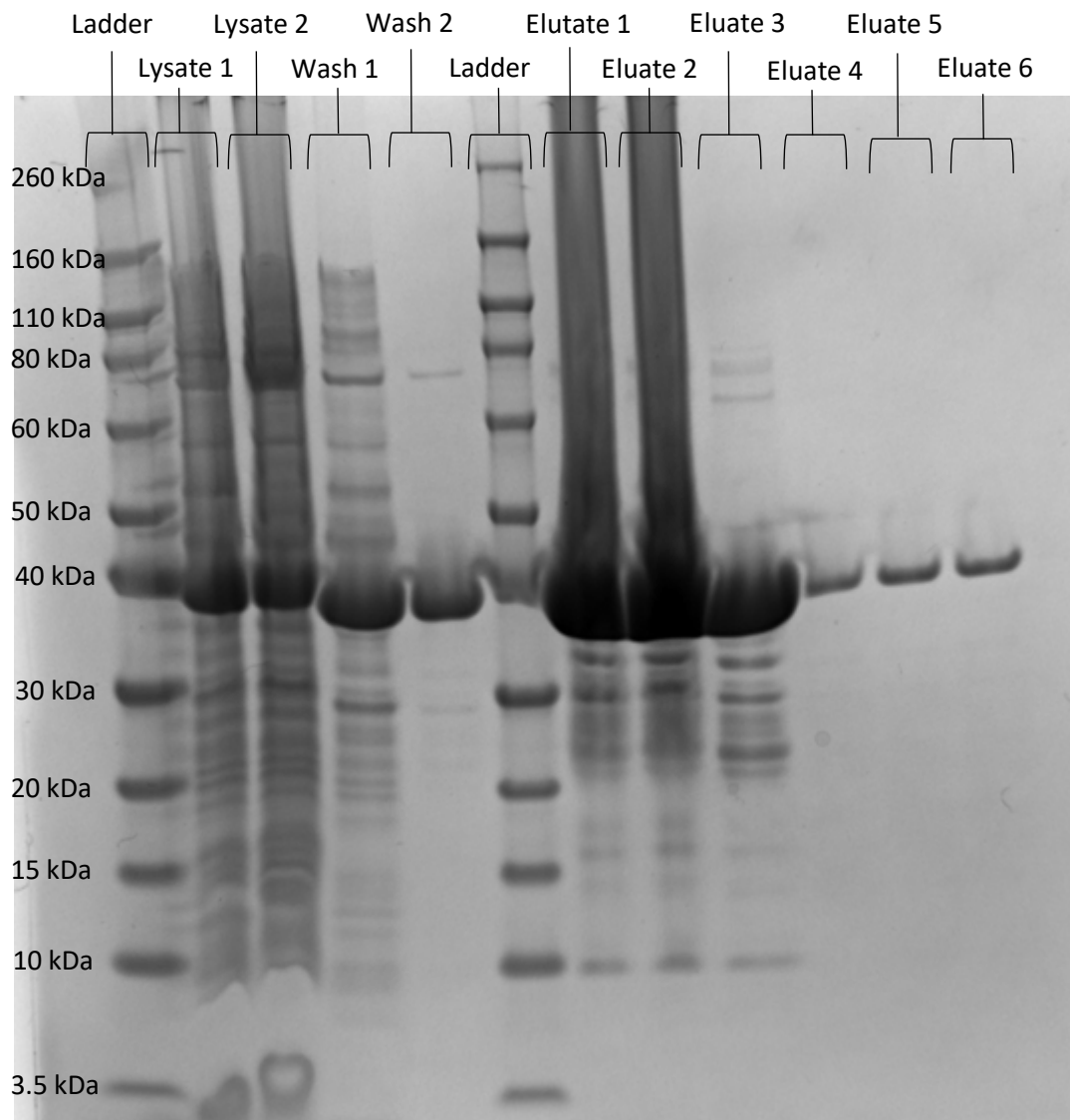


Figure 2.13. SDS-PAGE gel of extracted protein from CNA35 culture. Gel was stained with GelCode blue revealing larger amounts of protein at 35 kDa corresponding with the molecular weight of CNA35. Elutes 3 and 4 were pooled for subsequent use.

Eluates 3 and 4 were pooled together and added to an Amicon Ultra-15 centrifuge filter unit and centrifuged at 4000 g for 20 minutes, flow through was discarded. 10 ml of sodium bicarbonate buffer was then added to the membrane and the unit was again centrifuged at 4000 g for 15 minutes, flow through was discarded. The addition of sodium bicarbonate buffer and centrifugation was repeated twice. The concentrated protein was then suspended in 1.5 ml of buffer and recovered by pipetting out of the filter.

Protein concentration was measured using the BCA protein assay kit. The absorbance was found to be 1.155 resulting in a protein concentration of 17961.1 $\mu\text{g/ml}$. Next the DyLight

488 NHS ester dye was bound to the protein. To calculate the amount of dye needed the following equations were applied:

$$\text{Sample total protein} = \text{total volume (ml)} \times 17.96 = 0.117 \text{ ml} \times 17.96 = 3.13 \text{ mg} \quad [1]$$

$$\text{Amount of DyLight 488} = \frac{\text{total protein}}{\text{MW of protein}} \times \text{MW of fluor} \times \text{Molar fold excess} \quad [2]$$

$$= \frac{2.1}{35000} \times 1011 \times 15 = 0.9099 \text{ mg of fluor}$$

The molecular weight (MW) of protein was obtained from the manufacturer (ThermoFisher, Massachusetts, USA). The MW of DyLight 488 was found from the manufactures data sheet.

$$\text{Volume of dye to add} = \text{mg of fluor} \times \frac{100 \mu\text{l}}{1 \text{ mg}} \quad [3]$$

$$= 0.9099 \times 100 = 90.99 \mu\text{l NHS – ester fluor at } 10 \text{ mg/ml}$$

100 μl of Pierce Dimethylformamide (DMF) was added to DyLight 488 and pipetted up and down to mix. The solution was left to dissolve for 5 minutes at room temperature before vortexing. 90.09 μl of the DyLight 488 solution was added to 174 μl of the sample, mixed by pipetting up and down and incubated at room temperature for 1 hour in the dark. The now labelled protein was added to a fresh Amicon Ultra-15 centrifuge filter unit to remove excess dye. The filter was topped up with 10 ml sterile PBS and centrifuged at 4000 g for 20 minutes. The flow through was discarded, 10 ml of sterile PBS was added and the sample was re-centrifuged for 15 minutes at 4000 g. The sample was suspended by adding 10 mL PBS` to the filter and extracting carefully with a pipette.

Conformation that the DyLight 488 had bound to the protein was achieved by measuring the absorbance using the SPECTROstar Nano 2000 nanodrop (ThermoFisher, Massachusetts, USA) (Fig.2.14).

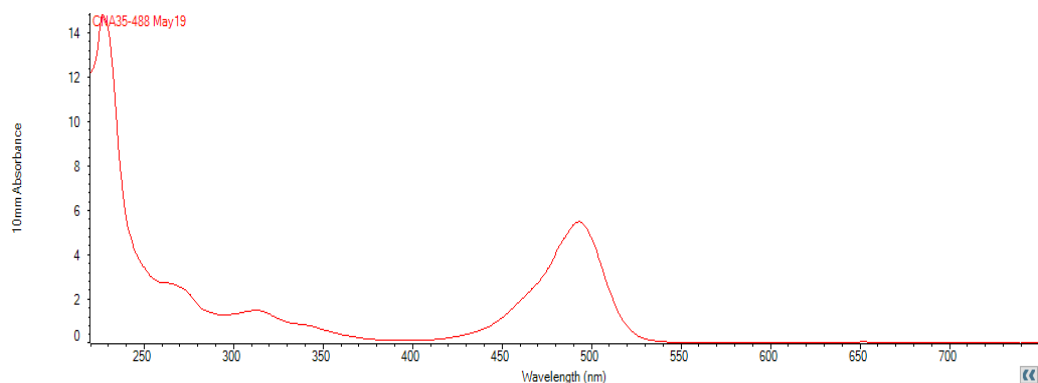


Figure 2.14. Nanodrop results to investigate the success of the DyLight 488 binding. Values for 280nm and 488nm recorded for calculations.

The A_{280} and A_{max} (max wavelength of DyLight 488 is 493 nm) values were recorded. A_{280} was found to be 1.72 and A_{max} was found to be 5.412. The following calculations were used to confirm the success of the DyLight binding:

$$\text{Protein Concentration (M)} = \frac{[A_{280} - (A_{max} \times CF)]}{\epsilon_{\text{protein}}} \quad [4]$$

Where CF is the correction factor, given by the manufacturer (ThermoFisher) as 0.147 for DyLight 488 and $\epsilon_{\text{protein}}$ is the protein molar extinction coefficient which is $33176 \text{ M}^{-1} \text{ cm}^{-1}$, given by the manufacturer (ThermoFisher).

$$\text{Protein Concentration (M)} = \frac{[1.72 - (5.412 \times 0.147)]}{33176} = 2.786 \times 10^{-5} \text{ M}$$

$$\text{Moles dye per mole protein} = \frac{A_{\text{max of the labeled protein}}}{\epsilon_{\text{fluor}} \times \text{protein concentration (M)}} \quad [5]$$

Where ϵ_{fluor} is the molar extinction coefficient at A_{max} , given by the manufacturer (ThermoFisher) for DyLight 488 as $70,000 \text{ M}^{-1} \text{ cm}^{-1}$.

$$\text{Moles dye per moles protein} = \frac{5.412}{70000 \times (2.786 \times 10^{-5})} = 2.77$$

CNA35 was therefore assumed to have almost 3 moles dye per moles protein, consistent with previous work (Krahn et al., 2006)

The CNA35 collagen-probe was applied to fixed triplicate tensile stimulated samples from each tensile stimulation group at the end of the three week loading period. Sample processing was applied through the combination of two protocols previously published, sample fixation and sectioning is outlined by Short et al. (2017) and CNA35 staining by Megens et al. (2007).

Short et al (2007) demonstrates the use of a vibratome to section the samples to $100 \mu\text{m}$ thick as vibratomes are frequently used for delicate tissues such as brain which has similar modulus to that of fibrin hydrogels (Miller et al., 2000, Breidenbach et al., 2015). At the end of the three week loading phase a sample from each tensile group was fixed in 1% NBF for 30 minutes within the bioreactor chamber. Once fixed the sample was removed and placed into a weighing boat dish. Low melting point agarose was mixed with PBS to a final concentration of 6% and melted. Once melted the agarose was poured over the sample in the weighing boat and left to set. A rectangle was cut around the sample encased in agarose removing excess, which was mounted onto a in house developed 3D printed platform on the

vibrotome and fixed in place with Loctite superglue (Fig.2.15). The sample was covered in PBS and the vibrotome set to speed 3 and frequency 8. 100 μm sections were cut from each sample in the longitudinal direction (along the fibre axis) and stored in 500 μl PBS in a 24 well plate (one well per sample) at 4°C.

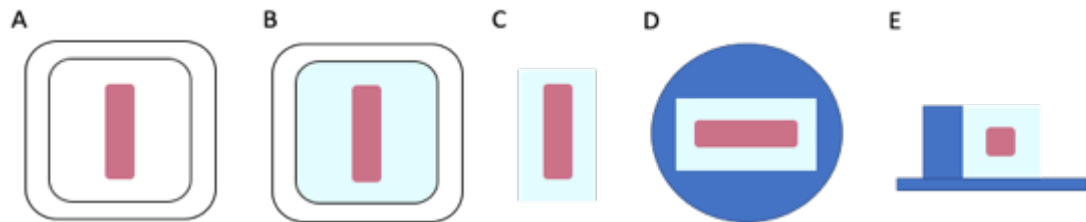


Figure 2.15. Schematic of the sample preparation process for vibrotome sectioning. (A) Fixed sample placed into weighing boat. (B) Weighing boat filled with low melting point agarose. (C) encased tissue engineered tendon removed from weighing boat and excess agarose cut away. (D) sample mounted onto 3D printed vibrotome platform and held in place with superglue (top view). (E) side view of the sample mount on the 3D printed platform.

Once all sections were cut they were stained with the CNA35 collagen-probe and DAPI. The samples were moved from PBS to Tris-buffered saline (TBS). The TBS was generated from 136.9 mM/l NaCl, 5 mM/l Trizma Base, 0.1% Tween 20 and 1% Bovine Serum Albumin. All solutions were suspended in TBS. First, endogenous peroxidase activity was blocked and each section was permeabilized with 3% hydrogen peroxide in methanol for 15 minutes at room temperature. The sections were then washed in three changes of TBS before incubation in 0.1% pepsin ($\geq 2,500$ U stock) in 0.01 M HCL for 30 minutes at room temperature. Sections were again washed with three changes of TBS and then incubated in 1 M CNA35 collagen-probe and 1:40 phalloidin 647 for one hour at room temperature in darkness. Dye was discarded and the sections were washed with three changes of TBS. 1% DAPI in TBS was then added to each section and samples were incubated for 20 minutes in darkness. Sections were washed in two changes of TBS and stored in a final change of TBS at 4°C.

Sections were imaged on the Confocal LMS800 (Zeiss). Acquisition information is shown in Appendix F. Phalloidin was not detected so is not shown in any images. Images were saved as CZI files for storage and TIFF files for analysis. Images were taken in two distinct regions, the mid region and the anchor point region (Fig.2.16). It was hypothesised that the anchor point region would be less aligned compared to the mid region as previous studies have shown a less uniform stresses in these regions (Lee et al., 2017, Atkinson et al., 2020). The anchor point region was therefore used as an internal control.

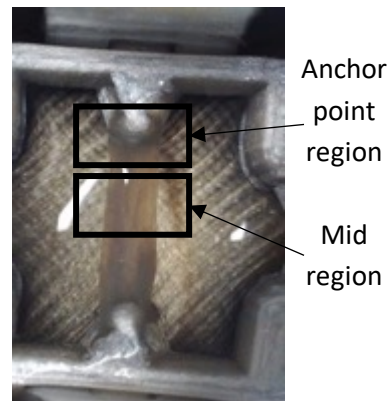


Figure 2.16. Anchor point region and Mid region highlight on fibrin hydrogel installed within the 3D printed chamber.

Image analysis was performed using the Image J plugin OrientationJ (BIG). Images were imported into ImageJ and transformed into 16-bit monochromatic images. The fluorescent channels were separated by selecting Image > Color > Split Channels. The channels not corresponding to the CNA35 collagen-probe were closed (Fig.2.17).

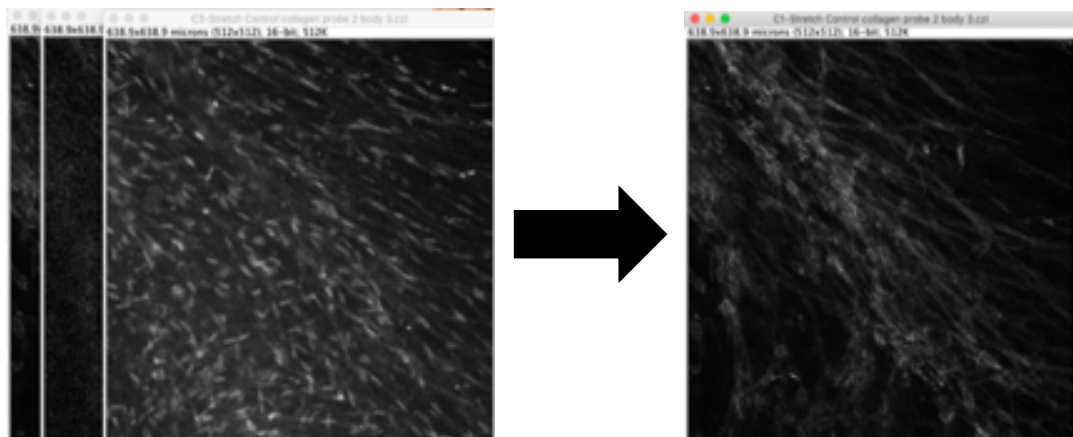


Figure 2.17. CNA35 image opened in Image J, channels split and non CNA35 collagen-probe channels closed.

Once the CNA35 channel was the only channel open the OrientationJ plugin was ready to be used. First the mode fibre angle was determined by selecting Plugin > OrientationJ > OrientationJ Dominant Direction. This value was later used to normalise the fibre angles across all images. Next all fibre angles were determined by selecting Plugins > OrientationJ > OrientationJ Distribution, from here the fibre angle was displayed as frequency of fibres at a particular angle, from -90° to 90° at 0.5° increments.

By subtracting the dominant direction from all values the mode across all images was normalised to 0° . To get all angles to lie between -90° to 90° any normalised angle that lay outside this range was either subtracted by 180° (if higher than 90°) or 180° was added to

the value if it was lower than -90° . The mean percentage frequency distribution was then found for each repeat sample and the mean was then found for each group for statistical analysis.

The angle distribution was visualised by selecting Plugin > OrientationJ > OrientationJ Analysis. Once ran a coloured representation of the original image is generated; here the fibres are designated a colour based on the angle of the fibre, the colour key is shown in Fig.2.18. The more aligned the fibres are in the image the more constant the colour is across the image, for example, 100% aligned fibres would all be one colour.

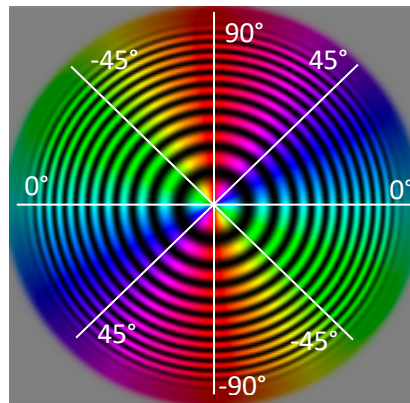


Figure 2.18. Colour key for OrientationJ images generation.

2.2.9. Mineralised Hydrogel Imaging by Micro-Computed Tomography

Following the completion of the experimental run (either one week of static culture followed by three weeks of hydrostatic pressure stimulation or three weeks of microgravity culture) six microtissues were randomly selected from each group and arranged within the imaging tube as required (Fig.2.19). Samples were spaced using cut polystyrene and the tube was sealed with parafilm.

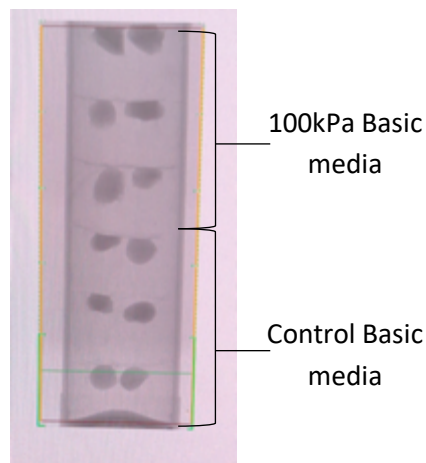


Figure 2.19. Example arrangement of samples in imaging tube for μ CT.

Samples were then scanned by μ CT using a Skyscan 1272 system (SKYSCAN, Belgium) with a rotation step size of 0.4° over 180° , an isotropic resolution set at $9\ \mu\text{m}$, X-ray source at 50 kV and $200\ \mu\text{A}$, 0.5 mm aluminium filter, 2x2 camera binning and average on. Images were reconstructed using Skyscan NRecon software (SKYSCAN, Antwerp, Belgium) which provides images of the analysed hydrogel slice-by-slice. Reconstructions were then reorientated in Skyscan's -Data-Viewer- software (SKYSCAN, Antwerp, Belgium) and volume of interest were selected for analysis. The volume of interested was then analysed using Skyscan CT-Analyser (SKYSCAN, Antwerp, Belgium) for mineralisation using a macro (details in Appendix G) with a fixed threshold to differentiate mineralised ECM from non-mineralised ECM. To find the hydrogel density the Skyscan 1272 system was calibrated using Bruker-MicroCT BMD calibration phantoms. The phantoms were supplied in pairs with concentrations of calcium hydroxyapatite of 0.25 and $0.75\ \text{g}/\text{cm}^3$. Due to the size of the hydrogels, 2 mm diameter phantoms were used (smallest available). Calibration was achieved using the attenuation coefficients following guidelines supplied by Bruker (Bruker-Mikro-CT, 2010). First the phantoms were imaged by the Skyscan 1272 system using the same settings as for the hydrogel samples. The image was then reconstructed using the NRecon software and region of interests generated using the -Data-Viewer- software. Finally the attenuation coefficient

was calculated using the CT-Analyser software with a macro (details in Appendix H) for both of the phantoms (found to be 0.029817 for the 0.25 g/cm³ phantom and 0.061498 for the 0.75 g/cm³ phantom), and this then factored into the density calibration. The density for the hydrogels was calculated using the same macro.

2.2.10. Tensile Mechanical Testing

Mechanical testing was performed on one sample from each tensile stimulation group (control, 3%, 5% and 10%) at the end of the three week loading phase from run 4, 5 and 6. To improve ease of handle of the engineered tendon, paper frames were used to hold samples in position (Fig.2.20). One paper frame was laid out on a flat surface and the engineered tendon sample was removed from the bioreactor chamber by breaking it away from the anchor frame before being laid lengthways in the middle of the paper frame. A second paper frame was then laid on top of the engineered tendon sandwiching it between the two frames (Fig.2.20).

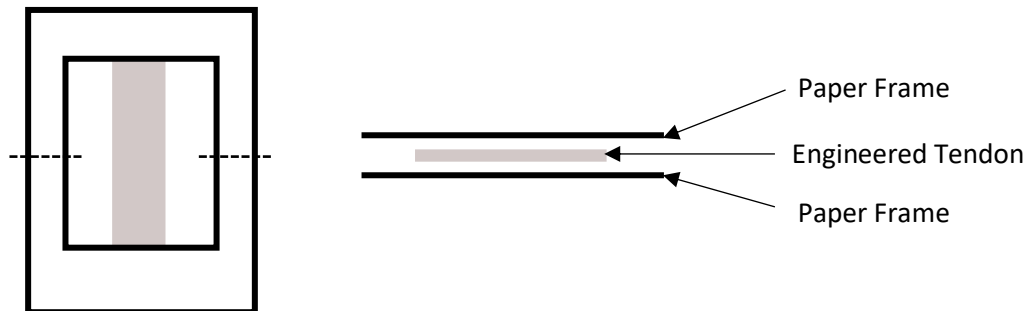


Figure 2.20. Schematic of fibrin hydrogel within paper frame.

Once the engineered tendon was secured within the paper frames it was moved to the tensile tester grips (Fig.2.21A). The system used for tensile testing was the Univert CellScale with a 1 N load cell. The fibrin hydrogels were tested for hysteresis, stress relaxation and stiffness, a graphical schematic of the testing regime is depicted in Fig.2.21B. Pre-conditioning was performed during the four cycles of hysteresis testing.

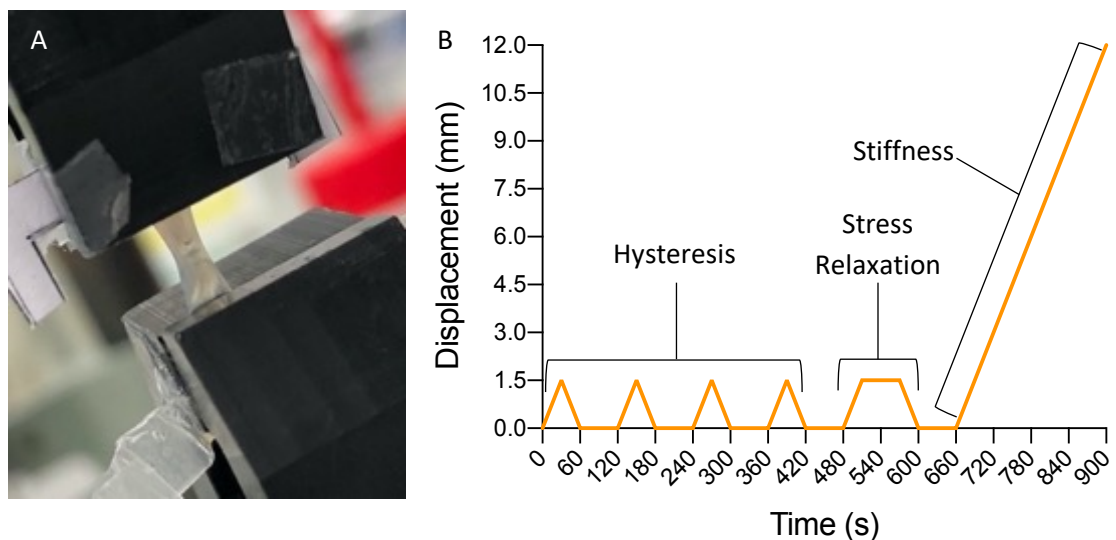


Figure 2.21. Tensile Mechanical testing. (A) Fibrin hydrogel sample loading into the Univert tensile tester (CellScale). (B) Graphical schematic of tensile testing loading regime

Following tensile testing the mechanical properties were calculated using the following equations:

$$\text{Stress: } \sigma = \frac{F}{A} \quad [6]$$

Where F is the recorded force and A is the cross sectional area (before loading)

$$\text{Strain: } \varepsilon = \frac{\Delta l}{l} \quad [7]$$

Where Δl is the change in length and l is the initial length

$$\text{Hysteresis (energy disipitated)} = \text{Area between curve} \quad [8]$$

$$\text{Hysteresis} = \text{Area below loading curve} - \text{Area below unloading curve}$$

$$\text{Percentage Energy loss} = \frac{\text{Hysteresis}}{\text{Area below loading curve}} \times 100 \quad [9]$$

$$\text{Rate of change of Stress} = \frac{\sigma_0 - \sigma_{60}}{T} \quad [10]$$

Where σ_0 is the initial stress (at 0s), σ_{60} is the final stress (at 60s) and T is the relaxation time (60s during this study).

$$\text{Young's Modulus: } E = \frac{\sigma}{\varepsilon} \quad [11]$$

2.3. Statistical Analysis

Cyclic Tensile Stimulation: A total of six experimental runs were performed, using three separate bioreactor chambers which were used for all loading conditions each to account for any hardware variation between bioreactor chambers. Samples taken for experimental repeats for each analysis were selected from across the six bioreactor wells by random determination using an online tool (www.random.org/sequences/) and varied across each run. In run #1, #2 and #3 two samples from each loading condition were taken for western blot analysis, and two samples for qPCR analysis, with two spare (n=6 total). In run #4, #5 and #6 one sample was taken for histology, one sample for collagen probe imaging, one sample for mechanical testing, and one sample for TEM with two spare samples (again n=6 total). One-way analysis of variance (ANOVA) with Tukey's post hoc test and multiple comparison tests was used for gene analysis, western blot analysis, collagen probe analysis and mechanical testing all carried out using GraphPad Prism 9. Where residuals did not meet assumptions of normality (Shapiro-Wilk test) or equal variance (Brown-Forsythe test) data were transformed before analysis. Two-way ANOVA with Tukey's post hoc test and multiple comparisons was used for the Alkaline Phosphatase analysis after data was confirmed to be normally distributed and equal variance confirmed with Spearman's test. Non-parametric data was analysed using the Kruskal-Wallis test.

Statistical analysis of collagen fibril diameters using TEM was undertaken in R (R, Version 4.0.3) (RCoreTeam, 2020) and performed by Mr. Daniel Green (University of Liverpool). The lmer function from the package lme4 was used to fit linear mixed models to assess differences in measured outcome variables between different loading conditions (Bates et al., 2015). In all cases, the measured outcome was specified as the response variable, the loading condition as the fixed effect and the run of the experiment as the random effect. For TEM analysis the means of the minimum diameters were determined for each image and different images accounted for with the specification of run as a random effect. Estimated marginal means and Tukey adjusted p values were extracted using the emmeans package (Lenth, 2020).

Hydrostatic Pressure: Samples taken from experimental repeats for each analysis were selected by random determination using an online tool (www.random.org/sequences/). One-way ANOVA with Tukey's post hoc test and multiple comparison tests was used for gene analysis of COL9A1 and COL24A1, densitometry for collagen $\alpha 1(XI)$ and the Alizarin red assay. Where residuals did not meet assumptions of normality (Shapiro-Wilk test) or equal variance

(Brown-Forsythe test) data were transformed before analysis. Two-way ANOVA with Tukey's post hoc test and multiple comparisons was used for all remaining analysis after data was confirmed to be normally distributed and equal variance confirmed with Spearman's test. Where residuals did not meet assumptions of normality or equal variance data were transformed before analysis non-parametric data was analysed using the Kruskal-Wallis test. All statistical analysis was carried out using Prism 9.

Microgravity culture: Samples taken from experimental repeats for each analysis were selected by random determination using an online tool (www.random.org/sequences/). One-way ANOVA with Tukey's post hoc test and multiple comparison tests was used for gene analysis, western blot analysis, sample weight and μ CT analysis. Principle component analysis (PCA) on the genes was based on eigenvalues and carried out in Prism 9. Where residuals did not meet assumptions of normality (Shapiro-Wilk test) or equal variance (Brown-Forsythe test) data were transformed before analysis. Two-way ANOVA with Tukey's post hoc test and multiple comparisons was used for ALP analysis after data was confirmed to be normally distributed and equal variance confirmed with Spearman's test. Non-parametric data was analysed using the Kruskal-Wallis test. All statistical analysis was carried out using Prism 9.

Chapter 3

**Design and validation of 3D printed universal
tensile bioreactor chamber**

3.1. Introduction

3.1.1. Bioreactors for Tendon Tissue Engineering

One of the fundamental obstacle to research in tissue engineering is the variety of bioreactors available, with very few research groups using identical or comparable platforms. This is highly apparent with tensile stimulation bioreactors were studies typically use custom made tensile bioreactors or commercially available systems such as the EBERS TC-3 and CellScale MC series. A search of literature published between January 2016 and March 2020 indicates that for cyclic loading studies focusing towards tendon tissue engineering, three groups published data generated using a CellScale bioreactor (Garcia et al., 2018, Wu et al., 2017, Sensini et al., 2019) and one group published using an EBERS TC-3 bioreactor (Deniz et al., 2020), with over twenty using custom designed bioreactors (Burk et al., 2016, Talò et al., 2020, Raveling et al., 2018, Engebretson et al., 2018, Youngstrom et al., 2016, Qiu et al., 2016, Carroll et al., 2017, Grier et al., 2017, Subramanian et al., 2017, Brandt et al., 2018, Lee et al., 2018, Liu et al., 2018, Patel et al., 2018, Raimondi et al., 2018, Wunderli et al., 2018, Grier et al., 2019, Hsiao et al., 2019, Atkinson et al., 2020, Banik and Brown, 2020, Ciardulli et al., 2020, Tohidnezhad et al., 2020). Furthermore, many research groups are moving towards combination strategies for tissue engineering, using increasingly complex combinations of scaffolds, cells and biomolecules. A clear requirement for greater reproducibility and consistency in approach is needed to enable repeatable consistency between these different approaches for both research and translation towards clinical therapies.

Regardless of the specific bioreactor (commercial brand or custom-built), all of these systems share similar design characteristics: a culture chamber enabling mechanical stimuli to be applied to the cells in a sterile environment, with the force applied by a linear actuator controlled by displacement software. To apply tensile forces to cells, the biological material must form an interface with the loading hardware *via* a direct friction grip or clamp, pinning a mature (usually *ex vivo*) tissue in place, or incorporation of the biological sample with a loading anchor during the formation of the tissue. In most tensile bioreactors, one end of the sample is typically held in a fixed position, while the second is attached to a linear actuator, permitting movement in just one axis.

3D printing is a now established technology for rapid prototyping and manufacturing of simple and complex parts and components. Usefully for the research community, it also enables free sharing of designs, tools and technologies to facilitate greater reproducibility of

experimental approaches and methodology. Here 3D printing has been used to design and test an optimised bioreactor chamber for engineering tissues under cyclic tensile loads. The first of these design criteria were that the bioreactor culture chamber should have six isolated wells to enable either simultaneous stretching of up to six differently treated samples, or an effective $n=6$ number of experimental repeats. This design criterion was paramount since many commercially available bioreactor chambers have a single unsegregated volume which does not allow for statistically distinct repeats (Carroll et al., 2017, Wu et al., 2017). This also overcomes a limitation imposed by the conventional single-well set up, which necessitates serial rather than parallel experimental runs and forces a compromise between experiment loading time and n -number. Based on the available literature, it was determined that each of the six wells should have a displacement volume of 6 ml to allow the culture of a variety of engineered tissues, whilst ensuring the tissues can remain submerged in 3-5 ml culture media subject to the application, for example, the size of the engineered tissue construct. The media volume was carefully considered based on the volumes typically used in a 6-well cell culture plate, and optimised to provide sufficient nutrient availability and buffering during culture, whilst minimising media wastage.

3.2. Hypothesis

3D printing will allow the design and fabrication of a universally usable bioreactor chamber that, with minimal manipulation, can be fitted to a wide range of custom and commercially available systems.

3.3. Aims

1. To design and manufacture a 3D printable system that allows for user friendly and reproducible cyclic uniaxial tensile stimulation.
2. Investigate the bio-compatibility of the fabrication materials for cell culture

3.4. Bioreactor Chamber Fabrication

3.4.1. 3D Printing

All prototypes and final components were designed using Creo Parametric (Fig.3.1). The designs were saved as an STL (StereoLithography) file and exported to CURA (Fig.3.2), where the software converts STL files to gcode files that can be read by the Ultimaker 2+ for 3D printing.

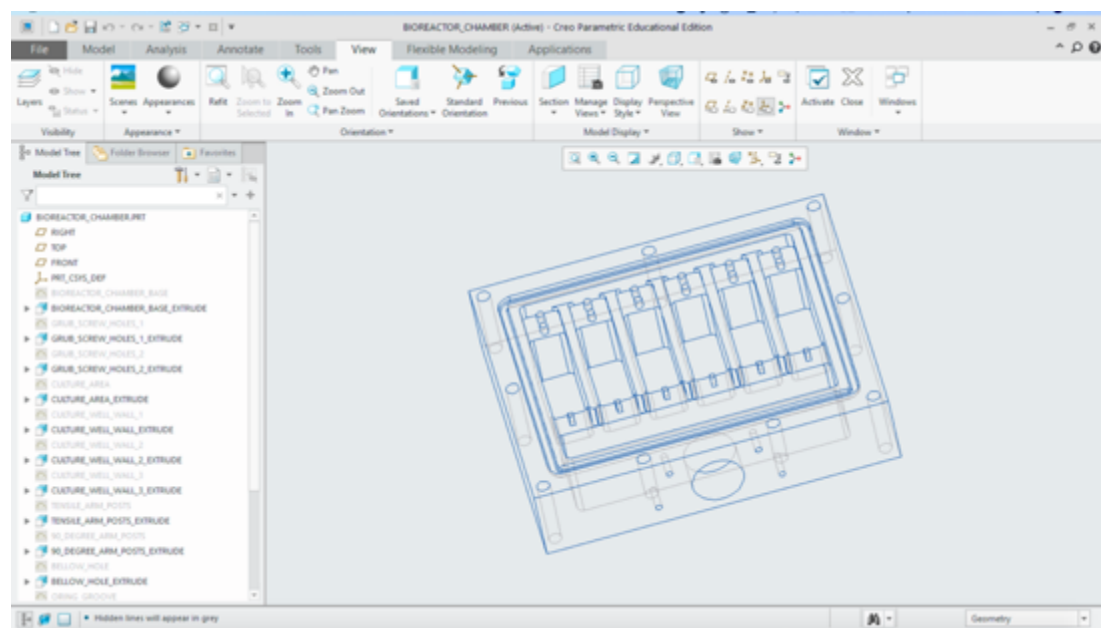


Figure 3.1. Bioreactor chamber CAD during design process in Creo Parametric.

For prototype prints the print settings were maintained as default; 0.4 mm nozzle, PLA filament, fine (0.1 mm) layer height and 100% infill (Fig.3.2A). Print setting for the bioreactor chamber were changed to reduce the time taken to complete the printing. If the print settings were maintained the main body would have taken two days, 14 hours and 54 minutes to 3D print. By increasing the nozzle size to 0.6 mm, increasing the layer height to 0.15 mm and reducing the infill to 40% the print time reduced to 12 hour and 58 minutes without compromising the quality of the print (Fig.3.2B). This option isn't available for smaller components as the larger nozzle doesn't have the resolution to print the more detailed sections.



Figure 3.2. CAD on CURA software. (A) 3D printed anchor post mark 5 generated in CURA. (B) Main body of culture chamber mark 1 design generated in CURA

For the final designs of the culture chamber three components required 3D printing: the chamber body, the 6-way tensile arm and the tensile runner (Fig.3.11). The print settings for the chamber body were (this includes support prints and no brim):

- Nozzle diameter – 0.6 mm
- Filament – PLA
- Layer height – 0.15 mm
- Infill – 30%

This took 23 hours and nine minutes to print using 243 g (30.72 m) of PLA filament.

The print setting for both the 6-way tensile arm and tensile runner were (this includes support prints and no brim):

- Nozzle diameter – 0.4 mm
- Filament – PLA
- Layer height – 0.1 mm
- Infill – 50%

The 6-way tensile arm took six hours and 15 minutes to print using 29 g (3.63 m) of PLA filament. The tensile runner took six hours and 12 minutes to print using 33 g (4.15 m) of PLA filament.

In total the 3D printed components took 35 hours and 36 minutes to print using 305 g (38.5 m) of PLA filament. To print with the ultimaker 2+ using PLA filament the build plate was first coated with glue stick, and then heated to 60°C. The nozzle was heated to 210°C to allow the PLA filament to extrude through. Once all components reach temperature the 3D printer automatically begins to print the component.

Once printed, finishing was applied to all components. Any support structures were cut away and rough areas were filed down. Thread inserts were installed using a pillar drill (on the top face for the grub screws and rear face for the tensile arm runner screws). The interior of the chamber body was coated with XTC-3D 'Smooth on' High Performance 3D print coating (an oxirane epoxy resin used to waterproof the chamber), cured overnight and washed with PBS. The XTC-3D was prepared as specified by the manufacturer; part A (resin) and part B (hardener) were mixed at a ratio of 2:1 and applied as a thin coat to the base and walls of each culture well. The chamber was then left to cure overnight. The base of each culture well was then coated with polydimethylsiloxane (PDMS) Sylgard-184 to prevent the cell embedded hydrogels from sticking to the well base during loading. The Sylgard-184 was prepared according to the manufacturer's instructions, and mixed with the curing reagent at a ratio of 9:1 in a 50 ml centrifuge tube, then left to mix on a rotomixer for 10 minutes at room temperature. 1 ml of the Sylgard-184 mixture was pipetted into the base of the culture well and a level coating was ensured by placing the chamber on a flat surface, then left to cure for three days at room temperature. Degassing was not required as bubbles were not observed in either the XTC-3D or the Sylgard-184. Once the XTC-3D and Sylgard-184 were fully cured and hardened the culture wells were washed through six changes of PBS to remove any residual cytotoxic monomers.

3.4.2. 3D Printed Culture Chamber Validation

3.4.2.1. 6-Way Tensile Arm Displacement

The displacement of the 6-way tensile arm was measured by monitoring the controlled movement of the arm and relating the observed displacement to the expected displacement. The bioreactor chamber was mounted onto the EBERS-TC3 base platform and attached to the linear actuator which was controlled by the EBERS software. The 6-way tensile arm was displaced in 5% iterations of the initial length of the fibrin hydrogel (8 mm). The displacement of the tensile arm was measured using a HD USB camera (MicroDirect, Celstron) (Fig.3.3), distances calculated using ImageJ/Fiji and analysed using GraphPad Prism 9.

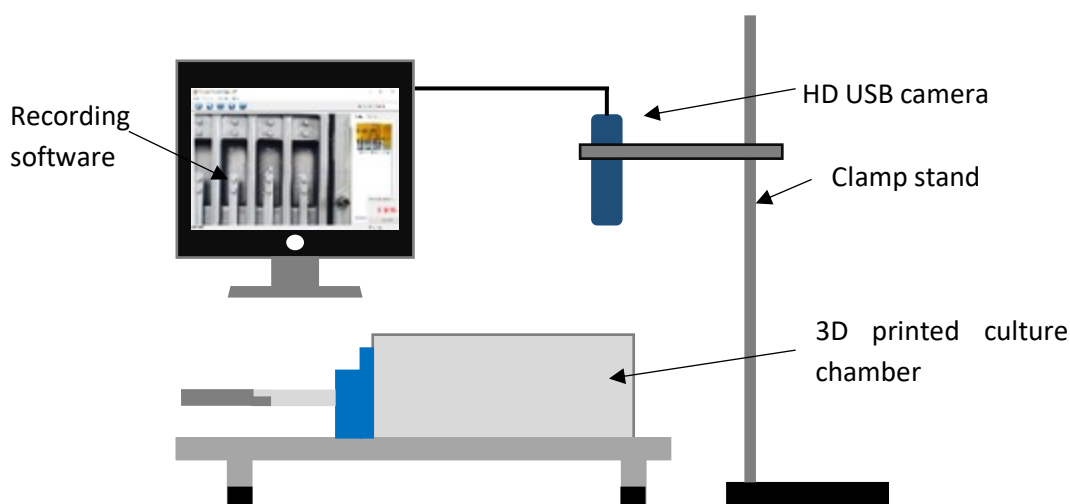


Figure 3.3. Schematic of displacement measurements for chamber validation.

3.4.2.2. Chamber Cytotoxicity

The lactate dehydrogenase (LDH) assay (Pierce, Thermo Scientific) was used to determine biocompatibility of the materials which interfaced with the cell culture media – PLA, XTC-3D 'smooth on' oxirane epoxy resin, and PDMS Sylgard-184. hMSCs (passage 3) were seeded in triplicate in wells of a 12-well plate at a density of 1.5×10^5 cells/ml and allowed to attach for 12 hours. Separately pieces of PLA and XTC-3D oxirane resin coated PLA (5 mm x 5 mm x 1 mm, ~5 g) were added in triplicate to experimental wells. In this initial test the XTC-3D oxirane resin was only washed once in PBS. The cells were incubated with the materials overnight and compared to unmodified control wells. The LDH activity within the media was quantified using the SPECTROstar Nano microplate reader (BMG LABTECH). The biocompatibility/cytotoxicity assay was then repeated using the fully coated, cured and washed bioreactor chamber, which included both the XTC-3D oxirane resin-coated walls and the Sylgard-184 coated well bases. The 3D printed culture chamber was sterilised with 70%

ethanol: initially all components were disassembled and washed in 70% ethanol before drying within a sterile cell culture hood for one hour. Once dry the 3D printed culture chamber was assembled and washed in 70% ethanol again and left to dry in a flow hood, washed again three times with PBS and left to dry. hMSCs were seeded onto cover slips at a density of 1.5×10^5 cells/ml and placed in the bioreactor wells, then incubated overnight at 37°C and assayed for LDH activity as described above.

3.5. Results

3.5.1. Development of Bioreactor Chamber

3.5.1.1. Anchor Post Design

Initially the anchor frame was considered the anchor post and went through a number of iterations (Table 3.1) to develop a design that would meet the design criteria.

Design Criteria - A rigid post that allows for a fibrin hydrogel to contract into a tendon like structure. Once contraction is complete the anchor post should attach to a tensile stimulation bioreactor to allow the stimulus to be applied to the fibrin hydrogel. The 3D printed posts should allow for consistent printing using the Ultimaker 2+ with high porosity within the attachment site (porosity >30%).

The porosity of initial designs (mark 1-5) was calculated using the equation:








$$Pt = \frac{V_p}{V_t} \quad [12]$$

Where Pt is the porosity, Vp is pore volume and Vt is the total volume. The volumes were calculated from only the attachment site, therefore excluding the solid section at the top of the anchor post. From the design criteria, posts mark 1 and 2's porosity was below the minimum requirement (30%) and were excluded.

The posts needed to be consistently printed. The consistency was measured by printing five of posts mark 3, 4 and 5 and judging the quality of the prints. Posts mark 3 and 4 did not print consistently with many of the holes throughout the structure being solid rather than open. Post mark 5 printed to a high consistency with low levels of post printing finishing required.

Bubbles formed when generating fibrin hydrogels within Post mark 5, this resulted in the hydrogel easily breaking. To prevent bubbles from forming within the hydrogel, a chamfer was added to the roof of the attachment site (post mark 6), allowing any bubbles to easily escape. When loading began with post mark 6 system it was found that the fibrin hydrogel 'peeled' away from the anchor post as only a small amount escaped the porous area. By removing half of the front face of the post, more of the hydrogel protruded generating a more stable structure and allowing stimulation to be applied without the hydrogel failing (mark 7).

Table 3.4. Design iterations of the 3D printed posts. Porosity measured using [Equation 12] and build quality measure by 3D printing five identical repeats.

Render							
Name	Anchor post mark 1	Anchor post mark 2	Anchor post mark 3	Anchor post mark 4	Anchor post mark 5	Anchor post mark 6	Anchor post mark 7
Porosity (%)	26.3	22.7	35.3	38.4	34.3	35.3	36.5
Build quality	Medium	Medium	Low	Low	High	High	High

3.5.1.2. Initial Concept Designs for 3D Printed Posts and Loading Supports

Anchor post mark 7 was taken forward to the loading phase. Initially two mark 7 posts were arranged within a six well plate and an alignment bridge was placed on top (Fig.3.4A). The alignment bridge ensured uniform positioning of the anchor posts and therefore a uniform length of the fibrin hydrogels. The fibrin hydrogels formed around the anchor posts and contracted to form tendon like structures (renders representation shown in Fig.3.4B). Once contracted the hydrogels were transferred to a bioreactor attachment and fixed in place via the anchor post (Fig.3.4C). The samples within the bioreactor attachments were then transferred into the EBERS TC-3 tensile culture chamber using sterile forceps. The 3D printed bioreactor attachment was fixed in place with 3D printed pins (Fig.3.4D). The culture chamber was then placed onto the EBERS TC-3 for tensile stimulation (Fig.3.4E). Once tensile stimulation was complete the process was reversed.

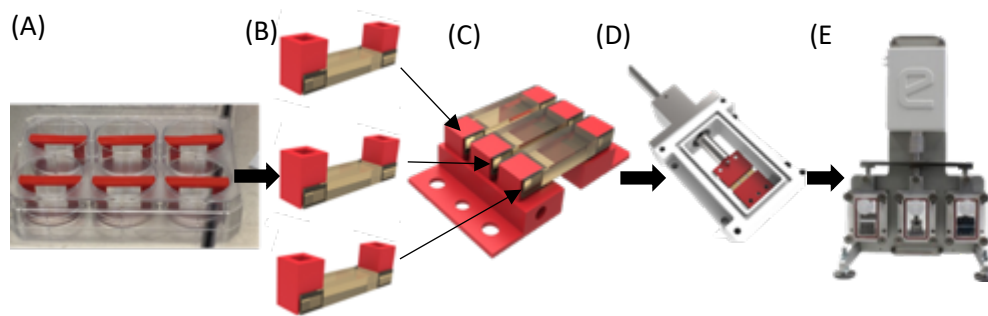


Figure 3.4. Schematic of the anchor posts from culture plate to bioreactor. (A) Anchor post layout in well plate before fibrin generation. (B) Render of fibrin hydrogel between anchor posts. (C) Fibrin hydrogels placed into bioreactor attachment via anchor posts. (D) Anchor posts within bioreactor culture chamber attached via bioreactor attachments. (E) Culture chamber mounted into EBERS TC-3 bioreactor

The anchor post was further edited (Fig.3.5) to overcome the faults of the previous design; primarily the unintentional movement of the hydrogel when moving between the six well plate and culture chamber. This was achieved with the addition of handles on the top of the anchor post. The alignment bridge fitted around the handles ensuring uniform fibrin hydrogel formation. Once the contraction was complete the fibrin hydrogel was picked up with sterile forceps with the alignment bridge in place, preventing the fibrin hydrogel for moving from its fixed position. The anchor post were designed to have an attachment point built in rather than needing the bioreactor attachment system. With these updates the fibrin hydrogels formed around the anchor posts and contracted to form the tendon like structure as before. The sample was then fixed into the EBERS TC-3 culture chamber (Fig.3.5C) with 3D printed pins (Fig3.5A). Samples remained in the culture chamber during loading before being placed back into the six well plate. This design completely removed the mid step of the bioreactor attachment.

However samples became infected within one week of entering the EBERS TC-3 culture chamber. The cause of infection was investigated to see if it was due to moving the samples between the culture chamber and six well plate before and after each tensile stimulation run (5% strain for 1 hour). The fibrin hydrogel was allowed to contract within the six well plate before moving into the culture chamber in triplicate where the samples remained for the loading regime (3 weeks). However, even with this mitigation the samples still became infected within one week. An alternative theory was that the flexible airtight membrane (the bellow) (Fig.3.5D) used to allow the tensile arm to move within the culture chamber whilst maintaining sterility was generating a liquid bridge for bacteria to travel.

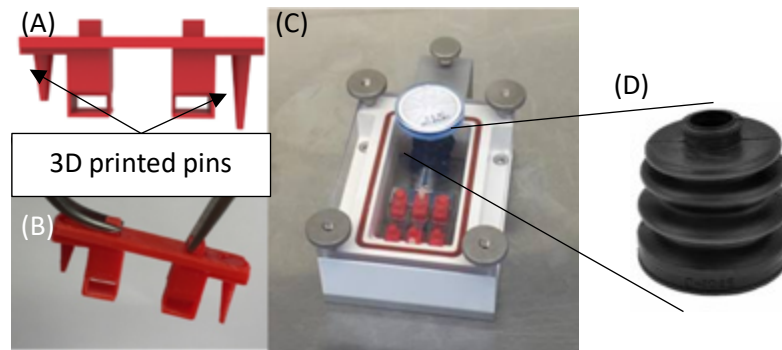


Figure 3.5. Anchor post in EBERS TC3 chamber. (A) Render of the updated anchor posts, the top of the post features a handle and the top rear of the posts features a built in bioreactor attachment site. An alignment bridge held the two anchor posts in place and pins ran through the alignment bridge and into the built in bioreactor attachment sites. (B) Example of how the system would be moved with sterile forceps. (C) Three sets of anchor posts fixed in place within the EBERS TC-3 bioreactor. The below has been highlighted to show assumed infection source.

3.5.1.3. Bioreactor Chamber Design mark 1

As the EBERS TC-3 culture chamber was being over manipulated to facilitate the anchor posts it was no longer a viable option for the experimental needs. A 3D printed bioreactor chamber was designed to accommodate the anchor posts and mount onto pre-existing bioreactor systems.

Design Criteria - The bioreactor chamber should have a minimum of three isolated culture wells and should not have a bellow that is submerged in cell culture media. The design should require minimal edits to allow it to mount onto a number of pre-existing bioreactors. The system should be able to be manufactured by 3D printing using bench top 3D printers (e.g. Ultimaker 2+) with minimal post manufacturing finishing required.

The first design of the bioreactor culture chamber was designated mark 1 (Fig.3.6). The system was composed of ten main components: The main body, the transparent base, the transparent base housing, the 6-way tensile arm, the arm housing, bellow barrier, the EBERS TC-3 arm and the lid (not shown in Fig.3.6). The main body, transparent base housing, bellow barrier, 6-way tensile arm and the arm housing were all 3D printed using the Ultimaker 2+ with PLA filament. The transparent base and lid were manufactured using transparent polycarbonate sheet machined using a milling machine and pillar drill. This design used pre-existing components from the EBERS TC-3 (EBERS TC-3 arm and runner) to ensure it would fit onto the EBERS TC-3. The sub-components were acquired as off the shelf parts and included: the O-rings, bellows, grub screws, thumb nuts and screws.

Once all the components were 3D printed and machined, screw threads were tapped to allow the screws to fix components together and grub screws to fix in place. However when fixing the components (main body, transparent base housing, bellow barrier, arm housing and EBERS TC-3 runner) with the screws it was found the resolution and consistency of the Ultimaker 2+ was not tight enough to ensure all components were printed exactly as the CAD designs specified. This prevented tight seals to form when mating two parts which is vital to create a sterile environment for cell culture. The mark 1 design was therefore not a viable option as a sterile environment could not be generated without substantial finishing.

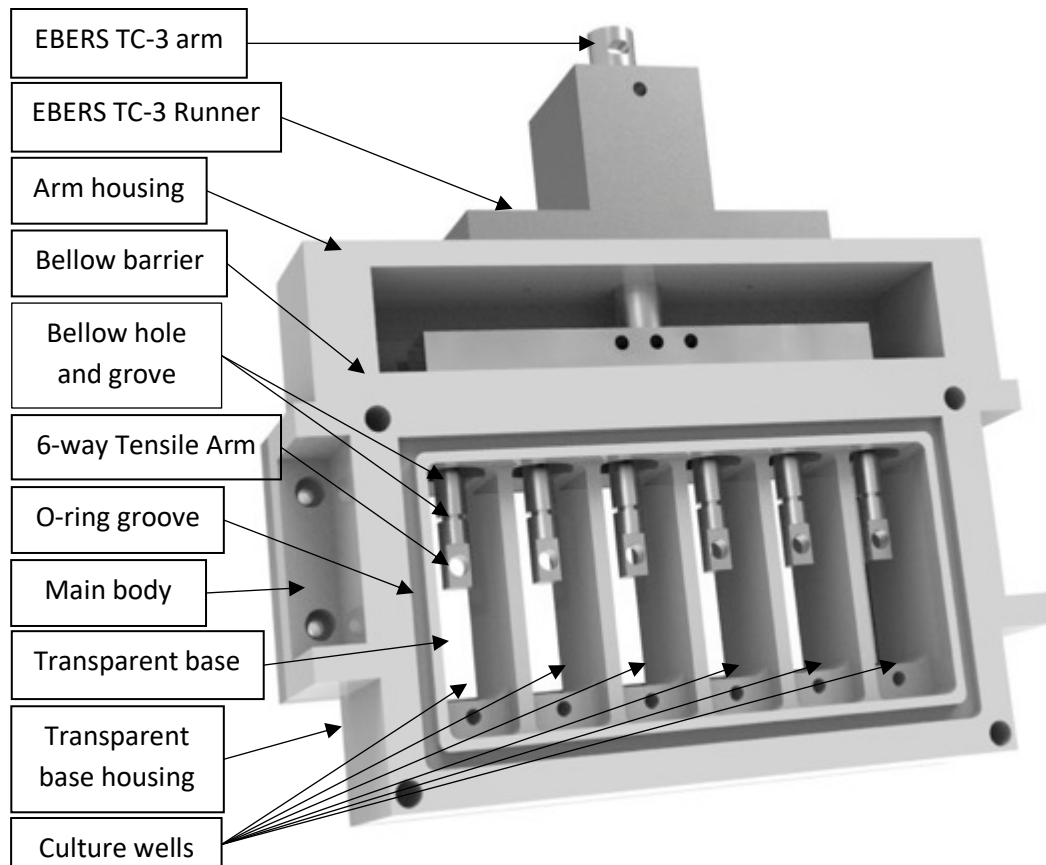


Figure 3.6. Initial design of 3D printed bioreactor chamber. The system included the runner from the EBERS TC-3 culture chamber and the tensile arm which connected to the 6-way tensile arm. The arm housing allowed for detachment from the chamber, allowing for multiple chambers to be used at once. The 6-way arm ran into six culture wells each with a bellow to provide a flexible air tight membrane. The main body connected to the transparent base via screws and sealed with an O-ring. The O-ring slotted into an O-ring groove on the base of the main body. Six culture wells allowed for isolated culture of hydrogels. A sterile seal at the top of the main body was provided by fixing the lid over grub screws with thumb nuts over a second O-ring placed into the upper O-ring groove.

3.5.1.4. Bioreactor Chamber Design mark 2

The complexity of the bioreactor chamber mark 1 design resulted in the 3D printed components not correctly mating preventing a sterile seal from forming. Mark 2 (Fig.3.7) was designed to limit the number of components as much as possible. Here the design was made up of four main components as opposed to ten in the mark 1 design. The four components were: the chamber body, the 6-way tensile arm, the tensile runner and the lid (shown in Fig.3.7B). The design removed the bellow from the culture wells and into a separate sterile area of the main body, this prevented the culture media generating a liquid bridge with the bellow.

3D printing was used to manufacture the chamber body, the 6-way tensile arm and the tensile runner. The lid was machined from polycarbonate sheet using a milling machine and pillar drill by Mr James Blackhurst in the William Henry Duncan building workshop (University of Liverpool). Sub components were acquired as off the shelf parts: the O-ring, the bellow, the grub screws and the screws.

Fig.3.7B shows a separated view of the mark 2 design post manufacturing. The 3D printed components, the 6-way tensile arm and chamber body were initially manufactured using PLA filament. The chamber body required minimal finishing (thread tapping and removal of support structures produced during 3D printing) to allow the mating of other components. Once tapped nine grub screws fixed into place around the perimeter of the chamber body. The O-ring slotted into the O-ring groove on the top face of the chamber body. The lid had nine holes drilled using a pillar drill around the perimeter that were complementary to the grub screws holes on the chamber body, allowing the lid to fit onto the chamber body. The lid was then fixed in place with nine thumb nuts, creating an airtight seal with the O-ring. Two holes were drilled and tapped on the lid above where the culture wells would be situated when the lid is fixed in position. The two holes allowed for two 0.2 μm nylon syringe filters to lock into Luer locks. This allowed for sterile air to circulate into the chamber body and culture wells. The bellow, acting as the flexible seal, fitted onto the 6-way tensile arm. The bellow and 6-way tensile arm then ran through the bellow hole into the chamber body. The tensile runner fitted onto the 6-way tensile arm and screwed into the rear of the chamber body creating a seal with the bellow. The tensile runner held the 6-way tensile arm in position whilst allowing for controlled linear movements into and out of the chamber body.

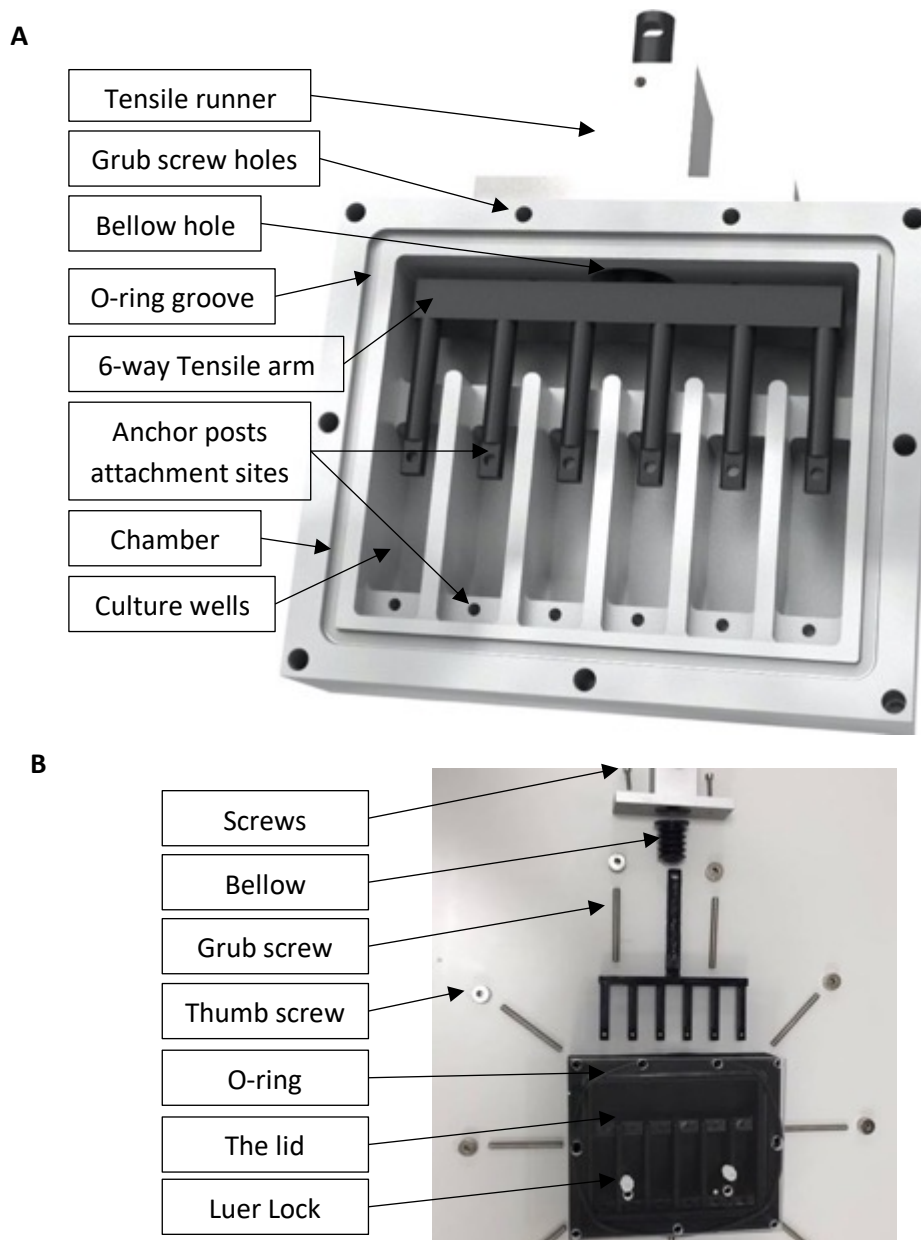


Figure 3.7. Bioreactor chamber mark 2. (A) The mark 2 design. Using a 3D printed tensile runner and 6-way tensile arm instead of the EBERS TC-3 parts, allowed for multiple systems to be printed and used at the same time. (B) Separated view of manufactured bioreactor chamber mark 2.

3.5.1.4.1. Updated Anchor Posts

The anchor posts shown in Fig.3.4 were updated to not require the culture period in a six well plate. Instead the anchor post were installed within the chamber body and the fibrin hydrogel was formed and contracted directly within the bioreactor chamber. This was achieved by adding a barrier to the rear of one of the anchor posts in the pair (Fig.3.8A). The barrier was designed to maintain a consistent length of fibrin hydrogel across all culture wells by preventing the fibrin from running past it. The anchor post featuring the barrier was attached to the 6-way tensile arm whilst the anchor post without the barrier is placed onto the chamber body (Fig.3.8B). The base of the anchor posts were reduced to allow better contraction around the post rather than sticking to the base.

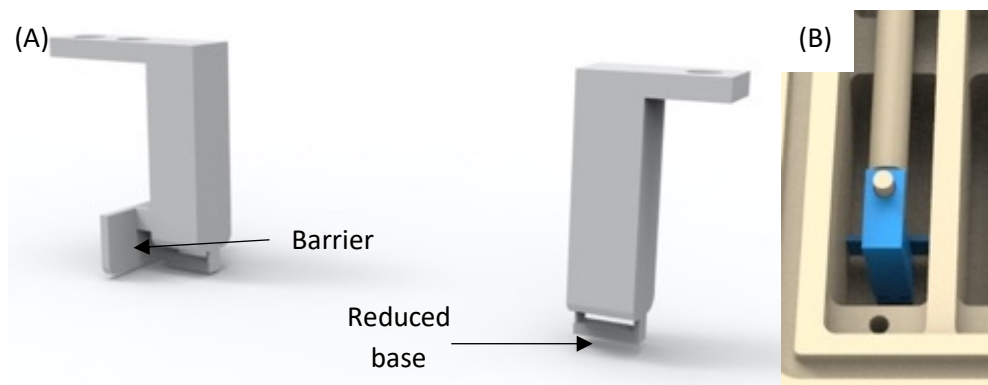


Figure 3.8. Render of updated anchor posts. (A) Rear of one anchor post features a barrier to ensure the fibrin hydrogel dimensions are consistent across all culture wells. Base of anchor post was removed to allow better contraction of fibrin hydrogel around the post. (B) Anchor post with barrier was placed within culture well. Barrier prevents fibrin hydrogel from running beyond set point controlled by the position of the 6-way tensile arm

3.5.1.5. Bioreactor Chamber Design Mark 2.1

Due to only one attachment post on each arm of the 6-way tensile arm and chamber body the anchor posts rotated away from intended position. This was overcome by adding an extra attachment point to the 6-way tensile arm and chamber body. An extra attachment hole was added to the anchor posts attachment sites (Fig.3.9). These additions generated the bioreactor chamber design mark 2.1, the final design.

The dimensions of the final bioreactor chamber are shown in (Fig.3.10). The main dimensions include:

The culture well – 40 mm x 15 mm x 11.5 mm, holding up to 6.9 ml of culture media.

The 6-way tensile arm run – 30 mm x 23 mm x 90 mm, when the 6-way tensile arm is installed it can move backwards and forwards by 8 mm.

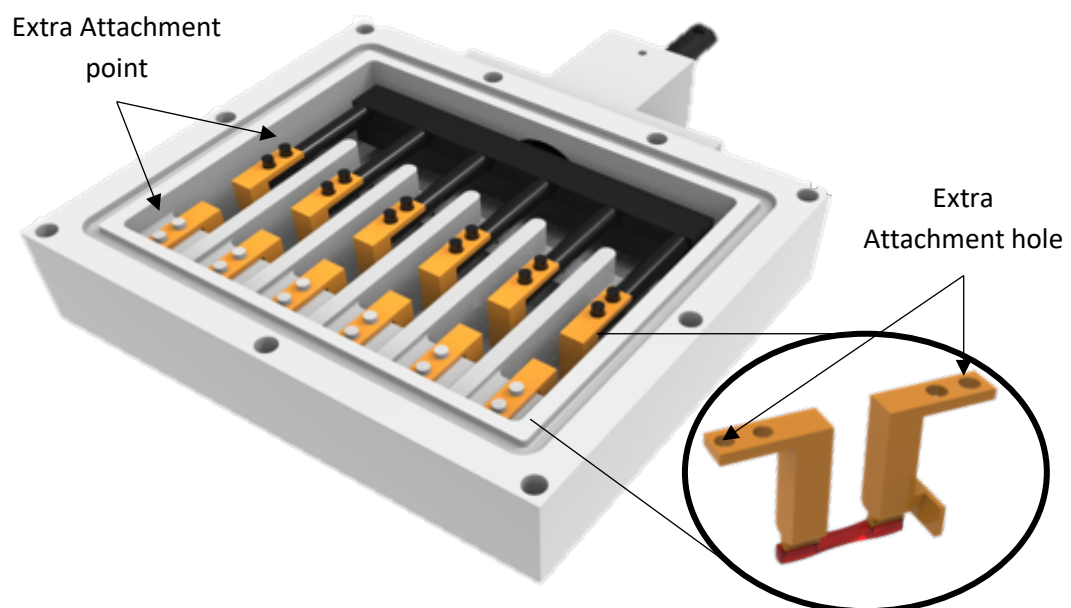


Figure 3.9. Render of updated bioreactor chamber and anchor posts. Extra attachment points have been added to the chamber body and an extra holes added to the attachment sites on the anchor posts.

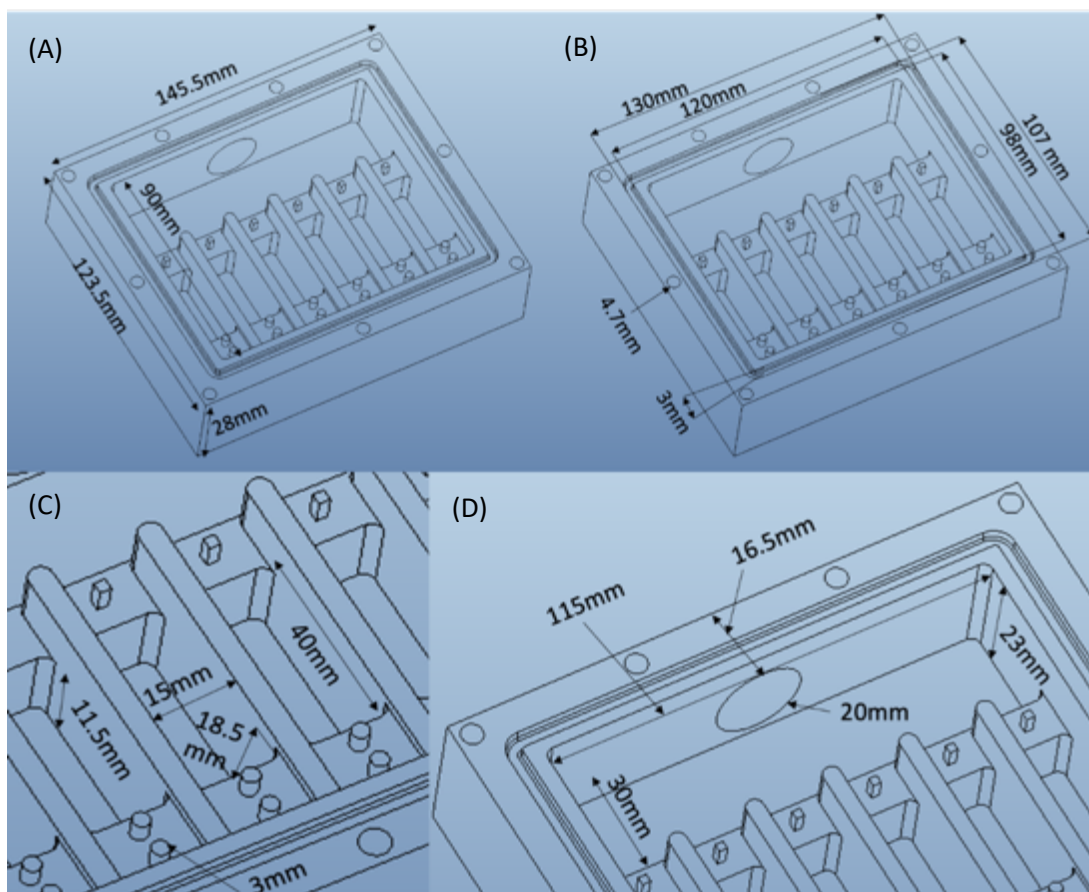


Figure 3.10. Dimensions of bioreactor chamber body mark 2.1. (A) Outer dimensions of chamber body and internal length of chamber body. (B) O-ring groove dimension and grub screw tap hole diameter. (C) Culture well dimension and attachment pin dimension. (D) 6-way tensile arm run area and bellow hole dimensions

The mark 2.1 design for the bioreactor chamber was taken forward as the final design. As in the mark 2 design the bioreactor chamber was made up of four main components. Fig.3.11Ai shows the CAD drawings of the 3D printed main components: the chamber body, 6-way tensile arm and tensile runner. The fourth main component, the lid, is shown in Fig.3.11B, and is identical to the mark 2 design. The sub-components (Fig.3.7B) were all acquired as off the shelf parts: the bellow, grub screws, thread insert, thumb screw, O-ring, Luer lock and screws. A list of components is shown in Table 3.2. The PLA grub screw holes were able to be threaded but not consistently, thread inserts were therefore used to fix the grub screws in place. The O-ring slotted into the O-ring groove, the lid then slotted onto the grub screws via complementary holes (Fig.3.11Aii) and was fixed in place via thumb nuts forming an airtight seal with the O-ring. The lid featured two threaded holes over the culture wells that Luer locks fix into, allowing for the fixing of two 0.2 μm nylon syringe filters for sterile air exchange. The bellow fitted onto the 6-way tensile arm and both slotted through the bellow

hole and were held in place by the tensile runner which fixed onto the chamber body via screws, creating an airtight seal with the rear of the bellow.

Following 3D printing the only steps required before the system was ready to use was to remove the 3D printing structural support, the insertion of the thread inserts, sealing the system with the XTC-3D waterproof resin and the addition of 1 ml of Sylgard 184 to each culture well.

The bioreactor chamber was designed to mount onto a wide range of commercial and custom tensile stimulation bioreactors with minimal edits. Fig.3.11B shows the bioreactor culture chamber mounted onto the EBERS TC-3. The 6-way tensile arm attaches to the bioreactors linear actuator, which is operated via a well-established software. The chamber body mounts onto the bioreactor via alignment pins and thumb screws. The bioreactor chambers CAD model was adapted to mount onto the CellScale MCT6 (Fig.3.11C). This was only done as far as the CAD design, which was not subsequently 3D printed therefore the adapted chamber was never mounted onto a real CellScale MCT6. For the CAD model to theoretically mount onto the MCT6, changes needed to be made to the base of the chamber body, the length of the tensile runner and the attachment point of the 6-way tensile arm. A separate part was developed to fix the linear actuator to the 6-way tensile arm. These edits took around 3 hours to implement.

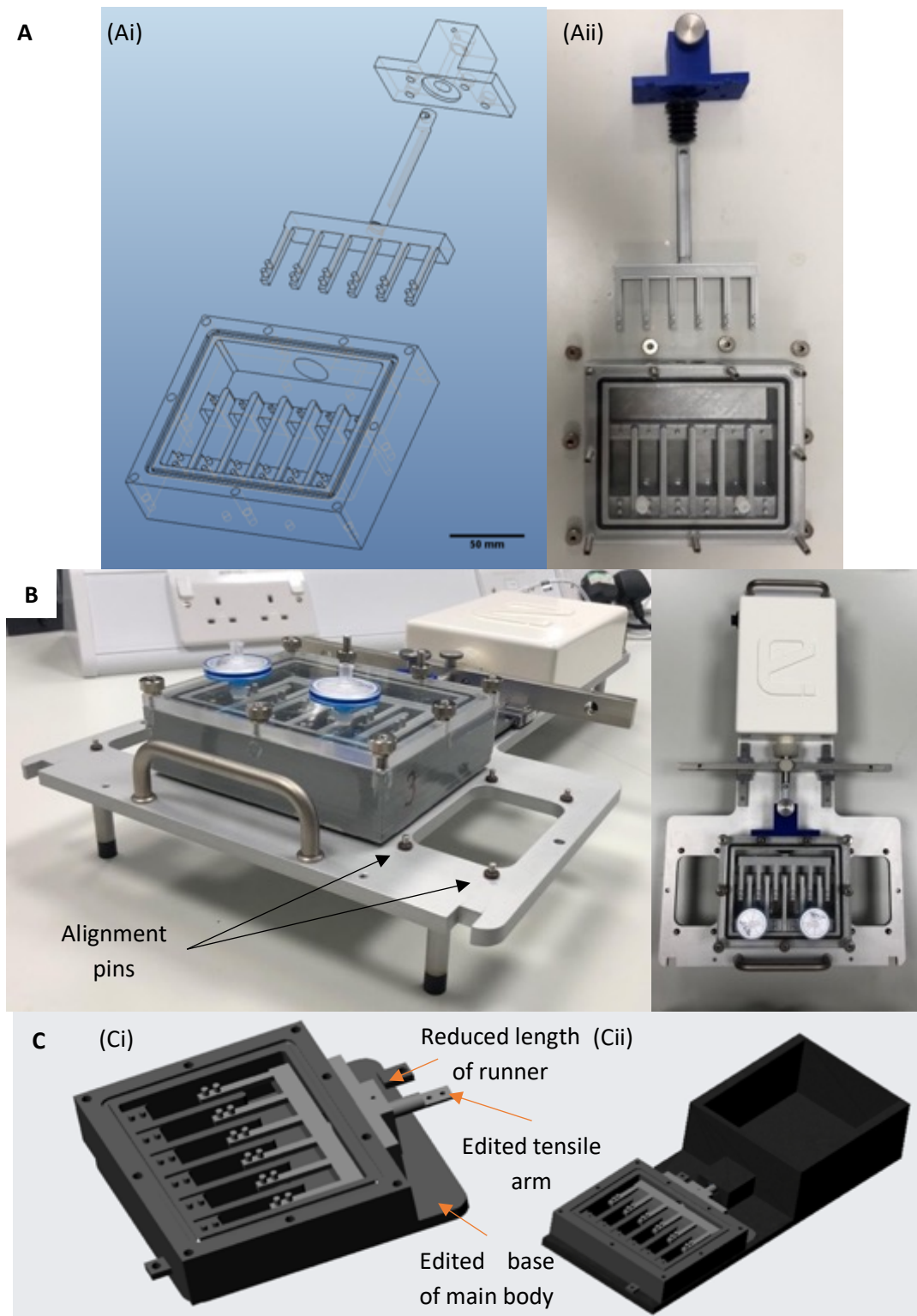


Figure 3.11. Final design of 3D printed culture chamber. (Ai) Separated CAD drawing of the final 3D printed culture chamber, scale bar is 50mm. (Aii) Manufactured 3D printed culture chamber, the main body, tensile arm and tensile arm runner were manufactured by 3D printing using PLA filament. (B) 3D printed culture chamber mount onto the EBERS TC-3 bioreactor. (Ci) CAD for 3D printed culture chamber adapted to the CellScale MCT6 bioreactor. (Cii) 3D printed culture chamber mounted onto the CellScale MCT6.

Table 3.5. Full components list for the bioreactor chamber.

Name	Description	Supplier	Product Code
Ultimaker 2+	FFF 3D printer	RS Components	918-8695
PLA filament	3D printing filament	RS Components	134-8190
Bellow	Flexible seal	Don Whitley Scientific	SP-90.007.006
Grub screw	M5 x 30 mm	Accu.co.uk	SSU-M5-30-A2
Polycarbonate sheet	1.25 m x 610 mm x 6 mm	RS components	681-665
O-ring	3mm cross section, 134mm circumference. VITON rubber	Simply Bearings	simplybearings.co.uk
XTC-3D	Waterproof resin	Smooth-on	benam.co.uk/xtc-3d
Thumb nut	M5	RS components	664-4886
Screw	M3	RS components	280-981
Sylgard 184	Low friction seal	Farnell	101697
Luer lock adapter	Attaches air filter	Cole Parmer	OU-30800-00
0.2 μ m syringe filter	Air filter	Cole Parmer	16534-----K
Thumb screw	M3	Accu.co.uk	SKT-M3-10-A1
M3 Thread insert	M3	Accu.co.uk	HSTI-M3-A2
M5 Thread insert	M5	Accu.co.uk	HSTI-M5-A2
CAD files	https://www.thingiverse.com/Janvier1/collections/tensile-stimulation-bioreactor		

3.5.1.6. Final Anchor Frame Design

The updated anchor posts featuring the barriers (Fig.3.8) did not function as designed. The fibrin hydrogel continued to run underneath the barrier generating non-uniform hydrogels. A final anchor post was designed to generate uniform fibrin hydrogels (Fig.3.12), this design was named the anchor frame. The solid PLA anchor frames were not coated in the XTC-3D resin or Sylgard-184. The design required the fibrin hydrogel to be formed within a six well plate. For the anchor frame system to initially fit within a 6-well plate before moving to the bioreactor chamber the design had to feature two main parts: the hydrogel attachment bracket (Fig.3.12i) and the 90° rotation arms (Fig.3.12ii). The hydrogel attachment bracket features breakable spars that maintain the uniformity of the structure during the fibrin hydrogel generation and contraction. Once the fibrin hydrogel had contracted (two week contraction phase) the 90° rotation arms are installed and the anchor frame system was moved into the appropriate culture well. The breakable spars were broken with sterile scissors, the fibrin then supported itself between the anchor frame allowing tensile loading to be applied directly to the fibrin hydrogel.

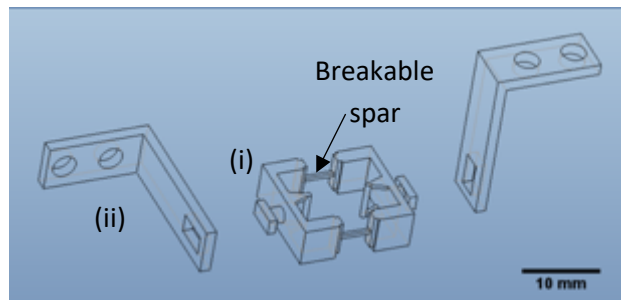


Figure 3.12. Anchor frame. CAD drawing of the final anchor frame. (i) the hydrogel attachment bracket, (ii) the 90° rotation arms.

The distance between the attachment posts on the hydrogel attachment bracket was 8 mm (12 mm from the wall behind the posts), the width of the main body was 7 mm and the depth of the main body was 4 mm (Fig.3.13). The volume of the fibrin hydrogels seeded within the hydrogel attachment bracket was 400 μ l. Once printed the hydrogel attachment bracket fitted into a well of a 6-well plate and was held in position with sterile 4% agarose (Fig.3.14A).

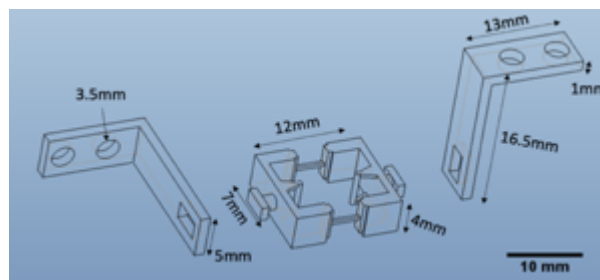


Figure 3.13. Dimensions of anchor frame system: the hydrogel attachment bracket and 90° rotation arms.

The breakable spars were covered with spar covers (Fig.3.14A) to prevent the fibrin hydrogel from running out below the breakable spars. Once the fibrin hydrogel contraction phase was completed, the spar covers were removed and the 90° rotation arms were installed. The anchor frame was then moved from the 6-well plate to the culture well with sterile forceps (Fig.3.14B). Once in the bioreactor chamber the breakable spars were broken with sterile scissors, the fibrin hydrogel then supported itself between the anchor frame (Fig.3.14C). The anchor frame was held in a fixed position by the 6-way tensile arm which in turn was held in position by the linear actuator. This maintained the length of the fibrin hydrogel (8 mm) until tensile strain was applied, displacing the hydrogel. The 6-way tensile arm could displace a further 8 mm backwards, equating to 100% the initial length of the hydrogel. The media volume was carefully considered based on the volumes typically used in a 6-well cell culture plate. For this particular study 3.5 ml of culture media ensured the tissue engineered tendon was fully submerged throughout culture and loading.

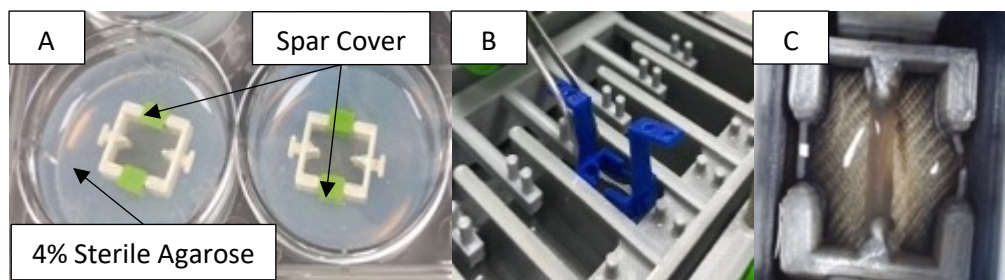


Figure 3.14. Flow of anchor frames from contraction to loading. (A) Anchor frame with spar covers installed, held in place with sterile 4% agarose. (B) Anchor frame moved to bioreactor chamber (C) Anchor frame within bioreactor chamber, breakable spars broken with sterile scissors.

3.5.1.7. 3D Printed Culture Chamber Validation

3.5.1.7.1. Well Displacement

The bioreactor chamber was validated by measuring the displacement of the 6-way tensile arm in each well when mounted onto the EBERS TC-3 bioreactor (Fig.3.3). The displacement of the tensile arm was recorded as percentage displacement of the hydrogels initial length (8 mm) (Fig.3.15). At 4 mm (50% strain) the displacement across all wells was within 0.6% of the programmed value, with no significant differences between wells at strain rates 5% to 50% across the wells ($p>0.09$) and a linear correlation between programmed and observed values.

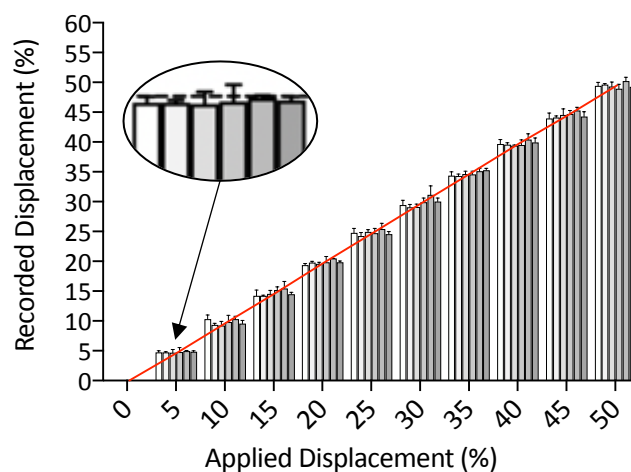


Figure 3.15. Linear displacement of the 6-way tensile arm by the software-controlled drive motor was shown to result in equal arm movement across each of the six wells of the printed chamber. $n=3$ technical repeats per well and $n=6$ experimental repeats across the chamber, significance measured using one-way ANOVA with Tukey's *post hoc* test and multiple comparison.

3.5.1.7.2. Lactate Dehydrogenase Assay

The biocompatibility and cytotoxicity of the bioreactor chamber was evaluated using the LDH assay ($n=3$), demonstrating that PLA has no cytotoxicity and was equivalent to tissue culture plastic controls (Fig.3.16A). The waterproof resin was found to induce significantly more LDH (2.5 fold increase, $p<0.05$), indicating toxicity (Fig.3.16A). The LDH assay was performed again, this time in the fully coated, cured and assembled bioreactor chamber. The culture wells were coated in XTC-3D oxirane resin and the base was coated in Sylgard-184. After the resins had completely cured the culture wells were thoroughly washed in six changes of PBS and the LDH assay was repeated within the bioreactor chamber, yielding equivalent LDH activity values to controls (6-well plate) (Fig.3.16B). This data indicates that repeat washing removes the toxic properties of the waterproof resin and renders it biocompatible. To further ensure biocompatibility a final layer of Sylgard was used to coat the inside of the chamber and provide a reduced friction surface for the moving parts of the arm and frame assembly. Maximum LDH production by the cells was induced by the addition of 10x Lysis Buffer. The maximum LDH was found to be 1.7 fold higher than the toxic Resin and 5.6 fold higher than the chamber (Fig.3.16).

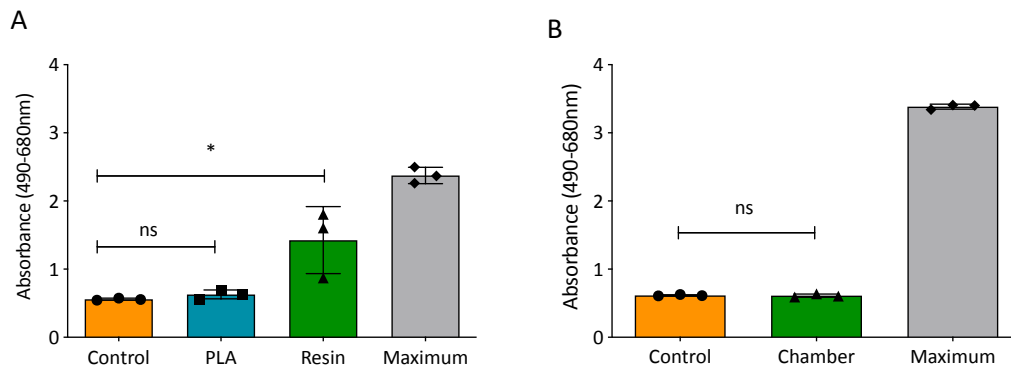


Figure 3.16. LDH assay for bioreactor chamber. (A) Cell viability as tested using the LDH assay within 6 well plate. (B) Cell viability tested using LDH assay with 3D printed culture chamber. Maximum represents induced LDH production. $n=3$ repeats. Error bars represent standard deviation. Significance tested using unpaired t-test (* indicates $p<0.05$).

3.6. Discussion

In this investigation it was shown that 3D printing is a useful method for producing customisable bioreactors; in this case to overcome technological challenges in tendon tissue engineering. The objective was to produce an easily replicable system that could be broadly adapted by the tissue engineering community to help improve the consistency and availability of research tools. The bioreactor chamber that was developed observed appropriate displacement when driven by commercially available software in comparison to existing commercial systems, and is adaptable to multiple base-platforms, for example those manufactured by EBERS and CellScale, enabling electronics, motor assemblies and software to be used. The bioreactor chamber was designed using the EBERS TC-3 bioreactor platform as a base, keeping the linear motor assembly and proprietary software to drive the actuator arm. Design of the original prototypes through to the final product validation took approximately 7 months with multiple redesigns used to improve the specification, optimise print quality and speed.

Several tests were performed to determine reliability and consistency across the bioreactor wells. Displacement of the 6-way tensile arm was measured and recorded as a percentage of the total hydrogel length (8 mm). The displacement was found to be uniform across each well and matched the programmed strain from 5% to 50% ($\pm 0.6\%$). The correlation between applied and recorded displacement was determined to be within acceptable engineering design limits, and is comparable to other published studies such as a biaxial loading bioreactor designed by Yusoff et al. (2011) which had a correlation of $\pm 0.95\%$.

The biocompatibility and cytotoxicity of the materials used to form the chamber was assessed using the LDH assay. The PLA base material was found to be non-toxic (no more LDH activity compared to tissue culture plastic controls), whilst the epoxy resin (oxirane) was initially discovered to be toxic. The toxicity was hypothesised to result from residual solvent and monomer leaching into the culture media, through repeat washing in PBS (6 washes) the resin-coated PLA showed no toxicity (LDH activity equal to tissue culture plastic controls). Other researchers have also shown that epoxy is compatible with cell culture (Pierce et al., 2012). The base of the wells were coated with PDMS (Sylgard-184), a widely used material for cell culture applications which provided a hydrophobic barrier, ensuring low protein adhesion and smooth operation, and was found to be non-toxic.

Poly(lactic acid) (PLA) is a versatile polymer and the most common material available for FFF desktop 3D printing, followed by acrylonitrile butadiene styrene (ABS) and nylon. ABS is not

recommended for manufacturing the bioreactor chamber as it has no material advantages to PLA in this application and needs to be used in a controlled environment (e.g. a class I fume hood) due to the production of toxic fumes and particulates during high temperature extrusion (Steinle, 2016, Hall et al., 2018). Nylon is known to swell and distort when exposed to humidified environments and was therefore not used (Park et al., 2016).

3.6.1. 150Conclusion

Using sharable CAD and 3D printing, a tensile stimulation bioreactor chamber that enables equal tensile forces to be applied to six isolated, independent samples in one chamber over a large displacement range has been designed, manufactured and tested. The materials used in the design are readily available for desktop manufacturing, easy to work with and were shown to be durable and non-toxic once the appropriate curing, washing and processing techniques had been applied. The bioreactor was successfully sterilised with 70% ethanol and was used for 18 months without infection, highlighting its reusability. The design and optimisation of this bioreactor chamber provides a freely available and globally reproducible platform for ongoing comparative research in tendon biology and tissue engineering. The ease and speed of the 3D printing process allows for multiple bioreactor chambers to be manufactured for each experiment ensuring the control chamber is identical to the experimental chambers, which is often a compromise with high-cost commercially available bioreactor systems where the number and availability of culture chambers is often limited to a single unit. With minimal editing to the design the system can be manipulated to mount onto a range of commercially available and custom-made bioreactor, for example the EBERS TC-3 and CellScale MCT6.

Chapter 4

Tensile Stimulation of hMSC Seeded Fibrin Hydrogels

4.1. Introduction

Tensile stimulation has long been used to drive the development of *de novo* tendons (Karamuk et al., 2004, Raif el and Seedhom, 2005). This approach derives from the role mechanotransduction plays during the development of musculoskeletal tissue from embryogenesis through to adulthood (Lee et al., 2017). Within the native environment the primary mechanical force applied to tendon is tensile stimulation (Wang, 2006). As muscle contracts the tendon is strained away from the bone acting as the transducer, transforming the generated force into skeletal movement (Glass et al., 2014). During development human tendon is thought to experience small amounts of cyclic strain coupled with constant strain resulting in an increase of up to 25% of the initial length (Kalson et al., 2011), whilst mature tendons are exposed to cyclic strain of up to 6% (Wang, 2006). The absence of tensile stimulation during *in vivo* embryonic growth of chicks has been shown to impair the development of the entire joint including tendons, highlighting the importance of mechanical stimulation for tissue generation (Mikic et al., 2000).

During embryonic development the modulus and ultimate tensile strength of tendons increases (Marturano et al., 2013), a trend that continues post-natally until tendons are fully mature (Ansoerge et al., 2009). Such properties are independent of increases in tendon length and diameter during tendon growth, which also improve extrinsic tensile biomechanical properties. Collagen type I, the most abundant protein in the tendons ECM, forms string-like fibrils primarily aligned with the long axis of the tendon, which provide tendons with mechanical durability and strength (Buckley et al., 2013). As fibrils progress through embryonic development the diameters increase from around 30 nm to 80nm (Fleischmajer et al., 1988) but have a predominantly unimodal diameter distribution. Mature tendons display a bimodal or trimodal fibril diameter distribution with fibril diameters reaching approximately ten times that of embryonic tendon (Ezura et al., 2000, Goh et al., 2012, Ribitsch et al., 2020).

Minor collagens occur in addition to type I collagen in healthy tendon, the minor collagens, comprise fibrillar types III, V, XI and FACIT collagens XII, and XIV (Riley et al., 1994). These less prominent collagens are often over looked in tissue engineering as a measure for the quality of the engineered tissues in favour of the more widely expressed ECM components. However the minor collagens play a key role in tendon homeostasis and without would render the tendon functionally impaired. Types V and XI form heterotypic (mixed) fibrils with type I collagen in tendon (Kadler et al., 2008). Type III reduces heterotypic fibril diameter and is

more abundant in elastic and distensible tissues (Asgari et al., 2017). During injury and aging the ratio of type III to type I increases, thereby altering tendon mechanical properties (Buckley et al., 2013). Types V and XI nucleate fibril assembly (Birk, 2001), with collagen type V influencing the diameter and number of fibrils assembled (Sun et al., 2015). Types XII and XIV are located at the surface of collagen fibrils with type XIV (Young et al., 2000) primarily present in developing tendon and replaced by collagen type XII during tendon maturation and ageing (Ansorge et al., 2009).

Mechanical stimulation has been applied in tendon bioengineering using an array of different scaffolds, bioreactors and conditions as outlined in Table 4.1. Here fibrin has been selected as the scaffold of choice with the biomaterial having been shown to be superior to collagen hydrogels, with improved tenogenic gene expression, ECM alignment, packing density of fibrils and increased linear modulus when cultured with 2.4% strain for 14 days (Breidenbach et al., 2015). Fibrin acts as a blank slate material for collagen synthesis as the only collagen detected is that synthesised by the cells. Table 4.1 further show the variability between studies as the rate of cyclic strain applied to tissues varies from 1-15%. Here three distinct strain rates, 3%, 5% and 10%, have been selected based on previous work by Wang (2006) which states that a strain up to 6% are routinely applied to tendon, therefore representing physiological loads, whilst greater than 6% may lead to degeneration or rupture. 3% represents low physiological strain, 5% high physiological strain and 10% excessive (degenerative) physiological strain.

In the present study cell-embedded hydrogels were generated using hMSCs in fibrin, which contracted around 3D printed attachment frames. To apply cyclic strain, the 3D printed bioreactor chamber was used as outlined in Chapter 3. The samples within their frames were incorporated into the bioreactor for 21 days, with one chamber for each condition (control, 3%, 5% and 10%) and cyclic strain delivered at 0.5Hz for 5h per day. A comprehensive multimodal end point analysis was performed using histology, qPCR and Western blotting for collagen isoform expression, transmission electron microscopy to quantify collagen fibril diameter and analysis of collagen fibre alignment with a fluorescent collagen probe (CNA35). Tensile testing was then used to measure viscoelastic and failure properties of the cell-engineered tendons in response to biomimetic cyclic strain.

Table 4.1. Published work on cyclic tensile stimulation for tendon tissue engineering, showing the range in loading platforms and conditions.

Study	Strain (%)	Duration (hr)	Frequency (Hz)	Overall Duration (day)	Cell type	Biomaterial	Sample Number	Bioreactor
Garvin et al. (2003)	1	1	1	8	Avian tendon internal fibroblasts	Collagen type I	n=6 isolated culture wells	Flexcell
Noth et al. (2005)	12	8	1	14	Human MSCs	Collagen type I	n=1	Custom
Webb et al. (2006)	10	8	0.25	7	Human fibroblasts	Polyurethane	n=4, shared culture well	Custom
Juncosa-Melvin et al. (2007)	2.4	8	0.2	12	Rabbit MSCs	Collagen type I	n=5, isolated culture wells	Custom
Joshi and Webb (2008)	5 or 12.5	1-24	0.1-1	7	Human dermal fibroblasts	Tecoflex	n=4, shared culture wells	Custom
Zhang and Wang (2010)	4 or 8	12	0.5	3	Rabbit tendon progenitor cells	Silicone membrane	n=6, isolated culture wells	Custom
Barber et al. (2013)	10	2	1	10	Human MSCs	Electrospun polylactic acid	n=4, isolated culture wells	Bose Electroforce
Morita et al. (2013)	5, 10 or 15	24 or 48	1	1-2	Human MSCs	Silicon monolayer	n=5, isolated culture wells	Custom
Breidenbach et al. (2015)	2.4	5	1	14	Murine tendon progenitor cells	Fibrin and collagen type I	n=5, isolated culture wells	Custom

Heher et al. (2015)	10 then 3	6 then 8	Static	6	C2C12		Fibrin	n=6, isolated culture wells	MagneTissue
Burk et al. (2016)	2	4, 8 or 24	1	1	Equine MSCs		Decellularised tendon	n=1	Custom
Qiu et al. (2016)	5	12	1	14	Human MSCs		NDGA-crosslinked	n=12, isolated culture wells	Custom
Youngstrom et al. (2016)	3	1	0.33	10	Tendon. Bone marrow and adipogenic derived MSCs		Decellularised tendon	n=1	Custom
Carroll et al. (2017)	5 or 10	4	0.5 or 1	21	Porcine MSCs		Fibrin	n=6, shared culture well	Custom
Grier et al. (2017)	10	0.7	1	6	Human MSCs		Collagen-GAG	n=24, isolated culture well	Custom
Subramanian et al. (2017)	2, 4 or 6	2	0.1 or 1	7	Human adipose derived MSCs		Collagen type I	n=4, isolated culture well	Custom
Wu et al. (2017)	4	2	0.5	12	Human adipose derived MSCs		PCL nanofibrous woven scaffold	n=6, shared culture well	CellScale MCT6
Brandt et al. (2018)	2	1	1	3	Human adipose derived MSCs		Decellularised tendon	n=3, shared culture well	Custom
Engbretson et al. (2018)	2	1	1	3 or 7	Rat MSCs		Decellularised umbilical vein	n=4, isolated culture well	CellScale MCT6

Garcia et al. (2018)	4	2	1	14	Rat MSCs	PCL/HA electrospun scaffold	n=6, shared culture well	Custom
Lee et al. (2018)	10	N/A	1	1, 3 or 7	Human MSCs	Decellularised tendon	n=2, shared culture well	Custom
Liu et al. (2018)	3	12	0.2	7	Canine MSCs	Decellularised tendon	n=6, shared culture well	Custom
Patel et al. (2018)	5	24	1	1	Bovine tenocytes	Poly(ethylene glycol) dimethacrylate	N/A	Custom
Raimondi et al. (2018)	10	12	0.5, 1 or 2	7 or 14	Porcine tenocytes	Collagen type I	n=4, shared culture well	Custom
Raveling et al. (2018)	10	12	0.05	3	Murine MSCs	Collagen tye I	n=1	Custom
Sensini et al. (2019)	5	1	1	7	Hs27	PLLA/Coll electrospun	n=1	CellScale MCB1
Wunderli et al. (2018)	1	8	1	6	Murine tenocytes	Murine tendon fascicles	n=8, shared culture wells	Custom
Grier et al. (2019)	5	1	1	6	Human MSCs	Collagen type I/GAG	n=24, isolated culture wells	Custom
Hsiao et al. (2019)	4 or 8	8	0.5	1	Rat tendon derived cells	Monolayer	n=12, isolated culture wells	Custom
Atkinson et al. (2020)	10	8	0.67	14	Equine tenocytes	Collagen type I	n=10, shared culture wells	Custom

Banik and Brown (2020)	3	2	0.01	21	Human MSCs	Poly-(ϵ -caprolactone)	Shared culture well	Custom
Ciardulli et al. (2020)	10	4	1	11	Human MSCs	Hyaluronate/Poly-Lactic-Co-Glycolic Acid (PLGA)/Fibrin	n=1	Custom
Deniz et al. (2020)	3 and 6	0.5 then 1	0.33	10	Human tenocytes	Poly (glycerol-sebacate) sheet	n=1	EBERS TC-3
Talò et al. (2020)	3	0.5, 1 or 2	0.33	7	Rabbit MSCs	Decellularised tendon	n=6, isolated culture wells	Custom
Tohidnezhad et al. (2020)	2.5	6	1	1 or 2	Rat tenocytes	Rat tendon	n=1	Custom

4.2. Hypothesis

Appropriate rates of intermittent, cyclic uniaxial tensile strain will drive the production of a complex collagen isoform repertoire (including types I, III, V, XI, XII and XIV), leading to improved structure and functional responses from tissue engineered tendon

4.3. Aims

1. Investigate the role of cyclic tensile strain on 3D culture hMSC differentiation and collagen production.
2. Investigate the structural development of 3D cultured hMSCs in response to varying cyclic tensile strains.

4.4. Experimental Setup

4.4.1. Chamber Run design

For this study four bioreactor chambers were 3D printed, one chamber for the control group and three for the tensile stimulated groups. To generate enough samples for the experimental analysis, six runs of complete tensile stimulation was required, this generated 36 samples per group (138 samples in total):

<u>Assay</u>	<u>Number of samples</u>
▪ Protein analysis (Western blotting)	[six samples]
▪ Gene expression analysis (qPCR)	[six samples]
▪ Fibril structural dimensions (TEM)	[three samples]
▪ Tissue microstructure (histology staining)	[three samples]
▪ Fibre Analysis (CNA35 Collagen-Probe)	[three samples]
▪ Mechanical testing	[three samples]

The extra twelve samples not accounted for in the analysis techniques were generated as six replacements for any failed samples during each run and six samples to be sent to the University of Georgia, USA, for external analysis.

As the bioreactor chamber was not mass produced but developed in-house, variations in the construction may have occurred during the manufacturing process. This variation was accounted for by rotating the stimulation groups chambers used during the experimental runs. The tensile stimulated bioreactor chambers were labelled 1, 2 or 3. On the first run chamber 1 was used for the 3% strain group, chamber 2 for the 5% strain group and chamber

3 for the 10% strain group. On run 2 chamber 1 was used for the 10% strain group, chamber 2 for the 3% strain group and chamber 3 for the 5% strain group. For run 3 chamber 1 was used for the 5% strain group, chamber 2 for the 10% strain group and chamber 3 for the 3% strain group. This rotation was repeated for runs 4, 5 and 6. Samples taken for experimental repeats varied across each run:

Run 1, 2 and 3 – two samples for protein analysis, two samples for gene analysis, two samples for the University of Georgia and one replacement sample per run.

Run 4, 5 and 6 – one sample for second harmonic generation, one sample for histology, one sample for collagen probe, one sample for mechanical testing, one sample for TEM and one replacement sample per run.

In order to efficiently generate the samples, each run was staggered over the five week experimental period (two week contraction phase, three week loading phase), this is shown in Fig.4.1.



Figure 4.1. Tensile stimulation experimental run. Each run was staggered to optimise experimental run time (20 weeks), each run was made up of two parts, the two week contraction phase and three week loading phase.

4.4.2. Tensile Stimulation

The varying rates of tensile stimulation were sequentially applied to fixed groups of fibrin hydrogels after the samples had been moved into the bioreactor chamber. The four chambers (control and three stimulated) were all kept within the same non-humidified incubator at 37°C in 5% CO₂ along with the EBERS TC3 bioreactor (Fig.4.2). When the culture chamber was mounted onto the EBERS TC-3, the 6-way tensile arm attached to the bioreactors linear actuator, this was how the tensile stimulation was applied to the fibrin hydrogels. When the linear actuator was displaced (controlled by the EBERS software) the 6-way tensile arm was also displaced. Each chamber was pre-determined as to which stimulation group it would be in, either control (0%), 3%, 5% or 10% strain. Strain was applied as a percentage of the initial length of the fibrin hydrogel (distance between posts), initial length was 8 mm; therefore 3% strain was 0.24 mm, 5% strain was 0.4 mm and 10% strain

was 0.8 mm. Stimulation was applied for five hours a day (19 hours at static length), at 0.5 Hz, five days a week (five days with stimulation, two days without) over three weeks. The stimulation was control by the EBERS software, the chamber was mounted onto the EBERS TC-3, and stimulation would begin. Once the five hours had elapsed the software would stop allowing the user to swap the chambers around. Stimulation was applied as a sinusoidal waveform as selected on the EBERS software.

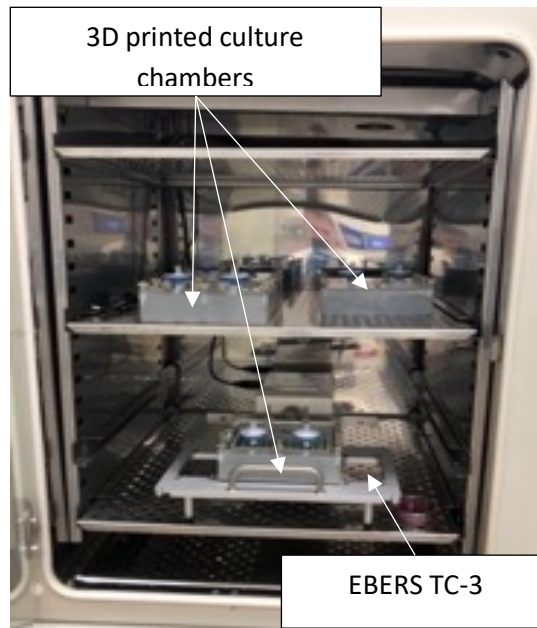


Figure 4.2. Bioreactor chambers and EBERS TC-3 in non-humidified incubator.

4.4.3. Histology

Qualitative histological analysis was used as an initial marker to determine the response of the tissue engineered tendons to the applied strain (Fig.4.3). H&E staining of the engineered tendon illustrates changes in tissue structure correlate with stain. Staining revealed that the static control group had little alignment within the structure. However, strained samples exhibited alignment to the direction of the strain. These results suggest that loading resulted in a more aligned structure compared to the static control.

Alcian blue staining highlighted GAG production within the engineered tissue. The staining suggested that cyclic strain did not influence the production of GAGs with no difference observed across loading conditions.

Alizarin red staining was used to investigate the calcium hydroxyapatite production within the engineered tissues. The control and 10% strain groups appeared to have produce significantly more calcium hydroxyapatite during culture than the 3% and 5% strain group. This suggests that physiologically appropriate rates of strain inhibit calcium hydroxyapatite production whilst the absence or excessive cyclic loading enables the production.

Under polarised light the Picrosirius red staining shows fibrillar collagen illuminated red, green and yellow. There appeared to be little difference in collagen production between all cyclically strained and the control groups. This suggests that total fibrillar collagen production was not driven by the cyclic strain.

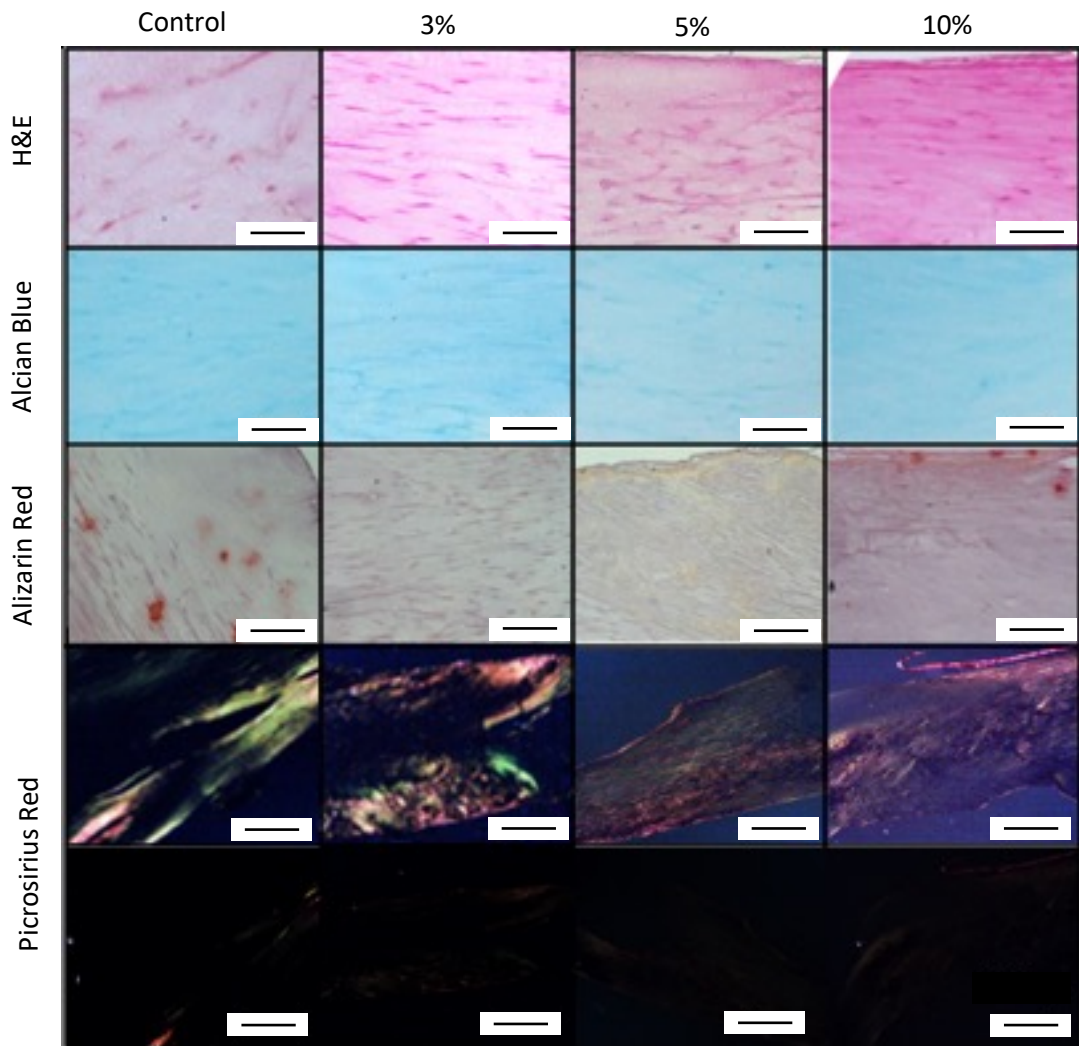


Figure 4.3. Histological analysis of tissue engineered tendons. Samples stained (from left to right) with H&E, Alcian blue, Alizarin red and Picrosirius Red (under polarized light). Both enhanced and original images are shown for Picrosirius Red staining highlighting how little collagen was initially detected before image enhancement. x10 objectives were used for each stain except Picrosirius red where x4 was used. n=2 experimental repeats. Scale bars represent 500 μm .

4.4.4. Alkaline Phosphatase Assay

ALP content in the cell culture media was measured at day 0 (end of contraction phase), 7, 14 and 21 (three week loading phase) (Fig.4.4). At day 0 no significant difference was seen across the three contraction plates. The control group peaked at day 7 being significantly higher than the three loaded groups ($p<0.001$). The 10% strained group peaked at day 14 and was significantly higher than the other groups ($p<0.001$). Both the 3% and 5% strain groups appeared to have very low levels of calcium hydroxyapatite deposition (Fig.4.3) and lower alkaline phosphatase activity.

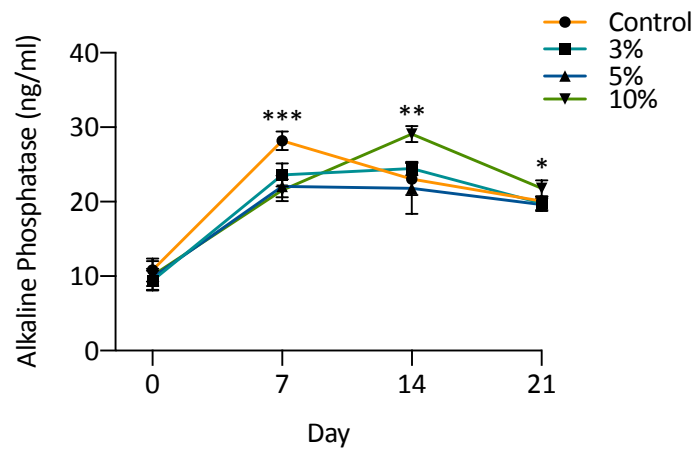


Figure 4.4. Alkaline phosphatase expression of tissue engineered tendons during cyclic loading phase. Day 0 marks the end of the contraction phase and sees the lowest ALP expression with no difference between loading condition, as expected. At day 7 the control group has a significantly higher ALP expression than all other groups ($p<0.05$). At both day 14 and 21 the 10% strain group has significantly higher ALP expression than all other groups ($p<0.05$). $n=6$. Significance was measured using two-way ANOVA with repeat measures and Tukey's *post hoc* test (*indicates $p<0.05$, ** $p<0.01$, *** $p<0.001$).

4.4.5. Tendon Gene Expression

The tendon markers decorin, scleraxis and tenomodulin were assessed using qPCR (Fig.4.5) for all experimental strain conditions and monolayer hMSCs. An increase was seen for TNMD between the 2D cultured hMSCs (monolayer) and the 3D cultured hMSCs with significance seen for the 5% group compared to the monolayer. SCXA was increased with mechanical stimulation, but only one sample from the monolayer expressed detectable SCXA. Expression of decorin, a key proteoglycan present in tendon, was highest in the control group and significantly higher in the 3% strain group than with 5% or 10% strain.

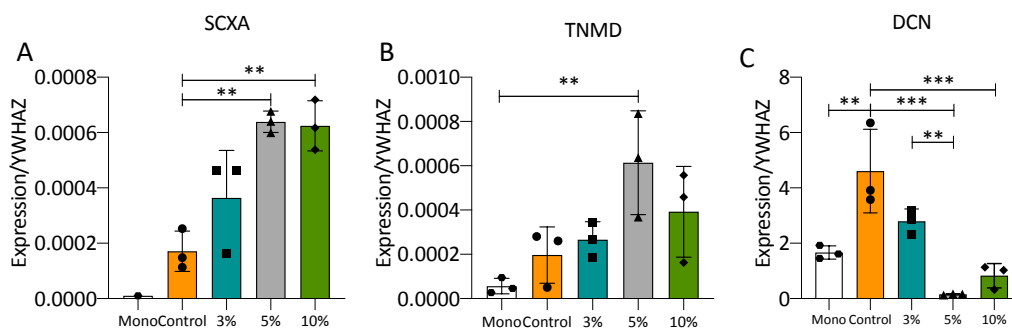


Figure 4.5. Gene expression analysis of tendon differentiation genes and a proteoglycan ECM gene. A) Screlaxis B) Tendomodulin and C) Decorin. Values shown normalised to YWHAZ. n=3 experimental repeats from three separate experimental runs. Significance measured using one-way ANOVA with Tukey's *post hoc* multiple comparisons test (*indicates $p < 0.05$, ** indicates $p < 0.01$, *** indicates $p < 0.001$).

Quantification by qPCR of the tendon collagen gene composition (COL1A1, COL3A1, COL5A1, COL11A1, COL12A1 and COL14A1) was assessed after 21 days of cyclic tensile strain (or static for control) (Fig.4.6). COL2A1 expression was also assessed and acted as a marker for non-tenogenic differentiation. COL2A1, COL3A1 and COL11A1 were found to be significantly higher with 5% cyclic strain than 3% cyclic strain or static conditions, with COL11A1 also higher than 10% cyclic strain. Conversely COL12A1 was significantly lower with 5% and 10% cyclic strain than the control group. A similar pattern was seen for COL1A1 and COL5A1 though no significance was seen.

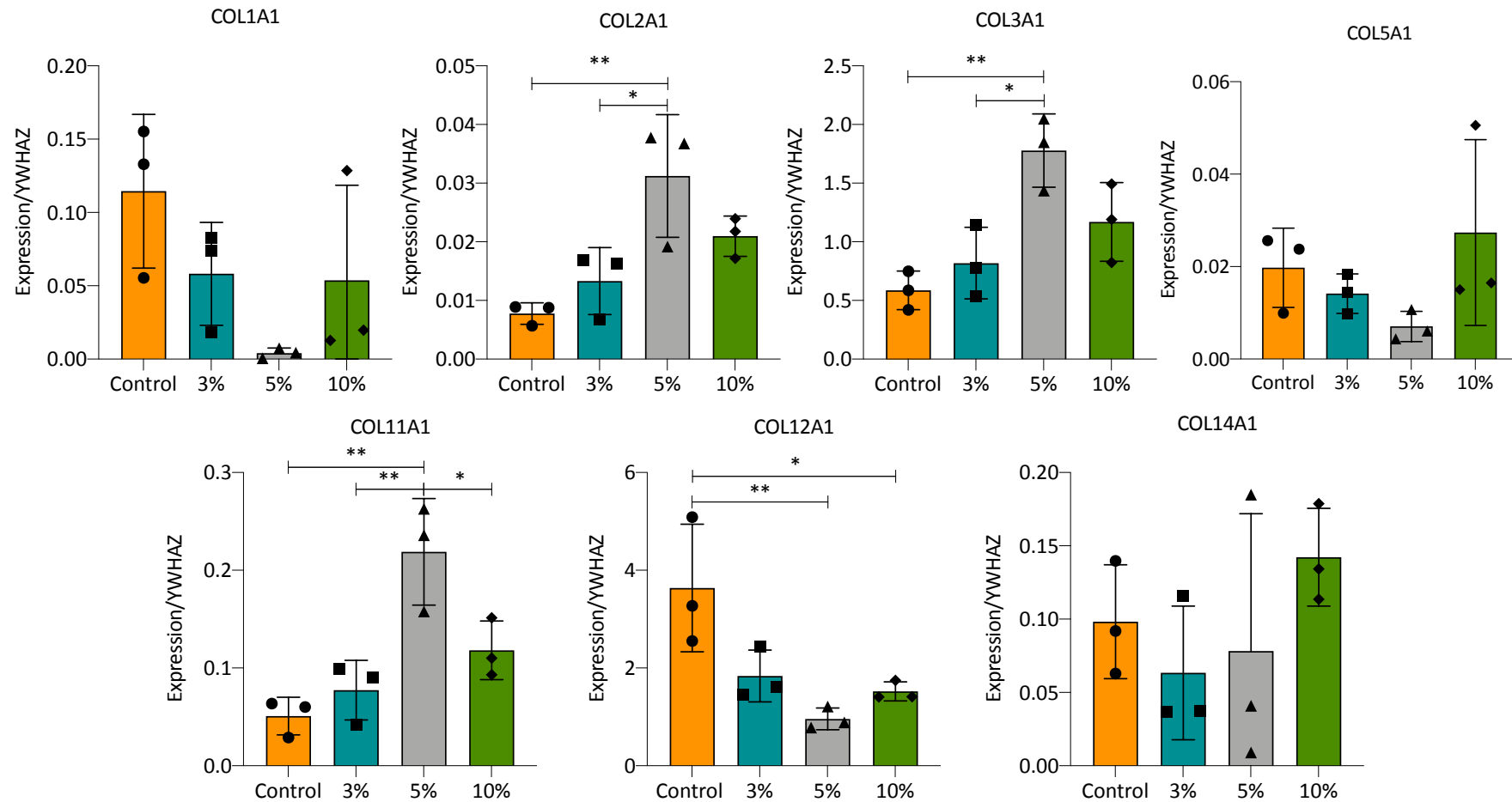


Figure 4.6. Gene expression analysis of collagen isoform composition in tissue engineered tendons. Relative expression is normalized to YWHAZ housekeeper. $n=3$ experimental repeats, each point designates one of three separate experimental runs. Significance was measured using a one-way ANOVA with Tukey's *post hoc* test and multiple comparisons (* indicates $p < 0.05$, ** indicates $p < 0.01$).

4.4.6. Complete Tendon Collagen Composition Expression

The tendon collagen composition (types I, III, V, XI, XII, XIV) was investigated by western blot and the detected expression was quantified by densitometry (Fig.4.7). However collagen type V and type XIV were not detected in any samples. Collagen type II was used as a negative marker. Procollagen $\alpha 1(I)$ and collagen $\alpha 1(I)$ beta chain were both detected on the western blot membrane for collagen I $\alpha 1$ and have been included in the analysis of protein expression. No significance was detected for collagen types I, XI or XII. Collagen $\alpha 1(II)$ was found to be significantly less abundant in the 3% and 10% cyclic strain groups compared to the control.

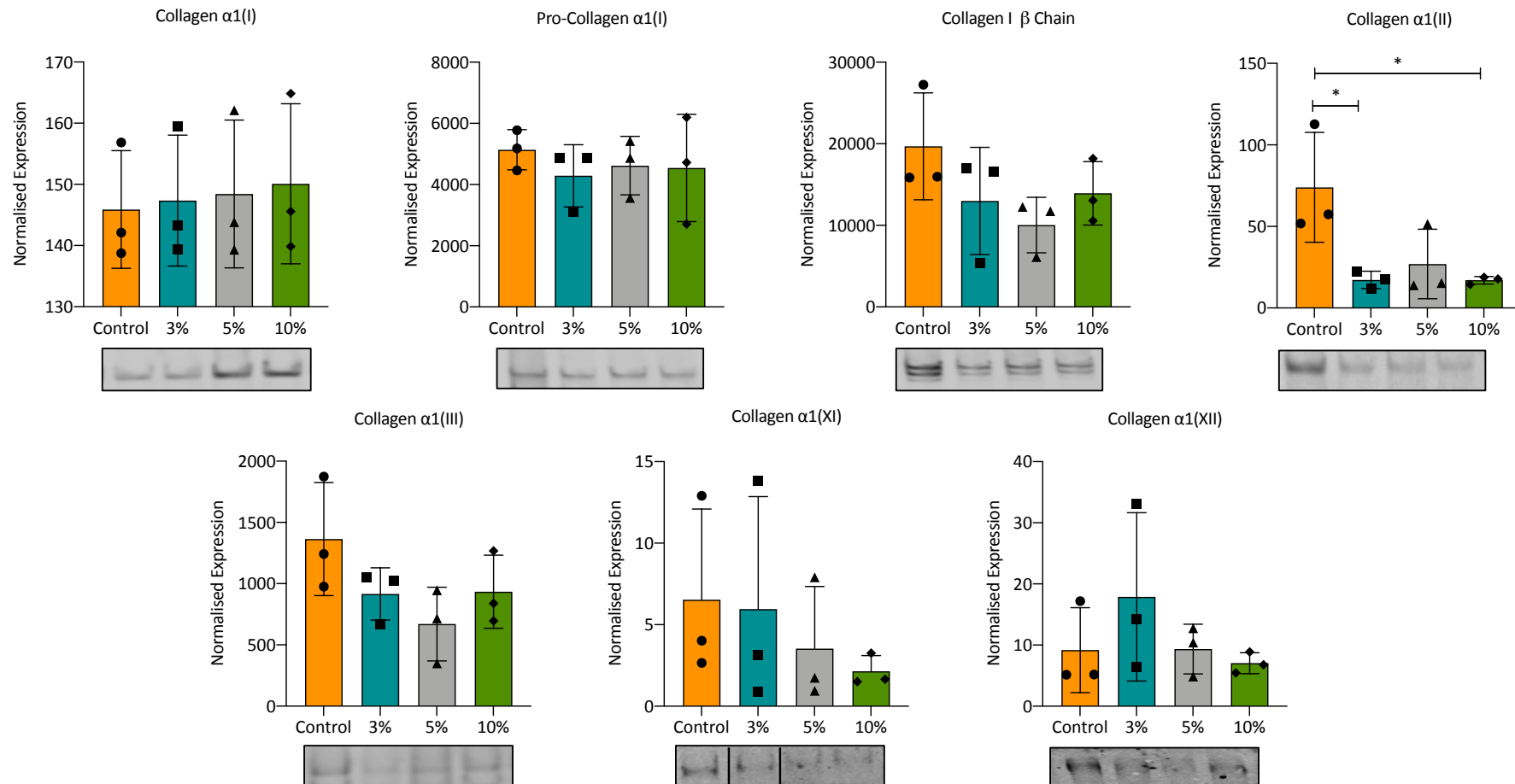


Figure 4.7. Western blot analysis of tendon collagen isoforms in tissue engineered tendons. Proteins were quantified using densitometry, with representative images of western blots show below each graph. Black bars indicate that a membrane has been cropped for the representative image. Values shown are normalised to total protein. Significance was measured using one-way ANOVA with Tukey's *post hoc* test and multiple comparisons (* indicates $p < 0.05$).

4.4.7. Transmission Electron Microscopy Analysis

Fig.4.8A shows representative images for TEM analysis of the samples after five weeks in culture. The upper row of images shows the transverse cross-sections of the collagen fibrils running through the engineered tendon. The lower row of images shows the longitudinal orientation of collagen fibrils and highlight the anticipated surface banding pattern. Both sets of images were taken using a x110,000 objective lens, scale bars represent 100 nm.

Fibrils in the 3% cyclic strain group developed the lowest diameter after the 21 day period with a median of 33.8 nm, this was found to be significantly lower than all other groups ($p<0.001$). The 10% strain group had the highest median diameter (41.2 nm), this was significantly higher than the control (36.3 nm) as well as the 3% strain group ($p<0.001$). The 5% strain group (39.7 nm) was only significantly greater than the 3% strain group.

The percentage frequency distribution of the fibril diameter (Fig.4.8Ci, ii and iii) was found for each sample using images of fibril cross sections across three experimental runs. The percentage frequency distribution of fibril diameter for each cyclically stimulated group was overlaid with the control groups diameter, highlighting the difference between static and cyclic conditions. The 3% strain group (Fig.4.8Ci) shows the same peak range as the control (30 nm to 36 nm). The 5% strain group (Fig.4.8Cii) has the same peak as the control group but the curve is wider than the 3% strain group or control groups curve (5% strain peaks at ~11%, control and 3% strain peak at ~15%). The 10% strain groups (Fig.4.8Ciii) mode shifts away from the control groups to 38 nm to 43 nm. Chi-squared tests between the control group and each of the strain groups showed significant differences for each strain rate, indicating that the application of any form of cyclic loading is resulting the a difference in the structure of the fibrin hydrogel. The 10% strain group showed the largest difference from the control group ($p<0.0001$).

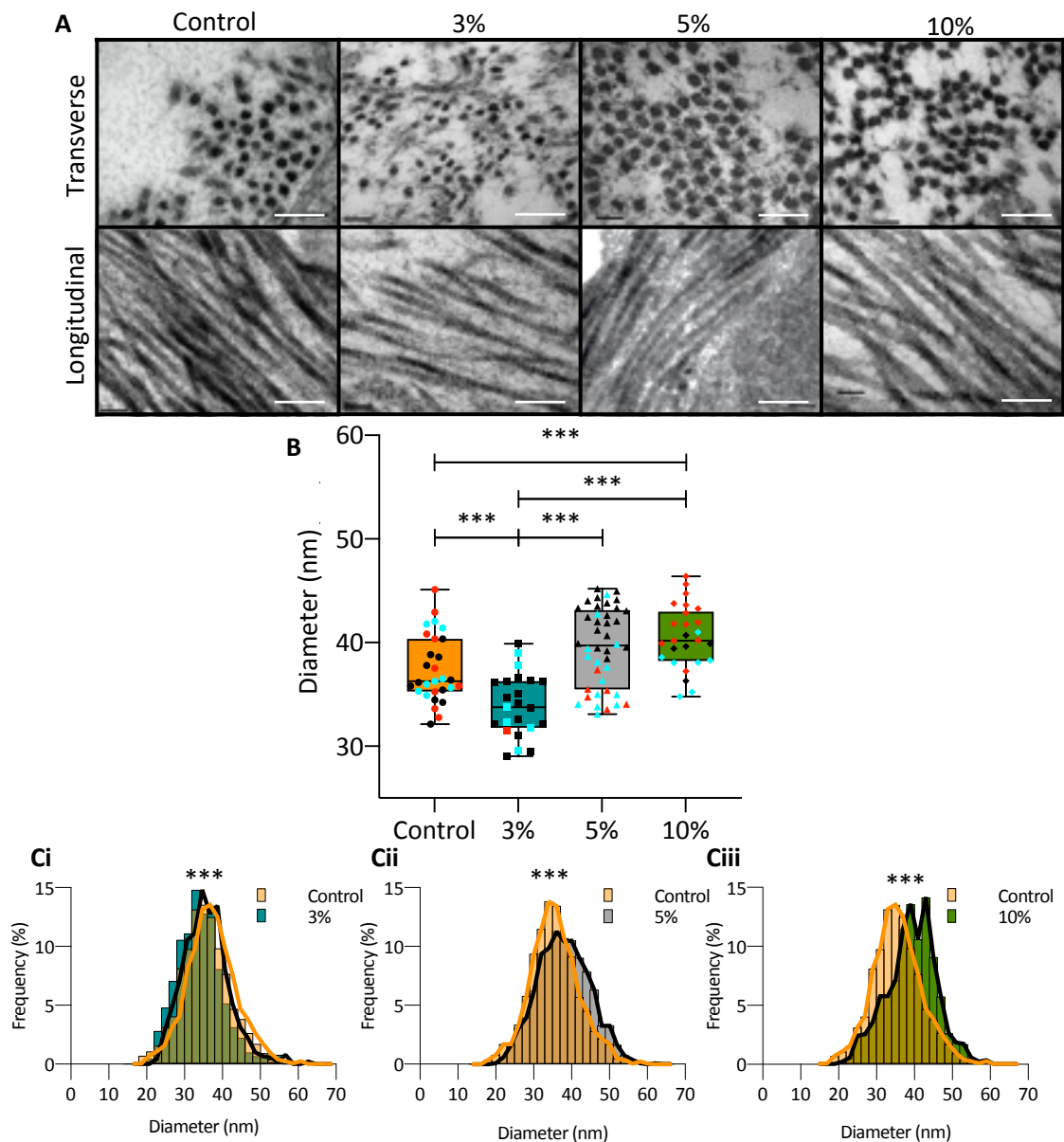


Figure 4.8. TEM analysis of tissue engineered tendons. (A) TEM images of engineered tendons showing collagen fibrils. Upper images show transverse cross-sections, lower images show longitudinal sections, all after 21 days of intermittent cyclic tensile strain and at x11,000 objective. Analysis of individual fibres in transverse sections by imageJ (B) showed differences in fibre diameter with the extent of tensile strain. Data was generated from n=3 experimental runs of each condition by analysing multiple images from each samples. Data from the same samples are indicated by identical coloured markers within each strain group. Fibril diameters are shown as frequency distributions for (Ci) 3% strain, (Cii) 5% strain and (Ciii) 10% strain, with the control group (orange) overlaid for comparison. Scale bars in (A) represent 200 nm. Statistical significance of the minimum diameters was determined using a linear mixed model whilst the distributions was measured with Chi-squared test (* indicates $p < 0.05$, ** indicates $p < 0.01$, *** indicates $p < 0.001$).

4.4.8. CNA35 Collagen-Probe Analysis

Representative images for DAPI, CNA35 collagen-probe staining and merged image are shown in Fig.4.9 for all stimulation groups. Images are shown at the anchor point (internal control) and the mid region (regions defined in section 2.2.8). Mid-region appeared to have greater alignment of collagen fibres compared to the anchor point region.

Fibre orientation was measured after normalising orientation to 0°. The percentage frequency distribution of the orientation is shown for the control, 3% strain, 5% strain and 10% strain groups, with the control mid region superimposed on the cyclically strained graphs (Fig.4.10). Representative images are shown from the alignment analysis, here colour has been assigned based on the orientation of the fibres (-90° to 90°): the more consistent the colour of the fibres, the more aligned the structure (colour key shown in section 2.2.8). It appears that the images from the mid region have more aligned fibres compared to the anchor point region. The control mid region versus the cyclically strained mid regions are shown above the x-axis whilst the anchor point region are shown below the x-axis. All groups had significantly increased alignment in the mid region compared to anchor point region except the control group (significance considered at 0°). All the strained groups had a more aligned mid region compared to the control mid region, however only the 10% strain group was significantly more aligned (above x-axis, significance considered at 0°), with 61.5% as compared to 40% alignment in the control group. Alignment in the 3% and 5% strain groups was intermediate between the control and 10% group at 45.7%, and 57.7% respectively.

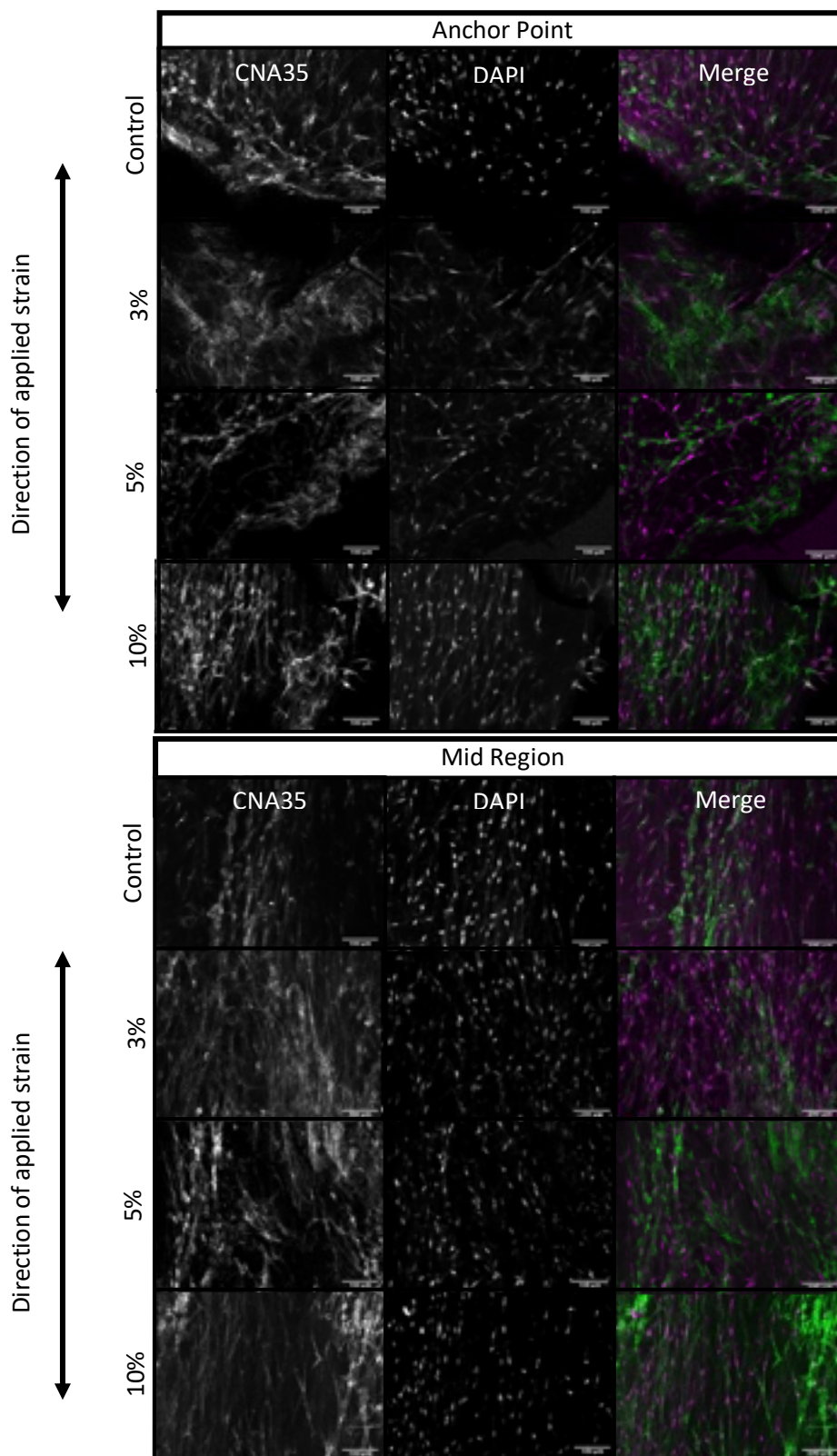


Figure 4.9. Tissue engineered tendons stained with CNA35 collagen-probe and DAPI representative images. Upper images show the anchor point region of the hydrogel, the lower images show the mid region of the hydrogel. Images appear to agree with the hypothesis indicating that the mid region was more aligned in all conditions compared to the anchor point region of the same sample.

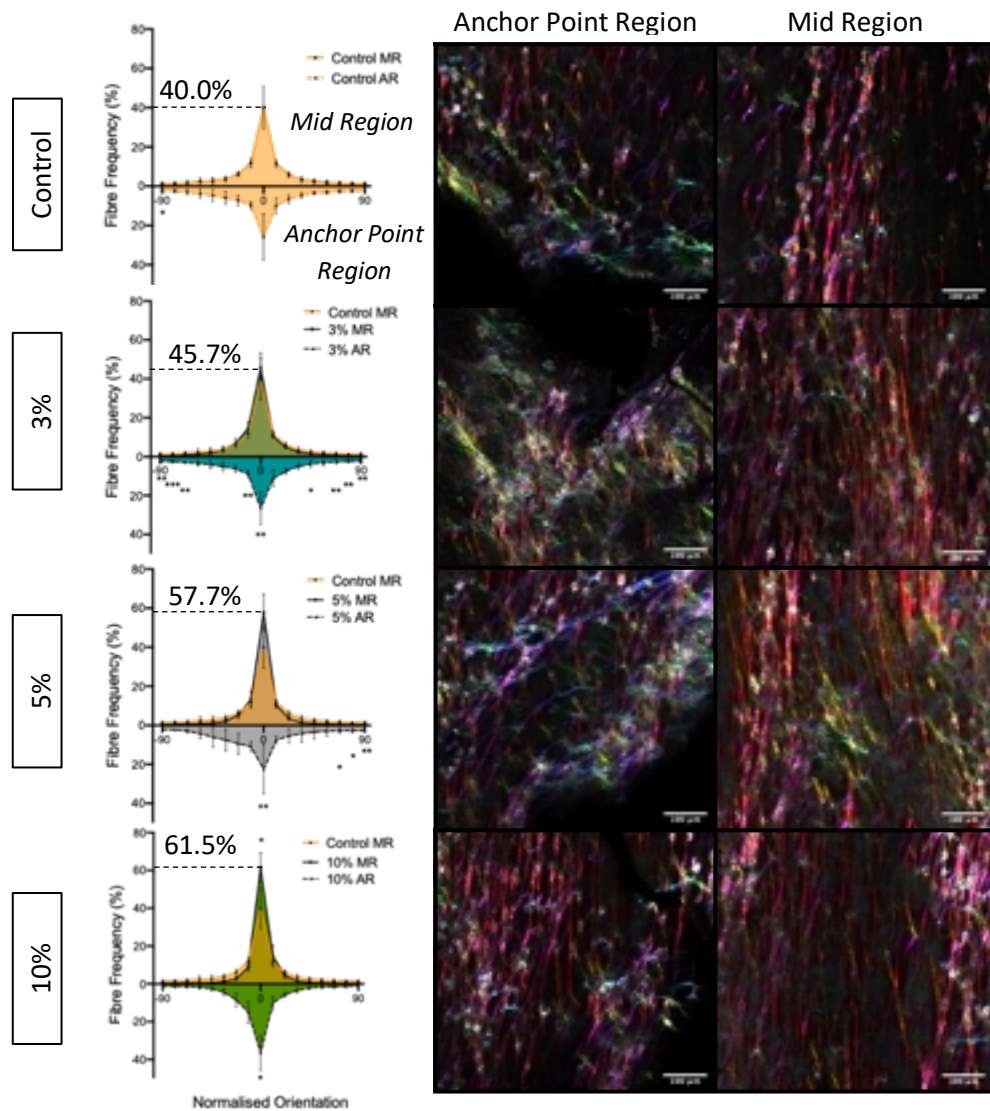


Figure 4.10. CNA35 collagen fibre analysis. The ImageJ plug-in (OrientationJ) was used to visualise and quantify fibril orientation from the CNA35 collagen-probe images parallel to the strain axis (0° = parallel, shown as vertical in these images) in both regions. Graphs show the frequency distribution of fibres aligned with the strain axis, with the mid-region shown above the x-axis and the anchor point region shown below the x-axis. An overlay of the control group mid region (in orange) is shown in for comparison. Images are representative of $n=3$ experimental repeats and scale bars represent $100\ \mu\text{m}$. Error bars represent standard deviation. Statistical significance cyclic strain vs static (above x-axis) and mid-point vs anchor point (below x-axis) was determined using one-way ANOVA with Tukey's *post hoc* test with multiple comparison ($p < 0.05$, $** p < 0.01$, $*** p < 0.001$).

4.4.9. Tensile Mechanical Testing

To determine how strain-induced differences in collagen isoform composition and collagen fibril diameter relate to biomechanical function, the tensile and viscoelastic properties of the engineered tendons were measured. No significant differences in construct diameters were found across experimental groups ($p>0.1$), with the mean diameter being 2.43 ± 0.32 mm. The stress against strain profile for each sample (Fig.4.11A) highlights the consistency of the trend for each stimulation, except for one control sample. The trend of the stress strain curves highlight the viscoelastic structure of the samples with the distinct “J” shape curve being apparent for each samples. In testing to failure the maximum stress, strain and Young’s modulus was found (Fig.4.11B-D). The 3% strain group had highest mean maximum stress (57.7 kPa) (Fig.4.11B). This is 2 fold higher than the maximum stress for the control and 10% strain group ($p<0.025$). The 5% strain group was 2.9 fold lower than the 3% group (20 kPa) ($p<0.004$). The maximum strain (Fig.4.11C) was not significantly different between experimental conditions. The static and 3% groups had the highest strain rates before rupture, whilst the 5% and 10% strain groups had the lowest. The Young’s modulus, calculated from the linear region of the stress strain curve was found to not be significantly different between experimental groups (Fig.4.11D).

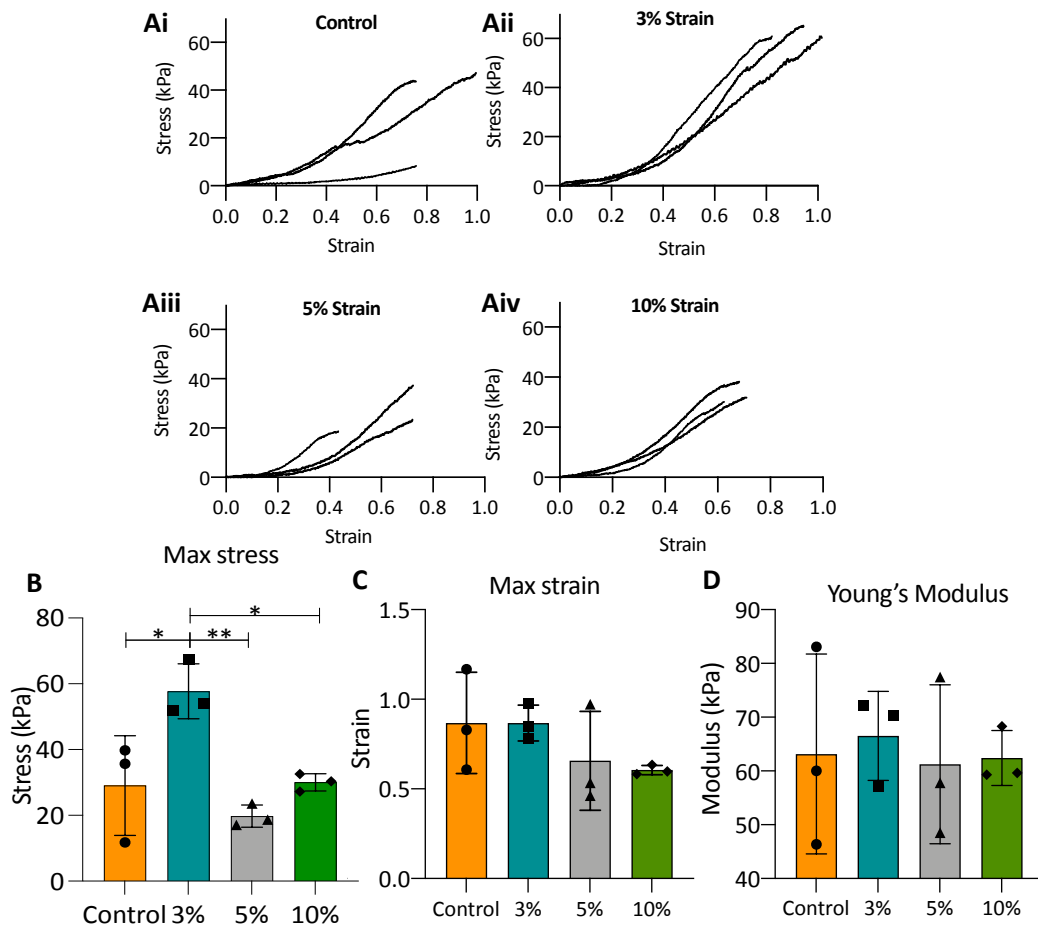


Figure 4.11. Stress vs strain profiles for all tissue engineered tendon samples after 21 days of intermittent cyclic tensile strain (Ai-Aiv). The maximum stress (B), maximum strain (C) and Young's modulus (D) were all calculated using the stress-strain profiles. The 3% strain group showed the highest maximum stress. The maximum strain and Young's modulus displayed no significant changes across groups. Error bars represent standard deviation of the mean. $n=3$ experimental repeats. Statistical significance was determined using one-way ANOVA with Tukey's *post hoc* test and multiple comparisons ($*p<0.05$, $**p<0.01$).

The fibrin hydrogels displayed further viscoelastic biomechanical properties, that were calculated from the preconditioning steps shown in (Fig.4.12B). Percentage energy loss was calculated from the hysteresis runs: the 10% strain group had the lowest energy loss (47%) whilst the 5% strain group had the highest (60%), however no significance was seen (Fig.4.12B).

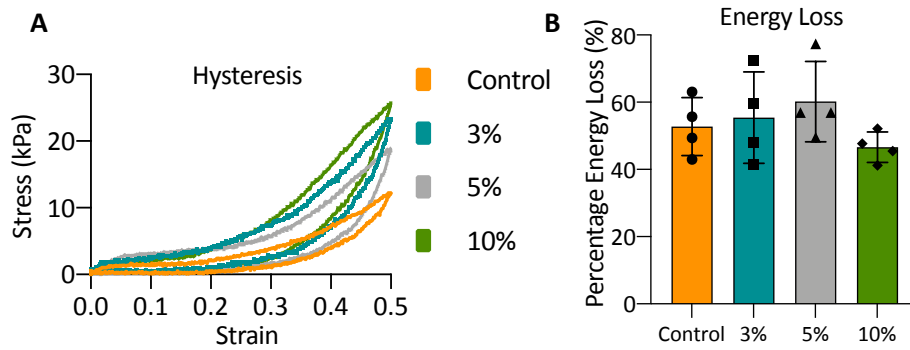


Figure 4.12. Viscoelastic profiles of tissue engineered tendons. (A) The hysteresis response shows the recorded strain during sample loading and unloading. (B) The percentage energy loss depicts how much energy is lost between the loading and unloading phase. Error bars represent standard deviation of the mean. $n=4$ experimental repeats. Significance was measured using one-way ANOVA with Tukey's *post hoc* test and multiple comparisons.

In addition to hysteresis the relaxation of the samples was investigated to further understand the viscoelastic properties. Staggered stresses are shown on the y-axis of Fig.4.13A to separate the samples. The rate of stress relaxation was found between 0 and 60 s. The rate of relaxation increased with increasing strain rate with 10% having the highest mean value and was found to be significantly higher than the control group ($p<0.05$) (Fig.4.13B).

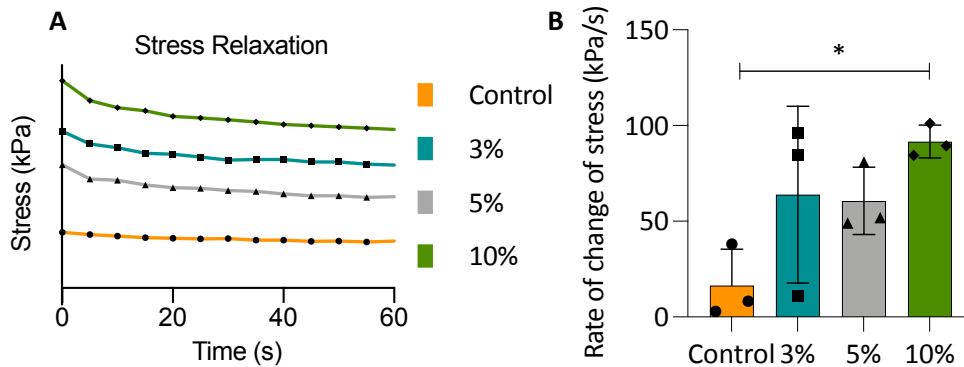


Figure 4.13. The stress relaxation profiles (A) for the samples shows that all groups displayed this viscoelastic characteristic. The start stresses are staggered to separate experimental conditions. The rate of stress relaxation (B) was found to be highest in the 10% strain group ($p<0.05$ vs control). Error bars represent standard deviation of the mean. $n=3$ experimental repeats. Statistical significance was determined using one-way ANOVA with Tukey's *post hoc* test and multiple comparisons ($*p<0.05$).

4.5. Discussion

Following the design and fabrication of the bioreactor chamber, the system was used to apply cyclic tensile strain to MSC embedded fibrin hydrogels. Following a 14 days contraction period the fibrin hydrogels were moved to the 3D printed chamber for 21 days of cyclic loading, or stasis for the control group. Gene and protein expression of tenogenic markers and collagens was altered by the extent of cyclic strain, as was collagenous tissue composition, fibril diameter, fibre alignment and mechanical properties.

H&E staining revealed that the tissue engineered tendons cultured with dynamic strain had a more visibly pronounced alignment and a greater abundance of cells and matrix at the surface than controls, supporting findings from previous studies (Noth et al., 2005, Benhardt and Cosgriff-Hernandez, 2009). Picrosirius red staining imaged under polarised light highlighted the areas rich in collagen due to the birefringent properties of collagen (Jett et al., 2020). The 5% and 10% strain group appeared to have the most aligned structures, with more widespread collagen supported by previous work showing increased collagen alignment with strain (Weidenhamer and Tranquillo, 2013).

Alizarin red staining highlighted matrix mineralisation in both the static (control) and 10% strain groups. The osteogenic products seen in the matrix was reinforced by increased ALP activity in both groups suggesting that strain below or above physiologically acceptable levels has detrimental effects on the development of tissue engineered tendon. The population of cells used did not undergo cell sorting, it is therefore possible that the osteogenic products are resultant of a sub population of the hMSCs pre-disposed to the osteogenic lineage. The early (day 7) ALP peak in the control group suggests that tensile stimulation initially inhibits the osteogenic differentiation. By day 14 the levels of ALP in the control media is not significantly different to the 3% or 5% groups however the 10% group had become significantly higher than the other groups. As the 10% group is considered beyond the physiologically acceptable levels of strain, it appears that these excessive strains see the tendons begin to undergo calcification, which is often a marker of degeneration in the native tissue (Bethune et al., 2007, Seil et al., 2006).

Tenogenic markers scleraxis and tenomodulin both saw changes between monolayer cells and 3D cultured cells. Scleraxis was only expressed by one monolayer sample whilst all 3D samples from each experimental group expressed the gene demonstrating that 3D culture alone results in greater expression of tendon markers. The highest loading group then saw

an significant increases in scleraxis compared to the control group suggesting that 5 and 10% cyclic strain results in a upregulation of tendon specific differentiation of MSCs. Tenomodulin was only found to be significant between the 5% strain group and the monolayer, this suggests that the 5% strain, physiologically appropriate strain, is upregulating both scleraxis and tenomodulin whilst the degenerative strain, 10%, is inhibiting tenomodulin.

The complete collagen composition of tendon was investigated to assess the success of different rate of tensile stimulation for tissue engineered tendon, to the authors knowledge this has not been previously done before. The negative marker COL2A1 was found to be significantly higher in the 5% strain group compared to the control and 3% strain groups, disagreeing with the tendon specific gene expression. It should be noted that the expression of COL2A1 was the lowest of all collagen genes investigated as seen previously (Maeda et al., 2010, Udeze et al., 2019). This demonstrates that despite the 5% strain group having a significantly higher expression it is not the dominant collagen being transcribed. Dynamic tensile stimulation increased collagen II inhibition as the detected protein collagen $\alpha 1(\text{II})$ was lower in all cyclically strained groups compared to the static control group (5% not significant). Alcian blue staining showed no obvious structural difference between conditions, aligning with the collagen II results and demonstrating that the 3D tendon culture inhibited chondrogenic differentiation which cyclic strain further suppressed.

Different studies have reported different collagen I and III responses to tensile stimulation. The rate of the stimulation and the 3D environment generate the largest variation across these studies. In collagen hydrogels increased expression of COL1A1 and COL3A1 has been reported with 2%, 4% and 6% strain at 0.1 Hz, and with 2% and 4% strain at 1 Hz, for 2 hours per day over 7 days (Subramanian et al., 2017). In crosslinked collagen scaffolds increased expression of COL3A1, but not COL1A1 has been reported (Qiu et al., 2016, Grier et al., 2017), whilst in decellularized tendon or synthetic scaffolds, increased expression of COL1A1 (Webb et al., 2006, Zhang and Wang, 2010, Xu et al., 2015) or both COL1A1 and COL3A1 (Xu et al., 2014, Barber et al., 2013, Lee et al., 2018, Wu et al., 2017, Engebretson et al., 2018) with cyclic strain has been reported. However in some situations expression of these collagens is unchanged. It may be that high level synthesis of type I collagen occurs during formation of the embryonic tendons and that expression and protein content then stabilises. Alterations in fibril diameter and fibre alignment with strain may not require alterations in type I collagen content.

Increased expression of collagen XI has been suggested, along with collagen V, to indicate a more developed structure as these regulatory collagens decrease in abundance as they are no longer required to organise the collagen I fibrils (Wenstrup et al., 2011). In the present study the COL11A1 gene expression was highest in the cyclically stimulated groups (peaking for 5%) but the collagen $\alpha 1(XI)$ protein detected was lowest in the stimulated groups, suggesting that cyclic stimulation drives the production of a more regulated ECM, therefore due to the high alignment the mRNA is not translated to protein. COL12A1 was the most highly expressed mRNA of all the collagens but with significantly lower expression in the 5% and 10% strained groups. Reductions in COL12A1 expression could indicate fibril remodelling although no significant alterations in protein levels were detected by western blotting. Type XIV collagen is highly expressed during embryonic tendon development (Young et al., 2000) and subsequently replaced with type XII (Ansorge et al., 2009). In the present study no type XIV was detected by western blot suggesting that the tissue engineered tendons had matured beyond the developmental stage or the type XIV antibody was less sensitive than that for type XII.

The initial hypothesis was that 10% strain would act as a degenerative level of stimulation and result in impaired tendon formation based on reports (Wang, 2006) suggesting that >6% strain may result in damage to the structure of native tendon, but this was not strongly supported by the data. TEM analysis was used to investigate how the application of cyclic tensile stimulation manipulated collagen fibril maturation. Both longitudinal and transverse sections were used for imaging. The longitudinal sections show the length of the fibrils and clearly display the collagen banding pattern (Shoulders and Raines, 2009). The transverse sections were used to investigate the cross-sectional dimensions of the fibrils. In native tendon the collagen fibrils in the ECM have a varying cross sectional areas due to the presence of multiple fibril types. Starborg et al. (2013) show the diameter of rat tail collagen fibrils range from 0 nm to 240 nm. In the present study the fibril diameter peaked at approximately 80 nm suggesting that the collagen fibrils in the engineered samples are not as developed as that in native tendons. However the native rat tail tendon has approximately 40% of all fibrils with a diameter of 0 to 80 nm. The fibril diameter was largest in the 10% group and lowest in the control and 3% groups. Similar results have been seen in previous studies where stimulation has resulted in an increase in the range of fibril areas (Breidenbach et al., 2015). Kalson et al. (2011) applied slow stretch which double the length of fibrin-based tendon-like constructs over 4 days and found an increase in fibril diameter from 34.4 to 38.4 nm (a 12% increase). The present studies results would therefore suggest a more developed

tendon with the application of cyclic tensile loading. A comparable increase in collagen fibril diameters in cell engineered tendons to native tendons may require a combination of slow stretching, cyclic strain or optimised concentrations of suitable combinations of growth factor cocktails (Hagerty et al., 2012, West et al., 2015).

Previous work by Lee et al. (2017) and Atkinson et al. (2020), both showed finite element analysis data for engineered tissue cyclically loaded between two posts (as with our study). The force displacement images across the sample showed that the highest and lowest value of force is located around the posts (high variation), whilst only the median force acts in the centre (low variation), it was therefore hypothesised that the highest alignment would be at the centre of the engineered tendons where the force is most consistent. Through staining with the CNA35 collagen-probe and image analysis this was observed for all groups. The 10% strain groups anchor point region was found to be the most aligned, however it is not currently known if this is due to purely mechanical processes, or if cell-directed fibril alignment or collagen isoform composition play a role in orientation.

Several publications have routinely showed an increase in fibril cross sectional area and alignment results in an increase in the mechanical properties of tissue engineered tendon (Liao and Vesely, 2003, Battaglia et al., 2003, Lin et al., 2004). In the present study the increased maximum stress corresponded with a decrease in collagen fibril diameter (3% strain group), although ultimate stress has previously been shown to be unrelated to collagen fibril diameter, in *ex-vivo* stress-deprived tendons (Lavagnino et al., 2005). An increased rate stress relaxation was detected with increasing strain rates. Changes in the rate of stress relaxation may be in response to a decrease in GAGs, as fluid flow is disrupted into and out of the tissue, or a decrease in SLRPs (Elliott et al., 2003, Legerlotz et al., 2013, Ahmadzadeh et al., 2015, Robinson et al., 2017, Screen et al., 2011). GAGs were only investigated through a qualitative measurement, Alcian blue staining, highlighting no apparent differences between loading conditions, however the gene expression of the SLRP decorin was investigated with a quantitative assay. The 10% group showed the lowest gene expression of DCN aligning with increased rate of stress relaxation, decreased decorin has also been related to increased collagen fibril diameters (Zhang et al., 2006), of which the 10% group was found to have the largest. However no difference was detected for maximum stress or Young's modulus across the strain groups whereas previous work has shown decorin null mice to be inhibited for these parameters (Zhang et al., 2006). No change in Young's modulus between the static and cyclically strained groups aligns with a previous study which applied

2.4% cyclic strain to fibrin-based tendon-like constructs (Breidenbach et al., 2015). Conversely application of cyclic strain to collagen hydrogels at 2.4% strain or to poly-(ϵ -caprolactone) scaffolds at 3% strain (Banik and Brown, 2020) was found to increase the final modulus (Juncosa-Melvin et al., 2007). The choice of material for 3D culture has a substantial effect on the final outcome of the tissue engineered structure, from fibril diameter and alignment to the mechanical capabilities, these parameters should all be considered when selecting an appropriate material.

4.5.1. Conclusion

The extent of cyclic strain influenced collagen isoform expression, fibril diameter and fibre alignment as well as the mechanical properties of the cell-engineered tendons-like biomaterials. 3% cyclic strain slightly decreased fibril diameter whilst increasing maximum stress two-fold. The 5% cyclically strained group showed increased expression of the tenogenic markers scleraxis and tenomodulin, as well as COL2A1, COL3A1 and COL11A1 genes but significantly lower expression of the COL12A1 gene and reduced type III collagen protein content. COL12A1 expression was also decreased in 10% strain as was type II collagen protein content. The 10% strain group had increased expression of scleraxis, increased collagen fibre alignment in the mid-region and increased collagen fibril diameter, as well as a higher stress relaxation, indicative of an improved ability to alter its internal structure in response to external stress. Most parameters tested had a non-linear response to increasing cyclic strain during culture although fibre alignment, which increased with increasing cyclic strain, was a notable exception. These results suggest that different rates of cyclic loading will have varying effects on the engineered tissue. The structural response of the engineered tissue, collagen alignment and diameter, appeared to be more driven by the cyclic tensile loading than the production of specific collagens which showed less of a trend with loading. This suggests that structural properties of collagen can be driven by varying cyclic tensile loading alone, however the addition of specific supplements such as FGF or TGF- β may be required to see a more pronounced response within the collagen type composition. Further work is needed to confirm if the complete collagen composition can be used to determine the state of the tissue engineered structure.

Chapter 5

**Hydrostatic pressure stimulation of hMSC-
seeded fibrin hydrogels**

5.1. Introduction

Compressive mechanical stimuli play important roles during bone and cartilage development, homeostasis and maintenance. These forces include hydrostatic pressure, which creates a mechanical-biological coupled relationship that translates macroscale forces to cells. Hydrostatic pressure is caused by confined compressive force acting on fluid-filled tissues. In bone, hydrostatic pressure has been repeatedly shown to stimulate differentiation and tissue building, with dynamic or cyclic pressures around 300 kPa associated with upregulation of osteogenic gene markers (e.g. Cox2, Runx2, Opn) and the mineralisation of the ECM (Liu et al., 2009b, Liu et al., 2010a, Sugimoto et al., 2017, Stavenschi et al., 2018). In cartilage, hydrostatic pressure has been shown to significantly upregulate chondrogenic gene expression (e.g. Sox9, aggrecan, collagen type II) (Angele et al., 2003, Wagner et al., 2008, Ogawa et al., 2009) and chondrogenic matrix production from MSCs in some studies, whilst other researchers have found little chondrogenic effect (Finger et al., 2007, Zeiter et al., 2009). These previous studies indicate that hydrostatic pressure is a primary physiological stimulus driving bone adaptation to load, and a secondary (or contributory) stimulus in cartilage.

MSCs have the potential to differentiate into chondrocytes and osteoblasts in response to appropriate chemical and mechanical stimulation. During chondrogenic differentiation MSCs differentiate first into chondroblasts which generate chondrogenic ECM (e.g. collagen II, collagen IX, and aggrecan), resulting in the chondroblasts separating from each other and terminally differentiating into chondrocytes with a distinctive spherical morphology and pericellular matrix, or chondron (Lefebvre and Smits, 2005). Under osteogenic stimuli, MSCs may differentiate into osteoblasts, resulting in the synthesis and secretion of bone ECM (e.g. collagen I, osteopontin) and in turn mineralisation of the structure which is mediated by alkaline phosphatase and embedded ECM proteins such as osteocalcin (Huang et al., 2007).

Mature bone and cartilage can be subjected to both underloading (lack of exercise) and mechanical overloading (e.g. trauma) – which is theoretically transduced into broadly healthy and unhealthy levels of hydrostatic pressure (Elder and Athanasiou, 2009, Stavenschi et al., 2018). MSCs are therefore a good candidates for studying the role that physiological levels of exercise play in skeletal development by correlating macroscale forces associated with activity, to hydrostatic pressures generated in the tissue, and a characteristic response by musculoskeletal cells.

It has been calculated that due to stress shielding the actual pressure experienced by osteocytes in the canalicula-lacuna network of load-bearing bones is in the order of 300 kPa, significantly lower than that of pressure generated in the joint synovial fluid during exercise (~18 MPa) (Zhang et al., 1998). Therefore, it has been theorised that chondrocytes typically experience higher mechanical loads than osteoblasts, one aim of this study is to investigate if relatively low pressure inhibits or accelerates chondrogenic differentiation of adult MSCs.

Chemical stimulation has also been widely used to induce differentiation in cultured MSCs. For chondrogenesis, TGF- β 3, dexamethasone, Insulin-Transferrin-Selenium and L-ascorbic acid are added to the culture medium (Murdoch et al., 2007) whilst for osteogenesis; dexamethasone, β -glycerophosphate and L-ascorbic acid are used (Jaiswal et al., 1997). Though it is accepted that the MSCs will differentiate to the desired lineage, the resulting bone or cartilage does not display exactly the same ECM composition, structure or morphology as native tissue, which is thought to be due to the lack of physiological multi-modal stimulation in cell culture (Wang and Chen, 2013). The application of mechanical stimulation to cells in culture has therefore become a major area of research in tissue engineering. Most published studies focus on the role of hydrostatic pressure as a stimulus in combination with a single type of differentiation media (e.g. osteogenic or chondrogenic), but rarely are these compared in a single experiment.

The application of hydrostatic pressure *in vitro* is typically achieved through the use of bioreactors. There are a number of commercially available and custom designed hydrostatic pressure bioreactors, including the CartiGen HP which was developed by Professor Alicia El Haj and Dr James Henstock, engineered by TissueGrowth Technologies and originally marketed by Instron. The bioreactor was validated and used for several bone culture experiments, showing for example that expression of osteogenic genes (osteonectin and osteopontin) were significantly upregulated when chick femurs were cultured within the system, together with proportional increases in bone formation and density as the magnitude and frequency of pressure was increased (Henstock et al., 2013). Using the El Haj groups bioreactor as a basis an updated version was produced for the present study featuring the same culture chamber but with a new air compressor, valve manifold and software.

The majority of published studies report the effects of hydrostatic pressure on key ECM genes/proteins, neglecting to investigate the less abundant ECM components which may nevertheless play an important role in regulating tissue neosynthesis and act as important biomarkers. Some of the most routinely overlooked ECM components are the minor

collagens. Eight collagens have been reported in adult cartilage ECM: I, II, V, VI, IX, X, XI, XII (Luo et al., 2017), whilst in bone there are eleven: I, II, III, V, VI, IX, X, XI, XII, XIV, and XXIV (Tzaphlidou, 2005). In this investigation some of the collagens that are expressed in both bone and cartilage have been investigated, therefore acting as conserved biomarkers to assay differential responses between chondrogenesis and osteogenesis in response to mechanical loading. Through these combinations of collagen isoform expression it is possible to determine the extent and 'quality' of the tissue which is formed, i.e. how closely the newly formed ECM corresponds to native tissue, and therefore assess functionality as bioengineered tissue for regenerative medicine.

The effect of hydrostatic pressure on the differentiation of hMSCs and the subsequent collagen production has been investigated in the present study. Whilst it is well established that hydrostatic pressure aids in the differentiation of hMSCs cultured in osteogenic or chondrogenic media (Liu et al., 2009a, Saha et al., 2017) the isolated role is not. This study will look to apply a range of hydrostatic pressures from 0 kPa to 300 kPa, the upper limit of the bioreactor in use, to hMSCs cultured in either chondrogenic, osteogenic or supplement free (basic) media, establishing how significant of a role hydrostatic pressure plays in the differentiation of MSCs.

5.2. Hypothesis

Differentiation is not solely driven by chemical stimulation (culture media supplements) but can be achieved by varying one consistent form of mechanical stimulation applied to the cells to better reflect that of native tissue. The differentiation can then be established by investigating the collagens produced in response to the mechanical stimulation.

5.3. Aims

1. Investigate the role of relatively low levels of cyclic hydrostatic pressure in stimulation of chondrogenic differentiation of MSCs through characterising the collagens produced by the cells.
2. Investigate the role of physiologically relevant levels of hydrostatic pressure in stimulation of osteogenic differentiation of MSCs through characterising the collagens produced by the cells.

5.4. Experimental setup

5.4.1. Hydrostatic Pressure

For the hydrostatic pressure study an in house developed bioreactor was utilised based on a previously published design outlined by Henstock et al. (2013). The system operates using a well plate placed within an airtight hydrostatic pressure chamber (HPC) (Fig.5.1). The chamber then connected to a valve manifold (Festo, UK) which was fed compressed air at 400 kPa by an air compressor (BAMBI, UK) (Fig.5.1). The valve manifold was controlled by an in house developed software which regulated the magnitude, frequency and duration of pressure applied to the HPC. The compressed air could be supplied at a maximum of 300 kPa and was sterilised by passing through an air filter at the entrance of the HPC (Fig.5.1).

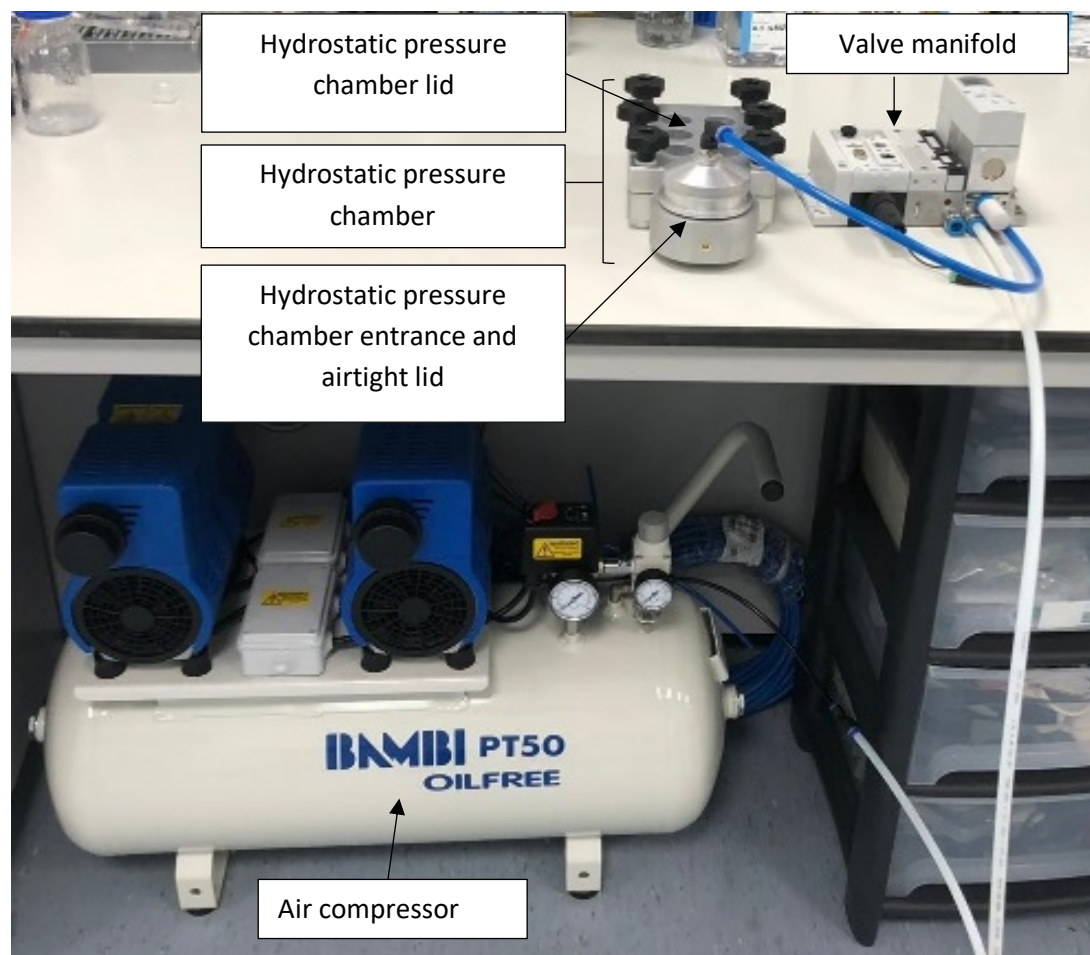


Figure 5.1. Hydrostatic pressure bioreactor setup.

Notes on usage: i) The temperature of the compressed air was not controlled, to account for this the none stimulated control group was left at room temperature for the same time period as the hydrostatically stimulated samples. ii) As the samples are stimulated with hydrostatic pressure a small amount of media was evaporated (higher in the higher-pressure

groups), this was controlled by replacing the vapourised media with sterile PBS at the end of the stimulation period.

Microtissues, the term used to denote the cell embedded fibrin hydrogels used throughout this study, were generated as explained in section 2.2.3.2. Briefly 1.25×10^6 cell/ml of hMSCs were seeded in fibrin hydrogels within a 48 well plate and allowed to contract for one week in basic media. Following the contraction phase the samples randomly were transferred by passive suction into a 24 well plate and cultured in designated culture media (basic, chondrogenic or osteogenic) for three weeks whilst being subjected to 0 kPa, 100 kPa, 200 kPa or 300 kPa hydrostatic pressure for one hour a day, five days a week at 1 Hz.

Analysis. Analysis of the microtissues was by the following techniques, for which the relevant n-numbers of samples are indicated in [brackets] (randomisation and statistical strategy described below):

<u>Assay</u>	<u>Number of samples</u>
▪ Protein analysis (Western blotting)	[six samples]
▪ Gene expression analysis (qPCR)	[six samples]
▪ 3D morphometry and densitometry (μ CT)	[six samples]
▪ Tissue microstructure (histology staining)	[three samples]

Experimental statistical design. All media types (basic, chondrogenic and osteogenic) were used across the plate to account for run variation. At the end of the contraction phase the microtissues were given a number (1-96) based on position in the 48 well plate (A1 on plate 1=1, F8 on plate 2=96), a random number sequence was generated (Random.org) with the first number in the sequence moved to position A1 in the control 24 well plate and the final number in the sequence to D6 on the 300 kPa plate. For each hydrostatic pressure individually each well in the 24 well plate was then given a new number (1-24) based on well position (A1=1, D6=24), the number sequence was randomised (random.org) with the first eight numbers being cultured in basic media, the second in chondrogenic media and the last eight in osteogenic media. Three experimental runs were required to generate enough samples. At the end of each run the eight samples within each media group for each loading condition were designated a number 1-8 and the sequence was randomised (Random.org), the first and second samples in the sequence were used for protein analysis, the third and fourth for gene analysis, fifth and sixth for μ CT, seventh for histology and eighth as a reserve.

5.4.2. Hydrostatic Pressure Loading Regime

After the one-week contraction period the samples were moved to a prepared 24 well plate and 500 μ l of the appropriate media was added to each sample. When not being stimulated

the well plates were kept in the same humidified incubator at 37°C in 5% CO₂. The HPC airline filter was sterilised using an autoclave whilst the HPC was sterilised with 70% ethanol and left to dry in a sterile cell culture hood. The air filter was then placed into the HPC and the air-tight lid was attached. Within the sterile cell culture hood the HPC lid was removed and the appropriate well plate was placed into the HPC. The well plate lid was then removed and the HPC lid was placed onto the HPC and secured. The HPC was then attached to the compressed air tank via the valve manifold and hydrostatic pressure was applied to the samples at either 100 kPa, 200 kPa or 300 kPa at 1 Hz for one hour a day, repeated for five days a week over three weeks. Stimulation was applied as a sinusoidal waveform as selected on the bioreactor control software. The control samples (not stimulated by pressure) were left in the sterile culture hood for one hour a day to replicate the temperature conditions of the loaded samples.

5.5. Results

5.5.1. Hydrogel weight and Appearance

After the hydrostatic pressure regime (three weeks stimulation) the samples were removed from the well plate and imaged using a dissecting microscope (Fig.5.2). Distinct differences can be seen between size, colour and opacity of the samples.

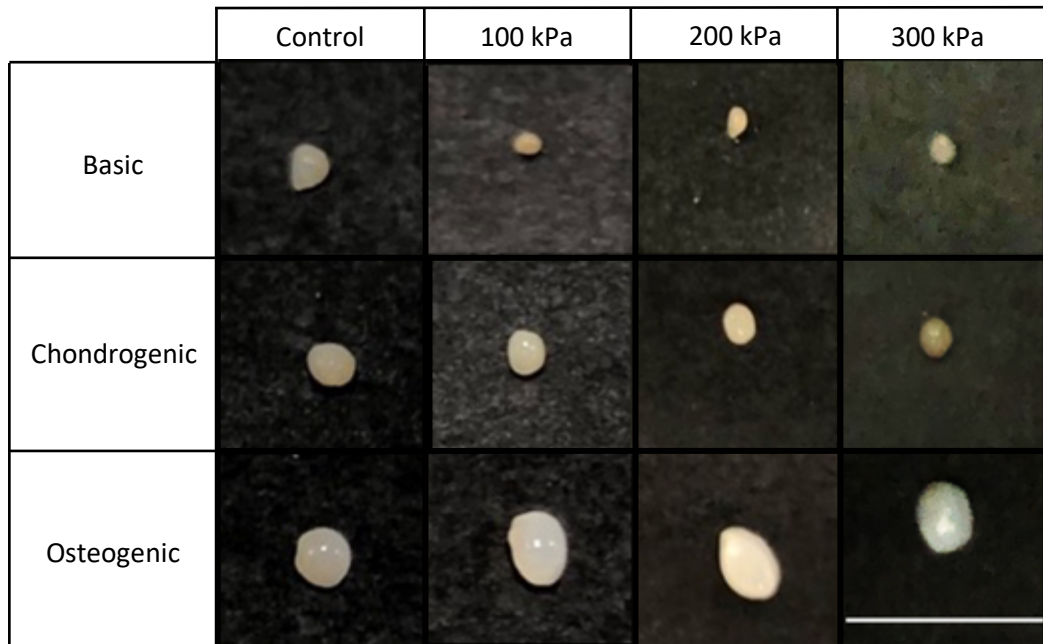


Figure 5.2. Representative images of microtissues cultured in basic, chondrogenic and osteogenic media following stimulation with intermittent, cyclic hydrostatic pressure for 21 days. Scale bar = 10 mm.

The wet weight of the samples was measured immediately after the completion of the experiment (Fig.5.3). Microtissues cultured in basic medium showed a decrease in weight with increasing pressure, while microtissues in chondrogenic medium showed no change in weight over the range of pressures used in this study. Microtissues cultured in osteogenic media generated the heaviest samples with the 200 kPa group being the heaviest overall (36.4 mg) - this was significantly higher than both the 100 kPa (23.2 mg, $p < 0.001$) and the 300 kPa (25.9 mg, $p < 0.05$) from the osteogenic group, whilst the control group was also significantly higher than the 100 kPa group (31.6 mg, $p < 0.001$).

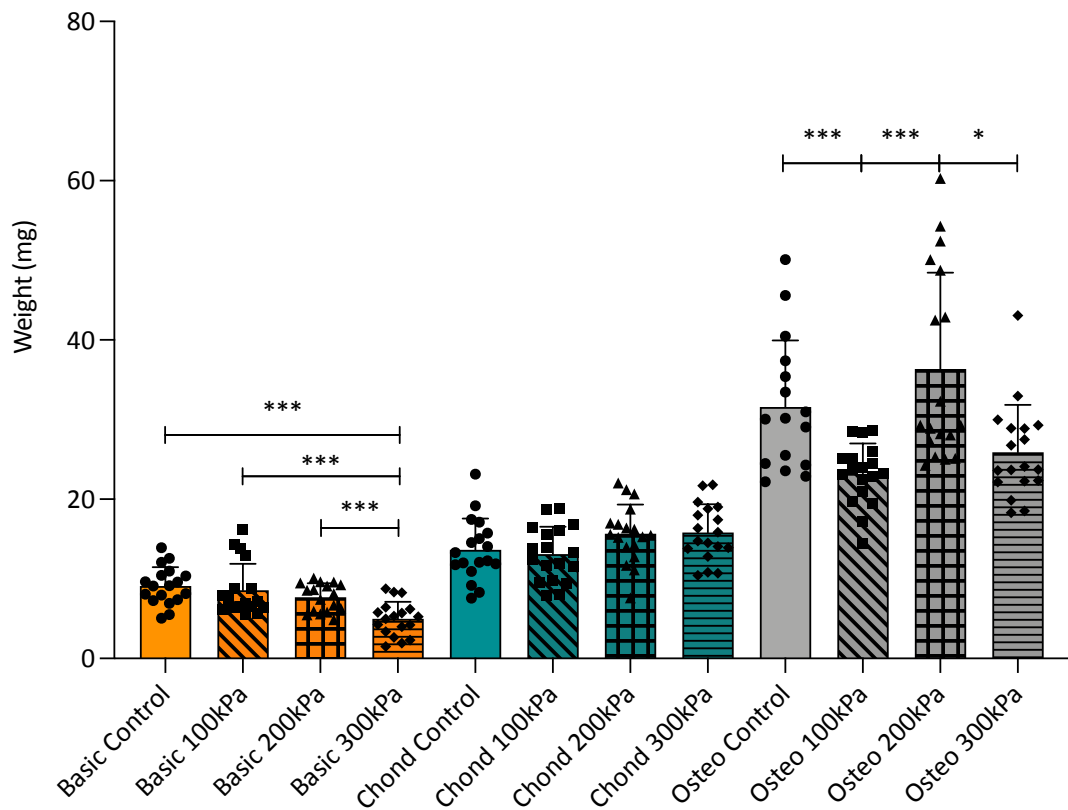


Figure 5.3. Weight of microtissues across basic, chondrogenic and osteogenic media groups. Error bars represent standard deviation. $n=18$ repeats. Statistical analysis using two-way ANOVA with Tukey's post hoc test and multiple comparisons, (* indicates $p < 0.05$, *** indicates $p < 0.001$).

5.5.2. Histology

5.5.2.1. H&E

Qualitative histology was used to visually assess the response of the microtissues to the applied hydrostatic pressure. H&E staining (Fig.5.4) highlighted differences in tissue structure caused by the differentiation medias, but with minimal noticeable differences within each group in response to hydrostatic pressure. The basic and chondrogenic groups appear similar, however the osteogenic group appeared significantly different to the two others with far less intense staining across the whole structure suggesting less ECM production by the cells in this condition.

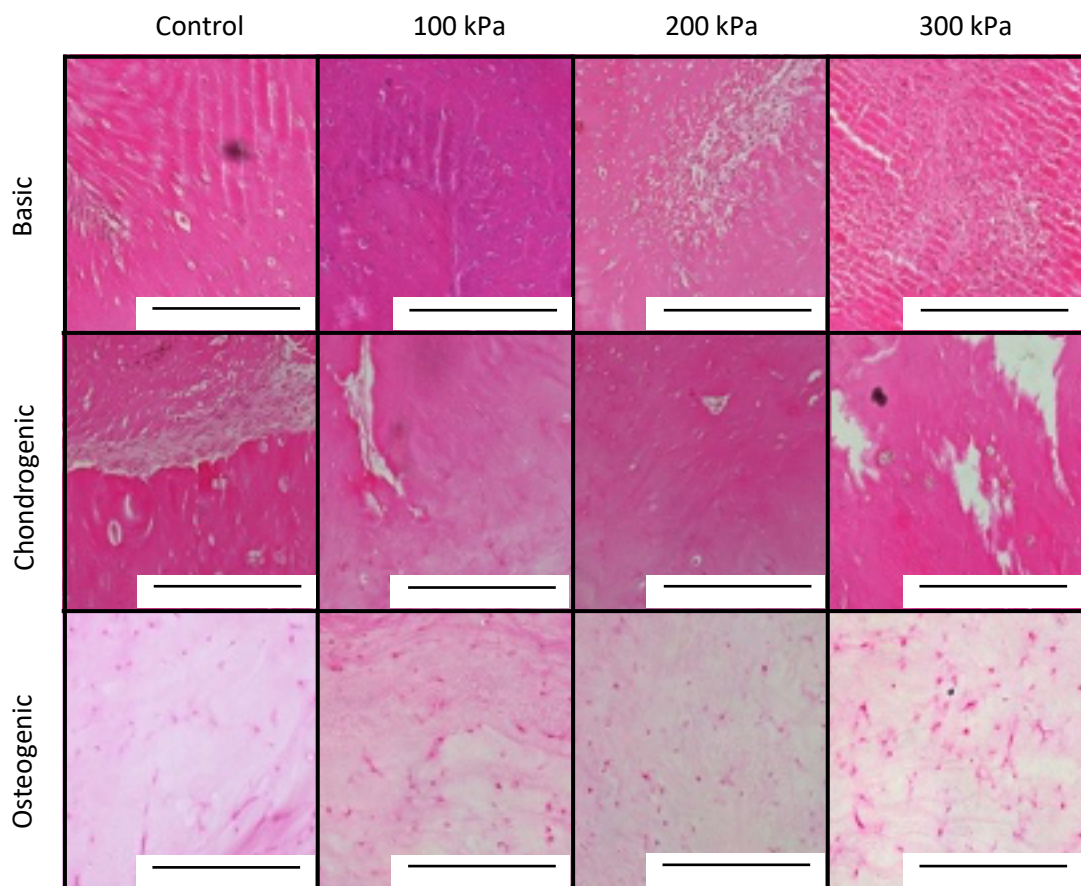


Figure 5.4. H&E staining of microtissues cultured in basic, chondrogenic or osteogenic media following 21-days hydrostatic pressure stimulation at 100 kPa, 200 kPa or 300 kPa. Representative images were taken with 10x objective, n=3 repeats. Scale bars represent 500 μm .

5.5.2.2. Alcian Blue

The basic and osteogenic media groups both displayed small amounts of GAG using Alcian blue staining (Fig.5.5) The most staining appears to be in the chondrogenic media group, where there appears to be an intense streak of blue running through the centre of the control and 300 kPa samples of the chondrogenic group, this suggests that the media is having driving effect on chondrogenic differentiation which low levels of hydrostatic pressure may be inhibiting. However the 100 kPa and 200 kPa microtissues from the chondrogenic media group still appear to have greater stain than other media groups, cross comparison is impaired by varying light intensity between groups. Networks of increased GAG deposition could be due to increased regional cell density (not seen on H&E), or due to localised deformations, or creases in the hydrogel matrix.

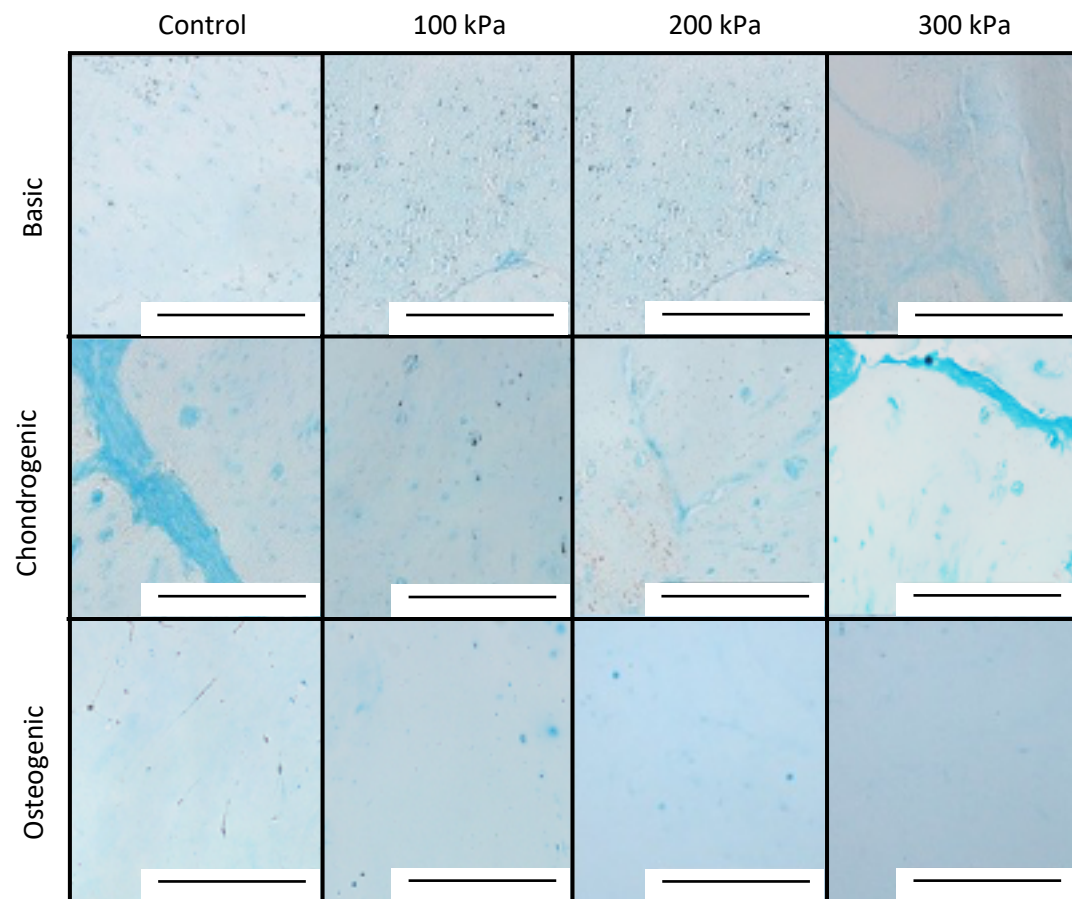


Figure 5.5. Alcian blue staining of microtissues cultured in basic, chondrogenic, or osteogenic media following 21-day period hydrostatic pressure stimulation at 100 kPa, 200 kPa or 300 kPa. Representative images were taken with 10x objective, n=3 repeats. Scale bars represent 500 μm .

5.5.2.3. Alizarin Red

Alizarin red stains calcium hydroxyapatite within the microtissue (Fig.4.6). Differences in overall staining intensity appear across the media groups, indicating various degrees of calcification occur in all samples, with noticeable changes in the pattern of mineralisation seen across hydrostatic pressure regimen.

Calcification was minimal in basic media, whilst in chondrogenic media areas of mineralisation were detected in microtissues exposed to 300 kPa pressure. All stimulated osteogenic media samples showed a distinctive pattern of mineralisation, which was not seen in the osteogenic media control, basic or chondrogenic media groups, indicating interaction between media supplementation and mechanical loading. The nodular pattern of mineralisation was most prominent in the osteogenic 300 kPa group.

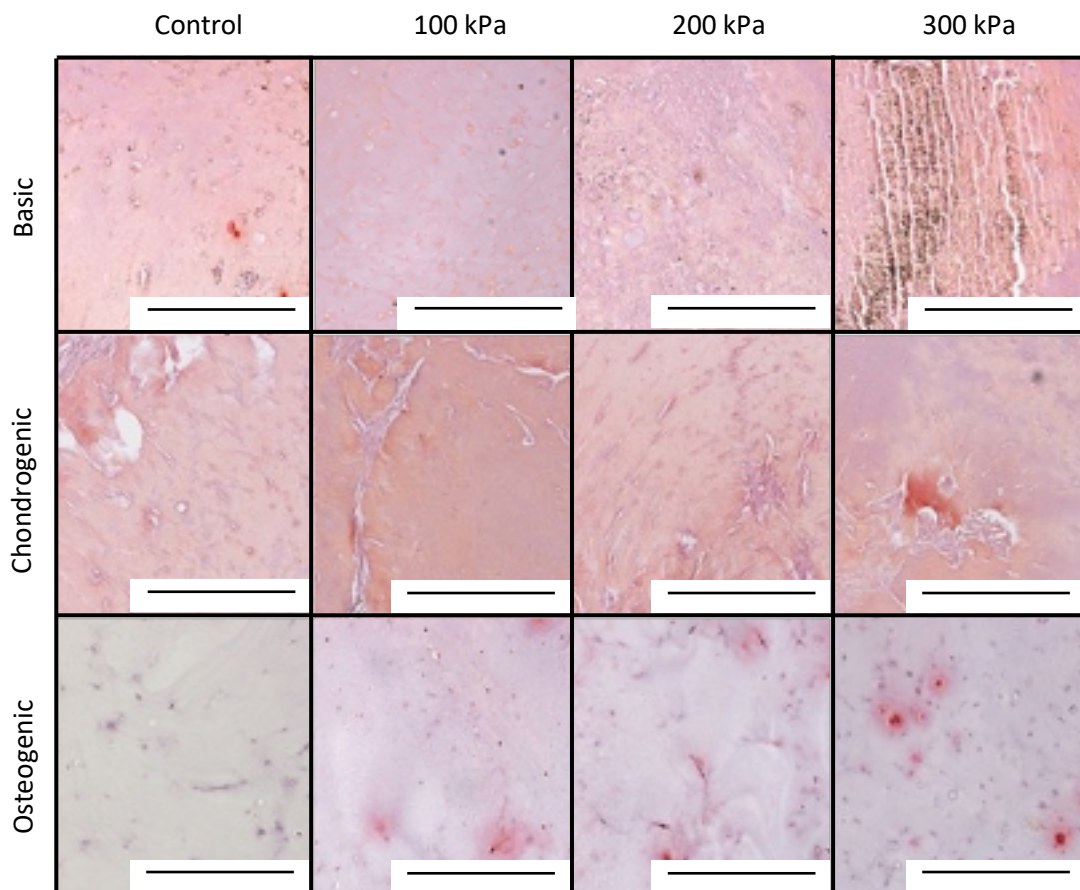


Figure 5.6. Alizarin red staining of microtissues cultured in basic, chondrogenic, or osteogenic media following 14-day period hydrostatic pressure stimulation at 100 kPa, 200 kPa or 300 kPa. Representative images were taken with 10x objective, n=3 repeats. Scale bar represents 500 μm .

The amount of calcium hydroxyapatite in the osteogenic media group was quantified by staining six samples from each regimen with Alizarin red and quantifying the extracted staining using cetylpyridinium chloride solution. The absorbance of the chelate was then measured to give a quantitative reading (Fig.5.7). The 300 kPa group was most calcified (0.237 Abs) and was significantly higher than all other groups.

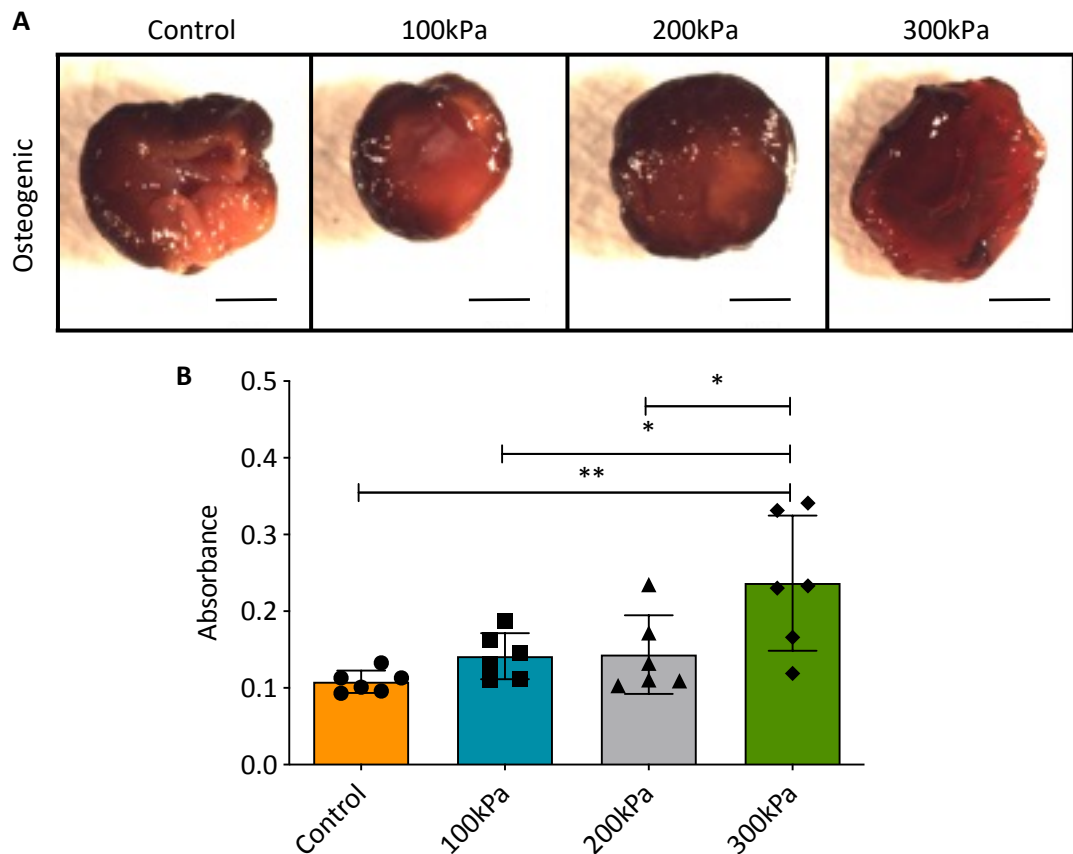


Figure 5.7. Alizarin red assay for osteogenic microtissues. (A) Representative images of Alizarin red stained hydrogels from the osteogenic media group. (B) Absorbance readings for these-stained hydrogels. n=6 repeats. Error bars represent standard deviation of the mean. Statistical significance measured using one-way ANOVA with multiple comparisons and Tukey's *post hoc* test (* indicates $p<0.05$, ** indicates $p<0.01$). Scale bar represents 1 mm.

5.5.2.4. Picrosirius Red

Under polarised light collagen stained with Picrosirius red illuminates red, green and yellow due to the birefringent properties of collagen (Fig.5.8). The illuminated staining appeared to be the lowest in the osteogenic media group, with none detected in the control group. The chondrogenic group appeared to have the highest density of collagen in the core of the hydrogel for all conditions whilst the basic media group appeared to have staining across the hydrogel, especially in the centre and edges. To highlight the collagen in the different groups different levels of exposure was required therefore little comparisons can be made across groups, however the osteogenic group required the highest increase in exposure to highlight any collagen, suggesting this group produced the least. The original un-enhanced images are found in Appendix I.

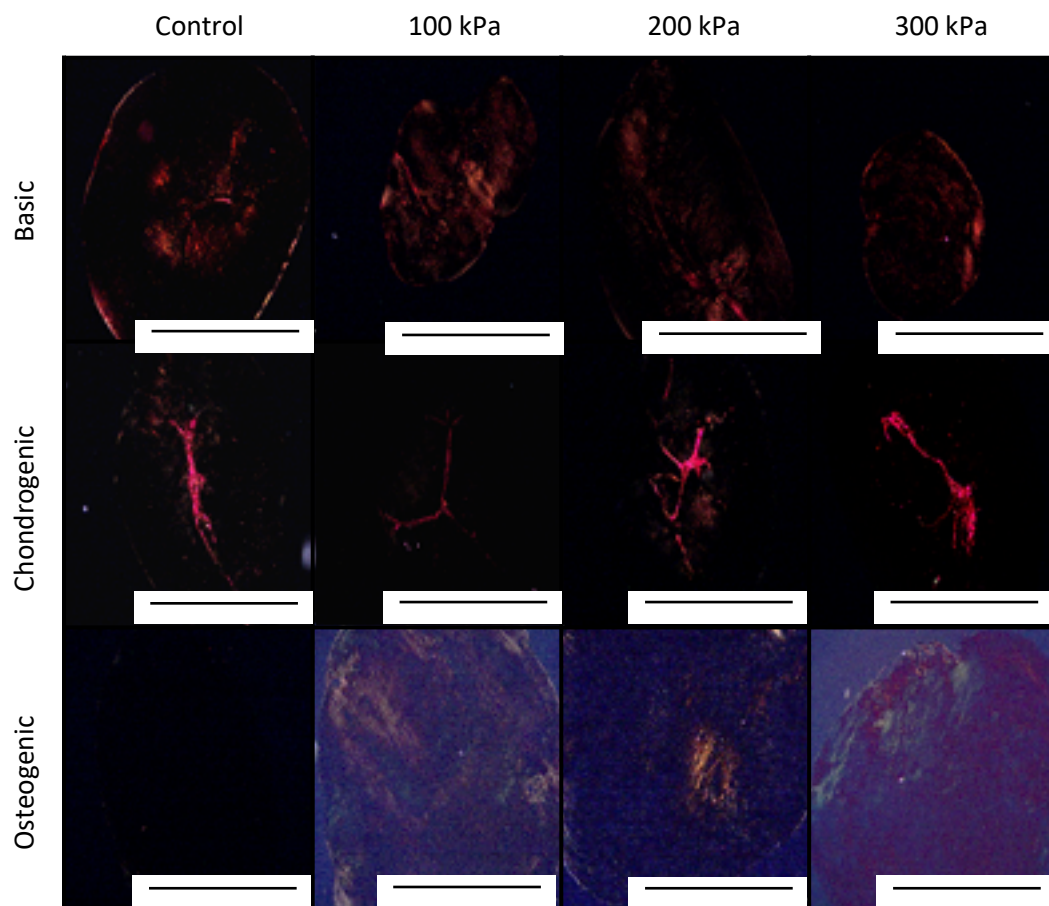


Figure 5.8. Picrosirius red staining of microtissues cultured in basic, chondrogenic, osteogenic media following 14-day period hydrostatic pressure stimulation at 100 kPa, 200 kPa or 300 kPa. Representative images are shown for Picrosirius Red to show collagen deposition under polarised light, the osteogenic group required increased exposure to detect any collagen, basic and chondrogenic were captured with same parameters. Representative images were taken with 4x objective, n=3 repeats. Scale bar represents 500 μm .

5.5.3. Alkaline Phosphatase Assay

ALP activity was measured in the culture medium at the end of each 7-day timepoint using the 4-methylumbelliferyl phosphate fluorescent substrate assay. No ALP activity was detected in samples cultured in chondrogenic media (fluorescence values were below the detection threshold / control even after extended incubation with the assay reagent).

In basic media (Fig.5.9A), the application of any hydrostatic pressure regime appeared to decrease ALP activity in the media compared to the unstimulated control, which was significant ($p < 0.01$) at the 7- and 21-day time points. This same general response was also observed in the ALP activity of samples cultured in osteogenic media (Fig.5.9B). Similarly, ALP activity decreased over time in both the basic media and osteogenic media groups.

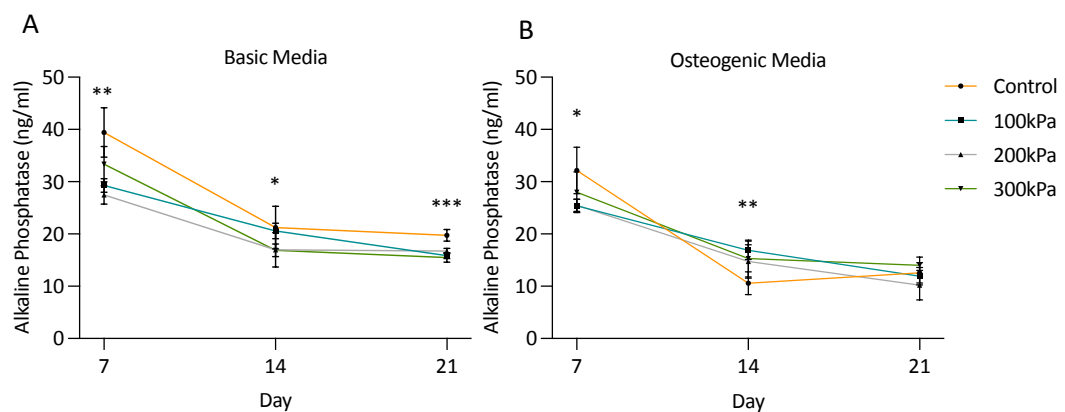


Figure 5.9. Graphs of alkaline phosphatase media content over the hydrostatic pressure stimulation period for Basic (A) and osteogenic (B) media groups. Error bars represent standard deviation. $n=6$ repeats. Significance measured using two-way ANOVA with multiple comparisons and Tukey's *post hoc* test and multiple comparisons (* indicates $p < 0.05$, ** indicates $p < 0.01$ and *** indicates $p < 0.001$).

5.5.4. Hydrostatic Pressure Collagen Gene Response

Collagen gene expression was measured for a range of collagen types found in bone and cartilage (Fig.5.10). COL2A1 was highest in the chondrogenic media group though no significance difference was seen across pressure regimen within the media groups. COL5A1 was significantly lower in the control microtissues of the basic media group versus the 200 kPa and 300 kPa microtissues. The basic 300 kPa microtissues were found to be significantly higher than the control microtissues for COL11A1. COL6A1 and COL9A1 were not detected in the basic media group.

COL9A1 and COL24A1 were not detected in the chondrogenic media group. COL10A1 showed a significant increase with hydrostatic pressure with both the 200 kPa and 300 kPa being higher than the control in the chondrogenic group. COL1A1, COL5A1, COL6A1 and COL11A1 all saw an increase with hydrostatic pressure peaking at different rates, none were significant. COL2A1 did not change across the pressure regime.

For the osteogenic media COL2A1 peaked at 100 kPa and but was not significantly higher than other pressures. Similarly COL10A1 peaked at 100 kPa which was significantly higher than 200 kPa. COL6A1 and COL11A1 also peaked at mid pressure regimes (100 kPa) but only COL11A1 saw significance with control, 100 kPa and 200 kPa being significantly higher than 300 kPa. COL5A1 was not detected in the control or 100 kPa regimes and only one sample expressed COL5A1 in the 200 kPa regime. COL24A1 was not detected.

Two-way ANOVA showed significance between media type for COL5A1 ($p < 0.05$). A significant interaction between media groups and pressure regimes was detected for COL10A1 and COL11A1 ($p < 0.001$).

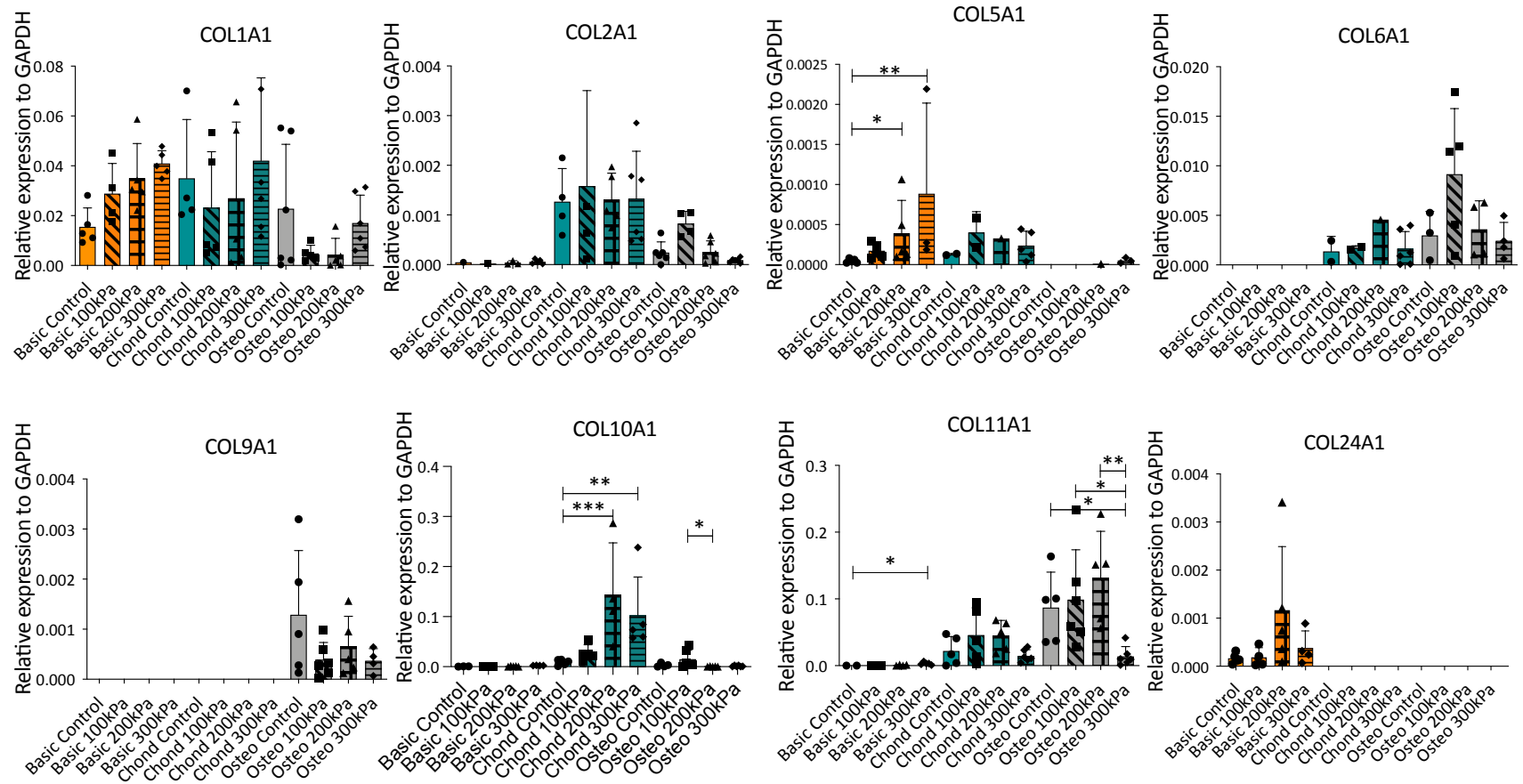


Figure 5.10. Collagen gene expression for hydrostatic pressure regimen. Values are shown normalised to GAPDH. Error bars depict standard deviation of the mean. $n \leq 6$ experimental repeats. Significance measured using one way ANOVA with multiple comparisons and Tukey's *post hoc* test for COL9A1 and COL24A1. Statistical significance measured using Two-way ANOVA with Tukey's *post hoc* test and multiple comparisons were performed on remaining genes. For non-parametric data a Kruskal-Wallis test was applied. (* indicates $p < 0.05$, ** indicates $p < 0.01$, *** indicates $p < 0.001$).

5.5.5. Collagen Composition in Response to Hydrostatic Pressure

Densitometry was performed following western blotting to analyse the collagen synthesis by the microtissues in response to hydrostatic pressure (Fig.5.11). Collagen V, VI and IX were not detected for any samples across all media conditions.

For basic media, mature alpha (tropocollagen), pro-form and beta (cross-linked) chain of collagen I all follow a similar trend of decreasing with increasing hydrostatic pressure. Collagen II and X follow a similar trend. Collagen XXIV sees an initial increase between the control group and 100 kPa and then a gradual decline up to 300 kPa, and all the pressure regimen are greater than the control group. Collagen XI was not detected.

Procollagen I, collagen I beta chain and collagen II all show a similar trend of increasing with hydrostatic pressure for the chondrogenic media group. Collagen I shows very little change across all pressure regimes. Collagen X, XI and XXIV decrease slightly with increasing pressure. No chondrogenic collagen expression was found to be significant.

Neither collagen II or XI was detected for any osteogenic media sample. Very little change is seen for collagen I, procollagen I or the collagen I beta chain across all pressure regimes with the 100 kPa group having the highest expression. Expression of collagen X did not change across pressure regimen. Collagen XXIV saw a decrease between the control and the hydrostatic pressure regimen, but was not found to be significant.

Two-way ANOVA showed significance across media for collagen $\alpha 1$ (XXIV) ($p < 0.001$). The interaction between media and pressure was significant for collagen $\alpha 1$ (I) beta chain and collagen $\alpha 1$ (X) ($p < 0.01$).

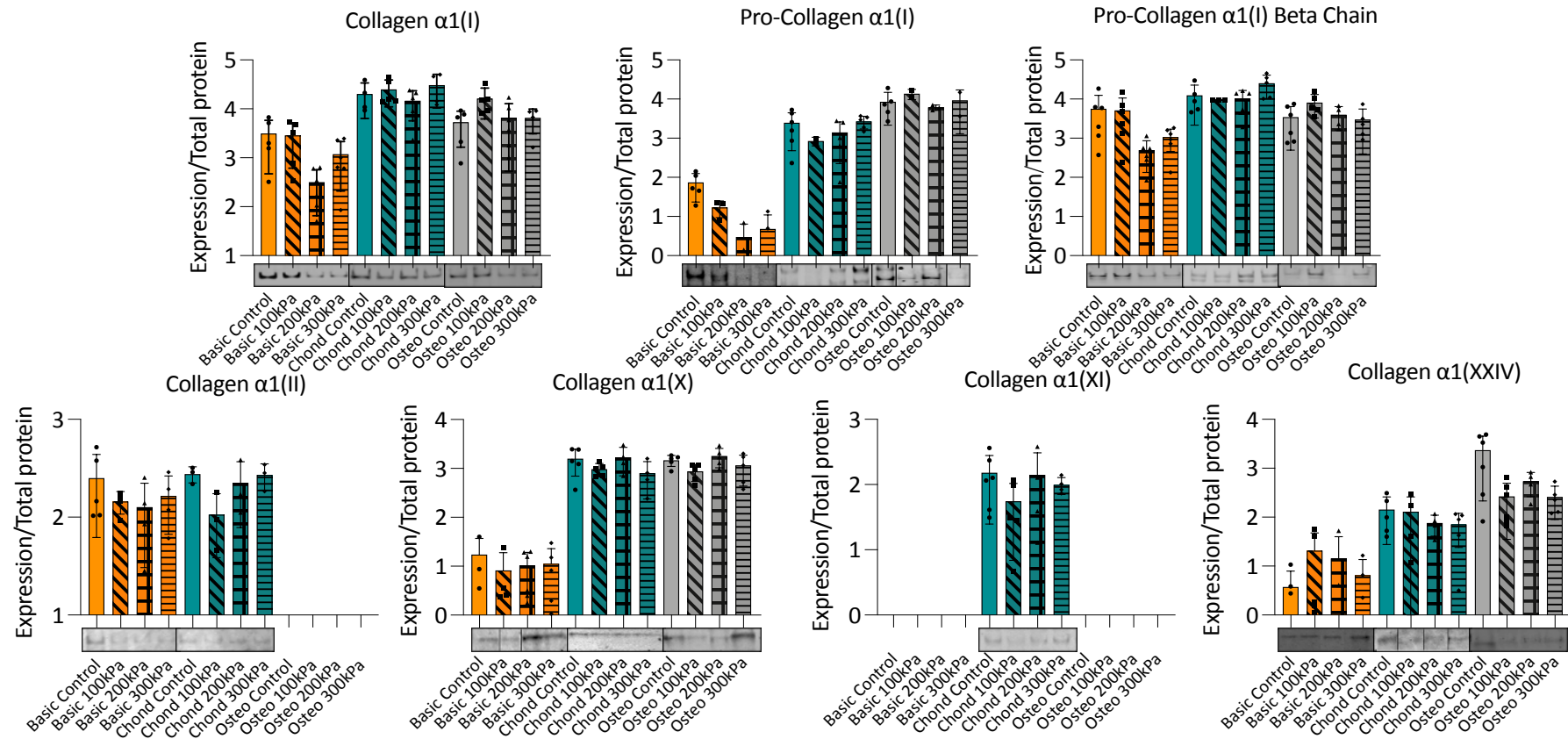


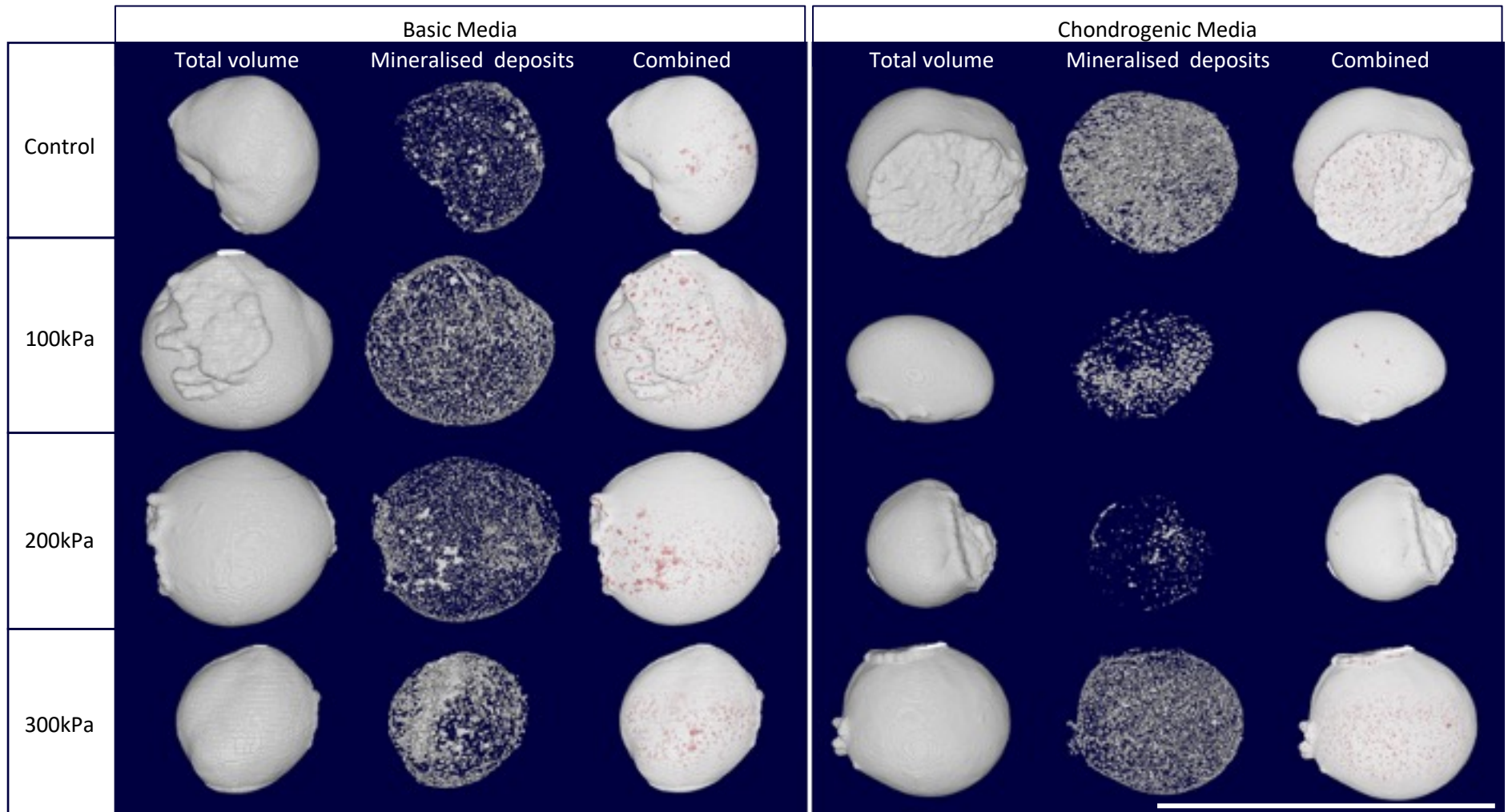
Figure 5.11. Densitometry of collagen types for hydrostatic pressure regimen. Representative images of western blots shown below graphs. Values are shown normalised to total protein. Error bars depict standard deviation of the mean. $n \leq 6$ experimental repeats. Statistical significance measured using one way ANOVA with Tukey's *post hoc* test and multiple comparisons for collagen $\alpha 1(XI)$. Significance measured using Two-way ANOVA with Tukey's *post hoc* test and multiple comparisons were performed on remaining collagen types.

5.5.6. Micro-Computed Tomography

Fig.5.12 depict representative μ CT images of the hydrogels for the basic, chondrogenic and osteogenic media groups. The first column of the figure shows the total microtissue volume, the second column shows the mineralised deposits within the microtissue volume and the third column shows the mineralised deposits (red) superimposed on the total volume. It appears that the basic media group had the most consistent mineralised deposits across all hydrostatic pressure conditions. The chondrogenic group appears to have a higher number of mineralised deposits in the control and 300 kPa groups. The osteogenic media group has a similar amount of mineralised deposits in the control and 100 kPa groups however this appeared to dramatically drop with the 200 kPa and 300 kPa groups.

The lowest percentage mineralised volume (Fig.5.13A) for all media types was the 200 kPa regime. The 300 kPa regime coupled with basic media had the highest overall percentage mineralised volume and was significantly higher than control ($p < 0.001$) and 200 kPa ($p < 0.001$). The control samples had the highest percentage volume for the chondrogenic media group, this was significantly higher than 100 kPa, 200 kPa and 300 kPa samples ($p < 0.001$). Both 100 kPa and 300 kPa were found to be significantly higher than 200 kPa ($p < 0.01$). The osteogenic control and 100 kPa samples were both significantly higher than the 200 kPa and 300 kPa samples ($p < 0.001$). Two-way ANOVA analysis showed that the interaction between pressure and media was significant ($p < 0.001$).

The density of the mineralised deposits (Fig.5.13B) was found to be highest overall in the 200 kPa and 300 kPa microtissues from the osteogenic media groups, with both the 200 kPa and 300 kPa samples being significantly higher than the osteogenic control ($p < 0.05$) and 100 kPa samples ($p < 0.01$). The 300 kPa basic media samples had the highest density whilst the control, 100 kPa and 200 kPa samples all have similar densities within the basic media group. The chondrogenic media group had the opposite trend to the basic media group with the control, 100 kPa and 200 kPa samples having similar and the highest densities in the media group. Two-way ANOVA analysis indicated a significant interaction between media and pressure for the density of the mineralised particles ($p < 0.001$).



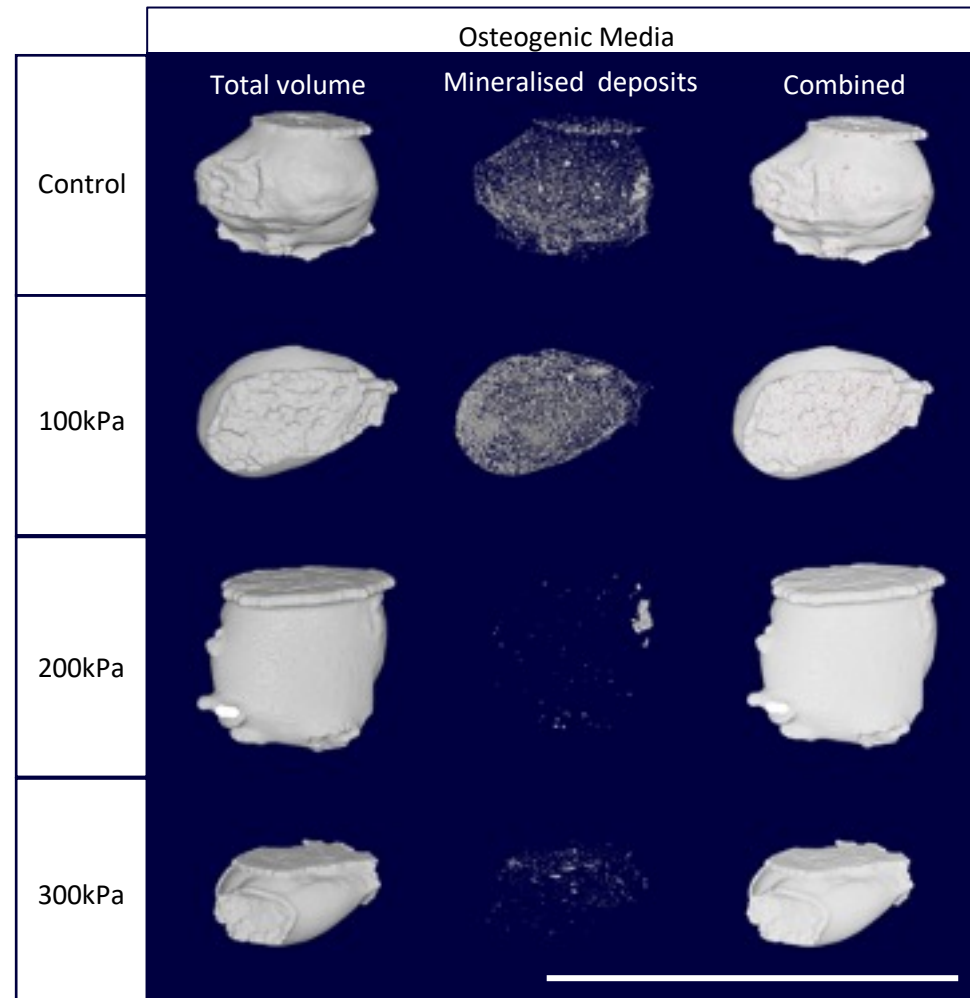


Figure 5.12. Representative μ CT images of microtissues from each media group and pressure regimen for total hydrogel volume, mineralised deposits and mineralised deposits superimposed onto total hydrogel volume. Scale bar = 10 mm.

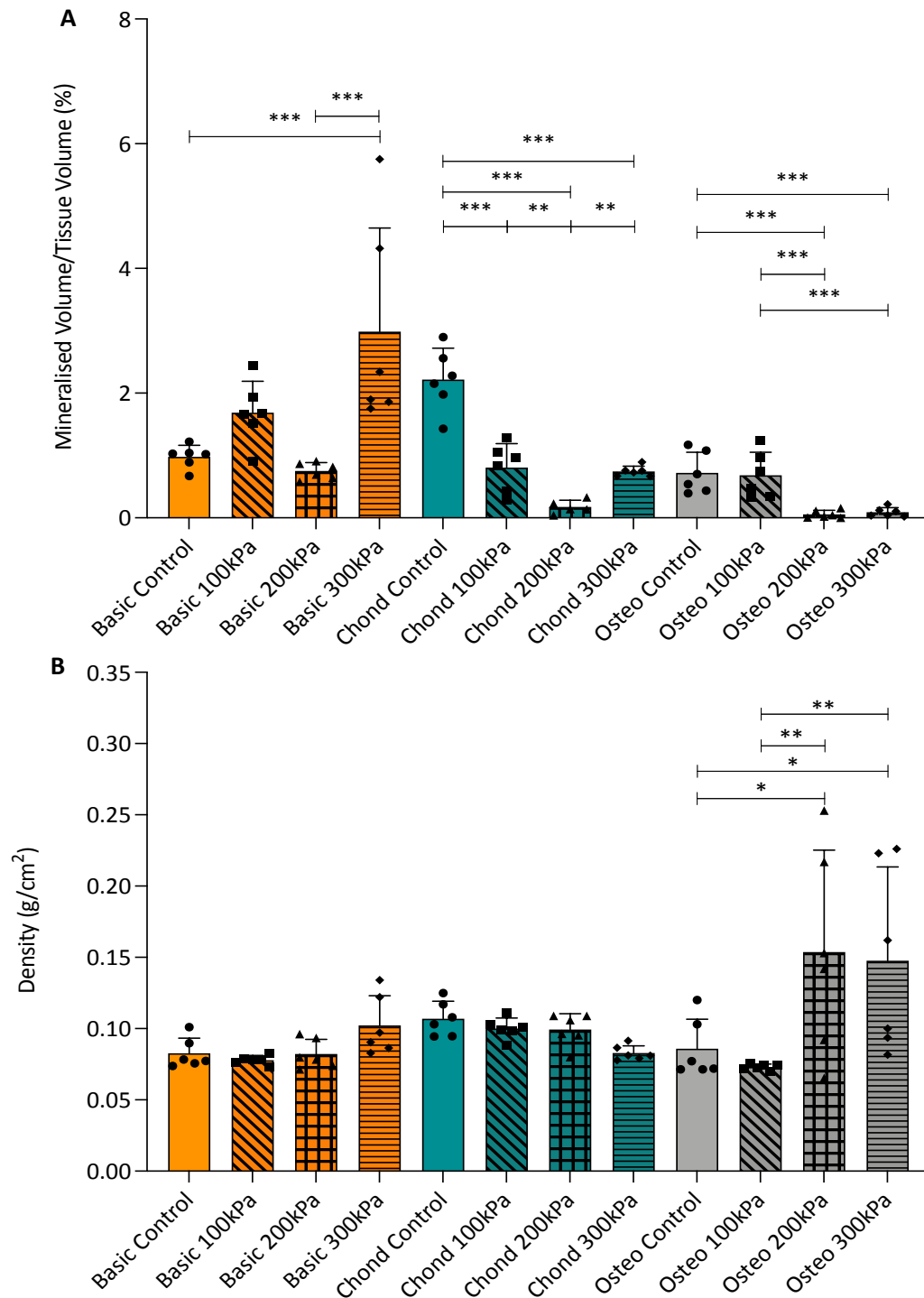


Figure 5.13. μ CT analysis of hydrostatic pressure microtissues. (A) Percentage of mineralised volume, comparison of all media groups. (B) Comparison of the density of mineralised deposits in microtissue across all media groups. Error bars depict standard deviation of the mean. $n=6$ repeats. Statistical significance measured using two-way ANOVA with Tukey's post *hoc* test and multiple comparisons (* indicates $p<0.05$, ** indicates $p<0.01$, *** indicates $p<0.001$).

5.6. Discussion

Hydrostatic pressure was applied to MSCs seeded within fibrin hydrogels at 100 kPa, 200 kPa and 300 kPa based on previous studies which found pressures of approximately 300 kPa to be consistent with pressure sensed by osteocytes in the canalicula-lacuna network of load-bearing bone (Zhang et al., 1998), this was also the upper limit of the bioreactor. The loading regimen was applied for three weeks at either 100 kPa, 200 kPa or 300 kPa, 1 Hz for 1 hour per day (five days on, two days off) following seven days of free swelling contraction in basic media. After the contraction period was completed the samples were either maintained in basic media or moved to osteogenic or chondrogenic differentiation media.

The microtissue appeared to change more due to the culture medium than the pressure applied, with colour and size varying between differentiation groups. The basic and chondrogenic media groups showed yellowing in colour and appeared similar in size (the chondrogenic slightly larger) whilst the osteogenic media group remained whiter and much larger. The basic media group was found to be the lightest of all groups with no significant differences across pressure regimens. The chondrogenic media group again showed no differences between pressure regimes and was found to be lighter than the osteogenic media group. The 200 kPa samples cultured in osteogenic media were found to be the heaviest overall and significantly heavier than the osteogenic 100 kPa and 300 kPa. Changes in construct size and weight has previously been seen as a result of hydrostatic pressure, aligning with the findings shown within the present study (Angele et al., 2003, Henstock et al., 2013). Results suggest that the media type drives the weight and size of the samples more so than the hydrostatic pressure regimen, however within the osteogenic media group (heaviest) the hydrostatic pressure begins to have an effect on the weight of the samples.

H&E staining intensity appeared consistent for the basic and chondrogenic media group but much lighter in the osteogenic media group (little effect across pressure regimen within media group), potentially due to a more sparse ECM owing to the significantly larger size of the hydrogel. A similar staining profile for Alcian blue, used to highlight GAG content within the ECM, was seen for the basic and osteogenic media groups suggested that hMSCs cultured in basic media were not differentiating towards the chondrogenic lineage. The chondrogenic media group appeared to have the most intense staining, particularly in the control and 300 kPa samples, this suggested that the media type was having a greater effect on the ECM production than the hydrostatic pressure regimen.

Alizarin red staining appeared to be highest in the 300 kPa osteogenic samples, aligning with previous work by Stavenschi et al. (2018). Quantified Alizarin red staining showed that the 300 kPa osteogenic samples were significantly more stained than all other regimens within the osteogenic media group. Staining in the chondrogenic and basic media groups appeared similar and lower than the osteogenic media group, which could suggest that the basic media alone is not enough to maintain differentiation as both Alcian Blue and Alizarin Red showed little expression of cartilage or bone markers within the ECM. Interestingly the 300 kPa chondrogenic samples appeared to show the highest level of Alizarin red staining. Previous work by Saha et al. (2017) also showed the highest amount of staining in the highest pressure group of cells cultured in chondrogenic media, suggesting that cells cultured under higher pressure may be undergoing hypertrophy. Hypertrophy would indicate bone formation beginning to occur within the microtissues as the MSCs have reached the end of the chondrogenic lineage and begin calcifying the cartilage (Mackie et al., 2008). However the alkaline phosphatase assay showed expression of ALP to be below the minimum detectable threshold for the chondrogenic samples, although this does not rule out that the cells may be undergoing hypertrophy in the higher pressure groups. The basic media group and osteogenic media group both expressed detectable levels of ALP, with highest expression at day 7 of hydrostatic pressure loading, aligning with previous work (Hess et al., 2010). The application of hydrostatic pressure sees the expression of ALP in the basic and osteogenic media groups to decrease after day 7, it therefore appears the highest level of osteogenic differentiation occurred during the first seven days of hydrostatic pressure.

Little difference was seen across the hydrostatic pressure regimes within the same media group for picrosirius red staining. The basic media group appeared to have the most widespread collagen within the ECM whilst the osteogenic media group had the lowest, further supporting the suggestion that the size of the osteogenic hydrogels resulted in a more sparse ECM (as seen in the H&E images).

Typically the minor collagen genes are not investigated when studies look to use mechanical stimulation to generate tissue engineered cartilage or bone. A range of major and minor collagens found within the ECM of both/either cartilage and bone has been investigated in the present study (I, II, V, VI, IX, X, XI, XXIV). Collagen I is the most abundant collagen in bone and seen as a marker of disease and ageing in cartilage. The expression of type I collagen at protein level was unexpectedly similar between the chondrogenic and the osteogenic media groups (osteogenic media group was expected to be higher), the basic media group had the

lowest expression of collagen $\alpha 1(I)$ with no significance seen in any group. However the gene expression of COL1A1 was more regulated by the pressure applied. For the basic media group the gene expression of COL1A1 increased with pressure, though not significantly. The control and 300 kPa samples had the highest expression within both the chondrogenic and osteogenic media group. Previous work sees hydrostatic pressure decreasing COL1A1 gene expression in chondrogenic media samples (Ogawa et al., 2015) and an increase in COL1A1 in osteogenic media samples (Huang and Ogawa, 2012) disagreeing with the results in the present study. As expected the trend in expression of pro-collagen $\alpha 1(I)$ and collagen $\alpha 1(I)$ beta chain was similar to that of collagen $\alpha 1(I)$.

As collagen II is the most abundant protein in cartilage it was expected to be highest in the chondrogenic media group and this was the case for the gene expression (COL2A1). There was no difference across the hydrostatic pressure regimens in any media group, therefore the main driver for COL2A1 expression appears to be media type. Despite the osteogenic media group having the second highest COL2A1 expression no protein was detected by western blot for this media group. The basic media group had very similar expression of collagen $\alpha 1(II)$ to the chondrogenic media group with no difference between hydrostatic pressure regimens. Previous work has shown that a mixed medium containing both chondrogenic and osteogenic supplements sees significant increases in COL1A1 and COL2A1 with 1000 kPa hydrostatic pressure (Wagner et al., 2008), this does not directly align with the present results and may suggest that a combination medium with higher levels of hydrostatic pressure is more appropriate than the relatively low levels applied with isolated medium types. It is also important to note that the Wagner et al. (2008) study used collagen I hydrogels not fibrin which may have significant effects on the COL1A1 and COL2A1 expression.

No protein expression was detected for collagen V, VI or IX in any media group. The gene expression for COL5A1 was highest in the basic media group with consistent increases with hydrostatic pressure, with 100 kPa and 300 kPa being significantly higher than the control. The lowest expression of COL5A1 was in the osteogenic media group, which was not anticipated as collagen V is typically found in tissues with high levels of collagen I (bone) (Birk et al., 1989). Collagen XI has a similar function to that of type V and is found in tissue with a high concentration of collagen II (Kadler et al., 2008). This is not observed at the gene level with the osteogenic media group having the highest expression (200 kPa osteogenic samples being the highest overall significantly). The basic media group had the lowest expression of

COL11A1. However at the protein level only the chondrogenic media group show any detectable expression, with no difference between hydrostatic pressure regimens. This is consistent across all protein expression for the different media groups (except collagen XXIV) suggesting that the media group is having a more pronounced effect on the collagen production than the hydrostatic pressure stimulation. COL6A1 and COL9A1 are typically found in chondrogenic ECM's however here the highest expression of COL6A1 was in the osteogenic media group and the only detectable expression of COL9A1 in the osteogenic media group.

COL10A1 had the highest expression in the chondrogenic media group with significance seen in the 200 kPa and 300 kPa microtissues vs the control, this aligns with previous work by Ogawa et al. (2009). As collagen X is a marker for endochondral ossification this supports the hypothesis that the cells are beginning to undergo hypertrophy as seen in the histological analysis. COL10A1 expression for the basic and osteogenic media groups is much lower than the chondrogenic media group and sees no difference between hydrostatic pressure regimens. A combination of hydrostatic pressure and shear forces has been suggested to inhibit the production of COL10A1 in cartilage tissue engineering (Nazempour et al., 2017). Therefore it may be important to combine multiple mechanical stimuli to engineer a more 'healthy' engineered chondrogenic structure and prevent hypertrophy.

COL24A1 is only detected in the basic media group despite being a marker for osteogenic differentiation (Wada et al., 2006, Matsuo et al., 2008). At the protein level the osteogenic media group has the highest expression, whilst the basic media group shows the lowest protein expression, further suggesting that the absence of chemical stimuli is limiting the differential potential of the hMSCs and preventing the cells from moving down a specific lineage, instead, based on collagen production, they appear to be moving between multiple lineages.

μ CT has been previously proposed as a technique for investigating tissue engineered hydrogels (Dorsey et al., 2009), here Dorsey et al (2009) argue that whilst fluorescence imaging offers high resolution, μ CT allows non-invasive imaging of more opaque structures and yields quantitative analysis. In the present study the representative images appear to show differences between samples within media groups exposed to different hydrostatic pressure regimens, for example there appears to be a low number of particles in the 300kPa osteogenic microtissues compared to the control microtissues whilst in the basic media group it appears to show the opposite. μ CT analysis showed that the highly pressurised

osteogenic samples (200 kPa and 300 kPa) had by far the lowest percentage mineralised tissue of all groups. This was surprising when comparing to the alizarin red staining and assay. However when investigating the density of what had been produced it was clear that the 200 kPa and 300 kPa samples from the osteogenic media group had produced the most dense mineral (significant), agreeing with previous work (Henstock et al., 2013). This suggest that the cells generated a more mature and developed mineralised component rather than a random production seen in other groups. Further it shows that for the production of appropriate mineral, the cells require the mechanical stimulation as well as the chemical stimulation as the control and 100kPa samples from the osteogenic media groups show very little difference in structure compared to samples in the basic and chondrogenic media groups.

5.6.1. Conclusion

The combination of the different analysis techniques appears to show that the chemical intervention is having the driving effect on the cell fate. The hydrostatic pressure regimen appeared to have a greater effect on the expression of the different collagen genes than the protein synthesis where the protein content was consistent across all hydrostatic pressure regimens with the only differences being generated between the different media types. This suggests that whilst the hydrostatic pressure is generating an intra-cellular response, the subsequent synthesis is being dictated by the media supplements. However the production of mineralised deposits within the osteogenic media group appears to be heavily influenced by the application of hydrostatic pressure. The synthesis of collagen $\alpha 1(I)$ did not significantly change across the osteogenic media group with pressure whilst the mineral density did, suggesting that the mechanical stimulation influenced the mineralisation of the tissue, potentially a response to stiffen the structure. Hydrostatic pressure acting without a differentiation media did not appear to enable lineage commitment from the MSCs with the microtissues displaying both chondrogenic and osteogenic responses without significant commitment to either. The present work shows that these rates of hydrostatic pressure alone are not enough to drive differentiation, a variation in media supplements or a change to the rate or amount of hydrostatic pressure may be required to generate a greater level of differentiation by the MSCs. Collagen synthesis was not an ideal tool for determining the MSC differentiation with hydrostatic pressure but appeared more useable with the media types, this suggests that to generate a detectable response the hydrostatic pressure regime needs optimising, with higher loading potentially required for chondrogenic differentiation.

Chapter 6

Differentiation of 3D Cultured hMSCs in Simulated Microgravity

6.1. Introduction

During their time in space astronauts show a distinct loss of bone mineral density of up to 20% in the lumbar spine, pelvis and proximal femur (Grigoriev et al., 1998). It is apparent that the lack of gravity has a significant effect on the astronauts cells leading to bone loss and muscle wastage, with this response being traced back to the astronauts MSCs. Microgravity reduces the mechanical load acting on cells, including those cultured *in vitro*, and therefore presents an opportunity to investigate how cells respond to an absence of mechanical loading, rather than applied, directional forces.

Research has shown that the reduction in loading caused by microgravity can suppress the osteogenic differentiation of MSCs, with one study indicating that this occurs through inhibition of the mechanotransduction pathway, MAPK (Meyers et al., 2004). Phenotypic analysis of cells shows that microgravity induces a rounded cell morphology with a distinctively reorganised cytoskeleton compared to normal gravity in MCF-7 cells (breast cancer cell line) (Li et al., 2009). Blaber et al. (2015) demonstrated that microgravity inhibits murine embryonic stem cell differentiation and therefore that mechanical unloading results in the preservation of stemness, suggesting that microgravity may be a useful culture condition for sustained 3D culture of undifferentiated MSCs.

A number of studies have shown greater expression of tissue specific genes from stem cells cultured under microgravity conditions compared to normal gravity culture. A consistent example across the literature is the increased neural potential for MSCs cultured in microgravity (Mitsuhara et al., 2013, Mattei et al., 2018, Otsuka et al., 2018), other have shown increased proliferation potential whilst maintaining the undifferentiated state of MSCs (Yuge et al., 2006, Yuge et al., 2011). The response of musculoskeletal tissue cells in microgravity varies with osteogenic cells typically showing impaired differentiation (Nabavi et al., 2011) and chondrogenic cells showing enhanced differentiation (Ulbrich et al., 2010). It is apparent that microgravity has a significant effect of the fate of cells and may be a useful tool in the long-term culture of MSCs for future therapies.

As it is not possible to remove or entirely shield the gravitational force on Earth, multiple systems have been developed to apply microgravity to cell culture for ground-based experimentation. The three main options for investigators are: “free fall”, counteracting gravity or spatially distributing the gravity vector (Grimm et al., 2018).

Rotating ‘free fall’ Bioreactors. The rotating cell culture system (RCCS) (Fig.6.1A) was developed by NASA (Begley and Kleis, 2000) and enables cells to be cultured in free fall through the use of a slow-turning lateral vessel (STLV) (Schwarz et al., 1992). For the present study the free fall method has been utilised, this is achieved via a rotating vessel, specifically the RCCS 4H bioreactor (Synthecon, Houston, USA).

Random positioning bioreactors. Random positioning machines work to make the average gravitational vector equal to zero (Hoson et al., 1997). In these bioreactors the vertical orientation at which cells grow is continuously changed so that the gravitational pull on the sample is distributed equally, spatially and temporally, therefore preventing the biological system to adapt to a single gravitational vector (Grimm et al., 2018).

Levitation strategies. The earth's gravitational field can be counteracted using buoyancy or magnetic levitation. For this to be achieved for tissue engineering, the cells or biomaterial scaffold requires modification to enable magnetic forces to act, preventing this being an option for many studies. An example of this technique is the study by Hammer et al. (2009), in which MC3T3-E1s (an osteoblast cell line) were cultured on a specifically designed microcarrier and then held within a magnetic field to counteract the gravitational force.

Short term ‘true’ microgravity on Earth. Short term microgravity can also be achieved through parabolic flight and drop towers. Parabolic flight can be used to stimulate space flight by capturing the early effects of hyper/microgravity and is achieved through an aeroplane performing repeat parabolas (Grosse et al., 2012). An alternative technique for short term microgravity is the drop tower, where the experimental sample is placed within specially designed vessels, the vessel is then moved to the top of the drop tower and released, allowing it to fall a fixed distance, in the case of the ZARM drop tower this is 110 m and takes 4.74 seconds (ESA, 2003), enabling very short experimental observations.

True microgravity. To provide long-term, true microgravity for extended and detailed biological research necessitates use of orbital platforms, such as microsatellites or facilities onboard the ISS. Several researchers have used the ISS for research, including a group at the University of Liverpool who aim to reach the ISS by the end of 2021 and are developing bioreactors for investigating links between muscle loss in astronauts and during ageing, with an emphasis on investigating the failure of adaptive responses to exercise in both situations (Jones et al., 2020). Several private companies now offer services to enable research groups to move their scientific investigations to the ISS, and national Space Agencies provide specific

funding for these activities. Consequently, research in true microgravity is a growing area with significant interest from a variety of stakeholders (Alwood et al., 2017, Afshinneko et al., 2020).

Previous work looking at MSCs cultured in microgravity has shown that the duration of the microgravity culture can have a major effect on the differentiation properties of the MSC. Xue et al. (2017) found that after 3 days of free fall simulated microgravity, rat MSCs showed enhanced potential to differentiate into endothelial, neuronal and adipogenic cells, whilst 10 days of culture promoted osteogenic differentiation. Studies have also focused on attempts to promote specific differentiation pathways in MSCs under microgravity culture. Mayer-Wagner et al. (2014), found that both hypertrophy and chondrogenesis differentiation was impaired for hMSCs cultured in microgravity, with downregulated COL10A1 and COL2A1 as highlighted outcome measures. Therefore, whilst microgravity is not ideal for chondrogenesis it may be a useful tool in inhibiting hypertrophy at later stages of cartilage tissue engineering (Mayer-Wagner et al., 2014).

The application of microgravity has been shown to partially regulate the differentiation of MSCs (Xue et al., 2017), work by Yuge et al. (2006) have gone on to show that MSCs cultured in microgravity preserve their stemness through strong proliferative characteristics typical of stem cells and the ability to differentiate whilst their 1 g counterparts largely lost these abilities. The inhibition of differentiation may be due to microgravity preserving the undifferentiated state of the MSCs, and therefore enabling long term culture of the cells before differentiation is required. MSC culture *in vitro* generally leads to either spontaneous differentiation or eventual senescence (McCulloch et al., 1991, Digirolamo et al., 1999, Banfi et al., 2000, Baksh et al., 2004), and so strategies that may preserve undifferentiated or uncommitted MSC *in vitro* have multiple applications, particularly for the development of cell therapies (Huang et al., 2020).

As reported in this chapter, the cells were cultured within a 3D fibrin hydrogel and maintained the culture in microgravity for 3 weeks using a rotating 'free fall' bioreactor, the RCCS 4H (Synthecon, Houston, USA) (Fig.6.1A). This bioreactor generates a microenvironment where high mass transfer is achieved with low shear stress. True microgravity would feature no downward gravitation force (Fig.6.1Bii) - this cannot be achieved on earth, therefore the sample will experience gravitational force (Fig.6.1Bi) but this will mostly be offset by the centrifugal force and drag force generated by rotating the sample within the vessel (Ronaldson and Vunjak-Novakovic, 2016). Through an inner co-rotating

cylinder with a gas exchange membrane, the microgravity chamber can rotate at specified rates, whilst supplying the culture with appropriate gas exchange. The control group were replicate 3D cultures maintained in static culture within a 12 well plate. To account for the fluid shear and increased nutrient diffusion generated by the rotating liquid (Khodabukus et al., 2018), a third group was used, in which replicates cultured within a 12 well plate were placed onto a plate rocker to provide increased nutrient perfusion and shear flow under a constant gravity vector (Juhas and Bursac, 2014). Whilst the rocker plate may not generate the same level of increased nutrient diffusion as the bioreactor, this condition went some way to highlight the effects of nutrient diffusion provided by the bioreactor helping to separate the role of microgravity. As in previous chapters, differentiation of the MSCs was characterised via collagen production, specifically in this case by considering several collagens that are characteristic of a broad range of musculoskeletal tissues (tendon, bone and cartilage).

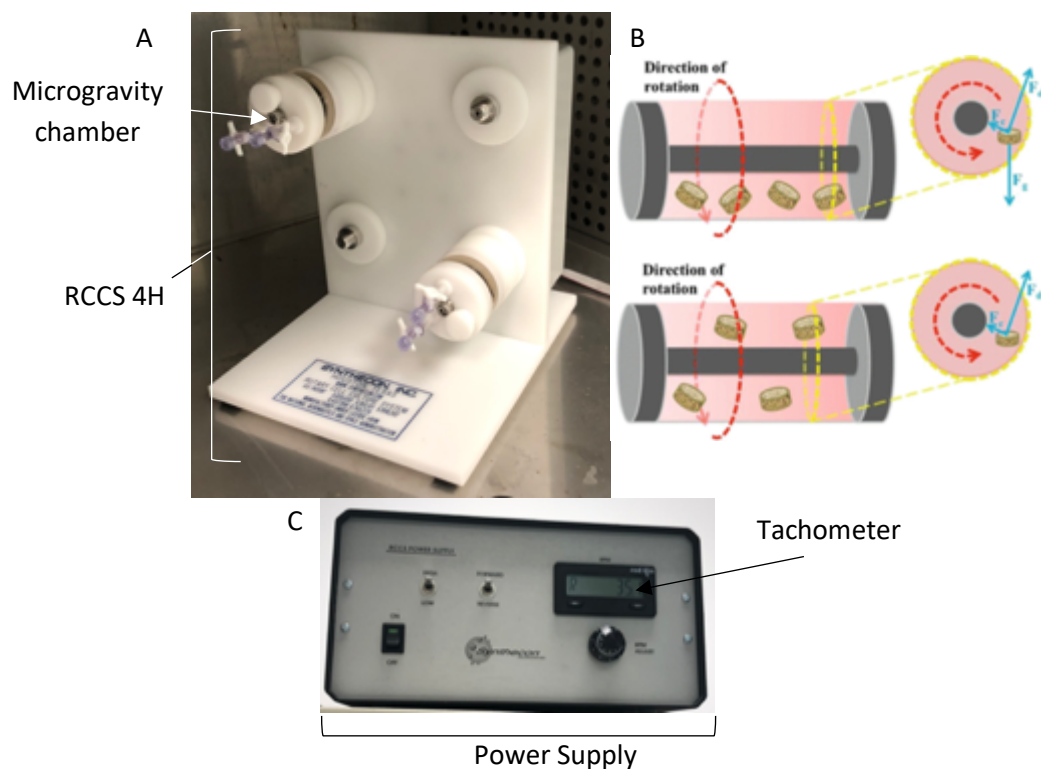


Figure 6.1. Free fall microgravity bioreactor setup. (A) Microgravity bioreactor RCCS 4H used to culture hMSCs under microgravity conditions. (B) Diagram of samples in simulated microgravity adapted from Ronaldson and Vunjak-Novakovic (2016). (C) Power supply displaying set RPM ensuring constant free fall of samples.

6.2. Hypothesis

The application of microgravity inhibits hMSC differentiation (preserves stemness) due to the lack of an over-riding mechanical stimulus. The collagen isoforms synthesised by the hMSCs during culture can be used to characterise the stemness of the cells.

6.3. Aims

1. Investigate the cell response to microgravity culture through the expression and synthesis collagen and microtissue structural changes.

6.4. Experimental Design

6.4.1. Microgravity Culture

The microtissues were generated as stated in section 2.2.3.2, briefly 1.25×10^6 cells/ml were seeded within fibrin hydrogels within the well of a 48 well plate and cultured with basic media. The samples were scored from the edge of the well with a 10 μ l pipette tip and allowed to free swell for one week. After the one-week contraction period the microtissues were moved to the three different culture chambers: microgravity bioreactor, static plate or dynamic plate. To select which microtissues were moved into which condition, each was given a number and a random number sequence was generated (RANDOM.org). The first 24 samples were placed under static condition, the second 24 under dynamic conditions and the final 27 in microgravity culture. The rotation speed of the microgravity bioreactor was defined as 35 rpm (Fig.6.1C) placing the samples in constant free fall and therefore under microgravity conditions (Maguire and Novik, 2010). The generated samples were used as:

<u>Assay</u>	<u>Number of samples</u>
▪ Protein analysis (Western blotting)	[six samples]
▪ Gene expression analysis (qPCR)	[six samples]
▪ 3D morphometry and densitometry (μ CT)	[six samples]
▪ Tissue microstructure (histology staining)	[three samples]

The extra samples not accounted for in the analysis techniques provided replacements for any failed samples. Due to an infection on one plate from the dynamic group no samples were generated for histology and only five for μ CT.

The final microtissues in the microgravity chambers were removed and placed into a 24 well plate (i.e. one sample per well, three samples stored as reserves). For all culture conditions each microtissue was given a number from 1-24 based on the position in the plate (A1 = 1, H8 = 24) and a random number sequence was generated (Random.org). The first six numbers were used for protein analysis, the second six for gene analysis, the third six for μ CT, the next three for histology and the remaining three as reserves

6.5. Results

6.5.1. Hydrogel Weight and Appearance

Representative images of the microtissues for each condition are shown in Fig.6.2A. These images were taken at the end of the experimental regime and appear to show differences in the size of the samples between the conditions. Dynamic stimulation generated the smallest microtissues whilst the microgravity and static culture were both similar in size, which was confirmed by analysis of the wet weight of the microtissues (Fig.6.2B). The microgravity samples were found to have a heaviest mass, with the dynamic group the lowest. The static group was not significantly different to either.

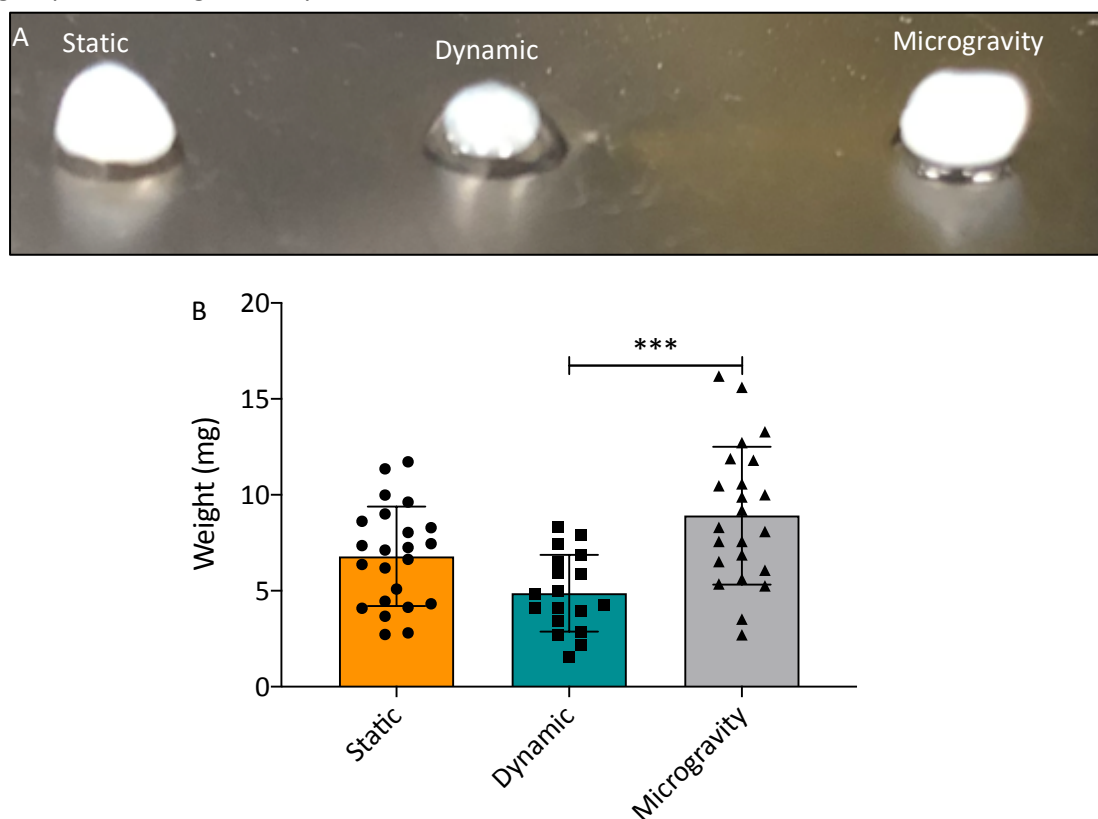


Figure 6.2. Size and weight of microgravity microtissues. (A) Representative images of the microtissues culture in normal gravity (static and dynamic) and microgravity conditions. (B) Weight of microtissues following one week contraction phase and three week microgravity or normal gravity phase. Error bars represent standard deviation. $n=23$ repeats. Statistical significance measured with one-way ANOVA with Tukey's *post hoc* test and multiple comparisons (***) indicates $p<0.001$).

6.5.2. Histology

Due to a cell culture infection in the dynamic stimulation group not enough microtissues were produced for histological analysis, here only static and microgravity are compared. Representative images of H&E staining (Fig.6.3) appear to show similar structures for both the static and microgravity groups.

Alcian blue staining (Fig.6.3) appeared to show increased GAG content in the core of the of the static group compared to the very low levels of staining in the microgravity group. Alizarin red staining highlighted one calcified nodule in the ECM (indicated with black arrow) of the static group, no nodule staining was seen in the microgravity group, whilst nodules were not widespread they may suggested increased osteogenic differentiation. Collagen was stained with Picosirius Red and imaged using polarised light. Both groups have some birefringent (organised) collagen, however more collagen appeared to be throughout the structure in the microgravity image, whilst the collagen distribution appears mostly on the microtissue's edge in the static group. The picosirius red images required a large amount of enhancement to highlight any illuminated collagen, the original un-enhanced images are included to highlight the difference.

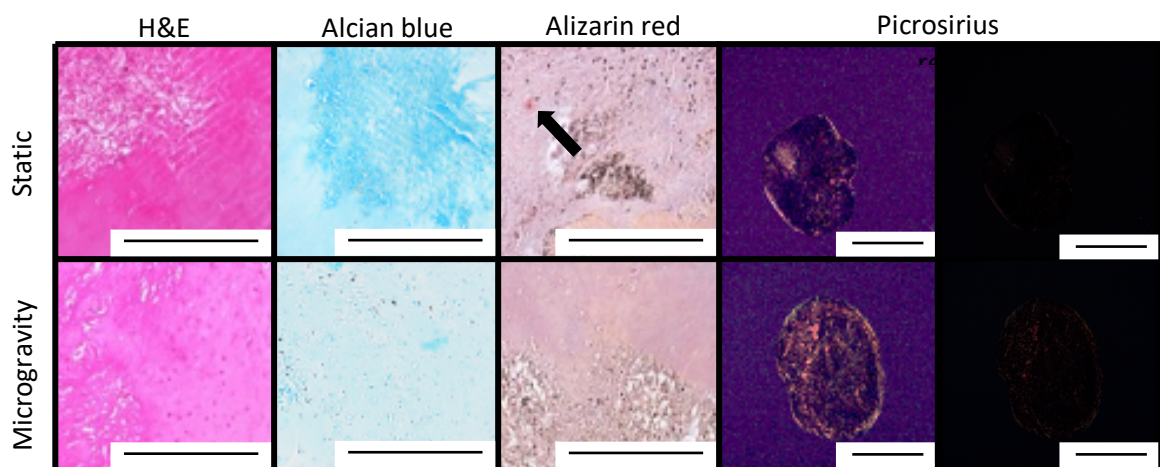


Figure 6.3. Histological sections of microtissues following 21-day microgravity and static culture. Representative images are shown for haematoxylin and eosin staining to show cell bodies and nuclei microscopy, Alcian blue staining highlighting GAGs within the ECM, Alizarin red staining for calcification and Picosirius Red staining to show collagen deposition under polarised light. Picosirius red staining is shown as both enhanced and original images. n=3 repeats, one representative sample shown. Scale bars represent 500 μm .

6.5.3. Alkaline Phosphatase Assay

ALP content in the culture medium was measured at the end of each 7-day timepoint using 4-methylumbelliferyl phosphate fluorescent substrate assay (Fig.6.4). The static and dynamic cultures followed the same pattern of activity over the three-week culture period with no significant difference seen between these two groups. In contrast, ALP activity in the microgravity group was significantly lower than both the static and dynamic cultures from day 7 onwards ($p<0.001$). ALP activity did increase in the microgravity group with time (day 21 having a significantly higher concentration than day 7; $p<0.001$), but at a slower rate to both static and dynamic cultured microtissues.

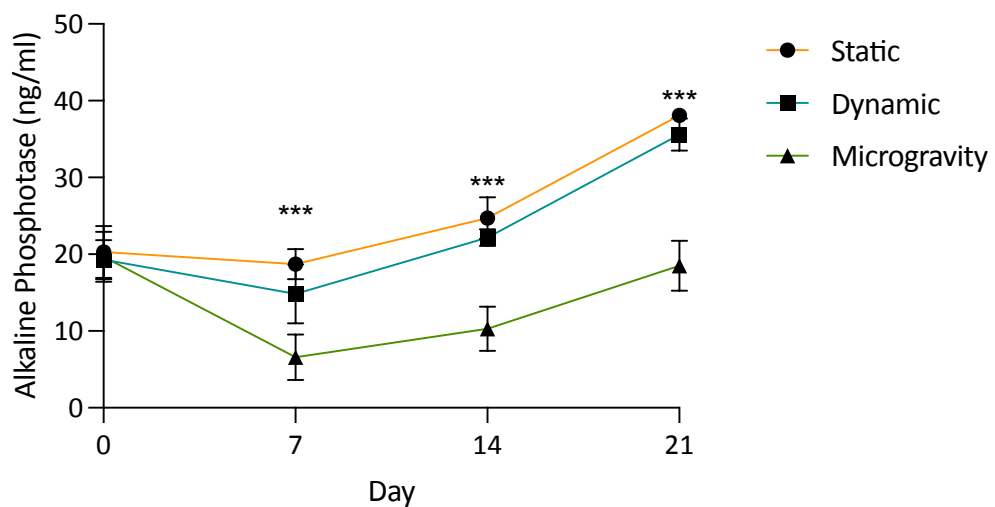


Figure 6.4. ALP activity in the media of static, dynamic and microgravity cultured microtissues. Absorbance measured at seven-day time points beginning at the end of the first week of culture and ending at the end of the experimental run. Error bars represent standard deviation. $n=18$ repeats for day 0 and $n=9$ for all later timepoints. Statistical significance measured using two-way ANOVA with Tukey's *post hoc* test and multiple comparisons (***) indicates $p<0.001$).

6.5.4. Microgravity Collagen Gene Response

The expression of a repertoire of collagen genes found across different musculoskeletal tissues (cartilage, bone and tendon) was investigated to determine the level of differentiation and identify any lineage commitment of the hMSCs (Fig.6.5). Only COL6A1 showed a significant differences with the static group being greater than the dynamic group. All other genes showed no significance at the experimental end-point between any of the groups, indicating a weak responses to the stimuli.

The ratio of COL14A1 to COL12A1 was found to be significantly higher for the microgravity group versus the static group showing a 9 fold increase (Fig.6.6).

The PCA showed evidence that the static culture grouped separately from the dynamic and microgravity culture (Fig.6.7A). The biplot (Fig.6.7B) highlights COL2A1, COL5A1, COL6A1, COL10A1 and COL12A1 as the variables that contributed the most to the separation.

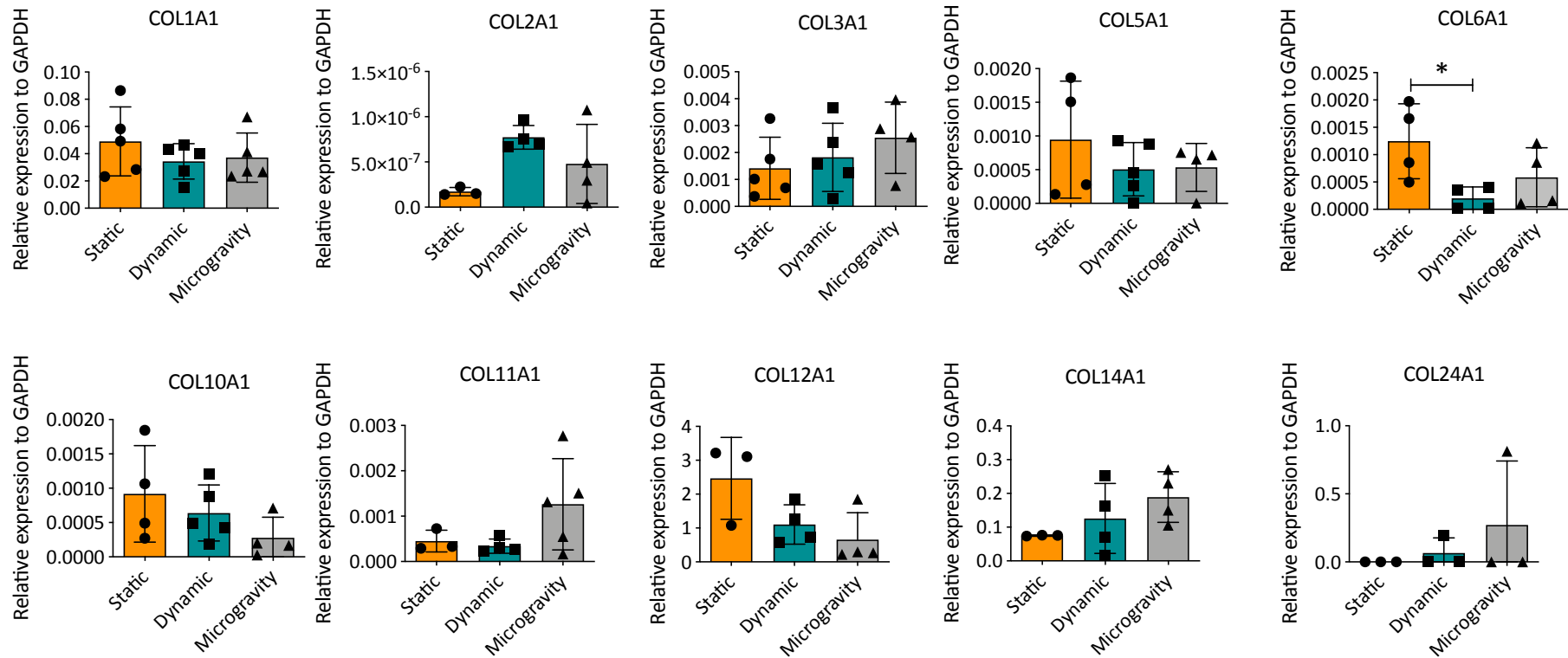


Figure 6.5. Collagen gene expression for microgravity microtissues. Error bars represent standard deviation of the mean. $n \leq 6$ repeats. Statistical significance measured using one-way ANOVA with Tukey's post *hoc* test and multiple comparisons (* indicates $p < 0.05$).

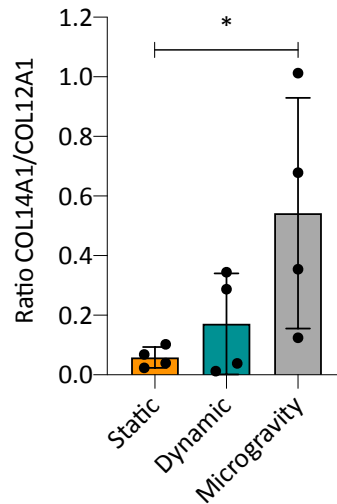


Figure 6.6. Ratio of COL14A1 to COL12A1 to investigate the maturation of the microtissues in different culture conditions. Error bars represent standard deviation of the mean. $n=4$ repeats. Statistical significance measured using one-way ANOVA with Tukey's *post hoc* test and multiple comparisons (* indicates $p < 0.05$).

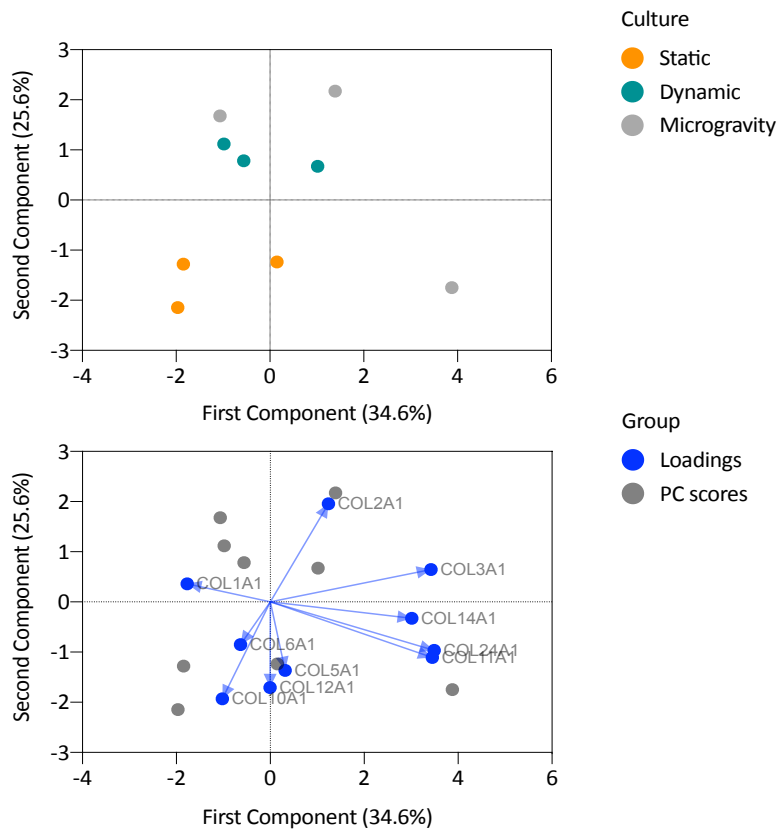


Figure 6.7. PCA of microgravity collagen gene expression. (A) PCA scores of all samples. Each point represents a sample with the colour designating the culture group (static-orange, dynamic-green and microgravity-grey). (B) Biplot of the PCA showing the variables that contribute to the most separation between the culture groups are COL2A1, COL5A1, COL6A1, COL10A1 and COL12A1.

6.5.5. Collagen Composition in Response to Microgravity

All collagen genes were measured at the protein level via western blot. The proteins synthesised due to the expression of COL2A1, COL5A1, COL6A1, COL10A1, COL11A1, COL12A1 and COL14A1, were not detected (Fig.6.8). This may be due to the concentration of these minor collagens being below the detectable threshold rather than being completely absent from the ECM.

The expression of collagen $\alpha 1(\text{III})$ was significantly highest in the microgravity group compared to both the control groups (dynamic having the lowest) (Fig.6.8). Both forms of collagen I and collagen XXIV did not significantly change between culture conditions, with the microgravity group being lower than the static control in all cases (Fig.6.8).

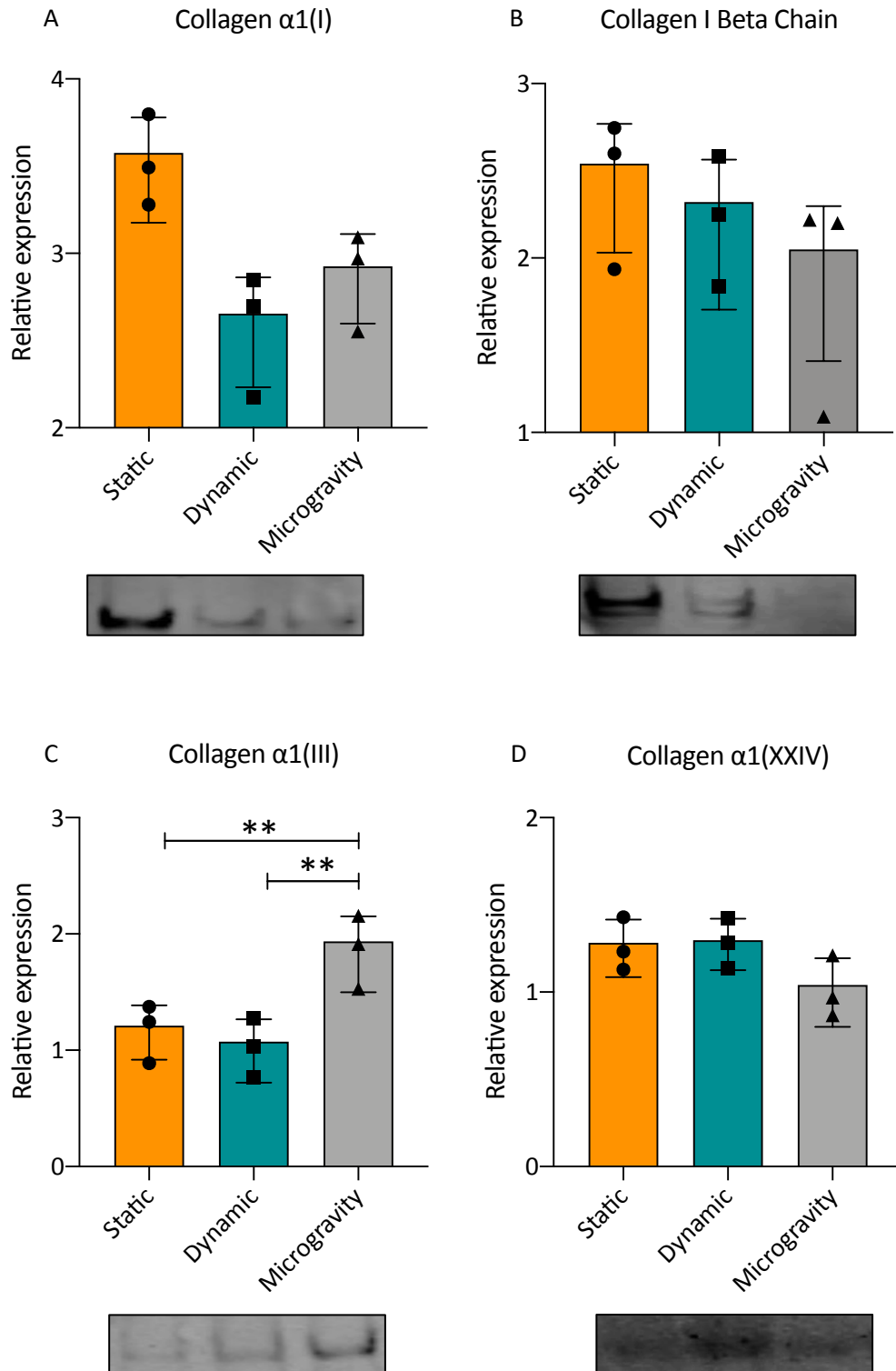


Figure 6.8. Densitometry of collagen extracted from microgravity microtissues. Representative images of western blots show below graph. Values shown are normalised to total protein. n=3 repeats. Error bars represent standard deviation of the mean. Statistical significance measured using one-way ANOVA with Tukey's *post hoc* test and multiple comparison (** indicates $p < 0.05$).

6.5.6. Micro-Computed Tomography

Representative μ CT images of the three culture conditions is shown in Fig.6.9A. The total volume of the microtissue is shown in the left column, the mineralised deposits are shown in the middle column and the mineralised deposits superimposed onto the total volume in the right column. No noticeable difference was seen between any condition with each group appearing to show a similar percentage of mineralised deposits. This is reflected in Fig.6.9B, the percentage mineralised volume. Fig.6.9C shows the difference in densities between the three culture groups. The static group was found to have a significantly higher density ($0.082\text{g}/\text{cm}^2$) than the dynamic group ($0.077\text{g}/\text{cm}^2$, $p < 0.05$) but not the microgravity groups ($0.078\text{g}/\text{cm}^2$).

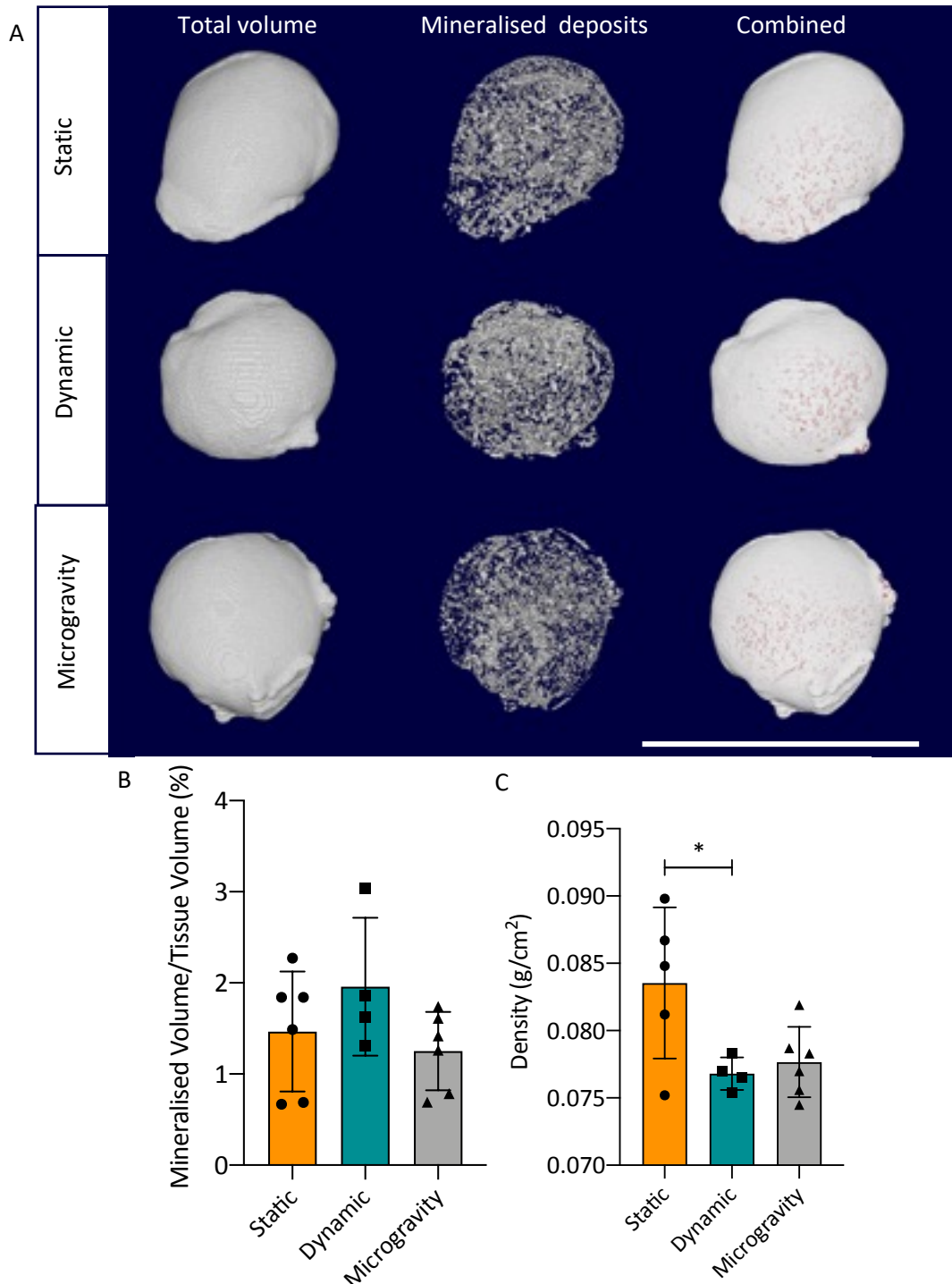


Figure 6.9. μ CT analysis of microgravity microtissues. (A) Representative images for μ CT of static, dynamic and microgravity cultured hMSC seeded fibrin constructs highlighting total volume, mineralised particles and combination. (B) percentage mineralised volume and (C) mineral density for static, dynamic and microgravity cultured hMSC seeded fibrin constructs. $n \leq 6$ repeats. Error bars represent standard deviation of the mean. Statistical significance measured using one-way ANOVA with Tukey's *post hoc* test and multiple comparisons (* indicates $p < 0.05$).

6.6. Discussion

Microgravity has the potential to be used as a tool to maintain and enhance the stem like properties of MSCs (Yuge et al., 2006, Lei et al., 2018). Collagen is typically used as a marker for cell differentiation, for example collagen type I is used as a tendon (Zhang et al., 2005) and bone marker (Cassella and Ali, 1992) whilst collagen type II is used for cartilage (Wardale and Duance, 1994). In the present study hMSCs were encapsulated in fibrin hydrogels and exposed to normal gravity (1 g) in either static or dynamic culture or microgravity (1×10^{-6} g) for three weeks. The dynamic culture was used to introduce a normal gravity condition with increased nutrient diffusion making it possible to assess whether microgravity was the driving stimuli for differentiation relative to the effects of increased nutrient diffusion seen with the bioreactor used (Khodabukus et al., 2018).

The size and weight of the microtissues was significantly increased for the samples cultured under microgravity compared to both normal gravity controls, suggesting that microgravity maintains a larger sized tissue engineered construct compared to normal gravity. This is supported by previous observations, here the study suggests that this increased size would be more suitable for a tissue engineered plug in a cell therapy application. (Sakai et al., 2009).

Sakai et al. (2009) cultured hMSCs in chondrogenic differentiation media and went on to find that the microgravity samples increased the expression of chondrogenic markers (GAGs and collagen II), indicating that microgravity was upregulating chondrogenic differentiation. The microgravity group in the present study did not show a strong affinity towards the chondrogenic lineage, it appeared that only small areas of intense Alcian blue staining occurred within the ECM. There looked to be equally low Alizarin red staining and low absorbance was detected in the media for ALP indicating low levels of osteogenic differentiation. Bradamante et al. (2018) found that microgravity had little effect on osteogenic differentiation. Similarly to Sakai et al. (2009), Bradamante et al. (2018) used specific differentiation media for culture (osteogenic in this case), whilst in the present study the microtissues were cultured in basic medium, which was chosen to show how the cells responded to microgravity solely. If spontaneous differentiation were to occur due to the culture medium it was hypothesised that it would be towards the osteogenic lineage as the basic medium more closely aligns to osteogenic differentiation medium than chondrogenic.

Only a small number of collagens are synthesised within the bone marrow niche; collagen type I, III, IV, V and VI along with a high percentage of proteoglycans, fibronectin and

laminins, among others (Gordon, 1988, Hamilton and Campbell, 1991). This goes some way to explain the low detection of collagen when only using basic media. Previous work looking at specific tissue types has seen a variation in the collagens synthesised. Cartilage tissue engineering typically sees beneficial responses with microgravity compared to normal gravity with an increased ratio of collagen II to collagen I (Ohyabu et al., 2009), and the downregulation of collagen X (Mayer-Wagner et al., 2014), a marker for hypertrophy that is often seen with cartilage tissue engineering (Jahangir et al., 2020). MSCs cultured in true microgravity (space) saw trans-differentiation from the osteogenic lineage towards the adipogenic lineage even with osteogenic medium (Zhang et al., 2018). It is apparent that the differential potential of MSCs in microgravity differs to MSCs in normal gravity, however the presence of differential medium appears to be required to show the true effects of microgravity.

6.6.1. Microgravity Culture Differentiation

The strongest expression of collagen genes within the microgravity culture group were for COL1A1, COL3A1, COL11A1, COL12A1, COL14A1 and COL24A1 (>0.001 relative to GAPDH), all collagen types that are found in tendon and bone ECM (Riley et al., 1994, Tzaphlidou, 2005). COL2A1, COL5A1, COL6A1 and COL10A1 (<0.001 relative to GAPDH) all had the lowest expression and are types typically found in the cartilage ECM (Luo et al., 2017). The gene profile therefore points towards the microgravity group moving along the osteogenic/tenogenic lineage rather than the chondrogenic. Further no collagen II was detected by western blot whilst the bone/tendon markers collagen I and III were, as was the bone marker, collagen XXIV. The molecular data therefore points towards the promotion of an osteo/tenogenic differentiation of the MSCs when culture under microgravity.

Functional outcomes were measured to clarify the differential lineage of the MSCs. ECM mineralisation was characterised by μ CT, and analysis found that the microgravity group had the lowest mineralised volume and density. Despite the gene and protein profiles, the microgravity group was not distinctively maturing along a strongly osteogenic lineage, supporting similar observations from Alizarin Red staining of the microtissues and reduced ALP activity. MSCs cultured in growth medium without intervention will often differentiate towards the osteogenic lineages, however when cultured in microgravity the spontaneous differentiation appears to be inhibited, therefore maintaining the stemness of these cells. Wall et al. (2007) showed that irrespective of media type hMSCs will eventually differentiate

towards the osteogenic lineage, suggesting that these cells are pre-disposed towards the osteogenic lineage and require significant intervention to inhibit this differentiation.

During early development of a native tissue's ECM the cells will secrete collagen XIV as a major FACIT collagen, then as the ECM continues to develop and mature the synthesis of collagen XIV reduces and is replaced by collagen XII (Ansorge et al., 2009), highlighting collagen XII and XIV's use as a measure of tissue maturity and development. Interestingly the ratio of COL14A1:COL12A1 gene expression was highest in the microgravity group indicating the delayed development of the tissue, demonstrating the inhibitory effect microgravity has on maturation and therefore spontaneous differentiation of the hMSCs. The work by Wall et al. (2007) found that later passages of hMSCs cultured within adipogenic media underwent spontaneous osteogenic differentiation, indicating that the more mature the cell the more likely it is to undergo the spontaneous differentiation. By delaying the maturation of the MSCs, the stemness of the cells will also be preserved.

ALP activity in the media indicated greater osteogenic differentiation in the static group compared to the microgravity group. Despite the absence of osteogenic differentiation supplements the cells appear to be undergoing spontaneous osteogenic differentiation, however the application microgravity is acting as an inhibitor.

6.6.2. Static Culture Differentiation

The gene profile for the static culture was similar to that of the microgravity group. The osteogenic/tenogenic collagen types had a higher expression (>0.001 relative to GAPDH) than the chondrogenic collagens. Protein expression of collagen II was not detected in the static group, whilst collagen I, III and XXIV were, implying that the cells were not spontaneously differentiating towards the chondrogenic group but more likely towards the osteogenic or tenogenic lineages.

The static group was found to have the lowest expression of the gene COL3A1 and the lowest expression of collagen $\alpha 1(\text{III})$ whilst microgravity had the highest expression for both the gene and protein (significantly). Fibrin is the biomaterial cells secreted at the site of a wound, initially the cells will then generate a unorganised matrix of collagen III before replacing it with organised collagen I and completing the healing process (maturation and development) (Clore et al., 1979). It is postulated that if the fibrin hydrogel is being matured by the cells as fibrin would be at a wound site it would suggest that a lower expression of collagen III and higher expression of collagen I would indicate a more mature structure, as seen with the

static versus the microgravity group. Inhibited wound healing with microgravity has previously been seen in rats, therefore suggesting the delayed maturation of the wound due to microgravity (Davidson et al., 1999).

μ CT analysis showed that the cells may have differentiated towards the osteogenic lineage in static culture as whilst the percentage of mineralised particles is similar to that of the microgravity culture, the density of the particles is highest in the static group, demonstrating a more advanced osteogenic ECM with dense hydroxyapatite regions.

6.6.3. Dynamic Culture Differentiation

The dynamic group expressed near identical ALP production within the media to the static group. The gene analysis showed a profile in between the static and microgravity groups with only COL2A1, COL6A1 and COL11A1 not lying between the other conditions. This would suggest that whilst gravity is having an effect which the microgravity bioreactor is somewhat removing there is an influence from the increased nutrient diffusion resulting in the dynamic group neither identically reflecting the static nor microgravity group. Again the osteogenic/tenogenic collagens have a higher expression than the chondrogenic genes, further indicating that within the basic media the cells are more likely to undergo spontaneous osteogenic/tenogenic differentiation. The PCA analysis of the collagen genes aligns the dynamic culture group more closely with the microgravity group, with COL2A1 having the largest contribution to the position of the dynamic and microgravity groups whilst COL10A1 (among others) has one of the largest effect of the static group. COL10A1 is seen as a transition marker during the endochondral ossification of cartilage to bone (Shen, 2005), suggesting that the static samples are more aligned to an osteogenic differentiation than the dynamic and microgravity cultures.

Protein analysis aligns the dynamic culture with the microgravity microtissues for collagen I and the static for collagen III and XXIV. Maturation of the dynamic microtissues appears to lie between the two cultures with the middle ratio of COL14A1 to COL12A1 and the lowest expression of collagen $\alpha 1(I)$ and $\alpha 1(III)$. Increased nutrient diffusion appears to inhibit the maturation of the cells seen with static culture, the absence of gravity further exaggerates the inhibitory effect. Further the PCA biplot shows that COL12A1 strongly contributes to the separation of the static group from the dynamic and microgravity group, suggesting that increased nutrient diffusion is a major contributor to the delayed maturation of the MSCs

By observing both the microgravity and dynamic microtissues particle densities together (both similar and lower than static) it appears that the increased nutrient diffusion does work to inhibit spontaneous osteogenesis. Majd et al. (2009) showed that a form of dynamic culture maintained stem cell phenotypes and differential capacity, Frith et al. (2010) found that dynamic 3D culture in spinner flasks maintain the MSC phenotype compared to MSCs cultured in 2D monolayer, both these studies support the observation of inhibited spontaneous osteogenic differentiation with the increased nutrient diffusion (dynamic cultures). The results of the dynamic culture highlight a major issue with the RCCS 4H bioreactor, and other free-fall systems, in that a static control group in well plates will be affected by not only normal gravity but also reduced nutrient diffusion, therefore not acting as a true control. Future studies with this system should continue to utilise dynamic and static controls for true comparison.

6.6.4. Conclusion

Through comparison of the three culture types it appears that each are differentiating towards the osteogenic lineage as expected due to the spontaneous differentiation of hMSCs in long term culture. PCA analysis appeared to show the presence of increased nutrient diffusion separating both the dynamic and microgravity groups from the static group with a more exaggerated separation seen in the microgravity group. This suggests that dynamic culture is having an initial effect on the MSCs which microgravity is amplifying. It was hypothesised that microgravity would help maintain the MSCs in a more naive state, inhibiting tissue specific collagen production and therefore ECM maturation. Microgravity had the greatest inhibitory effect as seen by the highest ratio of COL14A1 to COL12A1, whilst the static culture has the lowest, indicating the most mature ECM, the dynamic culture was found in between the two and significantly different to neither. COL12A1 was one of the main contributors in the separation of the static culture from the dynamic and microgravity, further indicating the maturation of the static ECM indicating the inhibitory effects of nutrient diffusion. The present study suggest microgravity may be an solution to prolonged growth of MSCs whilst maintaining the stemness of the cells, this would be a valuable solution to the bulk up of MSCs for autologous cell therapies. The present study suggests MSCs are in a less developed state after microgravity culture and the stemness is maintained, future work should look to investigate this by investigating the expansion and differential potential of MSCs following culture in microgravity.

Chapter 7

General Discussion

The overall aim of this thesis was to apply mechanical stimulation to hMSCs encased within 3D biomimetic constructs and monitor the collagen output from the cells. The collagen output was then used to investigate the differentiation of the MSCs and the 'quality' of the tissue engineering structure generated. Within healthy musculoskeletal tissues a specific composition of collagen isoforms are synthesised and form part of the ECM. Each of the collagens occur in different concentrations with the major fibril forming collagens typically accounting for the highest percentage of the dry protein weight. The minor collagen types, such as FACIT, MACIT and multiplexins are present along with proteoglycans and growth factors among other ECM components but at a smaller concentration. The composition, orientation and ratios of the different collagen types offer the tissue specific properties required to appropriately complete its routine task, such as force transduction between muscle and bone for tendons. Many tissue engineering studies do not investigate these minor collagens, generating an incomplete understanding of the tissue being generated. By investigating the complete collagen composition, a better understanding of how the cells are responding to the stimulus can be achieved enabling optimised tissue engineering.

Three different forms of mechanical stimulation have been used throughout this study, cyclic tensile strain, hydrostatic pressure and microgravity, with all three being applied to hMSCs encased in fibrin hydrogels. Whilst the fibrin hydrogel was constant throughout the study the initial formation and culture environment differed based on the mechanical loading. Identical fibrin hydrogels (microtissues) were used for both microgravity and hydrostatic pressure, here the fibrin was generated within the well of a 48 well plate. For tensile stimulation a purpose built 3D printed frame was designed with posts at either end. The fibrin was generated within the frame and around the posts forcing the fibrin into a rod like structure similar to that of a tendon and allowing uniaxial cyclic strain to be applied.

One of the main limitations seen in many studies when investigating the role of mechanical stimulation on cell differentiation and ECM production is the use of differentiation media, which, as seen with the hydrostatic pressure study, can have an overriding effect on the response of the cells subjected to the mechanical stimulation. Basic hMSCs proliferation media was used in all studies to show the sole effect of the mechanical stimulation on the cells collagen synthesis rather than the supplement driven production. However, it should be noted that the components of the basic media (DMEM, FBS, non-essential amino acids and ascorbic acid) more closely align with media used for osteogenic differentiation (missing dexamethasone and β -glycerophosphate), whilst culture media used for tenogenic and

chondrogenic differentiation typically remove FBS as a supplement and instead use a different combination of growth factors. It was therefore more likely that the hMSCs would spontaneously differentiate towards the osteogenic lineage due to the combination of media and the predisposition of bone marrow derived MSCs (Wall et al., 2007). Spontaneous differentiation appeared to be seen in all three studies when using the basic media and not subjecting the samples to any stimulation (the control groups), small amounts of osteogenic differentiation was present in the ECM through the formation of calcium hydroxyapatite nodules (Alizarin Red assay). This phenomenon has been previously reported by Zhang et al. (2016), here MSCs were seeded onto electrospun nanofibers and were cultured without osteogenic differentiation media, following 14 days of culture the cells showed increased expression of osteogenic markers Col1A1, OCN, ALP and Runx2.

The spontaneous differentiation of the cells may have been further driven by the non-sorted population used. The cells went through MSC verification by flow cytometry and the tri-lineage differentiation assay, demonstrating that this population could achieve adipogenic, chondrogenic and osteogenic differentiation. Flow cytometry showed that at the first passage the appropriate percentage of cells in the population (>95%) possessed the correct positive markers (CD73, CD90 and CD105) though the population exceeded the negative marker percentage by 0.83%. It is possible that a mixed cell population was used in this study and it contained cells that had already begun to differentiate down lineages, and may have then driven the spontaneous differentiation of other cells.

The expression of different collagens varied across the different mechanical stimulations, and appeared to show some regulatory effects for the varying stimuli. Without cyclic strain the tensile control group had the highest expression of collagen $\alpha 1(\text{II})$ as has been seen by previous studies (Maeda et al., 2010, Udeze et al., 2019). As collagen II is typically seen as a negative marker in tendon tissue engineering it demonstrates the beneficial properties of appropriate mechanical stimulation. However within the hydrostatic pressure study it appears that the media supplements had an overriding effect on the collagen synthesis with no significant differences seen between the different loading regimens for either the osteogenic or chondrogenic media groups. The COL10A1 expression was highest in the 200 kPa and 300 kPa samples from the chondrogenic media groups suggesting that hydrostatic pressure induces hypertrophy. Studies have shown that microgravity inhibits hypertrophy in cartilage tissue engineering (Mayer-Wagner et al., 2014), however whilst COL10A1 was found to have the lowest expression in the microgravity group it was not significantly lower

than the microgravity controls. A combination of hydrostatic pressure and microgravity may be beneficial for cartilage tissue engineering.

Gene expression is commonly used to investigate collagen synthesis in response to experimental intervention. This is typically due to the difficulty found when extracting collagen from tissue engineered tissues, due in part to the enzymatic digestion required but also because of the low abundance of the minor collagen. This was observed in all three studies with some collagens detected at the gene level not detected by western blot. However what was clear from the collagens that were detected by both qPCR and western blot was the low alignment between the two. The protein expression is a far greater way to judge the present ECM in the tissue engineered structure, it is therefore imperative to investigate the collagens at the protein level as well as gene level were possible to get a true representation of the cells response.

Changes between the loading and culture regimens was more apparent for the structural analysis than the molecular analysis, this indicated that whilst the collagen synthesis may not have been dramatically influenced by the stimulation applied, the way the collagens were embedding within the ECM was largely driven by these forces. In the tensile stimulation study the highest strain rate resulted in the largest diameter fibrils and the most aligned structure, whilst in the hydrostatic pressure study the highest pressures coupled with osteogenic medium resulted in the most dense mineral deposits indicating a more developed structure. The microgravity culture group had a lower mineralised density than the static group but this was also observed in the dynamic group suggesting here that the increased nutrient diffusion resulted in decreased osteogenic differentiation and therefore decreased mineralisation rather than the microgravity.

Through analysis of the ratio of COL14A1 to COL12A1 it was established that the microgravity group had the least developed ECM due to the highest ratio. This was established through the roles collagen XII and XIV play during development. Collagen XIV, a FACIT collagen typically found in embryonic tissue is replaced by collagen XII as the tissue matures (Ansoorge et al., 2009). These collagens were not investigated for hydrostatic pressure but in tensile stimulation an interesting trend occurred. At the gene level it appeared that the increase in cyclic stimulation resulted in a more immature construct with the 10% strain group having the highest expression of COL14A1 and lowest expression of COL12A1. This did not align with the more developed structural observations seen for the 10% strain group (diameter and alignment) but did support the mechanical properties seen.

7.1. Conclusion and Future Work

Mechanical stimulation is consistently used to drive the development of tissue engineered structures towards their native counterparts. From the present studies it is apparent that the type and variation of mechanical stimulation applied will have differing effects on the cells cultured within. For example microgravity appears to inhibit ECM development, as hypothesised in this study indicating longer preservation of the MSCs and delayed differentiation. Mapping the differentiation through the collagen profile is possible but does not appear to be as straight forward as initially anticipated.. If more studies investigate the complete composition of collagen a greater understating of how and why the collagens are synthesised in tissue engineered constructs will be developed. The profile of collagen is not a one dimensional measurement but appears to be dynamic and to vary with time and loading. Whilst the collagen profiles can be used to indicate the differentiation route taken by the cells it may be better used to indicate the developmental stage of the tissue.

From the work presented it appears that the mechanical stimulation applied has a greater effect on the structural development of the collagen, with high levels of tensile strain resulting in thicker and more aligned collagen fibrils. The lack of mechanical loading, microgravity, appeared to reduce the ECM, resulting in a less developed tissue than that cultured under normal gravity. The presence of differential medias in the hydrostatic pressure study appeared to override the role of mechanical stimulation, resulting in consistent collagen production regardless of the pressure applied. However, the mineralised deposits that formed in the osteogenic group did appear to be driven by the hydrostatic pressure regimen. It therefore appears that differentiation medias will drive the production of specific collagens but without mechanical stimulation these collagens will not be incorporated into the ECM in an appropriate way.

Future work with these studies should include more time point analysis. It is apparent that the collagen profile is continually changing but how this change progressed over time was not discovered. A larger protein and gene profile shown through proteomic analysis and RNA sequencing may indicate further collagens and other cellular and ECM components, therefore identifying ECM development missed during the present study. Combining these advanced analytical techniques with multiple time points may more clearly identify how the collagen profiles are changing with time.

Chapter 8

Appendices

8.1. Appendix A – Histology reagent recipes

Solutions for stains were generated using the following recipes:

Alcian blue solution:

- 1 g Alcian Blue 8GX
- 3% Acetic acid solution
 - 3 ml Glacial acetic acid
 - 97 ml distilled water
- Mix well and adjust pH to 2.5 with acetic acid

Alizarin red solution:

- 2 g Alizarin Red S
- 100 ml Distilled water
- Mix well and adjust pH to 4.1-4.3 with 10% ammonium hydroxide.

Mayer's Haematoxylin:

- 50 g Aluminium ammonium sulphate
- 5 g Haematoxylin
- 10 ml Ethanol
- 1 g Sodium iodate
- 20 ml Glacial acetic acid
- 300 ml Glycerol
- 700 ml Distilled water
- Dissolve the aluminium ammonium sulphate in 250 ml of distilled water on a heated stirrer, add remaining distilled water and leave to cool. Dissolve the haematoxylin in the ethanol and add solution to dissolved aluminium ammonium sulphate. Add the remaining components. Mix well.

Eosin:

- 100 ml 1% Eosin Y
 - 1 g Eosin Y
 - 100 ml Distilled water
- 10 ml 1% Aqueous phloxine
 - 1 g Phloxine B

- 100 ml Distilled water
- 775 ml 95% Ethanol
- 4 ml Glacial acetic acid

0.3% Acid Alcohol:

- 700 ml Ethanol
- 300 ml Distilled water
- 3 ml Hydrochloric acid

Weigert's Haematoxylin:

- Stock solution A
 - 1 g Haematoxylin
 - 95% Ethanol
- Stock solution B
 - 4 ml of 29% Ferric chloride
 - 2.9 g Ferric chloride
 - 10 ml Distilled water
 - 95 ml distilled water
 - 1 ml Hydrochloric acid
- Mix equal parts stock solution A and B.

Picrosirius red:

- 0.5 g Direct Red 80
- 500 ml of 1.3% Picric acid solution

Acidified water:

- 5 ml Glacial acetic acid
- 1 L distilled water

8.2. Appendix B – Designed Primer Parameters

Table 8.1. Table of primers used and their parameters.

Gene	Sequence	CG%	Melt Temp (°C)	Nucleotides
COL1A1 (FWD)	CGGCTCCTGCTCCTCTTAG	63	60.2	141-159 of 6728
COL1A1 (RVS)	CACACGTCTCGGTCATGGTA	55	60.6	258-277 of 6728
COL2A1 (FWD)	CCAGATTGAGAGCATCCGC	58	61.9	3585-3603 of 4257
COL2A1 (RVS)	CCAGTAGTCTCCACTCTCCAC	55	57.9	3669-3690 of 4257
COL3A1 (FWD)	GGGTGAGAAAGGTGAAGGAG	55	58.7	2049-2068 of 3234
COL3A1 (RVS)	CATTACTACCAGGAGGACCAG	52	56.3	2201-2221 of 3234
COL10A1 (FWD)	GCAACTAAGGGCCTCAATGG	55	61.9	1537-1556 of 3306
COL10A1 (RVS)	CTCAGGCATGACTGCTTGAC	55	59.6	1646-1665 of 3306
COL11A1 (FWD)	AATGGAGCTGATGGACCACA	50	61.5	3858-3877 of 6158
COL11A1 (RVS)	TCCTTTGGGACCGCCTAC	61	61	3972-3989 of 6158
COL12A1 (FWD)	TTTAGTTAGCACAGCGGGCA	50	61.8	2538-2557 of 3135
COL12A1 (RVS)	CGCTCGAAATACACAGCAGC	55	62	2605-2624 of 3135
GAPDH (FWD)	ATGGGGAAGGTGAAGGTCG	58	62.2	317-335 of 3855
GAPDH (RVS)	TAAAAGCAGCCCTGGTGACC	55	62.4	1999-2018 of 3855
YWHAZ (FWD)	CCGTTACTTGGCTGAGGTTG	55	60.7	29113-29132 of 37546
YWHAZ (RVS)	TGCTTGTTGTGACTGATCGAC	48	59.9	29776-29796 of 37546

8.3. Appendix C – Analysis of Primer Efficiencies and Melt Peaks

Primer efficiency was tested on hMSCs before use in experiments. cDNA was serially diluted between 0.3125 and 5 ng. The Ct values were plotted against the log value for the sample concentration and the efficiency curve calculated. Fig.8.1B shows the representative efficiency curve for COL12A1 which generated a efficiency of 97.04%. Fig.8.1C shows the melt peak for COL12A1 with one distinct amplification peak.

A

Template Concentration (ng)	Log (ng)	Ct.1	Ct.2	Ct.3	Average Ct
5	0.7	19.71	19.56	20.42	19.89667
2.5	0.4	20.77	20.82	20.48	20.69
1.25	0.1	21.79	21.06	23.01	21.95333
0.625	-0.2	23.6	25.77	23.47	24.28
0.3125	-0.51	27.99	22.93	-	25.46
Dilution Factor	2				
Slope	-3.39501				
Efficiency (%)	97.04				

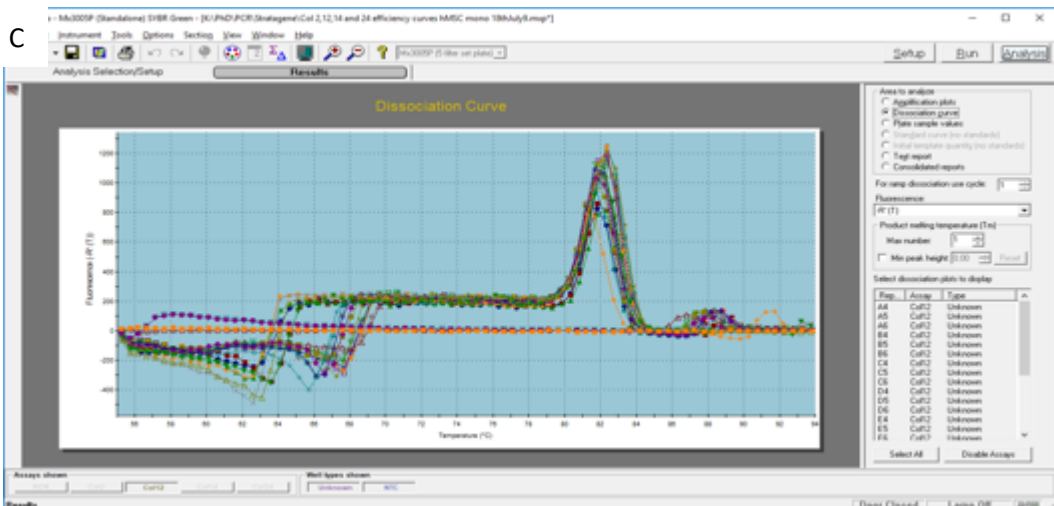
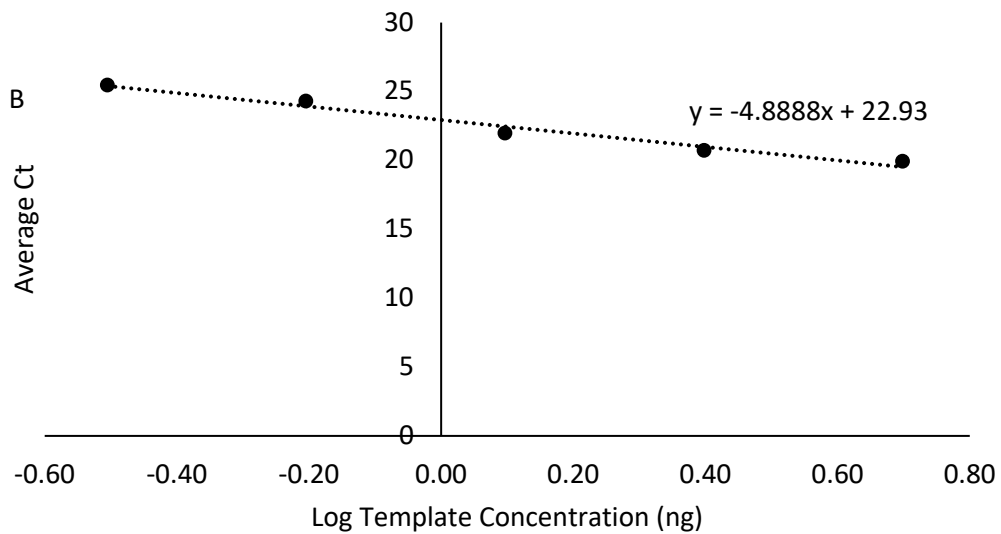


Figure 8.1. Example of primer efficiency calculation, (A) table shows extracted data for hMSC RNA and subsequent calculations, (B) graph shows scatter plot of the average Ct values vs the log concentration of the template to determine the linear equation. Efficiency for COL12A1 found to be 97.04%. (C) melt curve generated to show amplification of single PCR product.

8.4. Appendix D – Determination of House Keeper

Genes

House keeper genes were determined using the GeNorm algorithm (Vandesompele et al., 2002) for each experiment (tensile, hydrostatic and microgravity), utilising optimisation samples from each condition. A range of stable hMSC genes were trialled including GAPDH, GUSB, HPRT1, TBP and YWHAZ. The GeNorm results for the tensile condition is shown in Fig.8.2 with GAPDH and YWHAZ found to be the most stable, YWHAZ was taken forward.

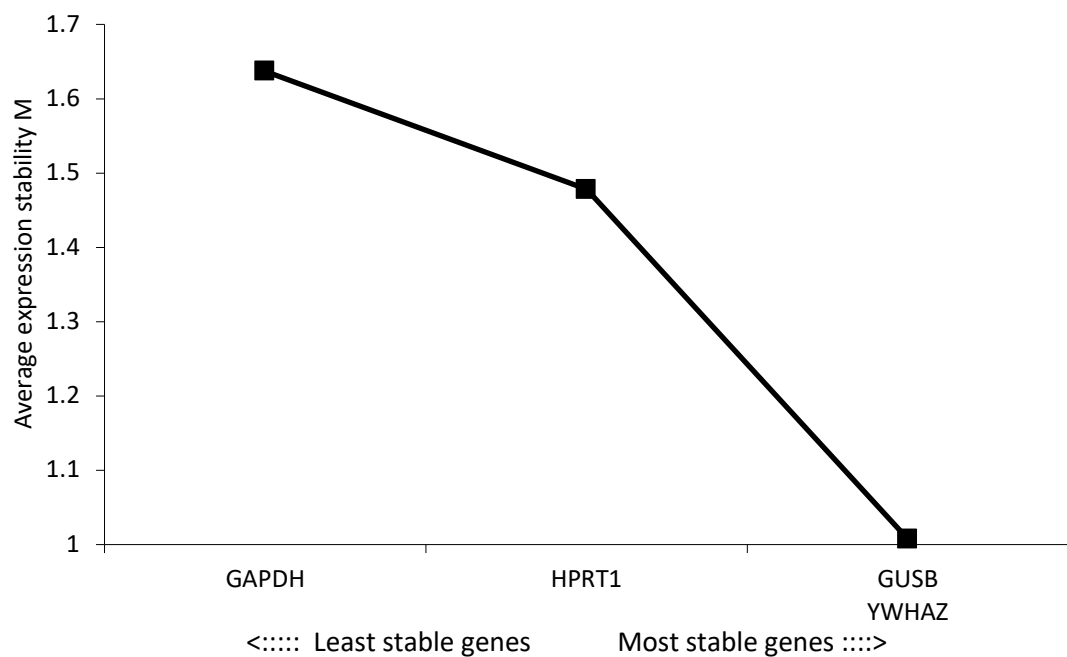


Figure 8.2. Graphical representation of GeNorm calculation highlighting the most stable hMSC housekeeper genes for tensile stimulation

8.5. Appendix E – CNA35 reagent recipes

100 ml Binding buffer – 50 mM NaH₂PO₄

300 mM NaCl

10 mM imidazole

35 ml wash buffer – 50 mM NaH₂PO₄

300 mM NaCl

20 mM imidazole

35 ml elution buffer – 50 mM NaH₂PO₄

300 mM NaCl

250 mM imidazole

8.6. Appendix F – CNA35 image acquisition




Acquisition Information			
Acquisition Start	18/12/2019 12:48:27		
Microscope	Axio Imager.Z2		
Objective	EC Plan-Neofluar 10x/0.30 M27		
	Track 1	Track 2	
Reflector	none	none	
Contrast Method	Fluorescence	Fluorescence	
Pinhole	0.89 AU / 28 μm	0.99 AU / 28 μm	
Laser Wavelength	488 nm: 0.4 % 640 nm: 0.5 %	405 nm: 1.60 %	
Laser Blanking	Enabled	Enabled	
Scan Mode	Frame	Frame	
Scan Zoom	1.0	1.0	
Rotation	0°	0°	
Pixel Time	1.03 μs	1.03 μs	
Line Time	4.95 ms	4.95 ms	
Frame Time	2.53 s	2.53 s	
Scan Direction	Unidirectional	Unidirectional	
Line Step			
Averaging	4	4	
	Channel 1	Channel 2	Channel 3
Channel Name	AF488-T1	AF647-T1	DAPI-T2
Channel Description			
Dye Name	AF488	AF647	DAPI
Channel Color			
Excitation Wavelength	493	653	353
Emission Wavelength	517	668	465
Effective NA	0.3	0.3	0.3
Detection Wavelength	515-620	656-700	400-515
Imaging Device	LSM800 GaAsP-Pmt3	LSM800 GaAsP-Pmt2	LSM800 GaAsP-Pmt1
Detector Type	GaAsP	GaAsP	GaAsP
Detector Gain	650 V	700 V	650 V
Detector Offset	0	0	0
Detector Digital Gain	0.3	0.3	0.3

Figure 8.3. Acquisition information for CNA35 collagen probe staining.

8.7. Appendix G – μ CT Analysis Macro for Hydrogel Mineralisation

Table 8.2. Table of macro used to determine hydrogel mineralisation.

Step 1: Filtering	
Mode	Median (2D space)
Kernel	Round
Radius	4
Step 2: Thresholding (3D space)	
Mode	Automatic (Otsu method)
Background	Dark
Lower grey threshold	35
Upper grey threshold	255
Step 3: Morphological operations	
Type	Erosion (2D space)
Kernel	Round
Radius	8
Apply to	Image
Step 3: Despeckle	
Type	Sweep (2D space)
Remove	All except the largest object
Apply to	Image
Step 4: Despeckle	
Type	Sweep (3D space)
Remove	All except the largest object
Apply to	Image

Step 5: Morphological operations	
Type	Dilation (3D space)
Kernel	Round
Radius	8
Apply to	Image
Step 6: Despeckle	
Type	Remove pores (2D space)
Detected by	By Image borders
Apply to	Image
Step 7: Morphological operations	
Type	Closing (3D space)
Kernel	Round
Radius	3
Apply to	Image
Step 8: Bitwise operations	
	<Regions of interest> = COPY<Image>
Step 9: Reload image	
Step 10: Thresholding	
Mode	Global
Lower grey threshold	90
Upper grey threshold	255
Step 11: Bitwise operations	
	<Image>=<Image>AND<Region of Interest>
Step 12: Save bitmaps (only ROI)	

File format	bmp	
Step 13: Save bitmaps		
	<Images>=COPY<Clipboard>	
Step 14: 3D analysis		
	Abbreviations	Unit
Tissue volume	TV	μm^3
Bone volume	BV	μm^3
Percentage bone volume	BV/TV	%
Tissue surface	TS	μm^2
Bone surface	BS	μm^2
Intersection surface	i.S	μm^2
Bone surface / volume ratio	BS/BV	1/ μm
Bone surface density	BS/TV	1/ μm
Trabecular pattern factor	Tb.Pf	1/ μm
Centroid (x)	Crd.X	μm
Centroid (y)	Crd.Y	μm
Centroid (z)	Crd.Z	μm
Trabecular thickness	Tb.Th	μm
Trabecular number	Tb.N	1/ μm
Trabecular separation	Tb.Sp	μm
Number of objects	Obj.N	
Number of closed pores	Po.N(cl)	
Volume of closed pores	Po.V(cl)	μm^3
Surface of closed pores	Po.S(cl)	μm^2
Closed porosity (percent)	Po(cl)	%

Volume of open pore space	Po.V(op)	μm^3
Open porosity (percent)	Po(op)	%
Total volume of pore space	Po.V(tot)	μm^3
Total porosity (percent)	Po(tot)	%
Euler number	Eu.N	
Connectivity	Conn	
Connectivity density	Conn.Dn	$1/\mu\text{m}^3$

8.8. Appendix H – μ CT Analysis Macro for Hydrogel

Density

Table 8.3. Table of macro used to determine hydrogel density.

Step 1: Filtering	
Mode	Median (2D space)
Kernel	Round
Radius	4
Step 2: thresholding (3D space)	
Mode	Automatic (Otsu method)
Background	Dark
Lower grey threshold	19
Upper grey threshold	255
Step 3: Morphological operations	
Type	Erosion (2D space)
Kernel	Round
Radius	8
Apply to	Image
Step 4: Despeckle	
Type	Sweep (2D space)
Remove	All except the largest object
Apply to	Image
Step 5: Morphological operations	
Type	Dilation (3D space)
Kernel	Round
Radius	8

Apply to	Image
Step 6: Despeckle	
Type	Remove pores (2D space)
Detected by	By image borders
Apply to	Image
Step 7: Morphological operations	
Type	Closing (3D space)
Kernel	Round
Radius	3
Apply to	Image
Step 8: Bitwise operations	
	<Region of Interest>=COPY<Image>
Step 9: Reload Image	
Step 10: Bitwise operations	
	<Clipboard>=COPY<Image>
Step 12: Thresholding	
Mode	Global
Lower grey threshold	45
Upper grey threshold	255
Step 13: Bitwise operations	
	<region of interest>=COPY<Image>
Step 14: Bitwise operations	
	<Image>=SWAP<Clipboard>
Step 15: Histogram (3D space) inside VOI	

Step 16: save bitmaps	
File format	bmp
Step 17: 3D analysis	
Mean density	
Standard deviation	
Standard error or mean	
95% confidence limit (minimum)	
95% confidence limit (maximum)	

8.9. Appendix I – Original Picrosirius red images for hydrostatic pressure study

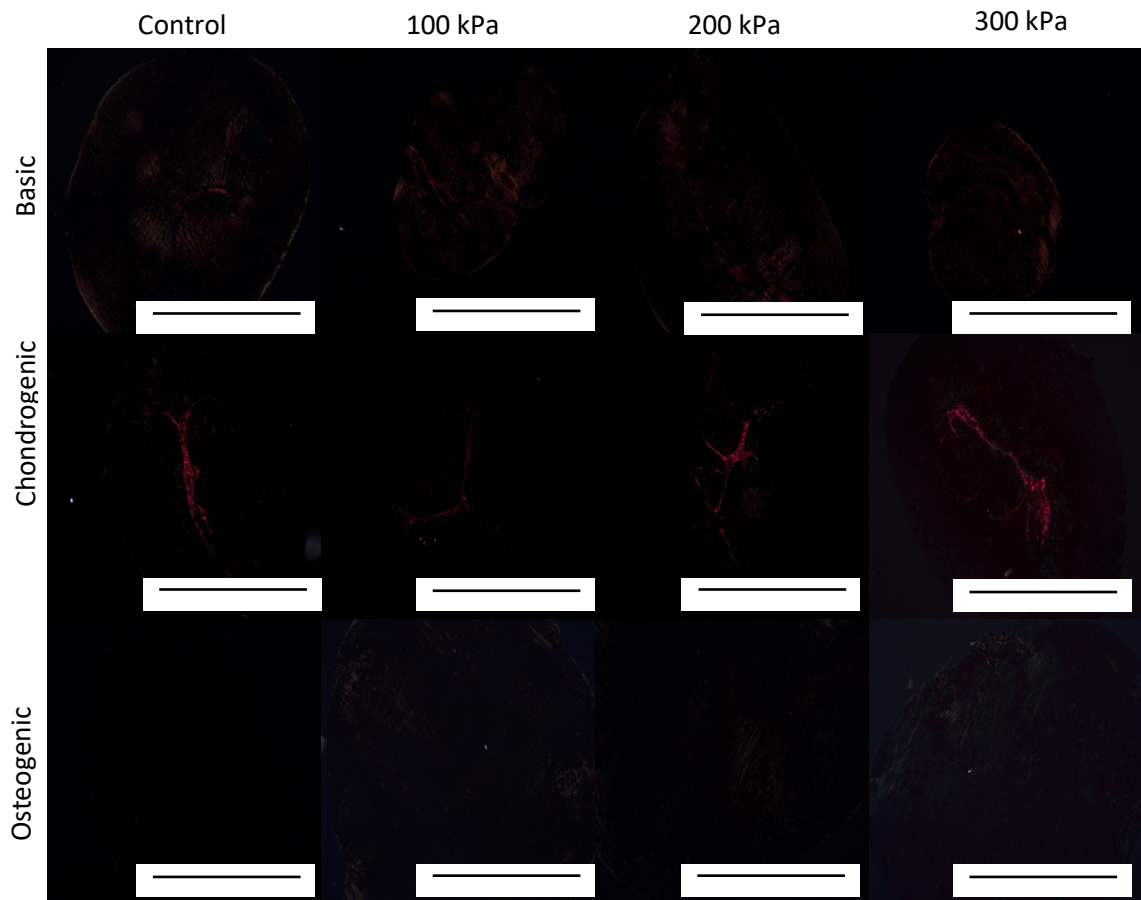


Figure 8.4. Original Picrosirius red images of microtissues cultured in basic, chondrogenic, osteogenic media following 14-day period hydrostatic pressure stimulation at 100 kPa, 200 kPa or 300 kPa. Representative images were taken with 4x objective, n=3 repeats. Scale bar represents 500 μm .

References

References

- ACKERS, I. & MALGOR, R. 2018. Interrelationship of canonical and non-canonical Wnt signalling pathways in chronic metabolic diseases. *Diab Vasc Dis Res*, 15, 3-13.
- ADAMOWICZ, J., POKRYWCZYNSKA, M., VAN BREDA, S. V., KLOSKOWSKI, T. & DREWA, T. 2017. Concise Review: Tissue Engineering of Urinary Bladder; We Still Have a Long Way to Go? *Stem Cells Transl Med*, 6, 2033-2043.
- AFOKE, N. Y., BYERS, P. D. & HUTTON, W. C. 1987. Contact pressures in the human hip joint. *J Bone Joint Surg Br*, 69, 536-41.
- AFSHINNEKOO, E., SCOTT, R. T., MACKAY, M. J., PARISET, E., CEKANAVICIUTE, E., BARKER, R., GILROY, S., HASSANE, D., SMITH, S. M., ZWART, S. R., NELMAN-GONZALEZ, M., CRUCIAN, B. E., PONOMAREV, S. A., ORLOV, O. I., SHIBA, D., MURATANI, M., YAMAMOTO, M., RICHARDS, S. E., VAISHAMPAYAN, P. A., MEYDAN, C., FOOX, J., MYRRHE, J., ISTASSE, E., SINGH, N., VENKATESWARAN, K., KEUNE, J. A., RAY, H. E., BASNER, M., MILLER, J., VITATERNA, M. H., TAYLOR, D. M., WALLACE, D., RUBINS, K., BAILEY, S. M., GRABHAM, P., COSTES, S. V., MASON, C. E. & BEHESHTI, A. 2020. Fundamental Biological Features of Spaceflight: Advancing the Field to Enable Deep-Space Exploration. *Cell*, 183, 1162-1184.
- AGARWAL, P., ZWOLANEK, D., KEENE, D. R., SCHULZ, J. N., BLUMBACH, K., HEINEGARD, D., ZAUCKE, F., PAULSSON, M., KRIEG, T., KOCH, M. & ECKES, B. 2012. Collagen XII and XIV, new partners of cartilage oligomeric matrix protein in the skin extracellular matrix suprastructure. *J Biol Chem*, 287, 22549-59.
- AHMADZADEH, H., FREEDMAN, B. R., CONNIZZO, B. K., SOSLOWSKY, L. J. & SHENOY, V. B. 2015. Micromechanical poroelastic finite element and shear-lag models of tendon predict large strain dependent Poisson's ratios and fluid expulsion under tensile loading. *Acta Biomater*, 22, 83-91.
- ALDRICH, S. 2020. *3D Bioprinting: Bioink Selection Guide* [Online]. www.sigmaaldrich.com. Available: [https://www.sigmaaldrich.com/technical-documents/articles/materials-science/3d-bioprinting-bioinks.html#:~:text=While%20a%20wide%20variety%20of,based%20materials%20\(Table%201\)](https://www.sigmaaldrich.com/technical-documents/articles/materials-science/3d-bioprinting-bioinks.html#:~:text=While%20a%20wide%20variety%20of,based%20materials%20(Table%201)). [Accessed 27/08/20 2020].
- ALENGHAT, F. J. & INGBER, D. E. 2002. Mechanotransduction: all signals point to cytoskeleton, matrix, and integrins. *Sci STKE*, 2002, pe6.
- ALEXOPOULOS, L. G., YOUN, I., BONALDO, P. & GUILAK, F. 2009. Developmental and osteoarthritic changes in Col6a1-knockout mice: biomechanics of type VI collagen in the cartilage pericellular matrix. *Arthritis Rheum*, 60, 771-9.
- ALMEIDA, H. V., ESWARAMOORTHY, R., CUNNIFFE, G. M., BUCKLEY, C. T., O'BRIEN, F. J. & KELLY, D. J. 2016. Fibrin hydrogels functionalized with cartilage extracellular matrix and incorporating freshly isolated stromal cells as an injectable for cartilage regeneration. *Acta Biomater*, 36, 55-62.
- ALMELKAR, S., PATWARDHAN, A., DIVATE, S., AGRAWAL, N., BHONDE, R. & CHAUKAR, A. 2014. Fibrin matrix supports endothelial cell adhesion and migration in culture. *OA Biology*, 2, 5.
- ALTMAN, G. H., HORAN, R. L., MARTIN, I., FARHADI, J., STARK, P. R., VOLLOCH, V., RICHMOND, J. C., VUNJAK-NOVAKOVIC, G. & KAPLAN, D. L. 2002. Cell differentiation by mechanical stress. *FASEB J*, 16, 270-2.
- ALWOOD, J. S., RONCA, A. E., MAINS, R. C., SHELHAMER, M. J., SMITH, J. D. & GOODWIN, T. J. 2017. From the bench to exploration medicine: NASA life sciences translational research for human exploration and habitation missions. *NPJ Microgravity*, 3, 5.
- AMENTA, P. S., SCIVOLETTI, N. A., NEWMAN, M. D., SCIANCALEPORE, J. P., LI, D. & MYERS, J. C. 2005. Proteoglycan-collagen XV in human tissues is seen linking banded collagen fibers subjacent to the basement membrane. *J Histochem Cytochem*, 53, 165-76.
- AN, Y. H. & MARTIN, K. L. 2003. *Handbook of histology methods for bone and cartilage*, Springer.
- ANGELE, P., YOO, J. U., SMITH, C., MANSOUR, J., JEPSEN, K. J., NERLICH, M. & JOHNSTONE, B. 2003. Cyclic hydrostatic pressure enhances the chondrogenic phenotype of human mesenchymal progenitor cells differentiated in vitro. *J Orthop Res*, 21, 451-7.
- ANSORGE, H. L., MENG, X., ZHANG, G., VEIT, G., SUN, M., KLEMENT, J. F., BEASON, D. P., SOSLOWSKY, L. J., KOCH, M. & BIRK, D. E. 2009. Type XIV Collagen Regulates Fibrillogenesis: PREMATURE COLLAGEN FIBRIL GROWTH AND TISSUE DYSFUNCTION IN NULL MICE. *J Biol Chem*, 284, 8427-38.
- ANTOINE, E. E., VLACHOS, P. P. & RYLANDER, M. N. 2014. Review of collagen I hydrogels for bioengineered tissue microenvironments: characterization of mechanics, structure, and transport. *Tissue Eng Part B Rev*, 20, 683-96.
- ANTTINEN, H., TUDERMAN, L., OIKARINEN, A. & KIVIRIKKO, K. I. 1977. Intracellular enzymes of collagen biosynthesis in human platelets. *Blood*, 50, 29-37.
- ARAI, F., MIYAMOTO, T., OHNEDA, O., INADA, T., SUDO, T., BRASEL, K., MIYATA, T., ANDERSON, D. M. & SUDA, T. 1999. Commitment and differentiation of osteoclast precursor cells by the sequential expression of c-Fms and receptor activator of nuclear factor kappaB (RANK) receptors. *J Exp Med*, 190, 1741-54.
- ARCHER, C. & RALPHS, J. 2010. *Regenerative medicine and biomaterials for the repair of connective tissues*, Elsevier.
- ARITA, N. A., PELAEZ, D. & CHEUNG, H. S. 2011. Activation of the extracellular signal-regulated kinases 1 and 2 (ERK1/2) is needed for the TGFbeta-induced chondrogenic and osteogenic differentiation of mesenchymal stem cells. *Biochem Biophys Res Commun*, 405, 564-9.

References

- ARMIENTO, A. R., ALINI, M. & STODDART, M. J. 2019. Articular fibrocartilage - Why does hyaline cartilage fail to repair? *Adv Drug Deliv Rev*, 146, 289-305.
- ARNOCZKY, S. P., TIAN, T., LAVAGNINO, M., GARDNER, K., SCHULER, P. & MORSE, P. 2002. Activation of stress-activated protein kinases (SAPK) in tendon cells following cyclic strain: the effects of strain frequency, strain magnitude, and cytosolic calcium. *J Orthop Res*, 20, 947-52.
- ASADA, N., SATO, M. & KATAYAMA, Y. 2015. Communication of bone cells with hematopoiesis, immunity and energy metabolism. *Bonekey Rep*, 4, 748.
- ASLAN, H., KIMELMAN-BLEICH, N., PELLED, G. & GAZIT, D. 2008. Molecular targets for tendon neof ormation. *J Clin Invest*, 118, 439-44.
- ASPBERG, A. 2016. Cartilage Proteoglycans. In: GRÄSSEL, S. & ASZÓDI, A. (eds.) *Cartilage: Volume 1: Physiology and Development*. Cham: Springer International Publishing.
- ATALA, A., BAUER, S. B., SOKER, S., YOO, J. J. & RETIK, A. B. 2006. Tissue-engineered autologous bladders for patients needing cystoplasty. *Lancet*, 367, 1241-6.
- ATKINSON, F., EVANS, R., GUEST, J. E., BAVIN, E. P., CACADOR, D., HOLLAND, C. & GUEST, D. J. 2020. Cyclical strain improves artificial equine tendon constructs in vitro. *J Tissue Eng Regen Med*.
- AUGST, A. D., KONG, H. J. & MOONEY, D. J. 2006. Alginate hydrogels as biomaterials. *Macromol Biosci*, 6, 623-33.
- AWAD, H. A., BUTLER, D. L., BOIVIN, G. P., SMITH, F. N., MALAVIYA, P., HUIBREGTSE, B. & CAPLAN, A. I. 1999. Autologous mesenchymal stem cell-mediated repair of tendon. *Tissue Eng*, 5, 267-77.
- BACHINGER, H. P. 1987. The influence of peptidyl-prolyl cis-trans isomerase on the in vitro folding of type III collagen. *J Biol Chem*, 262, 17144-8.
- BACHINGER, H. P., BRUCKNER, P., TIMPL, R. & ENGEL, J. 1978. The role of cis-trans isomerization of peptide bonds in the coil leads to and comes from triple helix conversion of collagen. *Eur J Biochem*, 90, 605-13.
- BACHINGER, H. P., BRUCKNER, P., TIMPL, R., PROCKOP, D. J. & ENGEL, J. 1980. Folding mechanism of the triple helix in type-III collagen and type-III pN-collagen. Role of disulfide bridges and peptide bond isomerization. *Eur J Biochem*, 106, 619-32.
- BAGNANINCHI, P. O., YANG, Y., EL HAJ, A. J. & MAFFULLI, N. 2007. Tissue engineering for tendon repair. *Br J Sports Med*, 41, e10; discussion e10.
- BAILEY, A. J. 2001. Molecular mechanisms of ageing in connective tissues. *Mech Ageing Dev*, 122, 735-55.
- BAILEY, A. J., WOTTON, S. F., SIMS, T. J. & THOMPSON, P. W. 1993. Biochemical changes in the collagen of human osteoporotic bone matrix. *Connect Tissue Res*, 29, 119-32.
- BAKSH, D., SONG, L. & TUAN, R. S. 2004. Adult mesenchymal stem cells: characterization, differentiation, and application in cell and gene therapy. *J Cell Mol Med*, 8, 301-16.
- BALDOCK, C., SHERRATT, M. J., SHUTTLEWORTH, C. A. & KIELTY, C. M. 2003. The supramolecular organization of collagen VI microfibrils. *J Mol Biol*, 330, 297-307.
- BANFI, A., MURAGLIA, A., DOZIN, B., MASTROGIACOMO, M., CANCEDDA, R. & QUARTO, R. 2000. Proliferation kinetics and differentiation potential of ex vivo expanded human bone marrow stromal cells: Implications for their use in cell therapy. *Exp Hematol*, 28, 707-15.
- BANIK, B. L. & BROWN, J. L. 2020. 3D-Printed Bioreactor Enhances Potential for Tendon Tissue Engineering. *Regenerative Engineering and Translational Medicine*, 1-10.
- BANYARD, J., BAO, L. & ZETTER, B. R. 2003. Type XXIII collagen, a new transmembrane collagen identified in metastatic tumor cells. *J Biol Chem*, 278, 20989-94.
- BARBER, J. G., HANDORF, A. M., ALLEE, T. J. & LI, W. J. 2013. Braided nanofibrous scaffold for tendon and ligament tissue engineering. *Tissue Eng Part A*, 19, 1265-74.
- BARD, F., CASANO, L., MALLABIABARRENA, A., WALLACE, E., SAITO, K., KITAYAMA, H., GUIZZUNTI, G., HU, Y., WENDLER, F., DASGUPTA, R., PERRIMON, N. & MALHOTRA, V. 2006. Functional genomics reveals genes involved in protein secretion and Golgi organization. *Nature*, 439, 604-7.
- BARD, F. & MALHOTRA, V. 2006. The formation of TGN-to-plasma-membrane transport carriers. *Annu Rev Cell Dev Biol*, 22, 439-55.
- BARNARD, K., LIGHT, N. D., SIMS, T. J. & BAILEY, A. J. 1987. Chemistry of the collagen cross-links. Origin and partial characterization of a putative mature cross-link of collagen. *Biochem J*, 244, 303-9.
- BARON, R., NEFF, L., LOUVARD, D. & COURTOY, P. J. 1985. Cell-mediated extracellular acidification and bone resorption: evidence for a low pH in resorbing lacunae and localization of a 100-kD lysosomal membrane protein at the osteoclast ruffled border. *J Cell Biol*, 101, 2210-22.
- BATES, D., MÄCHLER, M., BOLKER, B. & WALKER, S. 2015. Fitting Linear Mixed-Effects Models Using lme4. 2015, 67, 48.
- BATTAGLIA, T. C., CLARK, R. T., CHHABRA, A., GASCHEN, V., HUNZIKER, E. B. & MIKIC, B. 2003. Ultrastructural determinants of murine achilles tendon strength during healing. *Connect Tissue Res*, 44, 218-24.
- BAUD, C. A. 1968. Submicroscopic structure and functional aspects of the osteocyte. *Clin Orthop Relat Res*, 56, 227-36.
- BEGLEY, C. M. & KLEIS, S. J. 2000. The fluid dynamic and shear environment in the NASA/JSC rotating-wall perfused-vessel bioreactor. *Biotechnol Bioeng*, 70, 32-40.

References

- BELLA, J. 2016. Collagen structure: new tricks from a very old dog. *Biochem J*, 473, 1001-25.
- BELLA, J. & HULMES, D. J. 2017. Fibrillar collagens. *Fibrous proteins: structures and mechanisms*. Springer.
- BEN-ARYE, T. & LEVENBERG, S. 2019. Tissue engineering for clean meat production. *Frontiers in Sustainable Food Systems*, 3, 46.
- BENAVIDES DAMM, T., WALTHER, I., WÜEST, S. L., SEKLER, J. & EGLI, M. 2014. Cell cultivation under different gravitational loads using a novel random positioning incubator. *Biotechnology and bioengineering*, 111, 1180-1190.
- BENHARDT, H. A. & COSGRIFF-HERNANDEZ, E. M. 2009. The Role of Mechanical Loading in Ligament Tissue Engineering. *Tissue Engineering Part B-Reviews*, 15, 467-475.
- BENJAMIN, M. & RALPHS, J. 2004. Biology of fibrocartilage cells. *International review of cytology*, 233, 1-46.
- BENJAMIN, M. & RALPHS, J. R. 1998. Fibrocartilage in tendons and ligaments--an adaptation to compressive load. *J Anat*, 193 (Pt 4), 481-94.
- BERNAL, P. N., DELROT, P., LOTERIE, D., LI, Y., MALDA, J., MOSER, C. & LEVATO, R. 2019. Volumetric Bioprinting of Complex Living-Tissue Constructs within Seconds. *Adv Mater*, 31, e1904209.
- BETHUNE, R., BULL, A. M., DICKINSON, R. J. & EMERY, R. J. 2007. Removal of calcific deposits of the rotator cuff tendon using an intra-articular ultrasound probe. *Knee Surg Sports Traumatol Arthrosc*, 15, 289-91.
- BEZNOUSSENKO, G. V., PARASHURAMAN, S., RIZZO, R., POLISHCHUK, R., MARTELLA, O., DI GIANDOMENICO, D., FUSELLA, A., SPAAR, A., SALLESE, M., CAPESTRANO, M. G., PAVELKA, M., VOS, M. R., RIKERS, Y. G., HELMS, V., MIRONOV, A. A. & LUINI, A. 2014. Transport of soluble proteins through the Golgi occurs by diffusion via continuities across cisternae. *Elife*, 3.
- BIAN, W., JUHAS, M., PFEILER, T. W. & BURSAC, N. 2012. Local tissue geometry determines contractile force generation of engineered muscle networks. *Tissue Eng Part A*, 18, 957-67.
- BIAN, W., LIAU, B., BADIE, N. & BURSAC, N. 2009. Mesoscopic hydrogel molding to control the 3D geometry of bioartificial muscle tissues. *Nat Protoc*, 4, 1522-34.
- BIDANSET, D. J., GUIDRY, C., ROSENBERG, L. C., CHOI, H. U., TIMPL, R. & HOOK, M. 1992. Binding of the proteoglycan decorin to collagen type VI. *J Biol Chem*, 267, 5250-6.
- BIEWENER, A. A. 1998. Muscle-tendon stresses and elastic energy storage during locomotion in the horse. *Comparative Biochemistry and Physiology Part B: Biochemistry and Molecular Biology*, 120, 73-87.
- BILEZIKIAN, J. P., RAISZ, L. G. & MARTIN, T. J. 2008. *Principles of bone biology*, Academic press.
- BIRK, D. E. 2001. Type V collagen: heterotypic type I/V collagen interactions in the regulation of fibril assembly. *Micron*, 32, 223-37.
- BIRK, D. E. & BRUCKNER, P. 2005. Collagen suprastructures. *Collagen*. Springer.
- BIRK, D. E. & BRÜCKNER, P. 2011. Collagens, suprastructures, and collagen fibril assembly. *The extracellular matrix: an overview*. Springer.
- BIRK, D. E. & TRELSTAD, R. L. 1986. Extracellular compartments in tendon morphogenesis: collagen fibril, bundle, and macroaggregate formation. *J Cell Biol*, 103, 231-40.
- BIRK, D. E., ZYCBAND, E. I., WINKELMANN, D. A. & TRELSTAD, R. L. 1989. Collagen fibrillogenesis in situ: fibril segments are intermediates in matrix assembly. *Proc Natl Acad Sci U S A*, 86, 4549-53.
- BLABER, E. A., FINKELSTEIN, H., DVOROCHKIN, N., SATO, K. Y., YOUSUF, R., BURNS, B. P., GLOBUS, R. K. & ALMEIDA, E. A. 2015. Microgravity Reduces the Differentiation and Regenerative Potential of Embryonic Stem Cells. *Stem Cells Dev*, 24, 2605-21.
- BLAIR, H. C., TEITELBAUM, S. L., GHISELLI, R. & GLUCK, S. 1989. Osteoclastic bone resorption by a polarized vacuolar proton pump. *Science*, 245, 855-7.
- BLUMBACH, K., BASTIAANSEN-JENNISKENS, Y. M., DEGROOT, J., PAULSSON, M., VAN OSCH, G. J. & ZAUCKE, F. 2009. Combined role of type IX collagen and cartilage oligomeric matrix protein in cartilage matrix assembly: cartilage oligomeric matrix protein counteracts type IX collagen-induced limitation of cartilage collagen fibril growth in mouse chondrocyte cultures. *Arthritis Rheum*, 60, 3676-85.
- BOETTCHER, K., KIENLE, S., NACHTSHEIM, J., BURGKART, R., HUGEL, T. & LIELEG, O. 2016. The structure and mechanical properties of articular cartilage are highly resilient towards transient dehydration. *Acta Biomater*, 29, 180-187.
- BOHANDY, J., KIM, B. & ADRIAN, F. 1986. Metal deposition from a supported metal film using an excimer laser. *Journal of Applied Physics*, 60, 1538-1539.
- BONEWALD, L. F. & JOHNSON, M. L. 2008. Osteocytes, mechanosensing and Wnt signaling. *Bone*, 42, 606-15.
- BONFANTI, L., MIRONOV, A. A., JR., MARTINEZ-MENARGUEZ, J. A., MARTELLA, O., FUSELLA, A., BALDASSARRE, M., BUCCIONE, R., GEUZE, H. J., MIRONOV, A. A. & LUINI, A. 1998. Procollagen traverses the Golgi stack without leaving the lumen of cisternae: evidence for cisternal maturation. *Cell*, 95, 993-1003.
- BOOS, N., NERLICH, A. G., WIEST, I., VON DER MARK, K. & AEBI, M. 1997. Immunolocalization of type X collagen in human lumbar intervertebral discs during ageing and degeneration. *Histochem Cell Biol*, 108, 471-80.
- BOOT-HANDFORD, R. P., TUCKWELL, D. S., PLUMB, D. A., ROCK, C. F. & POULSOM, R. 2003. A novel and highly conserved collagen (pro(alpha)1(XVII)) with a unique expression pattern and unusual molecular characteristics establishes a new clade within the vertebrate fibrillar collagen family. *J Biol Chem*, 278, 31067-77.

References

- BORSCHEL, G. H., HUANG, Y. C., CALVE, S., ARRUDA, E. M., LYNCH, J. B., DOW, D. E., KUZON, W. M., DENNIS, R. G. & BROWN, D. L. 2005. Tissue engineering of recellularized small-diameter vascular grafts. *Tissue Eng*, 11, 778-86.
- BOTH, S. K., VAN APeldoORN, A. A., JUKES, J. M., ENGLUND, M. C., HYLLNER, J., VAN BLITTERSWIJK, C. A. & DE BOER, J. 2011. Differential bone-forming capacity of osteogenic cells from either embryonic stem cells or bone marrow-derived mesenchymal stem cells. *J Tissue Eng Regen Med*, 5, 180-90.
- BOURHIS, J. M., MARIANO, N., ZHAO, Y., HARLOS, K., EXPOSITO, J. Y., JONES, E. Y., MOALI, C., AGHAJARI, N. & HULMES, D. J. 2012. Structural basis of fibrillar collagen trimerization and related genetic disorders. *Nat Struct Mol Biol*, 19, 1031-6.
- BOYCE, B. F. & XING, L. 2008. Functions of RANKL/RANK/OPG in bone modeling and remodeling. *Arch Biochem Biophys*, 473, 139-46.
- BRADAMANTE, S., RIVERO, D., BARENGHI, L., BALSAMO, M., MINARDI, S. P., VITALI, F. & CAVALIERI, D. 2018. SCD—stem cell differentiation toward osteoblast onboard the International Space Station. *Microgravity Science and Technology*, 30, 713-729.
- BRANDT, L., SCHUBERT, S., SCHEIBE, P., BREHM, W., FRANZEN, J., GROSS, C. & BURK, J. 2018. Tenogenic Properties of Mesenchymal Progenitor Cells Are Compromised in an Inflammatory Environment. *Int J Mol Sci*, 19.
- BREIDENBACH, A. P., DYMENT, N. A., LU, Y. H., RAO, M., SHEARN, J. T., ROWE, D. W., KADLER, K. E. & BUTLER, D. L. 2015. Fibrin Gels Exhibit Improved Biological, Structural, and Mechanical Properties Compared with Collagen Gels in Cell-Based Tendon Tissue-Engineered Constructs. *Tissue Engineering Part A*, 21, 438-450.
- BRETSCHER, L. E., JENKINS, C. L., TAYLOR, K. M., DERIDER, M. L. & RAINES, R. T. 2001. Conformational stability of collagen relies on a stereoelectronic effect. *J Am Chem Soc*, 123, 777-8.
- BRITTBERG, M., LINDAHL, A., NILSSON, A., OHLSSON, C., ISAKSSON, O. & PETERSON, L. 1994. Treatment of deep cartilage defects in the knee with autologous chondrocyte transplantation. *N Engl J Med*, 331, 889-95.
- BROWN, A. C. & BARKER, T. H. 2014. Fibrin-based biomaterials: modulation of macroscopic properties through rational design at the molecular level. *Acta Biomater*, 10, 1502-14.
- BROWN, J. C., MANN, K., WIEDEMANN, H. & TIMPL, R. 1993. Structure and binding properties of collagen type XIV isolated from human placenta. *J Cell Biol*, 120, 557-67.
- BROWNING, J. A., WALKER, R. E., HALL, A. C. & WILKINS, R. J. 1999. Modulation of Na⁺ x H⁺ exchange by hydrostatic pressure in isolated bovine articular chondrocytes. *Acta Physiol Scand*, 166, 39-45.
- BRUCKNER, P. & EIKENBERRY, E. F. 1984. Formation of the triple helix of type I procollagen in cellulose. Temperature-dependent kinetics support a model based on cis in equilibrium trans isomerization of peptide bonds. *Eur J Biochem*, 140, 391-5.
- BRUKER-MIKRO-CT, C. 2010. Bone mineral density (BMD) and tissue mineral density (TMD) calibration and measurement by micro-CT using Bruker-MicroCT. *Bruker Method Note*, 1-30.
- BUCKLEY, M. R., EVANS, E. B., MATUSZEWSKI, P. E., CHEN, Y. L., SATCHEL, L. N., ELLIOTT, D. M., SOSLOWSKY, L. J. & DODGE, G. R. 2013. Distributions of types I, II and III collagen by region in the human supraspinatus tendon. *Connect Tissue Res*, 54, 374-9.
- BURDICK, J. A. & PRESTWICH, G. D. 2011. Hyaluronic acid hydrogels for biomedical applications. *Adv Mater*, 23, H41-56.
- BURK, J., PLENGE, A., BREHM, W., HELLER, S., PFEIFFER, B. & KASPER, C. 2016. Induction of Tenogenic Differentiation Mediated by Extracellular Tendon Matrix and Short-Term Cyclic Stretching. *Stem Cells Int*, 2016, 7342379.
- BURKE, J. F., YANNAS, I. V., QUINBY, W. C., JR., BONDOC, C. C. & JUNG, W. K. 1981. Successful use of a physiologically acceptable artificial skin in the treatment of extensive burn injury. *Ann Surg*, 194, 413-28.
- BURRIDGE, K., FATH, K., KELLY, T., NUCKOLLS, G. & TURNER, C. 1988. Focal adhesions: transmembrane junctions between the extracellular matrix and the cytoskeleton. *Annu Rev Cell Biol*, 4, 487-525.
- BYRNE, E. M., FARRELL, E., MCMAHON, L. A., HAUGH, M. G., O'BRIEN, F. J., CAMPBELL, V. A., PRENDERGAST, P. J. & O'CONNELL, B. C. 2008. Gene expression by marrow stromal cells in a porous collagen-glycosaminoglycan scaffold is affected by pore size and mechanical stimulation. *J Mater Sci Mater Med*, 19, 3455-63.
- BYRNES, J. R., DUVAL, C., WANG, Y., HANSEN, C. E., AHN, B., MOOBERRY, M. J., CLARK, M. A., JOHNSEN, J. M., LORD, S. T., LAM, W. A., MEIJERS, J. C., NI, H., ARIENS, R. A. & WOLBERG, A. S. 2015. Factor XIIIa-dependent retention of red blood cells in clots is mediated by fibrin alpha-chain crosslinking. *Blood*, 126, 1940-8.
- CADIGAN, K. M. & PEIFER, M. 2009. Wnt signaling from development to disease: insights from model systems. *Cold Spring Harb Perspect Biol*, 1, a002881.
- CAHILL, K. S., MCCORMICK, P. C. & LEVI, A. D. 2015. A comprehensive assessment of the risk of bone morphogenetic protein use in spinal fusion surgery and postoperative cancer diagnosis. *J Neurosurg Spine*, 23, 86-93.
- CALIARI, S. R. & BURDICK, J. A. 2016. A practical guide to hydrogels for cell culture. *Nat Methods*, 13, 405-14.

References

- CALIARI, S. R., RAMIREZ, M. A. & HARLEY, B. A. 2011. The development of collagen-GAG scaffold-membrane composites for tendon tissue engineering. *Biomaterials*, 32, 8990-8.
- CALORI, G. M., TAGLIABUE, L., GALA, L., D'IMPORZANO, M., PERETTI, G. & ALBISETTI, W. 2008. Application of rhBMP-7 and platelet-rich plasma in the treatment of long bone non-unions: a prospective randomised clinical study on 120 patients. *Injury*, 39, 1391-402.
- CALVE, S., DENNIS, R. G., KOSNIK, P. E., 2ND, BAAR, K., GROSH, K. & ARRUDA, E. M. 2004. Engineering of functional tendon. *Tissue Eng*, 10, 755-61.
- CALVERT, J. W., MARRA, K. G., COOK, L., KUMTA, P. N., DIMILLA, P. A. & WEISS, L. E. 2000. Characterization of osteoblast-like behavior of cultured bone marrow stromal cells on various polymer surfaces. *J Biomed Mater Res*, 52, 279-84.
- CAMERON, G. J., ALBERTS, I. L., LAING, J. H. & WESS, T. J. 2002. Structure of type I and type III heterotypic collagen fibrils: an X-ray diffraction study. *J Struct Biol*, 137, 15-22.
- CAMPBELL, J. J., BADER, D. L. & LEE, D. A. 2008. Mechanical loading modulates intracellular calcium signaling in human mesenchymal stem cells. *J Appl Biomater Biomech*, 6, 9-15.
- CAMPBELL, M. A., WINTER, A. D., ILIC, M. Z. & HANDLEY, C. J. 1996. Catabolism and loss of proteoglycans from cultures of bovine collateral ligament. *Arch Biochem Biophys*, 328, 64-72.
- CANTY, E. G. & KADLER, K. E. 2005. Procollagen trafficking, processing and fibrillogenesis. *J Cell Sci*, 118, 1341-53.
- CANTY, E. G., LU, Y., MEADOWS, R. S., SHAW, M. K., HOLMES, D. F. & KADLER, K. E. 2004. Coalignment of plasma membrane channels and protrusions (fibripositors) specifies the parallelism of tendon. *J Cell Biol*, 165, 553-63.
- CAO, D. J., ZHAI, H. L., LIU, W., CUI, L., ZHONG, B. & CAO, Y. L. 2004. [Preliminary study on in vitro tendon engineering using tenocytes and polyglycolic acids]. *Zhonghua Wai Ke Za Zhi*, 42, 110-3.
- CAO, Y., LIU, Y., LIU, W., SHAN, Q., BUONOCORE, S. D. & CUI, L. 2002. Bridging tendon defects using autologous tenocyte engineered tendon in a hen model. *Plast Reconstr Surg*, 110, 1280-9.
- CARBONE, A., CARBALLO, C., MA, R., WANG, H., DENG, X., DAHIA, C. & RODEO, S. 2016. Indian hedgehog signaling and the role of graft tension in tendon-to-bone healing: Evaluation in a rat ACL reconstruction model. *J Orthop Res*, 34, 641-9.
- CARLEVARO, M. F., CERMELLI, S., CANCEDDA, R. & DESCALZI CANCEDDA, F. 2000. Vascular endothelial growth factor (VEGF) in cartilage neovascularization and chondrocyte differentiation: auto-paracrine role during endochondral bone formation. *J Cell Sci*, 113 (Pt 1), 59-69.
- CARROLL, S. F., BUCKLEY, C. T. & KELLY, D. J. 2017. Cyclic Tensile Strain Can Play a Role in Directing both Intramembranous and Endochondral Ossification of Mesenchymal Stem Cells. *Frontiers in Bioengineering and Biotechnology*, 5.
- CARTER, W. G. 1982. Transformation-dependent alterations in glycoproteins of extracellular matrix of human fibroblasts. Characterization of GP250 and the collagen-like GP140. *J Biol Chem*, 257, 13805-15.
- CASHION, A. T., CABALLERO, M., HALEVI, A., PAPPA, A., DENNIS, R. G. & VAN AALST, J. A. 2014. Programmable mechanobioreactor for exploration of the effects of periodic vibratory stimulus on mesenchymal stem cell differentiation. *Biores Open Access*, 3, 19-28.
- CASSCELLS, S. W. 1990. Articular cartilage and knee joint function: Basic science and arthroscopy. *Arthroscopy*, 6, 167.
- CASSELLA, J. P. & ALI, S. Y. 1992. Abnormal collagen and mineral formation in osteogenesis imperfecta. *Bone Miner*, 17, 123-8.
- CELLINK. 2021. *Box X* [Online]. Available: <https://www.cellink.com/bioprinting/bio-x-3d-bioprinter/> [Accessed 2021].
- CHAMBERS, T. J. 2000. Regulation of the differentiation and function of osteoclasts. *J Pathol*, 192, 4-13.
- CHAN, A. S. H., COUCOUVANIS, E., TOUSEY, S., ANDERSEN, M. D. & NI, J. H. T. 2007. Improved Expansion of MSC Without Loss of Differentiation Potential. Available: <https://www.rndsystems.com/resources/posters/improved-expansion-msc-without-loss-differentiation-potential>.
- CHAN, B. P. & LEONG, K. W. 2008. Scaffolding in tissue engineering: general approaches and tissue-specific considerations. *Eur Spine J*, 17 Suppl 4, 467-79.
- CHAN, D., COLE, W. G., ROGERS, J. G. & BATEMAN, J. F. 1995. Type X collagen multimer assembly in vitro is prevented by a Gly618 to Val mutation in the alpha 1(X) NC1 domain resulting in Schmid metaphyseal chondrodysplasia. *J Biol Chem*, 270, 4558-62.
- CHANDRARAJAN, J. 1978. Separation of type III collagen from type I collagen and pepsin by differential denaturation and renaturation. *Biochem Biophys Res Commun*, 83, 180-6.
- CHANG, J., NAKAJIMA, H. & POOLE, C. A. 1997. Structural colocalisation of type VI collagen and fibronectin in agarose cultured chondrocytes and isolated chondrons extracted from adult canine tibial cartilage. *J Anat*, 190 (Pt 4), 523-32.
- CHATTERJEE, D., CHAKRABORTY, M., LEIT, M., NEFF, L., JAMSA-KELLOKUMPU, S., FUCHS, R., BARTKIEWICZ, M., HERNANDO, N. & BARON, R. 1992. The osteoclast proton pump differs in its pharmacology and catalytic subunits from other vacuolar H(+)-ATPases. *J Exp Biol*, 172, 193-204.

References

- CHATZIZACHARIAS, N. A., KOURAKLIS, G. P. & THEOCHARIS, S. E. 2008. Disruption of FAK signaling: a side mechanism in cytotoxicity. *Toxicology*, 245, 1-10.
- CHELLIAH, M., KIZER, N., SILVA, M., ALVAREZ, U., KWIATKOWSKI, D. & HRUSKA, K. A. 2000. Gelsolin deficiency blocks podosome assembly and produces increased bone mass and strength. *J Cell Biol*, 148, 665-78.
- CHEN, G., DENG, C. & LI, Y. P. 2012. TGF-beta and BMP signaling in osteoblast differentiation and bone formation. *Int J Biol Sci*, 8, 272-88.
- CHEN, H. C. & HU, Y. C. 2006. Bioreactors for tissue engineering. *Biotechnol Lett*, 28, 1415-23.
- CHEN, J. L., YIN, Z., SHEN, W. L., CHEN, X., HENG, B. C., ZOU, X. H. & OUYANG, H. W. 2010. Efficacy of hESC-MSCs in knitted silk-collagen scaffold for tendon tissue engineering and their roles. *Biomaterials*, 31, 9438-51.
- CHEN, P., CESCONE, M., ZUCCOLOTTO, G., NOBBIO, L., COLOMBELLI, C., FILAFERRO, M., VITALE, G., FELTRI, M. L. & BONALDO, P. 2015. Collagen VI regulates peripheral nerve regeneration by modulating macrophage recruitment and polarization. *Acta Neuropathol*, 129, 97-113.
- CHEN, Q., SHOU, P., ZHENG, C., JIANG, M., CAO, G., YANG, Q., CAO, J., XIE, N., VELLETRI, T., ZHANG, X., XU, C., ZHANG, L., YANG, H., HOU, J., WANG, Y. & SHI, Y. 2016. Fate decision of mesenchymal stem cells: adipocytes or osteoblasts? *Cell Death Differ*, 23, 1128-39.
- CHEN, W., LIU, J., MANUCHEHRABADI, N., WEIR, M. D., ZHU, Z. & XU, H. H. 2013. Umbilical cord and bone marrow mesenchymal stem cell seeding on macroporous calcium phosphate for bone regeneration in rat cranial defects. *Biomaterials*, 34, 9917-25.
- CHEN, X. D., DUSEVICH, V., FENG, J. Q., MANOLAGAS, S. C. & JILKA, R. L. 2007. Extracellular matrix made by bone marrow cells facilitates expansion of marrow-derived mesenchymal progenitor cells and prevents their differentiation into osteoblasts. *J Bone Miner Res*, 22, 1943-56.
- CHEN, Y. J., HUANG, C. H., LEE, I. C., LEE, Y. T., CHEN, M. H. & YOUNG, T. H. 2008. Effects of cyclic mechanical stretching on the mRNA expression of tendon/ligament-related and osteoblast-specific genes in human mesenchymal stem cells. *Connect Tissue Res*, 49, 7-14.
- CHENG, M. T., YANG, H. W., CHEN, T. H. & LEE, O. K. 2009. Isolation and characterization of multipotent stem cells from human cruciate ligaments. *Cell Prolif*, 42, 448-60.
- CHIEN, S. 2007. Mechanotransduction and endothelial cell homeostasis: the wisdom of the cell. *Am J Physiol Heart Circ Physiol*, 292, H1209-24.
- CHIQUET, M., BIRK, D. E., BONNEMANN, C. G. & KOCH, M. 2014. Collagen XII: Protecting bone and muscle integrity by organizing collagen fibrils. *Int J Biochem Cell Biol*, 53, 51-4.
- CHIU, C. L., HECHT, V., DUONG, H., WU, B. & TAWIL, B. 2012. Permeability of three-dimensional fibrin constructs corresponds to fibrinogen and thrombin concentrations. *Biores Open Access*, 1, 34-40.
- CHRISTIANO, A. M., GREENSPAN, D. S., LEE, S. & UITTO, J. 1994a. Cloning of human type VII collagen. Complete primary sequence of the alpha 1(VII) chain and identification of intragenic polymorphisms. *J Biol Chem*, 269, 20256-62.
- CHRISTIANO, A. M., HOFFMAN, G. G., CHUNG-HONET, L. C., LEE, S., CHENG, W., UITTO, J. & GREENSPAN, D. S. 1994b. Structural organization of the human type VII collagen gene (COL7A1), composed of more exons than any previously characterized gene. *Genomics*, 21, 169-79.
- CHRISTIANO, A. M., ROSENBAUM, L. M., CHUNG-HONET, L. C., PARENTE, M. G., WOODLEY, D. T., PAN, T. C., ZHANG, R. Z., CHU, M. L., BURGESSON, R. E. & UITTO, J. 1992. The large non-collagenous domain (NC-1) of type VII collagen is amino-terminal and chimeric. Homology to cartilage matrix protein, the type III domains of fibronectin and the A domains of von Willebrand factor. *Hum Mol Genet*, 1, 475-81.
- CHRISTIANSEN, D. L., HUANG, E. K. & SILVER, F. H. 2000. Assembly of type I collagen: fusion of fibril subunits and the influence of fibril diameter on mechanical properties. *Matrix Biol*, 19, 409-20.
- CHU, M. L., MYERS, J. C., BERNARD, M. P., DING, J. F. & RAMIREZ, F. 1982. Cloning and characterization of five overlapping cDNAs specific for the human pro alpha 1(I) collagen chain. *Nucleic Acids Res*, 10, 5925-34.
- CHUNG, C. & BURDICK, J. A. 2008. Engineering cartilage tissue. *Adv Drug Deliv Rev*, 60, 243-62.
- CHUNG, H. J. & UITTO, J. 2010. Type VII collagen: the anchoring fibril protein at fault in dystrophic epidermolysis bullosa. *Dermatol Clin*, 28, 93-105.
- CIARDULLI, M. C., MARINO, L., LOVECCHIO, J., GIORDANO, E., FORSYTH, N. R., SELLERI, C., MAFFULLI, N. & PORTA, G. D. 2020. Tendon and Cytokine Marker Expression by Human Bone Marrow Mesenchymal Stem Cells in a Hyaluronate/Poly-Lactic-Co-Glycolic Acid (PLGA)/Fibrin Three-Dimensional (3D) Scaffold. *Cells*, 9.
- CLARKE, B. 2008. Normal bone anatomy and physiology. *Clin J Am Soc Nephrol*, 3 Suppl 3, S131-9.
- CLORE, J. N., COHEN, I. K. & DIEGELMANN, R. F. 1979. Quantitation of collagen types I and III during wound healing in rat skin. *Proc Soc Exp Biol Med*, 161, 337-40.
- COCHIS, A., GRAD, S., STODDART, M. J., FARE, S., ALTOMARE, L., AZZIMONTI, B., ALINI, M. & RIMONDINI, L. 2017. Bioreactor mechanically guided 3D mesenchymal stem cell chondrogenesis using a biocompatible novel thermo-reversible methylcellulose-based hydrogel. *Sci Rep*, 7, 45018.
- COLIGE, A., LI, S. W., SIERON, A. L., NUSGENS, B. V., PROCKOP, D. J. & LAPIERE, C. M. 1997. cDNA cloning and expression of bovine procollagen I N-proteinase: a new member of the superfamily of zinc-

References

- metalloproteinases with binding sites for cells and other matrix components. *Proc Natl Acad Sci U S A*, 94, 2374-9.
- COLIGE, A., VANDENBERGHE, I., THIRY, M., LAMBERT, C. A., VAN BEEUMEN, J., LI, S. W., PROCKOP, D. J., LAPIERE, C. M. & NUSGENS, B. V. 2002. Cloning and characterization of ADAMTS-14, a novel ADAMTS displaying high homology with ADAMTS-2 and ADAMTS-3. *J Biol Chem*, 277, 5756-66.
- COLOMBO, F., SAMPOGNA, G., COCOZZA, G., GURAYA, S. Y. & FORGIONE, A. 2017. Regenerative medicine: Clinical applications and future perspectives. *J Microsc Ultrastruct*, 5, 1-8.
- COLOMBO, M., BRITTINGHAM, R. J., KLEMENT, J. F., MAJSTEREK, I., BIRK, D. E., UITTO, J. & FERTALA, A. 2003. Procollagen VII self-assembly depends on site-specific interactions and is promoted by cleavage of the NC2 domain with procollagen C-proteinase. *Biochemistry*, 42, 11434-42.
- CONNIZZO, B. K., FREEDMAN, B. R., FRIED, J. H., SUN, M., BIRK, D. E. & SOSLOWSKY, L. J. 2015. Regulatory role of collagen V in establishing mechanical properties of tendons and ligaments is tissue dependent. *J Orthop Res*, 33, 882-8.
- CORREIA, C., PEREIRA, A. L., DUARTE, A. R., FRIAS, A. M., PEDRO, A. J., OLIVEIRA, J. T., SOUSA, R. A. & REIS, R. L. 2012. Dynamic culturing of cartilage tissue: the significance of hydrostatic pressure. *Tissue Eng Part A*, 18, 1979-91.
- CORREIA, V., PANADERO, J. A., RIBEIRO, C., SENCADAS, V., ROCHA, J. G., GOMEZ RIBELLES, J. L. & LANCEROS-MENDEZ, S. 2016. Design and validation of a biomechanical bioreactor for cartilage tissue culture. *Biomech Model Mechanobiol*, 15, 471-8.
- COULSON-THOMAS, Y. M., COULSON-THOMAS, V. J., NORTON, A. L., GESTEIRA, T. F., CAVALHEIRO, R. P., MENEGHETTI, M. C., MARTINS, J. R., DIXON, R. A. & NADER, H. B. 2015. The identification of proteoglycans and glycosaminoglycans in archaeological human bones and teeth. *PLoS One*, 10, e0131105.
- CRAM, D. J. 1988. The design of molecular hosts, guests, and their complexes. *Science*, 240, 760-7.
- CRAPO, P. M., GILBERT, T. W. & BADYLAK, S. F. 2011. An overview of tissue and whole organ decellularization processes. *Biomaterials*, 32, 3233-43.
- CUI, L., LIU, B., LIU, G., ZHANG, W., CEN, L., SUN, J., YIN, S., LIU, W. & CAO, Y. 2007. Repair of cranial bone defects with adipose derived stem cells and coral scaffold in a canine model. *Biomaterials*, 28, 5477-86.
- CUKIERMAN, E., PANKOV, R., STEVENS, D. R. & YAMADA, K. M. 2001. Taking cell-matrix adhesions to the third dimension. *Science*, 294, 1708-12.
- DA SILVA MEIRELLES, L., CHAGASTELLES, P. C. & NARDI, N. B. 2006. Mesenchymal stem cells reside in virtually all post-natal organs and tissues. *Journal of cell science*, 119, 2204-2213.
- DANIELSON, K. G., BARIBAULT, H., HOLMES, D. F., GRAHAM, H., KADLER, K. E. & IOZZO, R. V. 1997. Targeted disruption of decorin leads to abnormal collagen fibril morphology and skin fragility. *J Cell Biol*, 136, 729-43.
- DARLING, E. M. & ATHANASIOU, K. A. 2003. Articular cartilage bioreactors and bioprocesses. *Tissue Eng*, 9, 9-26.
- DAVIDSON, J. M., AQUINO, A. M., WOODWARD, S. C. & WILFINGER, W. W. 1999. Sustained microgravity reduces intrinsic wound healing and growth factor responses in the rat. *FASEB J*, 13, 325-9.
- DE BARI, C., DELL'ACCIO, F., TYLZANOWSKI, P. & LUYTEN, F. P. 2001. Multipotent mesenchymal stem cells from adult human synovial membrane. *Arthritis Rheum*, 44, 1928-42.
- DE MATTEIS, M. A. & LUINI, A. 2008. Exiting the Golgi complex. *Nat Rev Mol Cell Biol*, 9, 273-84.
- DELANY, A. M. & HANKENSON, K. D. 2009. Thrombospondin-2 and SPARC/osteonectin are critical regulators of bone remodeling. *J Cell Commun Signal*, 3, 227-38.
- DENG, Z. L., SHARFF, K. A., TANG, N., SONG, W. X., LUO, J., LUO, X., CHEN, J., BENNETT, E., REID, R., MANNING, D., XUE, A., MONTAG, A. G., LUU, H. H., HAYDON, R. C. & HE, T. C. 2008. Regulation of osteogenic differentiation during skeletal development. *Front Biosci*, 13, 2001-21.
- DENIZ, P., GULER, S., CELIK, E., HOSSEINIAN, P. & AYDIN, H. M. 2020. Use of cyclic strain bioreactor for the upregulation of key tenocyte gene expression on Poly(glycerol-sebacate) (PGS) sheets. *Materials Science & Engineering C-Materials for Biological Applications*, 106.
- DERIDER, M. L., WILKENS, S. J., WADDELL, M. J., BRETSCHER, L. E., WEINHOLD, F., RAINES, R. T. & MARKLEY, J. L. 2002. Collagen stability: insights from NMR spectroscopic and hybrid density functional computational investigations of the effect of electronegative substituents on prolyl ring conformations. *J Am Chem Soc*, 124, 2497-505.
- DIAB, M., WU, J. J. & EYRE, D. R. 1996. Collagen type IX from human cartilage: a structural profile of intermolecular cross-linking sites. *Biochem J*, 314 (Pt 1), 327-32.
- DIAZ, L. A., RATRIE, H., 3RD, SAUNDERS, W. S., FUTAMURA, S., SQUIQUERA, H. L., ANHALT, G. J. & GIUDICE, G. J. 1990. Isolation of a human epidermal cDNA corresponding to the 180-kD autoantigen recognized by bullous pemphigoid and herpes gestationis sera. Immunolocalization of this protein to the hemidesmosome. *J Clin Invest*, 86, 1088-94.
- DIGIROLAMO, C. M., STOKES, D., COLTER, D., PHINNEY, D. G., CLASS, R. & PROCKOP, D. J. 1999. Propagation and senescence of human marrow stromal cells in culture: a simple colony-forming assay identifies samples with the greatest potential to propagate and differentiate. *Br J Haematol*, 107, 275-81.

References

- DILOGO, I. H., PRIMAPUTRA, M. R. A., PAWITAN, J. A. & LIEM, I. K. 2017. Modified Masquelet technique using allogeneic umbilical cord-derived mesenchymal stem cells for infected non-union femoral shaft fracture with a 12 cm bone defect: A case report. *Int J Surg Case Rep*, 34, 11-16.
- DOANE, K. J., HOWELL, S. J. & BIRK, D. E. 1998. Identification and functional characterization of two type VI collagen receptors, alpha 3 beta 1 integrin and NG2, during avian corneal stromal development. *Invest Ophthalmol Vis Sci*, 39, 263-75.
- DOMINICI, M., LE BLANC, K., MUELLER, I., SLAPER-CORTENBACH, I., MARINI, F., KRAUSE, D., DEANS, R., KEATING, A., PROCKOP, D. & HORWITZ, E. 2006. Minimal criteria for defining multipotent mesenchymal stromal cells. The International Society for Cellular Therapy position statement. *Cytotherapy*, 8, 315-7.
- DORSEY, S. M., LIN-GIBSON, S. & SIMON, C. G., JR. 2009. X-ray microcomputed tomography for the measurement of cell adhesion and proliferation in polymer scaffolds. *Biomaterials*, 30, 2967-74.
- DOYLE, A. D., CARVAJAL, N., JIN, A., MATSUMOTO, K. & YAMADA, K. M. 2015. Local 3D matrix microenvironment regulates cell migration through spatiotemporal dynamics of contractility-dependent adhesions. *Nat Commun*, 6, 8720.
- DUOCASTELLA, M., COLINA, M., FERNÁNDEZ-PRADAS, J., SERRA, P. & MORENZA, J. 2007. Study of the laser-induced forward transfer of liquids for laser bioprinting. *Applied surface science*, 253, 7855-7859.
- EHNIS, T., DIETERICH, W., BAUER, M., LAMPE, B. & SCHUPPAN, D. 1996. A chondroitin/dermatan sulfate form of CD44 is a receptor for collagen XIV (undulin). *Exp Cell Res*, 229, 388-97.
- EISENBERG, S. R. & GRODZINSKY, A. J. 1985. Swelling of articular cartilage and other connective tissues: electromechanochemical forces. *J Orthop Res*, 3, 148-59.
- EL SAYED, K., HAISCH, A., JOHN, T., MARZAHN, U., LOHAN, A., MULLER, R. D., KOHL, B., ERTEL, W., STOELZEL, K. & SCHULZE-TANZIL, G. 2010. Heterotopic autologous chondrocyte transplantation—a realistic approach to support articular cartilage repair? *Tissue Eng Part B Rev*, 16, 603-16.
- EL SAYED, K., MARZAHN, U., JOHN, T., HOYER, M., ZREIQAT, H., WITTHUHN, A., KOHL, B., HAISCH, A. & SCHULZE-TANZIL, G. 2013. PGA-associated heterotopic chondrocyte cocultures: implications of nasoseptal and auricular chondrocytes in articular cartilage repair. *J Tissue Eng Regen Med*, 7, 61-72.
- ELDER, B. D. & ATHANASIOU, K. A. 2009. Hydrostatic pressure in articular cartilage tissue engineering: from chondrocytes to tissue regeneration. *Tissue Eng Part B Rev*, 15, 43-53.
- ELLIOTT, D. M., ROBINSON, P. S., GIMBEL, J. A., SARVER, J. J., ABBOUD, J. A., IOZZO, R. V. & SOSLOWSKY, L. J. 2003. Effect of altered matrix proteins on quasilinear viscoelastic properties in transgenic mouse tail tendons. *Ann Biomed Eng*, 31, 599-605.
- ENGBRETSON, B., MUSSETT, Z., WILLIAMS, C., SIMMONS, A. & SIKAVITSAS, V. 2015. Tendon Tissue Engineering: Combined Tissue Engineering Approach for the Regeneration of Tendons. *Tendon Regeneration*. Elsevier.
- ENGBRETSON, B., MUSSETT, Z. R. & SIKAVITSAS, V. I. 2018. The effects of varying frequency and duration of mechanical stimulation on a tissue-engineered tendon construct. *Connective tissue research*, 59, 167-177.
- ENGEL, J. & PROCKOP, D. J. 1991. The zipper-like folding of collagen triple helices and the effects of mutations that disrupt the zipper. *Annu Rev Biophys Biophys Chem*, 20, 137-52.
- ENGLER, A. J., SEN, S., SWEENEY, H. L. & DISCHER, D. E. 2006. Matrix elasticity directs stem cell lineage specification. *Cell*, 126, 677-89.
- ERICKSON, G. R., GIMBLE, J. M., FRANKLIN, D. M., RICE, H. E., AWAD, H. & GUILAK, F. 2002. Chondrogenic potential of adipose tissue-derived stromal cells in vitro and in vivo. *Biochem Biophys Res Commun*, 290, 763-9.
- ESA. 2003. *The ZARM drop tower in Bremen, Germany* [Online]. The European Space Agency. Available: https://www.esa.int/Science_Exploration/Human_and_Robotic_Exploration/Research/Drop_towers [Accessed 2021].
- ESCAMILLA, R. F. 2001. Knee biomechanics of the dynamic squat exercise. *Med Sci Sports Exerc*, 33, 127-41.
- EYRE, D. 2002. Collagen of articular cartilage. *Arthritis Res*, 4, 30-5.
- EYRE, D. R., WU, J. J., FERNANDES, R. J., PIETKA, T. A. & WEIS, M. A. 2002. Recent developments in cartilage research: matrix biology of the collagen II/IX/XI heterofibril network. *Biochem Soc Trans*, 30, 893-9.
- EYRICH, D., BRANDL, F., APPEL, B., WIESE, H., MAIER, G., WENZEL, M., STAUDENMAIER, R., GOEPFERICH, A. & BLUNK, T. 2007. Long-term stable fibrin gels for cartilage engineering. *Biomaterials*, 28, 55-65.
- EZURA, Y., CHAKRAVARTI, S., OLDBERG, A., CHERVONEVA, I. & BIRK, D. E. 2000. Differential expression of lumican and fibromodulin regulate collagen fibrillogenesis in developing mouse tendons. *J Cell Biol*, 151, 779-88.
- FAN, D., CREEMERS, E. E. & KASSIRI, Z. 2014. Matrix as an interstitial transport system. *Circ Res*, 114, 889-902.
- FARNEBO, S., WOON, C. Y., SCHMITT, T., JOUBERT, L. M., KIM, M., PHAM, H. & CHANG, J. 2014. Design and characterization of an injectable tendon hydrogel: a novel scaffold for guided tissue regeneration in the musculoskeletal system. *Tissue Eng Part A*, 20, 1550-61.

References

- FERNANDES, R. J., HIROHATA, S., ENGLE, J. M., COLIGE, A., COHN, D. H., EYRE, D. R. & APTE, S. S. 2001. Procollagen II amino propeptide processing by ADAMTS-3. Insights on dermatosparaxis. *J Biol Chem*, 276, 31502-9.
- FERNANDES, R. J., WEIS, M., SCOTT, M. A., SEEGMILLER, R. E. & EYRE, D. R. 2007. Collagen XI chain misassembly in cartilage of the chondrodysplasia (cho) mouse. *Matrix Biol*, 26, 597-603.
- FERRARI, S. L., TRAIANEDES, K., THORNE, M., LAFAGE-PROUST, M. H., GENEVER, P., CECCHINI, M. G., BEHAR, V., BISELLO, A., CHOREV, M., ROSENBLATT, M. & SUVA, L. J. 2000. A role for N-cadherin in the development of the differentiated osteoblastic phenotype. *J Bone Miner Res*, 15, 198-208.
- FIDLER, A. L., BOUDKO, S. P., ROKAS, A. & HUDSON, B. G. 2018. The triple helix of collagens - an ancient protein structure that enabled animal multicellularity and tissue evolution. *J Cell Sci*, 131.
- FINGER, A. R., SARGENT, C. Y., DULANEY, K. O., BERNACKI, S. H. & LOBOA, E. G. 2007. Differential effects on messenger ribonucleic acid expression by bone marrow-derived human mesenchymal stem cells seeded in agarose constructs due to ramped and steady applications of cyclic hydrostatic pressure. *Tissue Eng*, 13, 1151-8.
- FITZGERALD, J. & BATEMAN, J. F. 2001. A new FACIT of the collagen family: COL21A1. *FEBS Lett*, 505, 275-80.
- FITZGERALD, J., HOLDEN, P. & HANSEN, U. 2013. The expanded collagen VI family: new chains and new questions. *Connect Tissue Res*, 54, 345-50.
- FITZGERALD, J., RICH, C., ZHOU, F. H. & HANSEN, U. 2008. Three novel collagen VI chains, alpha4(VI), alpha5(VI), and alpha6(VI). *J Biol Chem*, 283, 20170-80.
- FLEISCHMAJER, R., PERLISH, J. S., TIMPL, R. & OLSEN, B. R. 1988. Procollagen intermediates during tendon fibrillogenesis. *J Histochem Cytochem*, 36, 1425-32.
- FLORENCIO-SILVA, R., SASSO, G. R., SASSO-CERRI, E., SIMOES, M. J. & CERRI, P. S. 2015. Biology of Bone Tissue: Structure, Function, and Factors That Influence Bone Cells. *Biomed Res Int*, 2015, 421746.
- FONT, B., EICHENBERGER, D., ROSENBERG, L. M. & VAN DER REST, M. 1996. Characterization of the interactions of type XII collagen with two small proteoglycans from fetal bovine tendon, decorin and fibromodulin. *Matrix Biol*, 15, 341-8.
- FRANCHI, M., TRIRE, A., QUARANTA, M., ORSINI, E. & OTTANI, V. 2007. Collagen structure of tendon relates to function. *ScientificWorldJournal*, 7, 404-20.
- FRANCIS, S. L., DI BELLA, C., WALLACE, G. G. & CHOONG, P. F. M. 2018. Cartilage Tissue Engineering Using Stem Cells and Bioprinting Technology-Barriers to Clinical Translation. *Front Surg*, 5, 70.
- FRANK, E. H., JIN, M., LOENING, A. M., LEVENSTON, M. E. & GRODZINSKY, A. J. 2000. A versatile shear and compression apparatus for mechanical stimulation of tissue culture explants. *J Biomech*, 33, 1523-7.
- FRANZ-ODENDAAL, T. A., HALL, B. K. & WITTEN, P. E. 2006. Buried alive: how osteoblasts become osteocytes. *Dev Dyn*, 235, 176-90.
- FRASER, J. R., LAURENT, T. C. & LAURENT, U. B. 1997. Hyaluronan: its nature, distribution, functions and turnover. *J Intern Med*, 242, 27-33.
- FRIESS, W. 1998. Collagen--biomaterial for drug delivery. *Eur J Pharm Biopharm*, 45, 113-36.
- FRITH, J. E., THOMSON, B. & GENEVER, P. G. 2010. Dynamic three-dimensional culture methods enhance mesenchymal stem cell properties and increase therapeutic potential. *Tissue Eng Part C Methods*, 16, 735-49.
- GARA, S. K., GRUMATI, P., URCIUOLO, A., BONALDO, P., KOBBE, B., KOCH, M., PAULSSON, M. & WAGENER, R. 2008. Three novel collagen VI chains with high homology to the alpha3 chain. *J Biol Chem*, 283, 10658-70.
- GARCIA, A. G., LABRO, M. B., FARHAT, F., PEROT, J. B., DERMIGNY, Q., DUFRESNE, M., GROSSET, J. F., BEDOUI, F. & LEGALLAIS, C. 2018. Multi-scale approach to reconstruct a bioartificial system of system: the example of the bone-tendon-muscle continuum. *2018 13th Annual Conference on System of Systems Engineering (Sose)*, 408-410.
- GARVIN, J., QI, J., MALONEY, M. & BANES, A. J. 2003. Novel system for engineering bioartificial tendons and application of mechanical load. *Tissue Eng*, 9, 967-79.
- GELSE, K., POSCHL, E. & AIGNER, T. 2003. Collagens--structure, function, and biosynthesis. *Adv Drug Deliv Rev*, 55, 1531-46.
- GERBER, H. P., VU, T. H., RYAN, A. M., KOWALSKI, J., WERB, Z. & FERRARA, N. 1999. VEGF couples hypertrophic cartilage remodeling, ossification and angiogenesis during endochondral bone formation. *Nat Med*, 5, 623-8.
- GHARRAVI, A. M., ORAZIZADEH, M., ANSARI-ASL, K., BANONI, S., IZADI, S. & HASHEMITABAR, M. 2012. Design and fabrication of anatomical bioreactor systems containing alginate scaffolds for cartilage tissue engineering. *Avicenna J Med Biotechnol*, 4, 65-74.
- GHARRAVI, A. M., ORAZIZADEH, M. & HASHEMITABAR, M. 2016. Fluid-induced low shear stress improves cartilage like tissue fabrication by encapsulating chondrocytes. *Cell Tissue Bank*, 17, 117-22.
- GIANCOTTI, F. G. & RUOSLAHTI, E. 1999. Integrin signaling. *Science*, 285, 1028-32.
- GIULIANI, N., LISIGNOLI, G., MAGNANI, M., RACANO, C., BOLZONI, M., DALLA PALMA, B., SPOLZINO, A., MANFERDINI, C., ABATI, C., TOSCANI, D., FACCHINI, A. & AVERSA, F. 2013. New insights into osteogenic and chondrogenic differentiation of human bone marrow mesenchymal stem cells and

References

- their potential clinical applications for bone regeneration in pediatric orthopaedics. *Stem Cells Int*, 2013, 312501.
- GLASS, Z. A., SCHIELE, N. R. & KUO, C. K. 2014. Informing tendon tissue engineering with embryonic development. *J Biomech*, 47, 1964-8.
- GLICK, B. S. & NAKANO, A. 2009. Membrane traffic within the Golgi apparatus. *Annu Rev Cell Dev Biol*, 25, 113-32.
- GLIMCHER, M. J. 1989. Mechanism of calcification: role of collagen fibrils and collagen-phosphoprotein complexes in vitro and in vivo. *Anat Rec*, 224, 139-53.
- GOH, K. L., HOLMES, D. F., LU, Y., PURSLOW, P. P., KADLER, K. E., BECHET, D. & WESS, T. J. 2012. Bimodal collagen fibril diameter distributions direct age-related variations in tendon resilience and resistance to rupture. *J Appl Physiol (1985)*, 113, 878-88.
- GOLDRING, S. R. 2015. The osteocyte: key player in regulating bone turnover. *RMD Open*, 1, e000049.
- GOLDSTEIN, A. S., JUAREZ, T. M., HELMKE, C. D., GUSTIN, M. C. & MIKOS, A. G. 2001. Effect of convection on osteoblastic cell growth and function in biodegradable polymer foam scaffolds. *Biomaterials*, 22, 1279-88.
- GOMES, M. E., REIS, R. L. & RODRIGUES, M. T. 2015. *Tendon regeneration: understanding tissue physiology and development to engineer functional substitutes*, Academic Press.
- GOMES, M. E., SIKAVITSAS, V. I., BEHRAVESH, E., REIS, R. L. & MIKOS, A. G. 2003. Effect of flow perfusion on the osteogenic differentiation of bone marrow stromal cells cultured on starch-based three-dimensional scaffolds. *J Biomed Mater Res A*, 67, 87-95.
- GONCALVES, T. J. M., BOUTILLON, F., LEFEBVRE, S., GOFFIN, V., IWATSUBO, T., WAKABAYASHI, T., OURY, F. & ARMAND, A. S. 2019. Collagen XXV promotes myoblast fusion during myogenic differentiation and muscle formation. *Sci Rep*, 9, 5878.
- GONCALVES-NETO, J., WITZEL, S. S., TEODORO, W. R., CARVALHO-JUNIOR, A. E., FERNANDES, T. D. & YOSHINARI, H. H. 2002. Changes in collagen matrix composition in human posterior tibial tendon dysfunction. *Joint Bone Spine*, 69, 189-94.
- GONZALEZ DE TORRE, I., WEBER, M., QUINTANILLA, L., ALONSO, M., JOCKENHOEVEL, S., RODRIGUEZ CABELLO, J. C. & MELA, P. 2016. Hybrid elastin-like recombinamer-fibrin gels: physical characterization and in vitro evaluation for cardiovascular tissue engineering applications. *Biomater Sci*, 4, 1361-70.
- GOOCH, K. J., BLUNK, T., COURTER, D. L., SIEMINSKI, A. L., VUNJAK-NOVAKOVIC, G. & FREED, L. E. 2002. Bone morphogenetic proteins-2, -12, and -13 modulate in vitro development of engineered cartilage. *Tissue Eng*, 8, 591-601.
- GORDON, M. K., FOLEY, J. W., LIENMAYER, T. F. & FITCH, J. M. 1996. Temporal expression of types XII and XIV collagen mRNA and protein during avian corneal development. *Dev Dyn*, 206, 49-58.
- GORDON, M. K. & HAHN, R. A. 2010. Collagens. *Cell Tissue Res*, 339, 247-57.
- GORDON, M. Y. 1988. Extracellular matrix of the marrow microenvironment. *Br J Haematol*, 70, 1-4.
- GRÄSSEL, S. & ASZÓDI, A. 2016. Collagens in Hyaline Cartilage. *Cartilage*. Springer, Cham.
- GRAYSON, W. L., BHUMIRATANA, S., CANNIZZARO, C. & VUNJAK-NOVAKOVIC, G. 2011. Bioreactor cultivation of functional bone grafts. *Methods Mol Biol*, 698, 231-41.
- GREEN, W. T., JR. 1977. Articular cartilage repair. Behavior of rabbit chondrocytes during tissue culture and subsequent allografting. *Clin Orthop Relat Res*, 237-50.
- GREGORY, K. E., KEENE, D. R., TUFA, S. F., LUNSTRUM, G. P. & MORRIS, N. P. 2001. Developmental distribution of collagen type XII in cartilage: association with articular cartilage and the growth plate. *J Bone Miner Res*, 16, 2005-16.
- GRIER, W. G., MOY, A. S. & HARLEY, B. A. 2017. Cyclic tensile strain enhances human mesenchymal stem cell Smad 2/3 activation and tenogenic differentiation in anisotropic collagen-glycosaminoglycan scaffolds. *Eur Cell Mater*, 33, 227-239.
- GRIER, W. K., SUN HAN CHANG, R. A., RAMSEY, M. D. & HARLEY, B. A. C. 2019. The influence of cyclic tensile strain on multi-compartment collagen-GAG scaffolds for tendon-bone junction repair. *Connect Tissue Res*, 60, 530-543.
- GRIGORIEV, A. I., OGANOV, V. S., BAKULIN, A. V., POLIAKOV, V. V., VORONIN, L. I., MORGUN, V. V., SHNAIDER, V. S., MURASHKO, L. V., NOVIKOV, V. E., LEBLANK, A. & SHAKLEFORD, L. 1998. [Clinical and physiological evaluation of bone changes among astronauts after long-term space flights]. *Aviakosm Ekolog Med*, 32, 21-5.
- GRIMM, D., EGLI, M., KRUGER, M., RIWALDT, S., CORYDON, T. J., KOPP, S., WEHLAND, M., WISE, P., INFANGER, M., MANN, V. & SUNDARESAN, A. 2018. Tissue Engineering Under Microgravity Conditions-Use of Stem Cells and Specialized Cells. *Stem Cells Dev*, 27, 787-804.
- GROSSE, J., WEHLAND, M., PIETSCH, J., MA, X., ULBRICH, C., SCHULZ, H., SAAR, K., HUBNER, N., HAUSLAGE, J., HEMMERSBACH, R., BRAUN, M., VAN LOON, J., VAGT, N., INFANGER, M., EILLES, C., EGLI, M., RICHTER, P., BALTZ, T., EINSPANIER, R., SHARBATI, S. & GRIMM, D. 2012. Short-term weightlessness produced by parabolic flight maneuvers altered gene expression patterns in human endothelial cells. *FASEB J*, 26, 639-55.

References

- GUILAK, F., ALEXOPOULOS, L. G., UPTON, M. L., YOUN, I., CHOI, J. B., CAO, L., SETTON, L. A. & HAIDER, M. A. 2006. The pericellular matrix as a transducer of biomechanical and biochemical signals in articular cartilage. *Ann N Y Acad Sci*, 1068, 498-512.
- GUO, Y., SIRKIS, D. W. & SCHEKMAN, R. 2014. Protein sorting at the trans-Golgi network. *Annu Rev Cell Dev Biol*, 30, 169-206.
- GURKAN, U. A. & AKKUS, O. 2008. The mechanical environment of bone marrow: a review. *Ann Biomed Eng*, 36, 1978-91.
- HAGERTY, P., LEE, A., CALVE, S., LEE, C. A., VIDAL, M. & BAAR, K. 2012. The effect of growth factors on both collagen synthesis and tensile strength of engineered human ligaments. *Biomaterials*, 33, 6355-61.
- HAGG, P., REHN, M., HUHTALA, P., VAISANEN, T., TAMMINEN, M. & PIHLAJANIEMI, T. 1998a. Type XIII collagen is identified as a plasma membrane protein. *J Biol Chem*, 273, 15590-7.
- HAGG, P. M., HAGG, P. O., PELTONEN, S., AUTIO-HARMAINEN, H. & PIHLAJANIEMI, T. 1997. Location of type XV collagen in human tissues and its accumulation in the interstitial matrix of the fibrotic kidney. *Am J Pathol*, 150, 2075-86.
- HAGG, R., BRUCKNER, P. & HEDBOM, E. 1998b. Cartilage fibrils of mammals are biochemically heterogeneous: differential distribution of decorin and collagen IX. *J Cell Biol*, 142, 285-94.
- HAGLUND, L., TILGREN, V., ONNERFJORD, P. & HEINEGARD, D. 2013. The C-terminal peptide of chondroadherin modulates cellular activity by selectively binding to heparan sulfate chains. *J Biol Chem*, 288, 995-1008.
- HAGMANN, S., MORADI, B., FRANK, S., DREHER, T., KAMMERER, P. W., RICHTER, W. & GOTTERBARM, T. 2013. FGF-2 addition during expansion of human bone marrow-derived stromal cells alters MSC surface marker distribution and chondrogenic differentiation potential. *Cell Prolif*, 46, 396-407.
- HAKIM, F. T., CRANLEY, R., BROWN, K. S., EANES, E. D., HARNE, L. & OPPENHEIM, J. J. 1984. Hereditary joint disorder in progressive ankylosis (ank/ank) mice. I. Association of calcium hydroxyapatite deposition with inflammatory arthropathy. *Arthritis Rheum*, 27, 1411-20.
- HALL, A. C. 1999. Differential effects of hydrostatic pressure on cation transport pathways of isolated articular chondrocytes. *J Cell Physiol*, 178, 197-204.
- HALL, A. C., HORWITZ, E. R. & WILKINS, R. J. 1996. The cellular physiology of articular cartilage. *Exp Physiol*, 81, 535-45.
- HALL, S. 1997. Axonal regeneration through acellular muscle grafts. *J Anat*, 190 (Pt 1), 57-71.
- HALL, S., PENEGELLY, I., STAFF, J., PLANT, N. & EVANS, G. 2018. Measuring and Controlling Emissions from Polymer Filament Desktop 3D Printers. In: EXECUTIVE, H. A. S. (ed.). Research Reports.
- HAMILTON, R. & CAMPBELL, F. R. 1991. Immunohistochemical localization of extracellular materials in bone marrow of rats. *Anat Rec*, 231, 218-24.
- HAMMER, B. E., KIDDER, L. S., WILLIAMS, P. C. & XU, W. W. 2009. Magnetic Levitation of MC3T3 Osteoblast Cells as a Ground-Based Simulation of Microgravity. *Microgravity Sci Technol*, 21, 311-318.
- HAN, D. S., CHANG, H. K., KIM, K. R. & WOO, S. M. 2014. Consideration of bone regeneration effect of stem cells: comparison of bone regeneration between bone marrow stem cells and adipose-derived stem cells. *J Craniofac Surg*, 25, 196-201.
- HAN, Y., YOU, X., XING, W., ZHANG, Z. & ZOU, W. 2018. Paracrine and endocrine actions of bone-the functions of secretory proteins from osteoblasts, osteocytes, and osteoclasts. *Bone Res*, 6, 16.
- HANGODY, L., RATHONYI, G. K., DUSKA, Z., VASARHELYI, G., FULES, P. & MODIS, L. 2004. Autologous osteochondral mosaicplasty. Surgical technique. *J Bone Joint Surg Am*, 86-A Suppl 1, 65-72.
- HANKENSON, K. D., BAIN, S. D., KYRIAKIDES, T. R., SMITH, E. A., GOLDSTEIN, S. A. & BORNSTEIN, P. 2000. Increased marrow-derived osteoprogenitor cells and endosteal bone formation in mice lacking thrombospondin 2. *J Bone Miner Res*, 15, 851-62.
- HANSEN, N., GUDMANN, N. & KARSDAL, M. 2019. Type VIII collagen. *Biochemistry of Collagens, Laminins and Elastin*. Elsevier.
- HANSMA, P. K., TURNER, P. J. & RUOFF, R. S. 2006. Optimized adhesives for strong, lightweight, damage-resistant, nanocomposite materials: new insights from natural materials. *Nanotechnology*, 18.
- HANSON, A. D., MARVEL, S. W., BERNACKI, S. H., BANES, A. J., VAN AALST, J. & LOBOA, E. G. 2009. Osteogenic effects of rest inserted and continuous cyclic tensile strain on hASC lines with disparate osteodifferentiation capabilities. *Ann Biomed Eng*, 37, 955-65.
- HARDINGHAM, T. 2010. Cell- and tissue-based approaches for cartilage repair. *Altern Lab Anim*, 38 Suppl 1, 35-9.
- HARDINGHAM, T. E. 1979. The role of link-protein in the structure of cartilage proteoglycan aggregates. *Biochem J*, 177, 237-47.
- HARTIGAN, N., GARRIGUE-ANTAR, L. & KADLER, K. E. 2003. Bone morphogenetic protein-1 (BMP-1). Identification of the minimal domain structure for procollagen C-proteinase activity. *J Biol Chem*, 278, 18045-9.
- HASHIMOTO, T., WAKABAYASHI, T., WATANABE, A., KOWA, H., HOSODA, R., NAKAMURA, A., KANAZAWA, I., ARAI, T., TAKIO, K., MANN, D. M. & IWATSUBO, T. 2002. CLAC: a novel Alzheimer amyloid plaque

References

- component derived from a transmembrane precursor, CLAC-P/collagen type XXV. *EMBO J*, 21, 1524-34.
- HATTORI, T., MULLER, C., GEBHARD, S., BAUER, E., PAUSCH, F., SCHLUND, B., BOSL, M. R., HESS, A., SURMANN-SCHMITT, C., VON DER MARK, H., DE CROMBRUGGHE, B. & VON DER MARK, K. 2010. SOX9 is a major negative regulator of cartilage vascularization, bone marrow formation and endochondral ossification. *Development*, 137, 901-11.
- HEARD, M. E., BESIO, R., WEIS, M., RAI, J., HUDSON, D. M., DIMORI, M., ZIMMERMAN, S. M., KAMYKOWSKI, J. A., HOGUE, W. R., SWAIN, F. L., BURDINE, M. S., MACKINTOSH, S. G., TACKETT, A. J., SUVA, L. J., EYRE, D. R. & MORELLO, R. 2016. Sc65-Null Mice Provide Evidence for a Novel Endoplasmic Reticulum Complex Regulating Collagen Lysyl Hydroxylation. *PLoS Genet*, 12, e1006002.
- HEATH, D. E. 2019. A review of decellularized extracellular matrix biomaterials for regenerative engineering applications. *Regenerative Engineering and Translational Medicine*, 5, 155-166.
- HEDBOM, E. & HEINEGARD, D. 1989. Interaction of a 59-kDa connective tissue matrix protein with collagen I and collagen II. *J Biol Chem*, 264, 6898-905.
- HEHER, P., MALEINER, B., PRULLER, J., TEUSCHL, A. H., KOLLMITZER, J., MONFORTE, X., WOLBANK, S., REDL, H., RUNZLER, D. & FUCHS, C. 2015. A novel bioreactor for the generation of highly aligned 3D skeletal muscle-like constructs through orientation of fibrin via application of static strain. *Acta Biomater*, 24, 251-65.
- HEHLGANS, S., HAASE, M. & CORDES, N. 2007. Signalling via integrins: implications for cell survival and anticancer strategies. *Biochim Biophys Acta*, 1775, 163-80.
- HENRY, S. P., TAKANOSU, M., BOYD, T. C., MAYNE, P. M., EBERSPAECHER, H., ZHOU, W., DE CROMBRUGGHE, B., HOOK, M. & MAYNE, R. 2001. Expression pattern and gene characterization of asporin, a newly discovered member of the leucine-rich repeat protein family. *J Biol Chem*, 276, 12212-21.
- HENSTOCK, J. R., ROTHERHAM, M., RASHIDI, H., SHAKESHEFF, K. M. & EL HAJ, A. J. 2014. Remotely Activated Mechanotransduction via Magnetic Nanoparticles Promotes Mineralization Synergistically With Bone Morphogenetic Protein 2: Applications for Injectable Cell Therapy. *Stem Cells Transl Med*, 3, 1363-74.
- HENSTOCK, J. R., ROTHERHAM, M., ROSE, J. B. & EL HAJ, A. J. 2013. Cyclic hydrostatic pressure stimulates enhanced bone development in the foetal chick femur in vitro. *Bone*, 53, 468-77.
- HESS, R., DOUGLAS, T., MYERS, K. A., RENTSCH, B., RENTSCH, C., WORCH, H., SHRIVE, N. G., HART, D. A. & SCHARNWEBER, D. 2010. Hydrostatic pressure stimulation of human mesenchymal stem cells seeded on collagen-based artificial extracellular matrices. *J Biomech Eng*, 132, 021001.
- HESSLE, L., JOHNSON, K. A., ANDERSON, H. C., NARISAWA, S., SALI, A., GODING, J. W., TERKELTAUB, R. & MILLAN, J. L. 2002. Tissue-nonspecific alkaline phosphatase and plasma cell membrane glycoprotein-1 are central antagonistic regulators of bone mineralization. *Proc Natl Acad Sci U S A*, 99, 9445-9.
- HILL, T. P., TAKETO, M. M., BIRCHMEIER, W. & HARTMANN, C. 2006. Multiple roles of mesenchymal beta-catenin during murine limb patterning. *Development*, 133, 1219-29.
- HODGE, A. J. & SCHMITT, F. O. 1960. The Charge Profile of the Tropocollagen Macromolecule and the Packing Arrangement in Native-Type Collagen Fibrils. *Proc Natl Acad Sci U S A*, 46, 186-97.
- HOFFMAN, G. G., BRANAM, A. M., HUANG, G., PELEGRI, F., COLE, W. G., WENSTRUP, R. M. & GREENSPAN, D. S. 2010. Characterization of the six zebrafish clade B fibrillar procollagen genes, with evidence for evolutionarily conserved alternative splicing within the pro-alpha1(V) C-propeptide. *Matrix Biol*, 29, 261-75.
- HOLMGREN, S. K., BRETSCHER, L. E., TAYLOR, K. M. & RAINES, R. T. 1999. A hyperstable collagen mimic. *Chem Biol*, 6, 63-70.
- HOLTORF, H. L., DATTA, N., JANSEN, J. A. & MIKOS, A. G. 2005a. Scaffold mesh size affects the osteoblastic differentiation of seeded marrow stromal cells cultured in a flow perfusion bioreactor. *J Biomed Mater Res A*, 74, 171-80.
- HOLTORF, H. L., JANSEN, J. A. & MIKOS, A. G. 2005b. Flow perfusion culture induces the osteoblastic differentiation of marrow stroma cell-scaffold constructs in the absence of dexamethasone. *J Biomed Mater Res A*, 72, 326-34.
- HOLTROP, M. E. & KING, G. J. 1977. The ultrastructure of the osteoclast and its functional implications. *Clin Orthop Relat Res*, 177-96.
- HONG, J. H., HWANG, E. S., MCMANUS, M. T., AMSTERDAM, A., TIAN, Y., KALMUKOVA, R., MUELLER, E., BENJAMIN, T., SPIEGELMAN, B. M., SHARP, P. A., HOPKINS, N. & YAFFE, M. B. 2005. TAZ, a transcriptional modulator of mesenchymal stem cell differentiation. *Science*, 309, 1074-8.
- HOPKINS, D. R., KELES, S. & GREENSPAN, D. S. 2007. The bone morphogenetic protein 1/Tolloid-like metalloproteinases. *Matrix Biol*, 26, 508-23.
- HOPKINSON, S. B., FINDLAY, K., DEHART, G. W. & JONES, J. C. 1998. Interaction of BP180 (type XVII collagen) and alpha6 integrin is necessary for stabilization of hemidesmosome structure. *J Invest Dermatol*, 111, 1015-22.
- HOSON, T., KAMISAKA, S., MASUDA, Y., YAMASHITA, M. & BUCHEN, B. 1997. Evaluation of the three-dimensional clinostat as a simulator of weightlessness. *Planta*, 203 Suppl, S187-97.

References

- HOSPODIUK, M., DEY, M., SOSNOSKI, D. & OZBOLAT, I. T. 2017. The bioink: A comprehensive review on bioprintable materials. *Biotechnol Adv*, 35, 217-239.
- HOWELL, S. J. & DOANE, K. J. 1998. Type VI collagen increases cell survival and prevents anti-beta 1 integrin-mediated apoptosis. *Exp Cell Res*, 241, 230-41.
- HSIAO, M. Y., LIN, P. C., LIAO, W. H., CHEN, W. S., HSU, C. H., HE, C. K., WU, Y. W., GEFEN, A., IAFISCO, M., LIU, L. & LIN, F. H. 2019. The Effect of the Repression of Oxidative Stress on Tenocyte Differentiation: A Preliminary Study of a Rat Cell Model Using a Novel Differential Tensile Strain Bioreactor. *Int J Mol Sci*, 20.
- HUANG, C. & OGAWA, R. 2012. Effect of hydrostatic pressure on bone regeneration using human mesenchymal stem cells. *Tissue Eng Part A*, 18, 2106-13.
- HUANG, P., RUSSELL, A. L., LEFAVOR, R., DURAND, N. C., JAMES, E., HARVEY, L., ZHANG, C., COUNTRYMAN, S., STODIECK, L. & ZUBAIR, A. C. 2020. Feasibility, potency, and safety of growing human mesenchymal stem cells in space for clinical application. *NPJ Microgravity*, 6, 16.
- HUANG, W., YANG, S., SHAO, J. & LI, Y. P. 2007. Signaling and transcriptional regulation in osteoblast commitment and differentiation. *Front Biosci*, 12, 3068-92.
- HULMES, D. 2008. Collagen diversity, synthesis and assembly. *Collagen*. Springer.
- HULMES, D. J., KADLER, K. E., MOULD, A. P., HOJIMA, Y., HOLMES, D. F., CUMMINGS, C., CHAPMAN, J. A. & PROCKOP, D. J. 1989. Pleomorphism in type I collagen fibrils produced by persistence of the procollagen N-propeptide. *J Mol Biol*, 210, 337-45.
- INADA, M., WANG, Y., BYRNE, M. H., RAHMAN, M. U., MIYAURA, C., LOPEZ-OTIN, C. & KRANE, S. M. 2004. Critical roles for collagenase-3 (Mmp13) in development of growth plate cartilage and in endochondral ossification. *Proc Natl Acad Sci U S A*, 101, 17192-7.
- INGRAM, J. H., KOROSSIS, S., HOWLING, G., FISHER, J. & INGHAM, E. 2007. The use of ultrasonication to aid recellularization of acellular natural tissue scaffolds for use in anterior cruciate ligament reconstruction. *Tissue Eng*, 13, 1561-72.
- INOUE, K., SAKAKIBARA, S. & PROCKOP, D. J. 1976. Effects of the stereo-configuration of the hydroxyl group in 4-hydroxyproline on the triple-helical structures formed by homogenous peptides resembling collagen. *Biochim Biophys Acta*, 420, 133-41.
- INSOGNA, K. L., SAHNI, M., GREY, A. B., TANAKA, S., HORNE, W. C., NEFF, L., MITNICK, M., LEVY, J. B. & BARON, R. 1997. Colony-stimulating factor-1 induces cytoskeletal reorganization and c-src-dependent tyrosine phosphorylation of selected cellular proteins in rodent osteoclasts. *J Clin Invest*, 100, 2476-85.
- IOZZO, R. V. & SCHAEFER, L. 2015. Proteoglycan form and function: A comprehensive nomenclature of proteoglycans. *Matrix Biol*, 42, 11-55.
- ISHIKAWA, Y. & BACHINGER, H. P. 2013. A molecular ensemble in the rER for procollagen maturation. *Biochim Biophys Acta*, 1833, 2479-91.
- ITO, S. & NAGATA, K. 2017. Biology of Hsp47 (Serp1H1), a collagen-specific molecular chaperone. *Semin Cell Dev Biol*, 62, 142-151.
- IZU, Y., EZURA, Y., KOCH, M., BIRK, D. E. & NODA, M. 2016. Collagens VI and XII form complexes mediating osteoblast interactions during osteogenesis. *Cell Tissue Res*, 364, 623-635.
- IZU, Y., EZURA, Y., MIZOGUCHI, F., KAWAMATA, A., NAKAMOTO, T., NAKASHIMA, K., HAYATA, T., HEMMI, H., BONALDO, P. & NODA, M. 2012. Type VI collagen deficiency induces osteopenia with distortion of osteoblastic cell morphology. *Tissue Cell*, 44, 1-6.
- JAGODZINSKI, M., DRESCHER, M., ZEICHEN, J., HANKEMEIER, S., KRETTEK, C., BOSCH, U. & VAN GRIENSVEN, M. 2004. Effects of cyclic longitudinal mechanical strain and dexamethasone on osteogenic differentiation of human bone marrow stromal cells. *Eur Cell Mater*, 7, 35-41; discussion 41.
- JAHANGIR, S., EGLIN, D., POTTER, N., KHOZAEI RAVARI, M., STODDART, M. J., SAMADIKUCHAKSARAEI, A., ALINI, M., BAGHABAN ESLAMINEJAD, M. & SAFA, M. 2020. Inhibition of hypertrophy and improving chondrocyte differentiation by MMP-13 inhibitor small molecule encapsulated in alginate-chondroitin sulfate-platelet lysate hydrogel. *Stem Cell Res Ther*, 11, 436.
- JAISWAL, N., HAYNESWORTH, S. E., CAPLAN, A. I. & BRUDER, S. P. 1997. Osteogenic differentiation of purified, culture-expanded human mesenchymal stem cells in vitro. *J Cell Biochem*, 64, 295-312.
- JANG, J. Y., LEE, S. W., PARK, S. H., SHIN, J. W., MUN, C., KIM, S. H., KIM, D. H. & SHIN, J. W. 2011. Combined effects of surface morphology and mechanical straining magnitudes on the differentiation of mesenchymal stem cells without using biochemical reagents. *J Biomed Biotechnol*, 2011, 860652.
- JANG, Y., KOH, Y. G., CHOI, Y. J., KIM, S. H., YOON, D. S., LEE, M. & LEE, J. W. 2015. Characterization of adipose tissue-derived stromal vascular fraction for clinical application to cartilage regeneration. *In Vitro Cell Dev Biol Anim*, 51, 142-50.
- JANVIER, A. J., CANTY-LAIRD, E. G. & HENSTOCK, J. R. 2020. A universal multi-platform 3D printed bioreactor chamber for tendon tissue engineering. *Journal of Tissue Engineering*, 11, 1-15.
- JELINSKY, S. A., ARCHAMBAULT, J., LI, L. & SEEHERMAN, H. 2010. Tendon-selective genes identified from rat and human musculoskeletal tissues. *J Orthop Res*, 28, 289-97.
- JETT, S. V., HUDSON, L. T., BAUMWART, R., BOHNSTEDT, B. N., MIR, A., BURKHART, H. M., HOLZAPFEL, G. A., WU, Y. & LEE, C. H. 2020. Integration of polarized spatial frequency domain imaging (pSFDI) with a

References

- biaxial mechanical testing system for quantification of load-dependent collagen architecture in soft collagenous tissues. *Acta Biomater*, 102, 149-168.
- JIANG, Y., JAHAGIRDAR, B. N., REINHARDT, R. L., SCHWARTZ, R. E., KEENE, C. D., ORTIZ-GONZALEZ, X. R., REYES, M., LENVIK, T., LUND, T., BLACKSTAD, M., DU, J., ALDRICH, S., LISBERG, A., LOW, W. C., LARGAESPADA, D. A. & VERFAILLIE, C. M. 2002. Pluripotency of mesenchymal stem cells derived from adult marrow. *Nature*, 418, 41-9.
- JILKA, R. L., WEINSTEIN, R. S., BELLIDO, T., PARFITT, A. M. & MANOLAGAS, S. C. 1998. Osteoblast programmed cell death (apoptosis): modulation by growth factors and cytokines. *J Bone Miner Res*, 13, 793-802.
- JIN, M., EMKEY, G. R., SIPARSKY, P., TRIPPEL, S. B. & GRODZINSKY, A. J. 2003. Combined effects of dynamic tissue shear deformation and insulin-like growth factor I on chondrocyte biosynthesis in cartilage explants. *Arch Biochem Biophys*, 414, 223-31.
- JIN, M., FRANK, E. H., QUINN, T. M., HUNZIKER, E. B. & GRODZINSKY, A. J. 2001. Tissue shear deformation stimulates proteoglycan and protein biosynthesis in bovine cartilage explants. *Arch Biochem Biophys*, 395, 41-8.
- JOHNSON, K. A., HESSLE, L., VAINGANKAR, S., WENNBERG, C., MAURO, S., NARISAWA, S., GODING, J. W., SANO, K., MILLAN, J. L. & TERKELTAUB, R. 2000. Osteoblast tissue-nonspecific alkaline phosphatase antagonizes and regulates PC-1. *Am J Physiol Regul Integr Comp Physiol*, 279, R1365-77.
- JOHNSTONE, B., HERING, T. M., CAPLAN, A. I., GOLDBERG, V. M. & YOO, J. U. 1998. In vitro chondrogenesis of bone marrow-derived mesenchymal progenitor cells. *Exp Cell Res*, 238, 265-72.
- JOHNSTONE, I. L. 2000. Cuticle collagen genes. Expression in *Caenorhabditis elegans*. *Trends Genet*, 16, 21-7.
- JONES, S. W., JANVIER, A. J., SHIGDAR, S. M., HENSTOCK, J. R., MCARDLE, C., HOETTGES, K., MCARDLE, A. & JACKSON, M. J. 2020. Development of Functional, Contractile 3-D Human Muscle Constructs for Studies of the Effects of Microgravity on Muscle Mass and Function. *The FASEB Journal*, 34, 1-1.
- JOSHI, S. D. & WEBB, K. 2008. Variation of cyclic strain parameters regulates development of elastic modulus in fibroblast/substrate constructs. *J Orthop Res*, 26, 1105-13.
- JUHAS, M. & BURSAC, N. 2014. Roles of adherent myogenic cells and dynamic culture in engineered muscle function and maintenance of satellite cells. *Biomaterials*, 35, 9438-46.
- JULIN, J., JAMSEN, E., PUOLAKKA, T., KONTTINEN, Y. T. & MOILANEN, T. 2010. Younger age increases the risk of early prosthesis failure following primary total knee replacement for osteoarthritis. A follow-up study of 32,019 total knee replacements in the Finnish Arthroplasty Register. *Acta Orthop*, 81, 413-9.
- JUNCOSA-MELVIN, N., MATLIN, K. S., HOLDCRAFT, R. W., NIRMALANANDHAN, V. S. & BUTLER, D. L. 2007. Mechanical stimulation increases collagen type I and collagen type III gene expression of stem cell-collagen sponge constructs for patellar tendon repair. *Tissue Eng*, 13, 1219-26.
- JUNCOSA-MELVIN, N., SHEARN, J. T., BOIVIN, G. P., GOOCH, C., GALLOWAY, M. T., WEST, J. R., NIRMALANANDHAN, V. S., BRADICA, G. & BUTLER, D. L. 2006. Effects of mechanical stimulation on the biomechanics and histology of stem cell-collagen sponge constructs for rabbit patellar tendon repair. *Tissue Eng*, 12, 2291-300.
- KADLER, K. E., BALDOCK, C., BELLA, J. & BOOT-HANDFORD, R. P. 2007. Collagens at a glance. *J Cell Sci*, 120, 1955-8.
- KADLER, K. E., HILL, A. & CANTY-LAIRD, E. G. 2008. Collagen fibrillogenesis: fibronectin, integrins, and minor collagens as organizers and nucleators. *Curr Opin Cell Biol*, 20, 495-501.
- KADLER, K. E., HOJIMA, Y. & PROCKOP, D. J. 1987. Assembly of collagen fibrils de novo by cleavage of the type I pC-collagen with procollagen C-proteinase. Assay of critical concentration demonstrates that collagen self-assembly is a classical example of an entropy-driven process. *J Biol Chem*, 262, 15696-701.
- KADLER, K. E., HOJIMA, Y. & PROCKOP, D. J. 1990. Collagen fibrils in vitro grow from pointed tips in the C- to N-terminal direction. *Biochem J*, 268, 339-43.
- KADLER, K. E., HOLMES, D. F., TROTTER, J. A. & CHAPMAN, J. A. 1996. Collagen fibril formation. *Biochem J*, 316 (Pt 1), 1-11.
- KAIPATUR, N. R., MURSHED, M. & MCKEE, M. D. 2008. Matrix Gla protein inhibition of tooth mineralization. *J Dent Res*, 87, 839-44.
- KALAMAJSKI, S., ASPBERG, A., LINDBLOM, K., HEINEGARD, D. & OLDBERG, A. 2009. Asporin competes with decorin for collagen binding, binds calcium and promotes osteoblast collagen mineralization. *Biochem J*, 423, 53-9.
- KALSON, N. S., HOLMES, D. F., HERCHENHAN, A., LU, Y., STARBORG, T. & KADLER, K. E. 2011. Slow stretching that mimics embryonic growth rate stimulates structural and mechanical development of tendon-like tissue in vitro. *Dev Dyn*, 240, 2520-8.
- KANAFI, M. M., RAMESH, A., GUPTA, P. K. & BHONDE, R. R. 2014. Dental pulp stem cells immobilized in alginate microspheres for applications in bone tissue engineering. *Int Endod J*, 47, 687-97.
- KANAUJIYA, J., BASTOW, E., LUXMI, R., HAO, Z., ZATTAS, D., HOCHSTRASSER, M., REICHENBERGER, E. J. & CHEN, I. P. 2018. Rapid degradation of progressive ankylosis protein (ANKH) in craniometaphyseal dysplasia. *Sci Rep*, 8, 15710.
- KANNUS, P. 2000. Structure of the tendon connective tissue. *Scand J Med Sci Sports*, 10, 312-20.

References

- KAPOOR, R., BORNSTEIN, P. & SAGE, E. H. 1986. Type VIII collagen from bovine Descemet's membrane: structural characterization of a triple-helical domain. *Biochemistry*, 25, 3930-7.
- KAPOOR, R., SAKAI, L. Y., FUNK, S., ROUX, E., BORNSTEIN, P. & SAGE, E. H. 1988. Type VIII collagen has a restricted distribution in specialized extracellular matrices. *J Cell Biol*, 107, 721-30.
- KAPS, C., BRAMLAGE, C., SMOLIAN, H., HAISCH, A., UNGETHUM, U., BURMESTER, G. R., SITTINGER, M., GROSS, G. & HAUPL, T. 2002. Bone morphogenetic proteins promote cartilage differentiation and protect engineered artificial cartilage from fibroblast invasion and destruction. *Arthritis Rheum*, 46, 149-62.
- KARAGLANI, M., TOUMPOULIS, I., GOUTAS, N., POUIMPOURIDOU, N., VLACHODIMITROPOULOS, D., VASILAROS, S., RIZOS, I. & KROUPIS, C. 2015. Development of novel real-time PCR methodology for quantification of COL11A1 mRNA variants and evaluation in breast cancer tissue specimens. *BMC Cancer*, 15, 694.
- KARAMUK, E., MAYER, J. & RAEBER, G. 2004. Tissue engineered composite of a woven fabric scaffold with tendon cells, response on mechanical simulation in vitro. *Composites science and technology*, 64, 885-891.
- KARSDAL, M. 2019. *Biochemistry of collagens, laminins and elastin: structure, function and biomarkers*, Academic Press.
- KARSDAL, M. A., NIELSEN, S. H., LEEMING, D. J., LANGHOLM, L. L., NIELSEN, M. J., MANON-JENSEN, T., SIEBUHR, A., GUDMANN, N. S., RONNOW, S., SAND, J. M., DANIELS, S. J., MORTENSEN, J. H. & SCHUPPAN, D. 2017. The good and the bad collagens of fibrosis - Their role in signaling and organ function. *Adv Drug Deliv Rev*, 121, 43-56.
- KARYSTINO, A., ROELOFS, A. J., NEVE, A., CANTATORE, F. P., WACKERHAGE, H. & DE BARI, C. 2015. Yes-associated protein (YAP) is a negative regulator of chondrogenesis in mesenchymal stem cells. *Arthritis Res Ther*, 17, 147.
- KASSNER, A., HANSEN, U., MIOGGE, N., REINHARDT, D. P., AIGNER, T., BRUCKNER-TUDERMAN, L., BRUCKNER, P. & GRASSEL, S. 2003. Discrete integration of collagen XVI into tissue-specific collagen fibrils or beaded microfibrils. *Matrix Biol*, 22, 131-43.
- KATTAMIS, N. T., PURNICK, P. E., WEISS, R. & ARNOLD, C. B. 2007. Thick film laser induced forward transfer for deposition of thermally and mechanically sensitive materials. *Applied Physics Letters*, 91, 171120.
- KAUX, J. F., FORTHOMME, B., GOFF, C. L., CRIELAARD, J. M. & CROISIER, J. L. 2011. Current opinions on tendinopathy. *J Sports Sci Med*, 10, 238-53.
- KAWANISHI, M., OURA, A., FURUKAWA, K., FUKUBAYASHI, T., NAKAMURA, K., TATEISHI, T. & USHIDA, T. 2007. Redifferentiation of dedifferentiated bovine articular chondrocytes enhanced by cyclic hydrostatic pressure under a gas-controlled system. *Tissue Eng*, 13, 957-64.
- KEANE, T. J., DEWARD, A., LONDONO, R., SALDIN, L. T., CASTLETON, A. A., CAREY, L., NIEPONICE, A., LAGASSE, E. & BADYLAK, S. F. 2015. Tissue-Specific Effects of Esophageal Extracellular Matrix. *Tissue Eng Part A*, 21, 2293-300.
- KEARNEY, E. M., PRENDERGAST, P. J. & CAMPBELL, V. A. 2008. Mechanisms of strain-mediated mesenchymal stem cell apoptosis. *J Biomech Eng*, 130, 061004.
- KEENE, D. R., ENGVALL, E. & GLANVILLE, R. W. 1988. Ultrastructure of type VI collagen in human skin and cartilage suggests an anchoring function for this filamentous network. *J Cell Biol*, 107, 1995-2006.
- KEENE, D. R., LUNSTRUM, G. P., MORRIS, N. P., STODDARD, D. W. & BURGESSON, R. E. 1991. Two type XII-like collagens localize to the surface of banded collagen fibrils. *J Cell Biol*, 113, 971-8.
- KEENE, D. R., SAKAI, L. Y., LUNSTRUM, G. P., MORRIS, N. P. & BURGESSON, R. E. 1987. Type VII collagen forms an extended network of anchoring fibrils. *J Cell Biol*, 104, 611-21.
- KELLY, B. E., BHATTACHARYA, I., HEIDARI, H., SHUSTEFF, M., SPADACCINI, C. M. & TAYLOR, H. K. 2019. Volumetric additive manufacturing via tomographic reconstruction. *Science*, 363, 1075-1079.
- KERSTEEN, E. A. & RAINES, R. T. 2001. Contribution of tertiary amides to the conformational stability of collagen triple helices. *Biopolymers*, 59, 24-8.
- KESSLER, E., TAKAHARA, K., BINIAMINOV, L., BRUSEL, M. & GREENSPAN, D. S. 1996. Bone morphogenetic protein-1: the type I procollagen C-proteinase. *Science*, 271, 360-2.
- KHARAZ, Y. A., TEW, S. R., PEFFERS, M., CANTY-LAIRD, E. G. & COMERFORD, E. 2016. Proteomic differences between native and tissue-engineered tendon and ligament. *Proteomics*, 16, 1547-56.
- KHODABUKUS, A., PRABHU, N., WANG, J. & BURSAC, N. 2018. In Vitro Tissue-Engineered Skeletal Muscle Models for Studying Muscle Physiology and Disease. *Adv Healthc Mater*, 7, e1701498.
- KHOSHNOODI, J., PEDCHENKO, V. & HUDSON, B. G. 2008. Mammalian collagen IV. *Microsc Res Tech*, 71, 357-70.
- KHUNMANEE, S., JEONG, Y. & PARK, H. 2017. Crosslinking method of hyaluronic-based hydrogel for biomedical applications. *J Tissue Eng*, 8, 2041731417726464.
- KHURANA, J. S. 2009. *Bone pathology*, Springer Science & Business Media.
- KIELTY, C. M., WHITTAKER, S. P., GRANT, M. E. & SHUTTLEWORTH, C. A. 1992. Type VI collagen microfibrils: evidence for a structural association with hyaluronan. *J Cell Biol*, 118, 979-90.
- KIENZLE, C. & VON BLUME, J. 2014. Secretory cargo sorting at the trans-Golgi network. *Trends Cell Biol*, 24, 584-93.

References

- KIM, S. J., SHIN, Y. W., YANG, K. H., KIM, S. B., YOO, M. J., HAN, S. K., IM, S. A., WON, Y. D., SUNG, Y. B., JEON, T. S., CHANG, C. H., JANG, J. D., LEE, S. B., KIM, H. C. & LEE, S. Y. 2009. A multi-center, randomized, clinical study to compare the effect and safety of autologous cultured osteoblast(Ossron) injection to treat fractures. *BMC Musculoskelet Disord*, 10, 20.
- KIM, Y. & KUMAR, S. 2014. CD44-mediated adhesion to hyaluronic acid contributes to mechanosensing and invasive motility. *Mol Cancer Res*, 12, 1416-29.
- KINDBLOM, J. M., NILSSON, O., HURME, T., OHLSSON, C. & SAVENDAHL, L. 2002. Expression and localization of Indian hedgehog (Ihh) and parathyroid hormone related protein (PTHrP) in the human growth plate during pubertal development. *J Endocrinol*, 174, R1-6.
- KIRTON, J. P., CROFTS, N. J., GEORGE, S. J., BRENNAN, K. & CANFIELD, A. E. 2007. Wnt/beta-catenin signaling stimulates chondrogenic and inhibits adipogenic differentiation of pericytes: potential relevance to vascular disease? *Circ Res*, 101, 581-9.
- KISHIMOTO, Y., OHKAWARA, B., SAKAI, T., ITO, M., MASUDA, A., ISHIGURO, N., SHUKUNAMI, C., DOCHEVA, D. & OHNO, K. 2017. Wnt/beta-catenin signaling suppresses expressions of Scx, Mlx, and Tnmd in tendon-derived cells. *PLoS One*, 12, e0182051.
- KJAER, M. 2004. Role of extracellular matrix in adaptation of tendon and skeletal muscle to mechanical loading. *Physiol Rev*, 84, 649-98.
- KNIGHT, R. L., WILCOX, H. E., KOROSSIS, S. A., FISHER, J. & INGHAM, E. 2008. The use of acellular matrices for the tissue engineering of cardiac valves. *Proc Inst Mech Eng H*, 222, 129-43.
- KNOTT, L. & BAILEY, A. J. 1998. Collagen cross-links in mineralizing tissues: a review of their chemistry, function, and clinical relevance. *Bone*, 22, 181-7.
- KNUPP, C., PINALI, C., MUNRO, P. M., GRUBER, H. E., SHERRATT, M. J., BALDOCK, C. & SQUIRE, J. M. 2006. Structural correlation between collagen VI microfibrils and collagen VI banded aggregates. *J Struct Biol*, 154, 312-26.
- KNUPP, C. & SQUIRE, J. M. 2003. Molecular packing in network-forming collagens. *ScientificWorldJournal*, 3, 558-77.
- KOCH, M., FOLEY, J. E., HAHN, R., ZHOU, P., BURGESSON, R. E., GERECKE, D. R. & GORDON, M. K. 2001. alpha 1(Xx) collagen, a new member of the collagen subfamily, fibril-associated collagens with interrupted triple helices. *J Biol Chem*, 276, 23120-6.
- KOCH, M., LAUB, F., ZHOU, P., HAHN, R. A., TANAKA, S., BURGESSON, R. E., GERECKE, D. R., RAMIREZ, F. & GORDON, M. K. 2003. Collagen XXIV, a vertebrate fibrillar collagen with structural features of invertebrate collagens: selective expression in developing cornea and bone. *J Biol Chem*, 278, 43236-44.
- KOCH, M., SCHULZE, J., HANSEN, U., ASHWODT, T., KEENE, D. R., BRUNKEN, W. J., BURGESSON, R. E., BRUCKNER, P. & BRUCKNER-TUDERMAN, L. 2004. A novel marker of tissue junctions, collagen XXII. *J Biol Chem*, 279, 22514-21.
- KOCH, M., VEIT, G., STRICKER, S., BHATT, P., KUTSCH, S., ZHOU, P., REINDERS, E., HAHN, R. A., SONG, R., BURGESSON, R. E., GERECKE, D. R., MUNDLOS, S. & GORDON, M. K. 2006. Expression of type XXIII collagen mRNA and protein. *J Biol Chem*, 281, 21546-57.
- KOHN, A. D. & MOON, R. T. 2005. Wnt and calcium signaling: beta-catenin-independent pathways. *Cell Calcium*, 38, 439-46.
- KOMORI, T. 2006. Regulation of osteoblast differentiation by transcription factors. *J Cell Biochem*, 99, 1233-9.
- KOMORI, T. 2010. Regulation of bone development and extracellular matrix protein genes by RUNX2. *Cell Tissue Res*, 339, 189-95.
- KONG, X. B., TANG, Q. Y., CHEN, X. Y., TU, Y., SUN, S. Z. & SUN, Z. L. 2017. Polyethylene glycol as a promising synthetic material for repair of spinal cord injury. *Neural Regen Res*, 12, 1003-1008.
- KORHONEN, R. K. & JURVELIN, J. S. 2010. Compressive and tensile properties of articular cartilage in axial loading are modulated differently by osmotic environment. *Med Eng Phys*, 32, 155-60.
- KOSTENUIK, P. & MIRZA, F. M. 2017. Fracture healing physiology and the quest for therapies for delayed healing and nonunion. *J Orthop Res*, 35, 213-223.
- KRAHN, K. N., BOUTEN, C. V., VAN TUIJL, S., VAN ZANDVOORT, M. A. & MERKX, M. 2006. Fluorescently labeled collagen binding proteins allow specific visualization of collagen in tissues and live cell culture. *Anal Biochem*, 350, 177-85.
- KUO, H. J., MASLEN, C. L., KEENE, D. R. & GLANVILLE, R. W. 1997. Type VI collagen anchors endothelial basement membranes by interacting with type IV collagen. *J Biol Chem*, 272, 26522-9.
- KUPCSIK, L., ALINI, M. & STODDART, M. J. 2009. Epsilon-aminocaproic acid is a useful fibrin degradation inhibitor for cartilage tissue engineering. *Tissue Eng Part A*, 15, 2309-13.
- KURODA, R., USAS, A., KUBO, S., CORSI, K., PENG, H., ROSE, T., CUMMINGS, J., FU, F. H. & HUARD, J. 2006. Cartilage repair using bone morphogenetic protein 4 and muscle-derived stem cells. *Arthritis Rheum*, 54, 433-42.
- KWAN, A. P., CUMMINGS, C. E., CHAPMAN, J. A. & GRANT, M. E. 1991. Macromolecular organization of chicken type X collagen in vitro. *J Cell Biol*, 114, 597-604.

References

- KWAN, K. M., PANG, M. K., ZHOU, S., COWAN, S. K., KONG, R. Y., PFORDTE, T., OLSEN, B. R., SILLENCE, D. O., TAM, P. P. & CHEAH, K. S. 1997. Abnormal compartmentalization of cartilage matrix components in mice lacking collagen X: implications for function. *J Cell Biol*, 136, 459-71.
- LACEY, D. L., TIMMS, E., TAN, H. L., KELLEY, M. J., DUNSTAN, C. R., BURGESS, T., ELLIOTT, R., COLOMBERO, A., ELLIOTT, G., SCULLY, S., HSU, H., SULLIVAN, J., HAWKINS, N., DAVY, E., CAPPARELLI, C., ELI, A., QIAN, Y. X., KAUFMAN, S., SAROSI, I., SHALHOUB, V., SENALDI, G., GUO, J., DELANEY, J. & BOYLE, W. J. 1998. Osteoprotegerin ligand is a cytokine that regulates osteoclast differentiation and activation. *Cell*, 93, 165-76.
- LAHM, A., MROSEK, E., SPANK, H., ERGGELET, C., KASCH, R., ESSER, J. & MERK, H. 2010. Changes in content and synthesis of collagen types and proteoglycans in osteoarthritis of the knee joint and comparison of quantitative analysis with Photoshop-based image analysis. *Arch Orthop Trauma Surg*, 130, 557-64.
- LAMANDE, S. R., MORGELIN, M., ADAMS, N. E., SELAN, C. & ALLEN, J. M. 2006. The C5 domain of the collagen VI alpha3(VI) chain is critical for extracellular microfibril formation and is present in the extracellular matrix of cultured cells. *J Biol Chem*, 281, 16607-14.
- LANDIS, W. J. & JACQUET, R. 2013. Association of calcium and phosphate ions with collagen in the mineralization of vertebrate tissues. *Calcif Tissue Int*, 93, 329-37.
- LANZA, R., LANGER, R., VACANTI, J. P. & ATALA, A. 2020. *Principles of tissue engineering*, Academic press.
- LATVANLEHTO, A., FOX, M. A., SORMUNEN, R., TU, H., OIKARAINEN, T., KOSKI, A., NAUMENKO, N., SHAKIRZYANOVA, A., KALLIO, M., ILVES, M., GINIATULLIN, R., SANES, J. R. & PIHLAJANIEMI, T. 2010. Muscle-derived collagen XIII regulates maturation of the skeletal neuromuscular junction. *J Neurosci*, 30, 12230-41.
- LATVANLEHTO, A., SNELLMAN, A., TU, H. & PIHLAJANIEMI, T. 2003. Type XIII collagen and some other transmembrane collagens contain two separate coiled-coil motifs, which may function as independent oligomerization domains. *J Biol Chem*, 278, 37590-9.
- LAVAGNINO, M., ARNO CZKY, S. P., FRANK, K. & TIAN, T. 2005. Collagen fibril diameter distribution does not reflect changes in the mechanical properties of in vitro stress-deprived tendons. *J Biomech*, 38, 69-75.
- LAVIEU, G., ZHENG, H. & ROTHMAN, J. E. 2013. Stapled Golgi cisternae remain in place as cargo passes through the stack. *Elife*, 2, e00558.
- LAWRIE, A. S., MCDONALD, S. J., PURDY, G., MACKIE, I. J. & MACHIN, S. J. 1998. Prothrombin time derived fibrinogen determination on Sysmex CA-6000. *J Clin Pathol*, 51, 462-6.
- LAZARINI, M., BORDEAUX-REGO, P., GIARDINI-ROSA, R., DUARTE, A. S. S., BARATTI, M. O., ZORZI, A. R., DE MIRANDA, J. B., LENZ CESAR, C., LUZO, A. & OLALLA SAAD, S. T. 2017. Natural Type II Collagen Hydrogel, Fibrin Sealant, and Adipose-Derived Stem Cells as a Promising Combination for Articular Cartilage Repair. *Cartilage*, 8, 439-443.
- LEBLEU, V. S., MACDONALD, B. & KALLURI, R. 2007. Structure and function of basement membranes. *Exp Biol Med (Maywood)*, 232, 1121-9.
- LEE, J. H. & KIM, H. W. 2018. Emerging properties of hydrogels in tissue engineering. *J Tissue Eng*, 9, 2041731418768285.
- LEE, J. K., HUWE, L. W., PASCHOS, N., ARYAEI, A., GEGG, C. A., HU, J. C. & ATHANASIOU, K. A. 2017. Tension stimulation drives tissue formation in scaffold-free systems. *Nat Mater*, 16, 864-873.
- LEE, K. I., LEE, J. S., KANG, K. T., SHIM, Y. B., KIM, Y. S., JANG, J. W., MOON, S. H. & D'LIMA, D. D. 2018. In Vitro and In Vivo Performance of Tissue-Engineered Tendons for Anterior Cruciate Ligament Reconstruction. *Am J Sports Med*, 46, 1641-1649.
- LEE, Y. J., RICE, R. H. & LEE, Y. M. 2006. Proteome analysis of human hair shaft: from protein identification to posttranslational modification. *Mol Cell Proteomics*, 5, 789-800.
- LEFEBVRE, V. & SMITS, P. 2005. Transcriptional control of chondrocyte fate and differentiation. *Birth Defects Res C Embryo Today*, 75, 200-12.
- LEGERLOTZ, K., RILEY, G. P. & SCREEN, H. R. 2013. GAG depletion increases the stress-relaxation response of tendon fascicles, but does not influence recovery. *Acta Biomater*, 9, 6860-6.
- LEI, X., CAO, Y., ZHANG, Y., QIAN, J., ZHAO, Q., LIU, F., ZHANG, T., ZHOU, J., GU, Y., XIA, G. & DUAN, E. 2018. Effect of microgravity on proliferation and differentiation of embryonic stem cells in an automated culturing system during the TZ-1 space mission. *Cell Prolif*, 51, e12466.
- LEMMMA, S., AVNET, S., SALERNO, M., CHANO, T. & BALDINI, N. 2016. Identification and Validation of Housekeeping Genes for Gene Expression Analysis of Cancer Stem Cells. *PLoS One*, 11, e0149481.
- LENDECKEL, S., JODICKE, A., CHRISTOPHIS, P., HEIDINGER, K., WOLFF, J., FRASER, J. K., HEDRICK, M. H., BERTHOLD, L. & HOWALDT, H. P. 2004. Autologous stem cells (adipose) and fibrin glue used to treat widespread traumatic calvarial defects: case report. *J Craniomaxillofac Surg*, 32, 370-3.
- LENTH, R. 2020. emmeans: Estimated Marginal Means, aka Least-Squares Means. . 1.5-2.1 ed.
- LI, A., WEI, Y., HUNG, C. & VUNJAK-NOVAKOVIC, G. 2018. Chondrogenic properties of collagen type XI, a component of cartilage extracellular matrix. *Biomaterials*, 173, 47-57.
- LI, G., FU, N., YANG, X., LI, M., BA, K., WEI, X., FU, Y., YAO, Y., CAI, X. & LIN, Y. 2013. Mechanical compressive force inhibits adipogenesis of adipose stem cells. *Cell Prolif*, 46, 586-94.

References

- LI, J., BAO, Q., CHEN, S., LIU, H., FENG, J., QIN, H., LI, A., LIU, D., SHEN, Y., ZHAO, Y. & ZONG, Z. 2017a. Different bone remodeling levels of trabecular and cortical bone in response to changes in Wnt/ β -catenin signaling in mice. *J Orthop Res*, 35, 812-819.
- LI, J., ZHANG, S., CHEN, J., DU, T., WANG, Y. & WANG, Z. 2009. Modeled microgravity causes changes in the cytoskeleton and focal adhesions, and decreases in migration in malignant human MCF-7 cells. *Protoplasma*, 238, 23-33.
- LI, K., ZHANG, C., QIU, L., GAO, L. & ZHANG, X. 2017b. Advances in Application of Mechanical Stimuli in Bioreactors for Cartilage Tissue Engineering. *Tissue Eng Part B Rev*, 23, 399-411.
- LI, S. W., SIERON, A. L., FERTALA, A., HOJIMA, Y., ARNOLD, W. V. & PROCKOP, D. J. 1996. The C-proteinase that processes procollagens to fibrillar collagens is identical to the protein previously identified as bone morphogenic protein-1. *Proc Natl Acad Sci U S A*, 93, 5127-30.
- LIAO, J. & VESELY, I. 2003. A structural basis for the size-related mechanical properties of mitral valve chordae tendineae. *J Biomech*, 36, 1125-33.
- LIN, G. L. & HANKENSON, K. D. 2011. Integration of BMP, Wnt, and notch signaling pathways in osteoblast differentiation. *J Cell Biochem*, 112, 3491-501.
- LIN, T. W., CARDENAS, L. & SOSLOWSKY, L. J. 2004. Biomechanics of tendon injury and repair. *J Biomech*, 37, 865-77.
- LIN, X., PATIL, S., GAO, Y. G. & QIAN, A. 2020. The Bone Extracellular Matrix in Bone Formation and Regeneration. *Front Pharmacol*, 11, 757.
- LINDROOS, B., MAENPAA, K., YLIKOMI, T., OJA, H., SUURONEN, R. & MIETTINEN, S. 2008. Characterisation of human dental stem cells and buccal mucosa fibroblasts. *Biochem Biophys Res Commun*, 368, 329-35.
- LISIGNOLI, G., CODELUPPI, K., TODOERTI, K., MANFREDINI, C., PIACENTINI, A., ZINI, N., GRASSI, F., CATTINI, L., PIVA, R., RIZZOLI, V., FACCHINI, A., GIULIANI, N. & NERI, A. 2009. Gene array profile identifies collagen type XV as a novel human osteoblast-secreted matrix protein. *J Cell Physiol*, 220, 401-9.
- LIU, C., ZHAO, Y., CHEUNG, W. Y., GANDHI, R., WANG, L. & YOU, L. 2010a. Effects of cyclic hydraulic pressure on osteocytes. *Bone*, 46, 1449-56.
- LIU, C. F., BREIDENBACH, A., ASCHBACHER-SMITH, L., BUTLER, D. & WYLIE, C. 2013. A role for hedgehog signaling in the differentiation of the insertion site of the patellar tendon in the mouse. *PLoS One*, 8, e65411.
- LIU, J., ZHAO, Z., LI, J., ZOU, L., SHULER, C., ZOU, Y., HUANG, X., LI, M. & WANG, J. 2009a. Hydrostatic pressures promote initial osteodifferentiation with ERK1/2 not p38 MAPK signaling involved. *J Cell Biochem*, 107, 224-32.
- LIU, J., ZOU, L., WANG, J., SCHULER, C., ZHAO, Z., LI, X., ZHANG, J. & LIU, Y. 2009b. Hydrostatic pressure promotes Wnt10b and Wnt4 expression dependent and independent on ERK signaling in early-osteinduced MSCs. *Biochem Biophys Res Commun*, 379, 505-9.
- LIU, L., WU, W., TUO, X., GENG, W., ZHAO, J., WEI, J., YAN, X., YANG, W., LI, L. & CHEN, F. 2010b. Novel strategy to engineer trachea cartilage graft with marrow mesenchymal stem cell macroaggregate and hydrolyzable scaffold. *Artif Organs*, 34, 426-33.
- LIU, Q., HATTA, T., QI, J., LIU, H., THORESON, A. R., AMADIO, P. C., MORAN, S. L., STEINMANN, S. P., GINGERY, A. & ZHAO, C. 2018. Novel engineered tendon-fibrocartilage-bone composite with cyclic tension for rotator cuff repair. *J Tissue Eng Regen Med*, 12, 1690-1701.
- LIU, Z. J., ZHUGE, Y. & VELAZQUEZ, O. C. 2009c. Trafficking and differentiation of mesenchymal stem cells. *J Cell Biochem*, 106, 984-91.
- LOHAN, A., MARZAHN, U., EL SAYED, K., HAISCH, A., MULLER, R. D., KOHL, B., STOLZEL, K., ERTEL, W., JOHN, T. & SCHULZE-TANZIL, G. 2014. Osteochondral articular defect repair using auricle-derived autologous chondrocytes in a rabbit model. *Ann Anat*, 196, 317-26.
- LONG, F. 2011. Building strong bones: molecular regulation of the osteoblast lineage. *Nat Rev Mol Cell Biol*, 13, 27-38.
- LORENZ, J., SEEBACH, E., HACKMAYER, G., GRETH, C., BAUER, R. J., KLEINSCHMIDT, K., BETTENWORTH, D., BOHM, M., GRIFKA, J. & GRASSEL, S. 2014. Melanocortin 1 receptor-signaling deficiency results in an articular cartilage phenotype and accelerates pathogenesis of surgically induced murine osteoarthritis. *PLoS One*, 9, e105858.
- LORTHONGPANICH, C., THUMANU, K., TANGKIETTRAKUL, K., JIAMVORAPHONG, N., LAOWTAMMATHRON, C., DAMKHAM, N., Y, U. P. & ISSARAGRISIL, S. 2019. YAP as a key regulator of adipo-osteogenic differentiation in human MSCs. *Stem Cell Res Ther*, 10, 402.
- LOTIERE, D., DELROT, P. & MOSER, C. 2018. Volumetric 3D printing of elastomers by tomographic back-projection. Preprint at <https://doi.org/10.13140/RG.2>.
- LU, D. & KASSAB, G. S. 2011. Role of shear stress and stretch in vascular mechanobiology. *J R Soc Interface*, 8, 1379-85.
- LU, Y., MAPILI, G., SUHALI, G., CHEN, S. & ROY, K. 2006. A digital micro-mirror device-based system for the microfabrication of complex, spatially patterned tissue engineering scaffolds. *J Biomed Mater Res A*, 77, 396-405.

References

- LUO, Y., SINKEVICIUTE, D., HE, Y., KARSDAL, M., HENROTIN, Y., MOBASHERI, A., ONNERFJORD, P. & BAY-JENSEN, A. 2017. The minor collagens in articular cartilage. *Protein Cell*, 8, 560-572.
- LUYTEN, F. P., YU, Y. M., YANAGISHITA, M., VUKICEVIC, S., HAMMONDS, R. G. & REDDI, A. H. 1992. Natural bovine osteogenin and recombinant human bone morphogenetic protein-2B are equipotent in the maintenance of proteoglycans in bovine articular cartilage explant cultures. *J Biol Chem*, 267, 3691-5.
- MACKIE, E. J., AHMED, Y. A., TATARCZUCH, L., CHEN, K. S. & MIRAMS, M. 2008. Endochondral ossification: how cartilage is converted into bone in the developing skeleton. *Int J Biochem Cell Biol*, 40, 46-62.
- MAEDA, E., FLEISCHMANN, C., MEIN, C. A., SHELTON, J. C., BADER, D. L. & LEE, D. A. 2010. Functional analysis of tenocytes gene expression in tendon fascicles subjected to cyclic tensile strain. *Connect Tissue Res*, 51, 434-44.
- MAEHATA, Y., TAKAMIZAWA, S., OZAWA, S., IZUKURI, K., KATO, Y., SATO, S., LEE, M. C., KIMURA, A. & HATA, R. 2007. Type III collagen is essential for growth acceleration of human osteoblastic cells by ascorbic acid 2-phosphate, a long-acting vitamin C derivative. *Matrix Biol*, 26, 371-81.
- MAGID, A. & LAW, D. J. 1985. Myofibrils bear most of the resting tension in frog skeletal muscle. *Science*, 230, 1280-2.
- MAGNUSSON, S. P., HANSEN, P. & KJAER, M. 2003. Tendon properties in relation to muscular activity and physical training. *Scand J Med Sci Sports*, 13, 211-23.
- MAGUIRE, T. J. & NOVIK, E. 2010. *Methods in Bioengineering: Alternative Technologies to Animal Testing*, Artech House.
- MAJD, H., WIPFF, P. J., BUSCEMI, L., BUENO, M., VONWIL, D., QUINN, T. M. & HINZ, B. 2009. A novel method of dynamic culture surface expansion improves mesenchymal stem cell proliferation and phenotype. *Stem Cells*, 27, 200-9.
- MAJESKA, R. J. & WUTHIER, R. E. 1975. Studies on matrix vesicles isolated from chick epiphyseal cartilage. Association of pyrophosphatase and ATPase activities with alkaline phosphatase. *Biochim Biophys Acta*, 391, 51-60.
- MAK, K. K., CHEN, M. H., DAY, T. F., CHUANG, P. T. & YANG, Y. 2006. Wnt/beta-catenin signaling interacts differentially with Ihh signaling in controlling endochondral bone and synovial joint formation. *Development*, 133, 3695-707.
- MAK, K. M. & MEI, R. 2017. Basement Membrane Type IV Collagen and Laminin: An Overview of Their Biology and Value as Fibrosis Biomarkers of Liver Disease. *Anat Rec (Hoboken)*, 300, 1371-1390.
- MAK, K. M., PNG, C. Y. & LEE, D. J. 2016. Type V Collagen in Health, Disease, and Fibrosis. *Anat Rec (Hoboken)*, 299, 613-29.
- MAKRIS, E. A., GOMOLL, A. H., MALIZOS, K. N., HU, J. C. & ATHANASIOU, K. A. 2015. Repair and tissue engineering techniques for articular cartilage. *Nat Rev Rheumatol*, 11, 21-34.
- MALHOTRA, V. & ERLMANN, P. 2015. The pathway of collagen secretion. *Annu Rev Cell Dev Biol*, 31, 109-24.
- MALHOTRA, V., ERLMANN, P. & NOGUEIRA, C. 2015. Procollagen export from the endoplasmic reticulum. *Biochem Soc Trans*, 43, 104-7.
- MANDRYCKY, C., WANG, Z., KIM, K. & KIM, D. H. 2016. 3D bioprinting for engineering complex tissues. *Biotechnol Adv*, 34, 422-434.
- MANOLAGAS, S. C. 2000. Birth and death of bone cells: basic regulatory mechanisms and implications for the pathogenesis and treatment of osteoporosis. *Endocr Rev*, 21, 115-37.
- MARCACCI, M., KON, E., MOUKHACHEV, V., LAVROUKOV, A., KUTEPOV, S., QUARTO, R., MASTROGIACOMO, M. & CANCEDDA, R. 2007. Stem cells associated with macroporous bioceramics for long bone repair: 6- to 7-year outcome of a pilot clinical study. *Tissue Eng*, 13, 947-55.
- MARCELINO, J., CARPTEN, J. D., SUWAIRI, W. M., GUTIERREZ, O. M., SCHWARTZ, S., ROBBINS, C., SOOD, R., MAKALOWSKA, I., BAXEVANIS, A., JOHNSTONE, B., LAXER, R. M., ZEMEL, L., KIM, C. A., HERD, J. K., IHLE, J., WILLIAMS, C., JOHNSON, M., RAMAN, V., ALONSO, L. G., BRUNONI, D., GERSTEIN, A., PAPADOPOULOS, N., BAHABRI, S. A., TRENT, J. M. & WARMAN, M. L. 1999. CACP, encoding a secreted proteoglycan, is mutated in camptodactyly-arthropathy-coxa vara-pericarditis syndrome. *Nat Genet*, 23, 319-22.
- MARESCHI, K., FERRERO, I., RUSTICHELLI, D., ASCHERO, S., GAMMAITONI, L., AGLIETTA, M., MADON, E. & FAGIOLI, F. 2006. Expansion of mesenchymal stem cells isolated from pediatric and adult donor bone marrow. *J Cell Biochem*, 97, 744-54.
- MARINOVICH, R., SOENJAYA, Y., WALLACE, G. Q., ZUSKOV, A., DUNKMAN, A., FOSTER, B. L., AO, M., BARTMAN, K., LAM, V., RIZKALLA, A., BEIER, F., SOMERMAN, M. J., HOLDSWORTH, D. W., SOSLOWSKY, L. J., LAGUGNE-LABARTHET, F. & GOLDBERG, H. A. 2016. The role of bone sialoprotein in the tendon-bone insertion. *Matrix Biol*, 52-54, 325-338.
- MARTEL-PELLETIER, J., BOILEAU, C., PELLETIER, J. P. & ROUGHLEY, P. J. 2008. Cartilage in normal and osteoarthritis conditions. *Best Pract Res Clin Rheumatol*, 22, 351-84.
- MARTIN, I., WENDT, D. & HEBERER, M. 2004. The role of bioreactors in tissue engineering. *Trends Biotechnol*, 22, 80-6.
- MARTINSEN, A., SKJAK-BRAEK, G. & SMIDSRØD, O. 1989. Alginate as immobilization material: I. Correlation between chemical and physical properties of alginate gel beads. *Biotechnol Bioeng*, 33, 79-89.

References

- MARTURANO, J. E., ARENA, J. D., SCHILLER, Z. A., GEORGAKOUDI, I. & KUO, C. K. 2013. Characterization of mechanical and biochemical properties of developing embryonic tendon. *Proc Natl Acad Sci U S A*, 110, 6370-5.
- MATSUO, N., TANAKA, S., YOSHIOKA, H., KOCH, M., GORDON, M. K. & RAMIREZ, F. 2008. Collagen XXIV (Col24a1) gene expression is a specific marker of osteoblast differentiation and bone formation. *Connect Tissue Res*, 49, 68-75.
- MATTEI, C., ALSHAWAF, A., D'ABACO, G., NAYAGAM, B. & DOTTORI, M. 2018. Generation of Neural Organoids from Human Embryonic Stem Cells Using the Rotary Cell Culture System: Effects of Microgravity on Neural Progenitor Cell Fate. *Stem Cells Dev*, 27, 848-857.
- MAYER-WAGNER, S., HAMMERSCHMID, F., REDEKER, J. I., SCHMITT, B., HOLZAPFEL, B. M., JANSSON, V., BETZ, O. B. & MULLER, P. E. 2014. Simulated microgravity affects chondrogenesis and hypertrophy of human mesenchymal stem cells. *Int Orthop*, 38, 2615-21.
- MCBEATH, R., PIRONE, D. M., NELSON, C. M., BHADRIRAJU, K. & CHEN, C. S. 2004. Cell shape, cytoskeletal tension, and RhoA regulate stem cell lineage commitment. *Dev Cell*, 6, 483-95.
- MCCARTHY, H. E., BARA, J. J., BRAKSPEAR, K., SINGHRAO, S. K. & ARCHER, C. W. 2012. The comparison of equine articular cartilage progenitor cells and bone marrow-derived stromal cells as potential cell sources for cartilage repair in the horse. *Vet J*, 192, 345-51.
- MCCAUGHEY, J., STEVENSON, N. L., CROSS, S. & STEPHENS, D. J. 2019. ER-to-Golgi trafficking of procollagen in the absence of large carriers. *J Cell Biol*, 218, 929-948.
- MCCULLOCH, C. A., STRUGURESCU, M., HUGHES, F., MELCHER, A. H. & AUBIN, J. E. 1991. Osteogenic progenitor cells in rat bone marrow stromal populations exhibit self-renewal in culture. *Blood*, 77, 1906-11.
- MCMAHON, L. A., CAMPBELL, V. A. & PRENDERGAST, P. J. 2008. Involvement of stretch-activated ion channels in strain-regulated glycosaminoglycan synthesis in mesenchymal stem cell-seeded 3D scaffolds. *J Biomech*, 41, 2055-9.
- MCNEILLY, C. M., BANES, A. J., BENJAMIN, M. & RALPHS, J. R. 1996. Tendon cells in vivo form a three dimensional network of cell processes linked by gap junctions. *J Anat*, 189 (Pt 3), 593-600.
- MEGENS, R. T., OUDE EGBRINK, M. G., CLEUTJENS, J. P., KUIJPERS, M. J., SCHIFFERS, P. H., MERKX, M., SLAAF, D. W. & VAN ZANDVOORT, M. A. 2007. Imaging collagen in intact viable healthy and atherosclerotic arteries using fluorescently labeled CNA35 and two-photon laser scanning microscopy. *Mol Imaging*, 6, 247-60.
- MEINERT, C., SCHROBBACK, K., HUTMACHER, D. W. & KLEIN, T. J. 2017. A novel bioreactor system for biaxial mechanical loading enhances the properties of tissue-engineered human cartilage. *Sci Rep*, 7, 16997.
- MENDLER, M., EICH-BENDER, S. G., VAUGHAN, L., WINTERHALTER, K. H. & BRUCKNER, P. 1989. Cartilage contains mixed fibrils of collagen types II, IX, and XI. *J Cell Biol*, 108, 191-7.
- MESIMAKI, K., LINDROOS, B., TORNWALL, J., MAUNO, J., LINDQVIST, C., KONTIO, R., MIETTINEN, S. & SUURONEN, R. 2009. Novel maxillary reconstruction with ectopic bone formation by GMP adipose stem cells. *Int J Oral Maxillofac Surg*, 38, 201-9.
- MEYER, K. 1958. Chemical structure of hyaluronic acid. *Fed Proc*, 17, 1075-7.
- MEYERS, V. E., ZAYZAFON, M., GONDA, S. R., GATHINGS, W. E. & MCDONALD, J. M. 2004. Modeled microgravity disrupts collagen I/integrin signaling during osteoblastic differentiation of human mesenchymal stem cells. *J Cell Biochem*, 93, 697-707.
- MIENALTOWSKI, M. J. & BIRK, D. E. 2014. Structure, physiology, and biochemistry of collagens. *Adv Exp Med Biol*, 802, 5-29.
- MIKIC, B., JOHNSON, T. L., CHHABRA, A. B., SCHALET, B. J., WONG, M. & HUNZIKER, E. B. 2000. Differential effects of embryonic immobilization on the development of fibrocartilaginous skeletal elements. *J Rehabil Res Dev*, 37, 127-33.
- MILLER, E. A. & SCHEKMAN, R. 2013. COPII - a flexible vesicle formation system. *Curr Opin Cell Biol*, 25, 420-7.
- MILLER, E. J. & MATUKAS, V. J. 1969. Chick cartilage collagen: a new type of alpha 1 chain not present in bone or skin of the species. *Proc Natl Acad Sci U S A*, 64, 1264-8.
- MILLER, K., CHINZEI, K., ORSSENGO, G. & BEDNARZ, P. 2000. Mechanical properties of brain tissue in-vivo: experiment and computer simulation. *J Biomech*, 33, 1369-76.
- MINER, J. H. 2011. Basement membranes. *The extracellular matrix: An overview*. Springer.
- MIRONOV, V., BOLAND, T., TRUSK, T., FORGACS, G. & MARKWALD, R. R. 2003. Organ printing: computer-aided jet-based 3D tissue engineering. *Trends Biotechnol*, 21, 157-61.
- MISAWA, K., KANAZAWA, T., IMAI, A., ENDO, S., MOCHIZUKI, D., FUKUSHIMA, H., MISAWA, Y. & MINETA, H. 2014. Prognostic value of type XXII and XXIV collagen mRNA expression in head and neck cancer patients. *Mol Clin Oncol*, 2, 285-291.
- MISOF, K., RAPP, G. & FRATZL, P. 1997. A new molecular model for collagen elasticity based on synchrotron X-ray scattering evidence. *Biophys J*, 72, 1376-81.
- MITSUHARA, T., TAKEDA, M., YAMAGUCHI, S., MANABE, T., MATSUMOTO, M., KAWAHARA, Y., YUGE, L. & KURISU, K. 2013. Simulated microgravity facilitates cell migration and neuroprotection after bone marrow stromal cell transplantation in spinal cord injury. *Stem Cell Res Ther*, 4, 35.

References

- MIZOKAMI, A., KAWAKUBO-YASUKOCHI, T. & HIRATA, M. 2017. Osteocalcin and its endocrine functions. *Biochem Pharmacol*, 132, 1-8.
- MODDER, U. I. & KHOSLA, S. 2008. Skeletal stem/osteoprogenitor cells: current concepts, alternate hypotheses, and relationship to the bone remodeling compartment. *J Cell Biochem*, 103, 393-400.
- MONTAGNE, K., ONUMA, Y., ITO, Y., AIKI, Y., FURUKAWA, K. S. & USHIDA, T. 2017. High hydrostatic pressure induces pro-osteoarthritic changes in cartilage precursor cells: A transcriptome analysis. *PLoS One*, 12, e0183226.
- MOOREHEAD, C., PRUDNIKOVA, K. & MARCOLONGO, M. 2019. The regulatory effects of proteoglycans on collagen fibrillogenesis and morphology investigated using biomimetic proteoglycans. *J Struct Biol*, 206, 204-215.
- MORITA, Y., WATANABE, S., JU, Y. & XU, B. 2013. Determination of optimal cyclic uniaxial stretches for stem cell-to-tenocyte differentiation under a wide range of mechanical stretch conditions by evaluating gene expression and protein synthesis levels. *Acta Bioeng Biomech*, 15, 71-9.
- MOSS, D. W., EATON, R. H., SMITH, J. K. & WHITBY, L. G. 1967. Association of inorganic-pyrophosphatase activity with human alkaline-phosphatase preparations. *Biochem J*, 102, 53-7.
- MOW, V. C., HOLMES, M. H. & LAI, W. M. 1984. Fluid transport and mechanical properties of articular cartilage: a review. *J Biomech*, 17, 377-94.
- MOW, V. C. & WANG, C. C. 1999. Some bioengineering considerations for tissue engineering of articular cartilage. *Clin Orthop Relat Res*, S204-23.
- MUELLER, M. B. & TUAN, R. S. 2008. Functional characterization of hypertrophy in chondrogenesis of human mesenchymal stem cells. *Arthritis Rheum*, 58, 1377-88.
- MUNDLOS, S., CHAN, D., MCGILL, J. & BATEMAN, J. F. 1996. An alpha 1(II) Gly913 to Cys substitution prevents the matrix incorporation of type II collagen which is replaced with type I and III collagens in cartilage from a patient with hypochondrogenesis. *Am J Med Genet*, 63, 129-36.
- MUNDLOS, S. & OLSEN, B. R. 1997. Heritable diseases of the skeleton. Part II: Molecular insights into skeletal development-matrix components and their homeostasis. *FASEB J*, 11, 227-33.
- MURDOCH, A. D., GRADY, L. M., ABLETT, M. P., KATOPODI, T., MEADOWS, R. S. & HARDINGHAM, T. E. 2007. Chondrogenic differentiation of human bone marrow stem cells in transwell cultures: generation of scaffold-free cartilage. *Stem Cells*, 25, 2786-96.
- MURSHED, M., HARMEY, D., MILLAN, J. L., MCKEE, M. D. & KARSENTY, G. 2005. Unique coexpression in osteoblasts of broadly expressed genes accounts for the spatial restriction of ECM mineralization to bone. *Genes Dev*, 19, 1093-104.
- MURSHID, A. & PRESLEY, J. F. 2004. ER-to-Golgi transport and cytoskeletal interactions in animal cells. *Cell Mol Life Sci*, 61, 133-45.
- MYERS, J. C., CHU, M. L., FARO, S. H., CLARK, W. J., PROCKOP, D. J. & RAMIREZ, F. 1981. Cloning a cDNA for the pro-alpha 2 chain of human type I collagen. *Proc Natl Acad Sci U S A*, 78, 3516-20.
- MYERS, J. C., DION, A. S., ABRAHAM, V. & AMENTA, P. S. 1996. Type XV collagen exhibits a widespread distribution in human tissues but a distinct localization in basement membrane zones. *Cell Tissue Res*, 286, 493-505.
- MYERS, J. C., KIVIRIKKO, S., GORDON, M. K., DION, A. S. & PIHLAJANIEMI, T. 1992. Identification of a previously unknown human collagen chain, alpha 1(XV), characterized by extensive interruptions in the triple-helical region. *Proc Natl Acad Sci U S A*, 89, 10144-8.
- MYERS, J. C., LI, D., AMENTA, P. S., CLARK, C. C., NAGASWAMI, C. & WEISEL, J. W. 2003. Type XIX collagen purified from human umbilical cord is characterized by multiple sharp kinks delineating collagenous subdomains and by intermolecular aggregates via globular, disulfide-linked, and heparin-binding amino termini. *J Biol Chem*, 278, 32047-57.
- NABAVI, N., KHANDANI, A., CAMIRAND, A. & HARRISON, R. E. 2011. Effects of microgravity on osteoclast bone resorption and osteoblast cytoskeletal organization and adhesion. *Bone*, 49, 965-74.
- NARANDA, J., SUSEC, M., MAVER, U., GRADISNIK, L., GORENJAK, M., VUKASOVIC, A., IVKOVIC, A., RUPNIK, M. S., VOGRIN, M. & KRAJNC, P. 2016. Polyester type polyHIPE scaffolds with an interconnected porous structure for cartilage regeneration. *Sci Rep*, 6, 28695.
- NAZEMPOUR, A., QUISENBERRY, C. R., ABU-LAIL, N. I. & VAN WIE, B. J. 2017. Combined effects of oscillating hydrostatic pressure, perfusion and encapsulation in a novel bioreactor for enhancing extracellular matrix synthesis by bovine chondrocytes. *Cell Tissue Res*, 370, 179-193.
- NEBELUNG, S., GAVENIS, K., RATH, B., TINGART, M., LADENBURGER, A., STOFFEL, M., ZHOU, B. & MUELLER-RATH, R. 2011. Continuous cyclic compressive loading modulates biological and mechanical properties of collagen hydrogels seeded with human chondrocytes. *Biorheology*, 48, 247-61.
- NG, K. W., MAUCK, R. L., WANG, C. C., KELLY, T. A., HO, M. M., CHEN, F. H., ATESHIAN, G. A. & HUNG, C. T. 2009. Duty Cycle of Deformational Loading Influences the Growth of Engineered Articular Cartilage. *Cell Mol Bioeng*, 2, 386-394.
- NGO, T. D., KASHANI, A., IMBALZANO, G., NGUYEN, K. T. & HUI, D. 2018. Additive manufacturing (3D printing): A review of materials, methods, applications and challenges. *Composites Part B: Engineering*, 143, 172-196.

References

- NIELSEN, E. H. & BYTZER, P. 1979. High resolution scanning electron microscopy of elastic cartilage. *J Anat*, 129, 823-31.
- NISHIYAMA, T., MCDONOUGH, A. M., BRUNS, R. R. & BURGESSON, R. E. 1994. Type XII and XIV collagens mediate interactions between banded collagen fibers in vitro and may modulate extracellular matrix deformability. *J Biol Chem*, 269, 28193-9.
- NIYIBIZI, C. & EYRE, D. R. 1994. Structural characteristics of cross-linking sites in type V collagen of bone. Chain specificities and heterotypic links to type I collagen. *Eur J Biochem*, 224, 943-50.
- NOGUEIRA, C., ERLMANN, P., VILLENEUVE, J., SANTOS, A. J., MARTINEZ-ALONSO, E., MARTINEZ-MENARGUEZ, J. A. & MALHOTRA, V. 2014. SLY1 and Syntaxin 18 specify a distinct pathway for procollagen VII export from the endoplasmic reticulum. *Elife*, 3, e02784.
- NOHE, A., HASSEL, S., EHRlich, M., NEUBAUER, F., SEBALD, W., HENIS, Y. I. & KNAUS, P. 2002. The mode of bone morphogenetic protein (BMP) receptor oligomerization determines different BMP-2 signaling pathways. *J Biol Chem*, 277, 5330-8.
- NOTH, U., SCHUPP, K., HEYMER, A., KALL, S., JAKOB, F., SCHUTZE, N., BAUMANN, B., BARTHEL, T., EULERT, J. & HENDRICH, C. 2005. Anterior cruciate ligament constructs fabricated from human mesenchymal stem cells in a collagen type I hydrogel. *Cytotherapy*, 7, 447-455.
- NOURISSAT, G., BERENBAUM, F. & DUPREZ, D. 2015. Tendon injury: from biology to tendon repair. *Nat Rev Rheumatol*, 11, 223-33.
- O'CONNOR, W. J., BOTTI, T., KHAN, S. N. & LANE, J. M. 2000. The use of growth factors in cartilage repair. *Orthop Clin North Am*, 31, 399-410.
- OGAWA, R., MIZUNO, S., MURPHY, G. F. & ORGILL, D. P. 2009. The effect of hydrostatic pressure on three-dimensional chondroinduction of human adipose-derived stem cells. *Tissue Eng Part A*, 15, 2937-45.
- OGAWA, R., ORGILL, D. P., MURPHY, G. F. & MIZUNO, S. 2015. Hydrostatic pressure-driven three-dimensional cartilage induction using human adipose-derived stem cells and collagen gels. *Tissue Eng Part A*, 21, 257-66.
- OH, J. H., KIM, H. J., KIM, T. I. & WOO, K. M. 2014. Comparative evaluation of the biological properties of fibrin for bone regeneration. *BMB Rep*, 47, 110-4.
- OHYABU, Y., ADEGAWA, T., YOSHIOKA, T., IKOMA, T., SHINOZAKI, K., UEMURA, T. & TANAKA, J. 2009. A collagen sponge incorporating a hydroxyapatite/chondroitin sulfate composite as a scaffold for cartilage tissue engineering. *J Biomater Sci Polym Ed*, 20, 1861-74.
- OLDERSHAW, R. A. & HARDINGHAM, T. E. 2010. Notch signaling during chondrogenesis of human bone marrow stem cells. *Bone*, 46, 286-93.
- OLSEN, B. R. 1997. Collagen IX. *Int J Biochem Cell Biol*, 29, 555-8.
- OMARI, S., MAKAREEVA, E., GORRELL, L., JARNIK, M., LIPPINCOTT-SCHWARTZ, J. & LEIKIN, S. 2020. Mechanisms of procollagen and HSP47 sorting during ER-to-Golgi trafficking. *Matrix Biol*.
- ONNERFJORD, P., KHABUT, A., REINHOLT, F. P., SVENSSON, O. & HEINEGARD, D. 2012. Quantitative proteomic analysis of eight cartilaginous tissues reveals characteristic differences as well as similarities between subgroups. *J Biol Chem*, 287, 18913-24.
- OPTN. 2020. *Organ Procurement and Transplantation network (OPTN) Data Reports* [Online]. Available: <https://optn.transplant.hrsa.gov/data/> [Accessed 2020].
- OSATHANON, T., LINNES, M. L., RAJACHAR, R. M., RATNER, B. D., SOMERMAN, M. J. & GIACHELLI, C. M. 2008. Microporous nanofibrous fibrin-based scaffolds for bone tissue engineering. *Biomaterials*, 29, 4091-9.
- OTSUKA, T., IMURA, T., NAKAGAWA, K., SHRESTHA, L., TAKAHASHI, S., KAWAHARA, Y., SUEDA, T., KURISU, K. & YUGE, L. 2018. Simulated Microgravity Culture Enhances the Neuroprotective Effects of Human Cranial Bone-Derived Mesenchymal Stem Cells in Traumatic Brain Injury. *Stem Cells Dev*, 27, 1287-1297.
- OTT, S. M. 2018. Cortical or Trabecular Bone: What's the Difference? *Am J Nephrol*, 47, 373-375.
- OXLUND, H., BARCKMAN, M., ORTOFT, G. & ANDREASSEN, T. T. 1995. Reduced concentrations of collagen cross-links are associated with reduced strength of bone. *Bone*, 17, 365S-371S.
- OZBOLAT, I. T., PENG, W. & OZBOLAT, V. 2016. Application areas of 3D bioprinting. *Drug Discov Today*, 21, 1257-71.
- PACE, J. M., CORRADO, M., MISSERO, C. & BYERS, P. H. 2003. Identification, characterization and expression analysis of a new fibrillar collagen gene, COL27A1. *Matrix Biol*, 22, 3-14.
- PAIVA, K. B. S. & GRANJEIRO, J. M. 2017. Matrix Metalloproteinases in Bone Resorption, Remodeling, and Repair. *Prog Mol Biol Transl Sci*, 148, 203-303.
- PAKDEL, M. & VON BLUME, J. 2018. Exploring new routes for secretory protein export from the trans-Golgi network. *Mol Biol Cell*, 29, 235-240.
- PARFITT, A. M. 2002. Misconceptions (2): turnover is always higher in cancellous than in cortical bone. *Bone*, 30, 807-9.
- PARK, H. W., KIM, Y. C., YU, B., MOROISHI, T., MO, J. S., PLOUFFE, S. W., MENG, Z., LIN, K. C., YU, F. X., ALEXANDER, C. M., WANG, C. Y. & GUAN, K. L. 2015. Alternative Wnt Signaling Activates YAP/TAZ. *Cell*, 162, 780-94.

References

- PARK, J. Y., HA, S., PARK, E., KWON, D. & KIM, N. 2016. Hygroscopic Swelling Behavior of 3d Printed Parts Due to Changes in Environmental Conditions. *Proceedings of the Asme International Design Engineering Technical Conferences and Computers and Information in Engineering Conference, 2016, Vol 1a*.
- PARKIN, J. D., SAN ANTONIO, J. D., PERSIKOV, A. V., DAGHER, H., DALGLEISH, R., JENSEN, S. T., JEUNEMAITRE, X. & SAVIGE, J. 2017. The collalphen III fibril has a "flexi-rod" structure of flexible sequences interspersed with rigid bioactive domains including two with hemostatic roles. *PLoS One*, 12, e0175582.
- PARKINSON, J., SAMIRIC, T., ILIC, M. Z., COOK, J. & HANDLEY, C. J. 2011. Involvement of proteoglycans in tendinopathy. *J Musculoskelet Neuronal Interact*, 11, 86-93.
- PARSONS, J. R. & BLACK, J. 1979. Mechanical behavior of articular cartilage: quantitative changes with alteration of ionic environment. *J Biomech*, 12, 765-73.
- PARSONS, P., GILBERT, S. J., VAUGHAN-THOMAS, A., SORRELL, D. A., NOTMAN, R., BISHOP, M., HAYES, A. J., MASON, D. J. & DUANCE, V. C. 2011. Type IX collagen interacts with fibronectin providing an important molecular bridge in articular cartilage. *J Biol Chem*, 286, 34986-97.
- PATEL, D., SHARMA, S., SCREEN, H. R. C. & BRYANT, S. J. 2018. Effects of cell adhesion motif, fiber stiffness, and cyclic strain on tenocyte gene expression in a tendon mimetic fiber composite hydrogel. *Biochem Biophys Res Commun*, 499, 642-647.
- PAXTON, J. Z., WUDEBWE, U. N., WANG, A., WOODS, D. & GROVER, L. M. 2012. Monitoring sinew contraction during formation of tissue-engineered fibrin-based ligament constructs. *Tissue Eng Part A*, 18, 1596-607.
- PECINA, M., JELIC, M., MARTINOVIC, S., HASPL, M. & VUKICEVIC, S. 2002. Articular cartilage repair: the role of bone morphogenetic proteins. *Int Orthop*, 26, 131-6.
- PELHAM, R. J., JR. & WANG, Y. 1997. Cell locomotion and focal adhesions are regulated by substrate flexibility. *Proc Natl Acad Sci U S A*, 94, 13661-5.
- PELTONEN, S., HENTULA, M., HAGG, P., YLA-OUTINEN, H., TUUKKANEN, J., LAKKAKORPI, J., REHN, M., PIHLAJANIEMI, T. & PELTONEN, J. 1999. A novel component of epidermal cell-matrix and cell-cell contacts: transmembrane protein type XIII collagen. *J Invest Dermatol*, 113, 635-42.
- PEPPER, M. E., SESHADRI, V., BURG, T. C., BURG, K. J. & GROFF, R. E. 2012. Characterizing the effects of cell settling on bioprinter output. *Biofabrication*, 4, 011001.
- PEREZ, J. R., KOUROUPIS, D., LI, D. J., BEST, T. M., KAPLAN, L. & CORREA, D. 2018. Tissue Engineering and Cell-Based Therapies for Fractures and Bone Defects. *Front Bioeng Biotechnol*, 6, 105.
- PETERSON, B., ZHANG, J., IGLESIAS, R., KABO, M., HEDRICK, M., BENHAIM, P. & LIEBERMAN, J. R. 2005. Healing of critically sized femoral defects, using genetically modified mesenchymal stem cells from human adipose tissue. *Tissue Eng*, 11, 120-9.
- PFAFFL, M. W., TICHOPAD, A., PRGOMET, C. & NEUVIANS, T. P. 2004. Determination of stable housekeeping genes, differentially regulated target genes and sample integrity: BestKeeper--Excel-based tool using pair-wise correlations. *Biotechnol Lett*, 26, 509-15.
- PIERCE, B. F., PITTMANN, E., MA, N., GEBAUER, T., NEFFE, A. T., HOLSCHER, M., JUNG, F. & LENDLEIN, A. 2012. Viability of human mesenchymal stem cells seeded on crosslinked entropy-elastic gelatin-based hydrogels. *Macromol Biosci*, 12, 312-21.
- PIHLAJAMAA, T., LANKINEN, H., YLOSTALO, J., VALMU, L., JAALINOJA, J., ZAUCKE, F., SPITZNAGEL, L., GOSLING, S., PUUSTINEN, A., MORGELIN, M., PERANEN, J., MAURER, P., ALA-KOKKO, L. & KILPELAINEN, I. 2004. Characterization of recombinant amino-terminal NC4 domain of human collagen IX: interaction with glycosaminoglycans and cartilage oligomeric matrix protein. *J Biol Chem*, 279, 24265-73.
- PITTENGER, M. F., MACKAY, A. M., BECK, S. C., JAISWAL, R. K., DOUGLAS, R., MOSCA, J. D., MOORMAN, M. A., SIMONETTI, D. W., CRAIG, S. & MARSHAK, D. R. 1999. Multilineage potential of adult human mesenchymal stem cells. *Science*, 284, 143-7.
- POLISHCHUK, E. V., DI PENTIMA, A., LUINI, A. & POLISHCHUK, R. S. 2003. Mechanism of constitutive export from the golgi: bulk flow via the formation, protrusion, and en bloc cleavage of large trans-golgi network tubular domains. *Mol Biol Cell*, 14, 4470-85.
- POLLARD, T. D., EARNSHAW, W. C., LIPPINCOTT-SCHWARTZ, J. & JOHNSON, G. T. 2017. Connective Tissues. *Cell Biology*. 3 ed.: Elsevier.
- PORTER, B. D., LIN, A. S., PEISTER, A., HUTMACHER, D. & GULDBERG, R. E. 2007. Noninvasive image analysis of 3D construct mineralization in a perfusion bioreactor. *Biomaterials*, 28, 2525-33.
- PORTNER, R., NAGEL-HEYER, S., GOEPFERT, C., ADAMIETZ, P. & MEENEN, N. M. 2005. Bioreactor design for tissue engineering. *J Biosci Bioeng*, 100, 235-45.
- POWELL, D. W., PINCHUK, I. V., SAADA, J. I., CHEN, X. & MIFFLIN, R. C. 2011. Mesenchymal cells of the intestinal lamina propria. *Annu Rev Physiol*, 73, 213-37.
- QI, M. C., HU, J., ZOU, S. J., CHEN, H. Q., ZHOU, H. X. & HAN, L. C. 2008. Mechanical strain induces osteogenic differentiation: Cbfa1 and Ets-1 expression in stretched rat mesenchymal stem cells. *Int J Oral Maxillofac Surg*, 37, 453-8.

References

- QIAN, J., ITO, S., SATOH, J., GENG, H., TANAKA, K., HATTORI, S., KOJIMA, K., TAKITA, T. & YASUKAWA, K. 2017. The cleavage site preference of the porcine pepsin on the N-terminal alpha1 chain of bovine type I collagen: a focal analysis with mass spectrometry. *Biosci Biotechnol Biochem*, 81, 514-522.
- QIU, Y., LEI, J., KOOB, T. J. & TEMENOFF, J. S. 2016. Cyclic tension promotes fibroblastic differentiation of human MSCs cultured on collagen-fibre scaffolds. *J Tissue Eng Regen Med*, 10, 989-999.
- RADA, J. A., CORNUET, P. K. & HASSELL, J. R. 1993. Regulation of corneal collagen fibrillogenesis in vitro by corneal proteoglycan (lumican and decorin) core proteins. *Exp Eye Res*, 56, 635-48.
- RADA, T., REIS, R. L. & GOMES, M. E. 2009. Adipose tissue-derived stem cells and their application in bone and cartilage tissue engineering. *Tissue Eng Part B Rev*, 15, 113-25.
- RAIF EL, M. & SEEDHOM, B. B. 2005. Effect of cyclic tensile strain on proliferation of synovial cells seeded onto synthetic ligament scaffolds--an in vitro simulation. *Bone*, 36, 433-43.
- RAIMONDI, M. T., LAGANA, M., CONCI, C., CRESTANI, M., DI GIANCAMILLO, A., GERVASO, F., DEPONTI, D., BOSCHETTI, F., NAVA, M. M., SCANDONE, C., DOMENEGHINI, C., SANNINO, A. & PERETTI, G. M. 2018. Development and biological validation of a cyclic stretch culture system for the ex vivo engineering of tendons. *Int J Artif Organs*, 41, 400-412.
- RALSTON, S. H. 2017. Bone structure and metabolism. *Medicine*, 45, 560-564.
- RAMCHANDRAN, R., DHANABAL, M., VOLK, R., WATERMAN, M. J., SEGAL, M., LU, H., KNEBELMANN, B. & SUKHATME, V. P. 1999. Antiangiogenic activity of restin, NC10 domain of human collagen XV: comparison to endostatin. *Biochem Biophys Res Commun*, 255, 735-9.
- RAMESH, N., MORATTI, S. C. & DIAS, G. J. 2018. Hydroxyapatite-polymer biocomposites for bone regeneration: A review of current trends. *J Biomed Mater Res B Appl Biomater*, 106, 2046-2057.
- RAMSHAW, J. A., SHAH, N. K. & BRODSKY, B. 1998. Gly-X-Y tripeptide frequencies in collagen: a context for host-guest triple-helical peptides. *J Struct Biol*, 122, 86-91.
- RASI, K., HURSKAINEN, M., KALLIO, M., STAVEN, S., SORMUNEN, R., HEAPE, A. M., AVILA, R. L., KIRSCHNER, D., MUONA, A., TOLONEN, U., TANILA, H., HUHTALA, P., SOININEN, R. & PIHLAJANIEMI, T. 2010. Lack of collagen XV impairs peripheral nerve maturation and, when combined with laminin-411 deficiency, leads to basement membrane abnormalities and sensorimotor dysfunction. *J Neurosci*, 30, 14490-501.
- RATH, B., NAM, J., KNOBLOCH, T. J., LANNUTTI, J. J. & AGARWAL, S. 2008. Compressive forces induce osteogenic gene expression in calvarial osteoblasts. *J Biomech*, 41, 1095-103.
- RAVELING, A. R., THEODOSSIOU, S. K. & SCHIELE, N. R. 2018. A 3D printed mechanical bioreactor for investigating mechanobiology and soft tissue mechanics. *Methodsx*, 5, 924-932.
- RCORETEAM. 2020. *R: A language and environment for statistical computing* [Online]. Vienna: Foundation for Statistical Computing. Available: <https://www.R-project.org/> [Accessed 2020].
- REDMAN, S. N., OLDFIELD, S. F. & ARCHER, C. W. 2005. Current strategies for articular cartilage repair. *Eur Cell Mater*, 9, 23-32; discussion 23-32.
- REES, S. G., DAVIES, J. R., TUDOR, D., FLANNERY, C. R., HUGHES, C. E., DENT, C. M. & CATERSON, B. 2002. Immunolocalisation and expression of proteoglycan 4 (cartilage superficial zone proteoglycan) in tendon. *Matrix Biol*, 21, 593-602.
- REES, S. G., FLANNERY, C. R., LITTLE, C. B., HUGHES, C. E., CATERSON, B. & DENT, C. M. 2000. Catabolism of aggrecan, decorin and biglycan in tendon. *Biochem J*, 350 Pt 1, 181-8.
- REES, S. G., WAGGETT, A. D., KERR, B. C., PROBERT, J., GEALY, E. C., DENT, C. M., CATERSON, B. & HUGHES, C. E. 2009. Immunolocalisation and expression of keratan in tendon. *Osteoarthritis Cartilage*, 17, 276-9.
- REHN, M., HINTIKKA, E. & PIHLAJANIEMI, T. 1994. Primary structure of the alpha 1 chain of mouse type XVIII collagen, partial structure of the corresponding gene, and comparison of the alpha 1(XVIII) chain with its homologue, the alpha 1(XV) collagen chain. *J Biol Chem*, 269, 13929-35.
- REHN, M. & PIHLAJANIEMI, T. 1994. Alpha 1(XVIII), a collagen chain with frequent interruptions in the collagenous sequence, a distinct tissue distribution, and homology with type XV collagen. *Proc Natl Acad Sci U S A*, 91, 4234-8.
- REING, J. E., BROWN, B. N., DALY, K. A., FREUND, J. M., GILBERT, T. W., HSIONG, S. X., HUBER, A., KULLAS, K. E., TOTTEY, S., WOLF, M. T. & BADYLAK, S. F. 2010. The effects of processing methods upon mechanical and biologic properties of porcine dermal extracellular matrix scaffolds. *Biomaterials*, 31, 8626-33.
- REINWALD, Y., LEONARD, K. H., HENSTOCK, J. R., WHITELEY, J. P., OSBORNE, J. M., WATERS, S. L., LEVESQUE, P. & EL HAJ, A. J. 2015. Evaluation of the growth environment of a hydrostatic force bioreactor for preconditioning of tissue-engineered constructs. *Tissue Eng Part C Methods*, 21, 1-14.
- RESPONTE, D. J., LEE, J. K., HU, J. C. & ATHANASIOU, K. A. 2012. Biomechanics-driven chondrogenesis: from embryo to adult. *FASEB J*, 26, 3614-24.
- RHEE, D. K., MARCELINO, J., BAKER, M., GONG, Y., SMITS, P., LEFEBVRE, V., JAY, G. D., STEWART, M., WANG, H., WARMAN, M. L. & CARPTEN, J. D. 2005. The secreted glycoprotein lubricin protects cartilage surfaces and inhibits synovial cell overgrowth. *J Clin Invest*, 115, 622-31.
- RIBITSCH, I., GUELTEKIN, S., KEITH, M. F., MINICHMAIR, K., PEHAM, C., JENNER, F. & EGERBACHER, M. 2020. Age-related changes of tendon fibril micro-morphology and gene expression. *J Anat*, 236, 688-700.
- RICARD-BLUM, S. 2011. The collagen family. *Cold Spring Harb Perspect Biol*, 3, a004978.

References

- RICE, R. H. 2011. Proteomic analysis of hair shaft and nail plate. *J Cosmet Sci*, 62, 229-36.
- RILEY, G. P., HARRALL, R. L., CONSTANT, C. R., CHARD, M. D., CAWSTON, T. E. & HAZLEMAN, B. L. 1994. Tendon degeneration and chronic shoulder pain: changes in the collagen composition of the human rotator cuff tendons in rotator cuff tendinitis. *Ann Rheum Dis*, 53, 359-66.
- ROBERT, L., MOCZAR, M. & ROBERT, M. 1974. Biogenesis, maturation and aging of elastic tissue. *Experientia*, 30, 211-2.
- ROBERTSSON, O., STEFANSDOTTIR, A., LIDGREN, L. & RANSTAM, J. 2007. Increased long-term mortality in patients less than 55 years old who have undergone knee replacement for osteoarthritis: results from the Swedish Knee Arthroplasty Register. *J Bone Joint Surg Br*, 89, 599-603.
- ROBINSON, K. A., SUN, M., BARNUM, C. E., WEISS, S. N., HUEGEL, J., SHETYE, S. S., LIN, L., SAEZ, D., ADAMS, S. M., IOZZO, R. V., SOSLOWSKY, L. J. & BIRK, D. E. 2017. Decorin and biglycan are necessary for maintaining collagen fibril structure, fiber realignment, and mechanical properties of mature tendons. *Matrix Biol*, 64, 81-93.
- ROBUBI, A., BERGER, C., SCHMID, M., HUBER, K. R., ENGEL, A. & KRUGLUGER, W. 2014. Gene expression profiles induced by growth factors in in vitro cultured osteoblasts. *Bone Joint Res*, 3, 236-40.
- RODAN, G. A. & MARTIN, T. J. 1981. Role of osteoblasts in hormonal control of bone resorption--a hypothesis. *Calcif Tissue Int*, 33, 349-51.
- RONALDSON, K. & VUNJAK-NOVAKOVIC, G. 2016. Microgravity and Microgravity Analogue Studies of Cartilage and Cardiac Tissue Engineering. *Effect of Spaceflight and Spaceflight Analogue Culture on Human and Microbial Cells*. Springer.
- RONZIERE, M. C., PERRIER, E., MALLEIN-GERIN, F. & FREYRIA, A. M. 2010. Chondrogenic potential of bone marrow- and adipose tissue-derived adult human mesenchymal stem cells. *Biomed Mater Eng*, 20, 145-58.
- ROSSET, E. M. & BRADSHAW, A. D. 2016. SPARC/osteonectin in mineralized tissue. *Matrix Biol*, 52-54, 78-87.
- RUBIN, J., MURPHY, T. C., FAN, X., GOLDSCHMIDT, M. & TAYLOR, W. R. 2002. Activation of extracellular signal-regulated kinase is involved in mechanical strain inhibition of RANKL expression in bone stromal cells. *J Bone Miner Res*, 17, 1452-60.
- RUHLAND, C., SCHONHERR, E., ROBENEK, H., HANSEN, U., IOZZO, R. V., BRUCKNER, P. & SEIDLER, D. G. 2007. The glycosaminoglycan chain of decorin plays an important role in collagen fibril formation at the early stages of fibrillogenesis. *FEBS J*, 274, 4246-55.
- RUI, Y. F., LUI, P. P., NI, M., CHAN, L. S., LEE, Y. W. & CHAN, K. M. 2011. Mechanical loading increased BMP-2 expression which promoted osteogenic differentiation of tendon-derived stem cells. *J Orthop Res*, 29, 390-6.
- SAADA, J. I., PINCHUK, I. V., BARRERA, C. A., ADEGBOYEGA, P. A., SUAREZ, G., MIFFLIN, R. C., DI MARI, J. F., REYES, V. E. & POWELL, D. W. 2006. Subepithelial myofibroblasts are novel nonprofessional APCs in the human colonic mucosa. *J Immunol*, 177, 5968-79.
- SAARELA, J., REHN, M., OIKARINEN, A., AUTIO-HARMAINEN, H. & PIHLAJANIEMI, T. 1998. The short and long forms of type XVIII collagen show clear tissue specificities in their expression and location in basement membrane zones in humans. *Am J Pathol*, 153, 611-26.
- SABATELLI, P., GARA, S. K., GRUMATI, P., URCIUOLO, A., GUALANDI, F., CURCI, R., SQUARZONI, S., ZAMPARELLI, A., MARTONI, E., MERLINI, L., PAULSSON, M., BONALDO, P. & WAGENER, R. 2011. Expression of the collagen VI alpha5 and alpha6 chains in normal human skin and in skin of patients with collagen VI-related myopathies. *J Invest Dermatol*, 131, 99-107.
- SAHA, A., ROLFE, R., CARROLL, S., KELLY, D. J. & MURPHY, P. 2017. Chondrogenesis of embryonic limb bud cells in micromass culture progresses rapidly to hypertrophy and is modulated by hydrostatic pressure. *Cell Tissue Res*, 368, 47-59.
- SAITO, K., CHEN, M., BARD, F., CHEN, S., ZHOU, H., WOODLEY, D., POLISCHUK, R., SCHEKMAN, R. & MALHOTRA, V. 2009. TANGO1 facilitates cargo loading at endoplasmic reticulum exit sites. *Cell*, 136, 891-902.
- SAITO, K., YAMASHIRO, K., ICHIKAWA, Y., ERLMANN, P., KONTANI, K., MALHOTRA, V. & KATADA, T. 2011. cTAGE5 mediates collagen secretion through interaction with TANGO1 at endoplasmic reticulum exit sites. *Mol Biol Cell*, 22, 2301-8.
- SAKAGUCHI, Y., SEKIYA, I., YAGISHITA, K. & MUNETA, T. 2005. Comparison of human stem cells derived from various mesenchymal tissues: superiority of synovium as a cell source. *Arthritis Rheum*, 52, 2521-9.
- SAKAI, L. Y., KEENE, D. R., MORRIS, N. P. & BURGESSON, R. E. 1986. Type VII collagen is a major structural component of anchoring fibrils. *J Cell Biol*, 103, 1577-86.
- SAKAI, S., MISHIMA, H., ISHII, T., AKAOGI, H., YOSHIOKA, T., OHYABU, Y., CHANG, F., OCHIAI, N. & UEMURA, T. 2009. Rotating three-dimensional dynamic culture of adult human bone marrow-derived cells for tissue engineering of hyaline cartilage. *J Orthop Res*, 27, 517-21.
- SAKAI, T., LARSEN, M. & YAMADA, K. M. 2003. Fibronectin requirement in branching morphogenesis. *Nature*, 423, 876-81.
- SAKAO, K., TAKAHASHI, K. A., ARAI, Y., INOUE, A., TONOMURA, H., SAITO, M., YAMAMOTO, T., KANAMURA, N., IMANISHI, J., MAZDA, O. & KUBO, T. 2008. Induction of chondrogenic phenotype in synovium-derived progenitor cells by intermittent hydrostatic pressure. *Osteoarthritis Cartilage*, 16, 805-14.

References

- SALDIN, L. T., CRAMER, M. C., VELANKAR, S. S., WHITE, L. J. & BADYLAK, S. F. 2017. Extracellular matrix hydrogels from decellularized tissues: Structure and function. *Acta Biomater*, 49, 1-15.
- SALO, J., LEHENKARI, P., MULARI, M., METSIKKO, K. & VAANANEN, H. K. 1997. Removal of osteoclast bone resorption products by transcytosis. *Science*, 276, 270-3.
- SAMIRIC, T., ILIC, M. Z. & HANDLEY, C. J. 2004a. Characterisation of proteoglycans and their catabolic products in tendon and explant cultures of tendon. *Matrix Biol*, 23, 127-40.
- SAMIRIC, T., ILIC, M. Z. & HANDLEY, C. J. 2004b. Large aggregating and small leucine-rich proteoglycans are degraded by different pathways and at different rates in tendon. *Eur J Biochem*, 271, 3612-20.
- SANTOS, A. J., RAOTE, I., SCARPA, M., BROUWERS, N. & MALHOTRA, V. 2015. TANGO1 recruits ERGIC membranes to the endoplasmic reticulum for procollagen export. *Elife*, 4.
- SARASA-RENEADO, A. & CHIQUET, M. 2005. Mechanical signals regulating extracellular matrix gene expression in fibroblasts. *Scand J Med Sci Sports*, 15, 223-30.
- SASAI, Y., EIRAKU, M. & SUGA, H. 2012. In vitro organogenesis in three dimensions: self-organising stem cells. *Development*, 139, 4111-4121.
- SASAKI, T., FUKAI, N., MANN, K., GOHRING, W., OLSEN, B. R. & TIMPL, R. 1998. Structure, function and tissue forms of the C-terminal globular domain of collagen XVIII containing the angiogenesis inhibitor endostatin. *EMBO J*, 17, 4249-56.
- SASAKI, T., LARSSON, H., KREUGER, J., SALMIVIRTA, M., CLAESSION-WELSH, L., LINDAHL, U., HOHENESTER, E. & TIMPL, R. 1999. Structural basis and potential role of heparin/heparan sulfate binding to the angiogenesis inhibitor endostatin. *EMBO J*, 18, 6240-8.
- SASAKI, T., LARSSON, H., TISI, D., CLAESSION-WELSH, L., HOHENESTER, E. & TIMPL, R. 2000. Endostatins derived from collagens XV and XVIII differ in structural and binding properties, tissue distribution and anti-angiogenic activity. *J Mol Biol*, 301, 1179-90.
- SATO, K., YOMOIGIDA, K., WADA, T., YORIHUZI, T., NISHIMUNE, Y., HOSOKAWA, N. & NAGATA, K. 2002. Type XXVI collagen, a new member of the collagen family, is specifically expressed in the testis and ovary. *J Biol Chem*, 277, 37678-84.
- SATOH, M., HIRAYOSHI, K., YOKOTA, S., HOSOKAWA, N. & NAGATA, K. 1996. Intracellular interaction of collagen-specific stress protein HSP47 with newly synthesized procollagen. *J Cell Biol*, 133, 469-83.
- SCHAEFER, L., BABELOVA, A., KISS, E., HAUSSER, H. J., BALIOVA, M., KRZYZANKOVA, M., MARSCHE, G., YOUNG, M. F., MIHALIK, D., GOTTE, M., MALLE, E., SCHAEFER, R. M. & GRONE, H. J. 2005. The matrix component biglycan is proinflammatory and signals through Toll-like receptors 4 and 2 in macrophages. *J Clin Invest*, 115, 2223-33.
- SCHEGG, B., HULSMIEIER, A. J., RUTSCHMANN, C., MAAG, C. & HENNET, T. 2009. Core glycosylation of collagen is initiated by two beta(1-O)galactosyltransferases. *Mol Cell Biol*, 29, 943-52.
- SCHINDELIN, J., ARGANDA-CARRERAS, I., FRISE, E., KAYNIG, V., LONGAIR, M., PIETZSCH, T., PREIBISCH, S., RUEDEN, C., SAALFELD, S., SCHMID, B., TINEVEZ, J. Y., WHITE, D. J., HARTENSTEIN, V., ELICEIRI, K., TOMANCAK, P. & CARDONA, A. 2012. Fiji: an open-source platform for biological-image analysis. *Nat Methods*, 9, 676-82.
- SCHLESINGER, P. H., BLAIR, H. C., TEITELBAUM, S. L. & EDWARDS, J. C. 1997. Characterization of the osteoclast ruffled border chloride channel and its role in bone resorption. *J Biol Chem*, 272, 18636-43.
- SCHNEIDER, G. B., ZAHARIAS, R. & STANFORD, C. 2001. Osteoblast integrin adhesion and signaling regulate mineralization. *J Dent Res*, 80, 1540-4.
- SCHWARTZ, M. A. 2010. Integrins and extracellular matrix in mechanotransduction. *Cold Spring Harb Perspect Biol*, 2, a005066.
- SCHWARTZ, M. A. & DESIMONE, D. W. 2008. Cell adhesion receptors in mechanotransduction. *Curr Opin Cell Biol*, 20, 551-6.
- SCHWARZ, R. P., GOODWIN, T. J. & WOLF, D. A. 1992. Cell culture for three-dimensional modeling in rotating-wall vessels: an application of simulated microgravity. *J Tissue Cult Methods*, 14, 51-7.
- SCOTT, I. C., BLITZ, I. L., PAPPANO, W. N., IMAMURA, Y., CLARK, T. G., STEIGLITZ, B. M., THOMAS, C. L., MAAS, S. A., TAKAHARA, K., CHO, K. W. & GREENSPAN, D. S. 1999. Mammalian BMP-1/Tolloid-related metalloproteinases, including novel family member mammalian Tolloid-like 2, have differential enzymatic activities and distributions of expression relevant to patterning and skeletogenesis. *Dev Biol*, 213, 283-300.
- SCREEN, H., SETO, J., KRAUSS, S., BOESECKE, P. & GUPTA, H. 2011. Extrafibrillar diffusion and intrafibrillar swelling at the nanoscale are associated with stress relaxation in the soft collagenous matrix tissue of tendons. *Soft Matter*, 7, 11243-11251.
- SCREEN, H. R. 2009. Hierarchical approaches to understanding tendon mechanics. *Journal of Biomechanical Science and Engineering*, 4, 481-499.
- SCREEN, H. R., BERK, D. E., KADLER, K. E., RAMIREZ, F. & YOUNG, M. F. 2015. Tendon functional extracellular matrix. *J Orthop Res*, 33, 793-9.
- SCREEN, H. R., LEE, D. A., BADER, D. L. & SHELTON, J. C. 2004. An investigation into the effects of the hierarchical structure of tendon fascicles on micromechanical properties. *Proc Inst Mech Eng H*, 218, 109-19.

References

- SEET, L. F., TOH, L. Z., CHU, S. W. L., FINGER, S. N., CHUA, J. L. L. & WONG, T. T. 2017. Upregulation of distinct collagen transcripts in post-surgery scar tissue: a study of conjunctival fibrosis. *Dis Model Mech*, 10, 751-760.
- SEGEV, F., HEON, E., COLE, W. G., WENSTRUP, R. J., YOUNG, F., SLOMOVIC, A. R., ROOTMAN, D. S., WHITAKER-MENEZES, D., CHERVONEVA, I. & BIRK, D. E. 2006. Structural abnormalities of the cornea and lid resulting from collagen V mutations. *Invest Ophthalmol Vis Sci*, 47, 565-73.
- SEIF-NARAGHI, S. B., SINGELYN, J. M., SALVATORE, M. A., OSBORN, K. G., WANG, J. J., SAMPAT, U., KWAN, O. L., STRACHAN, G. M., WONG, J. & SCHUP-MAGOFFIN, P. J. 2013. Safety and efficacy of an injectable extracellular matrix hydrogel for treating myocardial infarction. *Science translational medicine*, 5, 173ra25-173ra25.
- SEIL, R., LITZENBURGER, H., KOHN, D. & RUPP, S. 2006. Arthroscopic treatment of chronically painful calcifying tendinitis of the supraspinatus tendon. *Arthroscopy*, 22, 521-7.
- SEN, B., XIE, Z., CASE, N., MA, M., RUBIN, C. & RUBIN, J. 2008. Mechanical strain inhibits adipogenesis in mesenchymal stem cells by stimulating a durable beta-catenin signal. *Endocrinology*, 149, 6065-75.
- SENSINI, A., CRISTOFOLINI, L., ZUCHELLI, A., FOCARETE, M. L., GUALANDI, C., A, D. E. M., KAO, A. P., ROLDO, M., BLUNN, G. & TOZZI, G. 2019. Hierarchical electrospun tendon-ligament bioinspired scaffolds induce changes in fibroblasts morphology under static and dynamic conditions. *J Microsc*.
- SHAPIRO, I. M., ADAMS, C. S., FREEMAN, T. & SRINIVAS, V. 2005. Fate of the hypertrophic chondrocyte: microenvironmental perspectives on apoptosis and survival in the epiphyseal growth plate. *Birth Defects Res C Embryo Today*, 75, 330-9.
- SHARIFI, N. & GHARRAVI, A. M. 2019. Shear bioreactors stimulating chondrocyte regeneration, a systematic review. *Inflamm Regen*, 39, 16.
- SHARMA, P. & MAFFULLI, N. 2006. Biology of tendon injury: healing, modeling and remodeling. *J Musculoskeletal Neuronal Interact*, 6, 181-90.
- SHAW, L. M. & OLSEN, B. R. 1991. FACIT collagens: diverse molecular bridges in extracellular matrices. *Trends Biochem Sci*, 16, 191-4.
- SHEN, G. 2005. The role of type X collagen in facilitating and regulating endochondral ossification of articular cartilage. *Orthod Craniofac Res*, 8, 11-7.
- SHEPHERD, J. H. & SCREEN, H. R. 2013. Fatigue loading of tendon. *Int J Exp Pathol*, 94, 260-70.
- SHERWIN, A. F., CARTER, D. H., POOLE, C. A., HOYLAND, J. A. & AYAD, S. 1999. The distribution of type VI collagen in the developing tissues of the bovine femoral head. *Histochem J*, 31, 623-32.
- SHI, G. X., ZHENG, X. F., ZHU, C., LI, B., WANG, Y. R., JIANG, S. D. & JIANG, L. S. 2017. Evidence of the Role of R-Spondin 1 and Its Receptor Lgr4 in the Transmission of Mechanical Stimuli to Biological Signals for Bone Formation. *Int J Mol Sci*, 18.
- SHIMIZU, T., TANAKA, T., ISO, T., MATSUI, H., OYOYAMA, Y., KAWAI-KOWASE, K., ARAI, M. & KURABAYASHI, M. 2011. Notch signaling pathway enhances bone morphogenetic protein 2 (BMP2) responsiveness of Msx2 gene to induce osteogenic differentiation and mineralization of vascular smooth muscle cells. *J Biol Chem*, 286, 19138-48.
- SHIMOKOMAKI, M., WRIGHT, D. W., IRWIN, M. H., VAN DER REST, M. & MAYNE, R. 1990. The structure and macromolecular organization of type IX collagen in cartilage. *Ann N Y Acad Sci*, 580, 1-7.
- SHORT, A. R., CZEISLER, C., STOCKER, B., COLE, S., OTERO, J. J. & WINTER, J. O. 2017. Imaging Cell-Matrix Interactions in 3D Collagen Hydrogel Culture Systems. *Macromol Biosci*, 17.
- SHOULDERS, M. D., GUZEI, I. A. & RAINES, R. T. 2008. 4-chloroprolines: synthesis, conformational analysis, and effect on the collagen triple helix. *Biopolymers*, 89, 443-54.
- SHOULDERS, M. D. & RAINES, R. T. 2009. Collagen structure and stability. *Annu Rev Biochem*, 78, 929-58.
- SIKAVITSAS, V. I., BANCROFT, G. N., LEMOINE, J. J., LIEBSCHNER, M. A., DAUNER, M. & MIKOS, A. G. 2005. Flow perfusion enhances the calcified matrix deposition of marrow stromal cells in biodegradable nonwoven fiber mesh scaffolds. *Ann Biomed Eng*, 33, 63-70.
- SIMMONS, C. A., MATLIS, S., THORNTON, A. J., CHEN, S., WANG, C. Y. & MOONEY, D. J. 2003. Cyclic strain enhances matrix mineralization by adult human mesenchymal stem cells via the extracellular signal-regulated kinase (ERK1/2) signaling pathway. *J Biomech*, 36, 1087-96.
- SINGH, A., GILL, G., KAUR, H., AMHMED, M. & JAKHU, H. 2018. Role of osteopontin in bone remodeling and orthodontic tooth movement: a review. *Prog Orthod*, 19, 18.
- SMITH, R. K., BIRCH, H., PATTERSON-KANE, J., FIRTH, E. C., WILLIAMS, L., CHERDCHUTHAM, W., VAN WEEREN, W. R. & GOODSHIP, A. E. 1999. Should equine athletes commence training during skeletal development?: changes in tendon matrix associated with development, ageing, function and exercise. *Equine Vet J Suppl*, 201-9.
- SMITH, R. L., RUSK, S. F., ELLISON, B. E., WESSELLS, P., TSUCHIYA, K., CARTER, D. R., CALER, W. E., SANDELL, L. J. & SCHURMAN, D. J. 1996. In vitro stimulation of articular chondrocyte mRNA and extracellular matrix synthesis by hydrostatic pressure. *J Orthop Res*, 14, 53-60.
- SOHN, H. S. & OH, J. K. 2019. Review of bone graft and bone substitutes with an emphasis on fracture surgeries. *Biomater Res*, 23, 9.

References

- SOLCHAGA, L. A., PENICK, K., GOLDBERG, V. M., CAPLAN, A. I. & WELTER, J. F. 2010. Fibroblast growth factor-2 enhances proliferation and delays loss of chondrogenic potential in human adult bone-marrow-derived mesenchymal stem cells. *Tissue Eng Part A*, 16, 1009-19.
- SOLCHAGA, L. A., PENICK, K., PORTER, J. D., GOLDBERG, V. M., CAPLAN, A. I. & WELTER, J. F. 2005. FGF-2 enhances the mitotic and chondrogenic potentials of human adult bone marrow-derived mesenchymal stem cells. *J Cell Physiol*, 203, 398-409.
- SOMMERFELDT, D. W. & RUBIN, C. T. 2001. Biology of bone and how it orchestrates the form and function of the skeleton. *Eur Spine J*, 10 Suppl 2, S86-95.
- SOMOZA, R. A., WELTER, J. F., CORREA, D. & CAPLAN, A. I. 2014. Chondrogenic differentiation of mesenchymal stem cells: challenges and unfulfilled expectations. *Tissue Eng Part B Rev*, 20, 596-608.
- SOPHIA FOX, A. J., BEDI, A. & RODEO, S. A. 2009. The basic science of articular cartilage: structure, composition, and function. *Sports Health*, 1, 461-8.
- SOUCACOS, P. N., DAILIANA, Z., BERIS, A. E. & JOHNSON, E. O. 2006. Vascularised bone grafts for the management of non-union. *Injury*, 37 Suppl 1, S41-50.
- SOYSA, N. S. & ALLES, N. 2016. Osteoclast function and bone-resorbing activity: An overview. *Biochem Biophys Res Commun*, 476, 115-20.
- SPINELLA-JAEGLE, S., RAWADI, G., KAWAI, S., GALLEA, S., FAUCHEU, C., MOLLAT, P., COURTOIS, B., BERGAUD, B., RAMEZ, V., BLANCHET, A. M., ADELMANT, G., BARON, R. & ROMAN-ROMAN, S. 2001. Sonic hedgehog increases the commitment of pluripotent mesenchymal cells into the osteoblastic lineage and abolishes adipocytic differentiation. *J Cell Sci*, 114, 2085-94.
- STARBORG, T., KALSON, N. S., LU, Y., MIRONOV, A., COOTES, T. F., HOLMES, D. F. & KADLER, K. E. 2013. Using transmission electron microscopy and 3View to determine collagen fibril size and three-dimensional organization. *Nat Protoc*, 8, 1433-48.
- STAVENSCHI, E., CORRIGAN, M. A., JOHNSON, G. P., RIFFAULT, M. & HOEY, D. A. 2018. Physiological cyclic hydrostatic pressure induces osteogenic lineage commitment of human bone marrow stem cells: a systematic study. *Stem Cell Res Ther*, 9, 276.
- STEADMAN, J. R., RODKEY, W. G., BRIGGS, K. K. & RODRIGO, J. J. 1999. [The microfracture technic in the management of complete cartilage defects in the knee joint]. *Orthopade*, 28, 26-32.
- STEINLE, P. 2016. Characterization of emissions from a desktop 3D printer and indoor air measurements in office settings. *J Occup Environ Hyg*, 13, 121-32.
- STENBECK, G. & HORTON, M. A. 2004. Endocytic trafficking in actively resorbing osteoclasts. *J Cell Sci*, 117, 827-36.
- STEPHAN, S., SHERRATT, M. J., HODSON, N., SHUTTLEWORTH, C. A. & KIELTY, C. M. 2004. Expression and supramolecular assembly of recombinant alpha1(viii) and alpha2(viii) collagen homotrimers. *J Biol Chem*, 279, 21469-77.
- STEWART, A. J. & KELLY, D. J. 2015. Mechanical regulation of mesenchymal stem cell differentiation. *J Anat*, 227, 717-31.
- STEWART, A. J., KELLY, D. J. & WAGNER, D. R. 2014. The role of calcium signalling in the chondrogenic response of mesenchymal stem cells to hydrostatic pressure. *Eur Cell Mater*, 28, 358-71.
- STOCKWELL, R. A. 1971. The interrelationship of cell density and cartilage thickness in mammalian articular cartilage. *J Anat*, 109, 411-21.
- STRICKER, S., FUNDELE, R., VORTKAMP, A. & MUNDLOS, S. 2002. Role of Runx genes in chondrocyte differentiation. *Dev Biol*, 245, 95-108.
- STRIOGA, M., VISWANATHAN, S., DARINSKAS, A., SLABY, O. & MICHALEK, J. 2012. Same or not the same? Comparison of adipose tissue-derived versus bone marrow-derived mesenchymal stem and stromal cells. *Stem Cells Dev*, 21, 2724-52.
- SUBRAMANIAN, G., STASUK, A., ELSAADANY, M. & YILDIRIM-AYAN, E. 2017. Effect of Uniaxial Tensile Cyclic Loading Regimes on Matrix Organization and Tenogenic Differentiation of Adipose-Derived Stem Cells Encapsulated within 3D Collagen Scaffolds. *Stem Cells Int*, 2017, 6072406.
- SUDA, T., TAKAHASHI, N., UDAGAWA, N., JIMI, E., GILLESPIE, M. T. & MARTIN, T. J. 1999. Modulation of osteoclast differentiation and function by the new members of the tumor necrosis factor receptor and ligand families. *Endocr Rev*, 20, 345-57.
- SUGIMOTO, A., MIYAZAKI, A., KAWARABAYASHI, K., SHONO, M., AKAZAWA, Y., HASEGAWA, T., UEDA-YAMAGUCHI, K., KITAMURA, T., YOSHIZAKI, K., FUKUMOTO, S. & IWAMOTO, T. 2017. Piezo type mechanosensitive ion channel component 1 functions as a regulator of the cell fate determination of mesenchymal stem cells. *Sci Rep*, 7, 17696.
- SUMANASINGHE, R. D., BERNACKI, S. H. & LOBOA, E. G. 2006. Osteogenic differentiation of human mesenchymal stem cells in collagen matrices: effect of uniaxial cyclic tensile strain on bone morphogenetic protein (BMP-2) mRNA expression. *Tissue Eng*, 12, 3459-65.
- SUN, M., CONNIZZO, B. K., ADAMS, S. M., FREEDMAN, B. R., WENSTRUP, R. J., SOSLOWSKY, L. J. & BIRK, D. E. 2015. Targeted deletion of collagen V in tendons and ligaments results in a classic Ehlers-Danlos syndrome joint phenotype. *Am J Pathol*, 185, 1436-47.

References

- SUN, S., GENOVESE, F. & KARSDAL, M. 2019. Type VI collagen. *Biochemistry of Collagens, Laminins and elastin*. Elsevier.
- SUND, M., VAISANEN, T., KAUKINEN, S., ILVES, M., TU, H., AUTIO-HARMAINEN, H., RAUVALA, H. & PIHLAJANIEMI, T. 2001. Distinct expression of type XIII collagen in neuronal structures and other tissues during mouse development. *Matrix Biol*, 20, 215-31.
- SUTMULLER, M., BRUIJN, J. A. & DE HEER, E. 1997. Collagen types VIII and X, two non-fibrillar, short-chain collagens. Structure homologies, functions and involvement in pathology. *Histol Histopathol*, 12, 557-66.
- SVEC, D., TICHOPAD, A., NOVOSADOVA, V., PFAFFL, M. W. & KUBISTA, M. 2015. How good is a PCR efficiency estimate: Recommendations for precise and robust qPCR efficiency assessments. *Biomol Detect Quantif*, 3, 9-16.
- TALÒ, G., D'ARRIGO, D., LORENZI, S., MORETTI, M. & LOVATI, A. B. 2020. Independent, Controllable Stretch-Perfusion Bioreactor Chambers to Functionalize Cell-Seeded Decellularized Tendons. *Annals of Biomedical Engineering*, 48, 1112-1126.
- TANAKA, T., WAKABAYASHI, T., OIZUMI, H., NISHIO, S., SATO, T., HARADA, A., FUJII, D., MATSUO, Y., HASHIMOTO, T. & IWATSUBO, T. 2014. CLAC-P/collagen type XXV is required for the intramuscular innervation of motoneurons during neuromuscular development. *J Neurosci*, 34, 1370-9.
- TEITELBAUM, S. L. 2000. Bone resorption by osteoclasts. *Science*, 289, 1504-8.
- TEITELBAUM, S. L. & ROSS, F. P. 2003. Genetic regulation of osteoclast development and function. *Nat Rev Genet*, 4, 638-49.
- TEN DIJKE, P. & ARTHUR, H. M. 2007. Extracellular control of TGFbeta signalling in vascular development and disease. *Nat Rev Mol Cell Biol*, 8, 857-69.
- TETI, A., BLAIR, H. C., TEITELBAUM, S. L., KAHN, A. J., KOZIOL, C., KONSEK, J., ZAMBONIN-ZALLONE, A. & SCHLESINGER, P. H. 1989. Cytoplasmic pH regulation and chloride/bicarbonate exchange in avian osteoclasts. *J Clin Invest*, 83, 227-33.
- THEOBALD, P., BENJAMIN, M., NOKES, L. & PUGH, N. 2005. Review of the vascularisation of the human Achilles tendon. *Injury*, 36, 1267-72.
- THORPE, C. T., BIRCH, H. L., CLEGG, P. D. & SCREEN, H. R. 2013. The role of the non-collagenous matrix in tendon function. *Int J Exp Pathol*, 94, 248-59.
- THORPE, C. T., CLEGG, P. D. & BIRCH, H. L. 2010. A review of tendon injury: why is the equine superficial digital flexor tendon most at risk? *Equine Vet J*, 42, 174-80.
- THORPE, C. T., GODINHO, M. S. C., RILEY, G. P., BIRCH, H. L., CLEGG, P. D. & SCREEN, H. R. C. 2015. The interfascicular matrix enables fascicle sliding and recovery in tendon, and behaves more elastically in energy storing tendons. *J Mech Behav Biomed Mater*, 52, 85-94.
- THORPE, C. T., RILEY, G. P., BIRCH, H. L., CLEGG, P. D. & SCREEN, H. R. 2014. Effect of fatigue loading on structure and functional behaviour of fascicles from energy-storing tendons. *Acta Biomater*, 10, 3217-24.
- TILLGREN, V., ONNERFJORD, P., HAGLUND, L. & HEINEGARD, D. 2009. The tyrosine sulfate-rich domains of the LRR proteins fibromodulin and osteoadherin bind motifs of basic clusters in a variety of heparin-binding proteins, including bioactive factors. *J Biol Chem*, 284, 28543-53.
- TIMPL, R. & BROWN, J. C. 1996. Supramolecular assembly of basement membranes. *Bioessays*, 18, 123-32.
- TIMPL, R., WIEDEMANN, H., VAN DELDEN, V., FURTHMAYR, H. & KUHN, K. 1981. A network model for the organization of type IV collagen molecules in basement membranes. *Eur J Biochem*, 120, 203-11.
- TOHIDNEZHAD, M., ZANDER, J., SLOWIK, A., KUBO, Y., DURSUN, G., WILLENBERG, W., ZENDEDEL, A., KWEIDER, N., STOFFEL, M. & PUFE, T. 2020. Impact of Uniaxial Stretching on Both Gliding and Traction Areas of Tendon Explants in a Novel Bioreactor. *Int J Mol Sci*, 21.
- TOMOAIA, G. & PASCA, R. D. 2015. On the Collagen Mineralization. A Review. *Clujul Med*, 88, 15-22.
- TSE, J. R. & ENGLER, A. J. 2010. Preparation of hydrogel substrates with tunable mechanical properties. *Curr Protoc Cell Biol*, Chapter 10, Unit 10 16.
- TULI, R., TULI, S., NANDI, S., HUANG, X., MANNER, P. A., HOZACK, W. J., DANIELSON, K. G., HALL, D. J. & TUAN, R. S. 2003. Transforming growth factor-beta-mediated chondrogenesis of human mesenchymal progenitor cells involves N-cadherin and mitogen-activated protein kinase and Wnt signaling cross-talk. *J Biol Chem*, 278, 41227-36.
- TWORKOSKI, E., GLUCKSBERG, M. R. & JOHNSON, M. 2018. The effect of the rate of hydrostatic pressure depressurization on cells in culture. *PLoS One*, 13, e0189890.
- TZAPHLIDOU, M. 2005. The role of collagen in bone structure: an image processing approach. *Micron*, 36, 593-601.
- TZAPHLIDOU, M. 2008. Bone architecture: collagen structure and calcium/phosphorus maps. *J Biol Phys*, 34, 39-49.
- UDEZE, C. P., JONES, E. R., RILEY, G. P., MORRISSEY, D. & SCREEN, H. R. C. 2019. An in vitro investigation into the effects of 10 Hz cyclic loading on tenocyte metabolism. *Scand J Med Sci Sports*, 29, 1511-1520.

References

- ULBRICH, C., WESTPHAL, K., PIETSCH, J., WINKLER, H. D., LEDER, A., BAUER, J., KOSSMEHL, P., GROSSE, J., SCHOENBERGER, J., INFANGER, M., EGLI, M. & GRIMM, D. 2010. Characterization of human chondrocytes exposed to simulated microgravity. *Cell Physiol Biochem*, 25, 551-60.
- UNSOLD, C., PAPPANO, W. N., IMAMURA, Y., STEIGLITZ, B. M. & GREENSPAN, D. S. 2002. Biosynthetic processing of the pro-alpha 1(V)2pro-alpha 2(V) collagen heterotrimer by bone morphogenetic protein-1 and furin-like proprotein convertases. *J Biol Chem*, 277, 5596-602.
- VAANANEN, H. K. & HORTON, M. 1995. The osteoclast clear zone is a specialized cell-extracellular matrix adhesion structure. *J Cell Sci*, 108 (Pt 8), 2729-32.
- VAANANEN, H. K., ZHAO, H., MULARI, M. & HALLEEN, J. M. 2000. The cell biology of osteoclast function. *J Cell Sci*, 113 (Pt 3), 377-81.
- VACANTI, J. P. 1988. Beyond transplantation. Third annual Samuel Jason Mixter lecture. *Arch Surg*, 123, 545-9.
- VALCOURT, U., GOUTTENOIRE, J., MOUSTAKAS, A., HERBAGE, D. & MALLEIN-GERIN, F. 2002. Functions of transforming growth factor-beta family type I receptors and Smad proteins in the hypertrophic maturation and osteoblastic differentiation of chondrocytes. *J Biol Chem*, 277, 33545-58.
- VAN HUIZEN, N. A., IJZERMANS, J. N. M., BURGERS, P. C. & LUIDER, T. M. 2019. Collagen analysis with mass spectrometry. *Mass Spectrom Rev*.
- VAN OSCH, G. J., MANDL, E. W., JAHR, H., KOEVOET, W., NOLST-TRENITE, G. & VERHAAR, J. A. 2004. Considerations on the use of ear chondrocytes as donor chondrocytes for cartilage tissue engineering. *Biorheology*, 41, 411-21.
- VANDESOMPELE, J., DE PRETER, K., PATTYN, F., POPPE, B., VAN ROY, N., DE PAEPE, A. & SPELEMAN, F. 2002. Accurate normalization of real-time quantitative RT-PCR data by geometric averaging of multiple internal control genes. *Genome Biol*, 3, RESEARCH0034.
- VAUGHAN, L., MENDLER, M., HUBER, S., BRUCKNER, P., WINTERHALTER, K. H., IRWIN, M. I. & MAYNE, R. 1988. D-periodic distribution of collagen type IX along cartilage fibrils. *J Cell Biol*, 106, 991-7.
- VAUGHAN-THOMAS, A., YOUNG, R. D., PHILLIPS, A. C. & DUANCE, V. C. 2001. Characterization of type XI collagen-glycosaminoglycan interactions. *J Biol Chem*, 276, 5303-9.
- VEIT, G., KOBBE, B., KEENE, D. R., PAULSSON, M., KOCH, M. & WAGENER, R. 2006. Collagen XXVIII, a novel von Willebrand factor A domain-containing protein with many imperfections in the collagenous domain. *J Biol Chem*, 281, 3494-504.
- VIDAL BDE, C. & MELLO, M. L. 2016. FT-IR Microspectroscopy of Rat Ear Cartilage. *PLoS One*, 11, e0151989.
- VINARDELL, T., ROLFE, R. A., BUCKLEY, C. T., MEYER, E. G., AHEARNE, M., MURPHY, P. & KELLY, D. J. 2012. Hydrostatic pressure acts to stabilise a chondrogenic phenotype in porcine joint tissue derived stem cells. *Eur Cell Mater*, 23, 121-32; discussion 133-4.
- VOGEL, K. G., PAULSSON, M. & HEINEGARD, D. 1984. Specific inhibition of type I and type II collagen fibrillogenesis by the small proteoglycan of tendon. *Biochem J*, 223, 587-97.
- VOGEL, K. G., SANDY, J. D., POGANY, G. & ROBBINS, J. R. 1994. Aggrecan in bovine tendon. *Matrix Biol*, 14, 171-9.
- VOGEL, V. & SHEETZ, M. P. 2009. Cell fate regulation by coupling mechanical cycles to biochemical signaling pathways. *Curr Opin Cell Biol*, 21, 38-46.
- VOLETI, P. B., BUCKLEY, M. R. & SOSLOWSKY, L. J. 2012. Tendon healing: repair and regeneration. *Annu Rev Biomed Eng*, 14, 47-71.
- VON DER MARK, K. 2006. Structure, biosynthesis and gene regulation of collagens in cartilage and bone. *Dynamics of Bone and Cartilage Metabolism. Principles and Clinical Applications*. Academic Press/Elsevier Burlington, MA.
- VON EISENHART, R., ADAM, C., STEINLECHNER, M., MULLER-GERBL, M. & ECKSTEIN, F. 1999. Quantitative determination of joint incongruity and pressure distribution during simulated gait and cartilage thickness in the human hip joint. *J Orthop Res*, 17, 532-9.
- WADA, H., OKUYAMA, M., SATOH, N. & ZHANG, S. 2006. Molecular evolution of fibrillar collagen in chordates, with implications for the evolution of vertebrate skeletons and chordate phylogeny. *Evol Dev*, 8, 370-7.
- WAGNER, D. R., LINDSEY, D. P., LI, K. W., TUMMALA, P., CHANDRAN, S. E., SMITH, R. L., LONGAKER, M. T., CARTER, D. R. & BEAUPRE, G. S. 2008. Hydrostatic pressure enhances chondrogenic differentiation of human bone marrow stromal cells in osteochondrogenic medium. *Ann Biomed Eng*, 36, 813-20.
- WALCHLI, C., KOCH, M., CHIQUET, M., ODERMATT, B. F. & TRUEB, B. 1994. Tissue-specific expression of the fibril-associated collagens XII and XIV. *J Cell Sci*, 107 (Pt 2), 669-81.
- WALDMAN, S. D., SPITERI, C. G., GRYPAS, M. D., PILLIAR, R. M. & KANDEL, R. A. 2003. Long-term intermittent shear deformation improves the quality of cartilaginous tissue formed in vitro. *J Orthop Res*, 21, 590-6.
- WALL, M. E., BERNACKI, S. H. & LOBOA, E. G. 2007. Effects of serial passaging on the adipogenic and osteogenic differentiation potential of adipose-derived human mesenchymal stem cells. *Tissue Eng*, 13, 1291-8.
- WALTERS, B. D. & STEGEMANN, J. P. 2014. Strategies for directing the structure and function of three-dimensional collagen biomaterials across length scales. *Acta Biomater*, 10, 1488-501.

References

- WANG, J. H., JIA, F., YANG, G., YANG, S., CAMPBELL, B. H., STONE, D. & WOO, S. L. 2003a. Cyclic mechanical stretching of human tendon fibroblasts increases the production of prostaglandin E2 and levels of cyclooxygenase expression: a novel in vitro model study. *Connect Tissue Res*, 44, 128-33.
- WANG, J. H. C. 2006. Mechanobiology of tendon. *Journal of Biomechanics*, 39, 1563-1582.
- WANG, M. & PENG, Z. 2015. Wear in human knees. *Biosurface and Biotribology*, 1, 98-112.
- WANG, N., TYTELL, J. D. & INGBER, D. E. 2009. Mechanotransduction at a distance: mechanically coupling the extracellular matrix with the nucleus. *Nat Rev Mol Cell Biol*, 10, 75-82.
- WANG, Q., HUANG, C., XUE, M. & ZHANG, X. 2011. Expression of endogenous BMP-2 in periosteal progenitor cells is essential for bone healing. *Bone*, 48, 524-32.
- WANG, W., LI, B., YANG, J., XIN, L., LI, Y., YIN, H., QI, Y., JIANG, Y., OUYANG, H. & GAO, C. 2010. The restoration of full-thickness cartilage defects with BMSCs and TGF-beta 1 loaded PLGA/fibrin gel constructs. *Biomaterials*, 31, 8964-73.
- WANG, X., HARRIS, R. E., BAYSTON, L. J. & ASHE, H. L. 2008. Type IV collagens regulate BMP signalling in *Drosophila*. *Nature*, 455, 72-7.
- WANG, X., MANNER, P. A., HORNER, A., SHUM, L., TUAN, R. S. & NUCKOLLS, G. H. 2004. Regulation of MMP-13 expression by RUNX2 and FGF2 in osteoarthritic cartilage. *Osteoarthritis Cartilage*, 12, 963-73.
- WANG, Y., UEMURA, T., DONG, J., KOJIMA, H., TANAKA, J. & TATEISHI, T. 2003b. Application of perfusion culture system improves in vitro and in vivo osteogenesis of bone marrow-derived osteoblastic cells in porous ceramic materials. *Tissue Eng*, 9, 1205-14.
- WANG, Y. K. & CHEN, C. S. 2013. Cell adhesion and mechanical stimulation in the regulation of mesenchymal stem cell differentiation. *J Cell Mol Med*, 17, 823-32.
- WARD, D. F., JR., SALASZNYK, R. M., KLEES, R. F., BACKIEL, J., AGIUS, P., BENNETT, K., BOSKEY, A. & PLOPPER, G. E. 2007. Mechanical strain enhances extracellular matrix-induced gene focusing and promotes osteogenic differentiation of human mesenchymal stem cells through an extracellular-related kinase-dependent pathway. *Stem Cells Dev*, 16, 467-80.
- WARDALE, R. J. & DUANCE, V. C. 1994. Characterisation of articular and growth plate cartilage collagens in porcine osteochondrosis. *J Cell Sci*, 107 (Pt 1), 47-59.
- WASSEN, M. H., LAMMENS, J., TEKOPPELE, J. M., SAKKERS, R. J., LIU, Z., VERBOUT, A. J. & BANK, R. A. 2000. Collagen structure regulates fibril mineralization in osteogenesis as revealed by cross-link patterns in calcifying callus. *J Bone Miner Res*, 15, 1776-85.
- WATKINS, J. 2009. *Pocket Podiatry: Functional Anatomy*, Elsevier Health Sciences.
- WATT, S. L., LUNSTRUM, G. P., MCDONOUGH, A. M., KEENE, D. R., BURGESSON, R. E. & MORRIS, N. P. 1992. Characterization of collagen types XII and XIV from fetal bovine cartilage. *J Biol Chem*, 267, 20093-9.
- WEBB, K., HITCHCOCK, R. W., SMEAL, R. M., LI, W., GRAY, S. D. & TRESKO, P. A. 2006. Cyclic strain increases fibroblast proliferation, matrix accumulation, and elastic modulus of fibroblast-seeded polyurethane constructs. *J Biomech*, 39, 1136-44.
- WEIDENHAMER, N. K. & TRANQUILLO, R. T. 2013. Influence of Cyclic Mechanical Stretch and Tissue Constraints on Cellular and Collagen Alignment in Fibroblast-Derived Cell Sheets. *Tissue Engineering Part C- Methods*, 19, 386-395.
- WEISEL, J. W. & LITVINOV, R. I. 2013. Mechanisms of fibrin polymerization and clinical implications. *Blood*, 121, 1712-9.
- WEN, L., CHEN, J., DUAN, L. & LI, S. 2018. Vitamin K dependent proteins involved in bone and cardiovascular health (Review). *Mol Med Rep*, 18, 3-15.
- WENSTRUP, R. J., SMITH, S. M., FLORER, J. B., ZHANG, G., BEASON, D. P., SEEGMILLER, R. E., SOSLOWSKY, L. J. & BIRK, D. E. 2011. Regulation of collagen fibril nucleation and initial fibril assembly involves coordinate interactions with collagens V and XI in developing tendon. *J Biol Chem*, 286, 20455-65.
- WEST, D. W., LEE-BARTHEL, A., MCINTYRE, T., SHAMIM, B., LEE, C. A. & BAAR, K. 2015. The exercise-induced biochemical milieu enhances collagen content and tensile strength of engineered ligaments. *J Physiol*, 593, 4665-75.
- WHEDON, D. G. & HEANEY, R. P. 2019. *Bone* [Online]. Encyclopaedia Britannica: Encyclopaedia Britannica, inc. Available: <https://www.britannica.com/science/bone-anatomy> [Accessed July 14 2020].
- WHITE, L. J., TAYLOR, A. J., FAULK, D. M., KEANE, T. J., SALDIN, L. T., REING, J. E., SWINEHART, I. T., TURNER, N. J., RATNER, B. D. & BADYLAK, S. F. 2017. The impact of detergents on the tissue decellularization process: A ToF-SIMS study. *Acta Biomater*, 50, 207-219.
- WIBERG, C., HEDBOM, E., KHAIRULLINA, A., LAMANDE, S. R., OLDBERG, A., TIMPL, R., MORGELIN, M. & HEINEGARD, D. 2001. Biglycan and decorin bind close to the n-terminal region of the collagen VI triple helix. *J Biol Chem*, 276, 18947-52.
- WIBERG, C., HEINEGARD, D., WENGLER, C., TIMPL, R. & MORGELIN, M. 2002. Biglycan organizes collagen VI into hexagonal-like networks resembling tissue structures. *J Biol Chem*, 277, 49120-6.
- WIBERG, C., KLATT, A. R., WAGENER, R., PAULSSON, M., BATEMAN, J. F., HEINEGARD, D. & MORGELIN, M. 2003. Complexes of matrilin-1 and biglycan or decorin connect collagen VI microfibrils to both collagen II and aggrecan. *J Biol Chem*, 278, 37698-704.

References

- WILKERSON, R. 2016. *Patellar Tendon Tear* [Online]. OrthoInfo.org. Available: <https://orthoinfo.aaos.org/en/diseases--conditions/patellar-tendon-tear/> [Accessed 2021].
- WILLIAMS, J. N., KAMBRATH, A. V., PATEL, R. B., KANG, K. S., MEVEL, E., LI, Y., CHENG, Y. H., PUCYLOWSKI, A. J., HASSERT, M. A., VOOR, M. J., KACENA, M. A., THOMPSON, W. R., WARDEN, S. J., BURR, D. B., ALLEN, M. R., ROBLING, A. G. & SANKAR, U. 2018. Inhibition of CaMKK2 Enhances Fracture Healing by Stimulating Indian Hedgehog Signaling and Accelerating Endochondral Ossification. *J Bone Miner Res*, 33, 930-944.
- WILSON, D. G., PHAMLUONG, K., LI, L., SUN, M., CAO, T. C., LIU, P. S., MODRUSAN, Z., SANDOVAL, W. N., RANGELL, L., CARANO, R. A., PETERSON, A. S. & SOLLOWAY, M. J. 2011. Global defects in collagen secretion in a Mia3/TANGO1 knockout mouse. *J Cell Biol*, 193, 935-51.
- WONG, A. J., POLLARD, T. D. & HERMAN, I. M. 1983. Actin filament stress fibers in vascular endothelial cells in vivo. *Science*, 219, 867-9.
- WOODRUFF, M. A. & HUTMACHER, D. W. 2010. The return of a forgotten polymer—Polycaprolactone in the 21st century. *Progress in polymer science*, 35, 1217-1256.
- WU, J. J., WEIS, M. A., KIM, L. S., CARTER, B. G. & EYRE, D. R. 2009. Differences in chain usage and cross-linking specificities of cartilage type V/XI collagen isoforms with age and tissue. *J Biol Chem*, 284, 5539-45.
- WU, S., WANG, Y., STREUBEL, P. N. & DUAN, B. 2017. Living nanofiber yarn-based woven biotextiles for tendon tissue engineering using cell tri-culture and mechanical stimulation. *Acta Biomater*, 62, 102-115.
- WUNDERLI, S. L., WIDMER, J., AMREIN, N., FOOLEN, J., SILVAN, U., LEUPIN, O. & SNEDEKER, J. G. 2018. Minimal mechanical load and tissue culture conditions preserve native cell phenotype and morphology in tendon—a novel ex vivo mouse explant model. *J Orthop Res*, 36, 1383-1390.
- WUTHIER, R. 1988. Mechanism of matrix vesicles-mediated mineralization of cartilage. *ISI Atlas Sci Biochem*, 1, 231-241.
- XIONG, J., ONAL, M., JILKA, R. L., WEINSTEIN, R. S., MANOLAGAS, S. C. & O'BRIEN, C. A. 2011. Matrix-embedded cells control osteoclast formation. *Nat Med*, 17, 1235-41.
- XU, Y., DONG, S., ZHOU, Q., MO, X., SONG, L., HOU, T., WU, J., LI, S., LI, Y., LI, P., GAN, Y. & XU, J. 2014. The effect of mechanical stimulation on the maturation of TSDCs-poly(L-lactide-co-ε-caprolactone)/collagen scaffold constructs for tendon tissue engineering. *Biomaterials*, 35, 2760-72.
- XU, Y., WANG, Q., LI, Y., GAN, Y., LI, P., LI, S., ZHOU, Y. & ZHOU, Q. 2015. Cyclic Tensile Strain Induces Tenogenic Differentiation of Tendon-Derived Stem Cells in Bioreactor Culture. *Biomed Res Int*, 2015, 790804.
- XU, Y., WU, J., WANG, H., LI, H., DI, N., SONG, L., LI, S., LI, D., XIANG, Y., LIU, W., MO, X. & ZHOU, Q. 2013. Fabrication of electrospun poly(L-lactide-co-ε-caprolactone)/collagen nanoyarn network as a novel, three-dimensional, macroporous, aligned scaffold for tendon tissue engineering. *Tissue Eng Part C Methods*, 19, 925-36.
- XUE, L., LI, Y. & CHEN, J. 2017. Duration of simulated microgravity affects the differentiation of mesenchymal stem cells. *Mol Med Rep*, 15, 3011-3018.
- YAMAGUCHI, Y., MANN, D. M. & RUOSLAHTI, E. 1990. Negative regulation of transforming growth factor-beta by the proteoglycan decorin. *Nature*, 346, 281-4.
- YEATTS, A. B. & FISHER, J. P. 2011. Bone tissue engineering bioreactors: dynamic culture and the influence of shear stress. *Bone*, 48, 171-81.
- YEUNG, C. Y., ZEEF, L. A., LALLYETT, C., LU, Y., CANTY-LAIRD, E. G. & KADLER, K. E. 2015. Chick tendon fibroblast transcriptome and shape depend on whether the cell has made its own collagen matrix. *Sci Rep*, 5, 13555.
- YLONEN, R., KYRONLAHTI, T., SUND, M., ILVES, M., LEHENKARI, P., TUUKKANEN, J. & PIHLAJANIEMI, T. 2005. Type XIII collagen strongly affects bone formation in transgenic mice. *J Bone Miner Res*, 20, 1381-93.
- YOUNG, B. B., GORDON, M. K. & BIRK, D. E. 2000. Expression of type XIV collagen in developing chicken tendons: association with assembly and growth of collagen fibrils. *Dev Dyn*, 217, 430-9.
- YOUNG, B. B., ZHANG, G., KOCH, M. & BIRK, D. E. 2002. The roles of types XII and XIV collagen in fibrillogenesis and matrix assembly in the developing cornea. *J Cell Biochem*, 87, 208-20.
- YOUNG, R. G., BUTLER, D. L., WEBER, W., CAPLAN, A. I., GORDON, S. L. & FINK, D. J. 1998. Use of mesenchymal stem cells in a collagen matrix for Achilles tendon repair. *J Orthop Res*, 16, 406-13.
- YOUNGSTROM, D. W., LADOW, J. E. & BARRETT, J. G. 2016. Tenogenesis of bone marrow-, adipose-, and tendon-derived stem cells in a dynamic bioreactor. *Connective Tissue Research*, 57, 454-465.
- YOUNGSTROM, D. W., RAJPAR, I., KAPLAN, D. L. & BARRETT, J. G. 2015. A bioreactor system for in vitro tendon differentiation and tendon tissue engineering. *J Orthop Res*, 33, 911-8.
- YUAN, X., CAO, J., HE, X., SERRA, R., QU, J., CAO, X. & YANG, S. 2016. Ciliary IFT80 balances canonical versus non-canonical hedgehog signalling for osteoblast differentiation. *Nat Commun*, 7, 11024.
- YUGE, L., KAJIUME, T., TAHARA, H., KAWAHARA, Y., UMEDA, C., YOSHIMOTO, R., WU, S. L., YAMAOKA, K., ASASHIMA, M., KATAOKA, K. & IDE, T. 2006. Microgravity potentiates stem cell proliferation while sustaining the capability of differentiation. *Stem Cells Dev*, 15, 921-9.
- YUGE, L., SASAKI, A., KAWAHARA, Y., WU, S. L., MATSUMOTO, M., MANABE, T., KAJIUME, T., TAKEDA, M., MAGAKI, T., TAKAHASHI, T., KURISU, K. & MATSUMOTO, M. 2011. Simulated microgravity maintains

References

- the undifferentiated state and enhances the neural repair potential of bone marrow stromal cells. *Stem Cells Dev*, 20, 893-900.
- YUSOFF, N., ABU OSMAN, N. A. & PINGGUAN-MURPHY, B. 2011. Design and validation of a bi-axial loading bioreactor for mechanical stimulation of engineered cartilage. *Med Eng Phys*, 33, 782-8.
- ZEITER, S., LEZUO, P. & ITO, K. 2009. Effect of TGF beta1, BMP-2 and hydraulic pressure on chondrogenic differentiation of bovine bone marrow mesenchymal stromal cells. *Biorheology*, 46, 45-55.
- ZELENCHUK, L. V., HEDGE, A. M. & ROWE, P. S. 2015. Age dependent regulation of bone-mass and renal function by the MEPE ASARM-motif. *Bone*, 79, 131-42.
- ZELZER, E., GLOTZER, D. J., HARTMANN, C., THOMAS, D., FUKAI, N., SOKER, S. & OLSEN, B. R. 2001. Tissue specific regulation of VEGF expression during bone development requires Cbfa1/Runx2. *Mech Dev*, 106, 97-106.
- ZHANG, D., WEINBAUM, S. & COWIN, S. C. 1998. Estimates of the peak pressures in bone pore water. *J Biomech Eng*, 120, 697-703.
- ZHANG, G., EZURA, Y., CHERVONEVA, I., ROBINSON, P. S., BEASON, D. P., CARINE, E. T., SOSLOWSKY, L. J., IOZZO, R. V. & BIRK, D. E. 2006. Decorin regulates assembly of collagen fibrils and acquisition of biomechanical properties during tendon development. *J Cell Biochem*, 98, 1436-49.
- ZHANG, G., YOUNG, B. B. & BIRK, D. E. 2003. Differential expression of type XII collagen in developing chicken metatarsal tendons. *J Anat*, 202, 411-20.
- ZHANG, G., YOUNG, B. B., EZURA, Y., FAVATA, M., SOSLOWSKY, L. J., CHAKRAVARTI, S. & BIRK, D. E. 2005. Development of tendon structure and function: regulation of collagen fibrillogenesis. *J Musculoskeletal Neuronal Interact*, 5, 5-21.
- ZHANG, J., HU, Q., WANG, S., TAO, J. & GOU, M. 2020. Digital Light Processing Based Three-dimensional Printing for Medical Applications. *Int J Bioprint*, 6, 242.
- ZHANG, J. & WANG, J. H. C. 2010. Mechanobiological response of tendon stem cells: implications of tendon homeostasis and pathogenesis of tendinopathy. *Journal of orthopaedic research*, 28, 639-643.
- ZHANG, L., TRAN, N., CHEN, H. Q., KAHN, C. J., MARCHAL, S., GROUBATCH, F. & WANG, X. 2008. Time-related changes in expression of collagen types I and III and of tenascin-C in rat bone mesenchymal stem cells under co-culture with ligament fibroblasts or uniaxial stretching. *Cell Tissue Res*, 332, 101-9.
- ZHANG, N., XIAO, Q.-R., MAN, X.-Y., LIU, H.-X., LÜ, L.-X. & HUANG, N.-P. 2016. Spontaneous osteogenic differentiation of mesenchymal stem cells on electrospun nanofibrous scaffolds. *RSC advances*, 6, 22144-22152.
- ZHAO, B., TUMANENG, K. & GUAN, K. L. 2011a. The Hippo pathway in organ size control, tissue regeneration and stem cell self-renewal. *Nat Cell Biol*, 13, 877-83.
- ZHAO, Q., EBERSPAECHER, H., LEFEBVRE, V. & DE CROMBRUGGHE, B. 1997. Parallel expression of Sox9 and Col2a1 in cells undergoing chondrogenesis. *Dev Dyn*, 209, 377-86.
- ZHAO, T., WEINHOLD, P. S., LEE, N. Y. & DAHNERS, L. E. 2011b. Some observations on the subfibrillar structure of collagen fibrils as noted during treatment with NKISK and cathepsin G with mechanical agitation. *J Electron Microsc (Tokyo)*, 60, 177-82.
- ZHENG, M. H., CHEN, J., KIRILAK, Y., WILLERS, C., XU, J. & WOOD, D. 2005. Porcine small intestine submucosa (SIS) is not an acellular collagenous matrix and contains porcine DNA: possible implications in human implantation. *J Biomed Mater Res B Appl Biomater*, 73, 61-7.
- ZHONG, W., TIAN, K., ZHENG, X., LI, L., ZHANG, W., WANG, S. & QIN, J. 2013. Mesenchymal stem cell and chondrocyte fates in a multishear microdevice are regulated by Yes-associated protein. *Stem Cells Dev*, 22, 2083-93.
- ZHU, J. & CLARK, R. A. F. 2014. Fibronectin at select sites binds multiple growth factors and enhances their activity: expansion of the collaborative ECM-GF paradigm. *J Invest Dermatol*, 134, 895-901.
- ZHU, J., ZHANG, X., WANG, C., PENG, X. & ZHANG, X. 2008. Different magnitudes of tensile strain induce human osteoblasts differentiation associated with the activation of ERK1/2 phosphorylation. *Int J Mol Sci*, 9, 2322-32.
- ZUK, P. A., ZHU, M., ASHJIAN, P., DE UGARTE, D. A., HUANG, J. I., MIZUNO, H., ALFONSO, Z. C., FRASER, J. K., BENHAIM, P. & HEDRICK, M. H. 2002. Human adipose tissue is a source of multipotent stem cells. *Mol Biol Cell*, 13, 4279-95.
- ZUR NIEDEN, N. I., KEMPKA, G., RANCOURT, D. E. & AHR, H. J. 2005. Induction of chondro-, osteo- and adipogenesis in embryonic stem cells by bone morphogenetic protein-2: effect of cofactors on differentiating lineages. *BMC Dev Biol*, 5, 1.

